

Investigation Of Melanoma Circulating Tumour Cell Clusters Using Biomaterial Surfaces

Rajeharish Rajendran
May 2023

A thesis submitted in partial fulfilment of the requirements of
Nottingham Trent University for the degree of Doctor of Philosophy

Copyright Statement

The copyright in this work is held by the author. You may copy up to 5% of this work for private study, or personal, non-commercial research. Any re-use of the information contained within this document should be fully referenced, quoting the author, title, university, degree level and pagination. Queries or requests for any other use, or if a more substantial copy is required, should be directed to the author.

Abstract

Circulating tumour cells (CTC) disperse from primary tumours to distal anatomical sites via lymphatic and haematological vessels. This process is known as metastasis, which contributes to the majority of cancer-related mortality. Though much rarer, CTC clusters are considerably more metastatic, up to 100-fold more, than their single CTC counterpart. Around 30 – 34% of patients suffering from metastatic melanoma present CTC clusters. However, the underlying molecular mechanisms governing cluster formation and contribution to metastasis remain unknown. Using hydrophobic fluoroalkylsilica (FS) surfaces that induce multicellular aggregation-disaggregation of FM3 melanoma cells as an *in vitro* model, this research project discovered novel signalling molecules, such as galectin-3, 4F2hc, and MMP2, involved in homotypic aggregation-disaggregation of melanoma CTC. To promote aggregation, oligomeric galectin-3 could cross-link coterminous 4F2hc glycoproteins on adjacent cells, via the formation of glycoprotein:galectin-3:glycoprotein (GGG) bridges. At distal metastatic sites, MMP2-dependent cleavage of oligomeric galectin-3 could dissociate GGG bridges to promote disaggregation. Studies reported that β -catenin-signalling could be regulated by 4F2hc. In FM3 cells, β -catenin expression was decreased during disaggregation, highlighting the importance of β -catenin interactome in aggregation. PU.1 transcription factor is likely involved in this non-canonical β -catenin-signalling. PU.1-inhibition resulted in increased 4F2hc levels, suggesting that 4F2hc expression could be regulated by β -catenin and PU.1 in melanoma CTC. Lastly, fibronectin and vitronectin undergo denaturation caused by conformational changes associated with intermolecular β -sheets and random coils, during adsorption onto tissue culture polystyrene (TCP) surfaces but not on FS surfaces. Denaturation could expose cell-binding motifs from cryptic sites, leading to increased cellular adhesion, and multicellular disaggregation. This explains why FM3 cells readily attach to TCP surfaces but aggregate on FS surfaces. This research project demonstrates the suitability of using FS surface-based approaches to study melanoma CTC clusters. Future research could use FS surfaces to interrogate GGG bridges and CTC cluster-mediated metastasis of other cancers.

Dedication

To my caring mother and sisters who supported me through thick and thin. To Marie Salomea Skłodowska–Curie, my greatest inspiration, who gave her life in the pursuit of a cure for cancer.

"Life is not easy for any of us. But what of that? We must have perseverance and above all confidence in ourselves. We must believe that we are gifted for something, and that this thing must be attained."

"Nothing in life is to be feared; it is only to be understood."

Marie Salomea Skłodowska–Curie (7th of November 1867 – 4th of July 1934)

Ancient Tamil proverbs:

எப்பொருள் யார் யார் வாய்க்கேட்பினும், அப்பொருள் மெய்ப்பொருள் காண்பது அறிவு.

To discern the truth in the matter yourself is the mark of one's wisdom.

கற்றது கை மண்ணளவு, கல்லாதது உலகளவு.

What we have learned is measured by grains of sand we can hold in our hands; what we have yet to learn is measured by all the grains of sand on the earth.

Acknowledgements

Firstly, I would like to express my deepest gratitude towards my supervisors Dr David Boocock, Professor Carole Perry, and Dr Amanda Coutts, who not only have been immensely supportive, exhortative, and inspirational, but often went beyond their duties to help during periods of tribulations.

I would like to acknowledge the following members of John van Geest Cancer Research centre and Biomolecular and Materials Interface Research Group:

- Dr Graham Hickman for support in surface synthesis and characterisation.
- Dr Jayakumar Vadakekolathu for support in molecular biology techniques.
- Dr David Belton for support in infrared spectroscopic techniques.
- Dr Clare Coveney for support in mass spectrometry and protein extraction.
- Mr Stephen Reeder for support in purchasing and help with protein extraction.
- Mrs Anne Schneider for support in cell culture.
- Dr Thomas Warwick for support in protein adsorption experiments.
- Dr Amanda Miles for support in mass spectrometry.

I acknowledge the support from fellow PhD students, who have made this journey even more enjoyable. Special thanks to my mother Mrs Rajeswary Rajeswaran for emotional and financial support during the last year of my PhD.

Lastly, I am grateful to Nottingham Trent University for the award of Vice Chancellor's PhD Scholarships, which allowed me to develop my research skills and discover novel findings pertaining to melanoma metastasis.

Abbreviations

4F2hc:	4F2 heavy-chain
ADPM:	Aggregation-disaggregation processes of metastasis
CHX:	Chlorhexidine
CRD:	Carbohydrate recognition domain
CTC:	Circulating tumour cells
ECM:	Extracellular Matrix
EMT:	Epithelial to Mesenchymal Transition
FDTES:	1 <i>H</i> ,1 <i>H</i> ,2 <i>H</i> ,2 <i>H</i> -perfluorodecyltriethoxysilane
Fn:	Fibronectin
FS:	Fluoroalkylsilica
GGG:	Glycoprotein:galectin-3:glycoprotein
GlcNAc:	<i>N</i> -Acetylglucosamine
GPI:	Glycosylphosphatidylinositol
IG:	Immunoglobulin G
MMP:	Matrix Metalloproteinase
oGal3:	Oligomeric galectin-3
PPI:	Protein-protein interaction
RCA:	Reduced cellular adhesion
RT-qPCR:	Reverse transcription quantitative polymerase chain reaction
TCP:	Tissue Culture Polystyrene
tGal3:	Truncated galectin-3
Vn:	Vitronectin

Contents

CHAPTER 1. INTRODUCTION.....	1
1.1 MELANOMA	2
1.1.1 Hallmarks of cancer.....	2
1.1.2 Melanoma carcinogenesis.....	4
1.1.3 Melanoma metastasis	5
1.2 CIRCULATING TUMOUR CELL (CTC) CLUSTERS.....	6
1.2.1 Single vs Clusters	6
1.2.2 Mechanisms of CTC cluster formation	7
1.3 ADVANCED TISSUE CULTURE SURFACES TO STUDY CTC CLUSTERS.....	8
1.3.1 Limitations of current CTC cluster models	8
1.3.2 Effects of surface chemistry and topography on cells.....	8
1.3.3 Effects of surface chemistry and topography on protein adsorption.....	10
1.3.4 Silica-modified surfaces.....	12
1.4 PROJECT AIMS AND OBJECTIVES	15
CHAPTER 2. MATERIALS & METHODS	17
2.1 SURFACE SYNTHESIS	18
2.1.1 Fluoroalkylsilica surface fabrication	18
2.1.2 Fluoroalkylsilica surface characterisation	18
2.2 CELL CULTURE & ASSAYS	19
2.2.1 Routine cell culture	19
2.2.2 Cell viability assay.....	19
2.2.3 Invasion and migration assay	19
2.2.4 Cell culture under hypoxic condition	20
2.2.5 Treatment of cells with inhibitor, antibody, or cytokine	20
2.2.6 Cellular aggregation assay.....	21
2.2.7 Immunofluorescence	21
2.3 PROTEOMICS & TRANSCRIPTOMICS	22
2.3.1 Cell lysis for mass spectrometry and western blot	22
2.3.2 Extracellular matrix isolation for mass spectrometry	22
2.3.3 Western blot.....	23
2.3.4 Mass spectrometry	23
2.3.5 Quantitative reverse transcription polymerase chain reaction (RT-qPCR).....	24
2.4 BIOINFORMATICS	25
2.4.1 Clinical patient data analyses	25
2.4.2 Protein docking	26

2.5 PROTEIN ADSORPTION.....	27
2.5.1 Amido black staining.....	27
2.5.2 FTIR-ATR and 2D correlation spectroscopy.....	27
2.6 STATISTICAL ANALYSES	28
CHAPTER 3. <i>IN VITRO</i> CELL CULTURE SURFACE-BASED MODEL OF MELANOMA CIRCULATING TUMOUR CELL CLUSTERS.....	30
3.1 INTRODUCTION	31
3.2 RESULTS.....	32
3.2.1 FM3 cell aggregation-disaggregation dynamics on FS surfaces	32
3.2.2 Cellular viability is reduced in FM3 aggregates	35
3.2.3 Cell-cell proteins are upregulated during FM3 multicellular aggregation.....	35
3.2.4 Cell-matrix proteins were upregulated during melanoma multicellular disaggregation.....	36
3.3 DISCUSSION	39
3.3.1 Melanoma FM3 cells aggregate under reduced cellular adhesion conditions....	39
3.3.2 Disaggregation occurs on remodelled extracellular matrix.....	40
3.3.3 Aggregation-disaggregation process results in a more invasive phenotype	41
3.3.4 Cellular viability is reduced in melanoma FM3 multicellular aggregates	43
3.3.5 ADPM of FM3 cells involve cell-cell, cell-matrix, and cytoskeletal regulatory pathways.....	44
3.3.6 FM3 cells remodel ECM by secreting vitronectin and fibronectin during disaggregation.....	45
3.3.7 Conclusions.....	46
3.4 SUPPLEMENTARY FIGURES	48
CHAPTER 4. INVOLVEMENT OF 4F2HC AND GALECTIN-3 IN MELANOMA MULTICELLULAR AGGREGATION	49
4.1 INTRODUCTION	50
4.2 RESULTS.....	51
4.2.1 Galectin-3 expression in FM3 multicellular aggregation-disaggregation	51
4.2.2 4F2hc expression during FM3 multicellular aggregation-disaggregation.....	53
4.2.3 Galectin-3 and 4F2hc colocalises at cell-cell facet of FM3 multicellular aggregate	55
4.2.4 4F2hc:oGal3:4F2hc bridges vs 4F2hc:4f2hc homophilic binding	55
4.2.5 4F2hc and galectin-3 predicted to contribute to clinical melanoma metastasis.	58
4.3 DISCUSSION	60
4.3.1 Galectin-3 is involved in FM3 multicellular aggregation-disaggregation	60
4.3.2 4F2hc plays a major role in FM3 multicellular aggregation-disaggregation.....	61
4.3.3 Galectin-3 and 4F2hc colocalises at FM3 cell-cell interface	63

4.3.4 4F2hc:oGal3:4F2hc bridges	63
4.3.5 4F2hc:4F2hc homophilic binding	65
4.3.6 4F2hc:oGal3:4F2hc bridges vs 4F2hc:4F2hc homophilic binding in melanoma FM3 aggregates	66
4.3.7 Glycoprotein:Galectin-3:Glycoprotein (GGG) Bridges in clinical melanoma.....	68
4.3.8 Conclusions	70
4.4 SUPPLEMENTARY FIGURES	71
CHAPTER 5. ROLE OF MMP2 IN MELANOMA MULTICELLULAR AGGREGATION AND DISAGGREGATION.....	78
5.1 INTRODUCTION	79
5.2 RESULTS.....	80
5.2.1 MMP2 expression during FM3 multicellular aggregation-disaggregation.....	80
5.2.2 4F2hc, β -catenin, and TIMP3 expression during MMP2-inhibition in FM3 cells	82
5.2.3 Galectin-3, 4F2hc, and MMP2 on melanoma survival outcome	83
5.3 DISCUSSION	86
5.3.1 FM3 cells reduce MMP2 expression to prevent untimely cellular disaggregation	86
5.3.2 MMP2-mediated control of β -Catenin and 4F2hc levels in FM3 cells	87
5.3.3 Concerted roles of Galectin-3, 4F2hc and MMP2 in melanoma ADPM.....	88
5.3.4 Conclusions	91
5.4 SUPPLEMENTARY FIGURES	92
CHAPTER 6. EPITHELIAL-MESENCHYMAL TRANSITION AND β-CATENIN IN MELANOMA MULTICELLULAR AGGREGATION-DISAGGREGATION... 	93
6.1 INTRODUCTION	94
6.1.1 EMT and MET	94
6.1.2 EMT-like process in melanoma.....	95
6.1.3 EMT-like process in CTC clusters	96
6.1.4 Crosstalk of TGF β and Wnt/ β -catenin signalling in EMT	97
6.1.5 β -catenin in melanoma CTC clusters.....	98
6.2 RESULTS.....	100
6.2.1 β -catenin expression during FM3 multicellular aggregation-disaggregation....	100
6.2.2 EMT in FM3 multicellular aggregation-disaggregation	102
6.2.3 Effect of EMT status on ADPM response of prostate cancer cells.....	103
6.2.4 β -catenin interactome changes during ADPM of FM3 cells.....	105
6.2.5 β -catenin interactome affects melanoma survival outcome	108
6.2.6 β -catenin-mediated transcriptional regulation of ADMP	111
6.3 DISCUSSION	114
6.3.1 β -catenin is involved in multicellular aggregation of FM3 cells.....	115

6.3.2 EMT does not occur during ADPM of FM3 cells.....	116
6.3.3 P4B6B cells sustain aggregation via expression of vitronectin, vimentin and shroom-3.....	116
6.3.4 β -catenin interactors, LDHB, PML, PABP1, PUR9, SPF45, RL11, and HS105 involvement during ADPM of FM3 cells	118
6.3.5 β -catenin interactors, LDHB, PML, PABP1, PUR9, SPF45, RL11, and HS105 impact on prognosis of metastatic melanoma	121
6.3.6 β -catenin and SPI1-mediated transcriptional regulation in ADPM of FM3 cells	126
6.3.7 Conclusions.....	127
6.4 SUPPLEMENTARY FIGURES	129
CHAPTER 7. PU.1-MEDIATED TRANSCRIPTIONAL REGULATION DURING MELANOMA MULTICELLULAR AGGREGATION-DISAGGREGATION	134
7.1 INTRODUCTION	135
7.1.1 PU.1 transcription factor	135
7.1.2 PU.1 in cancer.....	136
7.2 RESULTS.....	137
7.2.1 PU.1 on FM3 cellular responses during ADPM.....	137
7.2.2 PU.1-target genes in FM3 cells	140
7.2.3 PU.1-target genes in ADPM of FM3 cells.....	142
7.2.4 PU.1 in clinical melanoma metastasis	146
7.3 DISCUSSION	148
7.3.1 PU.1 is involved invasion and migration during ADPM of FM3 cells	148
7.3.2 PU.1 mediates key pathways involved in cellular proliferation, migration, and invasion in FM3 cells	151
7.3.3 PU.1 regulates expression of key proteins involved in ADPM of FM3 cells.....	154
7.3.4 PU.1 expression dictates clinical melanoma metastasis and survival outcome	156
7.3.5 Conclusions.....	158
7.4 SUPPLEMENTARY FIGURES	159
CHAPTER 8. CONFORMATIONAL CHANGES OF FIBRONECTIN AND VITRONECTIN DURING ADSORPTION ONTO HYDROPHOBIC FS AND TCP SURFACES	162
8.1 INTRODUCTION	163
8.2 RESULTS.....	165
8.2.1 Differential adsorption and fibril formation of fibronectin and vitronectin on FS and TCP surfaces	165
8.2.2 Conformational changes of fibronectin and vitronectin during adsorption onto FS and TCP surfaces.....	167

8.2.3 Sequential perturbation of secondary structures of fibronectin and vitronectin during adsorption onto FS and TCP surfaces	171
8.3 DISCUSSION	174
8.3.1 Conclusions	177
8.4 SUPPLEMENTARY FIGURES	178
CHAPTER 9. DISCUSSION	180
9.1 PROJECT OVERVIEW	181
9.2 4F2HC-CONTAINING GLYCOPROTEIN:GALECTIN-3:GLYCOPROTEIN (GGG) BRIDGES PROMOTE HOMOTYPIC AGGREGATION OF FM3 CELLS.	181
9.3 ROLE OF EPITHELIAL-TO-MESENCHYMAL (EMT) AND B-INTERACTOME IN ADPM OF FM3 CELLS	184
9.4 PU.1-MEDIATED TRANSCRIPTIONAL REGULATION DURING ADPM OF FM3 CELLS	185
9.5 CONFORMATION CHANGES OF FIBRONECTIN AND VITRONECTIN DURING ADSORPTION ON FS AND TCP SURFACES	186
9.6 CONCLUSION	187
9.7 FUTURE PROSPECTS	188
9.7.1 Novel silica-modified surfaces.....	188
9.7.2 Advances in melanoma therapeutics	189
CHAPTER 10. REFERENCES.....	191
10.1 APPENDIX.....	235

List of figures

- Fig. 1. Differences in molecular hallmark and properties between single CTC and CTC clusters.....6
- Fig. 1.2 Schematic depicting fabrication of FS surfaces from TCP surfaces.....14
- Fig. 3.1 Modelling melanoma CTC cluster aggregation-disaggregation dynamics using fluoroalkylsilica (FS) surfaces.....33
- Fig. 3.2 Proteomics of melanoma cell lysate reveal aggregation-disaggregation machinery upon FS surface.....37
- Fig. 3.3 Proteomics highlight key ECM components involved in aggregation-disaggregation of FM3 cells.....38
- Supplementary Fig. 3.1 Characterisation of FS and TCP surfaces.....48
- Fig. 4.1 Galectin-3 facilitates FM3 cellular aggregation-disaggregation.....52
- Fig. 4.2 4F2hc regulates FM3 cellular aggregation-disaggregation.....54
- Fig. 4.3 FM3 multicellular aggregation: [4F2hc-oGal3-4F2hc] bridges vs [4F2hc-4F2hc] homophilic interactions.....56
- Fig. 4.4 4F2hc predicted to contribute to clinical melanoma CTC aggregation-disaggregation.....59
- Supplementary Fig. 4.1 Treatment of FM3 cellular aggregates with Galectin-3 inhibitor (GB1107) inhibitor decreases aggregation.....71
- Supplementary Fig. 4.2 Galectin-3 colocalises with 4F2hc at cell-cell contact in FM3 multicellular aggregates.....72

- Supplementary Fig. 4.3 Change in MUC18 levels during FM3 multicellular aggregation-disaggregation.....73
- Supplementary Fig. 4.4 Possible molecular interactions of Galectin-3-CRD and 4F2hc-ED interface.....74
- Supplementary Fig. 4.5 Possible molecular interactions of 4F2hc-ED:4F2hc-ED homophilic interface.....75
- Supplementary Fig. 4.6 PPI score of Galectin-3/4F2hc or 4F2hc/4F2hc interactions.....77
- Supplementary Fig. 4.7 Galectin-3 predicted to contribute to clinical melanoma CTC aggregation-disaggregation.....77
- Fig. 5.1 MMP2-dependent cleavage of Galectin-3 oligomers regulates melanoma cellular disaggregation.....81
- Fig. 5.2 4F2hc, Galectin-3, and β -catenin expression in MMP2-inhibitor (CHX)-treated FM3 cells.....82
- Fig. 5.3 Concerted roles of galectin-3, 4F2hc and MMP2 define the survival of melanoma patients.....85
- Supplementary Fig. 5.1 Treatment of FM3 cellular aggregates with MMP2 inhibitor (CHX) decreases aggregation.....92
- Fig. 6.0 Parallel between EMT/MET and melanoma states.....95
- Fig. 6.1 Increased β -catenin levels promote FM3 multicellular aggregation.....101
- Fig. 6.2 Mesenchymal-like cells favour aggregation.....104
- Fig. 6.3. β -catenin interactome changes during FM3 multicellular aggregation-disaggregation.....107

- Fig. 6.4. β -catenin interactome expression on survival outcome of melanoma patients.....109
- Fig. 6.5. β -catenin interactome expression increased in metastatic melanoma patients.....110
- Fig. 6.6 Melanoma metastasis risk associated with β -catenin interactome.....111
- Fig. 6.7 Analysis of transcriptional regulation during ADPM of FM3 cells highlights SPI1 as the most influential master regulator.....113
- Fig. 6.8. Proposed cross-talk of TGF β -signalling, Wnt/ β -catenin-signalling and 4F2hc/Galectin-3/integrin signalling regulating β -catenin interactome during ADPM of FM3 cells and melanoma CTC clusters.....125
- Supplementary Fig. 6.1 Expression of EMT markers during ADPM of FM3 cells.....129
- Supplementary Fig. 6.2 No cadherin switch occurs during ADPM of FM3 cells.....130
- Supplementary Fig. 6.3 Hypoxia does not affect ADPM of FM3 cells.....131
- Supplementary Fig. 6.4 No cadherin switch occurs during ADPM of epithelial (P5B3) cells and mesenchymal (P4B6B) cells.....132
- Supplementary Fig. 6.5 Proteomic changes of β -catenin interactors during ADPM of FM3 cells.....133
- Fig. 7.0 PU.1 protein expression in anatomical sites.....135
- Fig. 7.1 PU.1 influences viability, invasiveness, and migration of FM3 cells during ADPM.....139
- Fig. 7.2 Inhibition of PU.1 in FM3 cells affects proteins involved in metabolism, regulation of cell shape and melanocyte differentiation.....141
- Fig. 7.3 Comparison of proteomic changes during inhibition of PU.1 and ADPM of FM3 cells.....143

- Fig. 7.4 PU.1-binding sites in candidate PU.1-target genes activated or repressed during ADPM of FM3 cells.....145
- Fig. 7.5 Melanoma metastasis risk associated with PU.1.....147
- Supplementary Fig. 7.1 DB2313 treatment of FM3 cells.....159
- Supplementary Fig. 7.2 Effect of DB2313 treatment on key proteins important for ADPM of FM3 cells.....160
- Supplementary Fig. 7.3. PU.1-binding sites in candidate PU.1-target genes activated or repressed during ADPM of FM3 cells.....161
- Fig. 8.0 Schematic of human fibronectin and vitronectin structures.....163
- Fig. 8.1 Adsorption and fibril formation dynamics of fibronectin and vitronectin on FS and TCP surfaces.....166
- Fig. 8.2 FTIR-ATR spectra of BSA and fibronectin fitted with conformer peaks.....169
- Fig. 8.3 Conformer composition of fibronectin and vitronectin after adsorption onto TCP and FS surfaces.....170
- Fig. 8.4 Two-dimensional (2D) correlation spectroscopy of FTIR spectra of fibronectin adsorbed onto TCP and FS surfaces.....173
- Supplementary Fig. 8.1 – 8.4 FTIR spectra.....178-179
- Fig 9.0 Scheme of aggregation-disaggregation process of metastasis of melanoma CTC.....182

List of Tables

- Table 2.1: Summary of treatments used in this study
- Supplementary Table. 4.1: Galectin-3-Binding Cell-Surface Glycoproteins
- Table 9.1. Number of *N*-glycosylation sites in cell-surface glycoproteins that are important for CTC cluster formation

Chapter 1. Introduction

Contents

1.1 MELANOMA	2
1.1.1 Hallmarks of cancer	2
1.1.2 Melanoma carcinogenesis	4
1.1.3 Melanoma metastasis	5
1.2 CIRCULATING TUMOUR CELL (CTC) CLUSTERS.....	6
1.2.1 Single vs Clusters	6
1.2.2 Mechanisms of CTC cluster formation.....	7
1.3 ADVANCED TISSUE CULTURE SURFACES TO STUDY CTC CLUSTERS.....	8
1.3.1 Limitations of current CTC cluster models.....	8
1.3.2 Effects of surface chemistry and topography on cells	8
1.3.3 Effects of surface chemistry and topography on protein adsorption	10
1.3.4 Silica-modified surfaces.....	12
1.4 PROJECT AIMS AND OBJECTIVES	15

1.1 Melanoma

1.1.1 Hallmarks of cancer

The International Agency for Research on Cancer, World Health Organization, reported that in 2022, there were almost 20 million new cancer incidents and 9.7 million cancer-related deaths occurred worldwide.¹ New cancer incidents are projected to rise to 29.9 million, and the number of deaths caused by cancer is expected to rise to 15.3 million by the year 2040. Recent scientific efforts have advanced our understanding of carcinogenesis, tumour progression, and prognosis of cancer, revealing new opportunities for therapeutic interventions for this deadly disease once considered as incurable.

Cancer is the broad-term used for describing a heterogenous group of diseases that exhibit fundamental abnormality in cellular behaviour: the uncontrolled, invasive, and sustained proliferation, which leads to incongruous, and often dangerous, growth into healthy tissue. Normal healthy cells vehemently and subserviently follow a set of strict rules and guidelines forced upon them by the human body. Growth factors and mitogenic factors tell cells to grow and undergo mitosis. Growth suppressors impede cellular growth. Cell-death programmes, such as apoptosis, tightly control where and when cells should die. And the ultimate rule which puts a time-limit on cellular replicative capabilities, which embodies the essence of mortality of all life-forms as they age. However, cancerous cells rebel against these rules. In defiance of nature, they gain advanced features that normal cells do not usually possess, features such as replicative immortality. These features, so-called 'hallmarks of cancer', are bestowed upon them by genomic instability and chromosomal abnormalities, that pave the path for carcinogenesis.

There are over two-hundred types of cancer that have been clinically described, each one manifesting as genotypically and phenotypically diverse compared to the next; though a myriad of commonalities, as described in the 'hallmarks of cancer' conceptual framework, allow for classification and treatment strategies. The hallmarks of cancer framework was initially conceptualised and codified by Hanahan and Weinberg in the year 2000,² based on a quarter century of advances in cancer research and discovery of oncogenes (dominant gain of function genes) and tumour suppressor genes (recessive loss of function genes).

Initially, it included six hallmarks:

1. **Self-sufficiency in growth signals** – e.g. overexpression of epidermal growth factor receptor in breast cancer, which induces cells to exit from G0 and enter G1 stage of the cell-cycle, thus perpetuating mitotic division and growth.³

2. **Insensitivity to anti-growth signals** - e.g. loss of the tumour suppressor gene p53 in almost half of all cancers, thus preventing p53-mediated senescence/apoptosis responses to cellular/genomic stresses.⁴
3. **Tissue invasion and metastasis** – e.g. reactivating developmental programmes, such as epithelial-to-mesenchymal transition (EMT) to obtain morphology required for motility and invasion.⁵
4. **Limitless replicative potential** – e.g. in cancer cells, telomerases are upregulated, which is an enzyme that maintains telomere tandem repeat sequences (TTAGGG)_n at the ends of chromosomes; gradual decrease of these telomere sequences with each cell-cycle normally preordains cells to senescence and eventual apoptotic-death during aging, which cancer cells intuitively avoid.⁶
5. **Sustained angiogenesis** – e.g. induction of angiogenesis, that is the formation of new blood vessels from old vessels, by overexpression of angiogenic factor VEGF by cancer cells.⁷
6. **Evading apoptosis** – e.g. upregulation of anti-apoptotic factors such as Bcl-2, whilst downregulating pro-apoptotic factors such as Bax.⁸

After another decade of discoveries that highlighted key roles that stromal cells, such as cancer-associated fibroblasts, as well as immune cells, play in progress of the disease, in year 2011,⁹ the hallmarks were expanded to include four more:

7. **Avoiding immune destruction** – e.g. to avoid immune-surveillance and subsequent destruction of abnormal cells, cancer cells downregulate cell-surface antigen presenting machinery by mutating or complete loss of MHC molecules.¹⁰
8. **Tumour-promoting inflammation** – e.g. inflammatory cells could infiltrate the tumour microenvironment, that could provide growth factors and cytokines to promote tumorigenesis.¹¹
9. **Genome instability and mutation** – e.g. for example, cancer cells contain large number of chromosomal aberrations (called chromosomal instability), that includes loss or gain of chromosomes, as well as translocation events, and hyper-mutability (called microsatellite instability) owing to faulty DNA mismatch repair system.¹²
10. **Deregulating cellular energetics** – e.g. as heightened rate of cell division of cancer cells demands large quantity of energy and biosynthetic materials, cancer cells seek to obtain these from glycolysis and lactate fermentation processes (referred to as the Warburg effect) which produce sufficient biosynthetic materials needed for increased cell division, as opposed to oxidative phosphorylation (OXPHOS) that normal cells use for the generation of ATP/energy.¹³

And more recently, emerging insights into epigenetics, phenotypic plasticity, response to cancer therapy, and discovery of novel perpetrators such as influences of the microbiome, all lead Douglas Hanahan to propose four more dimensions to this conceptual framework in 2022:¹⁴

11. **Nonmutational epigenetic reprogramming** – e.g. hypoxia-induced epigenetic changes confer resistance to anti-PD-1 immunotherapy.¹⁵
12. **Polymorphic microbiomes** – e.g. exotoxins secreted from tumour-promoting gut bacteria damage DNA of colon epithelial cells, contributing to colorectal carcinoma progress.¹⁶
13. **Senescent cells** – e.g. cancer cells can be induced to a transitory reversible senescent state, by therapy for instance, which allows them to escape from non-proliferative irreversible form of senescent state, and ultimately resume proliferative oncogenic state, leading to therapy-resistance and recurrence.¹⁷
14. **Unlocking phenotypic plasticity** – e.g. dedifferentiation by loss of expression of differentiation markers and transcription factors; SMAD4 in colonic epithelial cells lost in advanced colon carcinoma for instance.¹⁸

These advanced features allow cancer cells to more efficiently grow, survive, and successfully invade into neighbouring tissue as well as metastasise to distal anatomical sites. Abnormal growth of cancerous tissue in a secondary site, for example lungs or brain, leading to the formation of a tumour mass, would invariably and substantially decrease normal tissue function, causing organ failure and death.

1.1.2 Melanoma carcinogenesis

Melanoma is the most dangerous of all skin cancers, originating from melanin-producing melanocytes within the epidermis. Global incidence rates of cutaneous melanoma have been rising for the past decades and projected to continue to rise further.¹⁹ Early diagnosis is crucial for survival, as the '5-year post-diagnosis survival rate' of 99% for primary melanoma drops to a devastating 27% for late-stage metastatic melanoma.²⁰ A deeper understanding of tumour progression and metastasis of the disease is required to challenge this global burden.

The number one cause of melanoma is exposure to ultraviolet (UV) radiation from the sun.²¹ Mutation to certain genes, for example caused by UV radiation, may enhance proliferative and survival capabilities of melanocytes. The genes commonly affected by UV radiation are the *BRAF* and *NRAS* proto-oncogenes.^{22,23} Certain germ-line mutations, such as *MITF* gene, were also discovered to predispose melanocytes to transformation into melanoma.²⁴

The RAS→RAF→MEK→ERK signalling pathway is a mitogen-activated protein (MAP) kinase cascade which drives cellular proliferation and survival.²⁵ This signalling pathway is hyperactivated in most cases of melanoma, with NRAS (~52%) and BRAF (~28%) mutations being the predominant drivers of this pathway.²⁶ A melanocyte acquiring these driver mutations may lead to hyperplasia and development of naevi.²⁷

Progression from a benign naevus to melanoma *in situ* involves the transition from low to high mutational burden, accompanied by mutation of the *TERT* promoter gene.²⁸ This gene encodes for telomerase reverse transcriptase, which is the catalytic component of telomerase. Aberrantly high activity of telomerase in melanoma cells, meaning the prevention of shortening of telomeres with each cell cycle, essentially makes melanoma cells become replicative immortal.²⁹ Inactivating mutations of tumour suppressor genes, such as *TP53* gene (encodes for p53 protein) or *PTEN* gene (encodes for phosphatase and tensin homolog), contributes to genomic instability and dysregulated cell.^{30,31}

Pathways important for the development of primary melanoma tumours include phosphoinositide-3 kinase (PI3K) pathway which aids in cell survival,³² vascular endothelial growth factor (VEGF) and interleukin-8 (IL-8) which promotes angiogenesis,^{33,34} and programmed death-ligand 1 (PD-L1) which allows evasion from immune surveillance.³⁵

1.1.3 Melanoma metastasis

Metastasis is the term used to describe the dissemination of cancer cells from a primary tumour to a distal secondary site. This process begins with invasion into local stroma at the primary site, extravasation into vasculature and transit via hematologic circulation, intravasation into the stroma at distal sites, and finally formation of new tumour masses at distal peripheral tissues.³⁶ This incongruous tumour growth in vital organs, for example lungs, liver, gut, and brain for cutaneous melanoma,³⁷ is the cause for mortality.

Invasion into the surrounding stroma at the primary site requires hyperplastic cancer cells of epithelial origin to undergo drastic morphological transformation. This is known as Epithelial-to-Mesenchymal Transition (EMT). Here, immotile epithelial-like cells, which are woven tightly to their neighbouring extracellular matrix, becomes detached and develop mesenchymal cell-like motility.³⁸ Similar process has been described in malignant melanoma, where proliferatively-inclined but invasively-deficient population of cells, termed 'melanocytic state', undergo a transition wherein they evolve into invasively-inclined but proliferatively-deficient cell-types, termed 'undifferentiated state'.³⁹

1.2 Circulating tumour cell (CTC) clusters

1.2.1 Single vs Clusters

An overwhelming 90% of cancer-associated deaths are due to circulating tumour cells (CTC).⁴⁰ Tumour cells are shed into circulation as single cells or migrate collectively and shed cohesively into blood vessels as clusters. Tumour cells can also aggregate with each other within the vasculature to form homotypic clusters, as well as associate with stromal and immune cells to form heterotypic clusters.⁴¹

Clustered configuration augments CTC survivability in the circulation: it helps them escape from immune-surveillance (Fig. 1.1), provides resistant to detachment-induced cell death (called anoikis), and helps them withstand the shear-stress of blood.⁴¹ As such, CTC clusters are approximately 50-fold more metastatic than single CTC;⁴² in some cases, going up to 100-fold.^{43,44} Clusters, compared to single cells, confer shorter 'progression-free' and overall survival of patients with different cancers.⁴⁵⁻⁴⁸

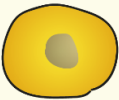
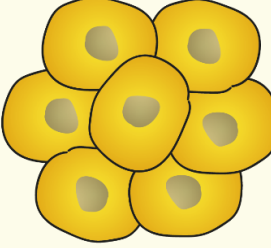
Single CTC	Properties	Molecular hallmark
	↑ Apoptosis ↓ Anoikis resistance ↓ Immune escape	↑ MHC II antigen presentation ↑ TNF signaling ↑ Interferon type II signaling
CTC clusters	Properties	Molecular hallmark
	↑ Shear stress resistance ↑ Anoikis resistance ↑ Immune escape ↓ Apoptosis	↑ Bcl-2 ↑ Plakoglobin ↑ CD44 ↑ Heparanase ↑ TMIGD2 ↑ Galectin-3 ↑ ICAM-1 ↓ MHC II antigen presentation

Fig. 1.1 Differences in molecular hallmark and properties between single CTC and CTC clusters. CTC: circulating tumour cells, ICAM-1: intercellular adhesion molecule-1 MHC II: major histocompatibility complex II, TMIGD2: transmembrane and immunoglobulin domain containing 2, TNF: tumour necrosis factor.

In CTC clusters, immune response pathways have shown to be downregulated; notable pathways include type II interferon and TNF signalling (Fig. 1.1).⁴⁹ Antigen presentation involving MHC class II was downregulated in CTC clusters compared to single CTC (Fig. 1.1).⁴³ These studies suggest that CTC clusters are much more capable of evading immune responses than single CTCs.

Lastly, the clustered configuration could provide survival advantage to CTC cells by enhancing anti-apoptosis signalling. The anti-apoptotic protein Bcl-2 was found overexpressed in breast cancer CTC clusters compared to single CTCs (Fig. 1.1).⁴⁹ Bcl-2 overexpression could also explain the anoikis-resistant observed in CTC clusters.^{50,51}

1.2.2 Mechanisms of CTC cluster formation

Several possible mechanisms of formation of clusters have been described so far for breast cancer CTCs. For example, CTC clusters isolated from patients with breast cancer showed elevated levels of the desmosomal junction protein plakoglobin (Fig. 1.1).⁴² Knock down of plakoglobin in mice model prevented CTC cluster formation and metastases to lungs. Within the primary tumour, high expression of plakoglobin demarcates regions which are more stringently tethered together;^{52,53} cohesive shedding of these regions would arguably give rise to CTC clusters with enhanced survivability.

CTC clusters originating from triple-negative breast cancer that were formed within the vasculature expressed high levels of CD44 cell-surface glycoprotein molecules (Fig. 1.1).⁴⁴ Using intravital multiphoton microscopic imaging to track individual oligoclonal cells, this study demonstrated that triple-negative breast cancer CTCs aggregated intravascularly as opposed to collective migration/cohesive shedding.⁴⁴ It was shown that CD44 could interact with other CD44 molecules on neighbouring cells. This homophilic interaction was essential for multicellular aggregation; depletion of CD44 resulted in disaggregation of CTC clusters.⁴⁴

The cell-surface protein heparanase was shown to be overexpressed in multicellular aggregates of breast cancer CTCs;⁵⁴ here, heparanase induced intravascular multicellular aggregation in a FAK/ICAM-1-dependent manner. A recent study has highlighted the role of ICAM-1 in initiating the formation of breast cancer CTC clusters, as well as aiding in transendothelial migration during pulmonary (Fig. 1.1).⁵⁵ Lastly, galectin-3BP has been shown to bridge Galectin-1 and other unknown surface molecules to induce homotypic cellular aggregation and promote metastasis of breast cancer CTCs.⁵⁶

For colon cancer, two studies have outlined the mechanism of CTC cluster formation. Firstly, TMIGD2 cell-surface protein (also called IGPR-1 and CD28H) has been shown to regulate multicellular aggregation of colon cancer CTCs (Fig. 1.1);⁵⁷ inhibition of TMIGD2 prevented multicellular aggregation. Secondly, colon cancer CTCs have been shown to aggregate by polarising the large interloping cell-surface MUC1 glycoproteins to one side of the cell, leading to the exposure and enrichment of the smaller cell-cell binding protein E-cadherin to the other

side of the cell.⁵⁸ The newly exposed E-cadherin molecules were suggested to form cell-cell junctions and promote multicellular aggregation. The polarisation of MUC1 was shown to be induced by galectin-3 binding to the glycosylated regions of MUC1 (Fig. 1.1).⁵⁸ Since galectin-3 could simultaneously bind to multiple molecules containing β -galactosides, it was suggested that galectin-3 could stick multiple MUC1 molecules.⁵⁸

As for melanoma, despite it being one of the cancer types with a high CTC cluster prevalence, approximately 30%⁵⁹ – 34%⁴⁸ of patients suffering from metastatic melanoma, the nature of melanoma CTC clusters, mechanisms of cluster formation, and their impact on metastasis all remain unknown.

1.3 Advanced tissue culture surfaces to study CTC clusters

1.3.1 Limitations of current CTC cluster models

Previous studies have used liquid biopsy samples from patients, isolated and enriched clusters using microfluidic techniques,⁶⁰ to better understand the nature of CTC clusters. Some limitations concerning these microfluidic approaches include: (i) scarcity of CTC clusters in liquid biopsies, approximately 1 cluster per over 10^7 leukocytes and 10^{10} red blood cells,⁶¹ (ii) risk of cluster dissociation during blood processing, (iii) and the need for tumour-specific cell-surface markers. The microfluidic techniques using cell-surface markers for detection could be inefficient, owing to most of the surface antigens being enclosed within the clusters, as well as shrouded by immune cells or platelets bound to the clusters.⁴¹ Therefore, a more reliable and facile approach is required for the investigation of CTC clusters *in vitro*, which arguably could both encourage and speed-up initial stages of research to uncover nature of CTC clusters and their contribution to metastasis cascade.

1.3.2 Effects of surface chemistry and topography on cells

Tissue culture polystyrene is by far the most used substrate for culturing adherent animal and human cells in research laboratories, due to its low production value, relatively straightforward synthesis, and optical clarity. In addition to two-dimensional surfaces, three-dimensional culture systems based on natural polymers such as polysaccharides and extracellular matrix-derived scaffold proteins, as well as synthetic hydrogel matrices have also gained popularity due to being more representative of the three-dimensional natural environment from which the cells were derived.⁶² More recently, advanced tissue culture

surfaces have been developed with tuneable surface characteristics, such as surface chemistry, topography, and wettability, that have been shown to produce interesting cellular behaviour that cannot be achieved via traditional tissue culture polystyrene or three-dimensional systems.⁶³

Surface chemistry: Many studies have demonstrated that surface chemistry and topology can be used to influence cellular behaviours, including proliferation, differentiation, adhesion, and morphology.^{64,65} Early studies highlighted that surface chemistry influences both cellular morphology and adsorbed extracellular matrix protein composition and architecture.⁶⁶ Development of self-assembled monolayers (SAM) has provided opportunities for exploring influences of surface chemistry and functional groups alone on cellular behaviour where effects due to topography could be controlled. Investigations using SAM functionalised with hydroxyl, amine, carboxylic, and methyl groups revealed influence of surface functional groups on protein adsorption kinetics (namely fibronectin) and subsequently cellular adhesion.⁶⁷ Another study show that SAM surfaces functionalised with hydroxyl groups induced human mesenchymal stem cell osteoblastic differentiation.⁶⁸ Recent study used silane-modified surfaces functionalised with CH₃, NH₂, OH groups to demonstrate that the hydrophobic surfaces suppressed cellular proliferation and induced apoptosis of breast cancer cells by upregulation of Bcl-2.⁶⁹ Surfaces functionalised with polyacrylate (high amine and low carboxyl group content) resulted in induction of mesenchymal stem cell chondrogenesis without needing to use a chondrogenesis-inducing cytokine that is normally required.⁷⁰ Interestingly, this study also highlighted that increase in hydrophobicity also induced aggregation of cells, still attached to the surface via basal layer of cells. It is conceivable that hydrophobic surfaces could induce aggregation of cells that could be used to model circulating tumour cell clusters. Furthermore, surface group-induced wettability (e.g. non-polar vs polar groups and hydrophobic vs hydrophilic surfaces) could also affect cellular adhesion capabilities and behaviour of cells.⁷¹

Surface topography: Topographical features have been shown to guide organisation of cellular morphology, in terms of both alignment and elongation, known as 'contact guidance',⁷² and where surface roughness,⁷³ surface free energy,⁷⁴ isotropy (same topography in all direction) and anisotropy (topography differ in different directions),⁷⁵ influence cellular morphology, growth, adhesion, and differentiation. Disordered nanotopographical feature, contrast to symmetrical features, has been shown to control mesenchymal cell differentiation and stimulate bone mineral *in vitro* without the need for osteogenic supplements, highlighting important clinical implications for bone tissue engineering.⁷⁶ Advanced techniques such as lithography and electrospinning have been used for precisely controlling topographical

features such as roughness, as well as mechanical features such as stiffness, from the nano to micro scale.⁷⁷ Microscale features (above one micrometre) solely depend on contact guidance-based mechanisms to exert their effect on cells; for example, guided nerve axonal outgrowth on polymethylmethacrylate-covered silicon chips patterned with 100–400 nm width 300 nm depth parallel groves with distance between two adjacent grooves over one micrometre.⁷⁸ Whereas nanopatterned surfaces with nanoscale topographical features such pits, columns, gratings, and islands all induce a plethora of different cellular responses ranging from differentiation to cell adhesion,⁷⁹ though cellular responses likely cell-type dependent. Roughness-dependent wettability, using nanoscale patterned silicon wafers, has also been associated with differential fibroblast cell adhesion responses.⁸⁰ Additionally, a study generated cell culture substrates with controlled nanotopographical features and demonstrated that surface roughness influenced cell adhesion, spreading, proliferation, whilst surface chemistry influenced cellular differentiation.⁸¹ Yeung et al. demonstrated that surface stiffness could also influence cell spreading, morphology and cytoskeletal structures.⁸²

1.3.3 Effects of surface chemistry and topography on protein adsorption

During two-dimensional cell culture, surface characteristics such as surface chemistry and surface topography could affect cellular behaviour. Although cells could directly interact with features of surfaces and elicit a cellular response, cells secrete extracellular matrix proteins such as fibronectin, laminin, and collagen IV, as well as those found in cell culture serum such as fibrinogen and albumin, that adsorb onto the surfaces, and it is these proteins that are in intimate contact with the surface. Cells use a class of cell-adhesion molecules, called integrins, that recognise a specific peptide motif, Arg-Gly-Asp (RGD motif), present on several extracellular proteins, to adhere onto the extracellular matrix scaffolds and subsequently adhere onto the surface.⁸³ Thus, cellular responses to surface features could be largely dependent upon surface-dependent adsorption kinetics of the various extracellular matrix proteins that cells secrete, as well as those found in the cell culture serum.⁸⁴

Surface chemistry: Protein adsorption on surfaces functionalised with various polar (e.g. carboxyl, phosphate, silanol, hydroxyl, and amino), and non-polar groups (e.g. methyl, and thiol) have been extensively studied previously,⁸⁵ due to relevancy and importance of protein-surface interactions for biosensors, biofilm formation, therapeutic devices, drug delivery, and nanomaterials.⁸⁶ Using model hydrophobic (methyl functionalised) and hydrophilic (hydroxyl functionalised) surfaces, early investigations revealed that albumin undergoes a single-step adsorption kinetic, whereas fibrinogen adsorption involves multistage process, and that

albumin had a stronger affinity towards the hydrophobic surface compared to the hydrophilic surface, whereas fibrinogen adsorb readily onto both surfaces.⁸⁷ Another study highlighted that bovine serum albumin adsorption increased as water contact angle (WCA) decreased.⁸⁸ Fibronectin adsorption notably increased on hydrophobic surfaces of polydimethylsiloxane functionalised with hydrophobic SAM and subsequently augmented cellular spreading.⁸⁹ Interestingly, using a superhydrophilic-to-superhydrophobic gradient, a study revealed that fibronectin adsorption induced conformational changes, with exposure of cell-binding epitopes (RGD motif) diminished on surfaces with superhydrophilic wetting properties, thus dramatically affecting cell-adhesion properties.⁹⁰ These studies provide insights into the surface-protein interface largely affecting adsorption kinetics and adsorption-dependent secondary structure conformational changes, which could promote cell-adhesive properties of the surface by exposure of cell-binding epitopes.

In a multiprotein system, for example cell culture media and serum, proteins adsorb competitively, wherein proteins at higher concentrations but low molecular size (e.g. albumin) which are described as high mobility/low affinity that adsorb first, that slowly become displaced by larger molecular size (e.g. fibrinogen) but less frequently-occurring proteins arriving much later which are described as low mobility/high affinity. This phenomenon, called the Vroman effect, was first noticed by Leo Vroman.⁹¹ Affinity for specific proteins to a particular surface could depend on surface functional groups. For example, surfaces functionalised with negatively charged/acidic groups such as carboxyl groups could have higher affinity towards proteins harbouring mostly positive charges, and surfaces functionalised with positively charged groups such as amino group could have higher affinity towards proteins whose charge is mostly negative. Though, it is noteworthy that proteins are not mono-charged entities, but rather have charge distribution, where hydrophobic moieties are buried in their cryptic sites, and hydrophilic moieties are exposed to aqueous phase. Therefore, both charge distribution as well as hydrophobicity could contribute towards protein adsorption. Generally, compared to bulk native protein in aqueous phase, several adsorbed proteins exhibit drastic conformational changes after prolonged contact with a solid substrate.⁹²

Surface topography: Similar to surface chemistry, surface topographical features such as roughness affect protein adsorption kinetics and dynamics. Early investigation using silica spheres suggested that BSA and fibrinogen both have distinct conformation profile during adsorption depending on surface curvature despite both proteins having similar binding affinity and saturation; BSA's conformation was increasingly less ordered on larger substrates, whilst fibrinogen was suggested to lose secondary structure during adsorption onto silica

spheres with high surface curvature,⁹³ indicating that silica nanospheres with these characteristics likely had a denaturation effect on larger proteins such as fibrinogen. Similarly, another study also showed that upon adsorption onto colloidal silica-coated surfaces with nanotopographic characteristics, fibronectin conformation changed dramatically, affecting human endothelial cell adhesion.⁹⁴ Additionally, BSA adsorption increased with nano-roughness of platinum surfaces.⁹⁵ Nearly globular protein BSA was less influenced by roughness, whereas the larger non-globular fibrinogen protein adsorption and saturation increase with increasing roughness.⁹⁶

Protein adsorption onto the surface can be influenced by surface characteristics, such as wettability, roughness, and surface chemistry.⁹⁷ Indeed, surface-induced adsorption-based approaches have provided much insight into conformational changes and fibrillogenesis of fibronectin,^{98,99} which is extracellular matrix protein important for melanoma metastasis.¹⁰⁰ Likewise, other notable extracellular matrix proteins such as fibronectin, laminin, and collagen IV, adsorption onto self-assembled monolayer (SAM)-modified gold substrates were recently investigated, highlighting that negatively charged proteins can adsorb onto negatively charged surfaces due to an interesting phenomenon called the adsorption-induced polarisation of proteins.¹⁰¹

1.3.4 Silica-modified surfaces

Our laboratory group has previously established the fabrication of silica-modified surfaces,¹⁰² that have been used to interrogate cancer cellular adhesion, aggregation, and differentiation capabilities. Melanoma cellular adhesion was investigated on hydrophilic silica surfaces,¹⁰² which demonstrated enhanced adhesion of cells onto silica surface compared to tissue culture polystyrene (TCP). Hydrophilic aminopropyl-functionalised silica surfaces were shown to enrich epithelial-like cells from a single clone containing both epithelial and mesenchymal-like subpopulation of prostate cancer cells.¹⁰³ Recently, it was demonstrated that epithelial-like prostate cancer cells adhere well onto the hydrophobic FS surfaces, whereas the mesenchymal-like prostate cancer cells adhere poorly; however this is reversed when cocultured with the epithelial-like cells.¹⁰⁴ Lastly, hydrophobic fluoroalkyl silica (FS) surface was developed, which induced fibronectin adsorption-dependent homotypic multicellular aggregation-disaggregation of breast cancer cells.¹⁰⁵ These FS surfaces could prove useful for the investigation of CTC clusters.

Fabrication of these silica-functionalised surfaces first involves polymerising a thin film of aniline onto TCP (Fig. 1.2 A & B),¹⁰² which adheres via hydrophobic interactions, using

ammonium persulphate as an oxidising agent to initiate the polymerisation process.¹⁰² This is followed by the immobilisation of glutaraldehyde (GDA) onto the polyaniline (PANI) film (Fig. 1.2 C); an aldehyde group of GDA reacts with the primary and secondary amine groups in PANI.¹⁰²

Lysozyme is next immobilised onto the surface (Fig. 1.2 D); the free aldehyde groups of GDA that are not bound to PANI reacts with the amine groups of lysozyme molecules.¹⁰² Silica film is next deposited onto the surface by condensation of orthosilicic acid (Fig. 1.2 E). Tetramethyl orthosilicate (TMOS, $\text{Si}(\text{OCH}_3)_4$) is pre-hydrolysed under acidic conditions to generate free orthosilicic acid for the silica condensation reaction.¹⁰² The resulting siloxane network is immobilised to lysozyme via electrostatic static interactions; positively charged amine groups of lysozyme catalyses silica condensation reaction.¹⁰²

The silica surfaces can then be functionalised with silanes. Hydrophobic surfaces are synthesised by reacting pre-hydrolysed 1h,1h,2h,2h-perfluorodecyltriethoxysilane (FDTES), so as to cleave off the ethoxy groups and to free the silanol groups (Si-OH), with the siloxane network on the silica surfaces (Fig. 1.2 F).¹⁰⁵ Condensation reaction results in the formation of siloxane bonds (Si-O-Si) between the silanol group of the aqueous silanes and the free silanol groups localised at the surface of the siloxane network.¹⁰⁵ The fluoroalkyl-functionalised FS surface is hydrophobic with a water contact angle of $\sim 115^\circ$,¹⁰⁵ where the water contact angle of the original TCP surfaces is $\sim 65^\circ$. FS surfaces (RMS roughness = ~ 119 nm) are also much rougher than the TCP surfaces (RMS roughness = ~ 20 nm).¹⁰⁵

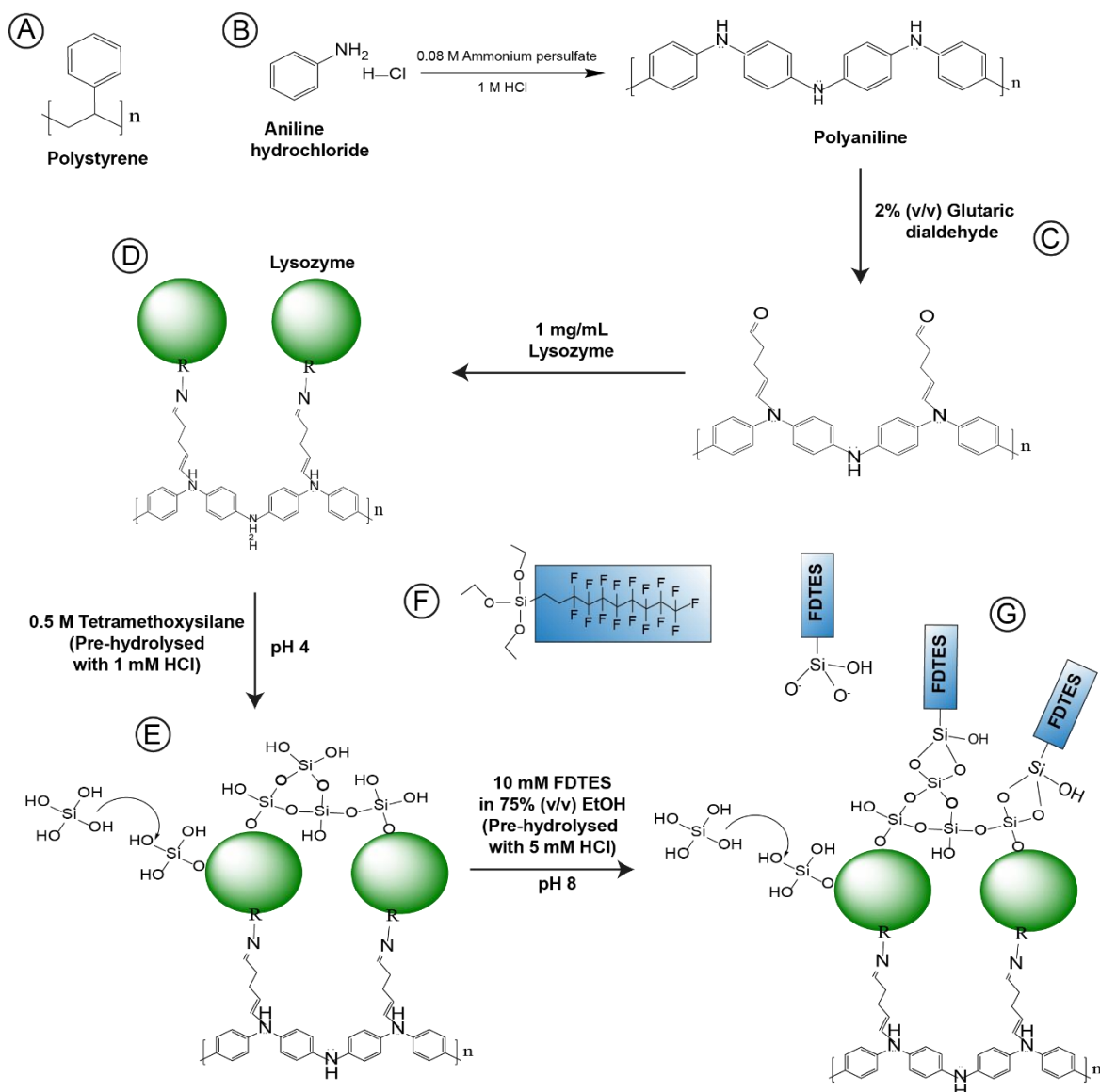


Fig. 1.2 Schematic depicting fabrication of FS surfaces from TCP surfaces. (A) Polystyrene monomer. **(B)** TCP coated with polyaniline by reacting aniline hydrochloride with ammonium persulfate at 1:1 ratio. **(C)** Glutaric dialdehyde is immobilised onto the polyaniline layer. **(D)** Free aldehyde group of glutaric dialdehyde reacts with amine groups present on lysozyme. **(E)** Aqueous orthosilicic acid, from pre-hydrolysed tetramethoxysilane, condensed upon lysozyme via formation of siloxane network. **(F)** FDTES molecule. **(G)** Fluoroalkyl functionalisation involves condensing FDTES onto the siloxane network and formation of siloxane bond between the silanol group of FDTES and silanol group of the free orthosilicic acid. EtOH: Ethanol, FDTES: 1h,1h,2h,2h-perfluorodecyltriethoxysilane,

1.4 Project aims and objectives

Nature of melanoma CTC clusters, including mechanism of multicellular aggregation, cell signalling pathways, and mechanism of disaggregation at distal metastatic sites, all remain elusive, owing to lack of a suitable *in vitro* cell culture model of melanoma CTC clusters that researchers could easily use in laboratory during the early stages of research, similar to tissue culture polystyrene that has been widely used for culturing adherent cancer cells, before carrying out further investigation using animal models or seek out scarce and labour-intensive isolation of patient-derived CTC cluster samples. Currently available models involve expensive microfluidic techniques, or three-dimensional cell culture or organoid-based models that may be suitable for studying primary or secondary tumours, whereas FS surface has been shown to induce multicellular aggregation-disaggregation as a single dynamic process which are comparatively more representative of intravascular CTC multicellular aggregation-disaggregation events.

Overarching aim: Therefore, this PhD research project aims to establish FS surface-induced multicellular aggregation-disaggregation of FM3 melanoma cells as an *in vitro* cell culture model to study nature of melanoma CTC clusters and unearth molecular players involved in multicellular aggregation-disaggregation events of FM3 melanoma cells.

Objective 1: Using quantitative mass spectrometry, proteins involved in cell-cell and cell-surface interactions and other cell signalling pathways important for FM3 melanoma multicellular aggregation and disaggregation will be identified.

Objective 2: Targeting candidate proteins identified from proteomics, commercially available antibody or inhibitors that have been shown to disrupt protein-protein interactions will be used to investigate whether disruption of normal protein-protein interaction will be sufficient to disrupt FM3 multicellular aggregation-disaggregation events.

Objective 3: To discern whether candidate proteins are also expressed in melanoma in the clinics, contribute to metastasis, proteomics or transcriptomics dataset of melanoma CTC clusters will be analysed if available, or at the very least primary and metastatic melanoma datasets obtained from online repositories will be analysed to prompt future detailed studies.

Objective 4: As EMT and EMT-like processes have been shown to influence melanoma metastasis, though unclear what their role in CTC cluster formation/multicellular disaggregation, influence of EMT status on FM3 melanoma multicellular aggregation-disaggregation will be investigated by treating FM3 cells with TGF β . Classical EMT markers expression, as well as associated EMT-like interactions will be explored using proteomics and pathway analyses. Our laboratory group also has access to a previously established fully

epithelial and fully mesenchymal cloned cancer cell line; albeit it is prostate cancer cell line (clones of OPCT cells), investigation using these cloned cells and how epithelial-like and mesenchymal-like state will influence multicellular aggregation-disaggregation events, alongside TGF β -treated FM3 cells will hopefully shed some light on influences of EMT/EMT-like processes on FM3 melanoma multicellular aggregation-disaggregation events.

Objective 5: Since protein adsorption likely play a part in cellular adhesion and could also be involved in surface-induced aggregation-disaggregation events, extracellular matrix proteins important for FM3 melanoma multicellular aggregation-disaggregation will be investigated by first isolating cell-secreted extracellular proteome and carrying out identification/quantification using quantitative mass spectrometry, then subsequently carrying out detailed study of conformation changes of secondary structure, during adsorption onto FS surfaces using FTIR spectroscopy.

Thesis hypothesis: Since multicellular aggregation CTC has been shown to involve cell-surface glycoprotein-mediated cell-cell interactions in breast and colon cancers, here it is predicted that FM3 multicellular aggregates will also involve cell-cell interactions using glycoprotein. This hypothesis will be tested using quantitative mass spectrometry as a discovery method to find candidate cell-surface glycoprotein and by treating with commercially available inhibitor or antibody that could disrupt protein-protein interaction of this glycoprotein, where it is predicted that the treated samples will show complete or partial disaggregation.

Molecular signatures of multicellular aggregates identified in this project could be utilised in the clinics; (i) to improve techniques of isolation of melanoma CTC clusters, (ii) to design therapeutic intervention of melanoma CTC cluster formation and metastasis, (iii) and to explore the predisposition of primary tumour cells in forming CTC clusters and metastasis.

Chapter 2. Materials & Methods

Contents

2.1 SURFACE SYNTHESIS	18
2.1.1 Fluoroalkylsilica surface fabrication	18
2.1.2 Fluoroalkylsilica surface characterisation.....	18
2.2 CELL CULTURE & ASSAYS	19
2.2.1 Routine cell culture.....	19
2.2.2 Cell viability assay	19
2.2.3 Invasion and migration assay.....	19
2.2.4 Cell culture under hypoxic condition.....	20
2.2.5 Treatment of cells with inhibitor, antibody, or cytokine.....	20
2.2.6 Cellular aggregation assay	21
2.2.7 Immunofluorescence.....	21
2.3 PROTEOMICS & TRANSCRIPTOMICS	22
2.3.1 Cell lysis for mass spectrometry and western blot.....	22
2.3.2 Extracellular matrix isolation for mass spectrometry.....	22
2.3.3 Western blot.....	23
2.3.4 Mass spectrometry.....	23
2.3.5 Quantitative reverse transcription polymerase chain reaction (RT-qPCR)	24
2.4 BIOINFORMATICS	25
2.4.1 Clinical patient data analyses	25
2.4.2 Protein docking.....	26
2.5 PROTEIN ADSORPTION.....	27
2.5.1 Amido black staining.....	27
2.5.2 FTIR-ATR and 2D correlation spectroscopy.....	27
2.6 STATISTICAL ANALYSES	28

2.1 Surface synthesis

2.1.1 Fluoroalkylsilica surface fabrication

Silica surfaces were synthesised on tissue culture polystyrene (TCP) (Sarstedt) plates following a previously described method,¹⁰² and subsequently functionalised with a silylperfluorocarbon compound. Briefly, TCP surfaces (Sarstedt; 10 cm, 24-well, and 96-well cell culture plates) were coated with an initial layer of polyaniline by polymerising 0.25 M aniline hydrochloride (Sigma-Aldrich, A8524) dissolved in 1 M HCl in the presence of an initiator, 0.08 M ammonium persulphate (Sigma-Aldrich, 248614) dissolved in ddH₂O. This reaction was conducted at 1:1 (v/v) ratio for 15 min at room temperature (RT). The surfaces were then coated with 2% (v/v) glutaric dialdehyde (Sigma-Aldrich, 340855) by incubating at 57 °C for 2 h.

Next, surfaces were coated with a layer of 1 mg/mL lysozyme (Sigma-Aldrich, 62971) dissolved in 0.1 M sodium-phosphate buffer (pH 7.2), incubating for 2 h at RT or overnight at 4 °C. Using these, superhydrophilic silica surfaces were fabricated by incubating with 0.5 M tetramethyl orthosilicate (TMOS) (Sigma-Aldrich, 218472) at RT for 2 h to allow thin layer of sol-gel formation from the colloidal TMOS monomers. Prior to use for surface coating, 0.5 M tetramethyl orthosilicate was hydrolysed in 1 mM HCl for 15 min and the pH raised to 4 with 0.1 M NaOH.

Lastly, the silica surfaces were functionalised with 10 mM 1H,1H,2H,2H-perfluorodecyltriethoxysilane (FDTES) (Alfa Aesar, L16585) dissolved in 75% (v/v) ethanol; FDTES was pre-hydrolysed with 5 mM HCl for 30 min at RT and the pH raised to 8 with 0.25 M NH₄OH prior to coating for 2 h at 57 °C. The functionalised FS surfaces were cured for 24 h at 57°C. The total coating volumes of each solution were kept the same but were only modified to account for the different sizes of the tissue culture plates (96-well: 300 µL, 24-well: 1.875 mL, 6-well/60x15 mm plates: 9.019 mL). Between coating with different solutions, surfaces were washed three times with ddH₂O (three times with ethanol and ddH₂O after incubation with FDTES). Before using these surfaces for cell culture, they were UV-sterilised for 15 min using a UV-crosslinker (UV stratalinker 2400).

2.1.2 Fluoroalkylsilica surface characterisation

Contact angle measurements were taken using an Attention Theta Lite tensiometer and sessile ddH₂O liquid droplets of 5 µL. Fourier transform infra-red attenuated total reflectance (FTIR-ATR) spectroscopy of the surfaces were obtained using a Spectrum 100 FTIR spectrometer

(Perkin Elmer) equipped with a diamond ATR golden gate accessory, at 2 cm^{-1} resolution, 32 scans for each sample, and between $650\text{--}4000\text{ cm}^{-1}$ wavenumber. Roughness of the surfaces was determined through atomic force microscopy (AFM) using a Dimensions Icon SPM (supplied by Bruker) in ScanAsyst mode, with a ScanAsyst-Air probe (Bruker, silicon tip on nitride lever, cantilever T: 650 nm, frequency 70 kHz). The root mean square (RMS) roughness was calculated using the built-in function of Nanoscale Analysis software.

2.2 Cell culture & assays

2.2.1 Routine cell culture

FM3 cells (human metastatic melanoma) were originally obtained from University of Tübingen, Germany, and cultured in RPMI-1640 growth media (Corning, 150-040-CVR) containing 10% (v/v) foetal bovine serum and 2 mM L-Glutamine, in an incubator set at $37\text{ }^{\circ}\text{C}$ and atmosphere of 5% CO_2 . P5B3 and P4B6B cell lines were obtained from a previous research project,¹⁰⁶ cultured in defined keratinocyte serum free medium (GIBCO) (Thermofisher, 10744019) supplemented with 2.5% (v/v) foetal bovine serum, in an incubator set at $37\text{ }^{\circ}\text{C}$ and atmosphere of 5% CO_2 .

2.2.2 Cell viability assay

Cell density was calculated using live cell-detection haematocytometer and seeded 20,000 cells per 300 μL for each well. Cellular viability assay in 96-well plate, and after 24 h or 72 h, live cells were measured using AlamarBlue cell viability reagent (Invitrogen, DAL1025) according to manufacturer's instructions.

2.2.3 Invasion and migration assay

Invasion and migration assays were carried out using 'Culturex basement membrane extract cell invasion assay kit' (R&D systems, 3455-096-K) according to manufacturer's instruction. Cells were first seeded at 20,000 cells per 300 μL for each well on FS or TCP surfaces. At 24 h or 72 h, cells were detached from the surfaces by means of repeated pipetting; this step was necessary for breaking off the clusters into single cells, and to be able to carry out the assays. Cells were centrifuged at $300 \times g$ for 5 min; pellets were resuspended in serum-free growth media. Cells were then immediately re-seeded into Boyden chambers containing basement

membrane extract to carry out the invasion assay, and into chambers without any basement membrane extract to test cell motility. For both assays, a chemotactic gradient was created by keeping the Boyden chamber serum-free and introducing 20% (v/v) foetal calf serum (FCS) in the bottom chamber. After 24 h, the number of cells present in the bottom chamber was quantified using calcein-AM which measures live cells. Fluorescence emission of calcein-AM was measured using a Tecan Ultra Microtiter Plate Reader (Tecan) at 485 nm excitation and 520 nm emission. A standard (fluorescence vs number of live cells) was used to calculate invaded or migrated cells as a percentage of the total cells that were initially seeded into the Boyden chamber.

2.2.4 Cell culture under hypoxic condition

For experiments concerning hypoxia, cells were maintained in incubator set at 37 °C, atmosphere of <1% O₂ and 5% CO₂.

2.2.5 Treatment of cells with inhibitor, antibody, or cytokine

Prior to experiments, full growth media was treated with the treatment as needed, and vortexed for 1 min to get an even mixture. Details of the treatment as follows:

Treatment	Function	Concentration*	Supplier	Catalogue #
GB1107	Galectin-3 inhibitor	10 µM	Cambridge Bioscience Ltd	HY-114409
Chlorhexidine dihydrochloride (CHX)	MMP2 Inhibitor	10 µM	Merck Sigma Aldrich	C8527-5G
DB2313	PU.1 inhibitor	10 µM	Cambridge Bioscience Ltd	HY-124629
Anti-galectin-3	Galectin-3 Inhibition	10 – 200 ng/mL	R&D Systems Inc.	AF1154
Anti-4F2hc	4F2hc inhibition	10 – 200 ng/mL	Merck Sigma Aldrich	HPA017980
Anti-MMP2	MMP2 inhibition	10 – 200 ng/mL	R&D Systems Inc.	AF902
Recombinant human TGFβ	EMT induction	10 ng/mL	PeptoTech	100-21

2.2.6 Cellular aggregation assay

Cells were seeded at 20,000 cells per 300 μ L for each well (unless otherwise stated) on UV-sterilised FS or TCP surfaces in full growth media. This cell density was chosen as it was the optimum density where there were not too much cells (contact inhibition) crowding the wells, and not too little, that 24 h time point would create small aggregates. After 24 h, 48 h or 72 h of culture, images were taken using a light microscope (Axio Observer.Z1 microscope, Zeiss) at 5x magnification. Image analysis was carried out using ImageJ software (Ver 1.52p). Aggregation and disaggregation events were quantified by drawing around the aggregates and non-aggregated cells using the freehand selection tool and adding the selection as a label onto the ROI manager, then measuring the area of each of the components as well as the total area so as to express the components as a percentage of total area of the image. On images with near-confluent cells, negative space was measured instead of the non-aggregated cells; the area of non-aggregated cells was then determined by subtracting the area of the sum of negative space and aggregates from the total area of the image.

2.2.7 Immunofluorescence

Cells were seeded at 20,000 cells per 300 μ L for each well into 96 well fluorescence compatible plates (BD Biosciences, 353219) – some of the wells were functionalised with FS prior to the immunofluorescence experiment. After 24 h or 72 h, media was removed, and cells were washed 3x with 300 μ L of PBS. Cells were then fixed by incubating with 100 μ L per well of 4% paraformaldehyde in PBS, at RT for 10 min. Fixed cells were blocked with 10% serum in PBST (0.1% Tween-20 in PBS), 100 μ L per well, for 1 hour at RT on a rocker. Primary antibodies were then added, diluted in PBST by a factor recommended by manufacturer, and incubated overnight at 4 °C. For EMT proteins, primary antibodies from the EMT antibody sampler kit (Cell signalling, 9782) were used. Excess primary antibodies were removed by 3x 5 min washes with PBS (300 μ L per well). Fluorescent-conjugated secondary antibodies were then applied, diluted in PBST by a factor recommended by manufacturer and incubated at RT for 2 h. Secondary antibodies used here were Alexa Fluor 488 anti-rabbit (Thermofisher, A-21206) and Alexa Fluor 568 (Thermofisher, A-11004). Wells were washed 3x 5 min washes with PBS (300 μ L per well) to remove excess secondary antibody, followed by incubation with 50 μ L per well DAPI nucleus staining solution (Vector laboratories, H-1200-10). Wells were washed 1x 5 min with PBS to remove excess DAPI staining, before visualisation using Axio Observer.71 microscope (ZEISS) and Nikon Eclipse Ts100 Light Microscope (Olympus).

2.3 Proteomics & Transcriptomics

2.3.1 Cell lysis for mass spectrometry and western blot

Cells were lysed using ice cold Pierce RIPA buffer (Thermo Scientific, 89900) containing 1% (v/v) protease inhibitor cocktail (Sigma, P8340), by 3x 10 min vortexing, followed by centrifugation at 14,000 x g at 4 °C for 10 min. The supernatant was transferred directly to Amicon ultra-0.5 centrifugal columns (Amicon, UFC500396) with a molecular weight cut off of 3 kDa; to concentrate protein, samples were centrifuged at 14,000 x g at 4 °C for 30 min, followed by 1,000 x g at 4 °C for 2 min, device upside down to recover the protein samples into fresh Eppendorf tubes. Protein concentration was determined through Pierce 660 nm protein concentration quantification assay (Thermo Scientific, 1861426). For this assay, 0.05 g/mL of ionic detergent compatibility reagent (Thermo Scientific, 22663) was added to the assay reagent as the RIPA buffer contained SDS detergent. An aliquot of the protein samples diluted in 0.8% Triton X-100 (Sigma, T8787) at a ratio of 1:10 was used for the assay. Samples containing 50 µg of cell lysate proteins were used for mass spectrometry analysis.

2.3.2 Extracellular matrix isolation for mass spectrometry

ECM was isolated using a protocol described by Hellewell, A.L. et al.¹⁰⁷ Briefly, cells were lysed by incubating in 20 mM ammonium hydroxide, followed by removal of cell debris by washing four times with copious amounts of sterilised ddH₂O. The insoluble ECM left on the surfaces were then isolated using SDS-PAGE buffer, containing 1 M Tris-HCl (pH 6.8), 2% (v/v) SDS, 10% (v/v) glycerol and 100 mM DTT. The buffer was heated to 95 °C for 2 min before applying onto the surface. This step was repeated twice, and the plates were scored and scratched in order ensure the isolation and pooling of the whole matrisome. Matrisome protein samples were concentrated using Amicon ultra-0.5 centrifugal columns (Amicon, UFC500396) with a molecular weight cut off of 3 kDa. Protein concentration was then determined using Pierce 660 nm protein concentration quantification assay as described in 6.2.4. Matrisome samples containing 50 µg of protein were used for mass spectrometry analysis. Dr Clare Coveney is thanked for her assistance with the ECM isolation.

2.3.3 Western blot

For each sample, 30 µg of protein was dissolved in 4x Laemmli buffer, heated at 95 °C for 10 min to denature the proteins, before loading wells of Mini-PROTEAN (4-20 %) Precast protein gels (Bio-Rad, 4561093). Protein lysate was separated by size via SDS polyacrylamide gel electrophoresis (SDS-PAGE) in running buffer (25.0 mM Trizma base, 191.8 mM Glycine & 3.5 mM SDS), at a current of 60 V for 10 min, followed by 100 V for 30 min. Size-separated protein was transferred from gel to PVDF membrane at a current of 30 V t at 4 °C overnight, using transfer buffer (25.0 mM Trizma base & 191.8 mM Glycine). After transfer, membranes were blocked for 1 hour at RT in 5% semi-skimmed bovine milk powder (Marvel Original) in TBST buffer (20.0 mM Trizma Base, 136.9 mM NaCl & 0.1% Tween-20, pH adjusted to 7.6 with HCl). Primary antibodies were then applied to membranes, diluted in TBST buffer containing 5% semi-skimmed milk by a factor recommended by the manufacturer, then incubated at 4 °C overnight. For EMT proteins, primary antibodies from the EMT antibody sampler kit (Cell signalling, 9782) were used. Membranes were then washed 3x 20 min using TBST buffer. Secondary antibodies were next applied to membranes by incubating at RT for 2 h, diluted in 5% semi-skimmed milk in TBST buffer by a factor recommended by the manufacturer. EMT markers were detected using the anti-rabbit HRB conjugated secondary antibody from the EMT antibody sampler kit (9782). After a final wash cycle of 3x 20 min of the membranes in TBST buffer, Clarity Western ECL substrate (Bio-Rad, 170-5061) was added to the membranes immediately prior to image acquisition using a Syngene G:box instrument. The protein bands were identified using a molecular weight ladder (Bio-Rad, 161-0376) as reference.

2.3.4 Mass spectrometry

Disulphides in the protein samples were reduced by incubating in 0.5 M DTT (Sigma, UK) at 56 °C for 20 min. Subsequently, the cysteine residues were alkylated by incubating in 0.5 M iodoacetamide (Sigma, UK) for 15 min at RT. Tryptic digestion, at a ratio of 1:10 (wt/wt) of trypsin to protein, was carried out through S-Trap Micro spin columns (Protifi, USA). Peptides were eluted from the columns using 50 mM TEAB buffer containing 0.2% (v/v) formic acid. Hydrophobic peptides were recovered from the elution columns using 50% (v/v) acetonitrile containing 0.2% (v/v) formic acid. The reduced, alkylated and SDS-free protein samples (3 µL) were injected into YMC (15 cm x 0.3 mm) Triart-C₁₈ columns (YMC, UK) linked to Eksigent NanoLC 425 HPLC system (Sciex) (5 µL/min flow rate). The fractionated and reverse phase-separated protein samples were then inserted into a TripleTOF 6600 mass spectrometer (Sciex) for analysis. Two acquisition methods were employed: Independent Data Acquisition (IDA) to

generate the initial spectral library, and targeted analysis by Sequential Window Activation of All Theoretical Mass Spectra (SWATH-MS) within 100 variable m/z windows for quantification. Protein identification and library generation were carried out by Protein Pilot 5.0.3 software (Sciex) searched against the Human Swissprot proteome database (www.uniprot.org). Library was aligned to SWATH data using iRT peptides (Biognosis AG), with calibration of the retention time of the library carried out using PeakView 2.1 SWATH microapp software (Sciex). This alignment normalised protein peaks and the normalised protein peak area (integral) were used for quantifying individual differences between replicates of the sample protein sample. Dr Clare Coveney and Dr David Boocock are thanked for assisting with mass spectrometry experiments.

2.3.5 Quantitative reverse transcription polymerase chain reaction (RT-qPCR)

Cell lysis and RNA extraction were conducted using RNeasy Mini kit (Qiagen, 74004) as per the manufacturer's protocol. RNA was quantified using NanoDrop 8000, and 260 nm/280 nm ratio of 1.9 and above considered to be uncontaminated RNA ready to be used for reverse transcription. 2 μg of total RNA per sample were used for reverse transcription. Reverse transcription was carried out using High-Capacity RNA-to-cDNA Kit (Thermofisher, 4388950) as per the manufacturer's protocol. RT-qPCR was conducted using iTaq Universal SYBR Green Supermix (Bio-Rad, 1725124) following the manufacturer's protocol, using a Qiagen Rotor-Gene Q real-time PCR instrument. Each reaction was carried out at total volume of 10 μL , containing 100 ng of cDNA, 500 nM of forward and reverse primers, and PCR-grade water to make up to the total volume. PCR cycle as follows: 5 min 95 °C denaturation, 40 cycles x [denaturation: 5 sec at 95 °C, annealing: 20 sec at 60 °C, elongation: 10 at sec 72 °C], and melt-curve analysis (65 – 95 °C at 0.5 °C increment, 2 – 5 sec per step) at the end to indicate amplification of gene of interest and not primer-dimers. Analysis was carried out using Rotor-Gene Q Software (2.3.1.49 ver) with normalised fluorescence threshold of 0.01. Fold change from control was calculated using the threshold cycle (CT) values of gene of interest, normalised to the CT value of a reference gene (Equation 1 & 2), using the Schmittgen & Livak (2008) method.¹⁰⁸

Equation 1:

$$\text{Fold change} = 2^{-\Delta\Delta\text{CT}}$$

Where, $2^{-\Delta\Delta\text{CT}}$ is described in Equation 2.

Equation 2:

$$2^{-\Delta\Delta CT} = [(CT1 - CT2) - (CT3 - CT4)]$$

Where, *CT1* = CT of gene of interest in treatment group, *CT2* = CT of reference gene in treatment group, *CT3* = CT of gene of interest in control group, and *CT4* = CT of reference gene in control group.

Two reference genes were used, *GUSB* (which encodes for Glucuronidase β) and *YWHAZ* (KCIP-1) just in case if one was affected by the treatment. Only the comparison to *GUSB* is graphically displayed. Fold change of three technical repeats were averaged to give fold change of one biological repeat. Details of primers can be found in the Appendix A.

2.4 Bioinformatics

2.4.1 Clinical patient data analyses

Melanoma datasets, obtained from cBioPortal¹⁰⁹ and OncoLnc¹¹⁰ online repositories were used in the analysis as follows: MEL_DFCI_2019,¹¹¹ MEL_TSAM_LIANG_2017,¹¹² MEL_UCLA_2016,¹¹³ SKCM_DFCI_2015,¹¹⁴ SKCM_MSKCC_2014,¹¹⁵ SKCM_TCGA_PAN_CAN_ATLAS_2018,¹¹⁶⁻¹²⁵ SKCM_TCGA_PUB_2015,²⁶ SKCM_VANDERBILT_MSKCC_2015.¹²⁶ Survival plots were generated using GraphPad Prism 9.1.0 software, from which median Overall Survival (OS) scores were determined; Log-Rank (Mantel-Cox) test was carried out to determine χ^2 and p-values. The PRECOG tool¹²⁷ was used to obtain Meta Z-score values of genes associated with melanoma and metastatic melanoma, and the datasets used here were as follows: PMID 20460471,¹²⁸ PMID 18505921,¹²⁹ and PMID 19915147.¹³⁰ Metastasis score was calculated from subtracting Meta Z-score of metastatic melanoma (Z_2) from Meta Z-score of melanoma (Z_1). A→D (aggregation-disaggregation) factor was calculated from Z-score of disaggregation and Z-score of aggregation. PANTHER classification system 17.0¹³¹ used for gene ontology-based identification of transcription regulatory proteins. The hTFtarget tool¹³² comprising chromatin immunoprecipitation sequencing (ChIP-Seq) databases was used for identification of transcription factors, co-regulators and their target genes.

2.4.2 Protein docking

Orthorhombic crystal structures of galectin-3-CRD (PDB ID: 1A3K)¹³³ and 4F2hc-ED (PDB ID: 2DH3)¹³⁴ obtained from the Protein Data Bank (<http://www.rcsb.org/>)¹³⁵ were used for protein-protein docking computations using the ClusPro tool.¹³⁶ Graphical depictions of the docking models were generated using PyMOL ver.1.7 software. Non-covalent interactions between the docking models were computed using LigPlot+.¹³⁷ Protein-Protein Interaction scores (*PPI*) for each model were calculated from the sum of normalised and weighted scores of Hydrogen bond score (*H*), Hydrophobic interaction score (*HP*), and Aryl-Aryl (*ArAr*) interaction score. Hydrogen bond score was calculated from the number predicted by LigPlot+. The Hydrophobic Interactions score was calculated by first counting the number of hydrophobic residues predicted to make hydrophobic interactions (spoked lines; Supplementary Fig. 4.4 & 4.5), then multiplying this number by a 'side-chain hydrophobicity factor' corresponding to each of these residues (normalised to the hydrophobicity of glycine).¹³⁸ Any residues with a negative side-chain hydrophobicity factor, that is they are less hydrophobic than glycine, were not included in this calculation, even if those residues were highlighted as spoked lines in LigPlot+, as the impact of their hydrophobicity on PPI would be negligible. The Aryl-Aryl interaction score was deduced by counting the number of aromatic residues pairs, Phenylalanine, Tyrosine and Tryptophan, present immediately opposite of each other of the interface. The Hydrogen bond score, Hydrophobic interaction score and Aryl-Aryl score were min-max normalised and weighted by their Bond Energy factor. The Bond Energy factor was deduced by first taking the median value of the range of bond energy of non-covalent interactions reported in literature, followed by min-max normalisation of these values. Median value of bond energy are as follows:¹³⁹ 5 Kcal mol⁻¹ for hydrogen bonds (weighted score multiplier = 1), 1.5 Kcal mol⁻¹ for hydrophobic interaction (weighted score multiplier = 0.125), 1 Kcal mol⁻¹ for Van der Waals (weighted score multiplier = 0), and 2 Kcal mol⁻¹ for π - π stacking (weighted score multiplier = 0.25).¹⁴⁰

Equation 3:

$$PPI = 1 \left[\frac{H - \min(H)}{\max(H) - \min(H)} \right] + 0.125 \left[\frac{HP - \min(HP)}{\max(HP) - \min(HP)} \right] + 0.25 \left[\frac{ArAr - \min(ArAr)}{\max(ArAr) - \min(ArAr)} \right]$$

Where, *H* = number of hydrogen bonds

HP = total sum of values of hydrophobic residues multiplied by their corresponding 'side-chain hydrophobicity factor'

ArAr = Number of aryl-aryl interactions

2.5 Protein adsorption

2.5.1 Amido black staining

Recombinant human vitronectin (PeproTech, 140-09) and human purified plasm fibronectin (Sigma-Aldrich, FC010) were used in this study. Proteins dissolved in ddH₂O (concentration between 0.05 – 0.5 mg/mL) were incubated at RT for 24 h on TCP or FS surfaces (both 96-well format). After 24 h of protein adsorption, surfaces were rinsed three times with ddH₂O (300 μ L per well) in order to remove unbound proteins. Next, staining solution (200 μ L per well) containing 1% (wt/wt) naphthol blue-black dye (Sigma), 10% (v/v) methanol (Fisher), 10% (v/v) glacial acetic acid (Fisher), and 80% ddH₂O, was added to each well and incubated at RT for 5 min. Afterwards, surfaces were rinsed three times with ddH₂O (300 μ L per well) and wash solution (300 μ L per well) containing 38% (v/v) methanol (Fisher), 2% (v/v) glacial acetic acid (Fisher), and 60% ddH₂O to remove any unbound dye. Dye that was bound to the adsorbed protein was then detached from the surface by adding eluent solution (250 μ L per well) containing 50% (v/v) ethanol (Fisher), 50 mM sodium hydroxide (Sigma) and 0.1 mM EDTA (Fisher) in ddH₂O, and incubating at RT for 30 min. An aliquot of 200 μ L from each well was then removed, added to a fresh 96-well TCP surface. Absorbance was measured at 620 nm using a Tecan Ultra Microtiter Plate Reader (Tecan).

2.5.2 FTIR-ATR and 2D correlation spectroscopy

Bovine serum albumin (ALB, Calbiochem #12659), recombinant human vitronectin (PeproTech, 140-09) and human purified plasm fibronectin (Sigma-Aldrich, FC010) were used in this study. Proteins were dissolved in ddH₂O; 5 μ L droplets were added on FS and TCP surfaces. Surfaces were then incubated at heat-controlled chamber at 37 OC for 24 h, covered tightly in paraffin film to prevent evaporation. Fourier transform infra-red attenuated total reflectance (FTIR-ATR) spectra were obtained using a Spectrum 100 FTIR spectrometer (Perkin Elmer) equipped with a diamond ATR golden gate accessory. FTIR spectra were collected between 4000 and 500 cm^{-1} , at resolution 2 cm^{-1} , followed by multipoint zero-baseline adjustment (including a linear subsection between \sim 1730 and 1470 cm^{-1} to highlight amide I and II regions). Commonly reported peaks of secondary structures were fit under the curve of the amide I band as outlined previously.¹⁴¹ Peak fitting was carried out using Thermo grams A1 software (Ver. 8.) Reported parameters were chosen for peak fitting corresponding to unique secondary structures:¹⁴²⁻¹⁴⁵ absorbance wavelength maxima at 1712 cm^{-1} for side chains, 1693 cm^{-1} for intermolecular β -sheet, 1680 cm^{-1} for β -turn, 1656 cm^{-1} for random coil, 1644 cm^{-1} for α -helix, 1628 cm^{-1} for intramolecular β -sheet, and 1615 cm^{-1} for intermolecular β -sheet. A further

peak at 1592 cm^{-1} was introduced to compensate for the non-baseline resolution of amide I & II bands. Peak widths were restrained between 10 and 30 cm^{-1} , and peak heights were allowed to assume any positive height to investigate changes in intensity of conformers. Dr Thomas Warwick is thanked for assisting with these experiments.

Lastly, for 2D correlation spectroscopy, either aqueous fibronectin or vitronectin samples ($10\text{ }\mu\text{M}$ concentration) dissolved in ddH₂O, were incubated on TCP or FS surfaces for 5 h, 24 h, or 72 h, as a $5\text{ }\mu\text{L}$ droplet (5 technical repeats each), washed once with ddH₂O to remove unbound proteins, leaving adsorbed protein layer. FTIR-ATR spectra were collected as described above, followed by smoothing (using Savitsky-Golay method) and normalisation to the consistent area of C-H peak at 1200 cm^{-1} using SpectraGryph software (ver. 1.2). One representative of the 5 technical repeats (good signal and in the middle of the 5 technical repeats) were chosen for further analyses (see Supplementary fig. 8.1 – 8.4). Smoothed and normalised spectra were used for carrying out 2D correlation spectroscopy using the 2Dshige computation software (ver. 1.3).

2.6 Statistical analyses

Parametric statistical analyses were performed for all dataset in this research as either no non-parametric distributions were observed or difficult to tell distribution due to low n number. For experiments testing differences in mean that included two treatment groups, Student's unpaired T-test (two-tailed, heteroscedastic) were carried out. For experiments testing differences in mean that included more than two treatment groups, Brown-Forsythe and Welch ANOVA test (equal SDs not assumed) were carried out, with Dunnett T3 post-hoc multiple comparisons test to highlight adjusted p-value. For experiments testing differences in mean that included more than two independent variables, Ordinary Two-way ANOVA with Tukey multiple comparisons post-hoc test was carried out. Note that in certain cases (e.g. mass spectrometry), Brown-Forsythe and Welch ANOVA tests were carried out for experiments that were testing effect of aggregation (FS-24h vs TCP-24h) and disaggregation (FS-72h vs FS-24h) on cellular proteomics, as these analyses were considered as One-way ANOVA, as opposed to Two-way ANOVA as effect of both surface and time-point were not being tested simultaneously. For survival plots, Median Overall Survival (OS) scores, high vs low expression statistics (χ^2 and p-values) were determined using Log-Rank (Mantel-Cox). The aforementioned statistical analyses were carried out using GraphPad Prism software (version 9). Precisely which statistical test were carried out for which experiment is included in the figure legends of each figure. Protein-surface adsorption data was fitted with the Langmuir

adsorption isotherm model ¹⁴⁶ (Equation 2) using Origin Pro (version 2022b). The Langmuir curve was used for calculating total surface saturation (Q_m), binding affinities (K), where Q and C represents the concentration of adsorbate on the surface and the concentration in the phase adjacent to the surface, respectively.

Equation 4:

$$\frac{Q}{Q_m} = \frac{KC}{1 + KC}$$

Chapter 3. *In vitro* cell culture surface-based model of melanoma circulating tumour cell clusters

Contents

3.1 INTRODUCTION	31
3.2 RESULTS.....	32
3.2.1 FM3 cell aggregation-disaggregation dynamics on FS surfaces	32
3.2.2 Cellular viability is reduced in FM3 aggregates.....	35
3.2.3 Cell-cell proteins are upregulated during FM3 multicellular aggregation	35
3.2.4 Cell-matrix proteins were upregulated during melanoma multicellular disaggregation	36
3.3 DISCUSSION	39
3.3.1 Melanoma FM3 cells aggregate under reduced cellular adhesion conditions ...	39
3.3.2 Disaggregation occurs on remodelled extracellular matrix	40
3.3.3 Aggregation-disaggregation process results in a more invasive phenotype.....	41
3.3.4 Cellular viability is reduced in melanoma FM3 multicellular aggregates.....	43
3.3.5 ADPM of FM3 cells involve cell-cell, cell-matrix, and cytoskeletal regulatory pathways.....	44
3.3.6 FM3 cells remodel ECM by secreting vitronectin and fibronectin during disaggregation	45
3.3.7 Conclusions	46
3.4 SUPPLEMENTARY FIGURES	48

3.1 Introduction

This chapter describes the behaviour of melanoma cells cultured on fluoroalkyl silica (FS) surfaces and discusses the suitability to use this surface-based approach as an *in vitro* model of melanoma circulating tumour cell (CTC) clusters observed in patients.

CTC clusters are substantially more metastatic than single CTC.⁴² Approximately 30 - 40% of patients with metastatic melanoma had clusters of CTC.^{48,59} The nature of melanoma CTC clusters still remain largely unknown. This is mainly due to the lack of appropriate *in vitro* models. Previously, studies have used microfluidic techniques to capture and investigate CTC clusters extracted from liquid biopsies.¹⁴⁷ Some studies have used intravital photoimaging techniques to track single CTC as they travel via the vasculature of mice,¹⁴⁸ as well as to visualise intravascular aggregation of CTC.⁴⁴ A melanoma-specific CTC capture method called the OncoBean (MelanoBean) platform has been developed.¹⁴⁹ However, these microfluidic-based approaches come with an intrinsic risk of mechanical disruption of the CTC clusters during blood processing. This limitation makes it difficult to investigate CTC cluster formation.

Our laboratory has previously described alternative cell culture surfaces and observed surface-induced multicellular aggregation and disaggregation of breast cancer cells.¹⁰⁵ MCF-7 breast cancer cells formed multicellular aggregates on FS surface during the initial 24 h of cell culture; by 72 h, disaggregation was observed.¹⁰⁵ The present chapter aims to study the multicellular aggregation-disaggregation dynamics of FM3 melanoma cells during culture on FS surface. Invasiveness, migratory properties, and cellular viability of aggregating and disaggregating FM3 cells will be compared to characteristics of clinical melanoma CTC clusters. This will aid in establishing FS surface as a suitable *in vitro* model of melanoma CTC clusters. As at present no such models exist, this research would encourage future *in vitro* studies of melanoma CTC clusters.

3.2 Results

3.2.1 FM3 cell aggregation-disaggregation dynamics on FS surfaces

FS surfaces were synthesised as before using tissue-culture polystyrene (TCP) as a starting material and a 'final-coating' functionalisation with FDTES to generate the hydrophobic FS surfaces.¹⁰⁵ ATR-IR spectroscopy confirmed the fluoroalkylsilica functionalisation as denoted by the presence of double C-F stretching vibrations (doublet peak between 1120-1350 cm^{-1})¹⁰⁵ (Supplementary Fig. 3.1 A). Water contact angle measurements (WCA) confirmed that FS surfaces were hydrophobic (WCA $\theta > 90^\circ$) and TCP surfaces as hydrophilic (WCA $\theta < 90^\circ$) (Supplementary Fig. 3.1 B). Roughness of the surfaces were assessed via AFM; root mean square (RMS) roughness of FS was ~5-fold higher than that of TCP (Supplementary Fig. 3.1 C - E).

FS induced aggregation of breast cancer cells (MCF-7 cells) by 24 h, followed by disaggregation at 72 h.¹⁰⁵ Therefore, it was hypothesised that melanoma cells would also undergo similar aggregation-disaggregation dynamics on FS surface. Similar to the MCF-7 breast cancer cells, in the present study, FS surface induced aggregation of a cutaneous melanoma cell line (FM3 cells) by 24 h, followed by disaggregation at 72 h (Fig. 3.1 A-B).

Raising seeding density from 5k cells/well to 40k cells/well resulted in disaggregation by 48 h rather than 72 h, as denoted by a significant increase in percentage of non-aggregated cells (Fig. 3.1 B). When CTC clusters encounter a microenvironment rich in cell-adhesive proteins and remodelled ECM suited for cancer cellular adhesion, CTC likely would disaggregate. It was hypothesised that the ECM composition present on FS surface at 72 h, that is ECM that had been remodelled by FM3 cells longer, favours disaggregation. To test this, FM3 cells were removed to expose 'bare' ECM at 24 h and 72 h to give '24 h ECM' (shorter period of remodelling by FM3 cells) and '72 h ECM' (longer period of remodelling by FM3 cells), respectively. On these isolated ECM-surfaces, *de novo* FM3 cells were then seeded. Upon the '72 h ECM', cells disaggregated much more readily (Fig. 3.1 C-D). Percentage of non-aggregated cells significantly increased on '72 h ECM' compared to the '24 h ECM' after 48 h of *de novo* seeding of cells. Undergoing aggregation-disaggregation promotes a more invasive phenotype.

During experimentation, one of the surfaces containing TCP control (5k cells; Fig. 3.1 B) was damaged, which is why this data is missing. It was not repeated as statistical comparison was only made within FS surfaces.

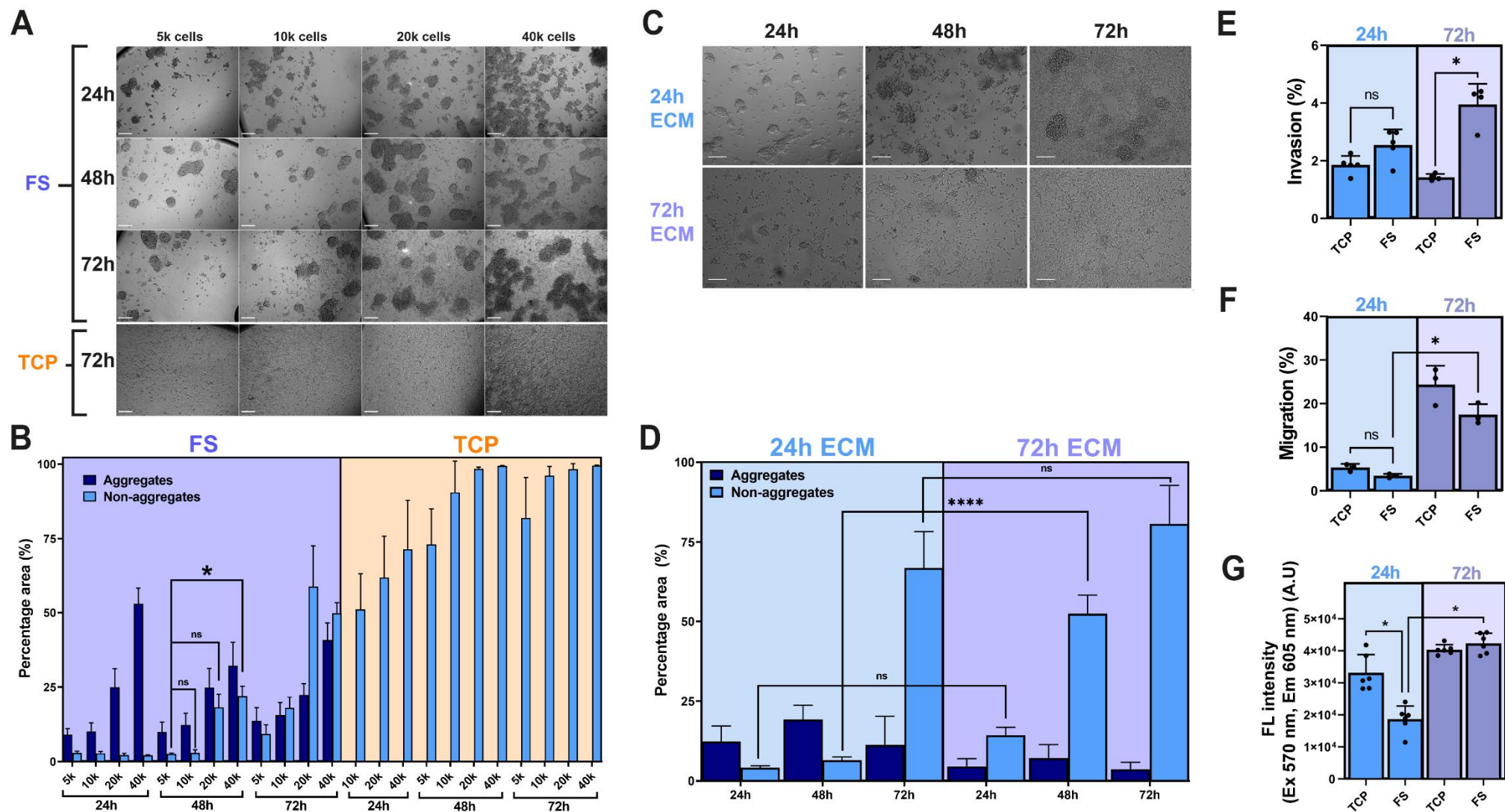


Fig. 3.1 Modelling melanoma CTC cluster aggregation-disaggregation dynamics using fluoroalkylsilica (FS) surfaces. (A-B) Effect of seeding density on FM3 cellular aggregation, (A) representative light micrograph images, scale = 200 μ m, and (B) quantification, n=4. (C-D) Aggregation-disaggregation propensity of cells cultured on ECM derived either from FS-24h or FS-72h surfaces, (D) quantification, n=6, and (C) representative light micrograph images. (E-G) (E) Invasiveness, n=5, (F) Migration, n=3, and (G) Proliferation, n=3, of aggregates (FS-24h) vs non-aggregates (FS-72h and TCP). Scale bar (white bottom left) = 200 μ m. Ordinary Two-way ANOVA with Tukey post-hoc multiple comparisons for B and D, Brown-Forsythe and Welch ANOVA tests (equal SDs not assumed) with Dunnett T3 post-hoc multiple comparison test for E – G. ECM: extracellular matrix, FS: fluoroalkylsilica, TCP: tissue culture polystyrene.

Metastatic melanoma is more invasive than primary tumours. This is because of aberrant overexpression of several key pathways responsible for cell-motility and secretion of matrix metalloproteinases (MMP); for example, Rac1 signalling and JAK-STAT signalling, respectively.¹⁵⁰ At metastatic sites, CTC clusters become entrapped in microvessels. Afterwards, CTC clusters disaggregate, extravasate out of vasculature, and invade neighbouring stroma.

Therefore, it was hypothesised that the ‘disaggregation’ phenotype seen at 72 h on FS surfaces was likely to be more invasive compared to the ‘aggregation’ phenotype seen at 24 h, as well as compared to those that have not undergone aggregation at all (cells cultured on TCP). To test this, invasion and migration assays were carried out using cells representing these phenotypes. Cells were first seeded onto FS or TCP surfaces. At 24 h or 72 h, cells were detached from the surfaces by means of repeated pipetting; this step was necessary for breaking off the clusters into single cells, and to be able to carry out the assays. Cells were then immediately re-seeded into Boyden chambers containing basement membrane extract to carry out the invasion assay, and into chambers without any basement membrane extract to test cell motility. For both assays, a chemotactic gradient was created by keeping the Boyden chamber serum-free and introducing 20% (v/v) foetal calf serum (FCS) in the bottom chamber. After 24 h, the number of cells present in the bottom chamber was quantified using calcein-AM reagent (which measures live cells).

The cells representing the ‘disaggregation’ phenotype (isolated from FS-72h) were significantly more invasive compared to those that did not undergo aggregation at all (isolated from TCP-72h) (Fig. 3.1 E). There was no difference in invasiveness between the ‘aggregation’ phenotype (isolated from FS-24h) and the TCP-24h control, suggesting that the ‘aggregation’ phenotype is not invasive. Cell migration assay showed that there was no difference in migration between cells grown on FS and TCP surfaces (Fig. 3.1 F). Together, these results suggest that cells that have gone through aggregation-disaggregation (‘disaggregation’ phenotype) representing CTC clusters at distal sites could be more invasive but not more motile, compared to aggregates (‘aggregation’ phenotype) representing intravascular CTC clusters, or when compared to those that have not undergone any aggregation-disaggregation events.

3.2.2 Cellular viability is reduced in FM3 aggregates

Since detachment from ECM or surfaces usually leads to cell-death by anoikis programmes and reduced cellular viability, it was hypothesised that cell viability would be reduced in the 'aggregation' phenotype compared to the cells that have attached to the surface (FS-72h and cells cultured on TCP). Cell viability during aggregation at FS-24h was significantly reduced compared to TCP-24h and the FS-72h 'disaggregation' phenotype (Fig. 3.1 G).

3.2.3 Cell-cell proteins are upregulated during FM3 multicellular aggregation

To discern molecular mechanisms governing melanoma cellular aggregation-disaggregation, quantitative proteomics was carried out (Fig. 3.2 A) on intracellular proteins isolated from cells representing the following phenotypes: (i) 'aggregation' phenotype (isolated from FS-24h; representing CTC clusters), (ii) 'disaggregation' phenotype (isolated from FS-72h; representing cells invading at metastatic site), (iii) 'single cell' phenotype (isolated from TCP-24h; representing single CTCs), and (iv) confluent-monolayer phenotype (isolated from TCP-72h; representing cells that did not undergo aggregation-disaggregation).

By comparing the intracellular proteome of 'aggregation' phenotype with 'single cell' phenotype (aggregation; FS-24h vs TCP-24h), the processes and molecules involved in cluster formation were identified. During aggregation, proteins involved in cell-cell contacts were upregulated (Fig. 3.2 B). Notably, the cell surface glycoprotein 4F2 (also known as 4F2hc and CD98) was upregulated during aggregation (FS-24h vs TCP-24h) (Fig. 3.2 B). Proteins involved in cell-matrix adhesion, for example collagen alpha-2(IV) chain (CO4A2), were downregulated during aggregation (Fig. 3.2 B).

Comparison of 'disaggregation' phenotype with 'aggregation' phenotype (disaggregation; FS-72h vs FS-24h), revealed processes and molecules underlying multicellular disaggregation. Cell-cell contact proteins, for example vinculin (VINC), were downregulated during disaggregation (Fig. 3.2 C). In contrast, cell-matrix proteins, for example integrin β 3 (ITB3), were upregulated (Fig. 3.2 C) during disaggregation.

Both aggregation and disaggregation involve drastic changes in cellular morphology. As such, proteins involved in cytoskeletal changes, for example unconventional myosin-X (MYO10), and epithelial-to-mesenchymal transition (EMT)-related proteins, such as thrombospondin-1 (THBS1), were also differentially expressed (Fig. 3.2 B & C).

3.2.4 Cell-matrix proteins were upregulated during melanoma multicellular disaggregation

Multicellular disaggregation appears to be influenced by changes in composition of ECM (section 3.3.1.2). Proteomic analysis of intracellular lysate also revealed upregulation of some ECM-remodelling proteins (Fig. 3.2 C). To outline the changes in ECM compositions during melanoma cellular aggregation-disaggregation, quantitative proteomics was carried out on the matrix proteins (Fig. 3.3 A), isolated and categorised using a previously established approach.¹⁵¹ By comparing differential expression (fold-change) against statistical significance (p-value), the most influential proteins were identified (Fig. 3.3 B-C). The vitronectin levels were significantly reduced during aggregation (FS-24h vs TCP-24h) and increased during disaggregation (FS-72h vs FS-24) (Fig. 3.3 D). Fibronectin levels also significantly reduced during aggregation (FS-24h vs TCP-24h (Fig. 3.3 E).

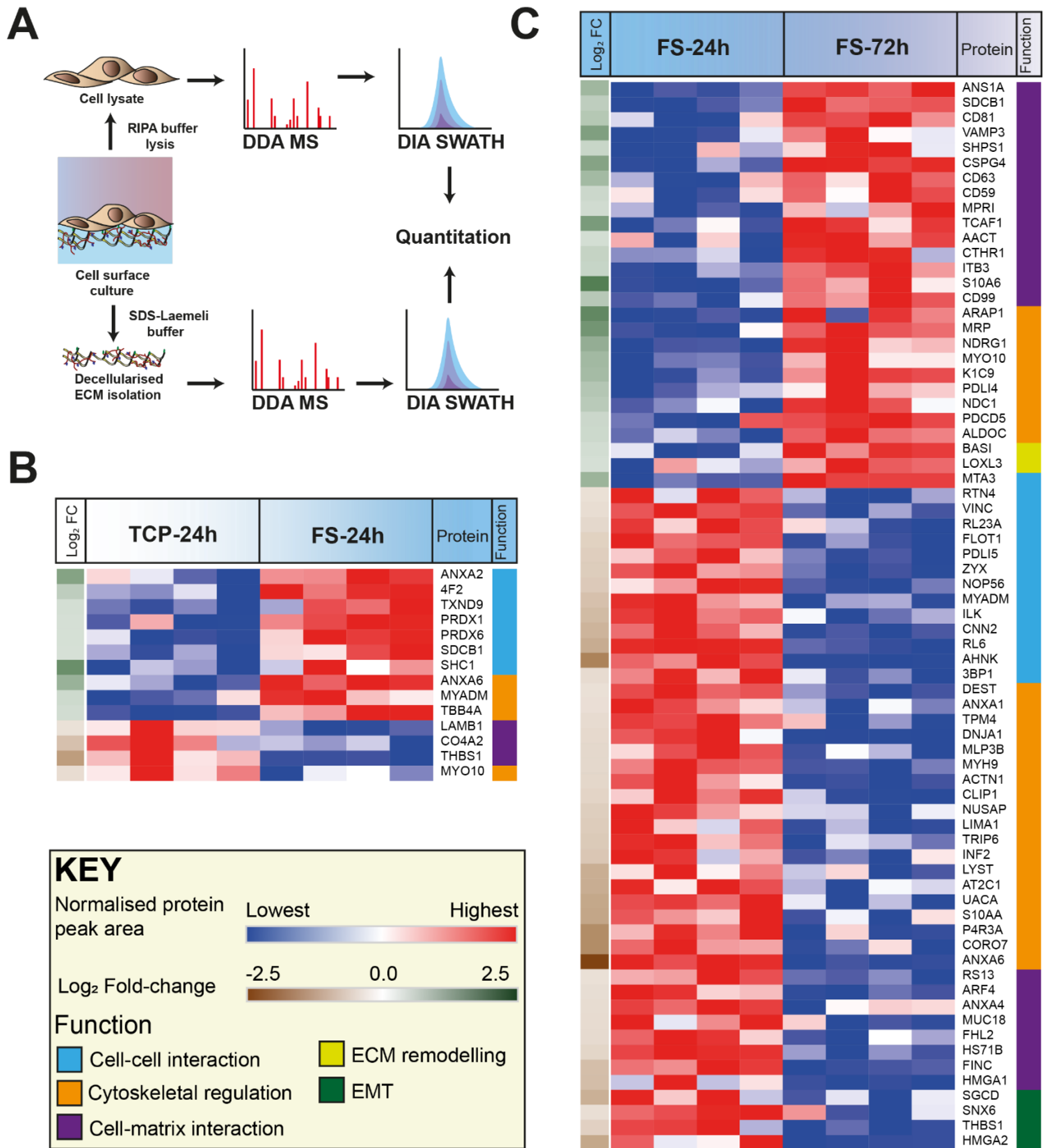


Fig. 3.2 Proteomics of melanoma cell lysate reveal aggregation-disaggregation machinery upon FS surface. (A) Scheme showing harvest of cell lysate and extracellular matrix protein followed by SWATH-MS. (B-C) Heat maps comparing differentially expressed proteins of (B) TCP-24h (non-aggregate) vs FS-24h (aggregate), n=4, and (C) FS-24h (aggregate) vs FS-72h (disaggregate), n=4. Proteins were chosen for analysis based on significant difference ($p < 0.05$) and Log₂ fold change ± 0.38 (3345 total hits). Log₂ fold change of the mean illustrated on the left most column, and protein function (cross-referenced from UniProt, MetaCore and DAVID 6.8) on the right most column. ECM: extracellular matrix. EMT: epithelial-mesenchymal transition, FS: fluoroalkylsilica, SWATH-MS: Sciex TripleTOF 6600 data-independent acquisition mass spectrometry. TCP: tissue culture polystyrene.

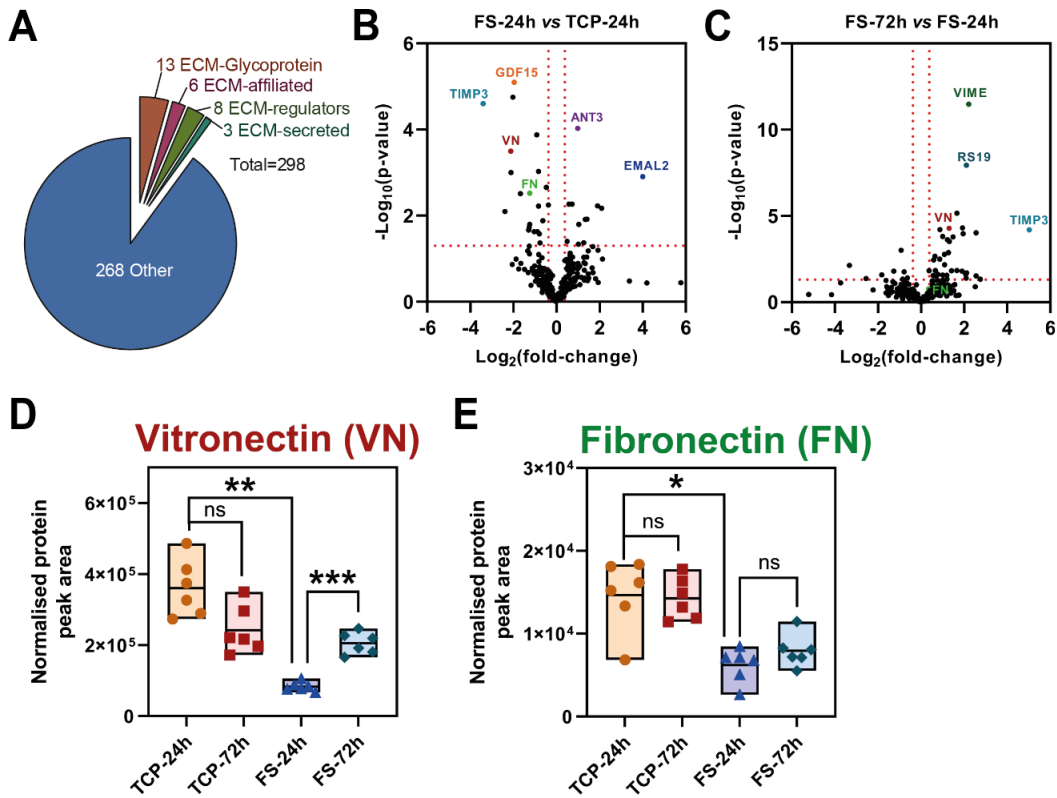


Fig. 3.3 Proteomics highlight key ECM components involved in aggregation-disaggregation of FM3 cells. (A) SWATH-MS proteomics of ECM secreted from FM3 cells upon TCP or FS surfaces, n=6 (298 hits), and categorised as outlined by A. Naba et al. (2016). (B & C) Key ECM proteins were identified using volcano plots with p-value < 0.05 ($-\text{Log}_{10}$) and Log_2 fold-change of ± 0.38 cut offs, (B) where FS-24h vs TCP-24h shows ECM composition during aggregation, and (C) FS-72h vs FS-24h shows ECM composition in disaggregation. (D & E) Change in expression during aggregation-disaggregation of matrisomal (D) Vitronectin (VN) and (E) Fibronectin (FN). Brown-Forsythe and Welch ANOVA tests (equal SDs not assumed) with Dunnett T3 post-hoc multiple comparison test. ECM: extracellular matrix, FS: fluoroalkylsilica, SWATH-MS: Sciex TripleTOF 6600 data-independent acquisition mass spectrometry, TCP: tissue culture polystyrene.

3.3 Discussion

3.3.1 Melanoma FM3 cells aggregate under reduced cellular adhesion conditions

During metastasis, single CTCs could aggregate upon collision with other CTCs or immune/stromal cells.^{54,152} These CTC clusters then disaggregate at secondary metastatic sites and invade through the local stroma to produce metastatic lesions. The aim of this chapter was to establish an *in vitro* model of melanoma CTC cluster formation and disaggregation. Currently, such models have not been described elsewhere. Skin organoid models¹⁵³ are suitable for studying CTC clusters originated via collective migration/cohesive shedding, but unsuitable for studying intravascular collision and multicellular aggregation.

Both FM3 cells (melanoma) and MCF-7 cells (breast cancer) originate from metastatic solid tumours, and as such, both are expected to behave in a similar, albeit not exact, fashion. Therefore, it was hypothesised that similar to MCF-7 cells,¹⁰⁵ FM3 cells would also aggregate under conditions of reduced cellular adherence (RCA). In line with this hypothesis, FM3 cells aggregated by 24 h of culture on FS surface (Fig. 3.1 A). One possible reason as to why FM3 cells aggregate under RCA conditions could be that it is important for cellular survival. The survival of cells increased when they aggregate or when cultured as 3D spheroids, as opposed to as 2D monolayers.¹⁵⁴ It is likely that mechanisms involving resistance to anoikis must be employed here. Anoikis is a process in which cells undergo apoptosis during RCA when cells are not attached to the matrix. As such, metastasising cancer cells, in most cases, adopt characteristics that promote resistance to anoikis.¹⁵⁵

A study showed that A549 lung cancer cells aggregated when cultured as suspension, where an elevation of anoikis-resistance during cellular aggregation was observed.¹⁵⁶ Similarly, CTC clusters also show resistant to anoikis even when under fluid shear stress.¹⁵⁷ Therefore, during instances of RCA, it would seem that CTC and FM3 cells aggregate to better their chances of survival. During the initial 24 h of culture upon the FS surfaces, the conditions mimic blood circulation as their adhesive capacity is significantly reduced due to the decreased adsorption of cell-adhesive proteins.¹⁰⁵ As such, at 24 h upon the FS surface, cells were influenced to aggregate.

A limitation when attempting to establish FS surface-induced aggregates as representative CTC clusters, is that the FS-surface induced aggregates, via its basal layer, attach to the matrix/surface. This means that at least some of the cells of the FS surface-induced aggregates were not under the same RCA conditions as the rest. However, since the majority of the cells within the FS surface-induced aggregates exist as that and experience RCA

conditions, FS-24h 'aggregate' phenotype is still an suitable representation of intravascular CTC clusters.

3.3.2 Disaggregation occurs on remodelled extracellular matrix

Upon FS surfaces, multicellular aggregates of MCF-7 cells disaggregated by 72 h.¹⁰⁵ Similarly, multicellular aggregates of FM3 cells also disaggregated by 72 h (Fig. 3.1 A). A reason for the disaggregation of FM3 aggregates could be similar to MCF-7 multicellular disaggregation, where adsorption of cell-adhesive proteins, such as fibronectin, onto the substrate increased overtime.¹⁰⁵

When FM3 cells were seeded onto ECM substrate that had been remodelled by other FM3 cells for a longer period ('72h ECM'), the multicellular aggregates rapidly disaggregated (Fig. 3.1 C), as compared to when FM3 cells were seeded onto ECM that had been remodelled by other FM3 cells for a shorter period of time ('24h ECM'). Indeed, ECM remodelling by metastasising cell has been shown to be necessary for successful invasion, infiltration, and colonisation.¹⁵⁸ For a successful infiltration of the lungs, tumour cells must stimulate within the stroma the expression of periostin; which is an ECM component that acts as a ligand for $\alpha V/\beta 3$ and $\alpha V/\beta 5$ integrins.¹⁵⁹ This in turn recruits Wnt ligands, signalling of which enhances the maintenance of cancer stem cells leading to a more efficient and sustained infiltration. During invasion of the brain, melanoma cells could coerce resident glial cells, such as astrocytes, to secrete pro-inflammatory cytokines, such as IL-23.¹⁶⁰ In turn, as part of a reciprocal signalling cascade, IL-23 can stimulate the expression of MMP2 by melanoma cells. MMP2 could remodel ECM and induce the blood-brain-barrier to become more permissive to infiltration by tumour cells.

Alternatives to FS surfaces, there are other ultra-low attachment tissue culture microplates, for example Corning™ Costar™, available on the market that researchers have used in the past to generate 3D spheroidal multicellular 'aggregates'.¹⁶¹ Poly-2-hydroxyethylmethacrylate (polyHEMA) has been widely used to coat tissue culture surfaces to generate water-absorbent surfaces, and produce mammosphere of MCF-7 breast cancer.¹⁶² Aggregates generated this way seldom undergo disaggregation. Similar to 3D Matrigel™ or Myogel™-based approaches, these aggregates grow in size over time and have a distinct necrotic core.¹⁶³ Having this growth pattern and necrotic core, permits these aggregates to be highly suitable models for primary and secondary tumours. Researchers have used these models to highlight many aspects of cancer biology, including resistance to chemotherapeutic agents, having an external proliferative zone and inner necrotic core,¹⁶⁴ as well as to highlight importance of 3D environment in cellular differentiation.¹⁶⁵ However, these aggregates might not be suitable for

studying CTC clusters that form by intravascular collision and aggregation. Whereas FS surface models are better suited for these types of CTC clusters, and disaggregation at metastatic site via remodelling of ECM as highlighted in the present contribution.

3.3.3 Aggregation-disaggregation process results in a more invasive phenotype

Metastatic melanoma cells are more invasive and migratory than their primary counterpart.¹⁶⁶ This is because invading cells need to have high invasive potential to be able invade through the basement membrane both at primary and secondary sites, and to infiltrate the stroma both at secondary sites. Here, they release matrix degrading proteins, such as collagenases and gelatinases, to permeate the basement membrane.¹⁶⁷ Moreover, it is the clusters, not single CTC, that are more metastatic;⁴² therefore, it is the CTC clusters likely to be more invasive and more migratory.

Following this, it was hypothesised that FM3 cells isolated from FS-24h 'aggregate' phenotype, representative of CTC clusters, that would be the most invasive and migratory than the 'disaggregated' phenotype from FS-72h and those that had not undergone aggregation-disaggregation (TCP-24h and TCP-72h). However, the experimental observations disproved this hypothesis; it was observed that the cells denoting FS-72h 'disaggregates' that were the most invasive (Fig. 3.1 E) and not the FS-24h 'aggregates or TCP-24h 'single cell' or TCP-72h 'monolayer' phenotypes. This indicates that the aggregation-disaggregation process itself augments cellular invasiveness; cells existing as aggregates is not enough to elicit a more invasive phenotype. This would suggest that upon a suitable and remodelled ECM that would promote multicellular disaggregation, CTC clusters cells undergo a transition that enhances their invasiveness.

Recent publications have highlighted that heterotypic melanoma CTC clusters contain mixture of epithelial-like cells and mesenchymal-like cells.¹⁶⁸ It was suggested that these mesenchymal-like cells take charge of invasiveness, whereas the epithelial-like cells carry out proliferative role as well as sustaining stemness and enhancing anoikis-resistance. Here, the neural crest transcription factor TFAP2 was noted as a master regulator of clustering and switch between proliferative vs invasive phenotypical states. These results imply that for successful metastasis, invasion, and seeding of secondary tumours, CTC clusters would need to be comprised of both epithelial-like and mesenchymal-like cells.¹⁶⁹ The present contribution builds onto this theory that, in addition to having a mixed population of cells, undergoing aggregation-disaggregation is important for invasion and infiltration at

metastatic site. Further research is required to address whether TFAP2 is important for the aggregation-disaggregation-dependent switch to an invasive phenotype.

Both FS-72h and TCP-72h showed increased cell migration compared to their 24h counterparts (Fig. 3.1 F); but no differences were observed between the FS-72h and TCP-72h phenotypes. This is likely due to the cells at 72 h reaching high confluency. When grown upon 2D surfaces such as TCP or FS, cells were forced to spread within the plane as a monolayer so as to decrease contact-induced inhibition of cellular proliferation.¹⁷⁰ Thus, it would seem that the increased cellular migration occurring at 72h both upon FS and TCP surfaces likely due to effects of confluency rather than aggregation-disaggregation. Even if aggregation-disaggregation events affected cell motility, it was hard to distinguish it from the confluency-dependent effects. One way to isolate and measure these effects separately would be to carry out the cell motility assay, but over varying cell density; that is, increasing cell density likely to pose a stronger confluency-effect. As such, if there was a noticeable effect, at 72h when cells disaggregate even at low cell density, then that could reveal any effect on cell motility caused by aggregation-disaggregation event; in this way, confluency-effect can be safely ruled out.

Another limitation of these experiments involving aggregates of cells and using Boyden chambers containing one-to-two cells-wide pores, is that to be able to carry out these assays, the aggregates were broken apart by pipetting up and down. Subsequently, the separated single cells, which at the time of beginning the experimentation standing as representative of the 'aggregate' phenotype, were seeded into the Boyden chambers. Other treatment groups in these experiments were treated the same so as to avoid any potential effects this process of pipetting up and down would have on cellular invasion and migration. Ideally, to test cellular motility of aggregates *in vitro*, live-cell imaging could have been carried out. One would still need to employ Boyden chambers to carry out the invasion assay; as it stands now, all available *in vitro* invasion assays that test the ability of a cancerous cell to invade through a basement membrane require a Boyden chamber of some kind. Currently, there are no appropriate invasion and migratory assays available that would overcome this limitation. Thus, to get a general overview of the invasive and migratory attributes of these phenotypes, the Boyden chamber-based assays were employed here.

One conclusion that can be drawn from these experiments, that is still valid in spite of the aforementioned limitations, is that the aggregation-disaggregation process results in a phenotype that is significantly more invasive than those cells that had not undergone aggregation-disaggregation. This explains why CTC clusters have much higher metastatic propensity and invasiveness compared to single CTC and primary tumours.⁴² It is not clear

how much EMT-like processes, that also influences invasiveness,¹⁷¹ contribute to the aggregation-disaggregation dynamics, or vice versa, and their concerted play in regulating invasion and migration. But it is clear that EMT processes and aggregation-disaggregation processes are separate, albeit similar, processes. Effects of EMT processes on metastasis and invasion can be imagined as occurring at the subcellular level, where effects due to aggregation-disaggregation processes occur at the multicellular level. Henceforth, aggregation-disaggregation processes of metastasis (ADPM) will be considered as a phenomenon that is separate but similar to EMT. Contribution of ADPM to invasiveness in other cancer types in addition to melanoma, and concerted play with EMT, needs to be investigated to get a more accurate picture of the metastasis cascade as a whole.

3.3.4 Cellular viability is reduced in melanoma FM3 multicellular aggregates

Cellular viability assay using AlamarBlue dye revealed that FM3 multicellular aggregates were significantly less proliferative compared to the other phenotypes (Fig. 3.1 G). There was no significant difference in viability between FS-72h and TCP-72h. Similarly, CTC clusters of small-cell lung cancer cells were shown to downregulate proliferative pathways.⁴⁶ Since there was no significant difference in viability of FM3 cells between FS-72h and TCP-72h (Fig. 3.1 G), the reduction in viability must be caused by the 'aggregate' phenotype, rather than the FS surface. That is, FS surfaces were not cytotoxic to FM3 cells.

Why is it important for CTC clusters and FM3 multicellular aggregates to slow down their rate of proliferation rate under RCA, only to resume their proliferative capabilities once they meet a suitable matrix? During the intravascular voyage, CTC clusters may use the resources that they would otherwise use for proliferation, for surviving the harsh conditions of circulation. For example, CTC clusters may increase their chances of survival by packing themselves tightly¹⁷² or repel adversarial immune cells by downregulating certain pathways that are involved in immune response, such as interferon- γ and tumour necrosis factor (TNF) signalling.⁴⁹ These responses require synthesis of proteins, where CTC cells would use the amino acids that they otherwise would use for cellular proliferations.

An important implication of this is that chemotherapeutic agents that target proliferative pathways, might not work as well as intended for melanoma CTC clusters. A commonly used chemotherapeutic agent for melanoma is dacarbazine, which targets cellular proliferation. A meta-analysis of nine randomised controlled trials, totalling 2,481 patients suffering from malignant melanoma, highlighted that dacarbazine-based combinatory therapies were substantially more effective, and yielded better overall response and 1-year survival

responses, when compared to treatment with dacarbazine alone.¹⁷³ In light of the present contribution, it is conceivable why Dacarbazine may work adequately for primary or secondary melanoma tumours,¹⁷⁴ but less so when targeting melanoma CTC clusters. A therapeutic approach that targets CTC clusters would be more effective than dacarbazine in preventing metastasis.

3.3.5 ADPM of FM3 cells involve cell-cell, cell-matrix, and cytoskeletal regulatory pathways

Various signalling pathways are likely to regulate ADPM of CTC clusters. It is conceivable that the underlying machinery of ADPM may vary vastly depending on the cancer subtype. For breast cancer CTC clusters utilise cell surface CD44 molecules to aggregate during intravascular passage,⁴⁴ whereas colorectal cancer CTC clusters seek the aid of galectin-3 and MUC1 for multicellular aggregation.⁵⁸ The signalling pathways that orchestrate ADPM of melanoma CTC clusters still remain elusive. To discover these, proteomics and ontology analysis were carried out on cytosolic proteome of FM3 cells extracted at various stages of FS surface-induced ADPM.

Proteins involved in cell-cell interaction were upregulated during FM3 multicellular aggregation (Fig. 3.2 B) as cell-cell contacts increased. During disaggregation, as cell-cell contacts decreased, cell-cell proteins were downregulated (Fig. 3.2 C). In contrast, proteins involved in cell-matrix interaction were downregulated during aggregation where there was minimal cell-matrix contact (Fig. 3.2 B). During disaggregation, as cell-matrix contacts increased, cell-matrix proteins were upregulated (Fig. 3.2 C). FM3 melanoma cells seem to follow similar pattern of tuning cell-cell proteins to aggregate as breast CTC clusters. Breast CTC clusters showed elevated cell-cell junctional proteins, such as plakoglobin⁴² and ICAM1.⁵⁴ These studies did not investigate disaggregation, as in CTC clusters at their final destination of metastasis; or at the very least, compared CTC clusters to the secondary metastatic lesions. Thus, it is difficult to compare FM3 cells to breast CTC clusters in terms of the signalling pathways underlying the disaggregation process, which is arguably the other half of the story. FS surface models, on the other hand, provide more of a holistic picture of ADPM.

Molecules and pathways that regulate cytoskeleton, as well as those involved in EMT, were differentially expressed during ADPM of FM3 cells (Fig. 3.2 B – C). FM3 cells were submitted to drastic morphological changes as they aggregated; they became more spherical in contrast to their usual elliptical shape, packed tightly, and had more cell-cell contacts, compared to their single-cell/monolayer phenotypes. This level of morphological changes seldom come

without changes to cellular cytoskeleton. For example, cells grown as 3D spheroids have vastly different cytoskeletal actin and intermediate filament arrangement compared to those grown as monolayers. Cells grown in 3D environment showed relaxation of cytoskeleton tension and seemingly increased expression of pluripotent genes in mesenchymal cells.¹⁷⁵ Similarly, FM3 cells were also likely to undergo genetic changes accompanying cytoskeletal relaxation/tension. Since EMT also involves morphological and cytoskeletal events, it is no surprise many molecules, or at the very least their related family members performing similar roles, also often differentially expressed during EMT, or its reverse mesenchymal-to-epithelial transition (MET).¹⁷⁶ These studies explain the differential expressions of cytoskeletal-regulatory and EMT-associated proteins during ADPM of FM3 cells.

More research is required to better understand exactly how each of these proteins regulate the cytoskeleton, identify positive and negative effects they have on each other, and how these effects culminate to bring about a spheroidal or an elliptical morphology, depending on RCA conditions. Further research could address this by inhibiting the proteins highlighted in the present contribution, individually, and in combination, and observing morphological changes at a single cell level, then at multicellular level.

3.3.6 FM3 cells remodel ECM by secreting vitronectin and fibronectin during disaggregation

Cell-matrix interactions and ECM remodelling both seem to play major parts in disaggregation than aggregation, as highlighted by ontological analysis. ECM-swap experiment (Fig 3.1 D) also confirmed that the FS-72h ECM favours multicellular disaggregation and spreading. To outline how the ECM is remodelled during ADPM of FM3 cells, mass spectrometry was carried out on cell-free ECM deposited on the surfaces.

Vitronectin levels decreased during aggregation (FS-24h vs TCP-24h) and increased during disaggregation (FS-72h vs FS-24h) (Fig. 3.3 D). Vitronectin is a cell-adhesive glycoprotein, often aiding in cell-matrix adhesion by linking cell-surface proteins to ECM scaffolds, using ligands, such as integrins (notably integrin alpha-V beta-3), plasminogen activator inhibitor-1 (PAI-1) and urokinase plasminogen activator receptor (uPAR).¹⁷⁷ These findings imply that melanoma CTC clusters could disaggregate by remodelling ECM; make the distal metastatic ECM more receptive for cellular adhesion by secreting vitronectin molecules. Further support for this comes from a clinical study that showed increased serum vitronectin levels in metastatic melanoma.¹⁷⁸

Fibronectin levels also decreased during aggregation (FS-24h vs TCP-24h) (Fig. 3.3 E). As fibronectin matrices are important for cellular adhesion,¹⁷⁹ this was expected as cell-matrix contacts decreased during aggregation. In metastatic melanoma, fibronectin levels were found to be increased.¹⁰⁰ These results are, however, in disagreement with a previous study that demonstrated that fibronectin levels increased during multicellular aggregation of breast and lung cancer cells;⁵¹ knockdown of fibronectin also decreased aggregation. The authors highlighted a non-matrisomal role of fibronectin in enhancing resistance to anoikis. An explanation for this disparity could be that fibronectin could serve different roles in melanoma ADPM (cell-matrix contact) compared to ADPM of breast and lung CTC clusters (resistance to anoikis). Metastatic cancer cells not only remodel the ECM at distal sites by reconstructing fibronectin networks,¹⁸⁰ and vitronectin networks,^{181,182} but they have also been shown to prime the distal ECM before they arrive by upregulating expression of these scaffold proteins in stromal fibroblast cells.¹⁸³

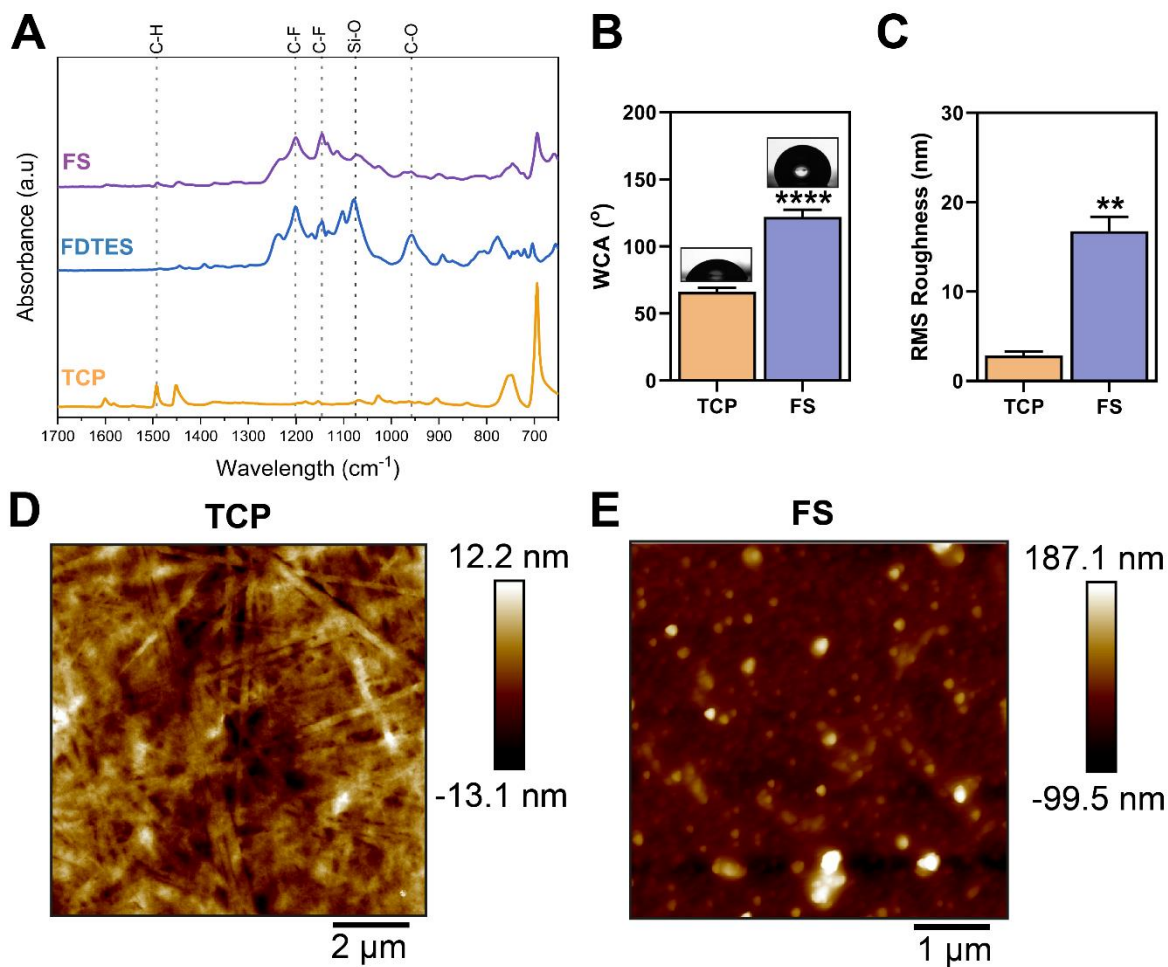
A notable limitation accompanying mass spectrometry of ECM in the present contribution is that the isolation of ECM was crude. Melanoma and melanocytes in general express matrisomal scaffolding proteins besides fibronectin and vitronectin, such as collagen¹⁸⁴ and chondroitin sulphates.¹⁸⁵ However, these were not detected in the mass spectrometry analysis. It could be that FM3 cells do not express these proteins. However, an obvious explanation could be that these matrisomal proteins were too scarce for this crude approach to effectively measure. An improvement here could be to include a further step, notably deglycosylation to remove glycosylated side chains that could otherwise obfuscate identification of the aforementioned proteins.¹⁸⁶ Another limitation with this study was that only one melanoma cell line (FM3 cells) was used. Ideally, another melanoma cell line needed to lend further support to the conclusions drawn. Though, due to lack of fund and time, only one set of experiment for one cell line was possible at this time. Future experiments could be repeated using a different melanoma cell line to lend further support.

3.3.7 Conclusions

The research used FS surfaces to explore aggregation-disaggregation events by FM3 melanoma cells and highlighted these surfaces as cost-effective and suitable *in vitro* models of melanoma CTC clusters that does not require patient samples or costly microfluidic instruments. FM3 cells aggregate under RCA conditions to increase their chances of survival. At distal metastatic sites, melanoma CTC clusters could disaggregate by remodelling the ECM, by secreting ECM scaffold proteins such as fibronectin and vitronectin. Cells that had undergone ADPM were more invasive than those that had not; this could why CTC clusters are more metastatic than single CTC. Cellular viability was reduced in multicellular aggregates,

which highlights the inadequacy of therapeutics that target proliferation in metastatic melanoma. Mass spectrometry revealed that FM3 cells aggregate by increasing cell-cell signalling and decreasing cell-matrix signalling; cells could disaggregate by doing the opposite. Morphological changes associated with ADPM arise from cytoskeletal regulations and EMT-like processes. Future research could use these FS surface models to investigate other important aspects of melanoma CTC cluster metastasis like resistance to anoikis and EMT.

3.4 Supplementary Figures



Supplementary Fig. 3.1 Characterisation of FS and TCP surfaces. (A) FTIR spectra of TCP, FDTES and FS. (B) Water contact-angle measurement of TCP and FS, n=3. (C) RMS roughness of TCP and FS, n=3, and representative micrographs (D-E). T-test (two-tailed, heteroscedastic). FS: fluoroalkylsilica, RMS: root mean square, TCP: tissue culture polystyrene, WCA: water contact-angle.

Chapter 4. Involvement of 4F2hc and galectin-3 in melanoma multicellular aggregation

Contents

CHAPTER 4. INVOLVEMENT OF 4F2HC AND GALECTIN-3 IN MELANOMA MULTICELLULAR AGGREGATION	49
4.1 INTRODUCTION	50
4.2 RESULTS.....	51
4.2.1 Galectin-3 expression in FM3 multicellular aggregation-disaggregation	51
4.2.2 4F2hc expression during FM3 multicellular aggregation-disaggregation.....	53
4.2.3 Galectin-3 and 4F2hc colocalises at cell-cell facet of FM3 multicellular aggregate	55
4.2.4 4F2hc:oGal3:4F2hc bridges vs 4F2hc:4f2hc homophilic binding	55
4.2.5 4F2hc and galectin-3 predicted to contribute to clinical melanoma metastasis.	58
4.3 DISCUSSION	60
4.3.1 Galectin-3 is involved in FM3 multicellular aggregation-disaggregation	60
4.3.2 4F2hc plays a major role in FM3 multicellular aggregation-disaggregation.....	61
4.3.3 Galectin-3 and 4F2hc colocalises at FM3 cell-cell interface	63
4.3.4 4F2hc:oGal3:4F2hc bridges	63
4.3.5 4F2hc:4F2hc homophilic binding.....	65
4.3.6 4F2hc:oGal3:4F2hc bridges vs 4F2hc:4F2hc homophilic binding in melanoma FM3 aggregates.....	66
4.3.7 Glycoprotein:Galectin-3:Glycoprotein (GGG) Bridges in clinical melanoma	68
4.3.8 Conclusions.....	70
4.4 SUPPLEMENTARY FIGURES	71

4.1 Introduction

This chapter focuses on the roles of 4F2-heavy chain (4F2hc) and galectin-3 proteins in driving multicellular aggregation of FM3 melanoma cells.

In chapter 3, quantitative proteomics revealed that the cell-surface glycoprotein 4F2hc levels increased during FM3 cellular aggregation (Fig. 3.2 B). Many cell-surface glycoproteins have been attributed to the formation of CTC clusters in different cancers; for example, CD44 in triple-negative breast cancer⁴⁴ and MUC1 in colon and breast cancer cells.⁵⁸ CD44 molecules form homophilic interactions with CD44 molecules on adjacent cells and induce cluster formation of breast cancer CTCs.⁴⁴ In both breast and colon cancer, galectin-3 molecules have been shown to link neighbouring MUC1 glycoproteins together, which allows for the formation of E-cadherin-dependent cell-cell adhesion and aggregation.⁵⁸ In FM3 melanoma cells, it is not clear, if at all, whether 4F2hc molecules induce multicellular aggregation, and whether it is via homophilic interactions similar to CD44 molecules, or via galectin-3-mediated similar to that of MUC1. Galectin-3 molecules could link 4F2hc molecules, since 4F2hc molecules possess four putative *N*-glycosylation sites that could be recognised by galectin-3.¹³⁴ Galectin-3 and 4F2hc interaction has been shown in HeLa cervical cancer cells.¹⁸⁷

Three principal characteristics separate galectin-3 from the other galectin types: (i) it functions both intracellularly and extracellularly, (ii) it oligomerises at high concentrations, (iii) and this oligomeric conformation allows for a greater flexibility in simultaneously binding to multiple glycans.¹⁸⁸ Physiological concentration of circulating galectin-3 is elevated in many different types of cancer, including breast¹⁸⁹ and melanoma.¹⁹⁰ In most of these cases, sera galectin-3 levels increased even further in patients with metastatic cancer compared to those with non-metastatic cancer. Immunohistochemistry staining for tissue galectin-3 revealed that compared to patients with precancerous naevus and dysplastic naevus, galectin-3 levels markedly increased in primary melanoma;¹⁹¹ however, expression levels notably dropped in secondary metastatic melanoma lesions. These findings suggest that galectin-3 must play a key role during early stages of melanoma progression and during CTC-cluster metastases through blood circulation; but is involved much less once metastasis has taken place.

Therefore, this chapter aims to study the potential interplay between 4F2hc and galectin-3 in regulating aggregation-disaggregation of FM3 melanoma cells. Whether it is through homophilic binding of 4F2hc, or through 4F2hc interacting with galectin-3, that melanoma CTC could undergo multicellular aggregation will be investigated using *in silico* protein docking experiments.

4.2 Results

4.2.1 Galectin-3 expression in FM3 multicellular aggregation-disaggregation

Galectin-3 has been reported to regulate CTC multicellular aggregation in malignancies.⁵⁸ Galectin-3 holds much potential in bridging multiple cell-surface glycoproteins on neighbouring cells during cellular aggregation. As such, in the present contribution, it was theorised that galectin-3 levels would rise during melanoma cellular aggregation. Indeed, both mass spectrometry and quantitative reverse transcription PCR (RT-qPCR) showed that intracellular galectin-3 levels were somewhat increased during melanoma cellular aggregation (Fig. 4.1 A & C). RT-qPCR also revealed a small reduction in expression of *LGALS3*, the gene that codes for galectin-3 protein, during cellular disaggregation (Fig. 4.1 C), although these results were not statistically significant, they follow the same pattern as the intracellular galectin-3 proteomic data. Conversely, matrisomal galectin-3 levels significantly reduced during cellular aggregation and increased during disaggregation (Fig. 4.1 B).

Silencing galectin-3 in MUC16-expressing breast and ovarian cancer cells reportedly inhibited metastasis in murine models.¹⁹² In this study, blocking galectin-3 with this antibody led to reduced lung-specific metastatic growth. In the present contribution, it was hypothesised that blocking galectin-3 signalling using an anti-galectin-3 antibody (AF1154) could reduce melanoma cellular aggregation. A concentration of 10 ng/mL of anti-galectin-3 antibody was sufficient to reduction in cellular aggregation (FS-24h) compared to that of IgG isotope control (Fig. 4.1 D), although not statistically significant. However, it is worth noting here that this was accompanied by a increase in cellular disaggregation (FS-72h). The antibody had no significant effect on cell viability (Fig. 4.1 E). These results highlight that galectin-3 could be important for intravascular aggregation of melanoma CTC.

A high-affinity galectin-3 inhibitor (GB1107; 37 nM) has been developed recently, with selectivity for galectin-3 over other Galectins.¹⁹³ In a mouse model, GB1107 decreased growth of human and mouse lung adenocarcinoma and blocked metastasis.¹⁹⁴ In the present study, treatment with GB1107 at 10 μ M decreased melanoma cellular aggregation (supplementary Fig. 4.1).

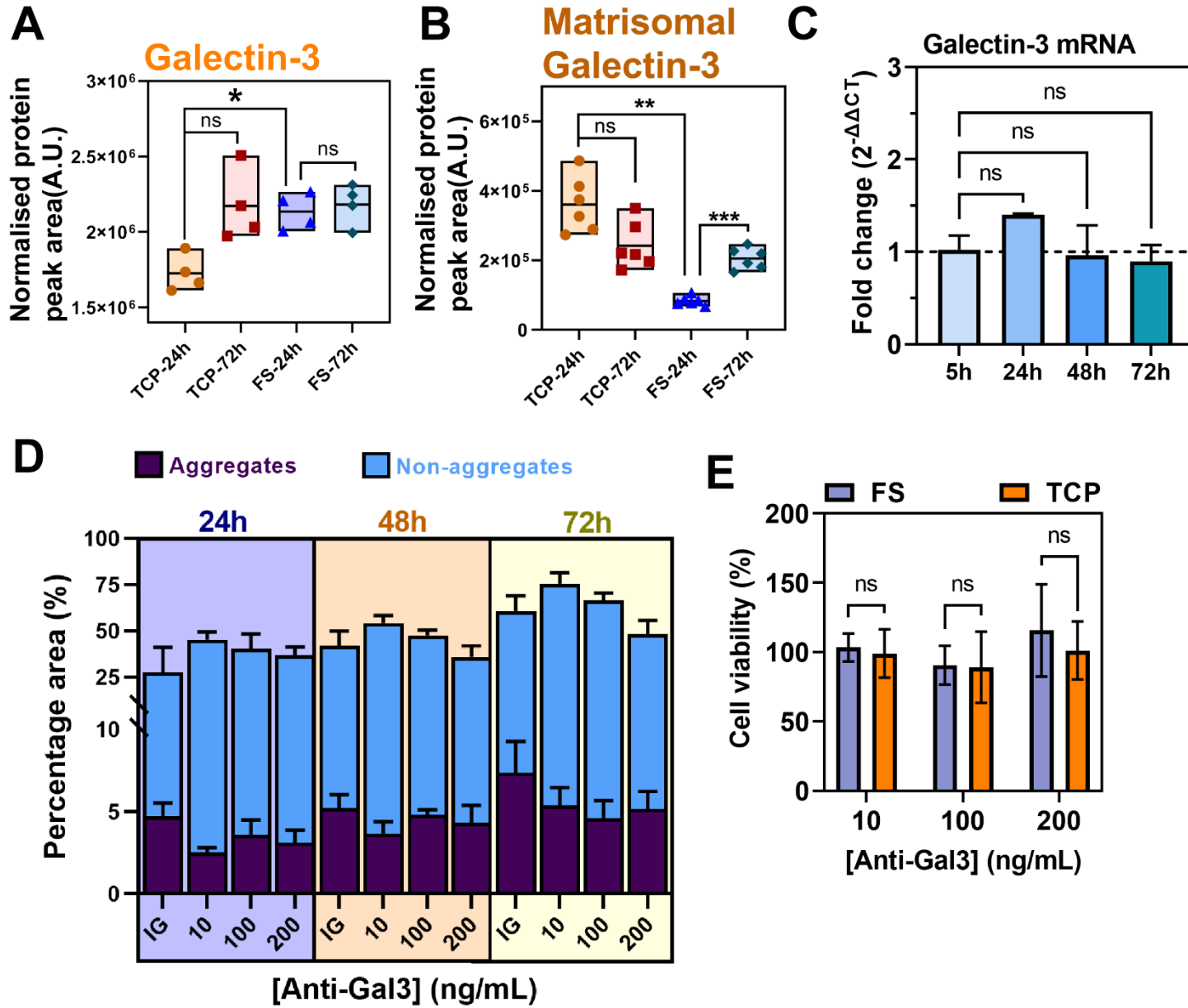


Fig. 4.1 Galectin-3 facilitates FM3 cellular aggregation-disaggregation. (A-B) Change in Galectin-3 levels during FM3 cellular aggregation (FS-24h vs TCP-24h) and disaggregation (FS-72h vs FS-24h) as measured by mass spectrometry; (A) Intracellular or cell-surface bound Galectin-3, n=4, or (B) extracellular or matrisomal Galectin-3, n=6. (C) Periodic expression of Galectin-3 mRNA during aggregation (5-24h) vs disaggregation (48-72h) as measured by RT-qPCR, n=3. Fold Change ($2^{-\Delta\Delta CT}$) represents comparison of FS surfaces vs TCP surfaces. (D-E) FM3 cells were treated with anti-Galectin-3 antibody (Anti-Gal3; AF1154) or immunoglobulin G (IG) isotope during culture upon FS surfaces. (D) Effect of increasing concentration of Anti-Gal3 on percentage area occupied by aggregates and non-aggregates, n=6. (E) Effect of increasing concentration of Anti-Gal3 on cellular viability after 72 h of culture, n=6. Brown-Forsythe and Welch ANOVA tests (equal SDs not assumed) with Dunnett T3 post-hoc multiple comparison test was carried out for mass spectrometry comparisons and RT-qPCR (A - C). Ordinary Two-way ANOVA with Tukey post-hoc multiple comparisons were carried out for antibody-treatment and cell viability experiments (D - E). Anti-Gal3: monoclonal antibody targeting galectin-3. FS: fluoroalkylsilica, Gal3: Galectin-3, IG: Immunoglobulin G Isotope, TCP: tissue culture polystyrene.

4.2.2 4F2hc expression during FM3 multicellular aggregation-disaggregation

Quantitative mass spectrometry revealed that 4F2hc and the large neutral amino acid transporter-1 (LAT1) proteins levels were significantly increased during cellular aggregation (Fig. 4.2 A-B). 4F2hc levels also significantly decreased during disaggregation. These two proteins compose the cell-surface glycoprotein CD98 heterodimer. RT-qPCR further confirmed that expression of *SLCA3A2*, the gene that codes for 4F2hc, was upregulated during melanoma cellular aggregation (significantly upregulated at 48 h), and subsequently downregulated during disaggregation (Fig. 4.2 C).

LAT1 is a membrane transport protein that transports branched-chain and aromatic amino acids. LAT1 has no reported glycosylation sites.¹⁹⁵ Whereas 4F2hc contains four glycosylation sites: *N*-Acetylglucosamine (GlcNAc) added to the amine nitrogen atom of asparagine residues at positions 365, 381, 424, and 506. All four of these asparagine residues are present within the extracellular topological domain of 4F2hc. Galectin-3 has been shown to bind to GlcNAc-R chains, and as such, exogenous galectin-3 has been reported to bind to 4F2hc.¹⁹⁶ When galectin-3 molecules were blocked in FM3 cells, reduced cellular aggregation was observed. Therefore, it was hypothesised that blocking 4F2hc/galectin-3 interaction would attenuate cellular disaggregation. For this, the anti-4F2hc antibody (HPA017980) was used. This antibody recognises an antigenic epitope within the extracellular region of 4F2hc, between amino acids 245-385; where 2 out of the 4 glycosylation sites are located.¹³⁴ Treating FM3 cells with 50 ng/mL of the anti-4F2hc antibody was sufficient to significantly reduce cellular aggregation at 24 h (Fig. 4.2 D). Unlike the galectin-3 antibody, this anti-4F2hc antibody did not induce a significant increase in cellular disaggregation at 72 h. Anti-4F2hc antibody significantly reduced cellular viability (Fig. 4.2 E)

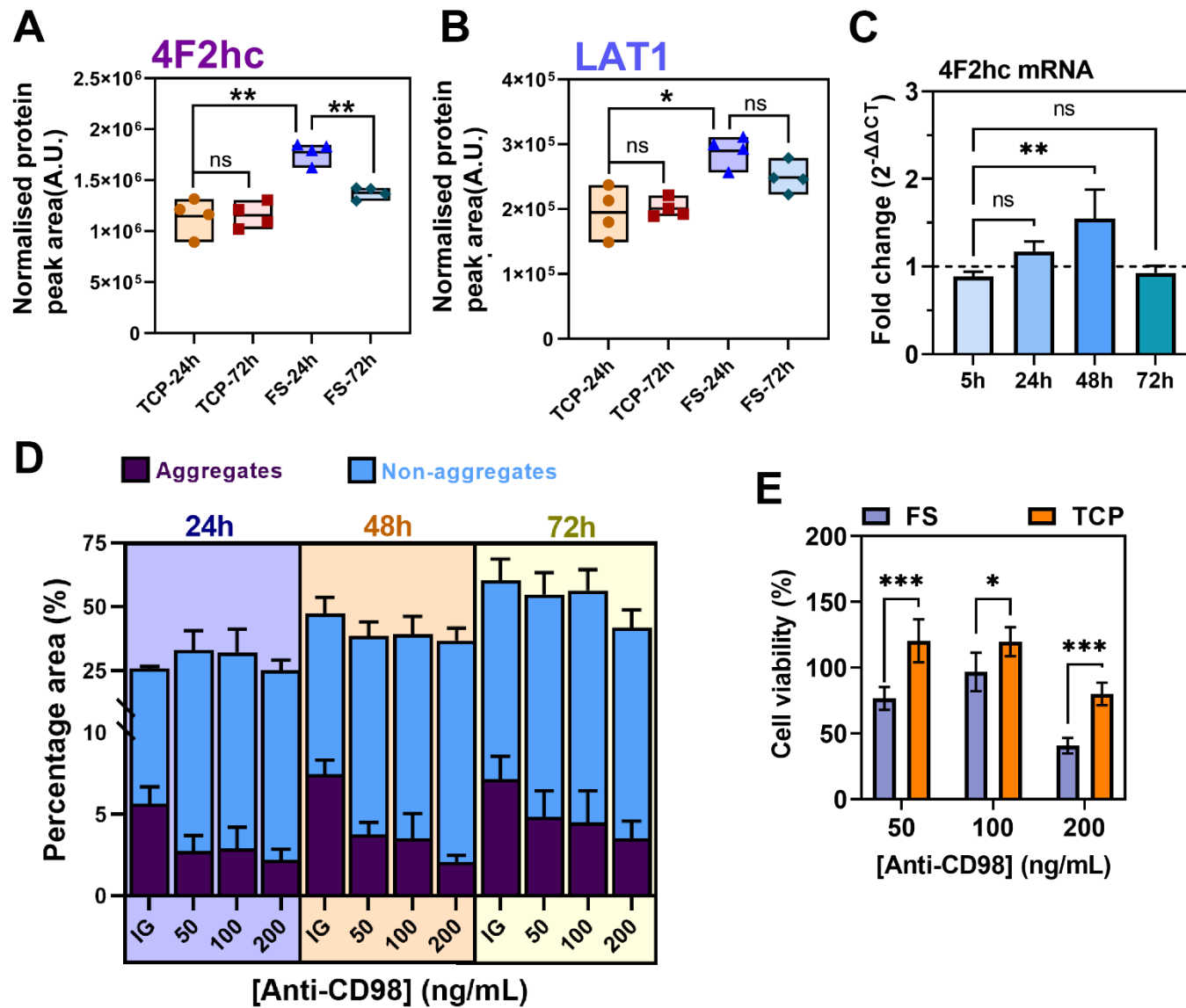


Fig. 4.2 4F2hc regulates FM3 cellular aggregation-disaggregation. Changes in protein levels of 4F2hc (A) and LAT1 (B) during FM3 cellular aggregation (FS-24h vs TCP-24h) and disaggregation (FS-72h vs FS-24h) as measured by mass spectrometry, n=4. (C) Periodic expression of 4F2hc mRNA during aggregation (5-24h) vs disaggregation (48-72h) as measured by RT qPCR, n=3. Fold Change ($2^{-\Delta\Delta CT}$) represents comparison of FS surfaces vs TCP surfaces. (D-E) FM3 cells were treated with anti-4F2hc antibody (Anti-CD98; HPA017980) or immunoglobulin G (IG) isotope during culture upon FS surfaces. (D) Effect of increasing concentration of Anti-CD98 on percentage area occupied by aggregates and non-aggregates, n=6. (E) Effect of increasing concentration of Anti-CD98 on cellular viability after 72 h of culture, n=6. Brown-Forsythe and Welch ANOVA tests (equal SDs not assumed) with Dunnett T3 post-hoc multiple comparison test was carried out for mass spectrometry comparisons and RT-qPCR (A – C). Ordinary Two-way ANOVA with Tukey post-hoc multiple comparisons were carried out for antibody-treatment, and cell viability experiments (D - E). FS: fluoroalkylsilica, IG: Immunoglobulin G Isotope, TCP: tissue culture polystyrene.

4.2.3 Galectin-3 and 4F2hc colocalises at cell-cell facet of FM3 multicellular aggregate

To investigate whether galectin-3 and 4F2hc colocalise at the cell-cell interface in FM3 multicellular aggregates, dual-stain immunofluorescence was carried out. Dual-staining of Galectin-3 and 4F2hc revealed that both proteins were colocalised at the cell-cell interface (Supplementary Fig. 4.2; as denoted by the white arrows). 4F2hc was predominantly localised to the cell-cell interface, whereas galectin-3 was predominantly localised to the outer periphery of the aggregates (Supplementary Fig. 4.2). This indicates that galectin-3 could serve a bigger role in the periphery than the core of the aggregates.

4.2.4 4F2hc:oGal3:4F2hc bridges vs 4F2hc:4f2hc homophilic binding

Co-expression of 4F2hc and oligomeric galectin-3 (oGal3) alone is insufficient to prove that galectin-3 binds to 4F2hc, and that this interaction is needed for multicellular aggregation. It is equally likely that 4F2hc could form homophilic interactions to promote aggregation. Since co-immunoprecipitation and pull-down binding assays require substantial time-investment and optimisation, *in silico* study was carried out to investigate the likelihood of 4F2hc:oGal3:4F2hc bridges, or homophilic interaction of 4F2hc:4F2hc, that would promote FM3 multicellular aggregation.

The orthorhombic crystal structures of 4F2hc ectodomain (4F2hc-ED) and galectin-3 carbohydrate recognition domain (galectin-3-CRD) have been solved via X-Ray Crystallography (PDB ID: 2DH3 and PDB ID: 1A3K, respectively). These crystal structures were chosen for this study as opposed to full molecules to limit interactions to the extracellular milieu. To test the bridge vs the homophilic interaction theory, human galectin-3-CRD was docked to 4F2hc-ED, or 4F2hc-ED to itself, via ClusPro computation¹³⁶ (Fig. 4.3 A-B), without including any molecules of water or solvent. The top ten models of each of the interactions were selected for further analysis, with the top two graphically depicted using PyMOL package (Fig. 4.3 A & B).

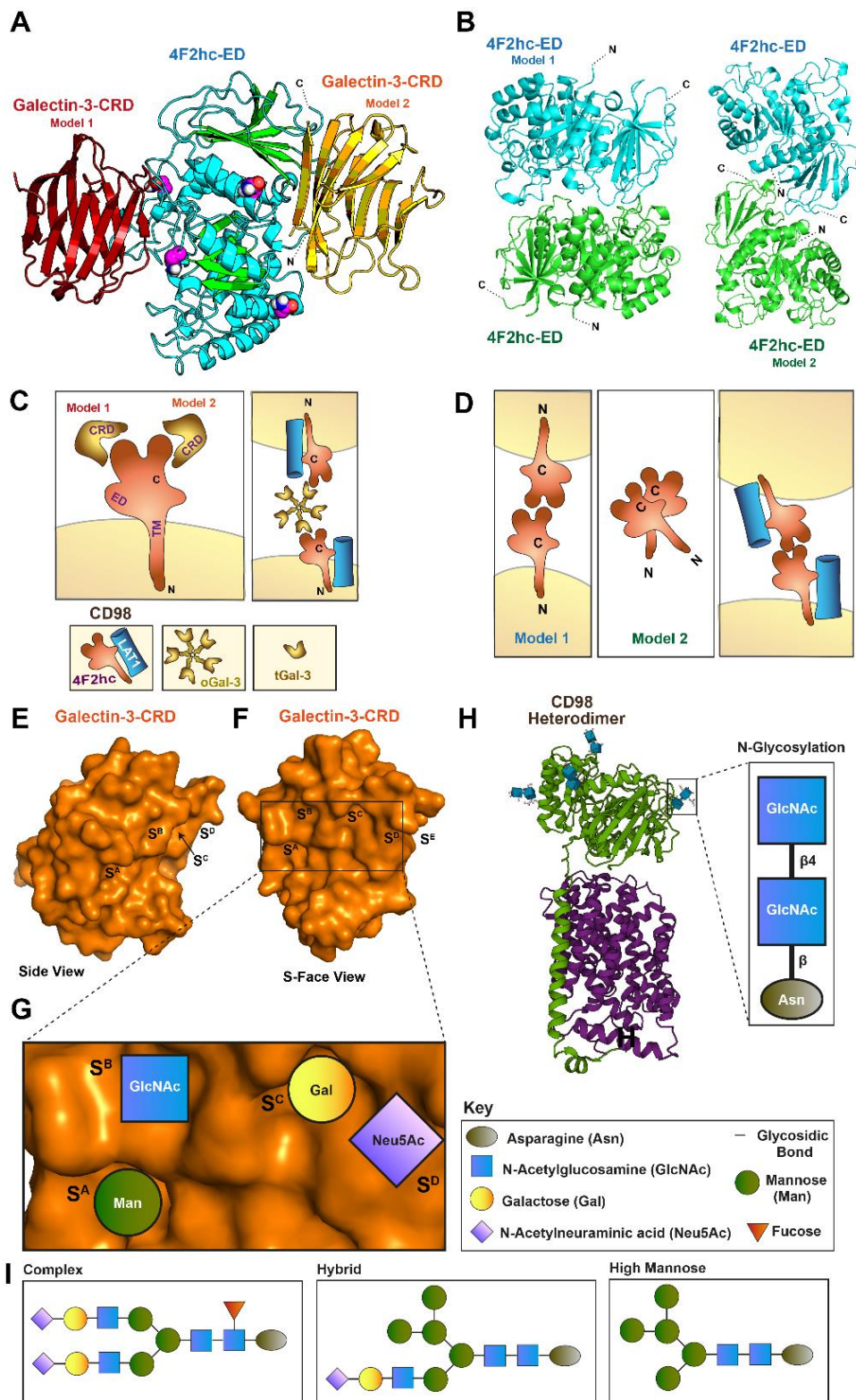


Fig. 4.3 FM3 multicellular aggregation: [4F2hc-oGal3-4F2hc] bridges vs [4F2hc-4F2hc] homophilic interactions. (A-B) Human 4F2hc ectodomain (4F2hc-ED) was docked to human galectin-3 carbohydrate domain (galectin-3- CRD) (A) or itself (B) *in silico* via ClusPro computation using crystal structures of 4F2hc-ED (PDB ID: 2DH3) and galectin-3-CRD (PDB ID: 1A3K). Top two docking models are shown for each interaction. (A) Highlighted in magenta are the four asparagine residues susceptible to N-Glycosylation. (C) Scheme of tGal-3-CRD binding to 4F2hc-ED (first panel), and scheme of oGal-3 binding to two coterminous 4F2hc-ED on adjacent cells to form cell-cell bridge (second panel). (D) Scheme of 4F2hc-ED homophilic binding in cell-cell interaction predicted by ClusPro protein docking computation (first and second panels) and scheme of homophilic interaction of CD98 molecules forming cell-cell contacts (third panel). (E-F) Crystal structure of human galectin-3-CRD was solved (PDB ID: 1A3K), allowing visualisation of the four-glycan binding pockets (S^{A-D}), and one protein-binding SE facet, within the S-Face of the CRD. (G) Scheme of a tetrasaccharide, containing GlcNAc, galactin and two additional sugars, fitting into the four S^{A-D} subsites of galectin-3-CRD. (H) Crystal structure of human CD98 heterodimer was solved (PDB ID: 6IRS); highlighted in blue are GlcNAc disaccharides N-Glycosylated to four asparagine residues. (I) Three classes of cell-surface glycosylation in mammalian cells. Asn: Asparagine, CRD: Carbohydrate recognition domain, ED: ectodomain, Gal: Galactose, oGal-3: oligomeric galectin-3, GlcNAc: N-acetylglucosamine, Man: mannose, tGal-3: truncated Galectin-3, Neu5Ac: N-acetylneuraminic acid.

4F2hc-ED possesses four asparagine residues (magenta in Fig. 4.3 A) which are susceptible to *N*-Glycosylation. Crystal structures revealed that the asparagine residues exist as pairs, with each pair on opposing sides of the ectodomain. Two of these (N264 and N323) pair is located on one side, and the other two (N280 and N405) pair residing on the other facet of the 4F2hc-ED. During *N*-Glycosylation, GlcNAc residues are added to the asparagine residues. Recent study, using Cryogenic Electron Microscopy (Cryo-EM) techniques solved structure of full CD98 heterodimer (PDB ID: 6IRS), LAT1-4F2hc; this further confirmed the presence of GlcNAc disaccharides on the four asparagine residues of 4F2hc-ED.

Since galectin-3-CRD recognises carbohydrates, it was hypothesised that it would bind at any of these four GlcNAc sites. Indeed, ClusPro computation revealed that seven out of the top ten models predicted galectin-3-CRD protomer to bind proximal to the N264 and N323 asparagine pair (Fig. 4.3 A; Model 2). Three out of the top ten models predicted galectin-3-CRD protomer to bind proximal to the N280 and N405 asparagine pair (Fig. 4.3 A; Model 1). Fig. 4.3 C shows a scheme of how these 4F2hc-galectin-3 interactions would lead to cell-cell bridges should the galectin-3 involved were to be oligomeric (oGal3) rather than the truncated variant (tGal3).

On the other hand, 4F2hc-ED self-docking involved two distinct orientations: (i) one model where the N-terminus domains, through which 4F2hc molecules tether to the plasma membrane, predicted to be opposite of the interface (Fig. 4.3 B; Model 1), and (ii) one model where the N-terminus domains predicted to be adjacent to the interface (Fig. 4.3 B; Model 2). Here, model 1 predicts homophilic interactions of 4F2hc-ED from adjacent cells during cell-cell contact, whereas model 2 predicts homophilic 4F2hc-ED interactions within the same cell (Fig. 4.3 D).

LigPlot+ computation¹³⁷ was used next to compare which of these two interactions, galectin-3-CRD:4F2hc-ED or 4F2hc-ED:4F2hc-ED, has higher propensity to occur. This analysis was carried out by focusing on non-covalent interactions, such as hydrogen bonds, hydrophobic and aryl-aryl interactions (Supplementary Fig. 4.4 & 4.5). Rather than comparing each of these non-covalent interactions individually, and since each of these non-covalent interactions could have varying degree of impact on the protein-protein interactions (PPI) as a whole, normalised and weighted PPI scores were calculated instead (Supplementary Fig. 4.6). 4F2hc/4F2hc model 2 yielded the highest PPI score and 4F2hc/4F2hc model 2 yielded the lowest. Both models of Gal3/4F2hc yielded similar PPI scores (Supplementary Fig. 4.6).

4.2.5 4F2hc and galectin-3 predicted to contribute to clinical melanoma metastasis

Malignant transformation of most solid tumours, including melanoma, is often accompanied by glycosylation of a plethora of cell-surface glycoproteins; this is carried out via post-translational modification by glycosyltransferases.¹⁹⁷ For melanoma CTC aggregation-disaggregation events, in addition to 4F2hc, other glycoproteins could also be linked by galectin-3. To deduce whether any other glycoproteins involved in ADPM of FM3 cells, quantitative proteomics dataset (from Chapter 3, Fig. 3.2 B & C) was compared to primary and metastatic melanoma datasets from clinical studies obtained from online repositories.

Literature from the past ~30 years reported fifty-one cell-surface proteins that could bind to galectin-3 (Supplementary Table. 4.1). Contribution of these proteins to the risk associated with melanoma (Z_1) and metastatic melanoma (Z_2) were obtained from PRECOG tool.¹²⁷ PRECOG tool matches RNA sequencing dataset to patient survival dataset to generate 'meta' Z-score (Fig. 4.4 A: Z_1 and Z_2). The dataset used here as follows: for melanoma, PMID 20460471¹²⁸ and PMID 18505921,¹²⁹ and for metastatic melanoma PMID 18505921¹²⁹ and PMID 19915147.¹³⁰

Next, Metastasis Z-score (Z_2-Z_1) was calculated for the fifty-one glycoproteins (Fig. 4.4 A). Since Z-score, classically, is a metric of statistical significance, where p-value of 0.05 of a two-tailed distribution equates to Z-score of 1.96, this Z-score was used to gauge the glycoproteins contributing to the most favourable and most unfavourable risks associated with the metastasis of melanoma. This revealed the following genes coding for the glycoproteins as most favourable: *ITGAM*, *TFRC*, *PTPRC*, *LAMP1*, *HPSE*, *FZD8*; and most unfavourable: *BSG*, *FZD9*, *CD44*, *FZD3*, *SLC3A2*, *LYPD3*, *LGALS3BP*. Notably, *SLC3A2*, the gene that codes for 4F2hc protein, was amongst the top five unfavourable prognostic markers for metastasis of melanoma.

To investigate whether these genes, also contribute to the *in vitro* FM3 multicellular aggregation-disaggregation model, Z-score was calculated for disaggregation (Z_D), aggregation (Z_A), and aggregation-disaggregation factor (Fig. 4.4 B: $A \rightarrow D$ ($|Z_D| + |Z_A|$)).

The glycoproteins considered to be important for both *in vitro* FM3 multicellular aggregation-disaggregation model (Fig. 4.4 B: $A \rightarrow D$), as well as metastasis of clinical melanoma (Fig. 4.4 A: Z_2-Z_1), were basigin (*BSG*) and 4F2hc (*SLC3A2*). Cell-surface proteins that seem to be only important for the *in vitro* model, but not necessarily clinical melanoma, were integrin $\beta 3$ (*ITGB3*) and LAT1 (*SLC7A5*).

Lastly, since human melanocytes and melanoma cells express a whole host of galectins, it was important to also identify galectins other than galectin-3, that could also serve as a cell-

cell bridge in multicellular aggregation. Meta Z-score obtained from PRECOG tool for different galectins, and metastasis factor (Z_2-Z_1) was calculated and stratified similar to glycoproteins (Supplementary Fig. 4.7). This investigation highlighted galectin-3 (*LGALS3*) and galectin-1 (*LGALS1*) as unfavourable risk factors for the metastasis of melanoma, and galectin-8 (*LGALS8*) as favourable risk factor (Supplementary Fig. 4.7).

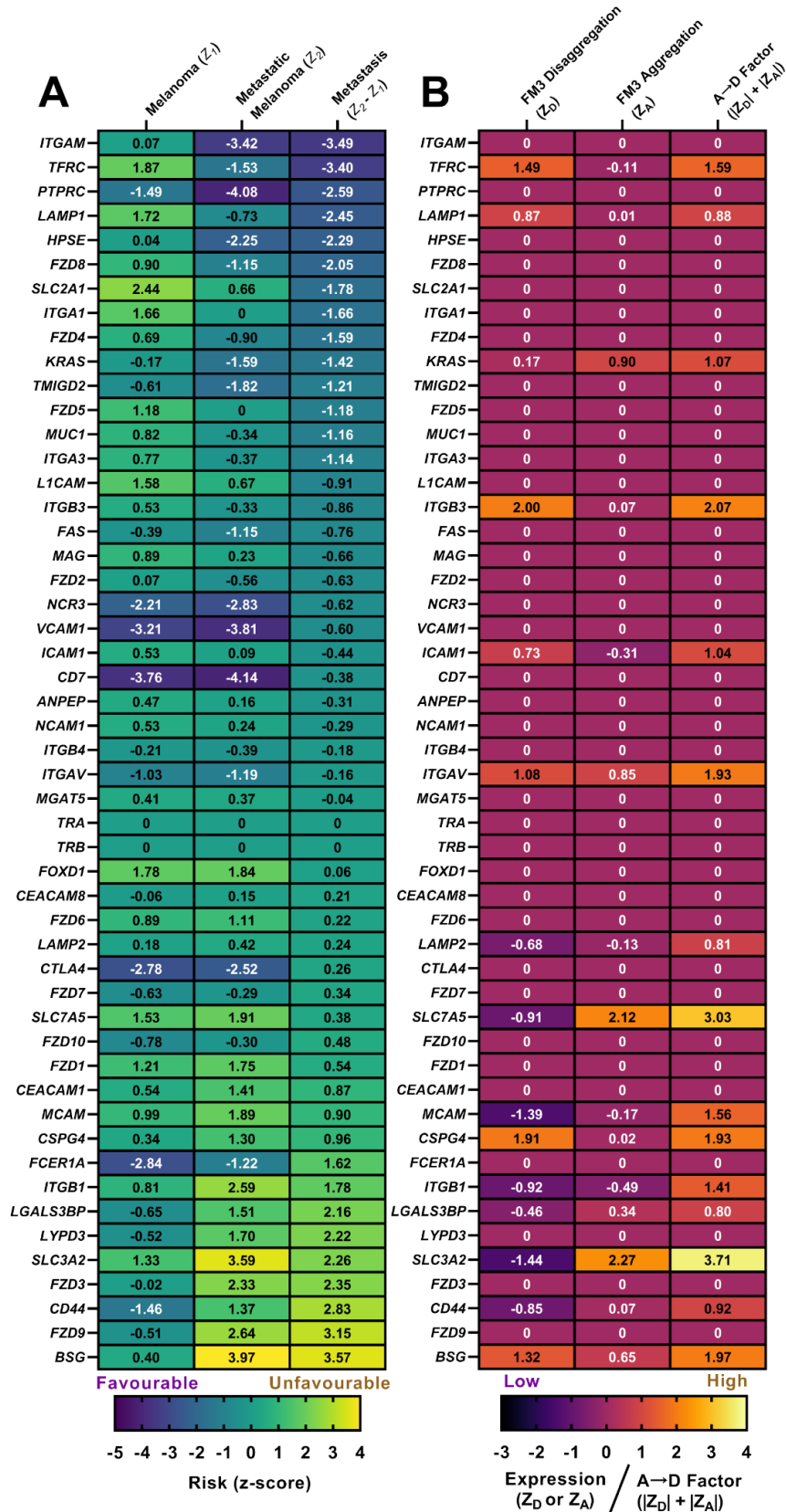


Fig. 4.4 4F2hc predicted to contribute to clinical melanoma CTC aggregation-disaggregation. **(A)** Clinical melanoma and metastatic melanoma Z-score (meta) obtained from PRECOG tool for galectin-3 binding cell-surface glycoproteins. Adjusted meta Z-score or 'metastasis score' (Z_2-Z_1) calculated from Z-score of melanoma (Z_1) and metastatic melanoma (Z_2). **(B)** Z-score was calculated using proteins expressed, as detected by mass spectrometry, during FM3 cellular aggregation (Z_A) and disaggregation (Z_D); from which Aggregation-disaggregation (A→D) contribution factor was calculated.

4.3 Discussion

4.3.1 Galectin-3 is involved in FM3 multicellular aggregation-disaggregation

In this chapter, the aim was to gain a deeper insight into FM3 multicellular aggregation-disaggregation by interrogating the interplay between galectin-3 and 4F2hc molecules.

Serum galectin-3 levels has been associated with melanoma growth and metastasis.¹⁹⁸ Galectin-3 also has been shown to promote multicellular aggregation of breast cancer cells, via cross-linking cell-surface MUC1 glycoproteins.⁵⁸ Therefore, it was hypothesised that galectin-3 levels could be elevated in FM3 multicellular aggregates, and that blocking galectin-3 could reduce aggregation. In line with these hypotheses, intracellular galectin-3 protein levels (Fig. 4.1 A), as well as *LGALS3* gene expression (Fig. 4.1 C), increased during FM3 multicellular aggregation. Transcriptomic analysis further highlighted that the *LGALS3* gene expression also decreased during disaggregation (Fig. 4.1 C). Blocking galectin-3 with anti-Gal3 antibody and inhibitory drug GB1107 decreased FM3 multicellular aggregation and increased disaggregation (Fig. 4.1 D & Supplementary Fig. 4.1). This reduction in galectin-3 levels during disaggregation agrees with previous findings that suggest galectin-3 expression decreases in metastatic lesions of malignant melanoma compared to primary tumours.¹⁹¹

Upon the plasma membrane of cells, galectin-3 could oligomerise, form lattices, and cross-link cell-surface glycoproteins, leading to the cell-activation and cell-cell contacts.¹⁹⁹ Two models galectin-3 conjectured to be at work here in promoting aggregation of FM3 cells. Model A: similar to breast and colon cancer aggregates,⁵⁸ galectin-3 could cross-link the otherwise interluding MUC1 surface glycoproteins and sequester them to the outer periphery of the aggregates, which ultimately allows cell-cell proteins to make cell-cell contacts.

Model B: galectin-3 could also cross-link cell-cell proteins, given that they possess GlcNAc sites, present on adjacent cells and promote aggregation. Lending support to Model B, galectin-3 has been shown in many studies, especially between immune cells,^{200,201} to cross-link multiple glycosylated membrane receptors, owing to the pentameric configuration of galectin-3 oligomers.²⁰² This configuration likely to form stable cell-cell contacts during intravascular transit of immune cells and CTC; unstable glycoprotein-glycoprotein bridges could result in cellular disaggregation. Exactly how much galectin-3 contributes to either model in during FM3 multicellular aggregation remains to be seen.

In contrast to intracellular galectin-3, extracellular matrix-associated galectin-3 levels decreased during aggregation and increased during disaggregation (Fig. 4.1 B). During multicellular aggregation, galectin-3 molecules theorised to be bound to cell cell-surface glycoproteins,

and thus would not be present within the ECM. During disaggregation, however, galectin-3 molecules would no longer be bound to cell-surface glycoproteins; free galectin-3 molecules can now interact with ECM glycoproteins. This would explain the increase in matrisomal galectin-3 observed during disaggregation (Fig. 4.1 B). Arguably, galectin-3 oligomers bound to the cell-surface are the ones that are pertinent for cellular aggregation, where galectin-3 found within the ECM could serve processes pertaining to cell-matrix adhesion during disaggregation. One such role galectin-3 could perform in the matrix is to stabilise matrisomal glycoprotein scaffolds and structures. Indeed, galectin-3 has been shown to directly bind to fibronectin, collagens IV, V and VI²⁰³ and regulate tumour cell motility by inducing fibronectin polymerisation.²⁰⁴

A drawback of the present contribution is that galectin-3 oligomers, free galectin-3 molecules, or exosomes containing galectin-3 that would be present secreted into the extracellular space were not investigated due to lack of time and resources. However, during the proteome extraction from the FM3 multicellular aggregates, the cell-culture serum was isolated and frozen at -80 °C, so that the dynamics of galectin-3 during ADPM of FM3 cells within the extracellular space investigated in the future. Nonetheless, the cell-lysate and matrix proteome studies, as well as *LGALS3* gene expression PCR, have provided a closer to full-picture of the role of galectin-3 in ADPM of FM3 cells.

4.3.2 4F2hc plays a major role in FM3 multicellular aggregation-disaggregation

Mass spectrometry revealed two notable glycoproteins, 4F2hc and LAT, the components of the CD98 heterodimer, were significantly upregulated during FM3 multicellular aggregation (FS-24h vs TCP-24h) (Fig. 4.2 A & B). Quantitative PCR showed that *SLC3A2* gene expression (encodes for 4F2hc protein) levels were significantly increased during aggregation and significantly reduced during disaggregation (Fig. 4.2 C). Since, 4F2hc possesses four GlcNAc sites,¹³⁴ whereas LAT1 zero GlcNAc sites, upon which galectin-3 likely to bind, 4F2hc was chosen for further detailed study of FM3 multicellular aggregation.

Treatment with the anti-4F2hc antibody (HPA017980; 50 ng/mL), which blocks two of these four glycosylation sites, resulted in a significant reduction in FM3 multicellular aggregation (Fig. 4.2 D), confirming the involvement of 4F2hc in aggregation. Perhaps, blocking all 4 glycosylation sites could completely prevent cellular aggregation. Similarly, another study has previously shown that CD98 molecules could promote homotypic aggregation of U937 promonocytic lymphoma cells, aided by CD43 and β 1 integrin.²⁰⁵

On the other hand, a study showed that treating Jurkat T cells with anti-CD147 or anti-CD98 monoclonal antibodies, as well as knock down of CD147 with RNA interference, all induced prominent homotypic aggregation.²⁰⁶ Thus, the authors concluded CD147 and CD98 could inhibit homotypic aggregation of Jurkat T cells. These results are not in line with the present contribution, as an increased expression of 4F2hc was observed in FM3 multicellular aggregate (Fig. 4.2 A) and inhibition of 4F2hc with anti-CD98 antibody decreased multicellular aggregation (Fig. 4.2 D). An explanation for this disparity between their study and the present contribution could be due to the promiscuous nature of 4F2hc. Various combinations of CD98 heterodimers exist, for example 4F2hc with LAT1 or 4F2hc with LAT2, at various levels in different cell lines, that could affect its trafficking to the plasma membrane.²⁰⁷ This would ultimately influence homotypic aggregation. For FM3 cells, the binding partner for 4F2hc likely to be LAT1, as LAT1 levels were increased during aggregation (Fig. 4.2 B) similar to 4F2hc; LAT2 or other binding partners of 4F2hc were not detected in the proteomics analyses.

Elevated levels of CD98 have been observed in almost all human melanoma cell lines²⁰⁸ as well as in many different cancers, including triple negative breast cancer,²⁰⁹ renal cancer²¹⁰ and lung adenocarcinomas.²¹¹ Overexpression of 4F2hc has been associated with development of neoplasms, progression, and increased metastatic potential.^{212,213} Moreover, CD98 levels has been shown to increase in proliferative normal tissues.²¹⁴ This explains why cell viability of FM3 cells upon both TCP and FS surfaces decreased with increasing concentration of anti-CD98 antibody (Fig. 4.2 E), but not with increasing concentration of anti-Galectin-3 antibody (Fig. 4.1 E). Moreover, overexpression of CD98, and interaction with β 1 Integrins, lead to malignant transformation.²¹⁵ Both 4F2hc and LAT1 levels were high in sites of metastases compared to primary tumours,²¹⁵ further alluding to the role of CD98 in metastasis.

The extracellular C-terminus domain of 4F2hc contains class II PDZ-binding domain.²¹⁶ As such, theoretically, 4F2hc could bind to any PDZ domain-containing proteins. This is important for cell-cell contacts, as many tight junctional proteins, such as the ZO-1, contain many PDZ domains.²¹⁷ This is also important for transferring syndecan/integrin-mediated signalling to the cytoskeleton, via the syntenin proteins, which also have several PDZ domains.²¹⁸ In chapter 3, proteomic studies highlighted the involvement of cytoskeletal regulation during ADPM of FM3 cells (Fig. 3.2 B & C). Together, these discoveries hint towards the major role 4F2hc could play in orchestrating cytoskeletal remodelling to cell-cell interactions and homotypic aggregation.

4.3.3 Galectin-3 and 4F2hc colocalises at FM3 cell-cell interface

CD98 molecules have been shown to interact with galectin-3.²¹⁹ Specifically, 4F2hc was shown to bind directly to galectin-3 via co-immunoprecipitation.²²⁰ In FM3 multicellular aggregates, 4F2hc and galectin-3 colocalised at the cell-cell interface (Supplementary Fig. 4.2). However, galectin-3 was mostly localised to the outer periphery of the aggregates. 4F2hc molecules were only localised to cell-cell interface, restricted to the core of the FM3 aggregates. These results suggest that galectin-3 could cross-link 4F2hc glycoproteins at cell-cell interface to promote multicellular aggregation. Since most galectin-3 proteins were localised to the outer periphery of the aggregates (Supplementary Fig. 4.2), perhaps an additional role of Galectin-3 could be to sequester Mucin-like proteins, for example MUC1, in melanoma cells much like colon and breast cancer cells.²²¹ Further experiments are needed to confirm this.

Since the dual-staining immunofluorescence was a preliminary experiment (n=1 was only possible at the time, due to lack of time and resources), having more repeats, and quantifying and statistical testing of the immunofluorescence of galectin-3 and 4F2hc signals at core vs periphery would provide further insights. An improvement of the dual-staining experiment could be to embed the aggregates in paraffin, section them into thin slices using a microtome, and carry out the dual-staining on the cross-section of the aggregates; this approach would highlight, if any, variation in galectin-3/4F2hc co-localisation signals from core to the periphery.

4.3.4 4F2hc:oGal3:4F2hc bridges

As opposed to the MMP2-cleaved truncated monomeric galectin-3 (tGal3), oligomeric galectin-3 (oGal3) could theoretically cross-link 4F2hc-ED and bridge coterminous CD98 molecules on adjacent cells. Three-dimensional orthorhombic structures of galectin-3-CRD (PDB ID: 1A3K) and 4F2hc-ED (PDB ID: 2DHC), that had been solved previously using X-Ray Crystallography, were used in the present study to carry out *in silico* protein docking analyses. As galectin-3-CRD recognises glycans, it was hypothesised that, if it were to interact with 4F2hc-ED, it would be proximal to any of the four *N*-glycosylable sites (Fig. 4.3 A). Top ten docking models, generated by ClusPro computation, predicted that galectin-3-CRD protomer likely to bind proximal to *N*-glycosylable sites upon the 4F2hc-ED, with 7 of the top ten (represented by model 2 on Fig. 4.3 A) favouring the asparagine pair N264 and N323. Evidence for whether these asparagine residues become *N*-glycosylated with GlcNAc comes from study that solved the structure of the full CD98 heterodimer (PDB ID: 6IRS). This study demonstrated

the presence of GlcNAc disaccharides present on all four of the *N*-glycosylable sites of the 4F2hc-ED.²²²

It is conceivable that if the CRD of galectin-3 presented to 4F2hc-ED is from oGal3 molecules instead of tGal3 molecules, this would lead to invariably cross-linking of 4F2hc-ED (Fig. 4.3 C; second panel). These cross-linking events are more likely to occur where oGal3 molecules are abundant, for example at and above physiological concentrations of Galectin-3, as oligomerisation increases with increasing concentration of Galectin-3.²²³ As concentration of serum galectin-3 was shown to increase above physiological levels in metastatic melanoma (median = 6.9 ng/mL in healthy control, median = 12 ng/mL in metastatic melanoma),²²⁴ the likelihood of oGal3-mediated cross-linking of 4F2hc increases in the blood circulation of patients suffering from metastatic melanoma.

Though the protein-protein docking analyses have provided much insight into galectin-3-CRD/4F2hc-ED interactions, arguably the interaction between the glycan-containing/glycan-recognition moieties of these two proteins, which the docking *in silico* analyses did not consider, likely would provide even a greater understanding. Protein-protein docking results may describe enfeebled and transient interactions. However, the strength of lectins lies in their ability to bind to carbohydrates. The conserved CRD of galectins comprise of several pockets in which glycans can fit snugly. Galectin-3-CRD has been described as having four distinct subsites S^{A-D}²²⁵ within its S-Face that can accommodate a tetrasaccharide (Fig. 4.3 E – G); with an additional site S^E that may bind to the protein part of a glycoprotein, an additional saccharide, or lipids.²²⁶ S^C pockets bind to putative β -Galactosides, which give these lectins its name; S^B pockets can accommodate GlcNAc, N-Acetylgalactosamine (GalNAc) and N-Acetylneuraminic acid (Neu5Ac); and subsites S^D and S^A can accommodate a variety of different saccharides, which allows for further variation in binding affinity of galectins.²²⁶ This hints towards how galectin-3 could not only bridge 4F2hc, but also other glycoproteins to induce homotypic multicellular aggregation of other cancers.

N-glycans often come as forked or branched structures (Fig. 4.3 H & I). The tail-end of these structures, usually 3 – 4 glycans long, are what may be presented to lectins. It is therefore likely that galectin-3 could recognise the tail-ends of both complex and hybrid glycan chains (Fig. 4.3 G), but not chains containing high levels of mannose due to the lack of β -Galactosides. Moreover, galectin-3 has the highest affinity towards triantennary- β 1,4 *N*-glycans ($K_d = 2.9 \mu\text{M}$), followed by tetraantennary *N*-glycans ($K_d = 3.8 \mu\text{M}$), and lower affinity towards biantennary *N*-glycans ($K_d = 6.3 \mu\text{M}$) and triantennary- β 1,4 *N*-glycans ($K_d = 7 \mu\text{M}$).²²⁷ 4F2hc molecules present on MCF7 breast cancer cells were shown to be predominantly *N*-glycosylated with tetraantennary, and small amounts of bi- and triantennary glycans.²²⁸

Therefore, it is conceivable how these complex or hybrid tetrasaccharide tail-end chains, composing tetraantennary structures, originating from an *N*-glycosylated asparagine residue of 4F2hc-ED, could bind feasibly within the four subsites (S^{A-D}) of galectin-3-CRD, and that the affinity for this interaction likely to be high.

4.3.5 4F2hc:4F2hc homophilic binding

4F2hc-ED self-docking analyses revealed that 4F2hc could interact with each other in two different orientations. As 4F2hc molecules tether to the plasma membrane via their N-terminus domain, the orientation in which the N-termini of two interacting 4F2hc-ED are adjacent to each other (Fig 4.3 D; second panel, Model 2), likely predicts the interaction of 4F2hc self-association that may occur within the same cell. It is important to note here that this self-association may not be feasible, as 4F2hc almost always trafficked to the plasma membrane bound to its heterodimeric light-chain partner (usually LAT1).²²⁹ These light chains likely would hinder the types of interactions as depicted by Model 2 (Fig. 4.3 B & D second panel). Whereas the orientation in which the N-termini are opposite of each other (Fig. 4.3 B & D; Model 1, first panel), likely predicts the interaction of 4F2hc molecules from two different cells. This interaction would not be hindered by light chain of the CD98 molecules.

PPI scores were calculated from LightPlot+ computation. Out of the two Gal3/4F2hc and two 4F2hc/4F2hc models, model 2 of 4F2hc/4F2hc interaction yielded the highest PPI score, contrasted to the model 1 of 4F2hc/4F2hc (Supplementary Fig. 4.6). This indicate that the likelihood of homophilic binding of 4F2hc/4F2hc molecules within the same plane, as in within the plasma membrane of the same cell, is arguably higher compared to the likelihood of homophilic binding of 4F2hc/4F2hc from adjacent cells. Whereas PPI scores of the two models of Gal3/4F2hc were comparable (Supplementary Fig. 4.6), indicating equivalence in likelihood. As such, PPI scores analyses indicate that the model 1 of 4F2hc/4F2hc, the model that predicts the orientation in which 4F2hc/4F2hc self-association would lead to the homotypic aggregation of FM3 cell, seems to be less likely compared to model 2 of 4F2hc/4F2hc.

Perhaps, model 2 of 4F2hc/4F2hc interactions that may occur within the same cell could aid in the formation of CD98 multicomponent cell-surface hubs. This is evident from 4F2hc molecules binding to other glycoproteins, such as CD147²³⁰ and β -integrins.²³¹ Conceivably, the more 4F2hc molecules a cell expresses on its surface, the more likely these 4F2hc self-associations may occur; a potential advantage of these types of homophilic binding is to perhaps cluster these proteins together to enhance downstream signalling. This conjecture is supported by how integrins are enriched to focal adhesions to enhance integrin-mediated

signalling.²³² 4F2hc/integrin interactions could also be amenable to similar enrichment and modulation mechanisms. 4F2hc homodimerisation has been predicted computationally, as well as shown experimentally in HeLa.²³³

4.3.6 4F2hc:oGal3:4F2hc bridges vs 4F2hc:4F2hc homophilic binding in melanoma FM3 aggregates

A recent study by Xia Liu et al. (2019) showed that CD44-CD44 homophilic interactions may lead to breast cancer multicellular aggregation.⁴⁴ It is entirely possible that, similar to 4F2hc molecules, CD44 molecules could also be bridged by oGal3 in order to promote breast cancer multicellular aggregation. Notable evidence for this is that CD44 molecules have been shown to bind to galectin-3,²³⁴ and CD44's lectin-like hyaluronate binding domain (HABD) contains five possible *N*-glycosylation sites,²³⁵ in its extracellular domain. Previous study truncated domain I of CD44, from N21-97, which resulted in reduced multicellular aggregation.²³⁶ The authors suggested that since domain I is located within the extracellular space, homophilic aggregation of breast cancer cells are governed by the interaction of two adjacent domain I of coterminous CD44 proteins on neighbouring cells. However, it is important to note here that domain 1 region between N21-97 contains 2 *N*-glycosylation sites (N25 and N57) (analysis carried out on neXtProt).²³⁷ Thus, the reduction in breast cancer aggregation could well be caused by the ablation of CD44:oGal-3:CD44 bridges.

The aforementioned study investigated CD44:CD44 homophilic binding by immobilising the extracellular domain of CD44 (CD44-ED) to a solid phase *in vitro* and tested for self-association by monitoring binding of secondary biotin-labelled CD44. Compared to BSA control, CD44 was shown to bind to other CD44 molecules more;⁴⁴ the authors concluded that this would allude to CD44-CD44 interaction that results in cellular aggregation. The only conclusion that can be drawn here is that relative to the CD44-BSA interaction, CD44 molecules have higher affinity for other CD44 molecules. It is inapposite to use these results to substantiate coterminous CD44-CD44 binding, as the results could also be explained by CD44-CD44 homodimerisation, which has been shown elsewhere;²³⁸ that is side-to-side within the same plasma membrane as opposed to end-to-end interaction from two different plasma membranes.

Furthermore, the study, via overexpression of CD44-FLAG and CD44-HA (full length) in two distinct subpopulations of HEK-293 cells, followed by co-immunoprecipitation pulldown of lysates, highlighted CD44-FLAG:CD44-HA interactions. This data, on the other hand, is

sufficient to show neighbouring cell CD44-ED:CD44-ED interaction and rule out CD44-CD44 binding by via homodimerisation within the same cell. Here still, it is imprudent to rule out CD44:oGal3:CD44 bridge as being the reason for cellular aggregation, given that there is evidence for CD44-galectin-3 directing binding.²³⁴ Indeed, galectin-3 has been associated with reduced tumorigenicity of breast cancer cells,²³⁹ and galectin-3 has been shown to enhance metastatic potential of breast cancer.²⁴⁰

A subsequent study from the same laboratory group showed that the extracellular domains, domain I and domain II, of both standard form CD44 (CD44s) and full-length CD44 (CD44fl), participate in breast cancer cellular aggregation.²³⁶ It is noteworthy that CD44s domain I mutant, which possessed, amongst many other, the mutation of the asparagine residue N94 into an alanine residue; this resulted in reduced cellular aggregation. The authors suggested that, due to the mutation of many residues and subsequent conformational change of domain I, the CD44 molecules are no longer able to associate with each other, and thus results in reduction in cellular aggregation. An important experiment here, to confirm involvement of galectin-3 in CD44-mediated breast cancer multicellular aggregation, would be to point-mutate just the N94 residue, and see if that would also result in reduced cellular aggregation.

For melanoma FM3 cells, it remains uncertain whether it is via 4F2hc-4F2hc or 4F2hc:oGal3:4F2hc melanoma cells aggregate. A future experiment that could uncover whether it is via CD44-CD44 or CD44:oGal3:CD44 breast cancer cells aggregate, and whether it is via 4F2hc-4F2hc or 4F2hc:oGal3:4F2hc melanoma cells aggregate, is to pulldown CD44 or 4F2hc molecule and their associated proteins using co-immunoprecipitation and carry out western blot analysis of the pulldown lysate, to show, if any, presence of Galectin-3. Furthermore, point mutagenesis of asparagine residues important for N-glycosylation, for example the N25 and N57 of CD44 molecules, or N365, N381, N424, and N506 asparagine residues of 4F2hc molecules, to show, possible, reduction in cancer cellular aggregation. This would conclusively confirm, one way or the other, interaction of CD44:CD44 or 4F2hc:4F2hc homophilic interaction, or whether its CD44:oGal3:CD44 or 4F2hc:oGal3:4F2hc bridges, that mediate cancer cellular aggregation.

A cost-effective experiment that could be carried out to investigate glycoprotein:galectin-3:glycoprotein (GGG) bridges vs glycoprotein:glycoprotein (GG) homophilic binding is through *in silico* computational analyses. For example, by using Molecular Dynamics (MD) simulation and the Amber99SB-ILDN forcefield²⁴¹ to study dynamics of galectin-3-CRD with random tetrasaccharide, galectin-3-CRD with 4F2hc-ED or domain I and II of CD44, and the oGal3 bridges (4F2hc:oGal3:4F2hc or CD44:oGal3:CD44). Then calculating the end-point binding free energy via Molecular Mechanics-Poisson Boltzmann Surface Area (MMPBSA-TΔS), which

combines continuum models with molecular interaction dynamics, similar to this study,²⁴² could ultimately reveal which of these aforementioned interactions would be more energetically favourable and thus would have more propensity to occur in the peripheral blood or lymphatic circulation.

4.3.7 Glycoprotein:Galectin-3:Glycoprotein (GGG) Bridges in clinical melanoma

Galectin-3 cross-linked MUC1 proteins in the periphery of colon cancer aggregates in order to promote E-cadherin-dependent multicellular aggregation.²²¹ In FM3 melanoma cells, MUC1 proteins were not detected in the mass spectrometry investigation. MUC18 is the only mucin protein that was detected; though, there was no significant difference in MUC18 levels between aggregates and non-aggregates (Supplementary Fig. 4.3), denoting to its lack of contribution to ADPM. It is equally likely that galectin-3 could be cross-linking and bridging a glycoprotein other than, or in addition to, 4F2hc, either at cell-cell interface or at the periphery or at mix of both interfaces, to promote homotypic aggregation of melanoma CTC clusters.

Moreover, CD44 and 4F2hc are both expressed simultaneously, albeit in varying degrees, in both melanoma and breast cancer; CD44 surface expression was shown on malignant melanoma²⁴³ and CD98 activation has been associated with clustering of $\beta 1$ Integrins in breast cancer cells.²⁴⁴ Therefore, it is within the realm of possibilities, that even in multicellular aggregates originating from a single clonal subpopulation of cells, there could be different compositions of GGG bridges using different glycoproteins as the cellular anchors. To identify composition of GGG bridges of cancer cellular aggregates, seeking a fractionation/co-immunoprecipitation method during protein harvest to isolate cell-membrane bound galectin-3/glycoprotein is preferred to crude cell-lysis, as the fractionation/co-immunoprecipitation method would isolate only membrane-bound galectin-3/glycoprotein conjugates, as well as disregarding monomers of galectin-3 and glycoproteins.

Since, the aforementioned protein-harvest approach was not carried out in the present study, to gain insights into the compositions of glycoproteins that could potentially partake in forming GGG bridges in melanoma CTC clusters, *in silico* analyses were carried out using 'meta Z-score' from melanoma and metastatic melanoma datasets obtained from PRECOG tool. The following genes coding for cell-surface glycoproteins were identified as markers of most favourable outcome: *ITGAM*, *TFRC*, *PTPRC*, *LAMP1*, *HPSE*, and *FZD8* (Fig. 4.4). The expression and risk associated with these glycoproteins reduce during metastasis; as such, it is unlikely that these glycoproteins partake in GGG bridges of melanoma CTC clusters.

Conversely, the following genes coding for glycoproteins were identified as harbingers of unfavourable outcome: *BSG*, *FZD9*, *CD44*, *FZD3*, *SLC3A2*, *LYPD3*, *LGALS3BP* (Fig. 4.4). As per nextprot sequence analyses (nextprot.org), in their extracellular domain, CD147 (also known as Basigin; coded by *BSG*) contains 3 *N*-linked GlcNAc sites, Frizzled-9 (coded by *FZD9*) contains 2 *N*-linked GlcNAc sites, CD44 (coded by *CD44*) contains 9 *N*-linked GlcNAc sites, Frizzled-3 (coded by *FZD3*) contains 1 *N*-linked GlcNAc site, C4.4A (also known as Ly6/PLAUR domain-containing protein 6; coded by *LYPD6*) contains 2 *N*-linked GlcNAc sites, Gp90 (previously known as Galectin-3 Binding Protein; coded by *LGALS3BP*) contains 6 viable *N*-linked GlcNAc sites and 1 high-mannose *N*-linked site; upon these glycosylation sites oGal3 could theoretically bind, cross-link coterminous glycoproteins, and form cell-cell GGG bridges. CD147 and 4F2hc are the only two cell-surface glycoproteins that seem to be involved in ADPM of both FM3 cells *in vitro* and clinical melanoma.

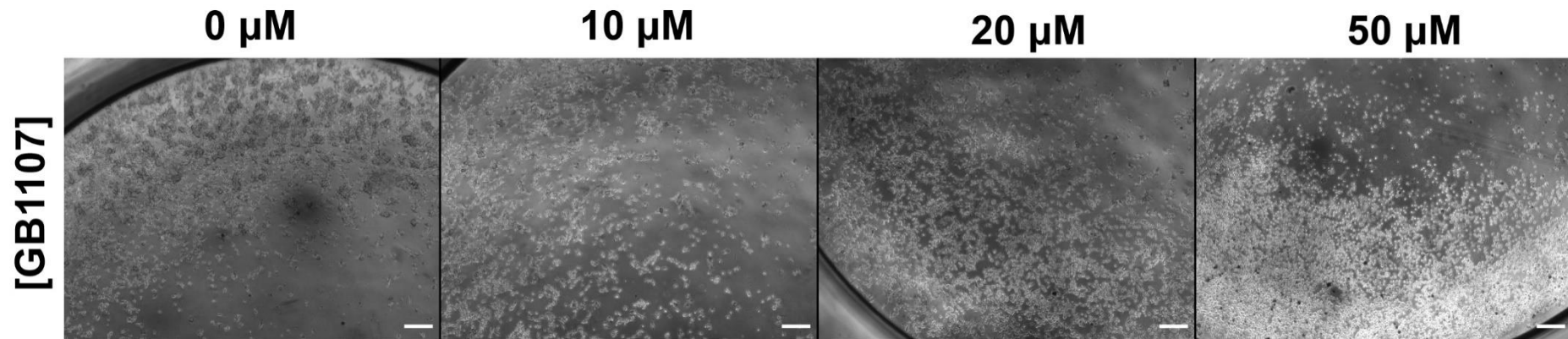
The focal galectin of the present study was galectin-3. Yet, many other galectins are also prone to multivalent and promiscuous binding owing largely to their well-conserved CRD. Notably, similar to galectin-3, dimeric galectins such as galectin-1, 2, 5, 7, 10, 11, 13 - 20, have been shown to cross-link glycoproteins including cell surface receptors and extracellular matrix proteins.²⁴⁵ As such, these aforementioned galectins could also be involved in GGG bridges and cell-cell interactions. Comparison of 'Metastatic Factor' score revealed that galectin-1 (*LGALS1*) and galectin-3 (*LGALS3*) as adverse risk factors for metastasis of melanoma, and galectin-8 (*LGALS8*) as favourable (Supplementary Fig. 4.7). A study showed that galectin-1 was expressed abundantly in dysplastic nevi, primary and metastatic melanomas, and that MCAM glycoproteins were the predominant ligand for Galectin-1.²⁴⁶

Another study also showed that galectin-1 levels were high in patients with metastatic melanoma compared to primary human melanoma.²⁴⁷ Interestingly, galectin-1 binding to Gp90 was shown to induce multicellular aggregation of breast cancer cells;²⁴⁸ though these cells expressed galectin-3 *mRNA*, they showed no surface localisation Galectin-3.²⁴⁹ The authors also suggested that the homotypic aggregation arise from the formation of galectin-1:galectin-3BP:galectin-1 bridges, where galectin-1 would be bound to another surface glycoproteins. In cases where oGal3 is absent in the extracellular space, cells could form galectin-1/Gp90-mediated bridges. Present study also suggested that perhaps Gp90 could serve a role in metastasis of clinical melanoma, but not in the *in vitro* FM3 cells. It could be that cancer cells may form galectin-3 or Galectin-1-based bridges or both; this requires further investigation.

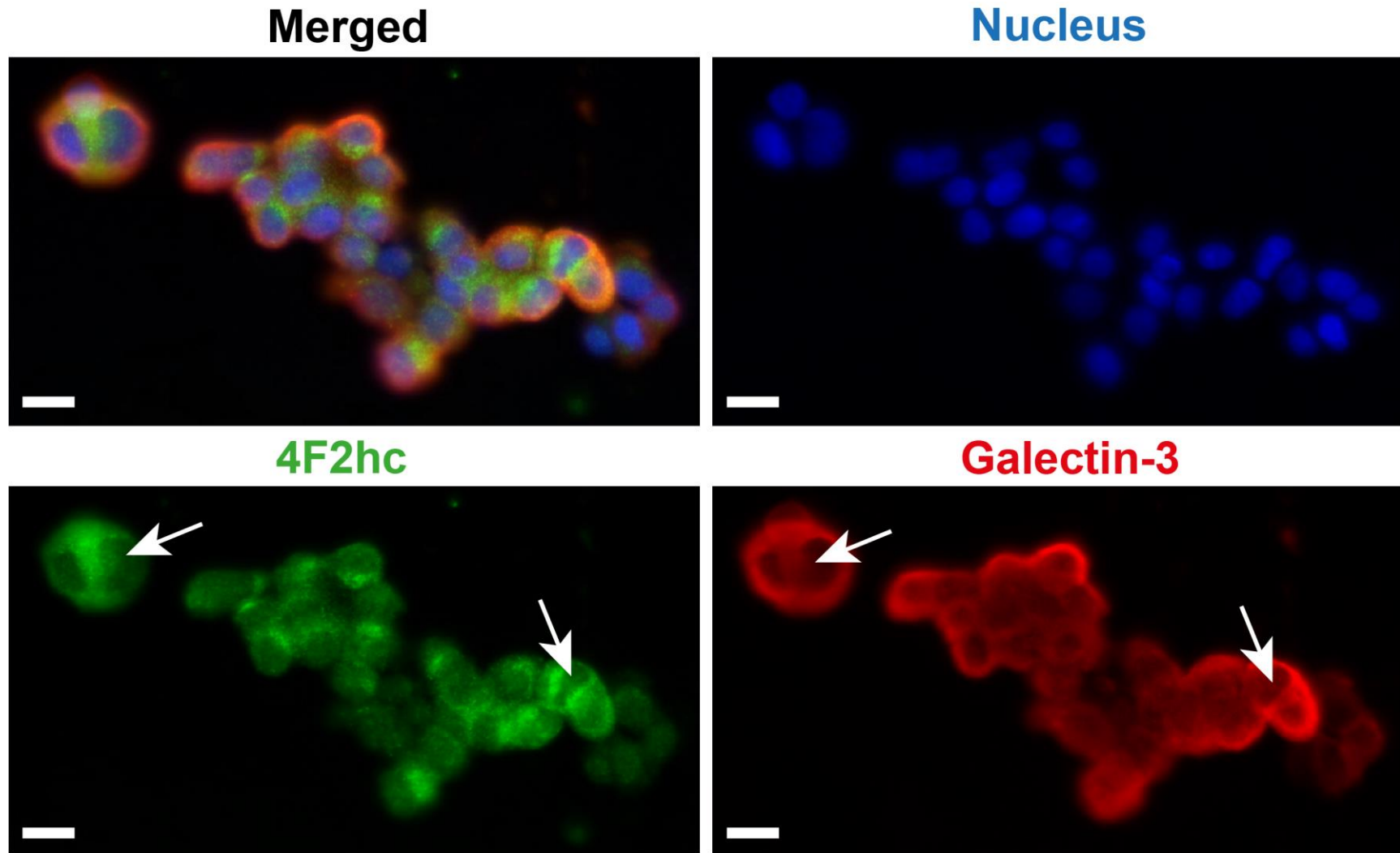
4.3.8 Conclusions

The present study uncovered that both 4F2hc and galectin-3 proteins are important for multicellular aggregation of FM3 cells. Galectin-3 could bridge coterminous cell-surface 4F2hc proteins on adjacent cells to induce homotypic aggregation of FM3 cells. Likewise, homotypic aggregation of melanoma CTC clusters likely occurs through formation of GGG bridge, for example 4F2hc:galectin-3:4F2hc, as opposed to homophilic binding of glycoproteins. Research into CTC clusters need to consider the potentiality of GGG bridges being responsible for cell-cell contacts; especially if CTC clusters express glycoprotein containing *N*-glycosylation sites, and if the patients present high levels of sera galectin-3 where oligomeric galectin-3 would be abundant enough to form GGG bridges and promote CTC clusters. Bioinformatics analyses revealed that, in addition to 4F2hc, other glycoproteins such as CD147, Frizzled-3 & 9, C4.4A, Gp90, CD44, all could theoretically form GGG bridges, and as such could regulate melanoma CTC cluster aggregation. It remains to be investigated which of these glycoproteins are the most notorious ones involved in building GGG bridges and driving ADPM of melanoma CTC clusters and CTC clusters of other cancers. Galectin-1 could also theoretically form GGG bridges much like galectin-3, however, extent to which Galectin-1 drives ADPM remains to be uncovered. In conclusion, the present contribution described for the first time the involvement of 4F2hc/Galectin-3-based GGG bridges in driving ADPM of melanoma.

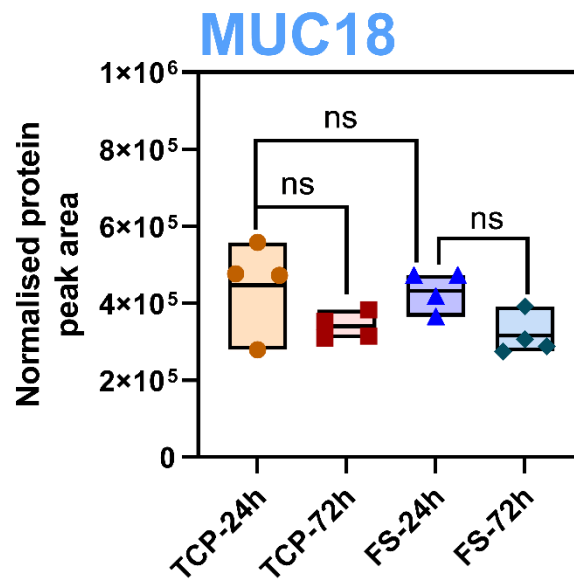
4.4 Supplementary Figures



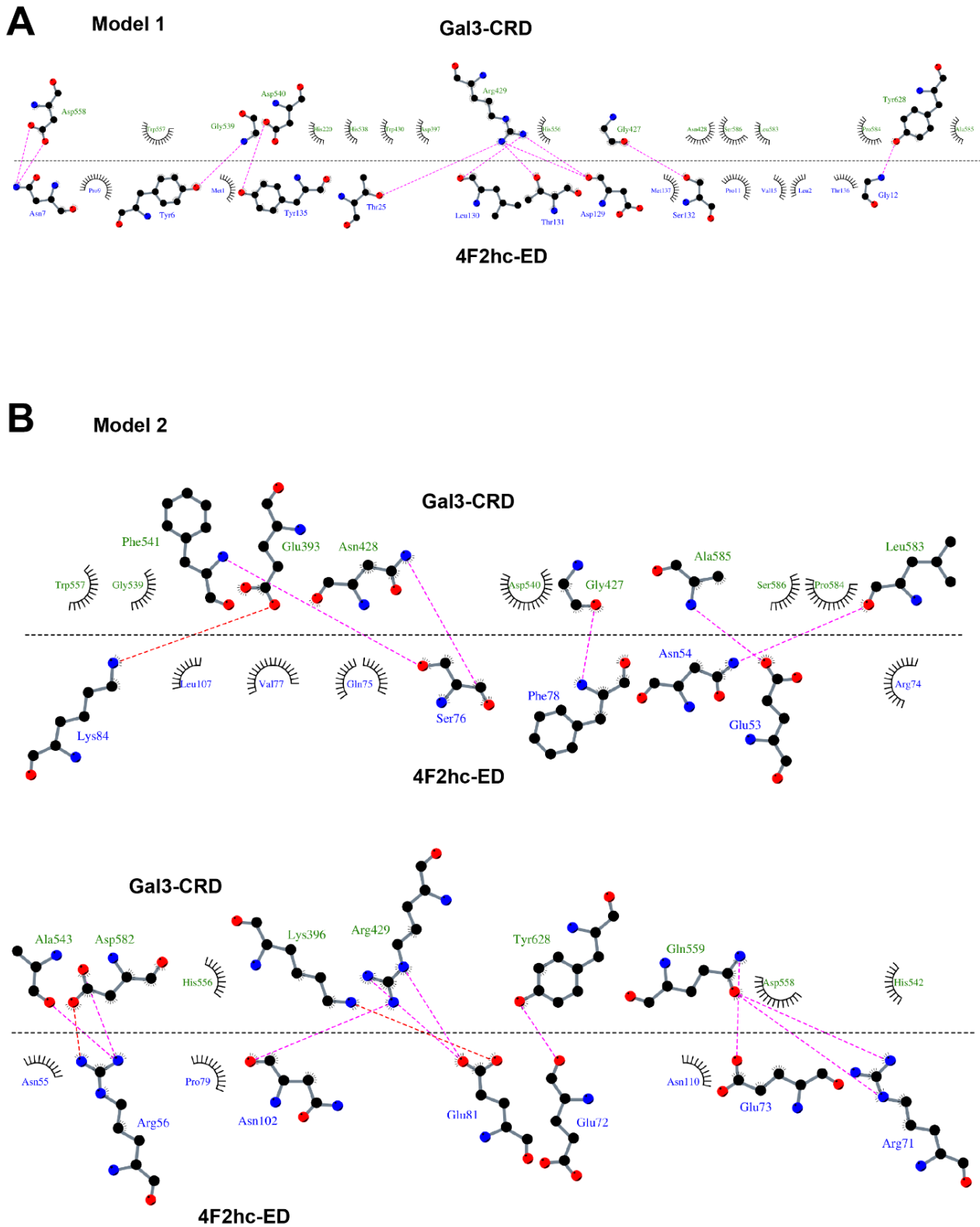
Supplementary Fig. 4.1 Treatment of FM3 cellular aggregates with galectin-3 inhibitor (GB1107) inhibitor decreases aggregation. Micrographs showing changes in multicellular aggregation of FM3 upon FS surface after 24 hours of treatment with increasing concentration of galectin-3 inhibitor (GB1107), (n=5). Scale = 200 μm. FS: fluoroalkylsilica.



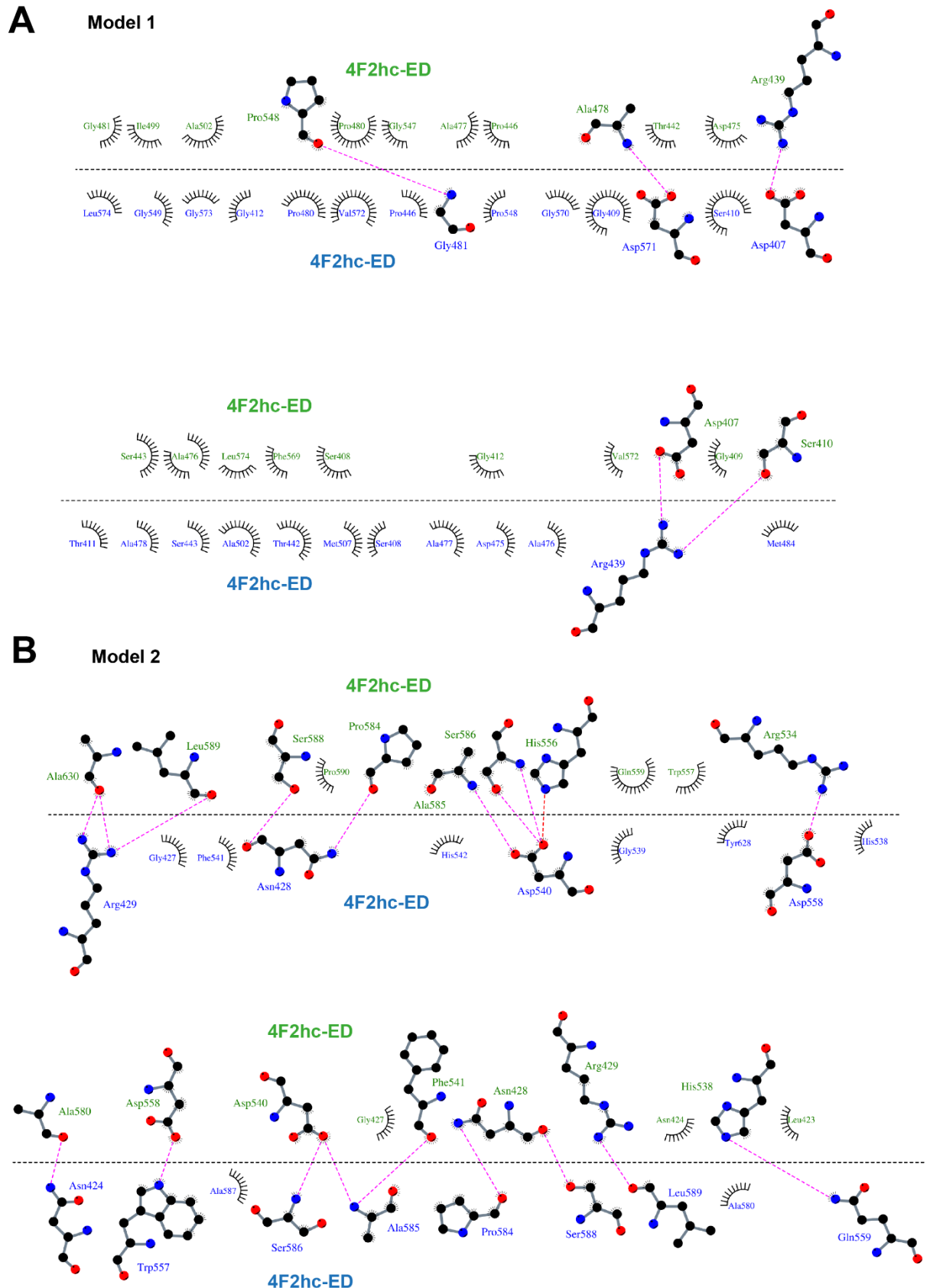
Supplementary Fig. 4.2 Galectin-3 colocalises with 4F2hc at cell-cell contact in FM3 multicellular aggregates. Immunofluorescence micrographs of FM3 multicellular aggregates on FS surfaces, shows 4F2hc localisation (Green Alexa-Fluor 488 nm dye; bottom left panel), galectin-3 localisation (Red Alexa-Fluor 594 nm dye; bottom right panel), and colocalisation of both 4F2hc and galectin-3 at the cell-cell interface as denoted by white arrows. Nucleus was stained with DAPI (top right). Top left image shows merged fluorescence micrograph. n=1 (preliminary experiment). Scale = 50 μ m.



Supplementary Fig. 4.3 Change in MUC18 levels during FM3 multicellular aggregation-disaggregation. MUC18 levels during FM3 cellular aggregation (FS-24h vs TCP-24h) and disaggregation (FS-72h vs FS-24h) as measured by mass spectrometry, n=4. Brown-Forsythe and Welch ANOVA tests (equal SDs not assumed) with Dunnett T3 post-hoc multiple comparison test was carried out for mass-spectrometry comparisons. FS: fluoroalkylsilica, TCP: tissue culture polystyrene.



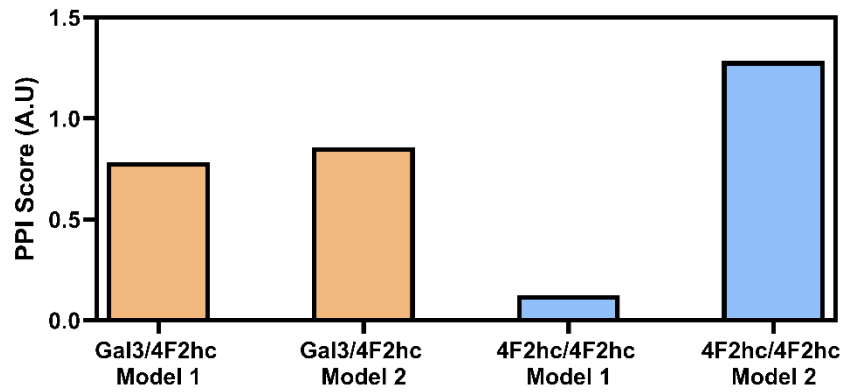
Supplementary Fig. 4.4 Possible molecular interactions of galectin-3-CRD and 4F2hc-ED interface. Interfaces of galectin-3-CRD:4F2hc-ED predicted by ClusPro docking (Fig 3.6 A) were further analysed using LigPlot+, with **(A)** showing model 1 and **(B)** showing model 2. Black dotted line depicts the interface and Magenta dotted line depicts hydrogen bonds. Spoked arcs around the amino acid residues, and ‘eye-lashes’ around individual atoms, both depict non-bonded hydrophobic contacts. CRD: Carbohydrate recognition domain, ED: ectodomain. LigPlot+ Plots were generated by Thomas Warwick.



Supplementary Fig. 4.5 Possible molecular interactions of 4F2hc-ED:4F2hc-ED homophilic interface. Interfaces of 4F2hc-ED:4F2hc-ED predicted by ClusPro docking (Fig 3.6 B) were further analysed using LigPlot+, with (A) showing model 1 and (B) showing model 2. Black dotted line depicts the interface and Magenta dotted line depicts hydrogen bonds. Spoked arcs around the amino acid residues, and ‘eye-lashes’ around individual atoms, both depict non-bonded hydrophobic contacts. CRD: Carbohydrate recognition domain, ED: ectodomain. LigPlot+ Plots were generated by Thomas Warwick.

Supplementary Table. 4.1: Galectin-3-Binding Cell-Surface Glycoproteins

<i>Protein (CD#)</i>	<i>Gene</i>	<i>Ref</i>	<i>Protein (CD#)</i>	<i>Gene</i>	<i>Ref</i>
4F2 (CD98)	SLC3A2 + SLC7A5	263	CSPG8 (CD44)	CD44	250
Galectin-3BP	LGALS3BP	264	T200 (CD45)	PTPRC	251
GP40 (CD7)	CD7	265	Transferrin Receptor (CD71)	TFRC	251
Integrin $\alpha 1\beta 1$	ITGA1 + ITGB1	266	FOXD1	FOXD1	252
Integrin $\beta 1$ (CD29)	ITGB1	252	GLUT1	SLC2A1	253
Integrin $\alpha V\beta 3$	ITGAV + ITGB3	267	Mgat5	MGAT5	254
Integrin $\beta 4$ (CD104)	ITGB4	268	Fc ϵ RI	FCER1A	255
Integrin $\alpha 3\beta 1$	ITGA3 + ITGB1	269	Fas (CD95)	FAS	256
Integrin αM (CD11B)	ITGAM	263	NCAM (CD56)	NCAM1	257
K-ras	KRAS	270	SIGLEC-4A	MAG	257
ICAM1 (CD54)	ICAM1	271	CAML1 (CD171)	L1CAM	257
MUC1 (CD227)	MUC1	272,273	C4.4A	LYPD3	258
MUC18 (CD146)	MCAM	274	Basigin (CD147)	BSG	259
Heparanase	HPSE	275	CTLA-4 (CD152)	CTLA4	260
NG2	CSPG4	269	VCAM-1 (CD106)	VCAM1	261
CEACAM1 (CD66a)	CEACAM1	276	Frizzled	FZD1	262
CEACAM2 (CD66b)	CEACAM8	276			
IGPR-1 (CD28H)	TMIGD2	277			
Aminopeptidase N (CD13)	ANPEP	278			
T-Cell Receptor	TRA + TRB	279			
Lamp-1 (CD107a)	LAMP1	263			
Lamp-2 (CD107b)	LAMP2	263			
Nkp30 (CD337)	NCR3	280			



Supplementary Fig. 4.6 PPI score of galectin-3/4F2hc or 4F2hc/4F2hc interactions. PPI Score calculated for the two Gal3/4F2hc models and two 4F2hc/4F2hc models, based on H-bonds, hydrophobic interactions and aryl/aryl interactions as determined from LigPlot+. PPI: Protein-protein interaction.



Supplementary Fig. 4.7 Galectin-3 predicted to contribute to clinical melanoma CTC aggregation-disaggregation. Clinical melanoma and metastatic melanoma Z-score (meta) obtained from PRECOG tool for the Galectins found in melanoma cells. Adjusted meta Z-score or 'metastasis score' ($Z_2 - Z_1$) calculated from Z-score of melanoma (Z_1) and metastatic melanoma (Z_2).

Chapter 5. Role of MMP2 in melanoma multicellular aggregation and disaggregation

Contents

CHAPTER 5. ROLE OF MMP2 IN MELANOMA MULTICELLULAR AGGREGATION AND DISAGGREGATION.....	78
5.1 INTRODUCTION	79
5.2 RESULTS.....	80
5.2.1 MMP2 expression during FM3 multicellular aggregation-disaggregation.....	80
5.2.2 4F2hc, β -catenin, and TIMP3 expression during MMP2-inhibition in FM3 cells	82
5.2.3 Galectin-3, 4F2hc, and MMP2 on melanoma survival outcome	83
5.3 DISCUSSION	86
5.3.1 FM3 cells reduce MMP2 expression to prevent untimely cellular disaggregation	86
5.3.2 MMP2-mediated control of β -Catenin and 4F2hc levels in FM3 cells	87
5.3.3 Concerted roles of Galectin-3, 4F2hc and MMP2 in melanoma ADPM.....	88
5.3.4 Conclusions	91
5.4 SUPPLEMENTARY FIGURES	92

5.1 Introduction

This chapter discusses the involvement of matrix metalloproteinase 2 (MMP2) in multicellular aggregation of FM3 melanoma cells, and outlines the concerted interplay of MMP2, galectin-3 and 4F2hc during melanoma metastasis of CTC clusters.

Stable silencing of 4F2hc impaired tumorigenicity of HeLa cells, perturbed integrin and hypoxia-dependent signalling, and reduced expression of MMP2.²²⁰ The integrin signalling cascade, FAK→PI3K→Akt→β-catenin, was shown to lie downstream of β1-integrins/4F2hc/CD147 cell-surface complexes. Silencing 4F2hc in HeLa cells reduced the activation of this pathway and prevented β-catenin translocation into the nucleus to regulate gene transcription binding to TCF/LEF family of transcription factors. As a notable target gene of these transcription factor are MMPs,²⁸¹ including MMP2, silencing 4F2hc in HeLa cells resulted in decrease in MMP2 levels.²²⁰

Additionally, the authors showed down-regulation of 4F2hc not only reduced MMP2 expression and activity, but also resulted in an exaggerated increase in extracellular, but not intracellular, galectin-3 levels.²²⁰ It was suggested that silencing 4F2hc leads to the inhibition of many galectin-3-mediated signalling events; likely due to reduced cleavage of galectin-3 by MMP2.²⁸² MMP2-cleaved galectin-3 has been thought to bind and stabilise 4F2hc multicomponent complexes, for example β1-integrins/4F2hc/CD147.²²⁰

Evidently, MMP2, galectin-3 and 4F2hc play an intricate role in relaying information from integrins, which are the primary receptors for many extracellular matrix proteins including fibronectin.²⁸³ Chapter 4 highlighted the involvement of galectin-3 and 4F2hc-dependent cell-cell bridges in FM3 multicellular aggregation. Chapter 3 revealed that multicellular disaggregation requires extracellular matrix proteins such as fibronectin. These findings lead to the question of whether MMP2 is involved in FM3 multicellular aggregation-disaggregation events and what, if any, part does MMP2 play in galectin-3/4F2hc-mediated aggregation. Answers to these questions would give further insights into the correlation between MMP2 expression and melanoma progression.²⁸⁴

Therefore, this chapter aims to investigate whether MMP2 is involved in multicellular aggregation-disaggregation of FM3 melanoma cells. Bioinformatic analyses will be carried out to uncover concerted interplay of MMP2, 4F2hc and galectin-3 expression in melanoma metastasis and prognosis.

5.2 Results

5.2.1 MMP2 expression during FM3 multicellular aggregation-disaggregation

Interaction of 4F2hc and galectin-3 molecules induces a non-canonical β -catenin-1 translocation into the nucleus²²⁰ and leads to the regulation of *MMP2* gene expression via TCF/LEF family of transcription factors.²⁸¹ Therefore, it was hypothesised that *MMP2* mRNA expression would be increased during FM3 cellular aggregation as 4F2hc, and Galectin-3 levels rise. However, RT-qPCR revealed that during aggregation (Fig. 5.1 A, from 5 h to 24 h), *MMP2* mRNA expression was decreased (effect statistically significant 5 h vs 72 h), and no change in *MMP2* mRNA expression was observed between aggregates and disaggregates (Fig. 5.1 A, 24 h vs 72 h).

Moreover, treating cells with 10 ng/mL of anti-MMP2 (AF902) antibody was sufficient to significantly reduce cellular aggregation (Fig. 5.1 B; 24 h). Notably, higher concentration of anti-MMP2 antibody (200 ng/mL) also significantly reduced disaggregation at all the time points tested. Similarly, treating cells with increasing concentration of chlorhexidine (CHX), a potent inhibitor of MMP2, MMP8 and MMP9,²⁸⁵ also reduced cellular aggregation (Supplementary Fig. 5.1).

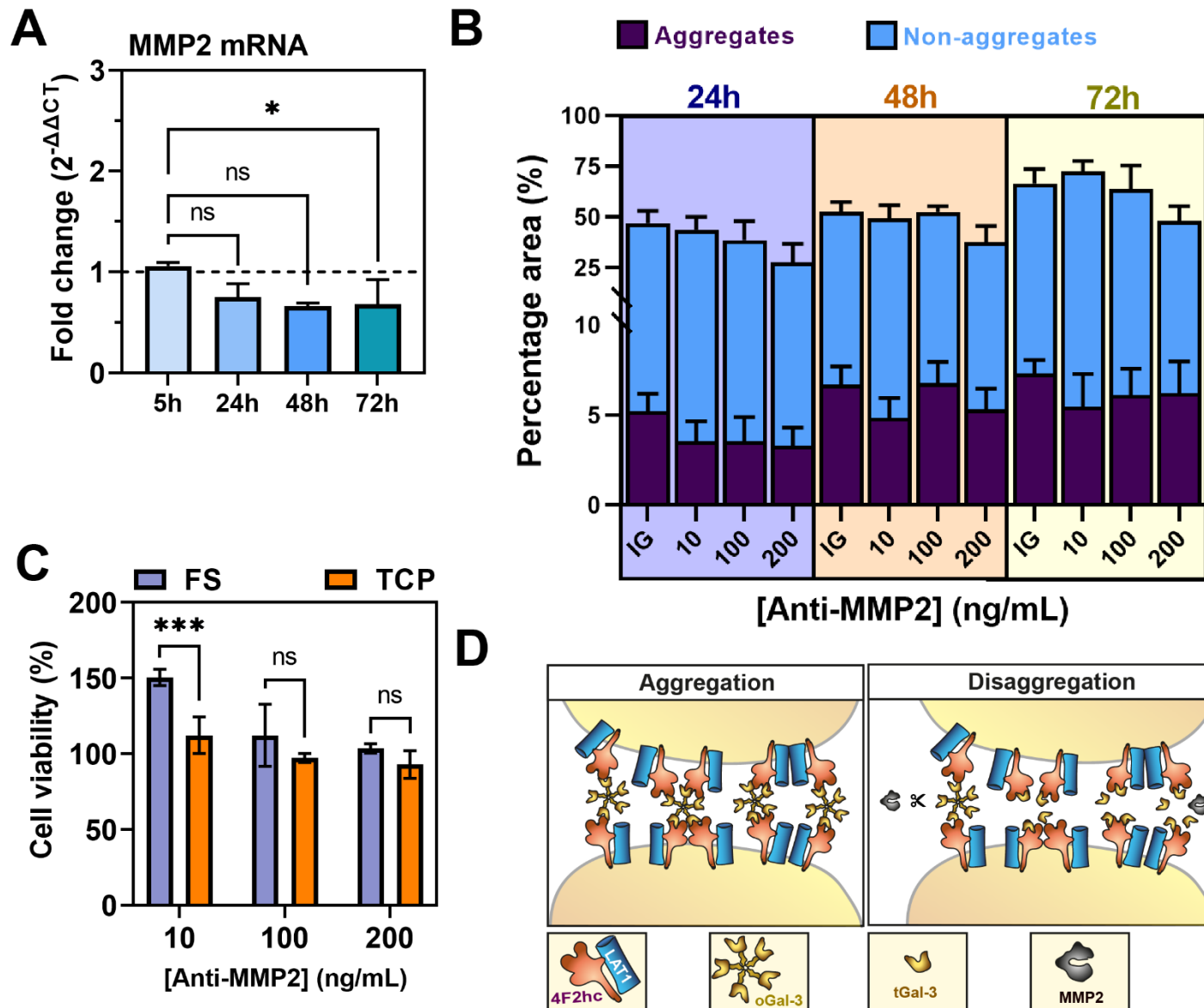


Fig. 5.1 MMP2-dependent cleavage of galectin-3 oligomers regulates melanoma cellular disaggregation. (A) Periodic expression of *MMP2* mRNA during aggregation (5-24h) vs disaggregation (48-72h) as measured by RT qPCR, n=3. Fold Change ($2^{-\Delta\Delta CT}$) represents comparison of FS surfaces vs TCP surfaces. (B-C) FM3 cells were treated with anti-MMP2 antibody (AF902) or immunoglobulin G (IG) isotope during culture upon FS surfaces. (B) Effect of increasing concentration of Anti-MMP2 on percentage area occupied by aggregates and non-aggregates, n=6. (C) Effect of increasing concentration of Anti-MMP2 on cellular viability after 72 h of culture, n=6. (D) Diagram depicting cleavage of galectin-3 oligomers by MMP2 during multicellular disaggregation. Brown-Forsythe and Welch ANOVA tests (equal SDs not assumed) with Dunnett T3 post-hoc multiple comparison test was carried out for RT-qPCR (A). Ordinary Two-way ANOVA with Tukey post-hoc multiple comparisons were carried out for antibody-treatment, and cell viability experiments (B - C). FS: fluoroalkylsilica, IG: Immunoglobulin G Isotope, oGal-3: Oligomers of galectin-3, tGal-3: truncated galectin-3, TCP: tissue culture

5.2.2 4F2hc, β -catenin, and TIMP3 expression during MMP2-inhibition in FM3 cells

To outline proteomic changes under the control of MMP2-dependent signalling in FM3 cells, cells were treated with 10 μ M of MMP2-inhibitor CHX for 24 h on TCP surface. Untreated FM3 cells (UT) were used as control. Cell lysate proteins were extracted, and quantitative mass spectrometry was carried out. This analysis revealed that 4F2hc protein levels significantly increased in FM3 cells treated with CHX (Fig. 5.2 A). No significant difference in galectin-3 levels was observed (Fig. 5.2 B). β -catenin levels significantly increased in FM3 cells treated with CHX (Fig. 5.2 C).

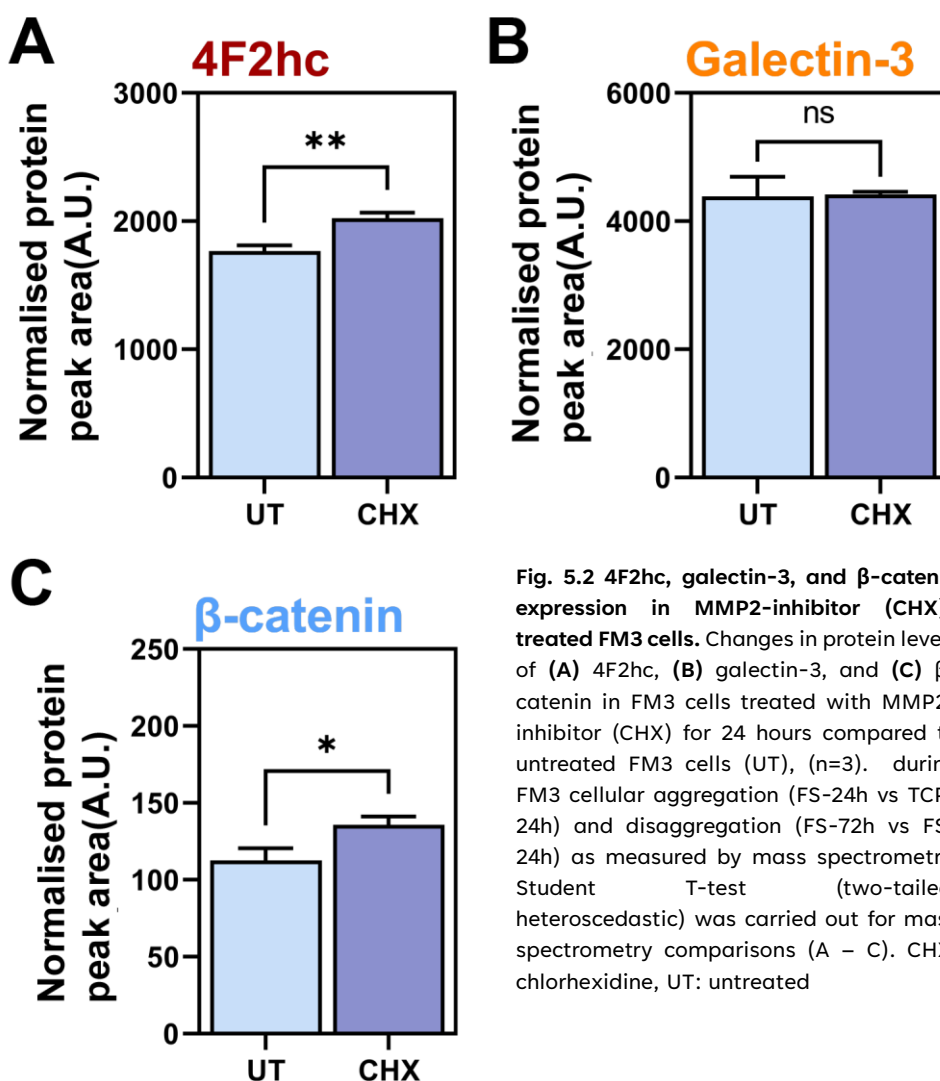


Fig. 5.2 4F2hc, galectin-3, and β -catenin expression in MMP2-inhibitor (CHX)-treated FM3 cells. Changes in protein levels of (A) 4F2hc, (B) galectin-3, and (C) β -catenin in FM3 cells treated with MMP2-inhibitor (CHX) for 24 hours compared to untreated FM3 cells (UT), (n=3). during FM3 cellular aggregation (FS-24h vs TCP-24h) and disaggregation (FS-72h vs FS-24h) as measured by mass spectrometry. Student T-test (two-tailed, heteroscedastic) was carried out for mass spectrometry comparisons (A – C). CHX: chlorhexidine, UT: untreated

5.2.3 Galectin-3, 4F2hc, and MMP2 on melanoma survival outcome

Galectin-3, 4F2hc and MMP2 appear to have concerted roles in FM3 multicellular aggregation-disaggregation *in vitro*. It is not apparent whether these three proteins also involved in CTC cluster aggregation-disaggregation of metastatic melanoma. To isolate and outline any concerted or inharmonious effects these three proteins have on the survival outcome of patients, *in silico* study was carried on melanoma (SKCM) dataset from the Cancer Genome Atlas project (TCGA). The following results shown are in part based on data generated by the TCGA Research Network (<https://www.cancer.gov/tcga>). The melanoma (SKCM) gene expression/alteration dataset and patient survival dataset were obtained via cBioPortal²⁸⁶ and OncoLnc,²⁸⁷ respectively.

Galectin-3, 4F2hc and MMP2 were differentially expressed during FM3 aggregation-disaggregation. As such, it was hypothesised that patients who presented alteration in *LGALS3* (gene coding for galectin-3), *SLC3A2* (gene coding for 4F2hc), and *MMP2* genes display shorter overall survival (OS) than those who presented unaltered version of these genes. Significant decrease in overall survival was observed for patients who presented altered *SLC3A2* (Fig 5.3 B) and *MMP2* (Fig. 5.3 C) genes compared to their unaltered counterparts. However, no significant difference in survival was observed for altered vs unaltered *LGALS3* gene (Fig. 5.3 A).

In FM3 cells, galectin-3 (Chapter 4: Fig. 4.1 A & C) and 4F2hc (Chapter 4: Fig. 4.2 A & C) increased during aggregation and subsequently decreased during disaggregation. MMP2 level decreased during aggregation and stayed the same during disaggregation (Fig. 5.1 A). Therefore, it was hypothesised that high expression of Galectin-3, 4F2hc and MMP2 would correlate with decreased patient survival. Each dataset was split by median expression of these three genes and Kaplan-Meier (KM) plots were generated to correlate changes in gene expression with patient survival (Fig. 5.3. D - F). However, similar to the gene alteration KM plots, significant reduction in overall survival was observed for patients who presented high expression of *SLC3A2* (Fig. 5.3 E) and *MMP2* (Fig. 5.3 F) genes compared to their low expression counterparts; but no significant difference in survival between high vs low was observed for *LGALS3* gene (Fig. 5.3 D).

To study effect of MMP2, 4F2hc and galectin-3 expression on melanoma patient survival, RNAseq dataset were obtained from TCGA (RNAseq TCGA-SKCM). Dataset was stratified based on high vs low expression of Galectin-3, MMP2 and 4F2hc, to give 8 strata of different combinations in expression of these three proteins (Fig. 5.3 G) (N=456 patients). Investigation of impact on patient survival each of these combinations had (Fig. 5.3 H), revealed that

Gal3^{low}-MMP2^{low}-4F2hc^{low} combination (median OS = 14 years) yielded the most favourable, and Gal3^{low}-MMP2^{high}-4F2hc^{high} combination (median OS = 4.43 years) the least favourable outcome (significance; p-value = 0.0004).

Next, the individual contribution each of these genes had on patient survival, genes were compared against the other two genes within the same cohort (Fig. 5.3 I-K). When all three genes were 'ON' (+), meaning that their expression level was above the median of the subset, the median OS of melanoma patients decreased by ~10 years compared to when all three genes were 'OFF' (-) (Fig. 5.3 K). When only MMP2 or 4F2hc genes were 'ON', the median OS decreased by ~7 years when compared to when only galectin-3 gene was 'ON' (Fig. 5.3 I). Interestingly, when considering the subsets with two genes being 'ON', it was clear that the reduction in median OS induced by MMP2 was offsetted by galectin-3 gene being 'ON'. However, the reduction in median OS as induced by 4F2hc was not offsetted by galectin-3 gene being 'ON' (Fig. 5.3 J).

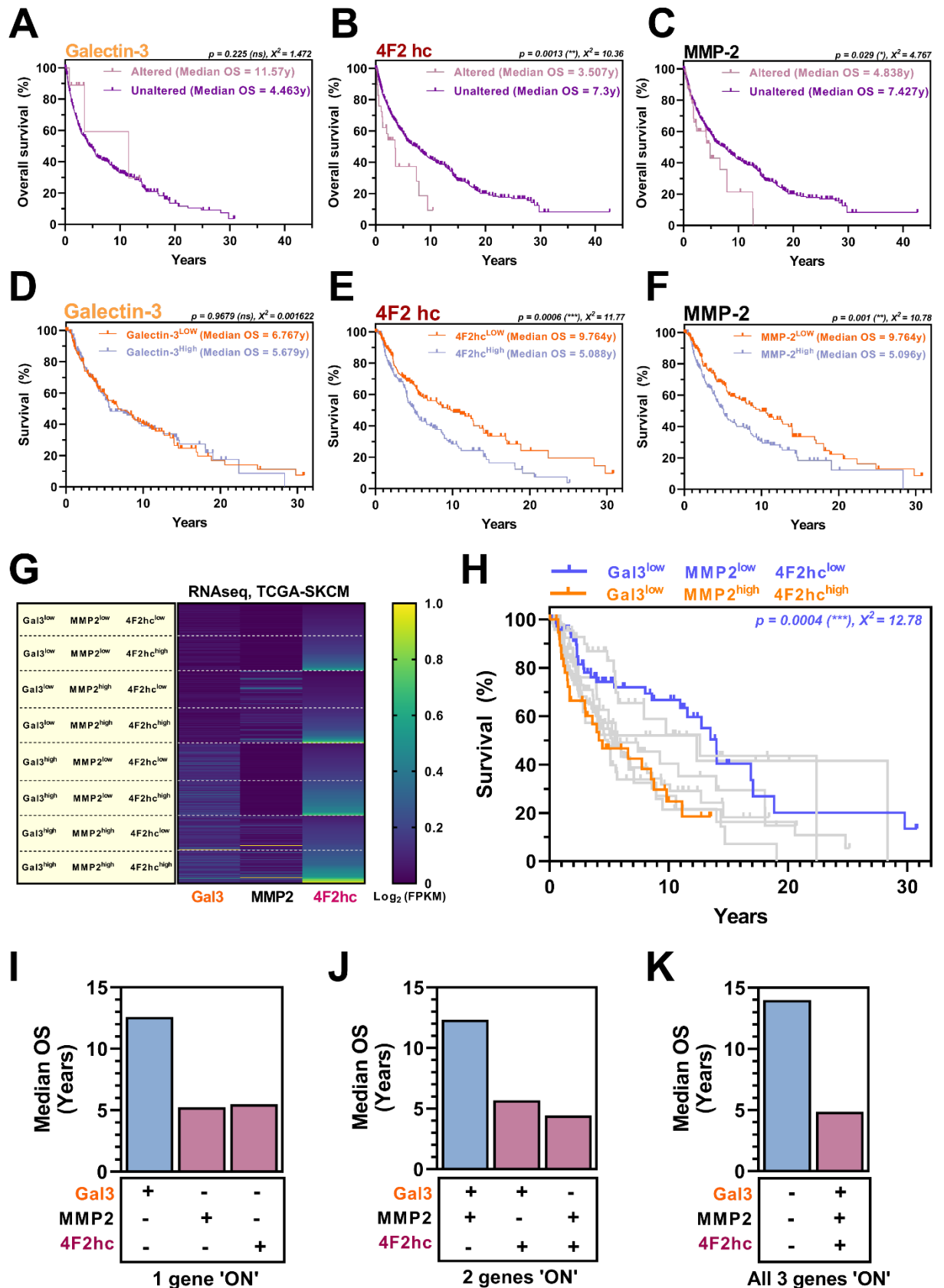


Fig. 5.3 Concerted roles of galectin-3, 4F2hc and MMP2 define the survival of melanoma patients. (A-C) Altered vs unaltered data obtained from cbiportal.org from multiple melanoma RNA-sequencing, to outline risk associated with gene alteration of (A) *LGALS3* gene (galectin-3), (B) *SLC3A2* gene (4F2hc), and (C) *MMP2* gene. (D-F) KM plot to show high vs low expression of (D) *LGALS3* gene (galectin-3), (E) *SLC3A2* gene (4F2hc), and (F) *MMP2* gene compared to patient survival. Median expression of the three genes was used to split patients expressing high vs low levels of each gene. Survival data set were obtained from oncolnc.org; data used here (from melanoma TCGA-SKCM) were adjusted and normalised in OncoLnc. (G-I) Normalised TCGA-SKCM (melanoma) dataset stratified (G) by based on high vs low expression of galectin-3, 4F2hc and MMP2 to give 8 possible combinations, (N=456 patients). (H) KM plot to show patient survival data, and (I-K) graphical representation of median OS survival of these 8 combinations, where blue is control cohort, pink is poor outcome. KM plot: Kaplan-Meier Plot, OS: Overall survival, TCGA: The Cancer Genome Atlas.

5.3 Discussion

5.3.1 FM3 cells reduce MMP2 expression to prevent untimely cellular disaggregation

This chapter aimed to address the involvement of MMP2 in FM3 multicellular aggregation and disaggregation. Since MMP2-cleaved galectin-3 was thought to interact with 4F2hc and stabilise 4F2hc/integrin macro-complexes,²²⁰ it was hypothesised that MMP2 expression would be increased during FM3 multicellular aggregation. Gene expression analysis of *MMP2* gene, via RT-qPCR, showed that this was not the case; MMP2 gene expression was significantly decreased during aggregation and expression levels stayed the same between aggregation and disaggregation (Fig. 5.1 A).

The gelatinases, MMP2 and MMP9 can both cleave galectin-3 at alanine⁶²-Tyrosine⁶³.²⁸⁸ This cleavage produces a truncated galectin-3 (tGal3) protein ~22 kDa. After cleavage, tGal3 retains its carbohydrate recognition domain (CRD), which can now bind more tightly to glycoconjugates at the cost of reduced self-association and oligomerisation.²⁸⁹ Therefore, MMP2-cleavage of galectin-3 in FM3 cells, and subsequent conversion of oGal3 to tGal3, most likely will eliminate glycoprotein:galectin-3:glycoprotein bridges (GGG) between cells (discussed in chapter 4). Thus, it is conceivable that MMP2-cleavage of galectin-3 ultimately leads to disaggregation of FM3 cells. Perhaps, this is the reason behind the decrease in *MMP2* mRNA expression by FM3 cells observed during aggregation (Fig. 5.1 A) so as to prevent untimely multicellular disaggregation.

In clinical melanoma, MMP2 expression almost doubles within the metastatic melanoma lesions compared to primary tumours;²⁹⁰ thus, it is conceivable that melanoma CTC clusters would disaggregate at metastatic sites where MMP2 levels and MMP2-cleavage of oGal3 likely to be high. As *MMP2* mRNA expression did not change between aggregation and disaggregation (Fig. 5.1 A), it is not clear whether MMP2 at metastatic sites are secreted from cancerous cells or MMP2-dependent disaggregation is caused by the secretion of MMP2 from stromal²⁹¹ or immune cells.²⁹² Further research could address the source of MMP2 at metastatic sites. In any case, these findings suggest that increased extracellular MMP2 activity would theoretically lead to more readily breaking of GGG bridges, separation of coterminous 4F2hc glycoproteins, and ultimately would lead to melanoma CTC disaggregation at metastatic sites and invasion through the stroma.

5.3.2 MMP2-mediated control of β -Catenin and 4F2hc levels in FM3 cells

MMP2 could have an intracellular role during ADPM of FM3 cells in addition to its extracellular role of cleavage of oGal3. Intracellular MMP2 has been shown to bind and cleave many intracellular proteins, including GSK-3 β .²⁹³ In cardiomyoblasts, this cleavage resulted in increased kinase activity of GSK-3 β .²⁹⁴ Increased activity of GSK-3 β could lead to the proteasomal degradation of β -Catenin.²⁹⁵ Inhibition of MMP2 by anti-MMP2 antibodies or CHX could lead to the reduction of intracellular MMP2-dependent cleavage of GSK-3 β , leading to a decrease in activation of GSK-3 β and GSK-3 β -dependent proteasomal degradation of β -Catenin. Thus, inhibition of intracellular MMP2 could lead to increased β -Catenin levels. In agreement, β -Catenin levels increased during inhibition of MMP2 in FM3 cells (Fig. 5.2 C).

β -Catenin molecules freely translocate to the nucleus and regulate gene expression.²⁹⁶ One or more of the β -Catenin-target genes could be involved in aggregation, for example galectin-3 or 4F2hc. Indeed, 4F2hc levels were increased during anti-MMP2 antibody or CHX treatment of FM3 cells (Fig. 5.2 A); galectin-3 levels stayed the same (Fig. 5.2 B). Further research is required to confirm that 4F2hc expression lies under the control of β -Catenin-mediated gene regulation in FM3 cells. In any case, inhibition of MMP2 leading to increased 4F2hc levels, meaning more likelihood of multicellular aggregation, could also explain why FM3 cells downregulated *MMP2* mRNA expression during aggregation (Fig. 5.1 A).

Additionally, GSK-3 β was shown to be inactivated by 4F2hc/integrin/FAK signalling,²²⁰ leading to increased β -Catenin levels and β -Catenin-dependent gene regulation. This suggests that β -Catenin levels in FM3 cells could potentially be under the control of both MMP2 expression and 4F2hc-mediated signalling. For instance, ADPM could be controlled by 4F2hc-mediated signalling and intracellular MMP2 levels. Further research could address the degree of control 4F2hc/integrin/FAK signalling and intracellular MMP2 have on β -Catenin and β -Catenin-target genes in ADPM.

Increase in extracellular MMP2 and subsequent MMP2-dependent cleavage of oGal3 could lead to increased multicellular disaggregation. Whereas an increase in intracellular MMP2 activity could result in decreased β -Catenin and 4F2hc levels, which could promote multicellular disaggregation. This could explain the observation where aggregation was decreased with anti-MMP2 antibody and CHX treatment (Fig. 5.1 B & Supplementary Fig. 5.1). As anti-MMP2 antibody and CHX could inhibit extracellular MMP2; however, uptake of anti-MMP2 antibody and CHX by cells could inhibit intracellular MMP2. This caveat confounds the effect of MMP2 on ADPM of FM3 cells. An improvement of this experiment could be to inhibit extracellular or intracellular MMP2 individually, for example via using an inhibitor that only

targets either one of these types of MMP2, in order to isolate effects of MMP2-inhibition on ADPM of FM3 cells.

5.3.3 Concerted roles of Galectin-3, 4F2hc and MMP2 in melanoma ADPM

Evidently, galectin-3, 4F2hc and MMP2 play major roles in ADPM of FM3 cells *in vitro*. To investigate whether they carry out similar roles in CTC clusters in clinical melanoma, patient survival and RNAseq dataset were analysed *in silico*. Patients who presented altered gene expression, as well as high RNA expression, of both *SLC3A2* and *MMP2* genes, had significantly reduced OS compared to the patients who presented unaltered genes or low RNA expression. However, no significant difference in OS were observed for *LGALS3* gene, for both gene alteration as well as between high vs low expression.

The poor prognosis of melanoma patients associated with increased 4F2hc expression could be explained in light of recent findings. A study showed that CD98 heterodimers levels were high in several cultured melanoma cell lines; notably, they highlighted, using tissue microarrays, increasingly higher expression of 4F2hc going from common dermal nevus to superficial spreading melanoma, to the highest expression in metastatic melanoma.²⁹⁷ Another study highlighted that loss of 4F2hc induced regression of Ras oncogene-driven melanoma tumours in mice;²⁹⁸ this study has also showed that 4F2hc acted as a stiffness/matrix-rigidity sensor by increasing Rho kinase (ROCK) activity, and subsequently increased gene transcription by YAP/TAZ transcriptional co-activators. Indeed, YAP (specifically YAP1), and TAZ (WWTR1) co-activators has been shown to drive cancer cell survival and growth of many different cancers including melanoma, in response to competing upstream signals from integrin/SRC, E-cadherin, and growth factor-induced PI3K/AKT signalling.²⁹⁹ These findings confirm that 4F2hc likely to be involved in RCA-detection, mechanosensing as well as promoting adherence-independent growth, and thus regulate ADPM of clinical melanoma.

Similar to 4F2hc, MMP2 expression also was shown to increase in metastatic melanoma (43%) compared to primary (25%) tumours as well as normal tissue (5%) and dysplastic nevi (10%).²⁹⁰ In accordance with the present study, they further showed that patients with high MMP2 had significantly poorer survival outcome. The prominent role of MMP2 in metastatic melanoma could be degradation of matrix proteins during invasion.³⁰⁰ The present study highlights a novel role of MMP2 in aiding ADPM of melanoma cells. Therefore, MMP2 could serve a range of different roles in melanoma metastasis, including degradation of matrix proteins,

contribution to EMT,³⁰¹ and as per the present contribution ADPM of melanoma, all contributing to the poorer survival of patients.

Unlike *SLC3A2* or *MMP2* genes, *LGALS3* gene showed no significant differences in OS between altered vs unaltered status, nor high vs low RNA expression. However, an overwhelming amount of research suggest that Galectin-3 does play a major role in melanoma. A study showed, using tissue microarray of melanocytic lesions, primary and metastatic melanoma expressed significantly higher level of Galectin-3 in both cytoplasm and nuclei compared to nevi tissue.³⁰² The role of Galectin-3 in metastatic melanoma though seems to be ambiguous. Indeed, primary melanoma tumours seem to express increased levels of Galectin-3 compared to benign nevus; somewhat puzzlingly, levels of Galectin-3 decrease in metastatic melanoma.^{303,304}

In contrast, galectin-3-depleted melanoma cells presented reduced tumorigenicity, reduced metastatic potential and reduced expression of certain tumour markers;³⁰⁵ notably, levels of Interleukin-8, Fibronectin-1, and MMP2 were significantly reduced. Discrepancy in these findings, that is galectin-3 levels decrease in metastatic melanoma whilst simultaneously lowers metastatic potential when levels of which are depleted, indicate that galectin-3 could be involved in initiating metastasis, but less so once metastasis has taken place. This explanation would be in line with the findings of the present research, which indicate that galectin-3 is involved in ADPM; but levels drop during disaggregation, which in terms of clinical melanoma would occur at distal sites after metastasis has taken place.

Melanoma cells have been shown to express extracellular galectin-3; subsequent activation of p38 mitogen-activated protein kinase pathway induced the secretion of MMP9.³⁰⁶ Evidently, galectin-3 regulate expression of MMP2 and MMP9 in melanoma. Reciprocally, MMP2 and MMP9 could regulate galectin-3 oligomerisation and binding by cleavage. Thus, to untangle this relationship between galectin-3, MMP2 and 4F2hc in clinical melanoma, expression patterns of these proteins were inquired within the same cohort. Unsurprisingly, the Gal3^{low}-MMP2^{low}-4F2hc^{low} combination yielded the most favourable prognosis, and expectedly, the combination Gal3^{low}-MMP2^{high}-4F2hc^{high} yielded the least favourable outcome; OS was significantly higher for the former combination, by about ~10 years (p-value = 0.0004). Even though this further substantiate the negative effect 4F2hc and MMP2 have on OS of melanoma patients, it remains to be uncovered the precise effects 4F2hc, MMP2 and galectin-3 have on each other during the progression of melanoma.

It would seem that either *SLC3A2* or *MMP2* gene being 'ON', here meaning that their expression level was above the median of the subset, by themselves were sufficient to result

in poor prognosis, with a decrease in median OS by ~7 years, compared to when only *LGALS3* gene was 'ON'. This suggests that the expression of 4F2hc or MMP2 alone is sufficient to make prognosis of melanoma worse; but this is not the case for galectin-3. As it stands, using galectin-3 inhibitors to target melanoma may be not as effective as targeting 4F2hc or MMP2.

The reduction in median OS caused by *MMP2* being 'ON' was counteracted when *LGALS3* gene was also 'ON'. This was surprising to find, as this indicates that galectin-3 provides protection against the negative effect MMP2 have on prognosis. As galectin-3 has been shown to attenuate survival of melanoma cells by negatively regulating autophagy,³⁰⁷ it is likely this role of galectin-3 offsets the pro-invasion role of MMP2. Galectin-3, however though, does not provide protection against the negative effect 4F2hc have on prognosis; the reduction in median OS induced by *SLC3A2* 'ON' was not offsetted by *LGALS3* being 'ON'. One way to interpret this finding, in light of the present contribution, is that galectin-3 expression alongside 4F2hc expression likely to lead to more successful CTC cluster formation and more efficient metastasis. If this was the case, seemingly, this pro-metastatic role of galectin-3 predominate the anti-autophagy role affecting prognosis. Following this, the protection against MMP2 expression exerted by galectin-3 expression, disappears when all three genes are expressed.

When both *SLCA3A2* and *MMP2* were 'ON' together, similar to when both were 'ON' individually, there was an adverse effect on prognosis. It is not clear whether this is an additive effect or whether 4F2hc and MMP2 separately drive this adverse prognosis. As silencing 4F2hc in HeLa cells (cervical cancer cells) resulted in decreased expression and activity of MMP2,²²⁰ it could be that, likewise, MMP2 expression lies downstream of 4F2hc signalling in melanoma as well. Further experiment is needed to confirm this; for example, by silencing 4F2hc in FM3 cells and see if that also would reduce MMP2 expression.

There is a lack of genetics studies or RNAseq studies carried on melanoma CTC clusters to isolate gene expression patterns during ADPM. As such, the present study attempted to gauge the gene expression pattern that are likely to take place during ADPM by looking at primary vs metastasis melanoma. However, the datasets were skewed largely towards primary tumours. To circumvent this, both primary and metastatic dataset were pooled together and investigated effect of each gene, together or alone, on prognosis of melanoma as a whole; this means that it would be illogical to draw any conclusion based on comparison between primary vs metastatic melanoma, but only logical statements would be pertaining to prognosis of melanoma as a whole. Furthermore, stratification of the RNAseq dataset meant each subset within the cohort had even fewer N number; as such, for when three genes were investigated for their concerted roles, statistical analyses were not feasible. Instead, the

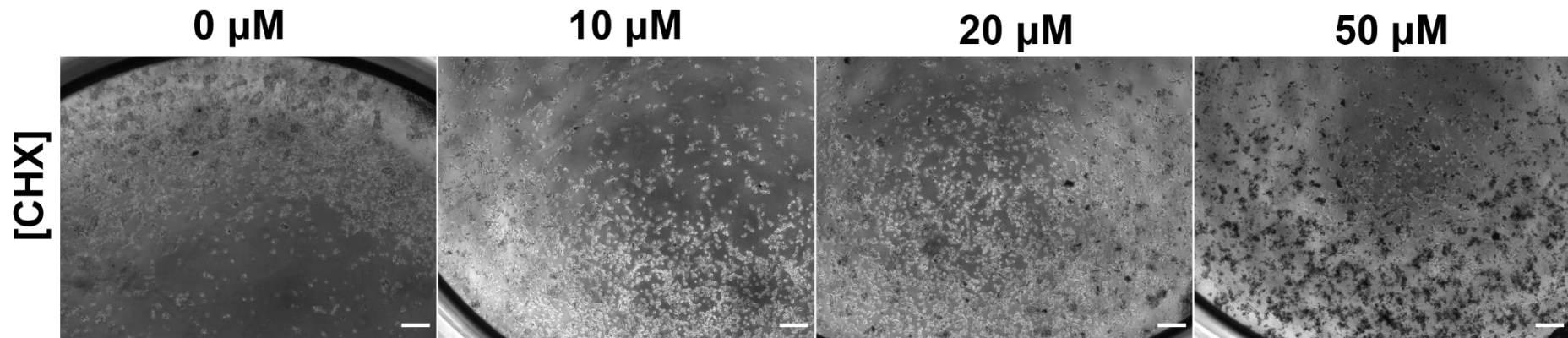
median OS of each subset were used as general guide to gauge adverse prognosis of one, two or all three genes being 'ON'. Despite these limitations, though, by looking at only the substantial differences (blue vs pink), and not any minor differences (pink vs pink; for example, if only MMP2 'ON' vs 4F2hc 'ON' was to be compared), conclusion based on median OS exerted by low vs high expression of the three genes would still be valid.

In any case, these findings suggest that 4F2hc and MMP2 expressions adversely affect melanoma prognosis in a concerted manner, whereas effect of galectin-3 expression on prognosis is more nuanced; that is, galectin-3 only provide adverse effect alongside 4F2hc, but disharmonious effect alongside expression of MMP2. Gaining insights into these effects is important for therapeutic intervention, as is genotyping of patients to discern expression patterns of these three genes; inappropriate inhibition of galectin-3 could impede the protective role it may play during later stages of melanoma and worsen prognosis.

5.3.4 Conclusions

This chapter revealed that FM3 cells could decrease MMP2 expression to prevent untimely multicellular disaggregation during ADPM, as MMP2-cleavage of galectin-3 oligomers and dissociation of GGG bridges would lead to disaggregation. In instances where MMP2 levels are high, for example in metastatic sites, GGG bridges could be readily broken by MMP2-cleavage of galectin-3, and thus CTC clusters could disaggregate and infiltrate the nearby stroma. Inhibition of MMP2 in FM3 cells resulted in increased β -Catenin and 4F2hc levels, suggesting that there intracellular MMP2 could serve a different role in ADPM compared to the extracellular role. Further research could address the control of β -Catenin levels and β -Catenin-dependent gene regulation by intracellular MMP2 activity or 4F2hc/FAK/integrin signalling. Lastly, bioinformatics analyses revealed that in clinical melanoma galectin-3 present poor prognosis when expressed alongside 4F2hc, but a protective effect when expressed alongside MMP2. As such, galectin-3 inhibitors should only be used to treat melanoma when 4F2hc levels are also high, and never when MMP2 is expressed so as to not disrupt this protective effect galectin-3 brings to prognosis. Combinatory treatment of galectin-3 inhibitor and 4Fh2c inhibitors could reduce the risk of CTC cluster/ADPM-dependent metastasis of melanoma.

5.4 Supplementary Figures



Supplementary Fig. 5.1 Treatment of FM3 cellular aggregates with MMP2 inhibitor (CHX) decreases aggregation. Representative micrographs showing changes in multicellular aggregation of FM3 upon FS surface after 24 hours of treatment with increasing concentration of MMP2 inhibitor (CHX), (n=5). Scale = 200 μm. CHX: chlorhexidine, FS: fluoroalkylsilica.

Chapter 6. Epithelial-Mesenchymal Transition and β -catenin in melanoma multicellular aggregation-disaggregation

Contents

CHAPTER 6. EPITHELIAL-MESENCHYMAL TRANSITION AND B-CATENIN IN MELANOMA MULTICELLULAR AGGREGATION-DISAGGREGATION...	93
6.1 INTRODUCTION	94
6.1.1 EMT and MET	94
6.1.2 EMT-like process in melanoma.....	95
6.1.3 EMT-like process in CTC clusters.....	96
6.1.4 Crosstalk of TGF β and Wnt/ β -catenin signalling in EMT	97
6.1.5 β -catenin in melanoma CTC clusters	98
6.2 RESULTS.....	100
6.2.1 β -catenin expression during FM3 multicellular aggregation-disaggregation....	100
6.2.2 EMT in FM3 multicellular aggregation-disaggregation.....	102
6.2.3 Effect of EMT status on ADPM response of prostate cancer cells.....	103
6.2.4 β -catenin interactome changes during ADPM of FM3 cells	105
6.2.5 β -catenin interactome affects melanoma survival outcome.....	108
6.2.6 β -catenin-mediated transcriptional regulation of ADMP.....	111
6.3 DISCUSSION	114
6.3.1 β -catenin is involved in multicellular aggregation of FM3 cells	115
6.3.2 EMT does not occur during ADPM of FM3 cells.....	116
6.3.3 P4B6B cells sustain aggregation via expression of vitronectin, vimentin and shroom-3.....	116
6.3.4 β -catenin interactors, LDHB, PML, PABP1, PUR9, SPF45, RL11, and HS105 involvement during ADPM of FM3 cells	118
6.3.5 β -catenin interactors, LDHB, PML, PABP1, PUR9, SPF45, RL11, and HS105 impact on prognosis of metastatic melanoma	121
6.3.6 β -catenin and SPI1-mediated transcriptional regulation in ADPM of FM3 cells	126
6.3.7 Conclusions.....	127
6.4 SUPPLEMENTARY FIGURES	129

6.1 Introduction

This chapter interrogates effect of Epithelial-to-Mesenchymal Transition (EMT) status on ADPM and explores the impact β -catenin (discussed in Chapter 5) interactome have on ADPM.

6.1.1 EMT and MET

Epithelial-to-Mesenchymal Transition (EMT) and its reversal, Mesenchymal-to-Epithelial Transition (MET) are fundamental cellular reprogramming events underlying many important biological processes, such as embryonic development, tissue regeneration, and metastasis of cancer cells.³⁰⁸ During EMT, epithelial cells undergo molecular and cytoskeletal changes that assist their transition from a 'compact and cuboidal' morphology to a mesenchymal-like 'motile and spindle-shaped' morphology.³⁰⁹ The opposite is true for MET. In carcinoma of epithelial origin, EMT drives metastasis and invasion; once dissemination from the primary tumour and invasion into secondary distal sites have taken place, MET promotes proliferation and growth of secondary neoplasms.³¹⁰

Epithelial cells present increased cell-cell contacts, whereas mesenchymal cells present minimal cell-cell contacts; in contrast, mesenchymal cells have comparatively enhanced locomotive capabilities.³⁰⁹ This is reflected in the molecular and cytoskeletal changes that accompany EMT. Indeed, proteins important for cell-cell contacts, such as E-cadherin and ZO-1, are upregulated in epithelial cells and downregulated in mesenchymal cells.³¹¹ Proteins that are important for motility, such as fibronectin and integrins, are comparatively elevated in mesenchymal cells.³¹¹

An important hallmark of EMT is the onset of the upregulation of several key transcription factors, for example snail (SNAI1), slug (SNAI2), twist1, and the zing finger E-box-binding homeobox (ZEB) family of transcription factors.³¹² The intricate interplay of the aforementioned, but not limited to, transcription factors govern the regulation of the vast and distinct proteomic changes and cellular processes that are involved in EMT. Unsurprisingly, these transcription factors are often highly employed in neoplastic transformation and metastasis of several cancers, including brain, breast, bladder, colorectal, gastric, and melanoma.³¹²

6.1.2 EMT-like process in melanoma

Several pieces of research highlight that an EMT-like process promotes melanoma metastasis. Two distinct subpopulations of melanoma were described as early as in 2006;³¹³ one was more proliferative but less invasive, termed ‘melanocytic state’, and the other was highly invasive, called the ‘undifferentiated state’.³¹⁴ Parallels, in terms of expression of EMT markers and morphology, can be drawn between the melanocytic state and epithelial cells, and between the undifferentiated state and mesenchymal cells³¹⁵ (Fig. 6.0). A notable parallel is that much like mesenchymal cells, undifferentiated melanoma showed loss of E-cadherin and gain of N-cadherin expression.³¹⁶ Moreover, transcription factors that regulate EMT, such as snail, twist1, and ZEB1, were expressed in the mesenchymal-like undifferentiated melanoma cells.³¹⁷ Similar to in mesenchymal cells, twist1 and ZEB1 suppressed E-cadherin expression and promoted dedifferentiation of melanocytic cells.³¹⁸

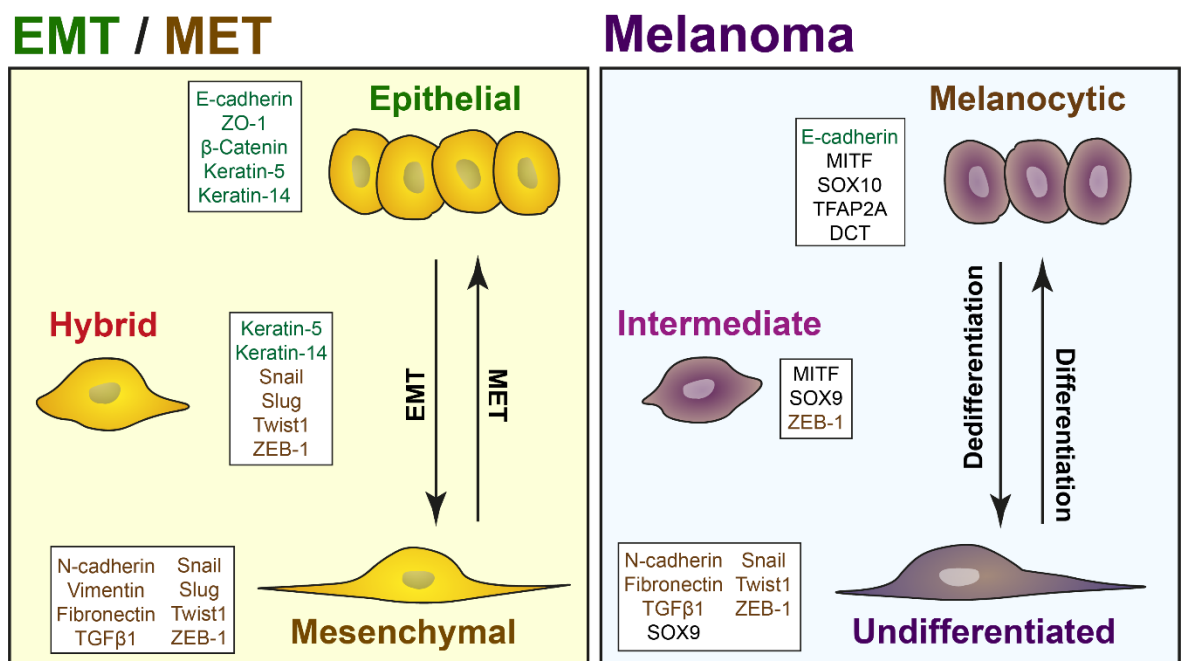


Fig. 6.0 Parallel between EMT/MET and melanoma states. Epithelial markers are highlighted in green and mesenchymal markers are highlighted in brown. EMT: Epithelial-to-Mesenchymal transition, MET: Mesenchymal-to-Epithelial transition. With permission, figure adapted from Pedri D. et al. (2021) with permission acquired from Dennis Pedri.

Melanocytes are differentiated, melanin-producing, subepidermal cells; neoplastic transformation into melanoma often elicits dedifferentiation.³¹⁹ Development and differentiation of melanocytes are governed by the microphthalmia-associated transcription factor (MITF),³²⁰ and other lineage-specific markers such as DCT³²¹ and SOX10.³²² Whereas undifferentiated melanoma cells show reduced MITF expression compared to melanocytic cells;³²³ high levels of MITF were associated with a proliferative phenotype. In contrast, cells containing low levels of MITF assume slow-cycling/low-proliferative but highly invasive

phenotype bearing resemblance to mesenchymal cells. MITF was shown to be downregulated in melanoma by extracellular stimuli, such as inflammatory signals such as $TNF\alpha$,³²⁴ mitogenic/EMT signals such as $TGF\beta$,³²⁵ hypoxia such as Wnt signalling,^{326,327} as well as various metabolic cues as glucose³²⁸ and amino acids.³²⁹ This indicates that, through MITF, melanoma cells could shift between differentiated and dedifferentiated states depending upon the tumour microenvironment.

Besides MITF, SOX10 also contributes to melanocyte development.³²² It has been shown that SOX10 could promote expression of MITF,³³⁰ as well as cooperating with MITF in transcriptional regulation of target genes involved in melanogenesis, for example *PMEL*,³³¹ or melanocyte proliferation such as *CDK2*.³³² Like MITF, downregulation of SOX10 was also shown to induce a slow-proliferative and mesenchymal-like state.³³³ Interestingly, SOX10 expression is inversely proportional to SOX9 expression.³³⁴ Indeed, upregulation of SOX9, and subsequent loss of SOX10 expression, was shown to drive a mesenchymal-like undifferentiated state in melanoma.³³⁵ SOX9 is one of the key mediators of EMT during embryogenesis.³³⁶ SOX9 was also shown to promote EMT, via Wnt/ β -catenin signalling pathway, in non-small-cell lung cancer.³³⁷

EMT in epithelial cancers and an EMT-like process in non-epithelial cancers like melanoma, should not be thought of as a binary system; cancer cells may not exist solely as epithelial-like or mesenchymal-like,³³⁸ and in melanoma, cells may not exist solely as melanocytic or in an undifferentiated state. But rather, cells could assume a phenotype somewhere within the spectrum of being mostly epithelial-like to being mostly mesenchymal-like, or in melanoma, being mostly proliferative/melanocytic to being mostly invasive/undifferentiated, depending on external factors such as metastasis state, inflammation, microenvironment, and metabolic cues.³³⁸ Recent advances in single cell RNA sequencing have highlighted that many metastatic cancer cells comprise subpopulations that exhibit expression signatures resembling both epithelial and mesenchymal cells (Fig. 6.0; hybrid).³³⁹ Likewise, melanoma cells may assume an intermediary state (Fig. 6.0; intermediate) in which they exhibit both proliferative and invasive phenotypes.³⁴⁰

6.1.3 EMT-like process in CTC clusters

As EMT appears to play an dominant role in augmenting cellular locomotion and invasiveness,³⁴¹ it was proposed that circulating tumour cells (CTC) likely would possess a mesenchymal-like phenotype.³⁴² However, another suggests that this may not be true as epithelial-like CTCs have been isolated from patients.³⁴³ Additionally, cells that had undergone

complete MET after transient induction of EMT were shown to have increased metastatic propensity.³⁴⁴ These studies question, to what extent EMT might be indispensable for metastasis, as previously thought, at least with regards to CTCs.

Moreover, CTC clusters are more metastatic, up to 100 times more, than a single CTC.³⁴⁵ This is especially true for melanoma.³⁴⁶ Here, the indispensability of EMT for metastasis seems to be even more implausible; clusters express many epithelial markers,³⁴⁷ especially those involved in cell-cell adhesion,³⁴⁸ and thus remain as clusters due to increased cell-cell contacts. In contrast, some CTC clusters were shown to exclusively express mesenchymal markers;³⁴⁹ here, it is unclear how cells remain as clusters, and which non-epithelial markers are utilised for making cell-cell contacts. As many CTC clusters are polyclonal and heterogenous, some researchers have proposed a 'Leader-Follower' model; wherein mesenchymal-like 'Leader' cells take charge of the invasion,³⁵⁰ and partial-EMT/hybrid cells³⁵¹ connect these 'leader' cells to the 'follower' cells comprising a mixture of hybrid and fully-epithelial cells.

This 'Leader-Follower' model seems to be true for melanoma as well. A recent study revealed that the metastasis of heterotypic melanoma CTC clusters was driven by the cooperation between a proliferative subpopulation (epithelial-like/melanocytic) and an invasive (mesenchymal-like/undifferentiated) subpopulation of cells.³⁵² Here, the neural crest transcription factor TFAP2A was shown to act as a master regulator governing the transition between proliferative and invasive states, as well as regulating the formation of clusters. Individual cells within the melanoma CTC clusters derived from patients showed varying degree of invasion-to-proliferation phenotype, as denoted by expression of SOX9 (representing invasive/undifferentiated phenotype), and expression of TFAP2A (representing proliferative/melanocytic phenotype). Given that TFAP2A is a component of the ZEB family transcription network that regulates gene transcription in response to TGF β -induced EMT,³⁵³ the involvement of TGF β and EMT-like process in melanoma CTC clusters are highly likely.

6.1.4 Crosstalk of TGF β and Wnt/ β -catenin signalling in EMT

TGF β plays a paradoxical role in tumour progression. During the early stages, TGF β acts as a tumour growth suppressor;³⁵⁴ however, during advanced stages of cancer progression, tumour cells become resistant to TGF β -mediated repression of growth.³⁵⁵ Additionally, during the later stages, TGF β acts as a pro-metastatic cytokine, whereby, it regulates the expression of EMT transcription factors such as snail, twist1 and ZEB.³⁵⁶ In melanoma, though, decreased TGF β signalling has been found to be associated with phenotypic plasticity, where cells exhibited

both highly proliferative and invasive phenotypes.³⁵⁷ These observations indicate that TGF β plays a complex role in mediating EMT in melanoma.

Using gene set enrichment analysis of BRAF-driven melanoma CTC, a study revealed that gene signatures of three key signalling pathways, TGF β signalling, non-canonical Wnt signalling, and bone morphogenetic protein (BMP) signalling were highly associated with EMT and tumour invasiveness of melanoma CTC.³⁵⁸ The canonical Wnt/ β -catenin pathway and TGF β signalling pathway have also been previously shown to crosstalk via cAMP-response element-(CREB)-binding protein (CBP) and mediate EMT.³⁵⁹ TGF β treatment increased β -catenin levels in a dose-dependent manner,³⁶⁰ additionally, TGF β repressed GSK-3 β , which signals for ubiquitin-mediated proteasomal degradation of β -catenin, thus further increasing β -catenin levels. Furthermore, a recent study revealed that, in patient-derived melanoma cells, TGF β /SMAD, YAP/TAZ and Wnt/ β -catenin, all were required, in that hierarchical order, for the transition from proliferative to invasive phenotype.³⁶¹ Thus, it is conceivable that β -catenin could be an important downstream signalling modulator of the TGF β signalling pathway that may fine-tune EMT-like processes during melanoma metastasis.

6.1.5 β -catenin in melanoma CTC clusters

β -catenin is involved in cell-cell adhesion protein alongside cadherins and other adherens junctional proteins,³⁶² as an intracellular signal transducer,³⁶³ and as a regulator of gene transcription.³⁶⁴ β -catenin primarily relays signal of the canonical Wnt pathway.³⁶⁵ Wnt ligand binding to Frizzled family of receptors, with subsequent phosphorylation of AXIN and GSK-3 β , leads to the disassembly of the destruction complex that would otherwise target β -catenin to ubiquitin-mediated proteasomal degradation.³⁶⁶ As cytosolic β -catenin levels increase, free β -catenin molecules translocate to the nucleus, where they are involved in regulation of gene transcription in a TCF/LEF-dependent/independent manner throughout metazoans.³⁶⁷ In the absence of Wnt, β -catenin levels are kept low through proteasomal degradation.

Wnt/ β -catenin signalling is likely to play an important role in melanoma metastasis. Canonical Wnt/ β -catenin signalling has been shown to drive metastasis of BRAF-driven melanomas.³⁶⁸ β -catenin signalling was shown to be markedly increased during melanoma progression.³⁶⁹ In primary melanoma, β -catenin may induce MITF to regulate cellular proliferation.³⁷⁰ In metastatic melanoma, a recent study suggested that Wnt/ β -catenin signalling inhibited SOX10 expression and thereby reduced melanoma proliferation.³⁷¹ This is further supported by another study that highlighted that, in both primary and metastatic melanoma, activation of Wnt-3a/ β -catenin signalling resulted in a less proliferative

phenotype and decreased tumour volume.³⁷² Together, these studies suggest that β -catenin could be crucial for repressing the proliferative/melanocytic phenotype; the extent to which β -catenin may be involved in promoting the invasive/undifferentiated phenotype remains unclear.

Wnt/ β -catenin have been implicated in aggregation of both normal and cancer cells. In normal cardiac myocytes, Wnt/Frizzled-2 signalling was shown to induce aggregation via formation of cadherin/ β -catenin complexes.³⁷³ Induction of Wnt/ β -catenin signals as short pulses by a small molecule (CHIR99021) increased aggregation capability of induced pluripotent stem cells (iPSC).³⁷⁴

In breast cancer, CTC clusters isolated from patients expressed high levels of plakoglobin and β -catenin.³⁴⁸ Here, the authors concluded that the poor prognosis due to high expression of plakoglobin and low E-cadherin expression was likely to be because of Wnt/ β -catenin and EMT-related signalling events. Moreover, in breast cancer, desmoglein-2 may promote CTC clustering and distant colonisation.³⁷⁵ The authors highlighted that hypoxia and HIF1 α may suppress gene expression of *DSG2* (the gene that codes for desmoglein-2). Notably, when hypoxic stress was alleviated, gene expression of *DSG2* was no longer suppressed, and CTCs reverted to clustering and distant colonisation. Interestingly, desmoglein-2 was shown to directly interact with β -catenin molecules and sequesters them to the peripheral membrane in order to suppress EMT induction.³⁷⁶ Moreover, hepatocellular carcinoma CTC clusters exhibited high levels of activation of Wnt/ β -catenin signalling.³⁷⁷ Single CTCs of hepatocellular carcinoma showed minimal Wnt/ β -catenin activation. These findings are indicative of the larger role β -catenin plays in CTC clustering and metastasis.

A recent study revealed that *CTNNB1*, the gene that codes for β -catenin, was highly overexpressed in single CTCs isolated from melanoma patients compared to non-disease donor blood cells.³⁷⁸ Involvement of β -catenin in melanoma CTC clusters, however, still remains largely unexplored. In this thesis, previous chapters highlighted that 4F2hc, Galectin-3 and MMP2 play important roles in the multicellular aggregation-disaggregation process of metastasis (ADPM) of FM3 melanoma cells. β -catenin signalling was shown to lie downstream of 4F2hc/Galectin-3/integrin in HeLa cervical cancer cells.²²⁰ It is not clear whether β -catenin lies downstream of 4F2hc/Galectin-3/integrin signalling or is even involved in FS surface-induced ADPM of FM3 cells.

Therefore, firstly, the present chapter will investigate whether β -catenin is involved in ADPM of FM3 cells. Secondly, as β -catenin may regulate EMT in melanoma, effect of EMT status on ADPM will be investigated using TGF β -treated FM3 cells, and by employing an EMT model of

prostate cancer cells that was previously generated in our laboratory.³⁷⁹ Thirdly, since β -catenin mediates a whole host of upstream signalling, including Wnt-dependent and independent signalling, and elicits a range of responses including transcriptional and cytosolic responses, changes in the β -catenin interactome during ADPM of FM3 cells will be explored in order to isolate key β -catenin-mediated responses. These investigations could highlight the extent to which β -catenin is involved in ADPM, potentially revealing whether if it is through EMT-related processes or something else entirely and could identify any β -catenin/EMT-related biomarkers that could be used to enrich and isolate melanoma CTC clusters. This chapter could shed light on how β -catenin and EMT-like processes could contribute to the grim prognosis associated with the presence of CTC clusters in melanoma patients.³⁸⁰

6.2 Results

6.2.1 β -catenin expression during FM3 multicellular aggregation-disaggregation

The Wnt/ β -catenin signalling pathway has been shown to increase in metastatic melanoma cells compared to nevi, primary, or non-metastatic cells.³⁶⁹ Moreover, it was shown that β -catenin plays an important role downstream of 4F2hc/galectin-3/integrin-mediated signalling in HeLa cervical cancer cells.²²⁰ Since 4F2hc and galectin-3 levels were increased during multicellular aggregation of FM3 melanoma cells (Chapter 4), it was hypothesised that β -catenin levels would also increase during aggregation. RT-qPCR showed no significant change in the levels of β -catenin mRNA during aggregation (between 0 to 24h) (Fig. 6.1 A); however, there was a significant decrease during disaggregation (between 48 – 72h). Quantitative SWATH mass spectrometry showed no significant difference in β -catenin protein levels (Fig. 6.1 B) during aggregation (FS-24h vs TCP-24h) or disaggregation (FS-72h vs FS-24h) of FM3 cells.

The TGF β cytokine has been shown to enhance β -catenin signalling in tumoral and non-tumoral fibroblasts;³⁶⁰ β -catenin protein levels increased in a dose-dependent manner following TGF β treatment. Increase in production of TGF β by melanoma has been associated with disease progression and malignancy.^{381,382} During malignant transformation, melanoma shows a transition from a proliferative melanocytic phenotype to an invasive mesenchymal-like phenotype; this transition was shown to be regulated by the cross-talk of TGF β /SMAD, YAP/TAZ, and β -catenin signalling pathways.³⁶¹ Therefore, it was hypothesised that TGF β treatment would promote FM3 multicellular aggregation by increasing β -catenin levels. In this study, treating FM3 multicellular aggregates with 10 ng/mL of TGF β , a concentration sufficient to induce expression of β -catenin,³⁸³ resulted in a significant increase in aggregate

to non-aggregate ratio (Fig. 6.1 C). Cells were treated with the cytokine for 24 h. Notably, at 72h, where disaggregation was expected to take place, there was a significant increase in aggregate to non-aggregate ratio.

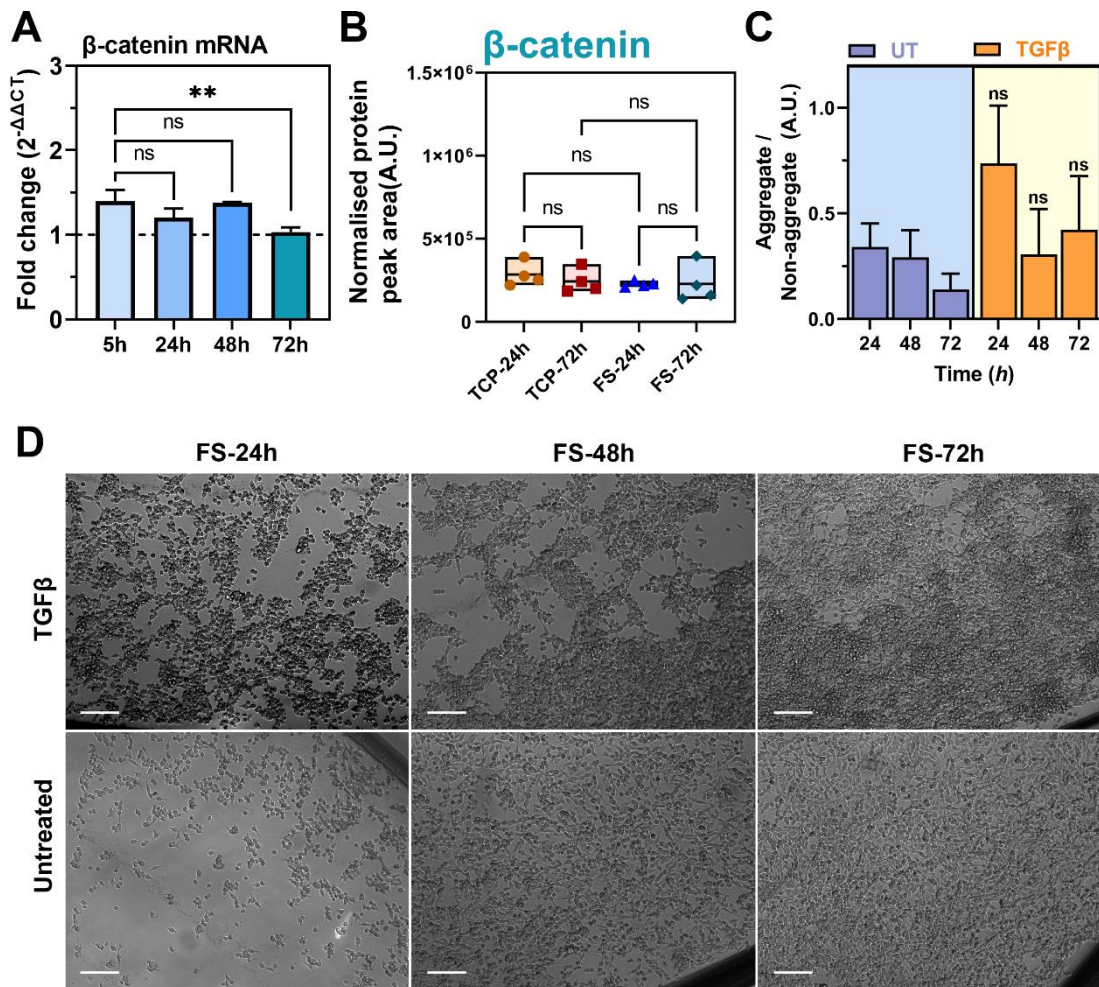


Fig. 6.1 Increased β-catenin levels promote FM3 multicellular aggregation. (A) Periodic expression of β-catenin mRNA during aggregation (5-24h) vs disaggregation (48-72h) as measured by RT-qPCR, n=3. Fold Change ($2^{-\Delta\Delta CT}$) represents comparison of FS surfaces vs TCP surfaces. (B) Change in β-catenin levels during FM3 cellular aggregation (FS-24h vs TCP-24h) and disaggregation (FS-72h vs FS-24h) as measured by mass spectrometry, n=4. (C-D) Effect of TGFβ treatment (10 ng/mL) on FM3 multicellular aggregation-disaggregation, (C) quantification of the micrographs depicted as ratio of aggregates (% area) to non-aggregates (% area), N = 5. (D) representative micrographs (scale = 200 μm), A.U.: arbitrary units. Brown-Forsythe and Welch ANOVA tests (equal SDs not assumed) with Dunnett T3 post-hoc multiple comparison test for RT-qPCR and mass spectrometry (A – B), and Ordinary Two-way ANOVA with Tukey post-hoc multiple comparisons were carried out for C. FS: fluoroalkylsilica, TCP: tissue culture polystyrene.

6.2.2 EMT in FM3 multicellular aggregation-disaggregation

TGF β has been shown to induce EMT and EMT-like processes; treatment of epithelial cells with TGF β induced a transformation from a cuboidal morphology to an elongated spindle morphology.³⁸⁴ This morphological change was accompanied by a decrease in epithelial markers and an increase in mesenchymal markers such as fibronectin and vimentin. As TGF β treatment resulted in increased aggregation, it was hypothesised that mesenchymal markers would be upregulated, and epithelial markers would be downregulated in FM3 multicellular aggregates. To investigate this, western blot, RT-qPCR, and quantitative mass-spectrometry were used for observing changes in epithelial markers such as E-cadherin and ZO-1, and in mesenchymal markers such as fibronectin, N-cadherin, slug, snail, vimentin, and ZEB1,³¹¹ during ADPM of FM3 cells. As SMAD family of proteins are signalled by TGF β receptors,³⁸⁵ these were also considered during this investigation.

Western blot analyses showed that the mesenchymal markers, fibronectin, N-cadherin, vimentin, and ZEB1 were not upregulated during aggregation (FS-24h vs TCP-24h) (Supplementary Fig. 6.1 A - C). β -catenin and vimentin were downregulated during disaggregation (FS-72h vs FS-24h) (Supplementary Fig. 6.1 A - C). The mesenchymal markers, transcription factors slug and snail, were not detected (Supplementary Fig. 6.1 A - B). RT-qPCR revealed that the mesenchymal marker *fibronectin* mRNA levels were significantly increased during disaggregation (Supplementary Fig. 6.1 D). Quantitative mass spectrometry showed no significant difference in cytosolic vimentin, SMAD2/4, however matrisomal vimentin levels significantly reduced during aggregation and increased during disaggregation (Supplementary Fig. 6.1 E - H). These results reject the hypothesis that mesenchymal markers would be upregulated during aggregation. The epithelial marker ZO-1 was downregulated during aggregation and upregulated during disaggregation (Supplementary Fig. 6.1 B). This result, however, is in line with the hypothesis.

An important hallmark of EMT during the cancer metastatic cascade is the upregulation of N-cadherin and downregulation of E-cadherin; this process is referred to as the 'cadherin switch'.³⁸⁶ To investigate whether the cadherin switch occurs during ADPM of FM3 cells, immunofluorescence, quantitative mass spectrometry, and RT-qPCR observations were used for this analysis. E-cadherin and N-cadherin immunofluorescence revealed no significant change in expression of these two proteins during ADPM of FM3 cells (Supplementary Fig. 6.2 A & B). Mass spectrometry confirmed no significant change in protein levels of N-cadherin (Supplementary Fig. 6.2 C); E-cadherin proteins were not detected. At the transcriptomic level, there was also no change in levels of *E-cadherin* mRNA and *N-cadherin* mRNA (Supplementary Fig. 6.2 D & E) during ADPM of FM3 cells.

Furthermore, hypoxia has been shown to stimulate TGF β activity.³⁸⁷ Hypoxia also was shown to induce EMT in cancers via HIF-1 α .³⁸⁸ Therefore, it was hypothesised that, under hypoxic conditions, FM3 multicellular aggregation would be enhanced. However, there was no difference in both aggregation and disaggregation of FM3 cells under hypoxic conditions compared to normoxic conditions (Supplementary Fig. 6.3).

6.2.3 Effect of EMT status on ADPM response of prostate cancer cells

Previously in our laboratory, stable epithelial (P5B3) and mesenchymal (P4B6B) subclonal populations were generated from the OPCT-1 prostate cancer cell line.³⁷⁹ P5B3 cells express high levels of E-cadherin and β -catenin compared to P4B6B cells;³⁸⁹ in contrast, P4B6B cells express high levels of fibronectin and vimentin compared to P5B3 cells.³⁸⁹ To investigate how EMT status (epithelial vs mesenchymal) and β -catenin levels (high in P5B3 vs low in P4B6B) affect ADPM, P5B3 and P4B6B cells were cultured upon FS and TCP surfaces. Upon TCP surfaces, P5B3 cells assumed a cuboidal morphology akin to cuboidal epithelial cells, and P4B6b cells assumed spindle-like morphology akin to that of mesenchymal cells (Fig. 6.2 A). Both cells adhered and grew as a monolayer upon TCP surfaces. Upon the FS surface, at 24h, both P5B3 and P4B6B cells formed aggregates; however, P5B3 cells underwent complete disaggregation by 72h, whereas P4B6B cells underwent minimal disaggregation. Since P5B3 cells expressed high levels of β -catenin,³⁸⁹ and decreased β -catenin expression was associated with disaggregation in FM3 cells (Fig. 6.1 A), it was hypothesised that P5B3 cells would display enhanced multicellular aggregation. However, P5B3 cells showed a significantly reduced aggregate/non-aggregate ratio compared to P4B6B cells at both 24 and 72h time points (Fig. 6.2 B).

FM3 melanoma cells showed no cadherin switching during ADPM (Supplementary Fig. 6.2 A & B). To test whether this was true also for P5B3/P4B6B cells, immunofluorescence staining was carried out. Upon both FS and TCP surfaces, P5B3 cells expressed high levels of E-cadherin, whereas P4B6B cells expressed high levels of N-cadherin (Supplementary Fig. 6.4 A & B). There was no significant difference in E-cadherin expression (in P5B3) or N-cadherin expression (in P4B6B) during the course of ADPM of P5B3 or P4B6B cells (Supplementary Fig. 6.4 B).

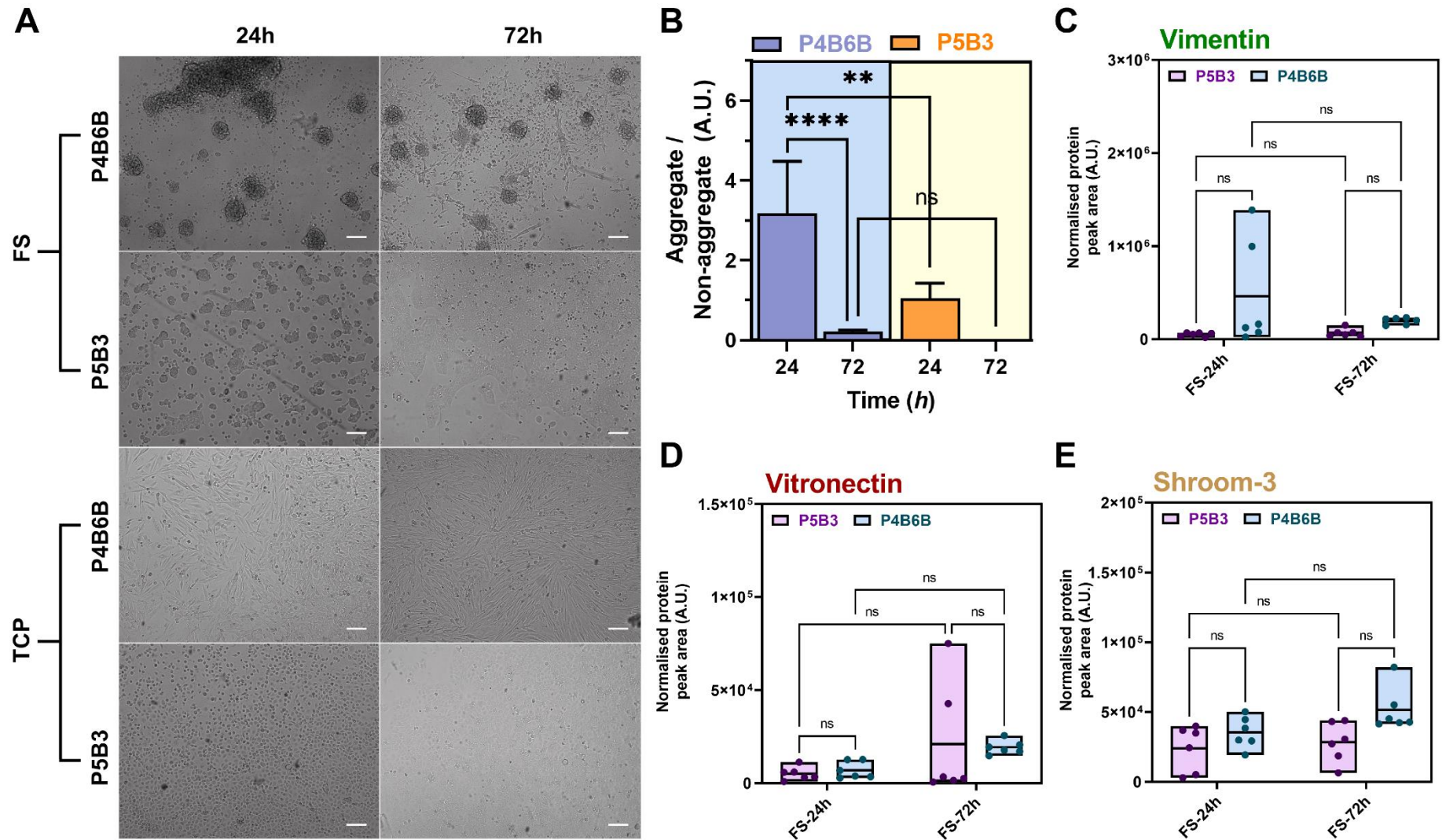


Fig. 6.2 Mesenchymal-like cells favour aggregation. (A-B) P4B6B mesenchymal-like subclones show increased aggregation compared to their P5B3 epithelial-like counterparts, (A) representative micrographs (scale = 200 μ m), (B) quantification of the micrographs depicted as ratio of aggregates (% area) to non-aggregates (% area), N = 5. (C-E) Change in (C) Vimentin, (D) Vitronectin, (E) Shroom-3 levels during P5B3 and P4B6B cellular aggregation (at FS-24h) and disaggregation (at FS-72h) as measured by quantitative SWATH mass spectrometry, N = 6. Ordinary Two-way ANOVA with Tukey post-hoc multiple comparisons were carried out for B - E. A.U.: arbitrary units. FS: fluoroalkylsilica, TCP: tissue culture polystyrene.

ADPM of FM3 cells was associated with changes in levels of the matrisomal proteins fibronectin and vitronectin, as well as matrix remodelling. To outline changes in matrisomal proteins that could be associated with ADPM of EMT status or difference in β -catenin levels, quantitative mass spectrometry was carried out using matrix harvested from P4B6B or P5B3 cells during ADPM. Multicellular disaggregation, rather than aggregation, set these two cell lines apart in their ADPM (Fig. 6.2 A). Investigation of disaggregation (FS-72h vs FS-24h) revealed that matrisomal vimentin levels significantly increased during disaggregation of P4B6B cells compared to P5B3 (Fig. 6.2 C). Matrisomal vitronectin levels increased in P4B6B cells during disaggregation (P4B6B FS-72h vs FS-24h); however, no significant difference was observed when P4B6B cells were compared to P5B3 cells at FS-72h (Fig. 6.2 D). Lastly, matrisomal shroom-3 levels significantly increased in P4B6B cells compared to P5B3 cells at 72h (Fig. 6.2 E).

6.2.4 β -catenin interactome changes during ADPM of FM3 cells

To investigate the role β -catenin plays in ADPM, other than as a mediator of TGF β signalling or EMT, proteins likely to be part of the interactome of β -catenin in ADPM need to be considered. Comparison of significantly altered proteins from quantitative mass spectrometry of FM3 cells, with that of known β -catenin interactors (obtained from experimental evidence from BioGRID³⁹⁰ Fig. 6.3 A), revealed 23 proteins in aggregation, 98 in disaggregation, and 12 in both aggregation and disaggregation, as potential candidates of the β -catenin interactome. To narrow down to a few important proteins, most differentially expressed (Log_2 fold-change) and most significantly altered ($-\text{Log}_{10}$ p-value) proteins were considered (Fig. 6.3 B & C). This revealed the following proteins (UniProt ID) as important in aggregation (Fig. 6.3 B): SPF45, HS105, LEG3 (Galectin-3), LDHB, PML, PUR9, PABP1, ZO1, and DNMT1; and in disaggregation (Fig. 6.3 C): RLA2, TCP4, H12, MRP, RL11, SQSTM, and UACA.

Differential expression of proteins due to ADPM needed to be separated out from differential expression due to other effects, for example confluency. To carry this out, quantified protein amount (normalised protein peak area) changes associated with aggregation (FS-24h vs TCP-24h) and disaggregation (FS-72h vs FS-24h) were compared. This revealed that PML (Fig. 6.3 D), PABP1 (Fig. 6.3 E), PUR9 (Fig. 6.3 G), SPF45 (Fig. 6.3 H), and LDHB (Fig. 6.3 I) as important for aggregation, RL11 (Fig. 6.3 F) for disaggregation, and HS105 (Fig. 6.3 J) as important for both aggregation and disaggregation. Other proteins from the Volcano plot analyses were also considered (Supplementary Fig. 6.5 A – H); however, they were not chosen for further

analyses as the differential expression was also seen to be due to confluency effects (TCP-72h vs TCP-24h).

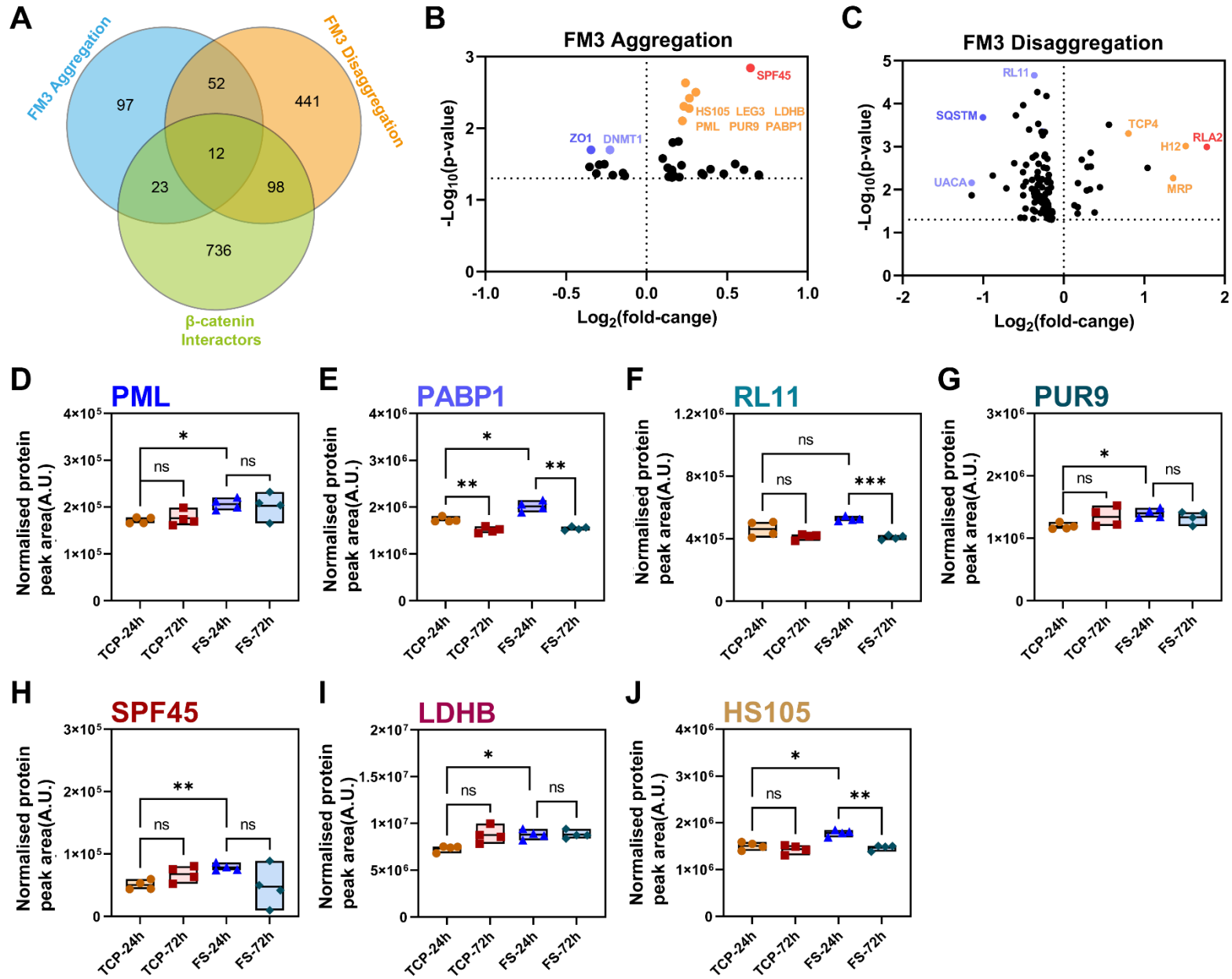


Fig. 6.3. β -catenin interactome changes during FM3 multicellular aggregation-disaggregation. (A) Comparison of β -catenin interactome (obtained from BioGRID with proteome of FM3 multicellular aggregation and disaggregation obtained from SWATH mass spectrometry, reveals changes in β -catenin interactome during ADPM. (B-C) Volcano plots reveal important β -catenin interactors (dotted line along the y-axis denotes p-value of 0.05); (B) Interactors involved in FM3 aggregation (FS-24h vs TCP-24h), and (C) Interactors involved in FM3 disaggregation upon FS surfaces. (D-J) Changes of β -catenin interactors observed during ADPM of FM3 cells, measured by SWATH mass spectrometry, N=4, Brown-Forsythe, and Welch ANOVA tests (equal SDs not assumed) with Dunnett T3 post-hoc multiple comparison test: (D) PML, (E) PABP1, (F) RL11, (G) PUR9, (H) SPF45, (I) LDHB, (J) HS10. Brown-Forsythe and Welch ANOVA tests (equal SDs not assumed) with Dunnett T3 post-hoc multiple comparison test for D – J was carried out. A.U. Arbitrary units, ADPM: Aggregation-Disaggregation Process of Metastasis, FS: fluoroalkylsilica, SWATH: Sequential Window Acquisition of All Theoretical, TCP: tissue culture polystyrene

6.2.5 β -catenin interactome affects melanoma survival outcome

To assess whether the important β -catenin interactors, expression of which altered during ADPM of FM3 cells, are also likely to play important roles in melanoma metastasis, *in silico* analyses were performed using TCGA melanoma datasets (SKCM) (TCGA research network). The following results shown are in part based on data generated by the TCGA Research Network (<https://www.cancer.gov/tcga>). Patient survival datasets were obtained from OncoLnc.²⁸⁷ Each patient survival datasets were divided into two subsets using the median expression of β -catenin interactors (high > median, low < median), and Kaplan-Meier (KM) plots were generated to correlate effect of high vs low expression with melanoma patient survival (Fig. 6.4 A – H). Significant difference in survival was observed for patients presented with low expression of PML (Fig. 6.4 B), and high expression of LDHB (Fig. 6.4 G). No significant difference in survival was observed for the other β -catenin interactome proteins: β -catenin (Fig. 6.4 A), PABP1 (Fig. 6.4 C), RL11 (Fig. 6.4 D), PUR9 (Fig. 6.4 E), SPF45 (Fig. 6.4 F), and HS105 (Fig. 6.4 H).

RNAseq gene expression datasets from clinical studies of melanoma (N = 1939) and metastatic melanoma (N = 358) were obtained from cBioPortal.²⁸⁶ The studies normalised the RNAseq datasets in a different order; melanoma datasets were normalised to the read depth that was mapped first then to individual gene expression to give 'reads per kilobase per millions mapped' (RPKM), and metastatic melanoma datasets were normalised to individual gene expression first then to read depth to give 'transcript per million' (TPM). Due to this, a further normalisation to a reference gene (GAPDH) was carried out, to be able to compare the melanoma dataset with that of the metastatic dataset, to give a ratio of Gene of interest (GoI) mRNA expression to GAPDH mRNA expression (Fig. 6.5 A – H). The gene expression of the corresponding proteins, β -catenin (Fig. 6.5 A), PML (Fig. 6.5 B), PABP1 (Fig. 6.5 C), RL11 (Fig. 6.5 D), PUR9 (Fig. 6.5 E), SPF45 (Fig. 6.5 F), and HS105 (Fig. 6.5 H), were significantly higher in metastatic melanoma compared to melanoma. No significant difference was observed for LDBH (Fig. 6.5 G).

Risk score (meta Z-score) associated with melanoma (Z_1) and metastatic melanoma (Z_2) were obtained from PRECOG.³⁹¹ PRECOG uses the following data sets: for melanoma, PMID 20460471¹²⁸ and PMID 18505921;³⁹² and for metastatic melanoma PMID 18505921³⁹² and PMID 19915147.¹³⁰ 'Metastasis factor' ($Z_2 - Z_1$) was generated to determine the risk associated with components of the β -catenin interactome in their contribution to metastasis of melanoma. This analysis revealed RL11 as the most adverse β -catenin interactor, and SPF45 as the second most, that are likely to induce metastasis of melanoma (Fig. 6.6).

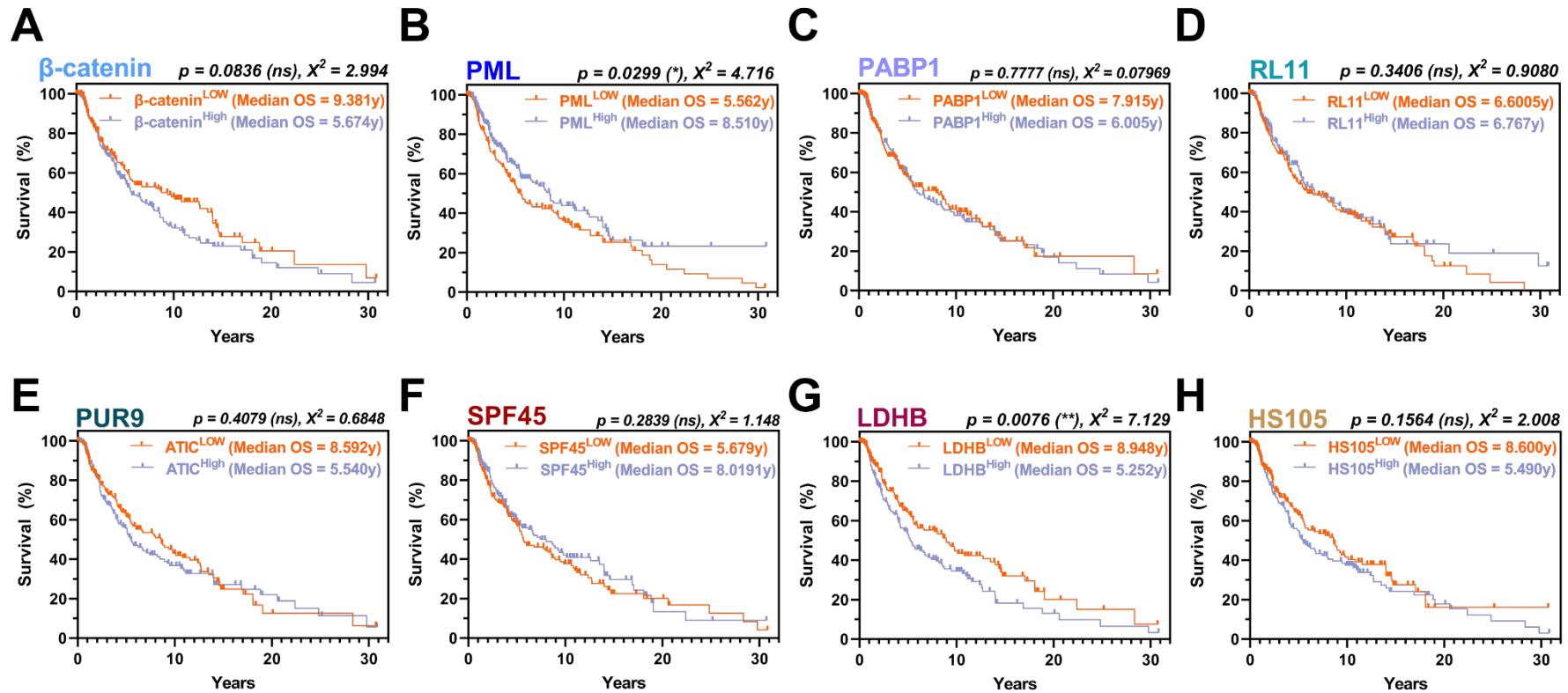


Fig. 6.4. β -catenin interactome expression on survival outcome of melanoma patients. (A – H) Data obtained from OncoLnc from multiple melanoma RNA-sequencing and patient survival studies, to outline survival outcome associated with high vs low expression of the following proteins: (A) β -catenin, (B) PML, (C) PABP1, (D) RL11, (E) PUR9, (F) SPF45, (G) LDHB, and (H) HS105. Median Overall Survival (OS) scores, high vs low expression statistics (χ^2 and p-values) were determined using Log-Rank (Mantel-Cox).

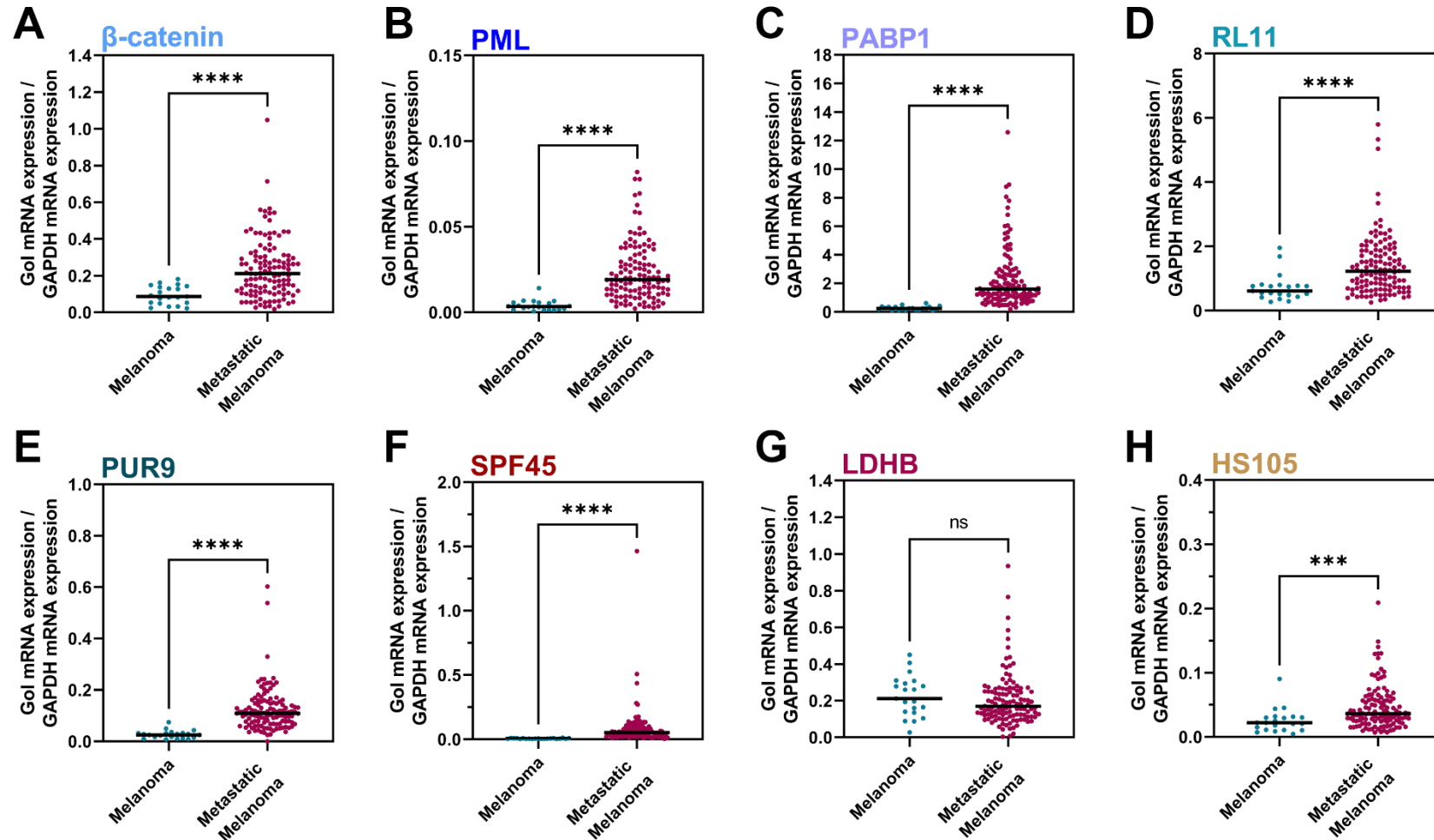


Fig. 6.5. β -catenin interactome expression increased in metastatic melanoma patients. (A – H) Data obtained from cBioPortal from multiple melanoma and metastatic melanoma RNA-sequencing and patient survival studies, to identify difference in expression between melanoma and metastatic melanoma in the following proteins: (A) β -catenin, (B) PML, (C) PABP1, (D) RL11, (E) PUR9, (F) SPF45, (G) LDHB, and (H) HS105. Student's T-tests (two-tailed distribution, heteroscedastic) were carried out for A – H. Gol: Gene of interest

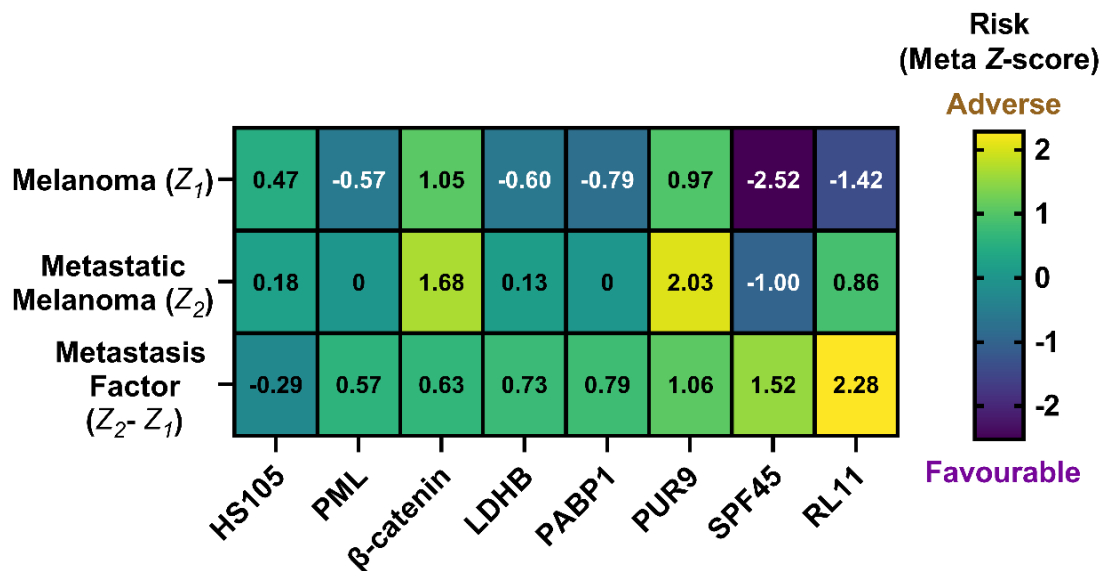


Fig. 6.6 Melanoma metastasis risk associated with β -catenin interactome. (A) Clinical melanoma and metastatic melanoma Z-score (meta) obtained from PRECOG tool for β -catenin interactome. Adjusted meta Z-score or ‘metastasis score’ ($Z_2 - Z_1$) calculated from Z-score of melanoma (Z_1) and metastatic melanoma (Z_2).

6.2.6 β -catenin-mediated transcriptional regulation of ADMP

Wnt/ β -catenin pathway depends upon many different transcription factors, the TCF/LEF family of proteins being the primary ones and FOXO4 in certain cases, to regulate transcription of target genes.³⁹³ Several bioinformatics tools were used in the present study for investigating which transcription factors and co-regulators could be relaying β -catenin-dependent and independent signalling to the transcriptional machineries involved in ADPM of FM3 cells.

The PANTHER classification system 17.0³⁹⁴ was used for the identification of transcription regulatory proteins within the significantly altered proteome during ADPM of FM3 cells as obtained from quantitative mass spectrometry, using the gene ontology terms ‘gene-specific transcriptional regulators’ (class ID PC00264). This analysis revealed 4 transcriptional regulators in aggregation (FS-24h vs TCP-24h; Fig. 6.7 A): FHL2, CEBPZ, MTA2, and STAT3; 8 transcriptional regulators in disaggregation (FS-72h vs FS-24h; Fig. 6.7 B): AFF4, CEBPZ, FHL2, GATAD2B, MAFF, MTA3, NCOA5, and STAT1.

Next, the hTFtarget tool³⁹⁵ was used to identify the number of target genes within the significantly altered proteome during ADPM of FM3 cells as obtained from quantitative mass spectrometry that could be potential targets of the transcriptional regulators. The hTFtarget database consists of a comprehensive repertoire of human transcription factors, co-regulators, and their target genes, obtained from several chromatin immunoprecipitation

sequencing (ChIP-Seq) studies.³⁹⁵ This analysis revealed STAT1 and STAT3, and to a lesser extent MAFF and MTA3, as important transcriptional regulatory proteins that could be involved in ADPM of FM3 cells (Fig. 6.7 C).

Nuclear β -catenin can act as a transcriptional activator.³⁹⁶ Alongside the TCF/LEF family of proteins, such as TCF1 (encoded by *TCF7*), TCF1 α (encoded by *LEF1*), TCF3 (encoded by *TCF7L1*), and TCF4 (encoded by *TCFL2*), β -catenin can stimulate the transcription of genes responsible for important cellular processes including differentiation, proliferation and many more.³⁶⁷ The hTFtarget tool was used to determine the number of target genes within the significantly altered proteome during ADPM of FM3 cells as obtained from quantitative mass spectrometry, that could be potential targets of β -catenin and/or TCF/LEF family members. Compared to potential targets of STAT1 and STAT3 within the proteins that were significantly altered during ADPM of FM3 cells, the targets of β -catenin and two TCF/LEF members, TCF1 α and TCF4 were much lower (Fig. 6.7 D).

These results lead to the hypothesis that perhaps master transcriptional regulators other than the putative TCF/LEF members acting downstream of β -catenin could be involved in ADPM of FM3 cells. To discover these master regulators, transcription factors that could regulate STAT1, STAT3, MAFF, MTA3, β -catenin, TCF1 α , and TCF3, were obtained from hTFtarget tool and delimited by anatomical expression zones to skin. Frequency density diagram was plotted based on the number of literature evidence that were reported (Fig. 6.7 E). This revealed that SPI1, CTCF, and FOXA2 as potential master regulators of ADPM of FM3 cells (Fig. 6.7 E). Investigation of the number of targets within the significantly altered proteome during ADPM of FM3 cells as obtained from quantitative mass spectrometry, revealed that SPI1, CTCF, and FOXA2, had many more targets within the significantly altered proteome during ADPM of FM3 cells compared to STAT1, STAT3, β -catenin, TCF1 α , and TCF3.

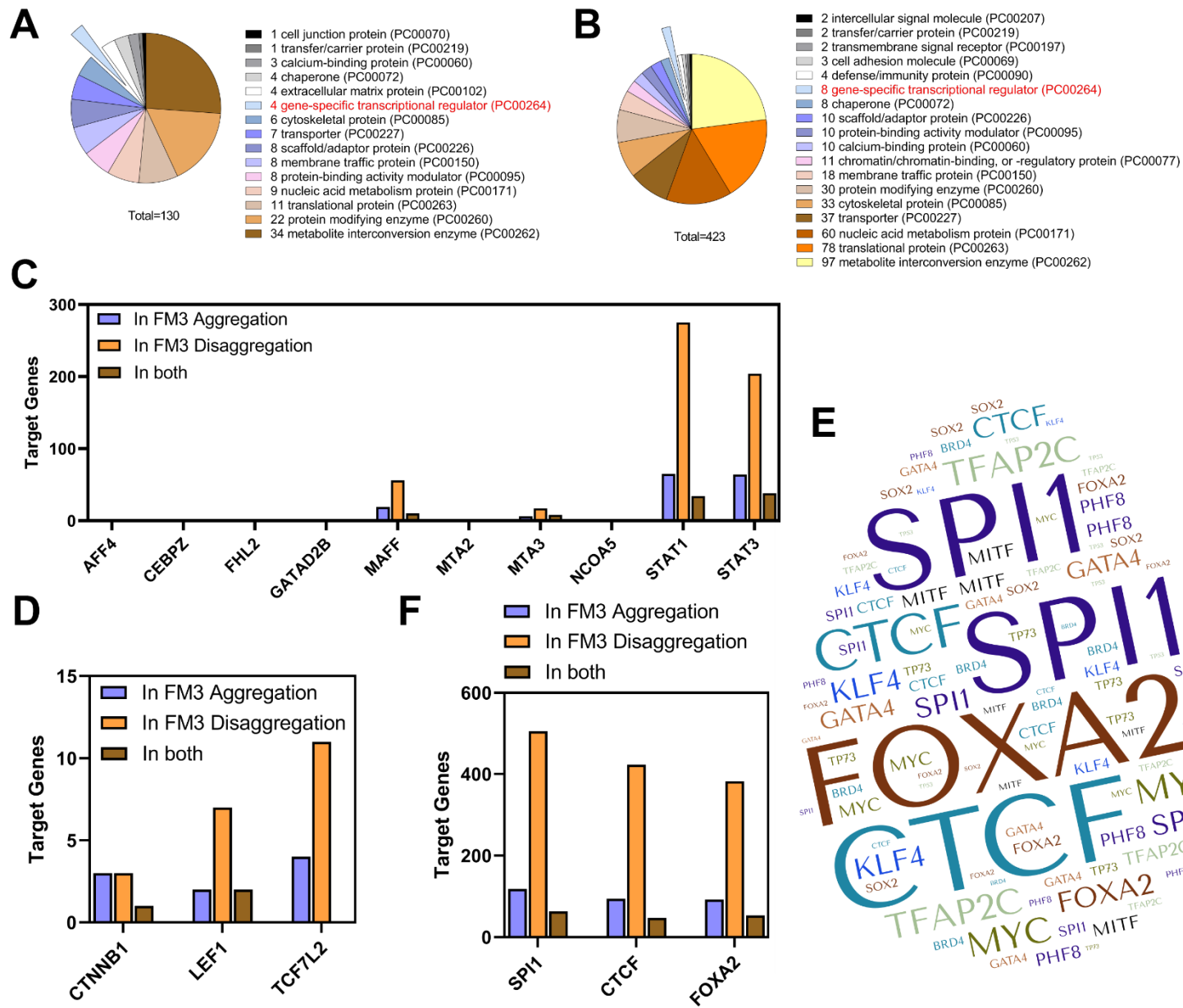


Fig. 6.7 Analysis of transcriptional regulation during ADPM of FM3 cells highlights SPI1 as the most influential master regulator. (A-B) Gene ontology-based classification of significantly altered proteome during ADPM of FM3 cells as obtained from quantitative mass spectrometry, classified using PANTHER classification system 17.0, during **(A)** aggregation (FS-24h vs TCP-24h), and during **(B)** disaggregation (FS-72h vs FS-24h). **(C)** Number of possible target genes of the transcriptional regulators (from gene ontology analysis), significantly altered during ADPM of FM3 cells, as identified using hTFtarget tool. **(D)** Number of possible target genes of *CTNBB1*, *LEF1*, and *TCFL2*, significantly altered during ADPM of FM3 cells, as identified using hTFtarget tool. **(E)** Frequency density of master transcriptional regulators, based on frequency of ChIP-Seq evidence (from hTFtarget tool), that interact with *STAT1*, *STAT3*, *MAFF*, *MTA3*, β -catenin, *TCF1a*, and *TCF3* in the skin. **(F)** Number of possible target genes of *SPI1*, *CTCF*, and *FOXA2*, significantly altered during ADPM of FM3 cells, as identified using hTFtarget tool.

6.3 Discussion

For many years, EMT was thought to spearhead the invasion-metastasis cascade of malignant tumour cells. When it comes to CTC clusters, though, the role of EMT does not seem as clear-cut. Single CTCs show mesenchymal-like characteristics;³⁹⁷ however, CTC clusters retain epithelial-like cell-cell connections as well as displaying mesenchymal-like invasive properties.³⁹⁸ This led to researchers concluding that CTC clusters could perhaps contain heterogenous phenotypes of epithelial and mesenchymal subpopulations,³⁹⁹ with some suggesting that the leading cells may be more mesenchymal-like in nature compared to the more epithelial-like tailing cells.³⁵⁰ Additionally, through single-cell sequencing, researchers have identified that single CTC and CTC clusters also show partial-EMT or hybrid phenotype, embellished with a high degree of EMT plasticity that allows phenotype switching, depending on spatiotemporal cues arising at various stages of the invasion-metastasis cascade.⁴⁰⁰ Though, some fundamental questions still remain unanswered: Does EMT status influence the formation of CTC clusters? What initiates metastases, EMT or CTC cluster formation, or is it a collaborative effort of both? Which EMT markers are important for CTC cluster formation, maintenance, and haematological transit?

β -catenin is a classical epithelial marker.⁴⁰¹ Through CREBP, β -catenin adjoins TGF β -signalling to Wnt signalling.³⁵⁹ Both TGF β -signalling, Wnt signalling, and their cross-talks have been heavily associated with EMT.⁴⁰² Interestingly, both TGF β -signalling and Wnt signalling have also been implicated in CTC clusters. Platelet-derived TGF β has been shown to induce EMT in CTC/platelet heterotypic clusters.⁴⁰³ Wnt/ β -catenin signalling has been shown to aggregate cardiac myocytes,³⁷³ and also hepatocellular carcinoma cells.³⁷⁷ As such, β -catenin likely lies at the nexus of EMT and CTC clusters – the two key strands of the invasion-metastasis cascade.

In melanoma metastasis, EMT-like processes regulate transition from a differentiated/melanocytic state to undifferentiated/mesenchymal state;⁴⁰⁴ this process is associated with the upregulation of key EMT-related markers.³³⁸ Similarly, Wnt/ β -catenin was shown to be crucial for metastasis of melanoma,³⁶⁸ as well as increased β -catenin-signalling events during melanoma progression.³⁶⁹ In melanoma CTC clusters, however, to the extent to which EMT-like processes and Wnt/ β -catenin signalling contribute to metastasis remains to be discovered. Therefore, the aim of this chapter was to investigate the role of EMT and β -catenin in melanoma CTC clusters, by using an *in vitro* surface-induced ADPM model of melanoma CTC clusters.

6.3.1 β -catenin is involved in multicellular aggregation of FM3 cells

β -catenin mRNA levels significantly decreased during FM3 multicellular disaggregation. This implies that β -catenin could play a larger role during aggregation, and levels were reduced during disaggregation as β -catenin was no longer needed to regulate this end of the process. This is further supported by the experiment in which FM3 cells were treated with TGF β cytokine, which resulted in an increased aggregate to disaggregate ratio. An assumption here was that TGF β treatment, similar to in fibroblasts,³⁶⁰ also increased the expression of β -catenin in FM3 cells. Here, further experimentation is needed, either at the transcriptomic level via RT-qPCR or at the proteomic level via western blot, to show the change in β -catenin levels with TGF β treatment in FM3 cells. In any case, the observation that β -catenin is associated with FM3 multicellular aggregation, is consistent with the earlier observations in breast cancer cells which showed high expression of β -catenin in plakoglobin^{high}/E-cadherin^{low} clusters.³⁴⁸

Similar to breast cancer clusters, FM3 cells also do not express E-cadherin. These observations imply that during multicellular aggregation, β -catenin may not be part of the E-cadherin/catenin adherens junction complex that mediates cell-cell contacts. Instead, β -catenin likely to be active within the cytoplasm or nucleus. As nuclear translocation of β -catenin often is due to Wnt signalling,⁴⁰⁵ or TGF β - signalling,⁴⁰⁶ or downstream of 4F2hc/galectin-3/integrin signalling,²²⁰ it could be that β -catenin might be responding to any of these pathways during aggregation. Since FM3 cells aggregated, as well as showed increased β -catenin levels, even without the need for external TGF β stimulation, TGF β -signalling might not be as important here; but TGF β -signalling could nonetheless work to enhance β -catenin-mediated responses. Platelet-derived,⁴⁰⁷ or other haematological or immune cell-derived,⁴⁰⁸ TGF β could sustain the clustered conformation during transit via lymph or blood circulation. Between 4F2hc/galectin-3/integrin signalling and Wnt signalling, though, only 4F2hc and galectin-3 levels, but not any of the Wnt ligands or Frizzled receptors, were increased during FM3 aggregation (see chapter 4). As such, it is more likely that β -catenin lies downstream of 4F2hc/galectin-3/integrin signalling rather than Wnt signalling during ADPM of FM3 cells.

6.3.2 EMT does not occur during ADPM of FM3 cells

TGF β that could be secreted from various stromal cells, such as fibroblasts, may induce EMT-like processes in cutaneous melanoma cells.⁴⁰⁹ Since TGF β treatment led to increased aggregate to non-aggregate ratio in FM3 cells, it seemed that perhaps TGF β is capable of driving EMT-like processes during ADPM. However, cell-cell signalling was upregulated during aggregation of FM3 cells, which invariably suggests that perhaps EMT, in its entirety, might not be as pertinent for multicellular aggregation. This led to the investigation of expression of epithelial and mesenchymal markers during ADPM of FM3 cells.

Mesenchymal markers, fibronectin, N-cadherin, vimentin, and ZEB1, were not upregulated during aggregation. Notable EMT-associated transcription factors, slug and snail, were not detected in FM3 cells. TGF β -driven mediators, SMAD2 and SMAD4, also showed no significant change in levels during ADPM. Additionally, FM3 cells showed no E-cadherin to N-cadherin switch during ADPM, which portends EMT-like events in epithelial cells.⁴¹⁰ Together, these observations imply that EMT-like processes do not take place during multicellular aggregation of FM3 cells. However, β -catenin and vimentin levels decreased during disaggregation, and fibronectin levels increased during disaggregation; this suggests that some EMT markers may still play vital roles in ADPM of FM3 cells.

6.3.3 P4B6B cells sustain aggregation via expression of vitronectin, vimentin and shroom-3

To probe influences of EMT and β -catenin in ADPM further, experiments were conducted using stable epithelial (P5B3) and mesenchymal (P4B6B) progeny of OPCT-1 prostate cancer cells. Both P5B3 and P4B6B clones aggregated at 24h. At 72h, P4B6B cells exhibited significantly higher aggregate to non-aggregate ratio compared to P5B3 cells, implying that perhaps mesenchymal cells are more likely to retain the aggregation state. An explanation for this observation is that P4B6B cells have been shown to express high levels of vimentin compared to P5B3 cells;³⁸⁹ indeed, vimentin-incorporated cytoskeletal architectures have been shown to be empowered with elasticity, which ultimately protects cells against compressive stress.⁴¹¹ Consistent with the present study, CTC clusters isolated from lung cancer patients exhibited strong expression of vimentin.⁴¹² Single CTC showed comparatively even higher expression of vimentin, suggesting that perhaps without the clustered conformation, more vimentin is required to withstand the sheer-stress of blood circulation.

P5B3 cells have been shown to express elevated levels of β -catenin compared to P4B6B cells.³⁸⁹ As an increase in *β -catenin* mRNA levels correlated with aggregation of FM3 cells, this led to the hypothesis that P5B3 cells would be more prone to aggregation than P4B6B cells. However, compared to P4B6B cells, P5B3 cells exhibited significantly reduced aggregate/non-aggregate ratio. This implies that mesenchymal-like state could be more important for multicellular aggregation than β -catenin expression, as the mesenchymal state already equips cells with the appropriate tools, such as vimentin expression, to aid cluster formation. Further experiments are needed here to rule out β -catenin in ADPM of the mesenchymal P4B6B; for example, measuring β -catenin levels in P4B6B cells during ADPM via western blot.

As P5B3 cells differed from P4B6B cells in their ability to disaggregate, and since extracellular matrix plays an important role in multicellular disaggregation,⁴¹³ exploring changes in matrisomal proteins is likely to explain the difference in disaggregation behaviour between these two cell lines. Levels of vitronectin significantly increased in P4B6B cells between 24h and 72h, however levels stayed the same in P5B3 cells. Perhaps, vitronectin-based scaffolds could be better suited to retain a clustered conformation. Alternatively, high levels of vitronectin could induce integrin α V β 3-dependent signalling,⁴¹⁴ that could promote and retain multicellular aggregation. Signalling via β 3 integrins has been shown to induce platelet aggregation.⁴¹⁵ Further investigation of scaffold proteins and their receptors is required to explore this 'out-side-in' integrin signalling that seemingly promotes differential multicellular aggregation-disaggregation responses depending on EMT status; indeed, different classes of integrins could be expressed on the cell surface based on EMT status or TGF β -signalling.⁴¹⁶

Matrisomal vimentin levels were higher in P4B6B cells than in P5B3 cells at 72h. Vimentin usually is restricted to the cytoplasm, where they line and reinforce cytoskeletal architecture.⁴¹⁷ However, vimentin can also be secreted into the extracellular space, which has been shown to bind to the cell surface of mesenchymal leader cells when they migrate during wound repair.⁴¹⁸ It could be that during ADPM of CTC clusters, mesenchymal leader cells could secrete vimentin into the matrix, where they could help complement migration. The exact mechanism in which vimentin could perform this extracellular function remains unclear; however, vimentin does seem to interact with certain cell surface receptors such as the IGF-1 receptor.⁴¹⁹

Matrisomal shroom-3 levels were significantly increased in P4B6B cells compared to P5B3 cells at 72h. Shroom-3 expression was shown to be downstream of TGF β / β -catenin/TCF7L2 signalling, and in turn shroom-3 facilitated canonical TGF β -signalling in renal tubular cells.⁴²⁰ This implies that perhaps mesenchymal cells secrete shroom-3 to sustain TGF β / β -catenin-

signalling, whereas epithelial cells lacking shroom-3 expression may not maintain sustained TGF β / β -catenin-signalling.

A limitation associated with these observations is that the intracellular mechanisms that could be taking place, that might also shed light onto the difference in aggregation-disaggregation behaviour of P5B3 and P4B6B cells, were not taken into consideration. During the matrisomal protein harvest, intracellular proteins were also isolated from P5B3 and P4B6B cells and were frozen in liquid nitrogen at -80 °C. Due to lack of time and resources, quantitative mass spectrometry of intracellular proteins was not carried out. However, this experiment could reveal cytoskeletal changes, signalling pathways, and cell-surface markers, that could be different between the epithelial and mesenchymal cells, potentially revealing the precise role epithelial and mesenchymal-like cells play in a mixed population within CTC clusters. For now, the conclusions that can be drawn is that mesenchymal-like cells may help CTC clusters retain the clustered conformation by increasing vitronectin, vimentin and shroom-3 levels, whereas epithelial-like cells within the CTC clusters could facilitate disaggregation; as of now, whether this is led by β -catenin expression in P5B3 cells remains unclear. Co-culturing P4B6B cells with P5B3 cells was shown to facilitate disaggregation of P4B6B cells.³⁸⁹ Further proteomic studies of the secretome/cell-lysate could reveal the manner in which the epithelial-like cells promote cellular disaggregation in a mixed heterogenous CTC cluster.

6.3.4 β -catenin interactors, LDHB, PML, PABP1, PUR9, SPF45, RL11, and HS105 involvement during ADPM of FM3 cells

In addition to mediating Wnt and TGF β -signalling, β -catenin serve diverse and multifaceted functions in cellular biology, ranging from contributing to the maintenance of cell polarity⁴²¹ to sustaining stemness.⁴²² In order to reveal these Wnt/TGF β -independent aspects of β -catenin in ADPM of FM3 cells, differentially expressed proteome during ADPM was compared against experimentally-established and known β -catenin interactors (obtained from BioGRID³⁹⁰). This analysis highlighted the following proteins as belonging to the β -catenin interactome partaking in ADPM: during aggregation, LDHB, PML, PABP1, PUR9, and SPF45 levels increased; during disaggregation, RL11 levels decreased; and HS105 levels increased during aggregation and decreased during disaggregation.

PML is a known tumour suppressor.⁴²³ It is required for the assembly of nuclear structures called the PML-nuclear bodies.⁴²⁴ PML has been shown to regulate p53/TP53.⁴²⁵ Cytoplasmic

PML affects TGF β -signalling.⁴²⁶ The gene encoding for PML (*PML*) is a target gene of the β -catenin and plakoglobin coactivated pathway⁴²⁷ (Fig. 6.8). In colorectal cancers, β -catenin inhibits the tumour suppressor function of PML.⁴²⁸ A recent study showed that degradation of PML, induced by PCI Domain Containing 2 (PCID2) protein, induced Wnt/ β -catenin signalling, and suppressed the ARF-p53 pathway.⁴²⁹

60S ribosomal protein L11 (RL11) is a component of the large ribonucleoprotein complex, involved in protein synthesis.⁴³⁰ RL11 links activation of p53/TP53 to ribosomal biogenesis.⁴³¹ RL11 has been shown to promote nucleolar translocation of PML⁴³² (Fig. 6.8). Knockdown of RL11 increased the level of *c-myc* mRNA.⁴³³ β -catenin signalling has been associated with stabilisation of *c-myc* mRNA via coding region instability determinant (CRD)-binding protein (CRD-BP).⁴³⁴ It remains unclear, however, whether RL11 binds to CRD-BP and acts downstream of β -catenin signalling. *C-myc* oncoproteins have been shown to localise to PML-nuclear bodies,⁴³⁵ implying that *c-myc* could be regulated at the post-transcriptional level via PML, and at the translational level via RL11. Since constitutive activation of *c-myc* is associated with proliferation of cancer cells⁴³⁶ and regulation of *MYC* (encodes *c-myc*) gene expression by aberrant Wnt/ β -catenin-signalling in cancers,⁴³⁷ it is likely that β -catenin could coordinate ADPM to cellular proliferation via this intricate multilevel RL11/PML-dependent regulation of *c-myc* (Fig. 6.8).

Polyadenylate-binding protein 1 (PABP1) is involved in mRNA turnover, by regulating mRNA metabolism and stability.⁴³⁸ Through affinity capture mass spectrometry, PABP1 was shown to be one of the proteins affected in the β -catenin-dependent signalling networks active within cancers.⁴³⁹ In hepatocellular carcinoma, PABP1 functioned as an effector of the small nucleolar RNA host gene 14 (SNHG14) oncogene.⁴⁴⁰ Another study highlighted that SNHG14 promotes hepatocellular carcinoma growth and metastasis via Wnt/ β -catenin pathway.⁴⁴¹ Together, these findings give some hints towards PABP1/ β -catenin interaction, be it direct or indirect via SNHG14. In any case, increased PABP1 levels during aggregation and decreased levels during disaggregation suggests that β -catenin interaction with PABP1 could prepare cells for mRNA processing and protein synthesis required for accommodating the vast proteomic changes accompanying ADPM of FM3 cells (Fig. 6.8).

PUR9, also known as 'bifunctional purine biosynthesis protein ATIC' and '5-Aminoimidazole-4-Carboxamide Ribonucleotide Formyltransferase/IMP cyclohydrolase (AICARFT/IMP Chase)', enzymatic activity of which catalyses the penultimate and last step of the *de novo* purine biosynthesis.⁴⁴² The link between PUR9 and β -catenin is not clear. However, evidence from affinity capture mass spectrometry lends some support towards this link.⁴³⁹ In addition, a study highlighting that methylenetetrahydrofolate dehydrogenase 2 (MTHFD2) knockdown in

lung cancer cells reduced tumorigenesis and stem-like properties, as well as notable accumulation of PUR9 and significant reduction in the expression of β -catenin.⁴⁴³ This implies expression of β -catenin could be tied to purine biosynthesis and cell replication, possibly via MTHFD2 and PUR9 (Fig. 6.8); increased levels of PUR9 during aggregation could prepare the cells for coordination of ADPM with cellular replication and proliferation.

Splicing factor 45 (SPF45) is an RNA binding protein, a component of the spliceosome complex, that is involved in alternate splicing by using cryptic splice sites.⁴⁴⁴ In addition to the support from SPF45- β -catenin interaction from affinity mass spectrometry,⁴³⁹ further evidence comes from experiments that suggests Jun N-terminal kinase 1 (JNK1) and p38 α MAPK could phosphorylate SPF45.⁴⁴⁵ Notably, JNK1 was associated with negative regulation of Wnt/ β -catenin pathway via GSK3 β ,⁴⁴⁶ and p38 α MAPK was also shown to regulate Wnt/ β -catenin pathway via inactivation of GSK3 β .⁴⁴⁷ These findings indicate that SPF45 and β -catenin, at the very least, could be part of the same network that couples Wnt signalling to protein synthesis. Increased SPF45 levels during aggregation of FM3 cells was likely due to accommodate the increased protein proteomic changes accompanying ADPM.

L-lactate dehydrogenase B chain (LDHB) is a component of lactate dehydrogenase, under normal conditions such as during oxidative phosphorylation, interconverts pyruvate and lactate with concomitant interconversion of NADH and NAD⁺.⁴⁴⁸ Cancer cells predominantly gain their energy from aerobic glycolysis (Warburg effect) as opposed to citric acid cycle/oxidative phosphorylation.⁴⁴⁹ As such, lactate dehydrogenases serve crucial role in cancers;⁴⁵⁰ in melanoma, a high level of glucose uptake and glycolysis lead to increased cytosolic pyruvate levels, and subsequent increased lactate dehydrogenases activity results in increased lactate fermentation.⁴⁵¹ Lactate is beneficial to cancer cells in many ways, such as induction of angiogenesis through activation of the vascular endothelial growth factor (VEGF),⁴⁵² and upregulation and activation of TGF β .⁴⁵³ Mass spectrometry of co-immunoprecipitated β -catenin complexes revealed that LDHB was associated with β -catenin within this complex.⁴⁵⁴ This indicates that β -catenin could couple cellular metabolism to ADPM via interaction with LDHB. In addition, increased LDHB levels during aggregation of FM3 cells points towards high lactate fermentation and subsequent incorporation into biomass.

Heat shock protein 105 kDa (HS105) is a member of the HSP70 superfamily⁴⁵⁵ and a nucleotide-exchange factor for certain chaperone proteins, such as HSPA1A and HSPA1B.⁴⁵⁶ Under stress, HS105 was shown to inhibit aggregation of denatured proteins.⁴⁵⁷ HS105 is a component of the β -catenin-degradation complex.⁴⁵⁸ Additionally, HS105 could recruit protein phosphatase 2A (PP2A) to dephosphorylate β -catenin,⁴⁵⁸ subsequently preventing phosphorylation-dependent ubiquitination and degradation of cytosolic β -catenin, leading to

increased β -catenin-signalling. HS105 levels increased in multicellular aggregation of FM3 cells and decreased during disaggregation. Aggregation/Stress-induced HS105 upregulation is likely to enhance β -catenin signalling. Decreased levels of HS105 during disaggregation of FM3 cells at 72h, points towards low levels of phosphorylation of β -catenin, which might or might not be via PP2A in FM3 cells; this is in line with the reduction in *β -catenin* mRNA levels observed during disaggregation. Collectively, these observations suggest that aggregation and stress-induced upregulation of HS105 upregulation are likely to enhance β -catenin signalling in FM3 cells.

It is unclear whether the above-mentioned β -catenin interactors indeed bind directly to β -catenin in FM3 cells. Co-immunoprecipitation experiments could highlight direct binding. β -catenin knock-out and observing changes in the interactors could lend further support to co-expression, and dual-stained immunofluorescence could reveal co-localisation. Regardless, the present study has highlighted co-expression of β -catenin and the above-mentioned interactors during ADPM of FM3 cells and gave a glimpse into the number of ways in which the β -catenin interactome could regulate cellular metabolism (via LDHB), protein synthesis (via SPF45 and PABP1), cellular replication (via PUR9), cellular proliferation (via PML and RL11), and stress-sensing/induced enhancement of β -catenin signalling (via HS105). Further research is needed to address how non-adherence/aggregation-induced stress is sensed by HS105 in CTC and CTC clusters.

6.3.5 β -catenin interactors, LDHB, PML, PABP1, PUR9, SPF45, RL11, and HS105 impact on prognosis of metastatic melanoma

Co-expression of β -catenin and some of its most important interactors was observed during ADPM of FM3 cells *in vitro*. In order to corroborate the β -catenin interactome changes with clinical observations, and to address how changes in the β -catenin interactome throughout melanoma progression and metastasis affect prognosis, bioinformatics analyses were carried out *in silico* using TCGA melanoma datasets (SKCM).

Although β -catenin expression levels had no significant impact on overall survival of melanoma patients, β -catenin levels were significantly higher in metastatic melanoma compared to melanoma. This highlights that β -catenin plays a vital role in metastasis. This is further substantiated by other studies which also showed that β -catenin signalling increased with progression of melanoma,³⁶⁹ and prominent involvement of β -catenin in metastasis of BRAF-activated melanoma.³⁶⁸ CTC clusters are more notorious than single CTCs in driving

metastasis of melanoma.³⁴⁵ Therefore, it is conceivable that β -catenin is likely to partake in either CTC cluster formation or maintenance of vital signalling cascades that promote the integrity and survival of these clusters during haematological transit. In breast cancer, however, there was no difference in the levels of β -catenin between CTC clusters and single CTCs.⁴⁵⁹ In contrast, β -catenin activation was associated with CTC clusters of hepatocellular carcinomas.³⁷⁷ Patient-derived colorectal cancer CTC clusters also exhibited heightened β -catenin and E-cadherin expression;⁴⁶⁰ here the authors showed that partial EMT status, wherein both E-cadherin and ZEB1 expression, was necessary for *in vivo* metastasis of CTC clusters. Lack of studies characterising melanoma patient-derived CTC clusters hampers gaining insights into β -catenin-driven responses that could support ADPM of melanoma. Through studying β -catenin interactome in the *in vitro* model of melanoma ADPM and validating clinical datasets of melanoma metastasis, these β -catenin-driven responses could be uncovered.

Melanoma patients who presented low PML expression had significantly worse overall survival. This is in line with the previous observations that suggest a tumour suppressive role of PML. Indeed, this was demonstrated first in increased incidence of tumour formation in PML^{-/-} mice.⁴⁶¹ The tumour suppressor activity of PML is primarily attributed to PML-dependent stabilisation of p53 in a positive feedback loop, thus promoting cellular apoptosis or senescence.⁴⁶² Most normal tissues expressed PML; in contrast, PML expression was markedly reduced or completely abolished in several cancers, including prostate adenocarcinomas, colon adenocarcinomas, breast carcinomas, lung carcinomas, lymphomas, CNS tumours, and germ cell tumours.⁴⁶³ Additionally, loss of PML expression was associated with lymph node metastasis during prostate and breast cancer progression.⁴⁶³

PML expression was significantly higher in metastatic melanoma compared to melanoma. Similarly, a study reported that PML levels in malignant melanoma cell lines increased with IFN α cytokine treatment; the majority of the protein localising to the nucleus in PML-nuclear bodies and some localisation to the cytoplasm.⁴⁶⁴ This study highlighted the role of helicase antigen HAGE (DDX43) and JAK-STAT pathway in maintaining low PML mRNA levels in malignant melanoma initiating cells. Upon induction of TGF β signalling, cytoplasmic PML promoted EMT-like phenotype in prostate cancer cells and increased their invasiveness by increasing phosphorylation of SMAD2/3 of the canonical TGF β pathway.⁴⁶⁵ Collectively, these findings suggest that the loss of PML and subsequent loss of tumour suppressive effects could contribute to melanoma progression during the early stages; in contrast, during advanced stages, increase in PML via cytokine signalling (IFN α or TGF β) could contribute to melanoma metastasis by promoting EMT-like processes. In light of the present contribution, it is

conceivable that increased PML in aggregates/CTC clusters would be advantageous to maintain EMT-like signalling during the metastatic cascade.

Unlike PML, high levels of LDHB in melanoma patients contributed to poor overall survival. No significant difference in expression of PML between melanoma and metastatic melanoma was observed. A high level of lactate dehydrogenase was correlated with poor survival in advanced melanoma,⁴⁶⁶ and an elevated serum level of LDHB has been shown to be a predictor of metastasis of melanoma and poor survival.⁴⁶⁷ Given that LDHB levels increased in FM3 aggregates, it is conjectured that the way in which LDHB contribute to metastasis is via the promotion of CTC clusters. Further research is needed to address how differences in environmental cues and respiration states, for example normoxic conditions during blood transit vs hypoxic conditions in tumour microenvironment, could affect LDHB-mediated regulation of lactate production, and in turn regulation of β -catenin-mediated EMT-like processes within CTC clusters based on these metabolic cues.

When considering impact on overall survival of melanoma patients, although no difference in high vs low expression of PABP1, RL11, PUR9, SPF45 and HS105 were observed, comparison of melanoma to metastatic melanoma revealed the expression of these 5 proteins were significantly higher in metastatic melanoma. PABP1 was identified as one of the hotspots in melanoma whole-exome sequencing data.⁴⁶⁸ In melanoma, both RL15 and RL11 has been shown to play a fundamental role in stabilising p53 by directly binding to MDM2 and preventing MDM2-mediated degradation of p53.⁴⁶⁹ Though PUR9 has not been studied in melanoma in detail; however, purine metabolism, especially inosine levels strongly correlate with enhanced melanoma cellular proliferation,⁴⁷⁰ and alteration in the ratio of adenosine to inosine ratio leads to increased invasiveness and metastasis of melanoma.⁴⁷¹

SPF45 has not been studied in melanoma thus far. However, its role in invasiveness in ovarian cancers,⁴⁷² and regulation of apoptosis, for example exon 6 skipping in *FAS* pre-mRNA (apoptosis death receptor) induced by SPF45,⁴⁴⁴ suggest that SPF45 could play similar roles in melanoma. On the other hand, HS105 has been extensively studied in melanoma. HS105 was overexpressed in melanoma compared to benign nevi.⁴⁷³ Notably, recurrent, and metastatic lesions were closely associated with elevated HS105 expression, suggesting an additional role in metastasis. Another study confirmed this and showed that compared to normal human skin and benign melanocytic nevi, malignant melanoma cells markedly overexpressed HS105.⁴⁷⁴

Comparison of the risk associated with metastasis of the β -catenin interactome, highlighted that RL11 as the factor that contributed to the most adverse metastasis-related outcome. In breast cancers, a recent publication reported that the RL11 \rightarrow c-myc \rightarrow snail \rightarrow N-cadherin

axis was important for invasion and metastasis.⁴⁷⁵ Another study highlighted that snail induces collective cellular migration by upregulation of claudin-11 and suppression of RhoA activity at the cell-cell junction.⁴⁷⁶ Therefore, in melanoma, perhaps RL11 could promote CTC-cluster based metastasis, alone or via RL11/PML/c-myc network; though, whether c-myc is involved in ADPM of FM3 cells, or in melanoma CTC cluster metastasis, needs further investigation.

An obvious limitation with the present analysis is that comparison of the β -catenin interactome in melanoma against metastatic melanoma alone is insufficient to give the full picture of the β -catenin interactome in CTC clusters. Once metastasis has taken place, most cells are likely to have undergone morphological changes similar to disaggregation of FM3 cells. As such, β -catenin interactome changes associated with aggregation will be overlooked. Although, ideally genomic and proteomic datasets of enriched CTC clusters and single CTC, alongside corresponding patient survival dataset, would be much more suitable for this analysis. In lieu of these datasets, an *in vitro* model of ADPM and *in silico* analyses of expression of melanoma vs metastatic melanoma, and risk pertaining to metastasis, present glimpses of the influences of the β -catenin interactome in orchestrating cellular metabolism, protein synthesis, cellular proliferation, and EMT-like processes.

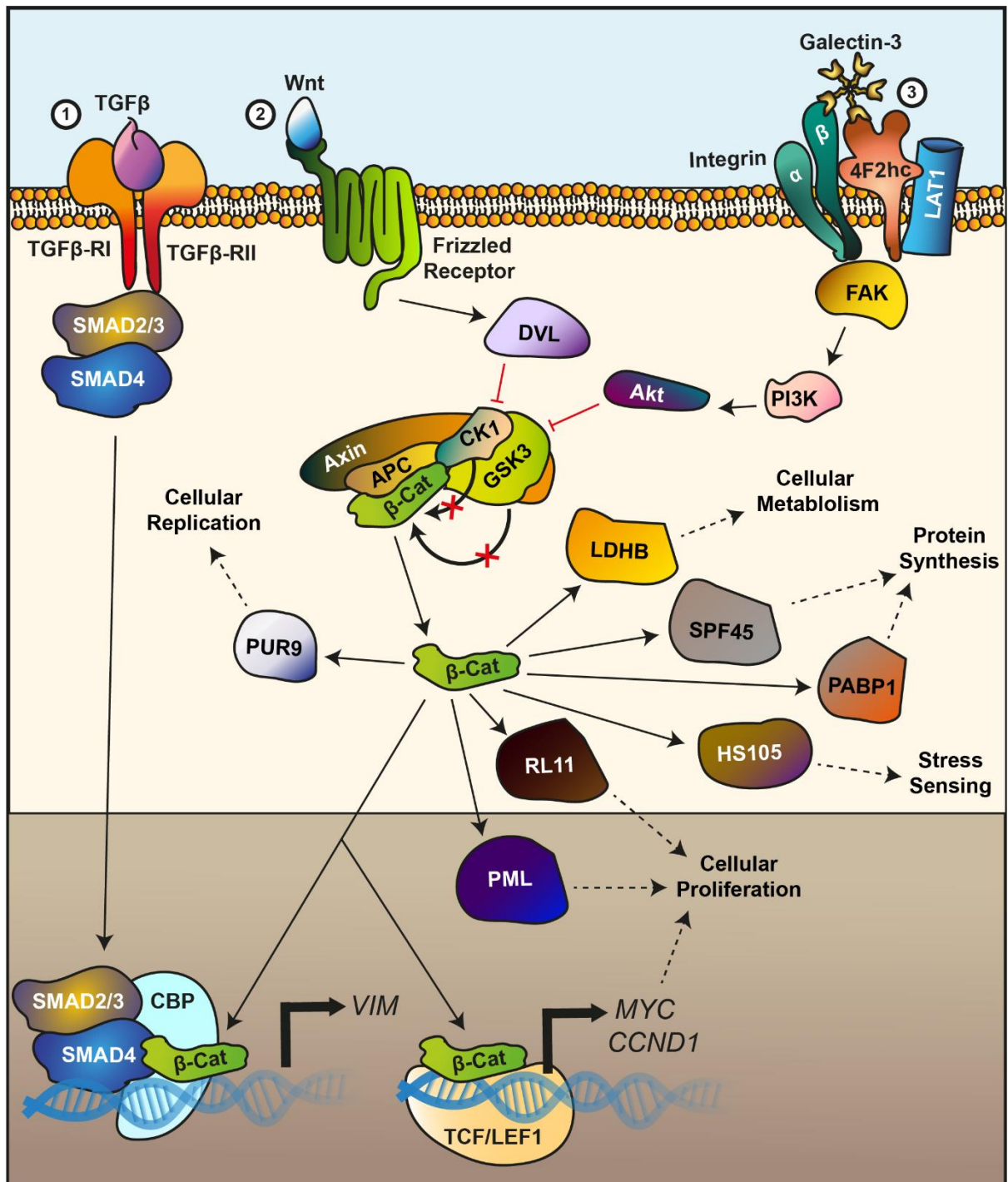


Fig. 6.8. Proposed cross-talk of TGF β -signalling, Wnt/ β -catenin-signalling and 4F2hc/galectin-3/integrin signalling regulating β -catenin interactome during ADPM of FM3 cells and melanoma CTC clusters. TGF β -signalling (1) through SMADs has been shown to conjoin with Wnt/ β -catenin-signalling (2) via CBP to upregulate gene regulation of EMT genes such as vimentin (encoded by *VIM* gene). Upon Wnt-ligand binding to frizzled receptors, dishevelled (DVL) becomes activated via phosphorylation and polymerises. This in turn recruits Axin and the destruction complex (made of Axin, APC, GSK3 β and CK1) is dismantled, preventing CK1 from phosphorylating β -catenin and directing towards phosphorylation-driven ubiquitination and proteasomal destruction. 4F2hc/galectin-3/integrin (3) complexes have also been shown to rescue β -catenin from destruction by concomitant phosphorylation and inhibition of GSK3 by FAK/PI3K/Akt activation. Accumulation of β -catenin in the cytoplasm and eventual translocation to the nucleus, allows β -catenin-mediated gene transcriptional regulation alongside its canonical partners, such as TCF/LEF1 family of transcription factors, or non-canonical gene transcriptional regulation via transcription factors such as the SAMDS. During ADPM of FM3 cells, or in melanoma CTC clusters, signalling via β -catenin interactome (HS105, LDHB, PABP1, PML, PUR9, SPF45, and PABP1) could regulate key cellular processes.

6.3.6 β -catenin and SPI1-mediated transcriptional regulation in ADPM of FM3 cells

The TCF/LEF family are the transcription factors of choice for the canonical Wnt/ β -catenin pathway.³⁹³ However, TCF/LEF family members were not detected in FM3 cells during ADPM. β -catenin interactome is extensive and may host a wide variety of transcription factors.⁴⁷⁷ To establish transcriptional activities that could be both TCF/LEF-dependent and independent during ADPM of FM3 cells, gene ontology classification (using PANTHER) and comparison of proteomics of FM3 cells ADPM with CHIP-Seq database (from hTFtarget tool) were carried out.

Gene ontology analysis revealed that of the 10 transcriptional regulators altered during ADPM of FM3 cells, only the target genes of the following transcriptional regulators STAT1, STAT3, MAFF and MTA3, were altered during ADPM. β -catenin/TCF/LEF transcriptional regulation was investigated next. Compared to the number of targets of STAT1 and STAT3 in ADPM of FM3 cells, the number of targets of β -catenin and two of the TCF/LEF family members TCF1 α (*LEF1*) and TCF4 (*TCFL2*), were much lower. This indicates that perhaps β -catenin-mediated transcriptional response is non-canonical, and other undetected transcriptional regulators must be at work. Investigation of transcriptional regulators that have been shown, via CHIP-Seq, to bind to STAT1, STAT3, MAFF, MTA3, β -catenin, TCF1 α and TCF4, within skin, highlighted SPI1, CTCF, and FOXA2. Comparing the number of targets of SPI1, CTCF, and FOXA2 in proteome of FM3 cells during ADPM, revealed that SPI1 as the most likely master regulator of ADPM in FM3 cells.

Cross-talk of Wnt/ β -catenin signalling and SPI1-mediated responses have been reported by a number of studies thus far. Monocyte to macrophage differentiation can be blocked by antagonising SPI1-targeted gene transcription via activation of Wnt/ β -catenin pathway.⁴⁷⁸ This finding not only highlights the possibility of regulation of SPI1-responses by Wnt β -catenin pathway, but also that SPI1 may be involved in regulation of morphological changes that accompany transition from monocytes containing minimal filopodial extrusions to macrophages containing extensive filopodium and lamellipodium.⁴⁷⁹ This could indicate that SPI1-targeted genes may be involved in amoeboid movement of cells. Additionally, Wnt8 overexpression was shown to repress expression of SPI1 during development of myeloid precursors.⁴⁸⁰ Cell-type specific effects of TGF β -signalling may be attributed to master transcriptional factors such as SPI1. Indeed, SPI1 may determine transcriptional activities of SMAD2/3 in pro-B cells, whereas Oct4 may determine SMAD3 activity in embryonic stem cells.⁴⁸¹ Evidently, TGF β or β -catenin-mediated transcription of target genes could rely on SPI1. More experiments are required to interrogate β -catenin and the SPI1 network in ADPM of FM3 cells, for example by observation of the β -catenin interactome in SPI1 -/- cells.

SPI1 was not detected in quantitative mass-spectrometry of FM3 cells during ADPM. Perhaps, levels of SPI1 were too low, or perhaps SPI1 might be more active during the initial pre-aggregation (before 24h) period. Carrying out RT-qPCR from 0 – 24 hours could show changes in SPI1 during the early stages of ADPM. However, others have highlighted that SPI1 levels were higher in melanoma compared to normal tissue.⁴⁸² Further research is required to confirm that SPI1 lies downstream of β -catenin-mediated signalling, or at the very least work alongside β -catenin interactome, and also confirm that the genes encoding the proteins responsible for producing the morphological and phenotypical changes during ADPM are indeed regulated by SPI1.

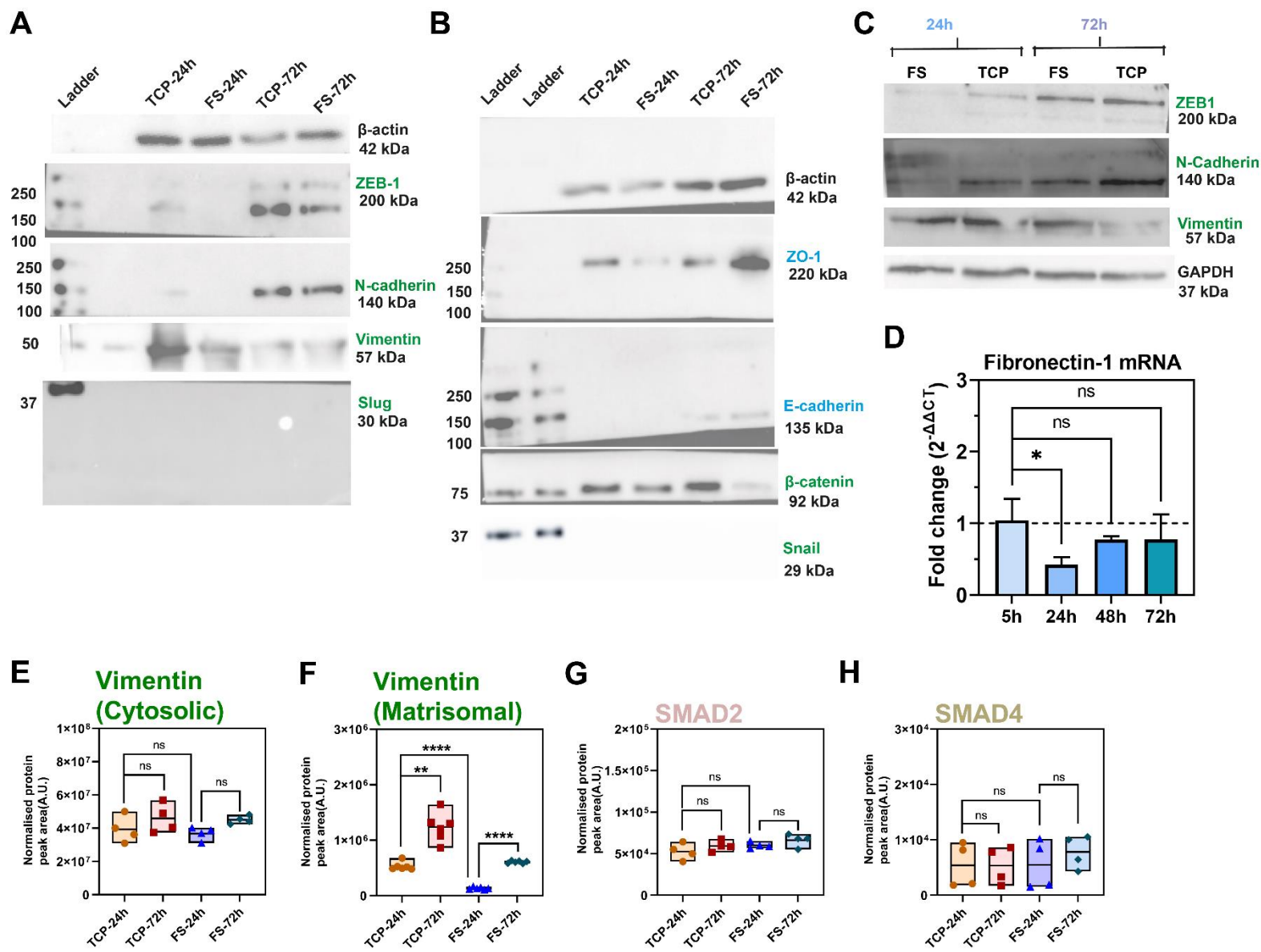
6.3.7 Conclusions

This research aimed to identify the roles of EMT status and β -catenin that could be key to unlocking the relationship between EMT-like processes and ADPM of melanoma CTC clusters. Though some of the classical EMT markers were not altered during ADPM, change in β -catenin and vimentin suggests that EMT-like processes do take place. TGF β -treatment leading to increased aggregation of FM3 cells, and P4B6B mesenchymal cells retaining aggregation but not P5B3 epithelial cells that express high levels of β -catenin, suggest that mesenchymal-like state more than β -catenin levels is required for the clustered conformation. This could be perhaps via reinforcement of the cytoskeleton with vimentin to withstand the tumultuous haematological circulation. Mesenchymal cells could prolong their clustered confirmation by secreting vitronectin, vimentin and shroom-3; this highlights an important part that mesenchymal cells could play within a heterogenous and mixed-population CTC cluster, in preventing disaggregation until a suitable distal site is reached.

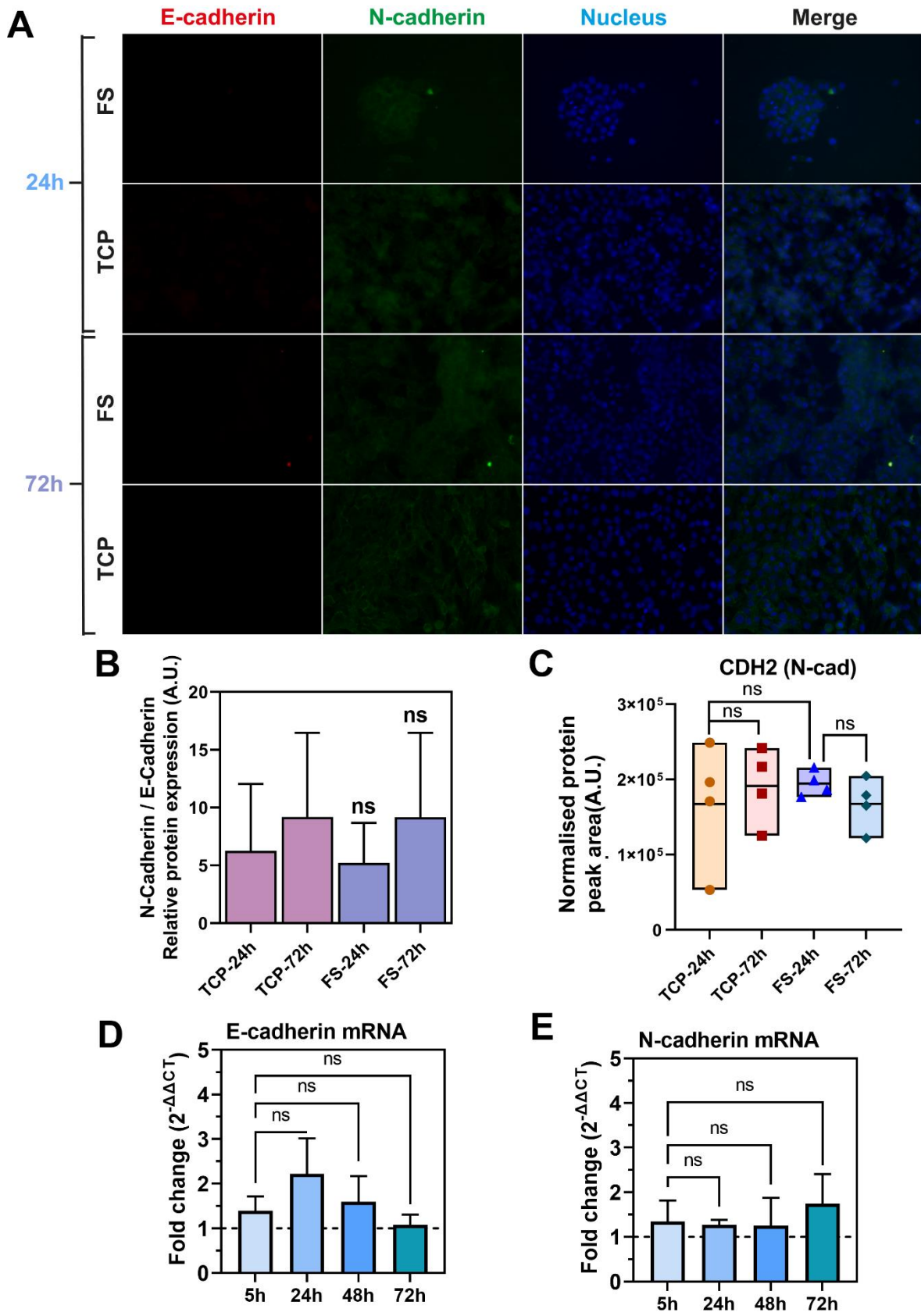
β -catenin involvement in ADPM of FM3 cells and increased levels of β -catenin in metastatic melanoma cells, point towards the dominant role β -catenin plays in metastasis of melanoma CTC clusters. This research elucidated the diverse ways in which the β -catenin interactome orchestrates important cellular processes during ADPM of melanoma CTC clusters: cellular metabolism via LDHB, protein synthesis via SPF45 and PABP1, cellular replication via PUR9, cellular proliferation via PML and RL11, and stress-sensing via HS105. Metastasis risk analysis revealed RL11 as the most notorious and adverse factor contributing to poor metastasis-related prognosis. The RL11/PML/c-myc network-mediated responses could be responsible for this, though this requires further detailed investigation. Analysis of transcriptional regulation revealed SPI1 as the potential master regulator of ADPM of melanoma cells; however, further research is needed to outline how SPI1-mediated transcription may be

regulated by EMT status, TGF β & β -signalling. This could illuminate how platelet-derived, or immune or stromal cells-derived, cytokines that could alter transcriptional regulations in CTC clusters during ADPM to make them more adept at metastasis compared to their single CTC counterparts as observed in the clinics.

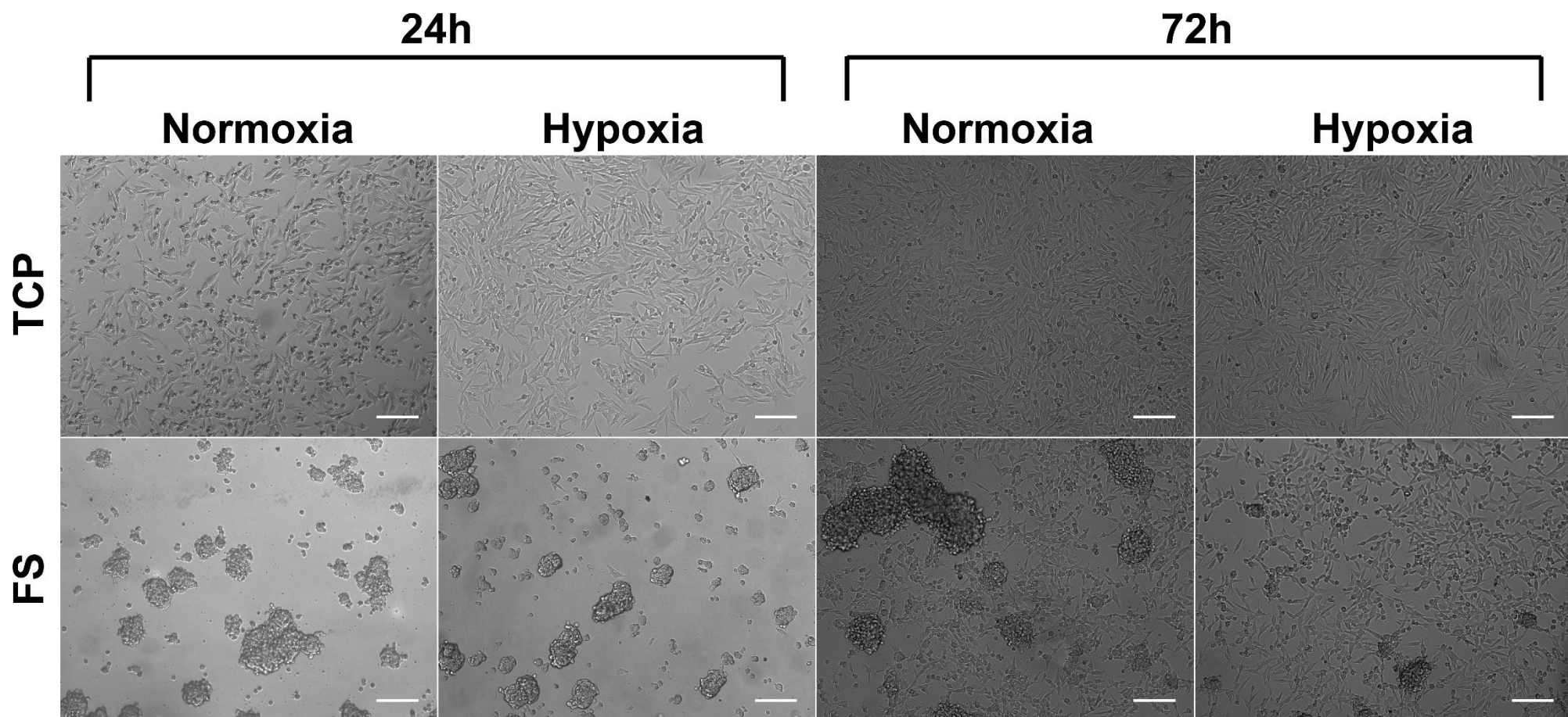
6.4 Supplementary Figures



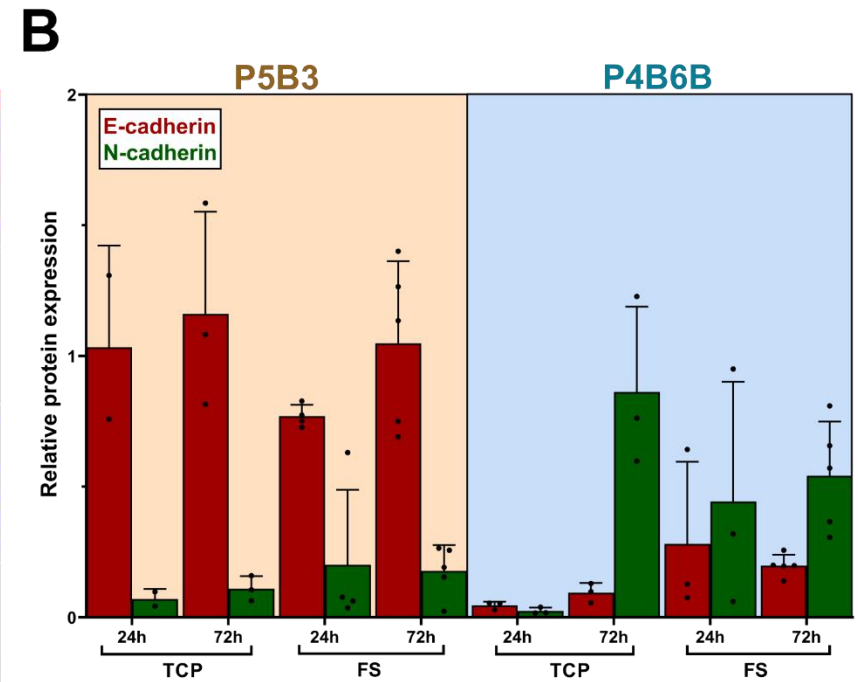
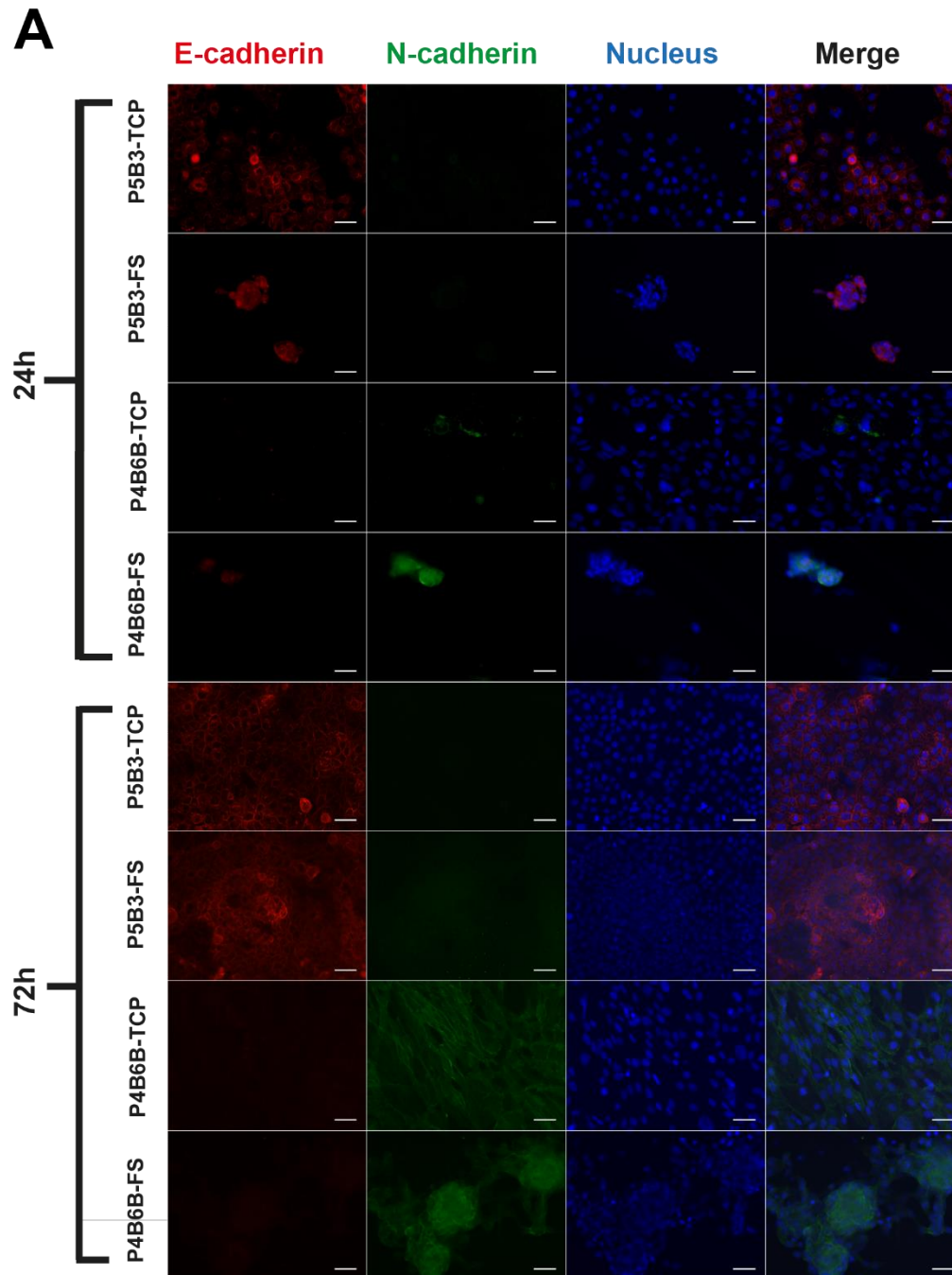
Supplementary Fig. 6.1 Expression of EMT markers during ADPM of FM3 cells. (A - C) Western blot showing changes in epithelial (blue) and mesenchymal markers (green) during ADPM of FM3 cells. **(D)** Periodic expression of fibronectin-1 mRNA during aggregation (5-24h) vs disaggregation (48-72h) as measured by RT-qPCR, n=3. **(E-H)** Change in **(E)** cytosolic vimentin, **(F)** matrisomal vimentin, **(G)**, SMAD2, and **(H)** SMAD4, during FM3 cellular aggregation (FS-24h vs TCP-24h) and disaggregation (FS-72h vs FS-24h) as measured by mass spectrometry, n=4. Brown-Forsythe and Welch ANOVA tests (equal SDs not assumed) with Dunnett T3 post-hoc multiple comparison test for D - H, FS: fluoroalkylsilica, TCP: tissue culture polystyrene.



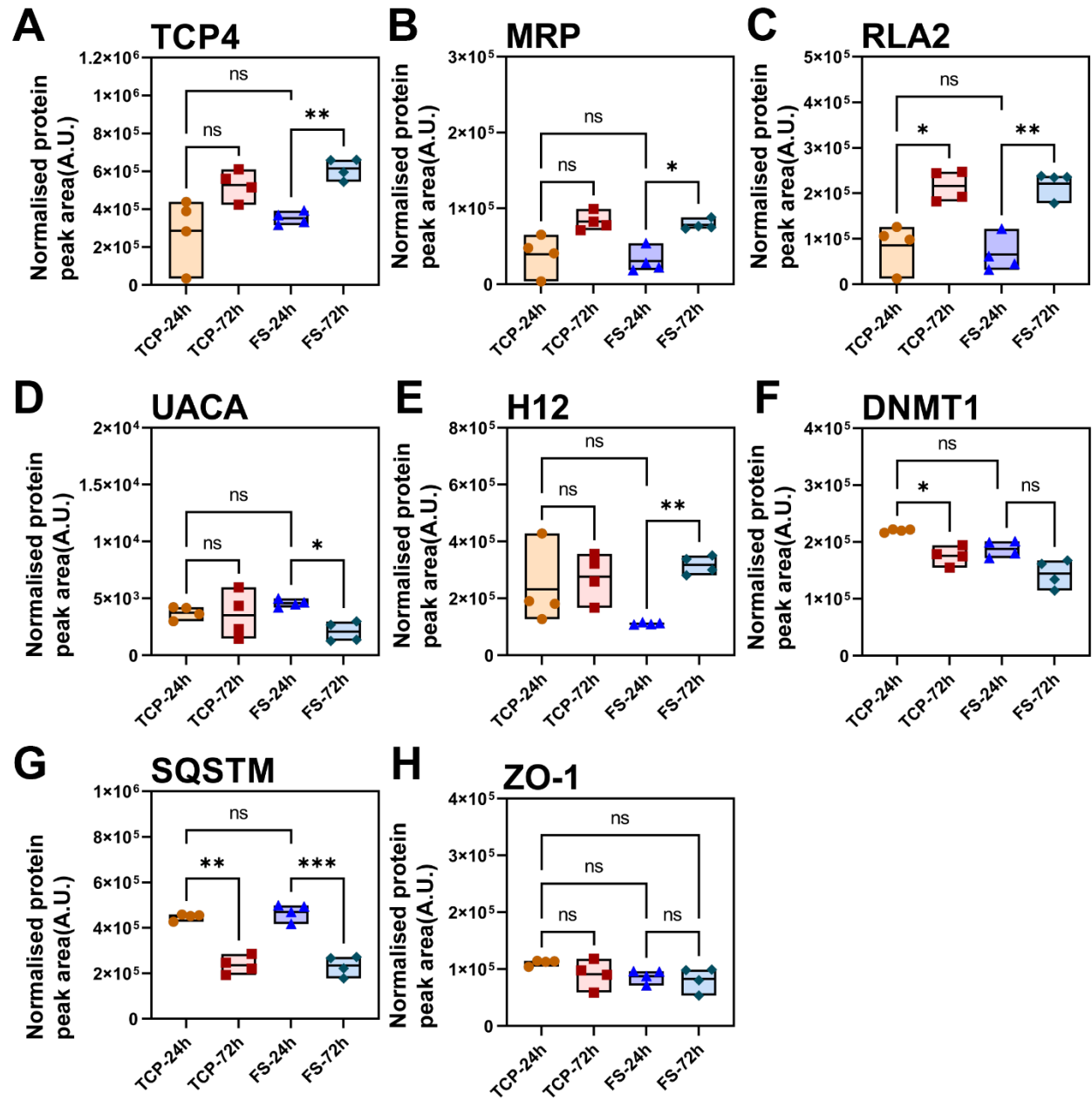
Supplementary Fig. 6.2 No cadherin switch occurs during ADPM of FM3 cells. (A-B) Immunofluorescence staining of E-cadherin (red), N-cadherin (green), and nucleus (blue) of FM3 cells during ADPM, (A) representative images, (B) quantification of colour intensity in each colour channel using Image J normalised to background, n=3. (C) Change in N-cadherin (CDH2) levels during FM3 cellular aggregation (FS-24h vs TCP-24h) and disaggregation (FS-72h vs FS-24h) as measured by mass spectrometry, N=4. (D – E) Periodic expression of (D) E-cadherin and (E) N-cadherin mRNA during aggregation (5-24h) vs disaggregation (48-72h) as measured by RT-qPCR, n=3. Fold Change (2^{-ΔΔCT}) represents comparison of FS surfaces vs TCP surfaces. Brown-Forsythe and Welch ANOVA tests (equal SDs not assumed) with Dunnett T3 post-hoc multiple comparison test for C -E, and Ordinary Two-way ANOVA with Tukey post-hoc multiple comparisons for B. FS: fluoroalkylsilica, TCP: tissue culture polystyrene.



Supplementary Fig. 6.3 Hypoxia does not affect ADPM of FM3 cells. FM3 cells were seeded onto FS or TCP surfaces, under normoxic or hypoxic conditions, n=6. FS: fluoroalkylsilica, TCP: tissue culture polystyrene. Scale = 200 μm .



Supplementary Fig. 6.4 No cadherin switch occurs during ADPM of epithelial (P5B3) cells and mesenchymal (P4B6B) cells. (A-B) Immunofluorescence staining of E-cadherin (red), N-cadherin (green), and nucleus (blue) of P4B6B and P5B3 cells during ADPM, **(A)** representative images, **(B)** quantification of colour intensity in each colour channel using Image J normalised to background, n=3. Ordinary Two-way ANOVA with Tukey post-hoc multiple comparisons for B. FS: fluoroalkylsilica, TCP: tissue culture polystyrene. Scale = 50 μ m.



Supplementary Fig. 6.5 Proteomic changes of β -catenin interactors during ADPM of FM3 cells. Change in levels of (A) TCP4, (B) MRP, (C) RLA2, (D) UACA, (E) H12, (F) DNMT1, (G) SQSTM, and (H) ZO-1 during FM3 cellular aggregation (FS-24h vs TCP-24h) and disaggregation (FS-72h vs FS-24h) as measured by mass spectrometry, $n=4$. Brown-Forsythe and Welch ANOVA tests (equal SDs not assumed) with Dunnett T3 post-hoc multiple comparison test for A – H. FS: fluoroalkylsilica, TCP: tissue culture polystyrene.

Chapter 7. PU.1-mediated transcriptional regulation during melanoma multicellular aggregation-disaggregation

Contents

CHAPTER 7. PU.1-MEDIATED TRANSCRIPTIONAL REGULATION DURING MELANOMA MULTICELLULAR AGGREGATION-DISAGGREGATION	134
7.1 INTRODUCTION	135
7.1.1 PU.1 transcription factor	135
7.1.2 PU.1 in cancer	136
7.2 RESULTS	137
7.2.1 PU.1 on FM3 cellular responses during ADPM	137
7.2.2 PU.1-target genes in FM3 cells.....	140
7.2.3 PU.1-target genes in ADPM of FM3 cells	142
7.2.4 PU.1 in clinical melanoma metastasis	146
7.3 DISCUSSION	148
7.3.1 PU.1 is involved invasion and migration during ADPM of FM3 cells.....	148
7.3.2 PU.1 mediates key pathways involved in cellular proliferation, migration, and invasion in FM3 cells.....	151
7.3.3 PU.1 regulates expression of key proteins involved in ADPM of FM3 cells	154
7.3.4 PU.1 expression dictates clinical melanoma metastasis and survival outcome	156
7.3.5 Conclusions	158
7.4 SUPPLEMENTARY FIGURES	159

7.1 Introduction

This chapter investigates whether the PU.1 transcription factor is affected during ADPM of FM3 cells. PU.1 transcription factor was identified in Chapter 6 as a potential master regulator that could act alongside β -catenin-dependent regulation of genes.

7.1.1 PU.1 transcription factor

PU.1 is a pioneer transcription factor that can directly bind to condensed chromatin, decompact heterochromatin, and recruit other transcription factors, co-regulators, and RNA polymerases to otherwise inaccessible genomic regions.⁴⁸³ In this manner, PU.1 promotes the transcription of several genes that are indispensable for self-renewal of haematopoietic stem cells or progenitor cells⁴⁸⁴ and commitment and/or maturation of B-lymphoid and myeloid lineages.⁴⁸⁵ In haematopoiesis, PU.1 acts as a euchromatin gatekeeper of pro- to pre-B cell transition.⁴⁸⁶

As a member of the E26 transformation-specific (ETS) family of transcription factors, PU.1 contains the ETS functional domain with a distinct winged helix-turn-helix pattern, which recognises DNA consensus sequences containing a core 5'-GGAA-3' motif.⁴⁸⁷ PU.1 preferentially binds to purine-rich DNA sequences, such as the 5'-GAGGAA-3'⁴⁸⁶ known as the 'PU-box'. In addition, PU.1 can regulate gene expression by interacting with a variety of other transcription factors, including the early haematopoietic factors GATA-2 and Runx-1, the erythroid factor GATA-1, and other general transcription factors such as TFIID, TBP, C/EBP α , C/EBP β , IRF4/8 and c-Jun.⁴⁸⁸ PU.1 can also antagonise certain transcription factors, such as GATA-1, by preventing GATA-1 from binding to putative 5'-GATA-3' consensus sequences.⁴⁸⁹ Other transcriptional factors could alter the transcriptional activity of PU.1; as such, PU.1-dependent gene regulation and its cell-specific activities are likely to be governed by the spatiotemporal expression of these co-regulators. Expression of *SPI1* (gene encoding for PU.1) is mostly restricted to haematopoietic cell.⁴⁹⁰ Surprisingly, high expression of PU.1 has also

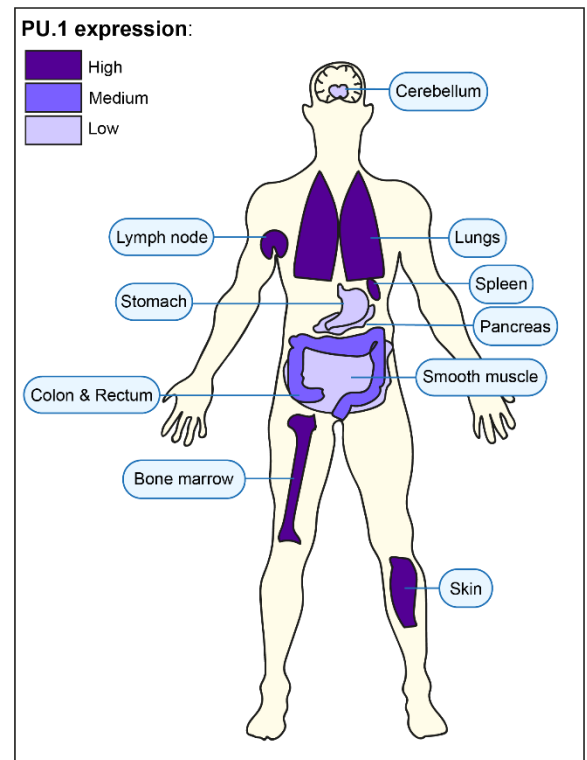


Fig. 7.0 PU.1 protein expression in anatomical sites. High levels of PU.1 protein expression in organs involved in haematopoiesis (lymph nodes, spleen, and bone marrow), as well as lungs and skin. Figure adapted from the Human Protein Atlas.

been observed in certain lung and skin cells ⁴⁹¹ (Fig. 7.0). However, the role of PU.1 in non-haematopoietic cells remain elusive.

7.1.2 PU.1 in cancer

Aberrant PU.1 activity has been highlighted in both haematological malignancies and solid tumours. PU.1 was shown to be a potent tumour suppressor in classical Hodgkin lymphoma.⁴⁹² Similarly, PU.1 functions as a tumour suppressor in acute myeloid leukaemia (AML). AML, which is the malignancy of myeloid lineage cells, show suppressed PU.1 expression; restoring endogenous PU.1 levels was shown to lead to differentiation of leukemic blasts to neutrophil-like cells, and subsequent suppression of PU.1 expression was shown to transform the cells back to a malignant state.⁴⁹³ This could be explained by earlier research that suggests that PU.1 could directly bind to, and impair the transcriptional activity of, the p53 family of tumour suppressors in B-cell precursor leukaemia cells.⁴⁹⁴

In contrast, PU.1 serves as an oncogene in erythroleukemia, which is a much rarer subset of AML where the disease manifests from erythrocytic precursors as opposed to myeloid precursors.⁴⁹⁵ In erythroleukemia, overexpression of PU.1 leads to decreased phosphorylation of the S-phase checkpoint protein CHK1, due to the increased expression of CHK1-phosphatase PP1 α .⁴⁹⁶ Without the ATR/CHK1-mediated governance during the S-phase, cells bypass this S-phase checkpoint and undergo cellular replication due to accelerated DNA replication fork progression. In murine erythroleukemia, histone deacetylase 1 (HDAC1) cooperates with PU.1 to repress gene transcription, for example GATA-1-mediated transcription of genes responsible for erythroid differentiation, by deacetylating PU.1-bound enhancer regions.⁴⁹⁷ These studies clearly illustrate that, in haematological malignancies at least, PU.1 may play important roles in subverting transcriptional programs underlying normal cellular differentiation and cellular replication.

In solid tumours, however, the actions of PU.1 seem to be much less obvious. In HER2-positive breast cancer, where the human epidermal growth factor receptor 2 (HER2) promotes cancerous growth, overexpression of PU.1 was correlated with shorter survival of patients;⁴⁹⁸ however, the interplay of HER2-mediated signalling and PU.1-dependent transcriptional regulation remains to be uncovered. A recent study highlighted that the *SPI1* gene was expressed substantially in colon tumours and the surrounding stroma.⁴⁹⁹ Here, PU.1 and its homologous partner SPI-B, was shown to promote aerobic glycolysis via increasing the expression of certain glycolytic genes such as *HK2* and *PGK1*. Interestingly, increased lactate resulted in the

polarisation of tumour-associated neutrophils, which in turn were shown to deliver *SPI1* mRNA enclosed in extracellular vesicles to cancer cells.

PU.1 expression was shown to be higher in lung adenocarcinoma compared to healthy lung tissue.⁵⁰⁰ As the transcription factor T-box-expressed in T cells (T-bet) levels were found to be decreased, the authors suggested that perhaps PU.1 could be antagonising T-bet activities in tumour sites, perhaps within anti-tumour Th1 cells as T-bet is involved in Th1 cell development. Furthermore, PU.1 expression was correlated with a favourable prognosis in adenocarcinoma, but poor prognosis in squamous cell lung carcinoma,⁵⁰¹ indicating that PU.1 may play a tumour suppressive role in the former and an oncogenic role in the latter. Another study revealed PU.1 as a master transcriptional activator of the tumour suppressor gene *LIMD1*,⁵⁰² which is downregulated in ~80% of lung cancers.

In melanoma, several ETS family members, including PU.1, were shown to be upregulated.⁴⁸² However, little is known of the contribution of PU.1 to melanoma progression and metastasis. In chapter 6, PU.1 was identified as the transcription factor with the highest number of target genes that were differentially expressed during ADPM of FM3 melanoma cells. The present chapter will further explore the involvement of PU.1 in melanoma metastasis and ADPM, by treating FM3 cells with a potent inhibitor of PU.1 (DB2313),⁵⁰³ and observing effects on ADPM, cellular proliferation, invasion, and migration. In order to identify target genes of PU.1 that could be involved in ADPM, quantitative mass spectrometry will be carried out on DB2313-treated cells. The results of these experiments will reveal cell-specific transcriptional regulation by PU.1 during ADPM and melanoma metastasis.

7.2 Results

7.2.1 PU.1 on FM3 cellular responses during ADPM

To outline changes in PU.1 expression during ADPM, RT-qPCR was carried out. This experiment revealed that *SPI1* mRNA levels did not significantly change throughout the course of ADPM of FM3 cells on FS surface (Fig. 7.1 A). A recent study developed a small-molecule inhibitor of PU.1 (called DB2313) that allosterically interferes with the binding of PU.1 to chromatin.⁵⁰³ To discern effect of DB2313 on the cell viability of FM3 cells, cells were treated with concentration of DB2313 ranging from 1 nM to 500 μ M, and cell viability was plotted as dose-response (Fig. 7.1 B). Non-linear fitting suggested that the most profound inhibition of PU.1 in FM3 cells occur between 10 to 50 μ M of the added chemical. Using this range of concentration, effect of inhibition of PU.1 on FM3 cell viability was tested, on both FS and TCP surfaces after 72 h

(during disaggregation on FS surface). The IC_{50} (best-fit value) for FS was 10.82 μM and TCP 19.81 μM (Fig. 7.1 C). Cell viability was significantly reduced on FS surfaces compared to TCP surfaces when treated with 20 and 50 μM of DB2313, but not 10 μM .

It was hypothesised that inhibition of PU.1 via treatment of FM3 cells with DB2313 would reduce ADPM responses. No significant change in aggregation (FS-24h) was observed with increasing concentration of DB2313 (Fig. 7.1 E). Though treatment of 50 μM seemed to have caused increased aggregation, a closer look at the representative images of the aggregates clearly shows that these were dead clumps of cells rather than living multicellular aggregates (Supplementary Fig. 7.1). There was a significant decrease in disaggregation indicated by reduction in percentage of non-aggregates at both 48 and 72 h when treated with 10 μM of DB2313; but no non-aggregates were observed when treated with 20 and 50 μM .

To test effect of inhibition of PU.1 via treatment with DB2313 on FM3 cellular invasiveness and motility, invasion and migration assay was carried out using a Boyden chamber (for both assays), basement membrane extract (for invasion assay only), and a chemotactic gradient (for both assays) of foetal calf serum (FCS) ranging from 0% (v/v) inside the Boyden chamber to 20% (v/v) in the bottom chamber. These experiments revealed that inhibition of PU.1 significantly increased invasiveness (Fig. 7.1 D) and migration (Fig. 7.1 F) of FM3 cells on both TCP and FS surfaces at 24 h. However, this increase in invasiveness (Fig. 7.1 D) and migration (Fig. 7.1 F) is significantly reduced in cells from aggregates (FS-24h) compared to single cells (TCP-24h).

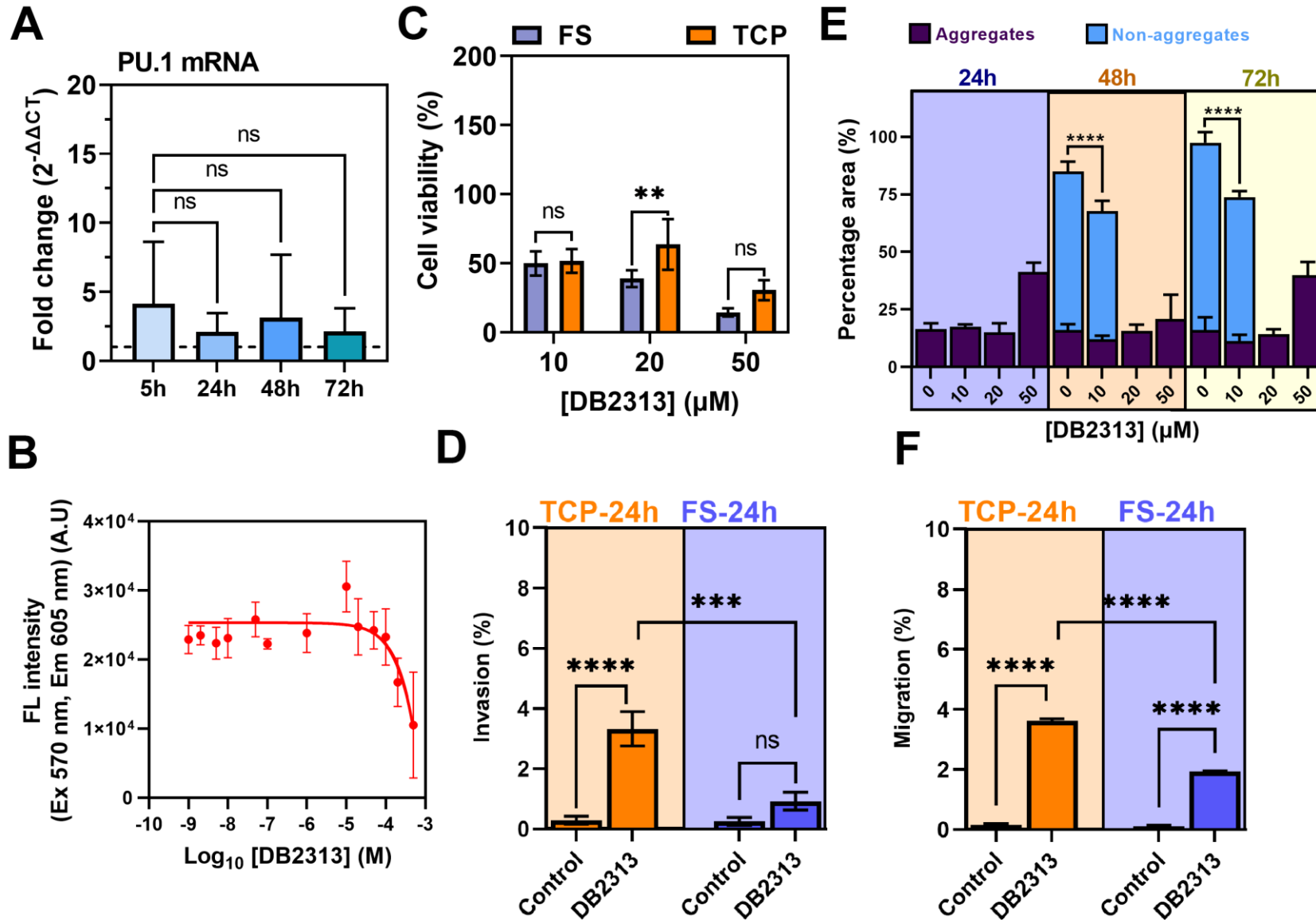


Fig. 7.1 PU.1 influences viability, invasiveness, and migration of FM3 cells during ADPM. **(A)** Periodic expression of *SPI1* mRNA during aggregation (FS surface; 5-24h) vs disaggregation (FS surface; 48-72h) as measured by RT-qPCR, n=3. Fold Change ($2^{-\Delta\Delta CT}$) represents comparison of FS surfaces vs TCP surfaces. **(B)** Effect of increasing concentration of PU.1 inhibitor (DB2313) on cellular viability after 24 h of culture on TCP surfaces, n=6. **(C)** Effect of increasing concentration of DB2313 on FM3 cellular viability after 72 h of culture on TCP and FS surfaces, n=6. **(D)** Invasion assay revealed increase in invasiveness of FM3 cells with DB2313 treatment (10 μ M), n=6. **(E)** Effect of increasing concentration of DB2313 on percentage area occupied by aggregates and non-aggregates of FM3 cells on FS surfaces, n=6. **(F)** Migration assay showed increase in migratory properties of FM3 cells with DB2313 treatment (10 μ M) on FS and TCP surfaces, n=6. Brown-Forsythe and Welch ANOVA tests (equal SDs not assumed) with Dunnett T3 post-hoc multiple comparison test was carried out for A, and Ordinary Two-way ANOVA with Tukey post-hoc multiple comparisons for C – F. FS: fluoroalkylsilica, TCP: tissue culture polystyrene.

7.2.2 PU.1-target genes in FM3 cells

To characterise target genes of PU.1 in FM3 cells, cells were treated with 10 μ M of DB2313 for 24 h on TCP surfaces, cell lysate proteins were harvested, and quantitative SWATH mass spectrometry was carried out. Out of the 6485 total proteins detected, 755 proteins were significantly altered ($p < 0.05$) in DB2313-treated FM3 cells. Gene ontology (GO) analysis highlighted some of the key proteins involved in notable melanoma cellular functions. With DB2313 treatment, proteins were upregulated (Fig. 7.2 A) that are involved in the tricarboxylic acid cycle (GO:0006099), actin cytoskeleton organisation (GO:0030036), regulation of cell shape (GO:0008360); and proteins were downregulated (Fig. 7.2 A) that are involved in purine nucleotide biosynthesis (GO:0006164), actin filament bundle assembly (GO:0051017), substrate-dependent cell migration (GO:0006929), and melanocyte differentiation (GO:0030318). PUR9, a protein involved in purine nucleotide biosynthesis, that was highlighted in chapter 6 as a member of the β -catenin interactome during ADPM of FM3 cells, significantly decreased in DB2313-treated FM3 cells (Fig. 7.2 A). MITF, an important melanocyte differentiation transcription factor was significantly decreased in DB2313-treated FM3 cells (Fig. 7.2 A).

In chapter 4, both 4F2hc and Galectin-3 were highlighted as important players of ADPM in FM3 cells. As PU.1 is conjectured to be the principal transcription factor of ADPM, it was hypothesised that 4F2hc and Galectin-3 could be the target genes of PU.1, and protein levels of 4F2hc and Galectin-3 would decrease in DB2313-treated cells. In line with the hypothesis, when cells were treated with DB2313, 4F2hc levels were significantly decreased (Fig. 7.2 B), however no significant difference was observed for Galectin-3 (Supplementary Fig. 7.2 A). Though, there was a significant increase in Galectin-3 binding protein (Galectin-3-BP) with DB2313 treatment (Fig. 7.2 E). Focal adhesion kinase-1 (FAK1) (Fig. 7.2 C) levels significantly decreased, whereas integrin- α 2 (Supplementary Fig. 7.2 D), and integrin- α 3 (Supplementary Fig. 7.2 E), and integrin- β 1 (Supplementary Fig. 7.2 F) levels significantly increased with DB2313 treatment. Similar to MITF, the melanocyte differentiation factor dopachrome tautomerase (DCT) (Fig. 7.2 D) also significantly decreased with DB2313 treatment. In contrast, levels of proteins involved in Wnt/ β -signalling, proteins LEF1 (Fig. 7.2 F) and Wnt-5a (Supplementary Fig. 7.2 C) significantly increased with DB2313 treatment. The levels of Histone deacetylase-1 (HADC1) (Fig. 7.2 G), involved in eukaryotic gene expression, significantly increased with DB2313 treatment. Lastly, the small GTPase RhoC (Supplementary Fig. 7.2 B), involved in cell motility and cytoskeletal remodelling, levels significantly decreased in DB2313-treated cells.

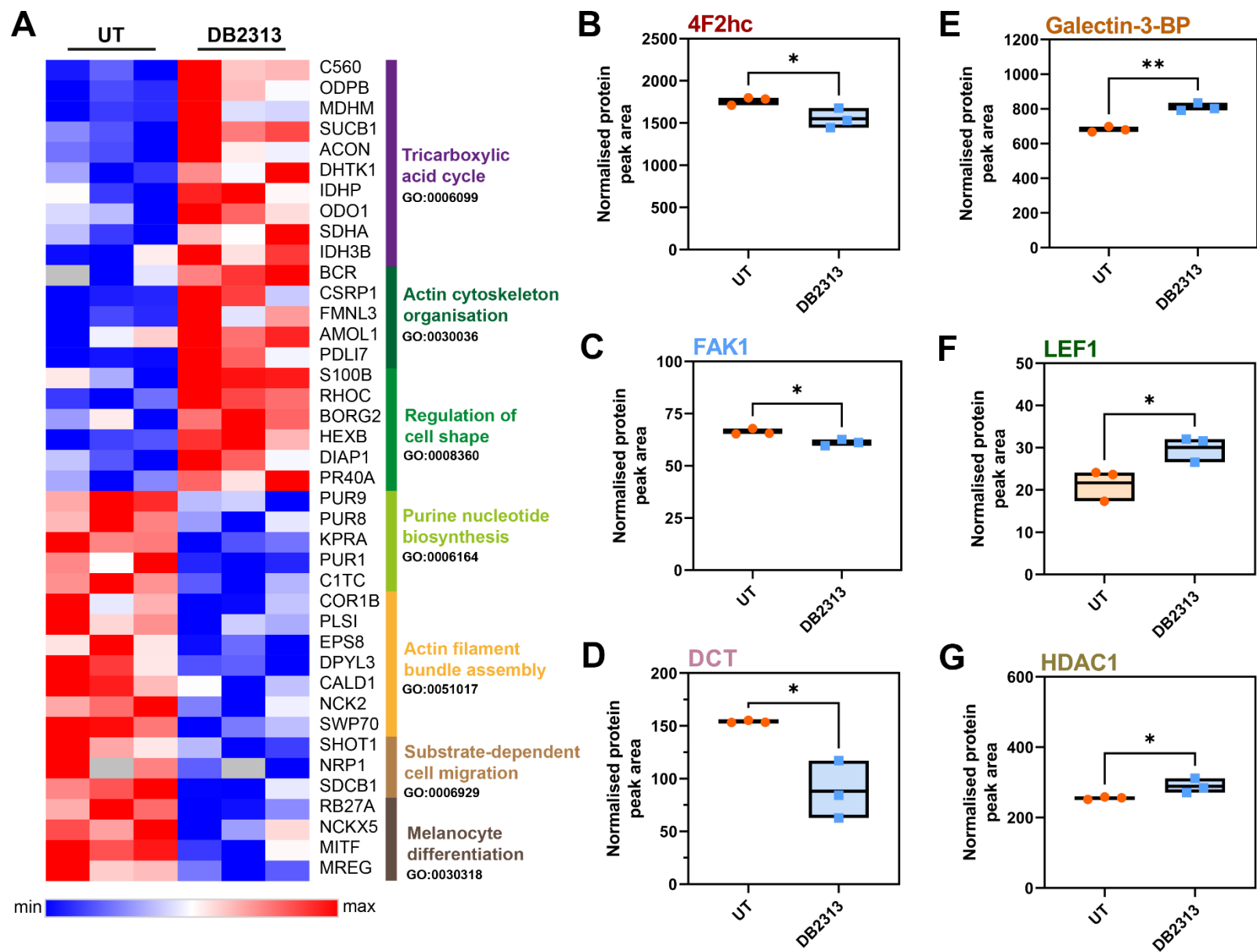


Fig. 7.2 Inhibition of PU.1 in FM3 cells affects proteins involved in metabolism, regulation of cell shape and melanocyte differentiation. (A) Heat map depicting some of the significant proteomic changes ($p < 0.05$) during DB2313 treatment ($10 \mu\text{M}$) of FM3 cells after 24 hours of culture on TCP surfaces, as obtained using quantitative SWATH-MS and categorised by gene ontology (GO) obtained from DAVID, $n=6$. (B-G) Levels of 4F2hc (B), FAK1 (C), and DCT (D) decreased with inhibition of SPI1, whereas levels of galectin-3-BP (E), LEF1 (F), and HDAC1 (G), increased with inhibition of SPI1 in FM3 cells, $n=3$. Student's T-tests (two-tailed distribution, heteroscedastic) were carried out for B – G. FS: fluoroalkylsilica, SWATH-MS: Sciex TripleTOF 6600 data-independent acquisition mass spectrometry, TCP: tissue culture polystyrene.

7.2.3 PU.1-target genes in ADPM of FM3 cells

In order to confirm that the inhibition of PU.1 by DB2313 treatment leads to perturbed transcription of PU.1-target genes in FM3 cells, target genes of PU.1 and PU.1/ β -catenin-associated transcription factors that were obtained from an online curated database of chromatin immunoprecipitation sequencing (ChIP-seq) (hTFtarget tool database,¹³² were compared to the significantly altered ($p < 0.05$) proteome of DB2313-treated FM3 cells. This analysis confirmed that over 90% of proteins that were significantly altered during DB2313-treatment were indeed targets of PU.1 (Fig. 7.3 A), followed by CTCF and FOXA2 (both over 70%). Targets of β -catenin-associated transcription factors (encoded by genes *TCF7L2* and *LEF1*) constituted less than 5% (Fig. 7.3 A).

The proteome (~90%) that was confirmed as target of PU.1 (via ChIP-seq) in DB2313-treated cells was subsequently compared to: (1) significantly altered cell-lysate proteome of aggregating FM3 cells (CL-agg; FS-24h vs TCP-24h), (2) significantly altered cell-lysate proteome of disaggregating FM3 cells (CL-disagg; FS-72h vs FS-24h), (3) significantly altered ECM proteome of aggregating FM3 cells (ECM-agg; FS-24h vs TCP-24h), and (4) significantly altered ECM proteome of disaggregating FM3 cells (ECM-disagg; FS-72h vs FS-24h). These comparisons (Fig. 7.3 B) revealed that PU.1-targets constitute 22.3% of CL-agg, 18.1% of CL-disagg, 12.8% of ECM-agg, and 13.8% of ECM-disagg. These shared proteins were used for the following analyses. Fold change values ($\text{Log}_2(\text{FC})$) of 'DB2313-treated vs untreated' proteome, were plotted against: (1) fold change values of CL-agg (Fig. 7.3 C), (2) fold change values of CL-disagg (Fig. 7.3 D), (3) fold change values of ECM-agg (Fig. 7.3 E), and (4) fold change values of ECM-disagg (Fig. 7.3 F). Proteins that were upregulated during PU.1-inhibition, assumed to be transcriptionally repressed by PU.1 in FM3 cells, that were downregulated during ADPM were highlighted in blue (Fig. 7.3 C-F). Proteins that were downregulated during PU.1-inhibition, assumed to be transcriptionally activated by PU.1 in FM3 cells, that were upregulated during ADPM were highlighted in orange (Fig. 7.3 C-F). Proteins not following these expression patterns assumed to be not transcriptionally regulated by PU.1 during ADPM (Fig. 7.3 C-F; are highlighted in grey).

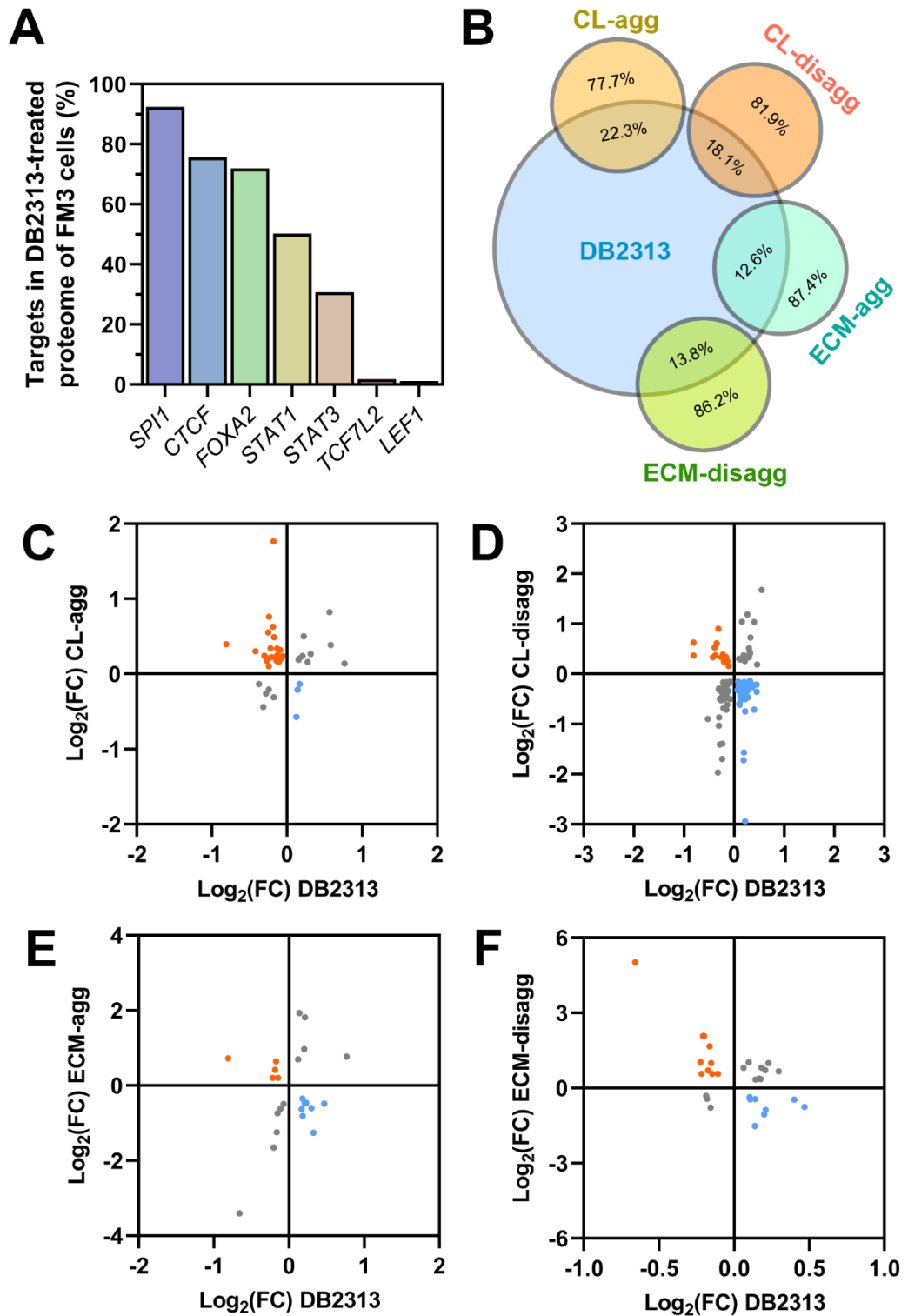
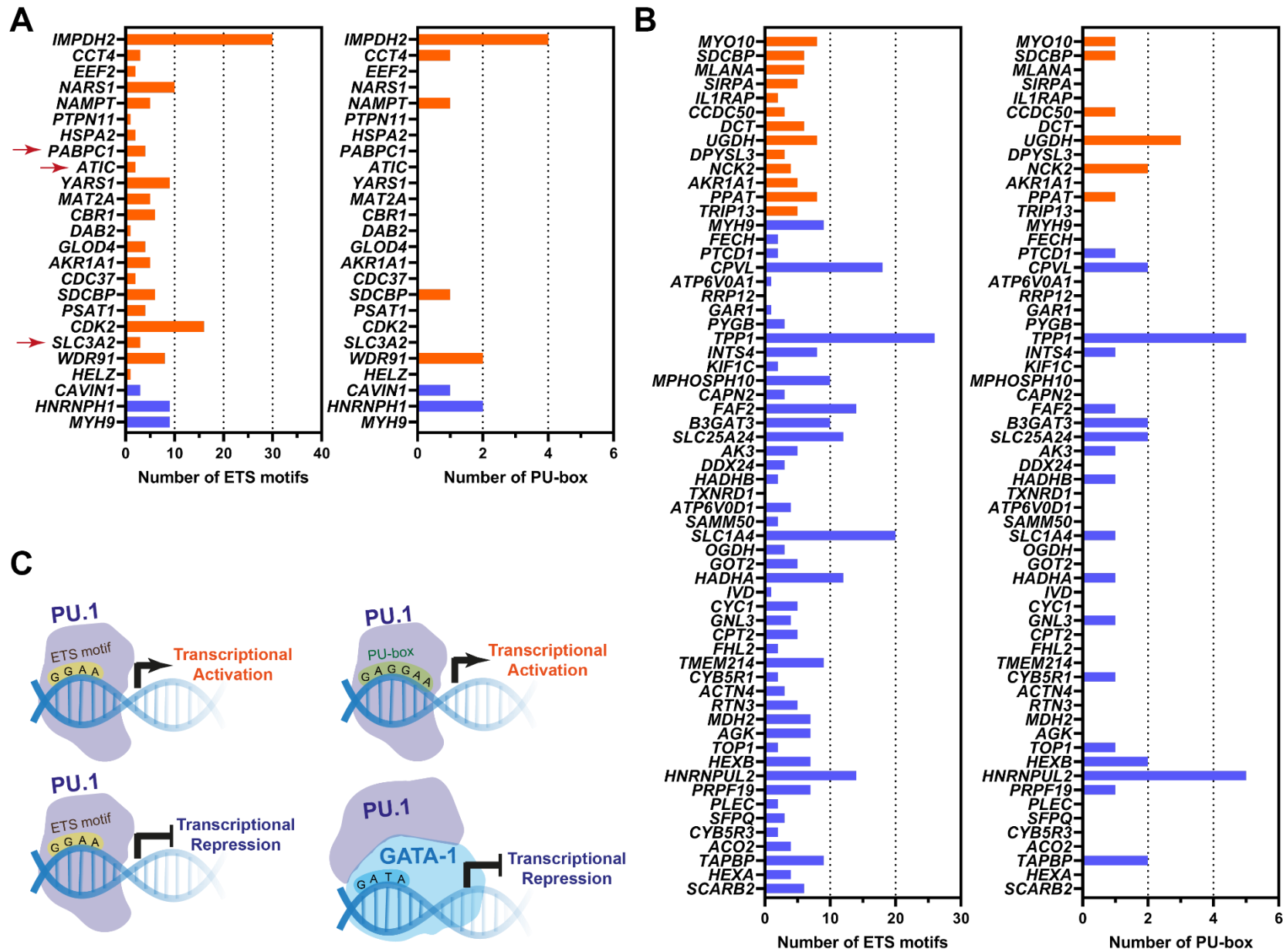


Fig. 7.3 Comparison of proteomic changes during inhibition of PU.1 and ADPM of FM3 cells. (A) Targets of PU.1 transcription factor and PU.1/ β -catenin-associated transcription factors (as obtained from hTFtarget tool ChIP-seq database found in the significantly altered ($p < 0.05$) proteome (measured via quantitative SWATH-MS) of DB2313-treated (10 μ M) FM3 cells. **(B)** Significantly altered ($p < 0.05$) proteome of DB2313-treated FM3 cells compared to cell-lysate proteome of aggregating FM3 cells (CL-agg; FS-24h vs TCP-24h), cell-lysate proteome of disaggregating FM3 cells (CL-disagg; FS-72h vs FS-24h), ECM proteome of aggregating FM3 cells (ECM-agg; FS-24h vs TCP-24h), and ECM proteome of disaggregating FM3 cells (ECM-disagg; FS-72h vs FS-24h). **(C-F)** Fold change ($\text{Log}_2(\text{FC})$) of DB2313-treated vs untreated proteome, compared to fold change of CL-agg proteome **(C)**, CL-disagg proteome **(D)**, ECM-agg proteome **(E)**, and ECM-disagg proteome **(F)**, to highlight candidate target proteins that could be transcriptionally regulated by PU.1; transcriptional activation highlighted in orange, transcriptional repression highlighted in blue, and proteins in grey denote whose transcription not regulated by PU.1 in ADPM. FS: fluoroalkylsilica, TCP: tissue culture polystyrene.

These gene-sets that could be transcriptionally activated or repressed by PU.1 during ADPM were next analysed for hypothetical PU.1 binding sites. These binding sites include ETS motif (5'-GGAA-3') and PU-box (5'-GAGGAA-3') upon which PU.1 could bind and activate gene transcription (Fig. 7.4 C). PU.1 could repress gene transcription by binding to an ETS motif, preventing other transcriptional activators from binding, or by interacting with the GATA-1 transcription factor that binds to GATA motifs (Fig. 7.4 C). Sequences of the transcriptionally activated or repressed gene-sets were obtained from Ensembl⁵⁰⁴ and analysed for the number of putative ETS motifs and PU-boxes present proximal to the promoter/Exon-1 region. Graphical depiction of these target genes is as follows: in the cell-lysate proteome during aggregation (Fig. 7.4 A; CL-agg) and disaggregation (Fig. 7.4 B; CL-disagg), and in the ECM proteome during aggregation (Supplementary Fig. 7.3 A; ECM-agg) and disaggregation (Supplementary Fig. 7.3 B; ECM-disagg). Notable genes that have been identified to be important for ADPM of FM3 cells in the previous chapters were highlighted with red arrows (Fig. 7.4): *SLCA3A2* gene that encodes the 4F2hc protein (identified in chapter 3-4), *ATIC* gene that encodes the PUR9 protein (identified in chapter 6), and *PABPC1* gene that encodes the PABP1 protein (identified in chapter 6).



7.2.4 PU.1 in clinical melanoma metastasis

To assess the impact of PU.1 expression on melanoma metastasis and prognosis, *in silico* analyses were performed using TCGA melanoma datasets (SKCM) (TCGA research network). The following results shown are in part based on data generated by the TCGA Research Network (<https://www.cancer.gov/tcga>). Patient survival datasets were obtained from OncoLnc.²⁸⁷ Each patient survival datasets were divided into two subsets using the median expression of PU.1 (high > median, low < median), and a Kaplan-Meier plot was generated to correlate effect of high vs low expression with melanoma patient survival (Fig. 7.5 A). Patients expressing low *SPI1* gene presented significantly poorer outcome (Fig. 7.5 A; median OS = 5.279y, compared to those presenting with high expression of the *SPI1* gene (Fig. 7.5 A; median = OS = 8.929y).

RNAseq gene expression datasets from clinical studies of melanoma (N = 1939) and metastatic melanoma (N = 358) were obtained from cBioPortal,²⁸⁶ and further normalised to a reference gene (*GAPDH*), to be able to compare the melanoma dataset with that of the metastatic dataset, to give a ratio of Gene of interest (GoI) mRNA expression to *GAPDH* mRNA expression (Fig. 7.5 B). No significant difference was observed in *SPI1* to *GAPDH* mRNA ratio between melanoma and metastatic melanoma (Fig. 7.5 B).

Risk score (meta Z-score) associated with melanoma (Z_1) and metastatic melanoma (Z_2) were obtained from PRECOG.³⁹¹ PRECOG uses the following data sets: for melanoma, PMID 20460471¹²⁸ and PMID 18505921;³⁹² and for metastatic melanoma PMID 18505921³⁹² and PMID 19915147.¹³⁰ 'Metastasis factor' ($Z_2 - Z_1$) was generated to determine the risk associated with PU.1 in contributing to metastasis of melanoma. The meta z-score associated with PU.1 in melanoma was -0.77 (Fig. 7.5 C), whereas the meta z-score associated with PU.1 in metastatic melanoma was -3.13 (Fig. 7.5 C), and the metastasis factor was -2.36 (Fig. 7.5 C). These observations suggest that prognostic risk associated with PU.1 expression was favourable for both metastatic melanoma and the process of metastasis.

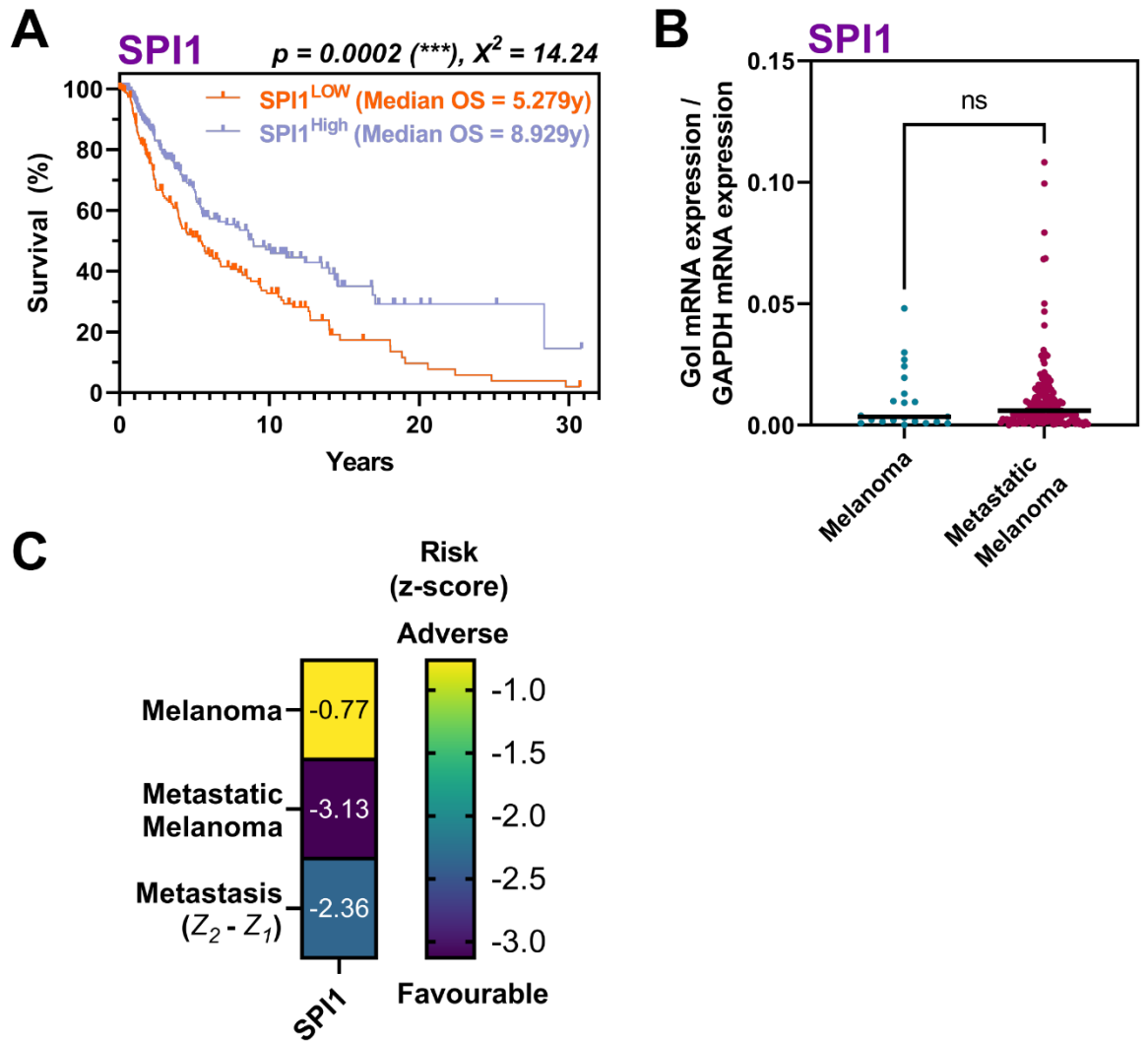


Fig. 7.5 Melanoma metastasis risk associated with PU.1. (A) Data obtained from OncoLnc from multiple melanoma RNA-sequencing and patient survival studies, highlight low *SPI1* expression is associated with poor patient survival, N=458. (B) Data obtained from cBioPortal from multiple melanoma and metastatic melanoma RNA-sequencing and patient survival studies, revealed no difference in *SPI1* mRNA levels between melanoma and metastatic melanoma, N=161. (C) Clinical melanoma and metastatic melanoma Z-score (meta) obtained from PRECOG tool associated with *SPI1* gene. Adjusted meta Z-score or ‘metastasis score’ ($Z_2 - Z_1$) calculated from Z-score of melanoma (Z_1) and metastatic melanoma (Z_2), indicates decreased *SPI1* expression during metastasis of melanoma associated with favourable outcome.

7.3 Discussion

PU.1 predominantly functions as the lineage-specific transcription factor for B-lymphoid and myeloid lineages;⁴⁸⁵ however, high expression of PU.1 in certain skin cells⁴⁹¹ raises the question of its function in the skin. Skin cells such as melanocytes originate from the neural crest during embryonic development; MITF and SOX10 transcription factors are responsible for the melanocytic lineage differentiation.³²⁰ Both MITF and PU.1 have been shown to cooperatively regulate over 1000 genes in osteoclast differentiation.⁵⁰⁵ Whether similar cooperativity between MITF and PU.1 occurs when driving early melanocytic differentiation or maintenance of the differentiated state remains to be elucidated. Melanoma cells often aberrantly reacquire early developmental transcription factors, such as MITF, to enhance their survival.⁵⁰⁶ Similarly, repurposing of PU.1 transcription factor could also occur during melanoma progression; this remains to be investigated.

PU.1 protein levels increased in fibroblasts isolated from fibrotic skin, compared to resting fibroblasts isolated from normal skin.⁵⁰⁷ Here, the authors revealed two notable functions of PU.1. Firstly, PU.1 expression was dependent upon TGF β /SMAD3-signalling. Secondly, expression of PU.1 induced a phenotypic switch similar to a mesenchymal-like/fibrotic-state, which involved the upregulation of many genes encoding pro-fibrotic extracellular matrix proteins, such as *COL1A1* (encodes collagen type I alpha 1 chain), *COL1A2* (encodes collagen type I alpha 2 chain), *ITGAV* (integrin subunit alpha V), and *THBS1* (encodes thrombospondin 1), as well as *TGFB1* (encodes TGF β 1) gene. In chapter 6, involvement of TGF β 1/ β -catenin-signalling and mesenchymal-like state in ADPM of melanoma FM3 cells were highlighted; bioinformatics analyses revealed PU.1 as candidate master transcription factor of ADPM. Though, PU.1 was shown to be upregulated in melanoma,⁴⁸² its role in progression or metastasis remains unclear. Therefore, this chapter aimed to reveal transcriptional regulation by PU.1 during ADPM of FM3 cells, in order to determine possible functional roles of PU.1 in the metastasis of melanoma.

7.3.1 PU.1 is involved invasion and migration during ADPM of FM3 cells

PU.1 expression during ADPM of FM3 cells was analysed via RT-qPCR, which revealed that *SPI1* mRNA (encodes for PU.1 protein) levels did not significantly change between aggregation (5h-24h) and disaggregation (48h-72h) (Fig. 7.1 A). Inhibition of PU.1 via DB2313-treatment did not affect FM3 multicellular aggregation (Fig. 7.1 E); though, there was a significant decrease in percentage of non-aggregates at 48 h and 72 h with 10 μ M of DB2313. However,

it is not clear whether the decrease in percentage of non-aggregates was due to PU.1-inhibition on multicellular disaggregation, or if it was due to the effect of PU.1-inhibition on cell-viability, as cell viability was significantly reduced DB2313-treatment at 10 μM (Fig. 7.1 C). No non-aggregates were observed at 48 and 72 h when cells were treated with 20 and 50 μM of DB2313, suggesting that at these concentrations DB2313-mediated cell-death responses highly eclipsed cellular disaggregation responses. Therefore, 10 μM of DB2313 was chosen as the concentration for subsequent experiments to investigate PU.1-mediated responses on ADPM without confounding the observations with PU.1-mediated responses on cell-death. An ideal experimental model for investigation of PU.1 on ADPM responses would be to use a cell-line which is not susceptible to PU.1-mediated cell-death responses, where effects on ADPM could be clearly observed. Alternatively, downstream targets of PU.1 responsible for these cell-death effects could be genetically knocked out in FM3 cells and study effects pertaining only to ADPM explored. For now, the conclusion that can be drawn from these experiments is that ADPM responses are not regulated by change in expression of PU.1.

Cellular viability assay revealed that treatment with 20 & 50 μM of the PU.1 inhibitor (DB2313) significantly decreased cellular viability of FM3 cells on both FS surfaces ($\text{IC}_{50} = 10.82 \mu\text{M}$) and TCP surfaces ($\text{IC}_{50} = 19.81 \mu\text{M}$) (Fig. 7.1 C); cellular viability was decreased even further on FS surfaces compared to TCP surfaces at 72h during disaggregation. DB2313-treatment inhibited cellular growth of AML cells at similar IC_{50} value ($\sim 7.1 \mu\text{M}$) as demonstrated by the study that developed DB2313.⁵⁰³ The reduced cellular-viability effect of inhibition of PU.1 could be attributed to one of its direct downstream targets *CDK6* gene,⁵⁰⁸ which encodes the cyclin dependent kinase 6 (CDK6) protein that associates with D-cyclins during the G1 phase and promotes progression through the cell cycle. As this was shown in erythroid cells, it remains to be seen whether PU.1 affects proliferation via CDK6 in melanoma and AML cells as well.

It is important to distinguish whether DB2313 had more of an inhibitory effect on FS surfaces compared to TCP surfaces, as even without DB2313-treatment FS surfaces exhibited reduced cellular-viability at 24 h (Chapter 3: Fig. 3.1 G), but not at the 72 h time point. An improvement of the cellular viability experiment in the present chapter could be to add two more controls, FM3 cells without any DB2313 on TCP and on FS surfaces, that would aid isolating reduction in cellular viability due to FS-surfaces from reduction in cellular viability due to DB2313-treatment. However, at 72 h, no difference in cellular viability was observed between FS surfaces and TCP surfaces (Chapter 3: Fig. 3.1 G), which suggests that the observed reduction in cell-viability on FS surfaces compared to TCP surfaces (Fig. 7.1 C) was likely due to DB2313-treatment. This suggests that PU.1 governs cellular proliferation more vigorously when cells disaggregated compared to when cells grew as a monolayer. This could be explained by the

following studies. When PU.1 was ectopically expressed in fibroblast cells, drastic macrophage-like cellular morphological changes was observed.⁵⁰⁹ PU.1 has been shown to connect cellular proliferation and differentiation programs in erythroid cells;⁵⁰⁸ erythroid differentiation accompanies major morphological changes. Moreover, PU.1 expression was shown to depend upon TGF β -signalling in fibrotic fibroblast cells;⁵⁰⁷ TGF β -signalling is highly involved in mesenchymal-like morphological changes.⁵¹⁰ These studies highlight PU.1 expression and its transcriptional regulation, including the genes involved in cellular proliferation, that may depend upon morphological cues. The morphological changes associated with ADPM of FM3 cells could reprogram PU.1-dependent regulation of cellular proliferation. This could be the mechanism in which metastasising CTC clusters reprogram their proliferation rates to be in line with ADPM state. A possible manner in which aggregated melanoma cells fine-tune PU.1-dependent gene regulation based on changes in morphology, could be via TGF β , β -catenin (highlighted in Chapter 6), or 4F2hc/Galectin-3 (highlighted in chapter 4). Future experiments could be carried out to determine which out of these signalling pathways convey morphological cues and influence PU.1-dependent gene regulation the most; the approach could be to inhibit these molecules via antibody and observe expression of the target genes of PU.1.

Invasiveness (Fig. 7.1 D) and migration (Fig. 7.1 F) of FM3 cells significantly increased when PU.1 was inhibited, on both TCP and FS surfaces. This implies that PU.1 could serve anti-invasive and anti-migratory functions in FM3 cells. In agreement with the present study, knockdown of PU.1 in hepatocellular carcinoma was also shown to promote invasion;⁵¹¹ the authors attributed the invasion-suppressive role of PU.1 to its transcriptional target gene *MIR615* that encodes the *miR-615-5p* microRNA. Previously, circulating cell-free *miR-615-3p* microRNA was detected in metastatic melanoma;⁵¹² though, in melanoma, its function remains unclear. Further experiments are needed to investigate *miR-615-5p* microRNA expression in FM3 cells during ADPM and during PU.1-inhibition. In contrast, in pancreatic ductal adenocarcinoma (PDAC), overexpression of *miR-615-5p* microRNA inhibited migration, and invasion;⁵¹³ however, as of now, studies have not investigated PU.1 function in PDAC. It is possible that target mRNAs that *miR-615-5p* microRNA could translationally repress differ between PDAC and melanoma cell; which could explain similar cellular responses caused by different treatments, i.e., inhibition of PU.1 in FM3 cells and overexpression of *miR-615-5p* microRNA in PDAC cells. However, both melanoma and PDAC cells exhibited dependency upon, PU.1 expression in the former (Fig. 7.1 C), and *miR-615-5p* microRNA in the latter,⁵¹³ for regulation of cellular proliferation. This is indicative of the primary function of PU.1 in cancer cells being the governance of cellular proliferation, and secondary cancer-type/cell-specific function being invasion/metastasis-suppression.

The increase in invasiveness (Fig. 7.1 D) and migration (Fig. 7.1 F) due to PU.1-inhibition was reduced in FM3 cells isolated from multicellular aggregates (FS-24h) compared to single cells (TCP-24h). This suggests that PU.1 exerted less of an inhibitory effect on invasiveness and migration on aggregated cells compared to single cells. Target genes of PU.1 that were responsible for PU.1-mediated suppression of invasiveness and migration, expression of which were likely reduced in aggregated cells compared to single cells are currently unknown. Characterising these target genes could provide further insights into metastasis-suppression by PU.1.

7.3.2 PU.1 mediates key pathways involved in cellular proliferation, migration, and invasion in FM3 cells

In haematological cells, PU.1 regulates certain cellular communication pathways, such as antibody receptor-signalling, cytokine receptor-mediated signalling to regulate growth, and cytokine receptor-mediated regulation of inflammation.⁵¹⁴ In FM3 cells, inhibition of PU.1 upregulated proteins involved in the tricarboxylic acid cycle pathway (Fig. 7.2 A). Similarly, other studies have also highlighted involvement of PU.1 in regulation of metabolic genes, such as genes involved in pyruvate metabolism,⁵¹⁵ as well as lipid metabolism.⁵¹⁶

Furthermore, during PU.1-inhibition in FM3 cells, proteins involved in actin cytoskeleton organisation and regulation of cell shape pathways were upregulated (Fig. 7.2 A). Notably, the small GTPase RhoC, which regulates cellular morphology and migration,⁵¹⁷ was upregulated during PU.1-inhibition (Supplementary Fig. 7.2 B). A previous study showed that exogenous induction of RhoC expression in cutaneous melanoma cells increased invasion and metastasis, and inhibition of RhoC reversed this phenotype both *in vitro* and *in vivo*.⁵¹⁸ Similarly, RhoC was upregulated in a highly metastatic melanoma cell line (DX3aza).⁵¹⁹ These findings provide an explanation for the increased invasion and metastasis during PU.1-inhibition in FM3 cells (Fig 7.1 D & F) where RhoC levels were likely elevated. As integrins act as the predominant upstream inducer of the Rho Family of GTPases,⁵²⁰ integrin- α 2 (Supplementary Fig. 7.2 D), Integrin- α 3 (Supplementary Fig. 7.2 E), and integrin- β 1 (Supplementary Fig. 7.2 F) were also upregulated during PU.1 inhibition. Members of the Wnt-signalling pathway, LEF1 (Fig. 7.2 F) and Wnt-5a (Supplementary Fig. 7.2 C), were also upregulated during PU.1-inhibition. Indeed, Wnt-signalling plays a major role in cellular motility and invasion both during development and in metastasis.⁵²¹ Through non-canonical signalling via dishevelled (Dvl), an effector protein that acts as the branchpoint for Wnt-signalling and Rho-signalling,⁵²² complexes of Dvl and Dvl-associated activator of

morphogenesis 1 (DAAM1) protein⁵²³ may activate Rho GTPase and Rho-associated kinase (ROCK), which subsequently modifies cytoskeletal architecture during cellular motility.

Certain proteins involved in the assembly of actin filament bundles and substrate-dependent cellular migration pathways were downregulated during PU.1-inhibition (Fig. 7.2 A). Notably, focal adhesion kinase 1 (FAK1) levels were decreased (Fig. 7.2 C). This was surprising as FAK relays signals from integrins at sites of focal adhesions in order to regulate cell migration.⁵²⁴ FAK was highlighted as a major player in melanoma progression, as phosphorylated/activated FAK was correlated with increased invasion and migration in aggressive uveal and cutaneous melanoma cells.⁵²⁵ A possible explanation for the decrease in FAK1 levels during PU.1-inhibition, where cellular motility/invasion was enhanced, could be that PU.1 may increase FAK1 turnover to sensitise cells to signals from integrins and growth factors. Indeed, several transcriptional regulatory elements and binding sites were shown to be upstream of the FAK promoter, including those associated with PU.1, NF- κ B, AP-1, AP-2, and TCF-1.⁵²⁶ This indicates that a variety of stimuli, including integrins and growth factors, could act to enhance FAK turnover to enhance cell motility. This highlights that PU.1, predominantly an anti-migratory/anti-invasive transcription regulator, depending on environmental/mitogenic cues, could work alongside other factors to fine-tune FAK-dependent cellular migratory signalling pathways.

Proteins involved in melanocyte differentiation (Fig. 7.2 A), most notably MITF (Fig. 7.2 A) and DCT (Fig. 7.2 D), were downregulated during PU.1-inhibition. Both MITF and DCT drives several key genetic transcriptional programs required for melanocyte differentiation.⁵²⁷ This suggests that downregulation of PU.1 could lead to an undifferentiated state, similar to that of a mesenchymal state (explored in more detail in Chapter 6), for example during metastasis, where such a state is more suitable for invasion and migration.⁵²⁸ Another protein involved in cellular differentiation and gene expression, histone deacetylase 1 (HDAC1) was upregulated during PU.1-inhibition (Fig. 7.2 G), suggesting that HDAC1-dependent gene transcription may continue in spite of depletion of PU.1, MITF and DCT activities. However, contradicting this observation, another study showed that treating melanoma cells with histone deacetylase inhibitors repressed MITF expression,⁵²⁹ clearly highlighting the collaboration between MITF and HDAC in maintaining a differentiated state. This must mean that HDAC1 likely works alongside MITF, DCT and PU.1 to keep a 'melanocyte-like' quasi-differentiated state in melanoma cells; where downregulation of PU.1 during metastasis could trigger a MITF^{low}/DCT^{low} 'undifferentiated state', in which HDAC1 could still maintain some elements of the differentiated state programs which could be beneficial for metastasis. Further research is required to isolate these gene regulatory programs carried out by MITF/DCT/HDAC1 in

driving differentiation that could be detrimental for metastasis, from that of HDAC1-dependent gene regulation involved in maintaining certain melanocyte-like traits that could be beneficial for metastasis.

Moreover, proteins involved in purine nucleotide biosynthesis were downregulated during PU.1-inhibition (Fig. 7.2 A). Notably, PUR9 levels were decreased when cells were treated with PU.1-inhibitor; PUR9 was highlighted as a member of the β -catenin-interactome involved in ADPM of FM3 cells in chapter 6. Purines are the most abundant and readily available substrates for the synthesis of DNA and RNA.⁵³⁰ Purines could also be metabolised to provide energy, and intermediates such as adenylate and guanylate that could be incorporated into many cofactors, for example coenzyme A.⁵³¹ As such, *de novo* purine nucleotide biosynthesis is intrinsically coupled to cellular proliferation. Therefore, the decrease in the levels of the members of the purine nucleotide biosynthesis pathway during PU.1-inhibition, could be one of the reasons for the decrease in cellular proliferation that was observed when FM3 cells were treated with DB2313 (Fig. 7.1 C). Interestingly, a recent study showed that depletion of purine nucleotides stimulated the serine synthesis pathway and promoted cellular migration, by triggering EMT-like processes, and metastatic colonisation in cancer models.⁵³² Together, these findings highlight that *de novo* purine synthesis could be altered by cancer cells by affecting PU.1 levels to both simultaneously increase invasive capabilities and reduce cellular proliferation during metastasis.

A limitation with the present analysis was that the DB2313-treated FM3 cells MS dataset was not corrected for multiple comparisons, as a vast number of proteins were detected (6485 total proteins) and statistical testing was carried out on all of these proteins to outline the 755 (11% of the total) significantly changed proteins. This meant that any correction for multiple comparisons to reduce false positive rates, for example via Bonferroni correction, would be too stringent and would lead to no significant discoveries. However, without correction for multiple comparisons, there could be false positive observations, at least 5% with a selection criterion of p-value < 0.05, that could weaken the validity of the dataset. One method by which the present study overcame this limitation was to carry out ontology-based discoveries, based on molecular function and biological processes, in which rather than observing expression changes of a single protein (that could potentially be a false positive), the ontology-based analyses take into consideration clusters of proteins. The chances of all proteins within a cluster being false positives are comparatively low. In cases where certain proteins were considered by themselves, to reduce the risk of the discovery being false positive and to lend further support, the comparison was carried out alongside their molecular function/biological processes related ontology-based protein clusters. Further experiments,

such as western blot, could be carried out to validate the changes in levels of these individual proteins associated with DB2313-treatment. At the very least, this dataset highlighted the involvement of PU.1 in FM3 cells in regulating key biological processes, including actin cytoskeletal organisation and melanocyte differentiation, that could be altered by melanoma cells via reduction in PU.1 levels during metastasis.

7.3.3 PU.1 regulates expression of key proteins involved in ADPM of FM3 cells

Both 4F2hc and Galectin-3 were revealed as important proteins for aggregation of FM3 cells (in chapter 4). Inhibition of PU.1 in FM3 cells leading to a significant reduction in 4F2hc levels (Fig. 7.2 B) but not Galectin-3 levels (Supplementary Fig. 7.2 A), implies that transcription of *SLC3A2* gene (that encodes for 4F2hc) could be regulated by PU.1, however transcription of *LGALS3* gene (that encodes for Galectin-3) might not be regulated by PU.1 in FM3 cells. The intron 1 *SLC3A2* gene contains several enhancer elements, including a consensus binding site for the inducible AP-1 transcription factor,⁵³³ which regulates gene expression in response to a plethora of stimuli, such as cytokines, growth factors, and stress.⁵³⁴ Thus, it is conceivable that PU.1, in conjunction with AP-1 as part of the ensemble of *cis*-acting elements, could regulate the transcription of the *SLC3A2* gene, in response to these stimuli. One stimulus could be stress/reduced adherence-induced response that could trigger the enhancement of 4F2hc expression via PU.1/AP-1 *cis*-acting enhancers, that could ultimately lead to multicellular aggregation during ADPM. However, no previous studies implicate PU.1 in the regulation of 4F2hc expression or reported consensus binding sites of PU.1, such as the PU-box or ETS motifs, in the promoter of the *SLC3A2* gene.

Moreover, an ideal experiment that could have been carried out to highlight PU.1-dependent regulation of 4F2hc expression during ADPM of FM3 cells, could be to treat FS-surface-induced aggregates with DB2313 and measure 4F2hc levels via western blot; however, this experiment was not carried out due to lack of time and resources. As such, PU.1-dependent regulation of 4F2hc during ADPM can only be indirectly inferred from observing change in 4F2hc levels in the MS dataset during inhibition of PU.1 in single FM3 cells (TCP-24h). Therefore, to corroborate PU.1-target genes, including the *SLC3A2* gene, within the proteomic changes associated with ADPM (FS-24h to FS-72h), DB2313-treated FM3 cell (TCP-24h) MS dataset was compared with both cell-lysate and ECM proteome of aggregating (FS-24h vs TCP-24h) and disaggregating (FS-72h vs FS-24h) FM3 cells (Fig. 7.3 B).

To narrow the discoveries strictly to PU.1-targets, the DB2313-treated FM3 cells proteome was first compared to PU.1-bound genes (Fig. 7.3 A) obtained from an online database of

ChIP-seq, called hTFtarget tool.³⁹⁵ This provided further support that the proteomic changes observed during DB2313-treatment were indeed due to depletion of PU.1 binding to the promoters of its target genes. At least 90% of the altered proteome of DB2313-treated FM3 cells were targets of the *SPI1* gene (that encodes PU.1) (Fig. 7.3 A), with *CTCF* and *FOXA2* genes that encodes the CCCTC-binding factor and Forkhead Box A2 transcription factors, respectively, possibly co-regulating the transcription of approximately 75% of these PU.1-target genes (Fig. 7.3 A). It is beyond the scope of the present study to address the co-regulation of PU.1-target genes by these two transcription factors. Further experiments, such as electrophoretic mobility shift assays or chromatin immunoprecipitation,⁵³⁵ could be carried out to test simultaneous binding of these transcription factors to nucleosomes.

Comparing the significantly altered proteome of DB2313-treated cells with significantly altered proteome CL-agg, CL-disagg, ECM-agg, and ECM-disagg, revealed that only ~12-22% (Fig. 7.3 B) of the altered proteome was likely regulated by PU.1 during ADPM of FM3 cells. This implies that the majority of the proteomic changes could be under the control of other transcription factors. Future research could address other important transcription factors involved in progression of melanoma, such as MITF, SOX10, p53, MYC, c-Jun, CREB and FOXO3a,⁵³⁶ that could also drive these proteomic changes associated with ADPM.

Next, considering only those proteins that could be altered by PU.1 (12-22%), transcriptional activation (Fig. 7.4 C), and transcriptional repression (Fig. 7.4 C) by PU.1, were deduced by plotting fold change values of DB2313-treated vs untreated proteome against fold change values of CL-agg (Fig. 7.3 C), CL-disagg (Fig. 7.3 D), ECM-agg (Fig. 7.3 E), ECM-disagg (Fig. 7.3 F). Proteins that were upregulated during ADPM but downregulated during DB2313-treatment were considered as transcriptionally activated by PU.1 during ADPM (Fig. 7.3 C-F; highlighted in orange). In contrast, proteins that were downregulated during ADPM but upregulated during DB2313-treatment were considered as transcriptionally repressed by PU.1 during ADPM (Fig. 7.3 C-F; highlighted in blue). Another assumption was that those proteins not following this pattern were not transcriptionally regulated by PU.1 during ADPM (Fig. 7.3 C-F; highlighted in grey). However, ChIP-sequencing revealed that all of these genes were bound to PU.1;³⁹⁵ this implies that PU.1 has the capability to regulate the expression of these proteins (highlighted in grey), but during ADPM, their expression could be regulated by other *cis*-acting regulatory elements that overwhelms PU.1-mediated responses. One such transcription factor could be GATA-1, which has been shown to negatively regulate *cis*-acting responses of PU.1.⁴⁸⁸

DNA sequence analyses of these PU.1-mediated transcriptionally regulated proteins, revealed that the genes of all of these proteins had several ETS motifs, 5'-GGAA-3' motif that PU.1

could bind,⁴⁸⁷ proximal to the promoter/Exon-1 (Fig. 7.4 A-B, Supplementary Fig. 7.3 A-B). However, only a select few of these genes had any PU-box, 5'-GAGGAA-3' sequences that PU.1 has been shown to preferentially bind to,⁴⁸⁶ proximal to the promoter/Exon-1 (Fig. 7.4 A-B, Supplementary Fig. 7.3 A-B). The *SLC3A2* gene that encodes for 4F2hc (in chapters 3-4), the *AT1C* gene that encodes for PUR9 (in chapter 6), the *PABPC1* gene that encodes for PABP1 (in chapter 6), highlighted as important for ADPM of FM3 cells, all contained several ETS motifs but no PU-box (Fig. 7.4 A: red arrows). The consequence of a gene possessing ETS motifs vs PU-box in the strength of PU.1-mediated transcriptional regulation requires further investigation. In any case, these analyses provided further insights into PU.1-binding to ETS motifs proximal to the promoter/Exon-1 region of 4F2hc, PUR9, and PABP1 that could potentially enhance the expression of these proteins during ADPM of FM3 cells. Carrying out future experiments such as ChIP sequencing to investigate the regional occupation of PU.1 near the transcription start site of these genes could lend further support. There still remain some unanswered questions. How is the transcriptional repression mediated by PU.1? Is it by PU.1 binding near to regions that are normally occupied by other transcriptional factors, such as GATA-1,⁴⁸⁸ thus preventing GATA-1-mediated transcriptional activation? Moreover, since PU.1 levels did not change during ADPM, how is PU.1-mediated transcriptional regulation controlled to fine-tune the differential expression of proteins observed during ADPM, for example elevated levels of 4F2hc in aggregates? Is it by changes in levels of co-regulators, such as AP-1, that could modulate PU.1-activity? Future research addressing these questions could provide further insights into the complex transcriptional regulation of important genes involved in ADPM of melanoma cells.

7.3.4 PU.1 expression dictates clinical melanoma metastasis and survival outcome

Bioinformatics analyses of RNAseq and melanoma patient survival data obtained from online repositories (TCGA, cBioPortal and PRECOG), revealed that patients expressing low levels of the *SPI1* gene presented significantly poorer overall survival compared to those expressing high levels (Fig. 7.5 A), and *SPI1* expression was associated with favourable outcome of both metastatic melanoma and the process of metastasis itself (Fig. 7.5 C). This implies that expression of PU.1 is somehow detrimental for melanoma metastasis, but good for survival outcome of patients. Melanoma could manifest as two distinct phenotypes, *SPI1*^{low} and *SPI1*^{high}, with vastly different patient survival outcome. The *SPI1*^{high} phenotype could be less migratory and less invasive, wherein PU.1 transcriptionally repress expression of RhoC and

integrins, which leads to favourable survival outcome. In contrast, *SPI1*^{low} phenotype might be less proliferative, but highly invasive, as RhoC and integrins expression could be elevated.

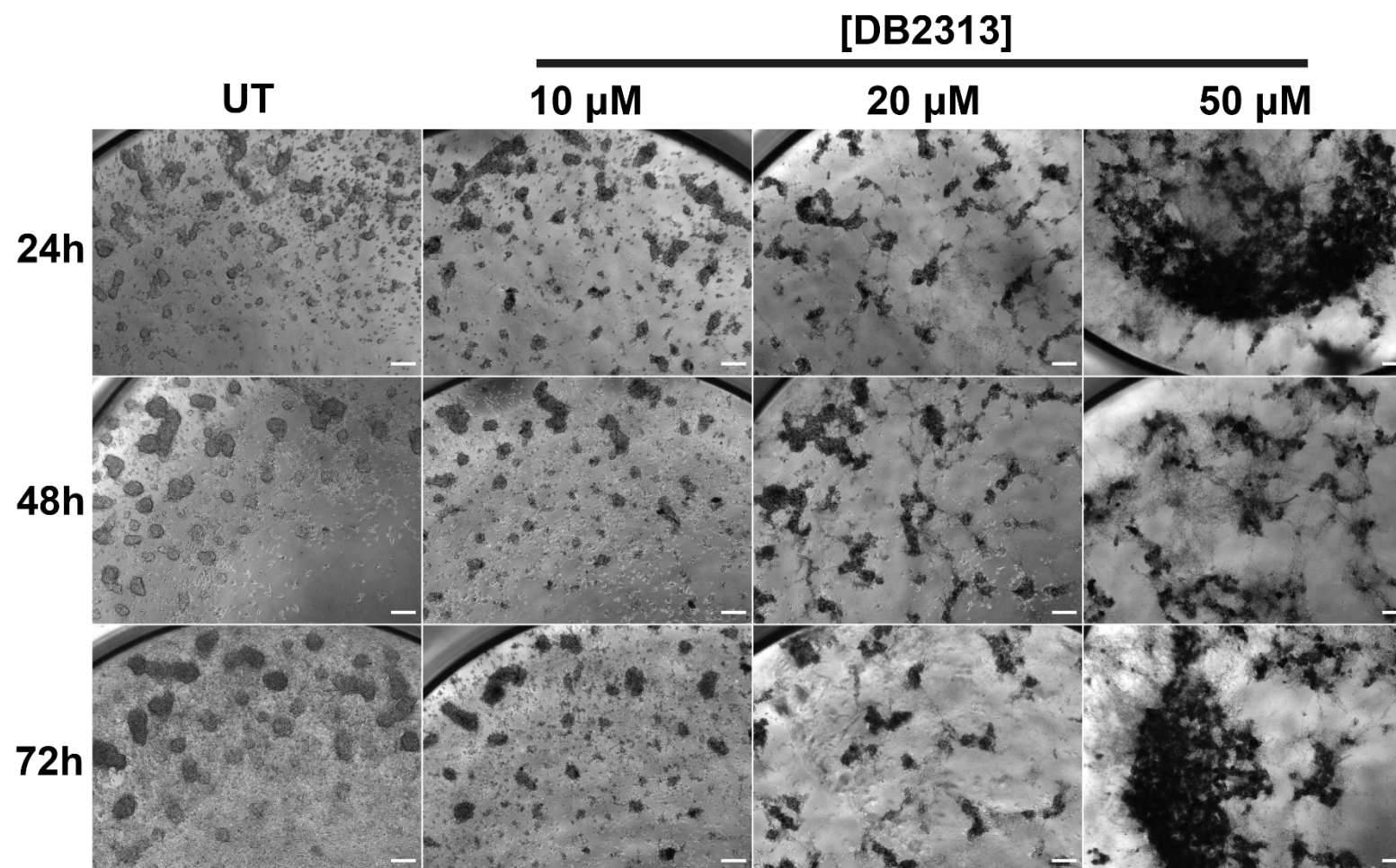
There was no significant difference in *SPI1* mRNA levels between melanoma and metastatic melanoma lesions (Fig. 7.5 B). Therefore, any influences of PU.1 on risk associated with melanoma metastasis must originate during haematological transit. Furthermore, it is paradoxical that in *SPI1*^{high} phenotype, 4F2hc levels would be elevated, and thus these cells would be more prone to multicellular aggregation and ultimately lead to increased metastasis risk due to the formation of melanoma CTC clusters;³⁴⁶ however, the overall risk associated with *SPI1*^{high} phenotype is favourable. An explanation for this could be that *SPI1*^{low} phenotype represent a population of melanoma cells that is undifferentiated, due to reduced MITF and DCT expression, which could readily disaggregate and readily invade through the stroma at distal metastatic sites. The *SPI1*^{low} phenotype could still undergo multicellular aggregation via 4F2hc, as PU.1 expression could be exogenously induced, for example via TGFβ/SMAD3-signalling.⁵⁰⁷ An important source of TGFβ for CTC clusters during haematologic transit could be platelets.⁵³⁷ Sustained TGFβ/SMAD3-signalling could lead to upregulated PU.1 expression in *SPI1*^{low} phenotype, which could lead to 4F2hc expression and multicellular aggregation. Interestingly, inhibition of PU.1 leading to increase in invasiveness (Fig. 7.1 D) and migration (Fig. 7.1 F) was more pronounced when cells were single (TCP-24h) compared to when they were aggregated (FS-24h), which indicates that perhaps CTC clusters could possess molecular machinery that can override the anti-invasive effects of PU.1 whilst still maintaining the pro-aggregation effects. Further research is required to address precisely which molecules or pathways allows this in melanoma CTC clusters.

A limitation with the present analysis is that an ideal dataset here would be RNA-seq of CTC clusters and cognate patient survival outcomes. As this was not available, the meta z-score risk associated with the metastasis factor was used to gain some insights into the risk changes in PU.1 levels in CTC clusters could pose. A future experiment could be to transplant genetically modified melanoma cells representing *SPI1*^{low}/*SPI1*^{-/-} and *SPI1*^{high} phenotypes, into mice and observe frequency of CTC cluster formation, frequency of secondary metastasis, and associated survival outcome. This could provide further insights into ADPM of these distinct melanoma phenotypes. All things considered, the present study provided insights into the molecular signatures of the different melanoma phenotypes, and what these signatures entail for their propensity to form CTC clusters and metastasis.

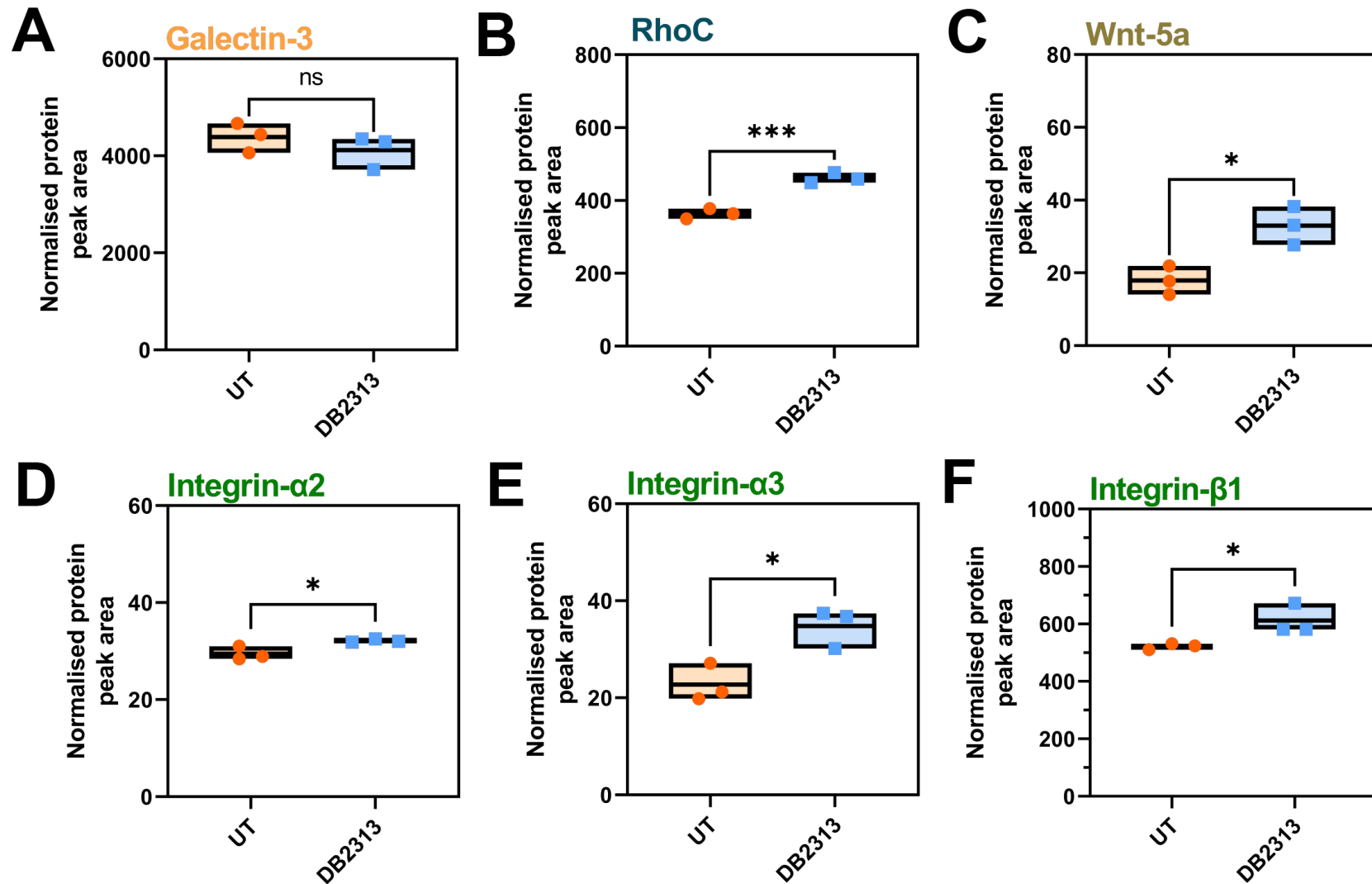
7.3.5 Conclusions

This chapter aimed to explore the involvement of the transcription factor PU.1 in ADPM of FM3 cells. Though *SPI1* mRNA levels did not change during ADPM, inhibition of PU.1 resulted in increased invasiveness and migration, and reduced viability. This anti-invasive effect of PU.1 was less pronounced when cells were aggregated compared to single cells. This could be the way in which CTC clusters may override the anti-invasive effects of PU.1, whilst maintaining pro-aggregation responses, such as increased 4F2hc levels; though, further research is required to address the specific molecules that allows this complex transcriptional regulation by PU.1. In FM3 cells, inhibition of PU.1 resulted in changes in proteins associated with actin cytoskeleton organisation, notably RhoC and integrins were upregulated, which explains the anti-invasive effects of PU.1. Proteins important for melanocyte differentiation, namely MITF and DCT, were downregulated when PU.1 was inhibited; this explains the undifferentiated state observed in metastatic melanoma. Around 12-22% of the altered proteome during ADPM of FM3 cells were likely transcriptionally regulated by PU.1; this raises the question as to which master transcription factors could regulate the transcription of the majority of proteins. PU.1, however, does seem to transcriptionally activate important proteins for ADPM of FM3 cells, namely 4F2hc, PUR9 and PABP1, likely by binding to ETS motifs proximal to the promoters of their genes. This research clearly illustrates the transcriptional regulation by PU.1 in melanoma, the differential molecular signatures that could be brought upon by the two *SPI1*^{low} and *SPI1*^{high} phenotypes, that could ultimately dictate the propensity of CTC cluster formation and metastasis, and prognosis of disease for patients.

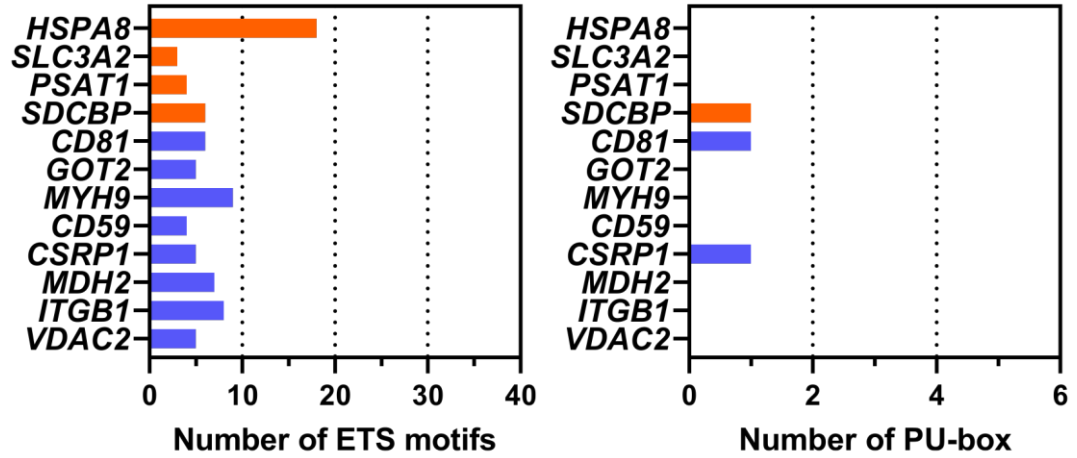
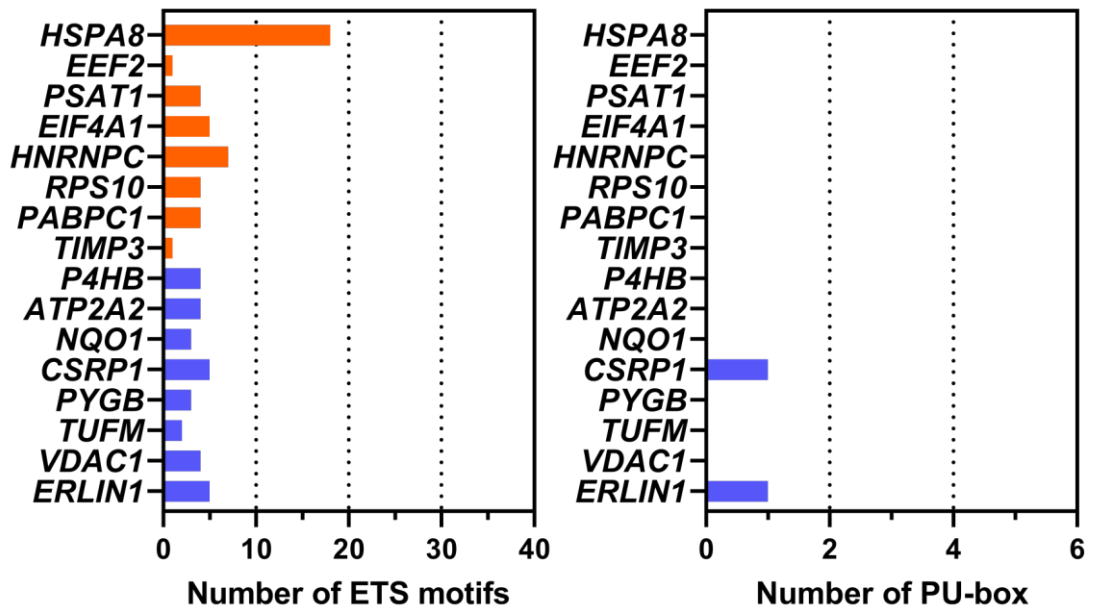
7.4 Supplementary Figures



Supplementary Fig. 7.1 DB2313 treatment of FM3 cells. Representative micrographs of FM3 cells treated with increasing concentration of DB2313 on FS surfaces, n=6. Scale = 200 μM . FS: fluoroalkylsilica,



Supplementary Fig. 7.2 Effect of DB2313 treatment on key proteins important for ADPM of FM3 cells. (A - F) Quantitative SWATH-MS (n=3) reveals changes associated with DB2313 treatment (10 μ M) in levels of (A) Galectin-3, (B) RhoC, (C) Wnt-5a, (D) Integrin- α 2, (E) Integrin- α 3, and (F) Integrin- β 1. Student's T-tests (two-tailed distribution, heteroscedastic) were carried out for A - F. FS: fluoroalkylsilica, SWATH-MS: Sciex TripleTOF 6600 data-independent acquisition mass spectrometry, TCP: tissue culture polystyrene.

A**B**

Supplementary Fig. 7.3. PU.1-binding sites in candidate PU.1-target genes activated or repressed during ADPM of FM3 cells. (A-C) Sequences of PU.1-target genes were obtained from Ensembl. Number of ETS-motif and PU-box found in genes likely to be transcriptionally activated (highlighted in orange), or transcriptionally repressed (highlighted in purple), by PU.1 within the ECM proteome of aggregating cells (ECM-agg) (A) or ECM proteome of disaggregating cells (ECM-disagg) (B) of FM3 cells.

Chapter 8. Conformational changes of fibronectin and vitronectin during adsorption onto hydrophobic FS and TCP surfaces

Contents

CHAPTER 8. CONFORMATIONAL CHANGES OF FIBRONECTIN AND VITRONECTIN DURING ADSORPTION ONTO HYDROPHOBIC FS AND TCP SURFACES	162
8.1 INTRODUCTION	163
8.2 RESULTS.....	165
8.2.1 Differential adsorption and fibril formation of fibronectin and vitronectin on FS and TCP surfaces.....	165
8.2.2 Conformational changes of fibronectin and vitronectin during adsorption onto FS and TCP surfaces.....	167
8.2.3 Sequential perturbation of secondary structures of fibronectin and vitronectin during adsorption onto FS and TCP surfaces.....	171
8.3 DISCUSSION	174
8.3.1 Conclusions	177
8.4 SUPPLEMENTARY FIGURES	178

8.1 Introduction

Two important matrisomal proteins, fibronectin and vitronectin, were identified to be involved in FM3 multicellular aggregation-disaggregation on FS surfaces (Chapter 3: Fig. 3.3 D & E). Fibronectin is a glycoprotein (~230 to 270 kDa), commonly exists as a dimer covalently linked by a pair of disulphide bonds proximal to the C-terminus⁵³⁸ (Fig. 8.0 C). The fibronectin sequence consists of repeating units of three different types of domains (type I, II, and III) (Fig. 8.0 A). All three domains consist of two antiparallel β -sheets, forming a β -sandwich, with type III differing from the other two types by not possessing any intra-chain disulphide bonds.⁵³⁹

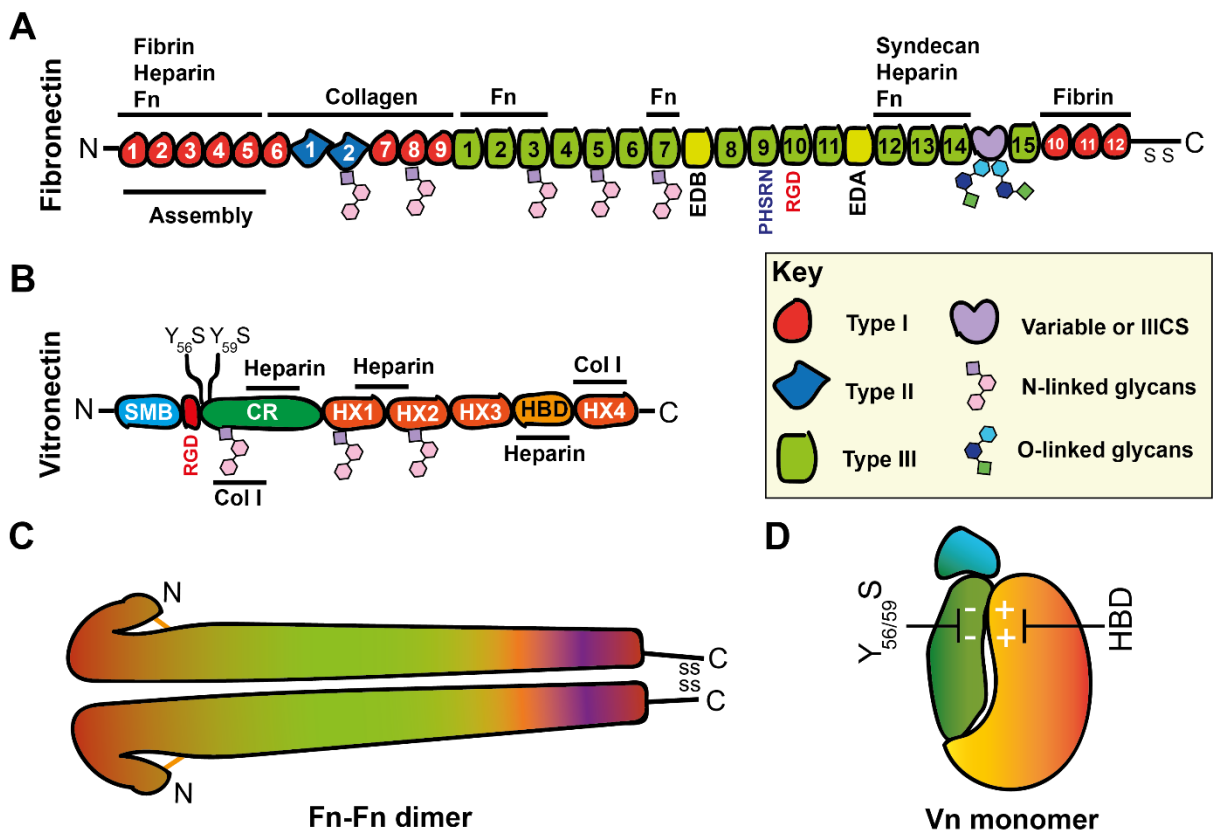


Fig. 8.0 Schematic of human fibronectin and vitronectin structures. (A) Unfolded structure of fibronectin; highlighted are domain types, glycosylation sites and sites for association with other matrisomal proteins. (B) Unfolded structure of vitronectin; highlighted are domain types, glycosylation sites and sites for association with other matrisomal proteins. (C) Structure of fibronectin dimer. (D) Folded structure of vitronectin monomer. Fn: fibronectin, HBD: heparin binding domain, Vn: vitronectin.

On the other hand, vitronectin is a much smaller glycoprotein (54 kDa), consisting of three distinct domains (Fig. 8.0 B): N-terminal somatomedin B (SMB) domain, central hemopexin homology

domains (HX 1-3) and C-terminal hemopexin homology domain (HX4), and heparin binding domain (HBD).⁵⁴⁰ SMB and HX1 domains often are linked by a connecting region (CR). NMR spectroscopic studies revealed that SMB domain is comprised of a single-turn α -helix, loosely defined 3_{10} helix, and flexible loops.⁵⁴¹ Structure of hemopexin has also been resolved; contains four-bladed β -propeller fold, with each blade consisting of four stranded antiparallel β -sheets.⁵⁴²

Both fibronectin and vitronectin interact and activate integrin family of cell surface receptors.⁵⁴³ As such, these glycoproteins play important roles in various biological phenomena, cellular adhesion to basement membrane, cell migration and wound healing.^{544,545} Expectedly, these two proteins have been heavily implicated in tumorigenesis^{546,547} and tumour metastasis.^{548,549} In melanoma, fibronectin has been shown to promote cellular proliferation and metastasis.¹⁰⁰ Likewise, intact vitronectin molecules have been shown to enhance invasion of melanoma cells by induction of matrix metalloproteinase-2.⁵⁵⁰

FM3 melanoma cells were shown to aggregate on FS surfaces at 24 h, however they grew as a monolayer on TCP surfaces (Chapter 3: Fig. 3.1 A). At 72 h, these multicellular aggregates achieved near-complete disaggregation on the FS surfaces (Chapter 3: Fig. 3.1 A). Mass spectrometry analyses of the underlying matrisomal proteins during this aggregation-disaggregation cascade revealed both fibronectin and vitronectin levels were reduced during aggregation (at 24 h) (Fig. Chapter 3: Fig. 3.3 D & E), and levels of both proteins notably increased during disaggregation (at 72 h), reaching levels comparable to those deposited on TCP surfaces (at 72 h). These results clearly highlighted the importance of these proteins in driving multicellular disaggregation. However, the extent to which these proteins contribute to multicellular aggregation remains elusive.

Therefore, this chapter aims to study conformational changes of fibronectin and vitronectin accompanying adsorption onto TCP and FS surfaces, using FTIR-ATR spectroscopy, conformer fitting, and two-dimensional (2D) correlation spectroscopy analyses. These analyses could provide insights into changes in secondary structures of fibronectin and vitronectin, and subsequent effect on cellular adhesion, during the early stages of adsorption onto the hydrophobic TCP and FS surfaces.

8.2 Results

8.2.1 Differential adsorption and fibril formation of fibronectin and vitronectin on FS and TCP surfaces

To determine adsorption kinetics of fibronectin and vitronectin on FS and TCP surfaces, recombinant human fibronectin and vitronectin molecules were incubated on the surfaces for 24 hours. Subsequently, amido black assay was carried out as outlined previously,⁵⁵¹ followed by Langmuir curve fitting. Amido black assay showed that after 24 h of incubation, the amount of fibronectin adsorbed onto FS surface was higher compared to TCP surface (Fig. 8.1 A). In contrast, vitronectin adsorption was higher on TCP surface compared to FS surface (Fig. 8.1 B).

Immunofluorescence was carried out to visualise the micro-architecture of fibronectin or vitronectin-based matrices deposited by FM3 cells. FM3 cells were grown on FS or TCP surfaces. After 24 h or 72 h, cells were removed to expose the deposited matrices. Fibronectin or vitronectin molecules were detected using protein-specific primary antibodies and illuminated using fluorescence-tagged secondary antibodies. Immunofluorescence images confirmed that similar to the amido black assay of recombinant human protein incubation (Fig. 8.1 B), higher amount of vitronectin was deposited onto TCP surface compared to FS surface (Fig. 8.1 D). In contrast to amido black assay using recombinant fibronectin, cell-based deposited fibronectin and subsequent adsorption was higher on TCP surface compared to FS surface (Fig. 8.1 C). Interestingly, both fibronectin (Fig. 8.1 C) and vitronectin (Fig. 8.1 D) formed extensive fibrillar network on FS surface at 72 h. Whereas on TCP surface, the matrix architecture of fibronectin was less extensive and disjointed (Fig. 8.1 C), and vitronectin matrices were restricted to the boundaries marked by the cells (Fig. 8.1 D; visible cell-sized circular structures).

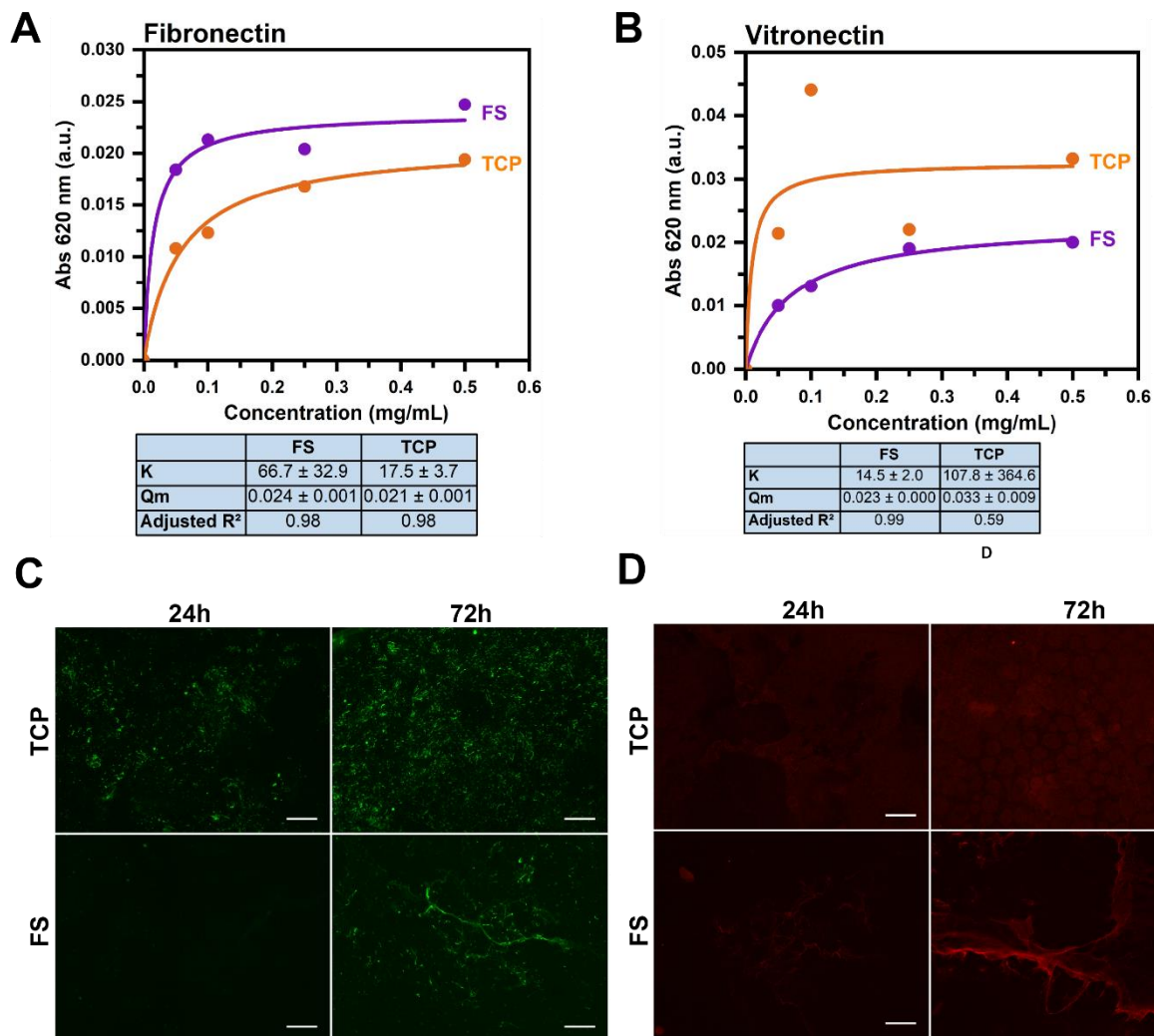


Fig. 8.1 Adsorption and fibril formation dynamics of fibronectin and vitronectin on FS and TCP surfaces. (A - B) Saturation Langmuir-fit curves of fibronectin (**A**) and vitronectin (**B**) adsorption on FS and TCP surfaces ($n=1$). (**C - D**) Representative immunofluorescence micrographs depicting fibronectin (**C**) and vitronectin (**D**) extracellular matrix network after cells have been removed ($n=3$). Scale bar = 100 μm . FS: fluoroalkylsilica, TCP: tissue culture polystyrene.

8.2.2 Conformational changes of fibronectin and vitronectin during adsorption onto FS and TCP surfaces

Surface chemistry has been widely shown to affect protein adsorption kinetics, denaturation, and conformational changes.⁵⁵² Fibrillogenesis of fibronectin has also shown to involve conformational changes.⁵³⁸ Therefore, it was hypothesised that fibronectin and vitronectin adsorption likely to result in conformational changes. In order to study these conformational and secondary structural changes in detail FTIR was carried out. FTIR of lyophilised bovine serum albumin (BSA) (Fig. 8.2 A) and fibronectin (Fig. 8.2 B) revealed amide A (highlighted in purple) between 3280 – 3225 cm^{-1} , amide I (highlighted in red) between 1700 – 1600 cm^{-1} , Amide II (highlighted in blue) between 1580 – 1510 cm^{-1} , and the complex amide III band (highlighted in green) between 1350 – 1250 cm^{-1} . Amongst the amide vibrations due to peptide backbone, Amide I band (between 1700 – 1600 cm^{-1}) in particular, which is mainly associated with peptide backbone C=O stretching vibrations, holds important secondary structural information.⁵⁵³ Examples of amide I peak-fitting of lyophilised BSA and fibronectin highlighted in Fig. 8.2 C & D, respectively. Examples of amide I peak-fitting of BSA (0.2 mM) and fibronectin (4.55 μM) adsorbed onto TCP surfaces after 24 hours of incubation highlighted in Fig. 8.2 E & F, respectively. Composition of conformers were expressed as % Conformers denoting percentage area under the curve of each conformer when compared to the total amide I peak area.

Protein concentration of 1–50 μM yielded signals where both amide I band and simultaneously the strong signals of C–H vibrations (~ 1500 and 1450 cm^{-1}) for TCP surface, or C–F vibrations (1200 and 1150 cm^{-1}) for FS surface were visible. Protein concentration of over 50 μM dampened the aforementioned surface-related signals. As such, 10 μM of protein was deemed to be suitable to detect the adsorbed proteins that were likely to be at the protein-surface interface (assumed as monolayer), as opposed to detecting those that could be adsorbing on top of other already adsorbed proteins that likely to occur at $> 50 \mu\text{M}$ concentrations.

In order to investigate the conformational changes of fibronectin and vitronectin during the early stages of adsorption onto FS and TCP surfaces, 10 μM of fibronectin or vitronectin were incubated as a 5 μL droplet onto each surface for 5 h. FTIR spectra and % conformer analyses revealed that there was a significant reduction in % conformer of intermolecular β -sheet (highlighted in orange, 1693 cm^{-1}) and random coil of fibronectin adsorbed onto FS surface compared to TCP surface (Fig. 8.3 A). In contrast, there was a significant increase in % conformer of α -helix of fibronectin adsorbed onto FS surface compared to TCP surface (Fig. 8.3 A). No significant differences in %

conformer of β -turn, intramolecular β -sheet, or intermolecular β -sheet (highlighted in purple, 1615 cm^{-1}) of fibronectin adsorbed onto FS surface compared to TCP surface (Fig. 8.3 A).

Similar to fibronectin, there was a significant increase in % conformer of intermolecular β -sheet (highlighted in orange, 1693 cm^{-1}) and random coil of vitronectin adsorbed onto FS surface compared to TCP surface (Fig. 8.3 B). Unlike fibronectin, there was no significant increase in % conformer of α -helix of vitronectin adsorbed onto FS surface compared to TCP surface (Fig. 8.3 B). Moreover, there was a significant increase in % conformer of intermolecular β -sheet (highlighted in purple, 1615 cm^{-1}) of vitronectin adsorbed onto FS surface compared to TCP surface (Fig. 8.3 B). No significant differences in % conformer of β -turn or intramolecular β -sheet of fibronectin adsorbed onto FS surface compared to TCP surface (Fig. 8.3 B).

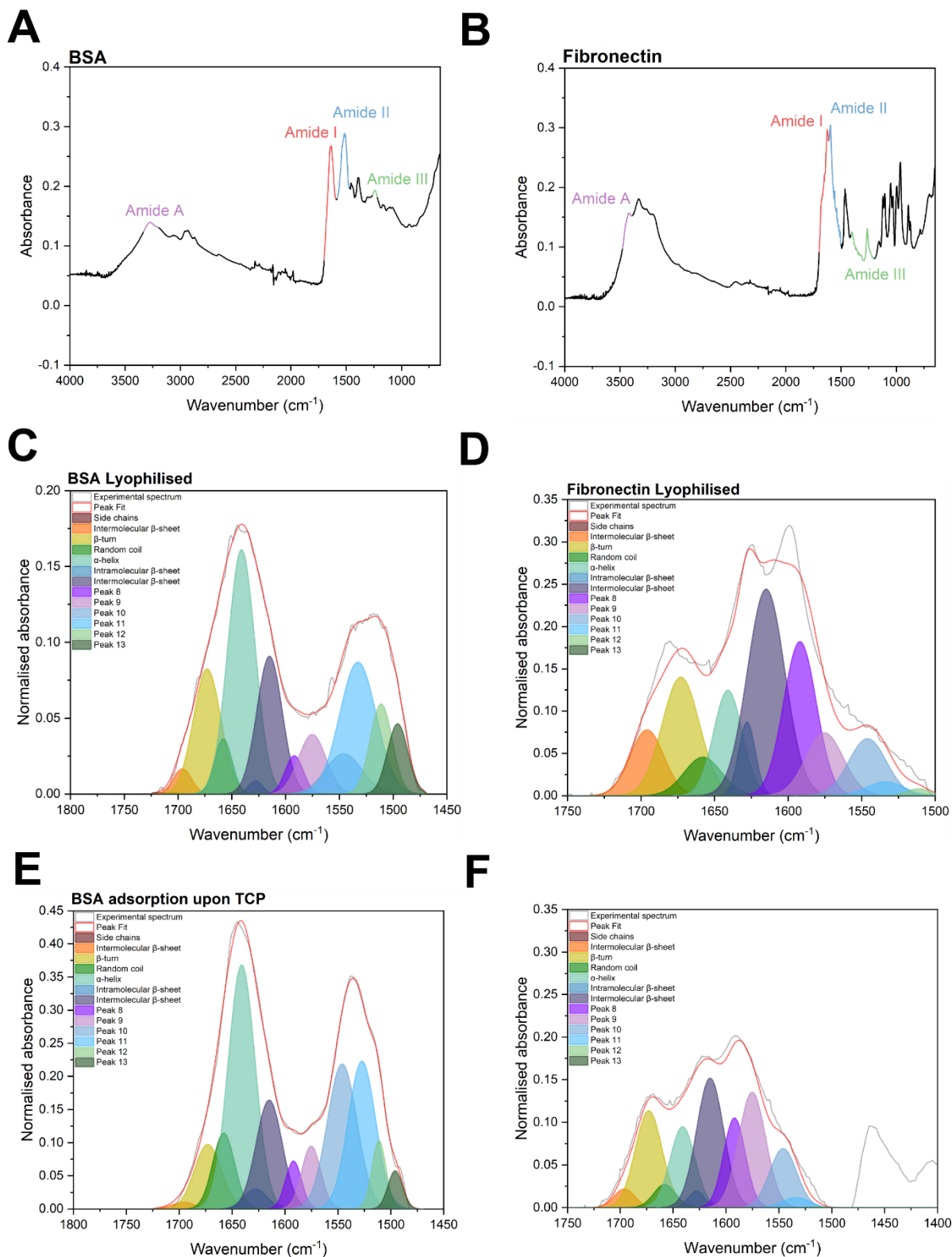


Fig. 8.2 FTIR-ATR spectra of BSA and fibronectin fitted with conformer peaks. (A - B) Amide A, amide I, amide II and amide III bands highlighted on FTIR spectra of BSA (A) and fibronectin (B). (C - F) Normalised and zero-base-line adjusted FTIR spectra fitted with peaks representing conformers composing the amide I and II bands. (C) Peak fitted amide I and II bands of lyophilised BSA. (D) Peak fitted amide I and II bands of lyophilised fibronectin. (E) Peak fitted amide I and II bands of 0.2 mM BSA adsorbed onto TCP surfaces after 24 h of incubation. (F) Peak fitted amide I and II bands of 4.55 μ M fibronectin adsorbed onto TCP surfaces after 24 h of incubation. BSA: Bovine serum albumin, FS: fluoroalkylsilica, TCP: tissue culture polystyrene.

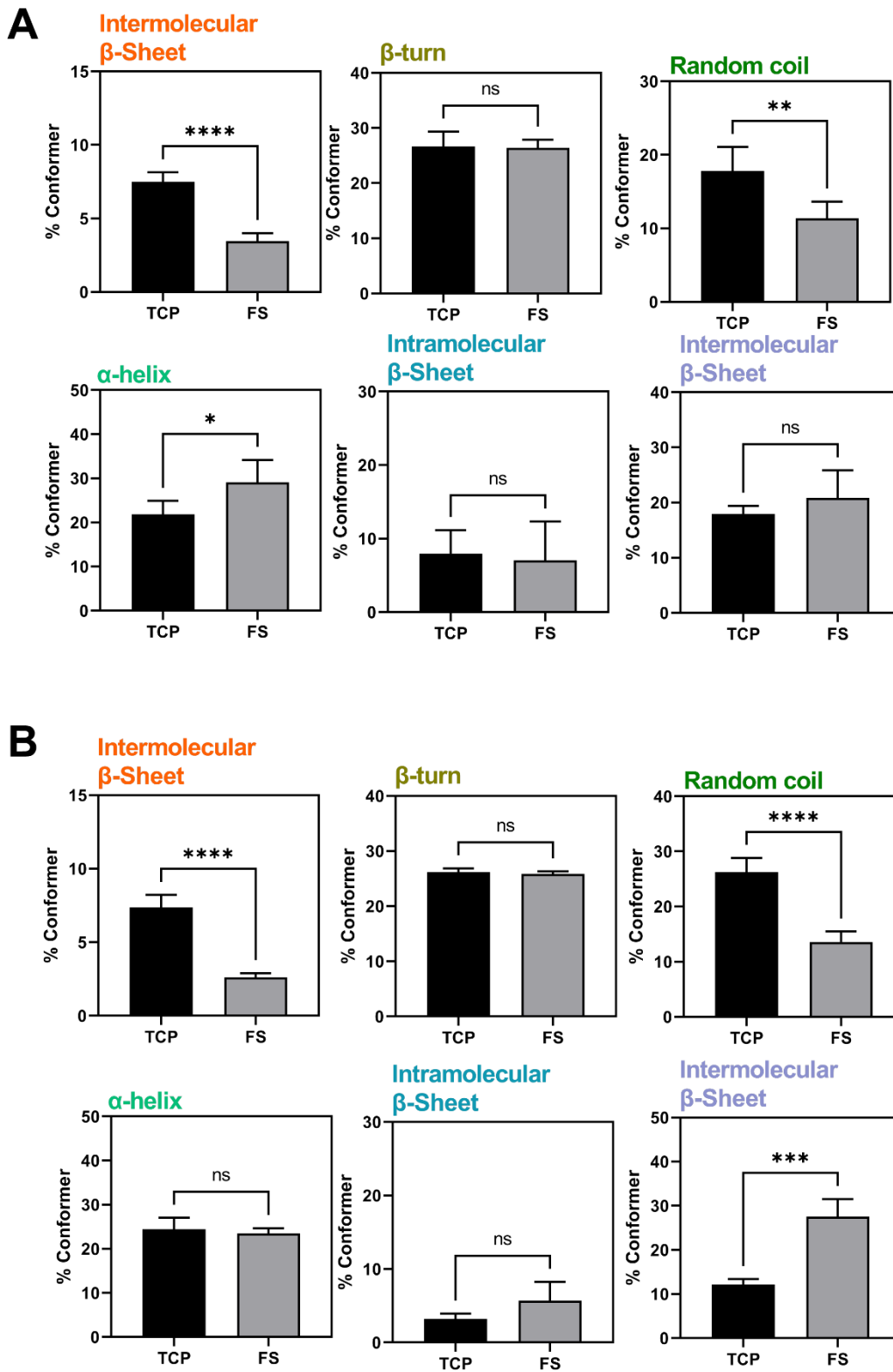


Fig. 8.3 Conformer composition of fibronectin and vitronectin after adsorption onto TCP and FS surfaces. (A - B) % conformer represented as integral area of peak-fitted curves as a percentage of total integral area of amide I band, (N = 5). (A) Conformer composition of fibronectin. (B) conformer composition of vitronectin. Student's T-tests (two-tailed distribution, heteroscedastic) were carried out for A - B. FS: fluoroalkylsilica, TCP: tissue culture polystyrene.

8.2.3 Sequential perturbation of secondary structures of fibronectin and vitronectin during adsorption onto FS and TCP surfaces

In order to investigate sequential conformational changes of fibronectin and vitronectin during adsorption onto FS and TCP surfaces, two-dimensional (2D) correlation spectroscopic analyses were carried out. In essence, 2D correlation spectroscopy highlights systemic variations in the spectral intensities induced by an external perturbation, by carrying out 2D-mapped cross correlation analysis of dynamic spectra.^{554,555} Usually studied perturbations include changes in temperature or pH, addition of a catalyst, or a time-dependent phenomenon. The present study considered adsorption of proteins onto the surface as the perturbation. 2D correlation spectroscopy were useful for when spectral regions consist of many overlapped peaks, such as in the amide I region.⁵⁵⁵

Table 8.1. Conformers within the Amide I region

Conformer	Wavenumber (cm ⁻¹)
Intermolecular β -sheet	1615
Intramolecular β -sheet	1628
α -helix	1644
Random coil	1656
β -turn	1680
Intermolecular β -sheet	1693

Simultaneous and sequential changes in secondary structures of fibronectin and vitronectin during adsorption onto TCP and FS surfaces were determined using the sequential order rules (Noda's rules).⁵⁵⁶ Noda's rule states that:

1. Synchronous 2D plot will yield in positive cross peaks at (x,y) if the spectral intensities of the bands at x and y are changing in the same direction during perturbation.
2. Synchronous 2D plot will yield in negative cross peak at (x,y) if the spectral intensities of the bands at x and y are changing in the opposite direction during perturbation.
3. Asynchronous 2D cross peak at (x,y) will be positive if the change at x precedes change in y during perturbation.
4. Asynchronous 2D cross peak at (x,y) will be negative if the change at x follows change in y during perturbation.

5. Lastly, if the synchronous 2D cross peak at (x,y) is negative, then rule 3 and 4 will be reversed.

All synchronous peaks show positive sign (Fig. 8.4 A – D), indicating that amide I spectral intensity increases from 5 h to 72 h caused by the increase in adsorbed protein amount on both TCP and FS surfaces for both proteins.

Highest synchronous auto-peak spectral intensity observed for fibronectin adsorption onto TCP (Fig. 8.4 A) and FS surfaces (Fig. 8.4 B) was for intermolecular β -sheet (1615 cm^{-1}) suggesting increase in β -sheet content during adsorption of fibronectin regardless of surface type. Whereas highest synchronous auto-peak spectral intensity observed for vitronectin adsorption onto both TCP (Fig. 8.4 C) and FS surfaces (Fig. 8.4 D) was for α -helix (1644 cm^{-1}), suggesting increase in α -helix content during adsorption of vitronectin regardless of surface type.

Large positive off-diagonal asynchronous cross-peak (1680, 1615) was observed during fibronectin adsorption onto TCP surfaces (Fig. 8.4 A), indicating that β -turn preceded intermolecular β -sheet (1615 cm^{-1}). Four positive asynchronous cross-peak (1628, 1615), (1656, 1615), (1680, 1615), and (1680, 1644) were observed during fibronectin adsorption onto FS surfaces (Fig. 8.4 B), indicating that intramolecular β -sheet (1628 cm^{-1}), random coil (1656 cm^{-1}), and β -turn (1680 cm^{-1}) all preceded intermolecular β -sheet (1615 cm^{-1}), and β -turn (1680 cm^{-1}) preceded α -helix (1644 cm^{-1}).

Positive off-diagonal asynchronous cross-peak (1628, 1615) was observed during vitronectin adsorption onto TCP surfaces (Fig. 8.4 C), indicating intramolecular β -sheet (1628 cm^{-1}) preceded intermolecular β -sheet (1615 cm^{-1}). Negative asynchronous cross-peak from (1680, 1615 to 1660) observed during vitronectin adsorption onto TCP surfaces (Fig. 8.4 C) indicate that β -turn (1680 cm^{-1}) mostly follows the other conformations within amide I region except intermolecular β -sheet (1693 cm^{-1}). Additionally, negative asynchronous cross-peak (1656, 1628) observed during vitronectin adsorption onto TCP surfaces (Fig. 8.4 C), suggests that random coil (1656 cm^{-1}) followed intramolecular β -sheet (1628 cm^{-1}).

Lastly, positive off-diagonal asynchronous cross-peaks (1615 to 1660, 1680) observed during vitronectin adsorption onto FS surfaces (Fig. 8.4 D) suggests that β -turn follows other conformations within amide I region except region except intermolecular β -sheet (1693 cm^{-1}) similar to vitronectin adsorption onto TCP surfaces. Negative cross peak at (1628, 1615) observed during vitronectin adsorption onto FS surfaces (Fig. 8.4 D) suggests that intermolecular β -sheet (1615 cm^{-1}) preceded intramolecular β -sheet (1628 cm^{-1}).

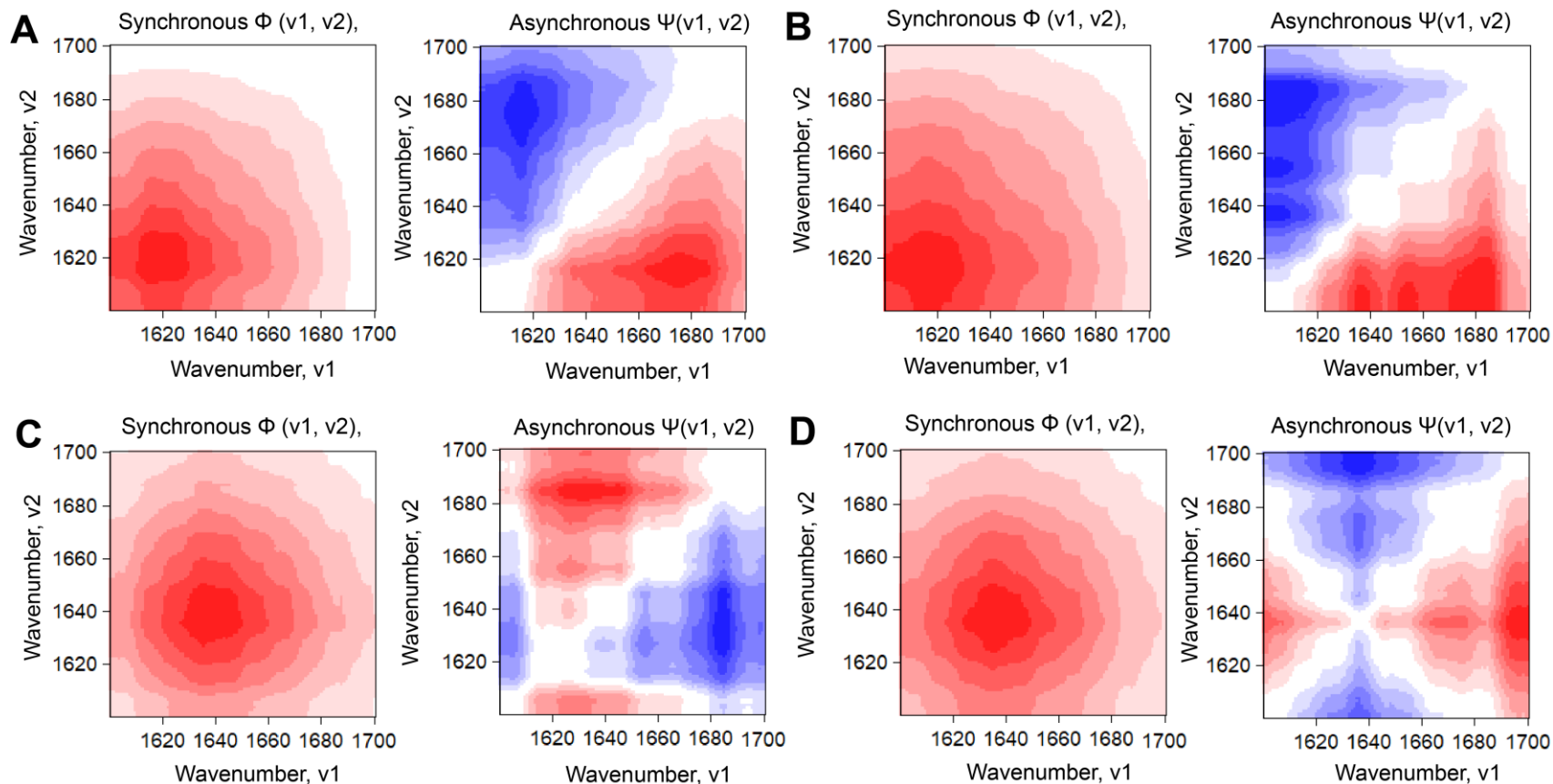


Fig. 8.4 Two-dimensional (2D) correlation spectroscopy of FTIR spectra of fibronectin and vitronectin reveal adsorption dynamics onto TCP and FS surfaces at 5 h, 24 h and 72 h period. (A - D) Fibronectin or vitronectin in aqueous phase at concentration of 10 μM were incubated on TCP or FS surfaces. After 5 h, 24 h, and 72 h of incubation at room temperature, unbound proteins washed off, and FTIR spectra were collected on the adsorbed protein layer. FTIR spectra were smoothed (Savitsky-Golay method), normalized to the consistent area of C-H peak at 1200 cm^{-1} , before carrying out 2D correlation spectroscopic analyses using 2Dshige software computation (Shigeaki Morita et al. 2005) to generate synchronous and asynchronous contour plots of the amide I region (1600 – 1700 cm^{-1}). (A) Synchronous and asynchronous plots of fibronectin adsorption on TCP surfaces. (B) Synchronous and asynchronous plots of fibronectin adsorption on FS surfaces. (C) Synchronous and asynchronous plots of vitronectin adsorption on TCP surfaces. (D) Synchronous and asynchronous plots of vitronectin adsorption on FS surfaces. Colours of contour indicate gradient from positive (red), neutral (white), to negative spectral (blue) in spectral intensity variations at cross-peaks.

8.3 Discussion

FM3 cells aggregated at 24 h on FS surfaces but not on TCP surfaces (Chapter 3; Fig. 3.1 A). Two notable matrisomal proteins, fibronectin and vitronectin involved in cellular adhesion,⁵⁵⁷ levels of both decreased during FM3 cellular aggregation (at 24h) and increased during disaggregation (at 72h) (Chapter 3; Fig. 3.3 D & E). Therefore, it was theorised that the increase in levels of fibronectin and vitronectin secreted onto FS surface at 72 h compared to 24 h, likely to lead to increased cellular disaggregation at 72 h compared to 24 h. The latent adsorption of fibronectin onto the FS surfaces could be explained by Vroman effect,⁴¹³ which explains how abundant, high-motile but low-affinity proteins may initially adsorb and saturate a surface, where low-motile proteins with higher-affinity to the surface begin to slowly replace the former adsorbates. Although, it remains unclear how adsorption of fibronectin and vitronectin onto hydrophobic FS and TCP surfaces may lead to the observed multicellular aggregation-disaggregation events. Thus, in order to gain answers for this question, this chapter aimed to explore the adsorption of fibronectin and vitronectin on TCP and FS surfaces, during the initial period of aggregation (5 h 24 h), and to probe whether conformational changes of these proteins during adsorption could hold any further insights into surface-induced cancer cellular behaviour.

Amido black protein adsorption assay revealed that fibronectin more readily adsorbed onto FS surface (Fig. 8.1 A) at 24 h, whereas vitronectin more readily adsorbed onto TCP surface at 24 h (Fig. 8.1 B). Immunofluorescence staining revealed that both fibronectin and vitronectin were deposited more on TCP surfaces than FS surfaces (Fig. 8.1 C-D). However, both fibronectin and vitronectin established extensive fibrillar network on FS surfaces at 72 h, whereas the matrisomal structures were disjointed and non-fibrillar upon TCP surfaces at 72 h. These results indicated that even though fibronectin and vitronectin may not readily adsorb onto FS surfaces at 24 h, the way in which they do adsorb could prime them to produce fibrillar structures during disaggregation. This could explain the increase in invasiveness of FM3 cells that had undergone aggregation-disaggregation (Chapter 3: Fig. 3.1 E) at 72 h on FS surfaces compared to their 72 h TCP counterparts. Indeed, several studies highlighted the importance of fibrillar matrix for cancer cellular invasion.⁵⁵⁸⁻⁵⁶⁰ Due to the cost of recombinant human proteins, only one repeat of the amido black assay was carried out. Having more repeats could lend further support for the Langmuir isotherm fit, especially for vitronectin adsorption on TCP, where the curve fit was poor (adjusted $R^2 = 0.59$). Langmuir adsorption isotherm model assumes that the proteins adsorb onto the surface as a monolayer. However, it could be that the amido black assay detected proteins that were adsorbed onto other proteins, and not the proteins at the protein-surface interface. A future improvement could be to supplement this

experiment with measurements of the cross-section of the adsorbate layer via atomic force microscopy (AFM) to ensure only the monolayer adsorption at the protein-surface interface is detected via the amido black assay.

FTIR spectroscopic analyses and % conformer analyses revealed that at 5 h, there was a significant reduction in intermolecular β -sheet (1693 cm^{-1}) and random coils (1656 cm^{-1}) when fibronectin and vitronectin molecules adsorbed onto FS surface compared to TCP surface (Fig. 8.3 A & B). As protein denaturation has been associated with formation of random coil secondary structures,⁵⁶¹ the decrease in random coils in fibronectin and vitronectin upon FS surfaces compared to TCP surfaces indicated reduced denaturation of proteins (maintenance of native-like state) when they adsorbed onto FS surfaces. Similarly, during denaturation, induced via increase in temperature above $60\text{ }^{\circ}\text{C}$, bands associated with intermolecular β -sheet aggregates (at 1626 and 1693 cm^{-1}) were observed.⁵⁶² This further confirms that fibronectin and vitronectin reduced denaturation (maintenance of native-like state) during adsorption upon FS surfaces by 5 h, whereas both proteins began undergoing denaturation during adsorption upon TCP surfaces by 5 h. Denaturation of extracellular proteins likely expose cryptic cell-binding RGD motifs to cells,⁵⁶³ thereby increasing cellular adhesion. As such, during the initial period of adsorption, decreased fibronectin and vitronectin denatured proteins upon FS surfaces, likely lead to decreased exposure of RGD-motifs from cryptic sites, subsequently creating a reduced-adhesion environment. This theory could be further supported by measuring the presence of RGD motifs exposed on adsorbed fibronectin and vitronectin molecules, accessible by cells. A future experiment could be to take spatial mapping of adsorbed proteins on surfaces using 2D Raman spectroscopic imaging and compare the intensity signatures to those of RGD peptides. Alternatively, antibody that recognises RGD motifs could be used in an Enzyme-linked immunosorbent (ELISA) assay to quantify the exposure of RGD motifs during the course of protein adsorption on FS and TCP surfaces.

Evidence against the theory of reduced denaturation during adsorption on FS surfaces arose with the observation that there was a significant increase in α -helix (1644 cm^{-1}) of adsorbed fibronectin on FS surface compared to TCP surface (Fig. 8.3 A). Denaturation of native proteins has been shown to disrupt α -helical secondary structures.⁵⁶⁴ An explanation for the increase in α -helix structures within FS-surface adsorbed proteins could be that non-native α -helical structures could form during adsorption. Further experiments, such as X-ray crystallography, are required to investigate the increase in α -helical structures in fibronectin but not in vitronectin, during adsorption on FS surface.

Moreover, there was a significant increase in intermolecular β -sheets (1615 cm^{-1}), commonly associated with intermolecular β -sheets amyloid aggregates,⁵⁶⁵ in vitronectin during adsorption on FS compared to TCP surface (Fig. 8.3 B). A study has shown that a C-terminal protease-resistant fragment of vitronectin fibrils could form the core regions required for amyloid formation.⁵⁶⁶ Together these results points towards an increase in the propensity of amyloidal fibrillogenesis of vitronectin on during adsorption on FS surface; this might not be the case on TCP surfaces. This explains the extensive fibrillar structures of vitronectin observed upon FS surfaces, but not TCP surfaces (Fig. 8.1 D). Since, there was no significant increase in intermolecular β -sheets (1615 cm^{-1}) of fibronectin (Fig. 8.3 A) adsorbed onto FS compared to TCP, fibronectin fibrillogenesis may not occur through amyloidal fibril formation. Further experiments, such as thioflavin T fluorescence assay,⁵⁶⁷ required to investigate amyloid fibril formation, which could lend further support to the vitronectin amyloid fibril formation theory.

A drawback of the present study was that the band wavenumber assignment of different conformers was carried out using a previously established method, which focused on silk fibroin protein.⁵⁶⁸ An improvement could be to develop a similar approach in which conformer band-fitting could be carried out using the band wavenumber peak maxima of conformers of fibronectin and vitronectin reported in previous studies. Since the peak maxima of amide I band and conformers silk proteins and extracellular matrix proteins are virtually the same, the conclusions drawn from the present study are still valid.⁵⁶⁹

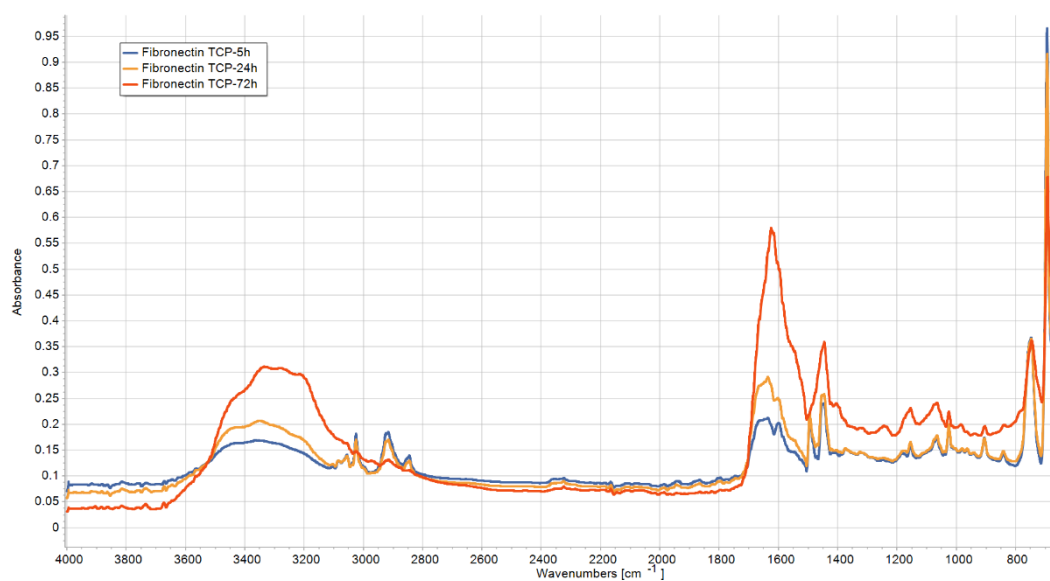
Lastly, 2D correlation spectroscopy was carried out to outline the simultaneous and sequences of events surrounding conformational changes during adsorption of fibronectin and vitronectin upon TCP and FS surfaces, from 5 h to 72 h of adsorption. These analyses revealed sequential order of conformation changes during protein adsorption of fibronectin and vitronectin on TCP and FS surfaces. These results could be used to aid future experiments, for example in computational modelling and Molecular dynamics (MD) simulation, to support sequential structural changes of fibronectin and vitronectin as they adsorb onto TCP and FS hydrophobic surfaces. A recent study, using computation methods, has described vitronectin adsorption on negatively charged, positively charged, neutral hydrophobic and neutral hydrophilic surfaces,⁵⁷⁰ highlighting RGD accessibility to cells in response to differential surface-induced protein adsorption. Future investigations could expand on these findings by investigating fibronectin and vitronectin self-assembly via exposure of self-assembly motifs⁵⁷¹ in addition to RGD motifs and investigate surface-chemistry-dependent matrisomal fibrillogenesis together with cellular-surface adhesion.

A limitation associated with these analyses was that the amide I band drastically changed in during 72 h of incubation where adsorption of both proteins reached saturation point, compared to 5 h and 24 h of incubation where amide I band was weak. Ideally, for accurate 2D correlation spectroscopy, one need amide I band normalised and stacked neatly on top, so that any small changes due to conformation can be isolated via this approach. An improvement of the current study could be to obtain saturation point of at 5 and 24 h to improve amide I band signal, with careful choice of protein concentration to measure proteins that are in immediate contact with the surfaces as opposed to sedimented on top of the initially adsorbed layer of proteins.

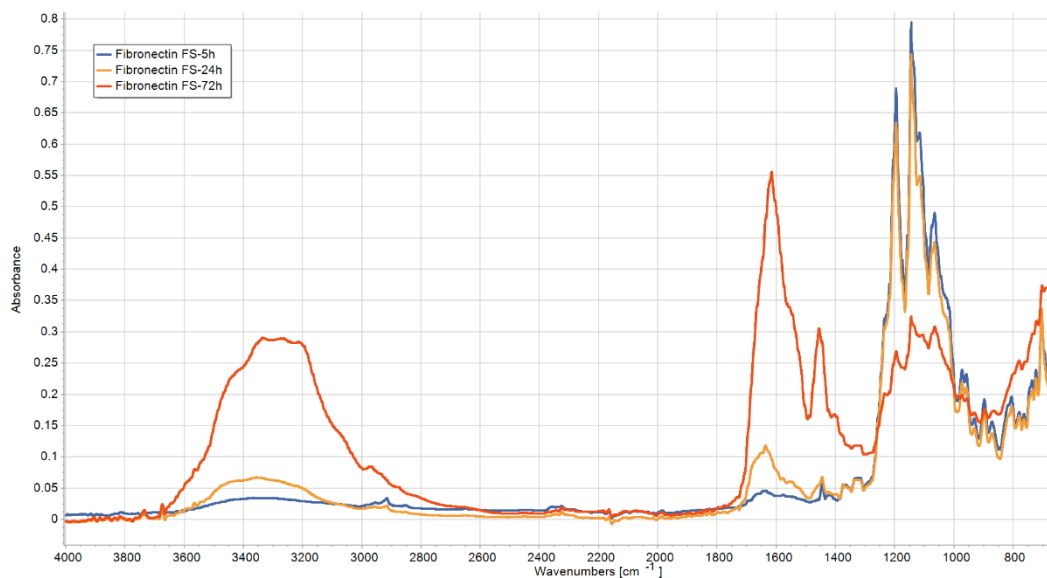
8.3.1 Conclusions

This chapter aimed to investigate adsorption dynamics and secondary structural changes associated with adsorption of fibronectin and vitronectin proteins onto TCP and FS hydrophobic surfaces. Conformational changes, such as decrease in intermolecular β -sheet and random coils of both fibronectin and vitronectin during adsorption on FS surfaces compared to TCP surfaces, highlighted that these proteins readily denature on TCP but not FS surfaces during initial stages of adsorption. Reduction in denaturation and maintenance of native-like states of fibronectin and vitronectin hints towards prevention of exposure of RGD cell-binding motifs from cryptic sites on FS surfaces, which in turn explains the reduced-cellular adhesion and multicellular aggregation properties of FS surfaces. Further research, such as computational modelling, could elaborate on surface-induced exposure of RGD motifs, which could lend further support to this theory. Increased intermolecular β -sheets (1615 cm^{-1}) of vitronectin, associated with intermolecular β -sheets amyloid aggregates, were observed as vitronectin adsorbed on FS surfaces compared to TCP surfaces, which explains the extensive fibrillar structures observed on FS but not TCP surfaces. This research illustrates the importance of surface-chemistry approaches in studying matrisomal protein conformational changes, and how these changes could dictate cell-adhesion via exposure of RGD motifs or exposure of self-assembly motifs to induce fibrillogenesis. Gaining insights into these cellular and matrisomal aspects are fundamental to understanding cancer metastasis.

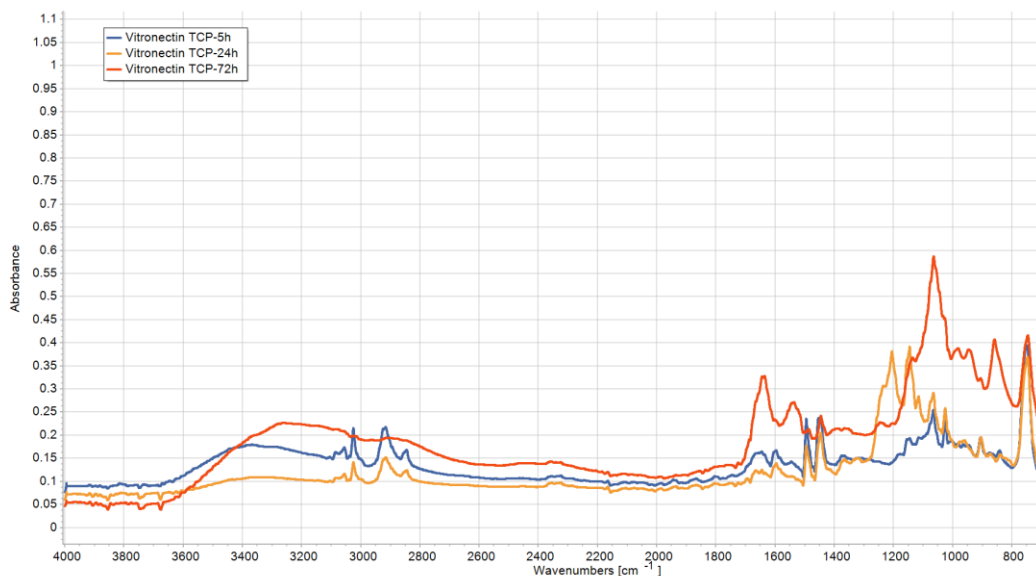
8.4 Supplementary Figures



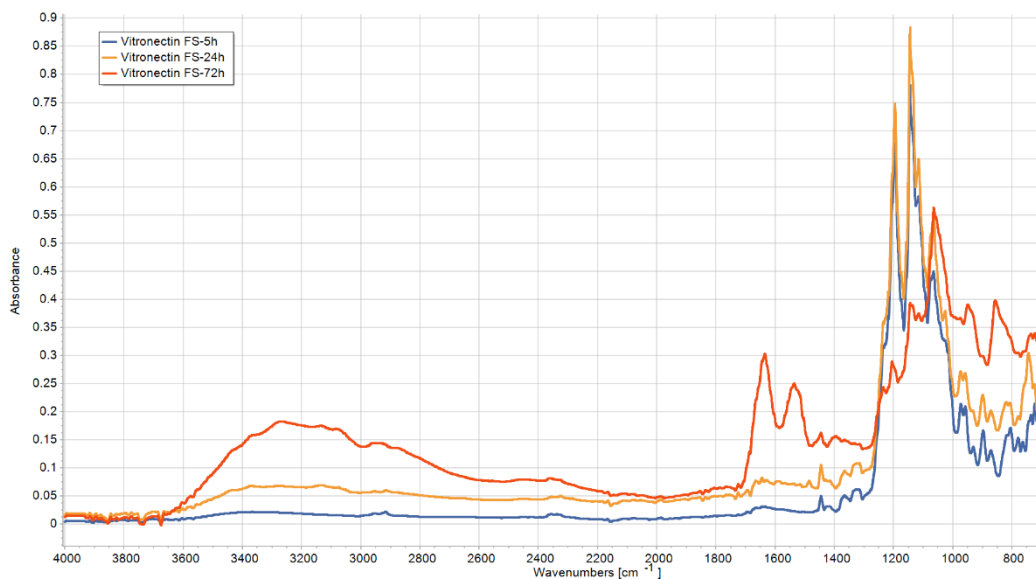
Supplementary Fig. 8.1 FTIR spectra of fibronectin adsorption onto TCP surfaces. Fibronectin in aqueous phase at concentration of 10 μM were incubated on TCP surfaces. After 5 h, 24 h, and 72 h of incubation at room temperature, unbound proteins washed off, and FTIR spectra were collected on the adsorbed protein layer. FTIR spectra were smoothed (Savitsky-Golay method), normalized to the consistent area of C-H peak at 1200 cm^{-1} . Representative spectra from five technical repeats shown here.



Supplementary Fig. 8.2 FTIR spectra of fibronectin adsorption onto FS surfaces. Fibronectin in aqueous phase at concentration of 10 μM were incubated on FS surfaces. After 5 h, 24 h, and 72 h of incubation at room temperature, unbound proteins washed off, and FTIR spectra were collected on the adsorbed protein layer. FTIR spectra were smoothed (Savitsky-Golay method), normalized to the consistent area of C-H peak at 1200 cm^{-1} . Representative spectra from five technical repeats shown here.



Supplementary Fig. 8.3 FTIR spectra of vitronectin adsorption onto TCP surfaces. Fibronectin in aqueous phase at concentration of 10 μM were incubated on TCP surfaces. After 5 h, 24 h, and 72 h of incubation at room temperature, unbound proteins washed off, and FTIR spectra were collected on the adsorbed protein layer. FTIR spectra were smoothed (Savitsky-Golay method), normalized to the consistent area of C-H peak at 1200 cm^{-1} . Representative spectra from five technical repeats shown here.



Supplementary Fig. 8.4 FTIR spectra of vitronectin adsorption onto FS surfaces. Fibronectin in aqueous phase at concentration of 10 μM were incubated on FS surfaces. After 5 h, 24 h, and 72 h of incubation at room temperature, unbound proteins washed off, and FTIR spectra were collected on the adsorbed protein layer. FTIR spectra were smoothed (Savitsky-Golay method), normalized to the consistent area of C-H peak at 1200 cm^{-1} . Representative spectra from five technical repeats shown here.

Chapter 9. Discussion

Contents

CHAPTER 9. DISCUSSION	180
9.1 PROJECT OVERVIEW.....	181
9.2 4F2HC-CONTAINING GLYCOPROTEIN:GALECTIN-3:GLYCOPROTEIN (GGG) BRIDGES PROMOTE HOMOTYPIC AGGREGATION OF FM3 CELLS.	181
9.3 ROLE OF EPITHELIAL-TO-MESENCHYMAL (EMT) AND B-INTERACTOME IN ADPM OF FM3 CELLS	184
9.4 PU.1-MEDIATED TRANSCRIPTIONAL REGULATION DURING ADPM OF FM3 CELLS	185
9.5 CONFORMATION CHANGES OF FIBRONECTIN AND VITRONECTIN DURING ADSORPTION ON FS AND TCP SURFACES	186
9.6 CONCLUSION.....	187
9.7 FUTURE PROSPECTS	188
9.7.1 Novel silica-modified surfaces.....	188
9.7.2 Advances in melanoma therapeutics.....	189
CHAPTER 10. REFERENCES.....	191
10.1 APPENDIX.....	235

9.1 Project overview

CTC clusters are 50 to 100-fold more metastatic compared to their single CTC counterpart.^{44,572,573} Though melanoma is one of the cancer types that present elevated levels of CTC clusters enriched in liquid biopsies,⁵⁷⁴ characteristics of melanoma CTC clusters has remained elusive thus far. This is partly due to the lack of an appropriate *in vitro* model of melanoma CTC clusters. This research project addressed this issue by establishing FS surface as a suitable *in vitro* model to investigate melanoma CTC clusters. These surfaces were used successfully to discover important aspects of melanoma CTC cells that undergo aggregation-disaggregation events, for instance during intravascular collision-dependent aggregation and subsequent disaggregation at metastatic sites. This research project discovered novel signalling molecules and pathways important for melanoma CTC clusters, as well as establishing methodology to study surface-driven protein adsorption.

9.2 4F2hc-containing Glycoprotein:Galectin-3:Glycoprotein (GGG) bridges promote homotypic aggregation of FM3 cells.

A novel mechanism underlying the formation of melanoma CTC clusters was discovered in this research project. FM3 cells formed multicellular aggregates by increasing cell-cell signalling and decreasing cell-matrix signalling (Chapter 3). Protein levels of galectin-3 and the cell-surface glycoprotein 4F2hc was increased during aggregation and decreased during disaggregation (Chapter 4). Galectin-3 and 4F2hc proteins colocalised at the cell-cell interface (Chapter 4). Co-expression and colocalisation indicated towards the interaction of these two proteins. Others have highlighted the direct binding of galectin-3 and 4F2hc through co-immunoprecipitation assays.²²⁰ Therefore, galectin-3 and 4F2hc interaction at the cell-cell interface was considered to be important for multicellular aggregation of FM3 cells. Indeed, inhibition of galectin-3 via anti-galectin-3 antibody and the galectin-3 inhibitor GB1107, as well as inhibition of 4F2hc via anti-4F2hc antibody, decreased multicellular aggregation (Chapter 4).

A recent study revealed that multicellular aggregation of breast cancer CTC occurs through the homophilic interaction of CD44 molecules on adjacent cells.⁴⁴ Likewise, the multicellular aggregation of FM3 melanoma cells could also occur through the homophilic interaction of 4F2hc. In contrast, galectin-3 molecules have been shown to promote aggregation of monocytic cells by cross-linking coterminous cell-surface CD13 glycoproteins expressed on

adjacent cells.⁵⁷⁵ Therefore, it was theorised that galectin-3 could also cross-link coterminous 4F2hc molecules on adjacent FM3 cells to promote multicellular aggregation (Fig. 9.0 A). Comparison of 4F2hc:4F2hc homophilic interactions and 4F2hc:galectin-3 interactions using protein docking computation revealed that 4F2hc:galectin-3 interaction is more likely to occur (Chapter 4).

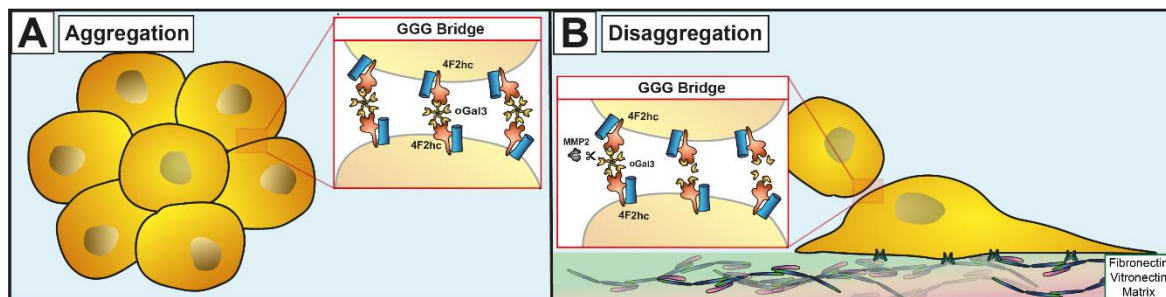


Fig. 9.0 Scheme of aggregation-disaggregation process of metastasis of melanoma CTC. Metastatic melanoma CTC could undergo homotypic multicellular aggregation via the formation of GGG bridges between adjacent cells during intravascular transit; for example, cross-linkage of coterminous 4F2hc by galectin-3. At metastatic sites, these aggregates could undergo disaggregation via MMP2-dependent cleavage of oGal3 and subsequent dissociation of GGG bridges. CTC: circulating tumour cells, GGG bridge: glycoprotein:galectin-3:glycoprotein bridge, oGal3: oligomeric galectin-3

Melanoma CTC expresses a plethora of cell-surface glycoproteins in addition to 4F2hc, such as CD147, frizzled-3 & 9, C4.4A, Gp90, and CD44, that could also be cross-linked via the formation of GGG bridges (Chapter 4). Further research is required to identify which of these cell surface proteins are important for melanoma CTC cluster aggregation, and whether if there is any heterogeneity in cell-surface glycoproteins expression by melanoma CTC that could influence ADPM of melanoma CTC.

Breast cancer CTCs were reported to cluster using cell-surface glycoproteins such as CD44,⁴⁴ heparanase,⁵⁷⁶ ICAM-1,⁵⁷⁷ and galectin-3BP.²⁴⁹ Whereas colon cancer CTCs were shown to cluster using the glycoprotein TMIGD2.⁵⁷⁸ These studies suggested that CTC cluster formation occur through the homophilic interaction of glycoproteins expressed on adjacent cells. However, these glycoproteins contain numerous *N*-glycosylation sites that could become glycosylated with β -Galactosides (Table 9.1), which could be recognised by galectin-3.⁵⁷⁹ This implies that GGG bridges could mediate cluster formation of breast and colon CTC as opposed to homophilic interaction of these glycoproteins. Future research could expand on these findings by investigating GGG bridges that could be driving cluster formation of CTC of breast and colon cancers.

N-GLYCOSYLATION SITES

CD44	2
HEPARANASE	7
ICAM-1	1
GALECTIN-3BP	6
TMIGD2	3

Table 9.1. Number of *N*-glycosylation sites in cell-surface glycoproteins that are important for CTC cluster formation. Glycosylation site information was observed using GlyGen.⁵⁸⁰

Furthermore, *MMP2* mRNA expression was decreased during aggregation of FM3 cells (Chapter 5). Since *MMP2* has been shown to cleave oligomeric galectin-3,²⁸⁸ extracellular *MMP2* could break GGG bridges. As such, *MMP2* expression was decreased during aggregation to prevent untimely disaggregation. Metastatic lesions of melanoma expressed considerably more *MMP2* compared to primary tumours.²⁹⁰ This implies that, at metastatic sites, GGG bridges could be more readily broken, and CTC clusters could be forced to disaggregate and invade through the distal metastatic site (Fig. 9.0 B). *MMP2* has been widely shown to cleave extracellular matrix protein and facilitate invasion of metastatic cells.⁵⁸¹ The present contribution highlighted a novel role of *MMP2* in melanoma metastasis.

Bioinformatics analyses of metastatic melanoma revealed that *MMP2* and 4F2hc expression adversely affect prognosis. Whereas galectin-3 expression provides a protective effect when expressed alongside *MMP2*, but adversely affect prognosis when expressed alongside 4F2hc. This suggests that galectin-3 and 4F2hc in melanoma CTC clusters could form GGG bridges and promote cluster formation much like in FM3 multicellular aggregates. It is worth noting that inappropriate therapeutic inhibition of galectin-3, that is when 4F2hc is not expressed, could hinder the protective role galectin-3 plays when *MMP2* is expressed, and could worsen prognosis. Therefore, genotyping to gauge 4F2hc, *MMP2*, and galectin-3 expression levels in patients is recommended before considering galectin-3 inhibition as a therapeutic option.

Lastly, phytohemagglutinin has been shown to increase CD98 mRNA levels.⁵⁸² Thus, it is prudent for patients suffering from primary melanoma to avoid food containing high levels of phytohemagglutinin, such as fresh red kidney beans,⁵⁸³ in order to reduce risk of homotypic aggregation and CTC clusters-associated metastasis.

9.3 Role of Epithelial-to-Mesenchymal (EMT) and β -interactome in ADPM of FM3 cells

Epithelial-to-Mesenchymal (EMT)-like processes have been reported in melanoma metastasis.^{313,314} It is not clear whether EMT-like processes contribute to ADPM of CTC clusters. Some studies highlighted that CTC clusters were exclusively made of mesenchymal-like cells⁵⁸⁴ and some CTC clusters have been shown to contain a mixed population of epithelial-like and mesenchymal-like cells.³⁹⁹ The 'Leader-Follower' model was proposed to describe this heterogeneous CTC clusters, in which mesenchymal-like leader cells are responsible for invasion through the stroma;³⁵⁰ partial-EMT/hybrid cells link leader and follower cells.³⁵¹ A recent study highlighted subpopulation of cells within melanoma CTC clusters were invasive (mesenchymal-like), and another subpopulation of cells that were more proliferative (epithelial-like).³⁵²

TGF β is a cytokine that has been shown to promote EMT-like processes in cutaneous melanoma cells.⁴⁰⁹ TGF β treatment of FM3 cells increased aggregation compared to untreated cells (Chapter 6). Additionally, culturing epithelial (P5B3) and mesenchymal (P4B6B) progeny of OPCT-1 prostate cancer cells on FS surface highlighted that mesenchymal cells retain clustered conformation longer than epithelial cells (Chapter 6). Together, these findings suggest that CTC clusters could be more mesenchymal in nature, though EMT-like processes do not occur during ADPM of FM3 cells (Chapter 6).

A decrease in β -catenin mRNA levels was associated with disaggregation of FM3 cells (Chapter 6). Comparison of β -catenin interactors with differentially expressed proteome of FM3 cells during ADPM, highlighted key proteins that could be involved in regulating various cellular processes as a response to β -catenin signalling. LDHB, PML, PABP1, PUR9, RL11 and SPF45 levels were increased during aggregation of FM3 cells (Chapter 6), RL11 levels were decreased during disaggregation (Chapter 6). HS105 levels increased during aggregation and decreased during disaggregation (Chapter 6). In FM3 cells, β -catenin signalling could control the following cellular processes: cellular metabolism via LDHB, protein synthesis via PABP1 and SPF45, cellular replication via PUR9, cellular proliferation via PML and RL11, and stress-dependent responses via HS105. Bioinformatics analyses highlighted that PML and LDHB in particular worsened survival outcome of melanoma patients (Chapter 6). RL11 was highlighted as the β -catenin interactor with the most adverse metastasis-related outcome compared to the other β -catenin interactor considered in this study (Chapter 6). Since β -catenin has been implicated in breast cancer⁵⁸⁵ and colon cancer⁵⁸⁶ future research could

examine the involvement of β -catenin interactors in ADPM of breast and colon cancer using FS surfaces.

Lastly, since β -catenin signalling has been shown to lie downstream of 42hc/integrin signalling,²²⁰ it could be that certain extracellular cues such as reduced cellular adhesion (RCA) conditions, could be detected by 4F2h/integrin/ β -catenin signalling, and in turn, cells can respond by multicellular aggregation to increase their chances of survival (Chapter 3). Future work can interrogate this signalling cascade further to determine other components of this cascade; for example, GSK-3 β -dependent proteasomal degradation of β -catenin³⁶⁶ and influences of MMP2-cleaved GSK-3 β (Chapter 5).

9.4 PU.1-mediated transcriptional regulation during ADPM of FM3 cells

PU.1 transcription factor, a member of the ETS family, was upregulated in melanoma.⁴⁸² Bioinformatics analyses of β -catenin-dependent transcriptional regulation of differentially expressed proteome, during ADPM of FM3 cells, highlighted PU.1 as a transcription factor of interest (Chapter 6). However, expression of *SPI1* mRNA (that encodes for PU.1 protein) did not change during ADPM of FM3 cells (Chapter 7). Inhibition of PU.1 using DB2313 (PU.1 inhibitor) also did not affect ADPM (Chapter 7). These results suggest that PU.1 is not involved in the regulation of ADPM in FM3 cells.

During inhibition of PU.1 via DB2313-treatment, invasiveness and migration capabilities were reduced in FM3 cells isolated from aggregates compared to single cells (Chapter 7). This suggests that the anti-invasion role of PU.1 was abated in aggregated cells. In FM3 cells, inhibition of PU.1 resulted in upregulation of the small GTPase RhoC (Chapter 7), which is involved in cellular motility.⁵¹⁷ Exogenous induction of RhoC in cutaneous melanoma has been shown to increase invasion and metastasis.⁵¹⁸ This suggests that PU.1 inhibits RhoC in FM3 cells and reduce invasion and migration; inhibition of PU.1 reversed this anti-invasion effect. Further research is required to isolate these anti-invasion effects by PU.1 and explore why this is less prominent in aggregated cells compared to single cells.

Moreover, inhibition of PU.1 resulted in a reduction in 4F2hc levels, but not galectin-3 levels (Chapter 7), indicating that transcription of *SLC3A2* gene (that encodes for 4F2hc) could be regulated by PU.1. Investigation of the number of ETS motif (5'-GGAA-3') and PU-box (5'-GAGGAA-3'), upon which PU.1 likely to bind, present in genes associated with ADPM of FM3

cells, revealed that *SLC3A2* gene (that encodes for 4F2hc), *ATIC* gene (that encodes for PUR9) and *PABPC1* gene (that encodes for PABP1) all had several PU.1 binding sites proximal to their transcription start site (Chapter 7). Future research could address PU.1-dependent transcription of these genes in ADPM of CTC clusters of various cancers, especially breast⁴⁹⁸ and lung cancer⁵⁰⁰ where high PU.1 expression has been reported.

9.5 Conformation changes of fibronectin and vitronectin during adsorption on FS and TCP surfaces

Matrisomal proteins fibronectin and vitronectin levels were decreased during aggregation and increased during disaggregation of FM3 cells (Chapter 3). These two proteins are pertinent for cellular adhesion as they contain arginine-glycine-aspartic acid (RGD) motifs, recognised by integrins during cellular adhesion.⁵⁵⁷ To probe how the FS surface induced aggregation-disaggregation events of FM3 cells, conformational changes of fibronectin and vitronectin that may arise during protein adsorption onto the surface were investigated. This revealed that levels of intermolecular β -sheet (1693 cm^{-1}) and random coils (1656 cm^{-1}) of both fibronectin and vitronectin were decreased during the initial stages of adsorption onto FS surfaces as compared to TCP surfaces (Chapter 8). As random coil formation,⁵⁶¹ as well as increase in intermolecular β -sheet aggregates (at 1626 and 1693 cm^{-1}),⁵⁶² are associated with denaturation of proteins, it was concluded that fibronectin and vitronectin likely to undergo denaturation on TCP surfaces, whereas there was a maintenance of native-like state on FS surfaces. Denaturation of extracellular matrix proteins is predicted to expose cryptic cell-binding motifs, such as arginine-glycine-aspartic acid (RGD) motifs.⁵⁶³ As such, on TCP surfaces, denaturation of fibronectin and vitronectin leads to cellular adhesion at 24 h (Chapter 3), whereas the maintenance of native-like state of fibronectin and vitronectin leads to reduced cellular adhesion (subsequent multicellular aggregation) on FS surfaces (Chapter 3).

Furthermore, intermolecular β -sheets (1615 cm^{-1}) content was increased in vitronectin during adsorption onto FS surfaces as compared to TCP surfaces (Chapter 8). This is indicative of the formation of cross- β -sheets⁵⁶⁵ and fibril formation.⁵⁸⁷ These findings explain the fibril formation at 72 h on FS surfaces, but not TCP surfaces, observed via immunofluorescence (Chapter 8).

Lastly, two-dimensional (2D) correlation spectroscopy was carried out to examine the sequences of the conformation changes associated with protein adsorption of fibronectin.

These sequences of events could be used to guide computational modelling, for example via Molecular Dynamics (MD), which could provide further insights into exposure of RGD motifs or self-binding motifs. Future research could explore how exposure of these motifs could result in fibrillogenesis and RGD-dependent cell-adhesion. This would, in essence, give greater insights into surface-induced ADPM, as well as extracellular remodelling by melanoma cells at metastatic sites.

9.6 Conclusion

This research project identified novel signalling molecules, 4F2hc, MMP2 and galectin-3, involved in multicellular aggregation of FM3 cells. GGG bridges could cross-link coterminous 4F2hc and promote multicellular aggregation of melanoma CTC clusters; MMP2-dependent cleavage of galectin-3 at metastatic site could promote disaggregation. Further research is needed to examine whether GGG bridges drive breast and colon cancer CTC cluster formation as well.

Homotypic melanoma CTC clusters are likely to be mesenchymal like in nature, as this would help them retain their clustered-conformation the longest. Heterotypic CTC clusters could involve heterogenous subpopulation consisting of epithelial-like, mesenchymal-like and hybrid cells. In FM3 cells, β -catenin expression was decreased during disaggregation, suggesting its role during aggregation. 4F2hc/integrin/ β -catenin signalling likely to sense RCA conditions and mediate multicellular aggregation by altering β -catenin interactor responses.

Expression of PU.1 did not change during ADPM of FM3 cells and inhibition of PU.1 did not affect ADPM of FM3 cells; this suggests that PU.1 is not involved in the regulation of ADPM of FM3 cells. However, inhibition of PU.1 resulted in decreased 4F2hc levels and region proximal to transcription start site of the *SLC3A2* gene contained many PU.1-binding sequences; these findings suggest that PU.1 could transcriptionally control 4F2hc levels amongst many other transcription factors. An open question here is what conditions, for example EMT status, β -catenin-signalling, that could promote PU.1-mediated transcription of 4F2hc levels. Further, PU.1 serves an anti-invasion role in FM3 cells, by regulating RhoC levels; however, this anti-invasion role was abated in aggregated cells, which also requires further detailed investigation.

Lastly, this research project revealed that fibronectin and vitronectin undergo denaturation during adsorption on TCP surfaces, where RGD motifs could be exposed from cryptic sites leading to cell-adhesion; whereas native-like state of fibronectin and vitronectin is

maintained on FS surfaces, where RGD motifs are buried in cryptic sites, leading to reduced cellular adhesion and multicellular aggregation.

9.7 Future prospects

9.7.1 Novel silica-modified surfaces

On August 3rd, 2020, European Commission restricted the use of perfluorocarboxylic acids containing 9 to 14 carbon atoms in the chain, as well as their salt variants and related substances. Restriction is outlined in the 'amending Annex XVII to Regulation (EC) NO 1907/2006 of European Parliament and of the Council', concerning Registration, Evaluation, Authorisation and Restrictions of Chemicals (REACH)(REACH Annex XVII Entry 68). The restriction will come in force 18 months after publication (2021). Our laboratory ceased to fabricate FS surface fabrication using 1*H*,1*H*,2*H*,2*H*-perfluorodecyltriethoxysilane (FDTES) and committed to being perfluorocarbon-free. Therefore, a suitable substitute silane is needed for the fabrication of hydrophobic surfaces that induce ADPM, comparable to FS surface in physicochemical characteristics.

Preliminary experiments were carried out in collaboration with Kuda P. A. Kasuri S. Kulasinghe to find a suitable substitute. A range of different silanes were used for functionalisation, containing chemical group of amines, bicyclic, halides, methacrylate, alkene, or hydrocarbon chains. Trimethoxy(octadecyl)silane (ODT) (CAS 3069-42-9) and (3-Iodopropyl)trimethoxysilane (IDP) (CAS 14867-28-8) yielded surfaces that elicited FS surface-like ADPM of FM3 cells. ODT surfaces exhibited water contact angle of ~ 115°, which was closer to the water contact angle of FS surface (~115°); whereas IDP functionalisation produced surfaces with water contact angle of ~80°. Surface free energy of ODT and IDP surfaces however were not comparable to FS surfaces. These findings suggest that ODT and IDP could be used as an alternative to FS surfaces; however, differences in surface free energy and water contact angle may affect protein adsorption of matrix proteins different to FS surface, leading to altered ADPM responses.

Further experiments are needed to tailor surfaces whose physicochemical characteristics are as close to FS surfaces as possible, for example via co-functionalisation with multiple silanes. Suitability for replacement for FS surface requires examination of biomarkers, such as 4F2hc, galectin-3, and MMP2 expression during ADPM of FM3 cells. Nonetheless, these preliminary experiments represent a new avenue for research of surface-induced ADPM and surface-

induced protein adsorption using silica-modified surfaces. Data discussed here are from thesis of Kuda P. A. Kasuri S. Kulasinghe submitted for master's degree.

9.7.2 Advances in melanoma therapeutics

Targeting melanoma CTC clusters during intravascular transit may prove to be difficult. A possible approach could be to design nanoparticles conjugated with glycans similar to those found on 4F2hc molecules. Galectin-3 molecules could bind to these nanoparticles instead of 4F2hc molecules on CTC clusters. Silver, gold, and Fe₂O₃ magnetic nanoparticles could be conjugated to glycans.⁵⁸⁸ Longer glycan chains could also be conjugated to graphene or carbon nanotubes.⁵⁸⁸ Self-assembled glycodendrimers or metal containing metalloglycodendrimers with branched chain glycans⁵⁸⁸ could also be used here to target complex and hybrid glycans that might be present on 4F2hc molecules. As 4F2hc-galectin-3 interaction could be important for various normal biological functions, nanoparticle design must consider CTC cluster specific glycans.

Scientific Communication

Manuscript for publication at preparation state:

- Galectin-3 Bridges Coterminous Cell-Surface CD98 Glycoproteins and Mediates Homotypic Aggregation-Disaggregation of Melanoma Cells.
- Modification of β -catenin Interactome During Aggregation-Disaggregation of Melanoma Cells.
- Conformational Changes Associated with Fibronectin and Vitronectin During Adsorption On Hydrophobic Fluoroalkyl Surfaces.

Poster presentations:

- Rajeharish Rajendran, Clare Coveney, Carole C Perry, and David J Boocock (2021), Investigation of Cancer Cellular Homotypic Aggregation-Disaggregation Events using Co-functionalised Silica Surfaces. Biointerfaces International Zurich online conference, 2021.
- Rajeharish Rajendran, Graham J Hickman, Carole C Perry, and David J Boocock (2019), Next-generation 2.5D tissue culture surfaces to study cancer cell aggregation. Royal Society of Chemistry Biomaterials Chemistry Annual Conference, 2019.

Oral presentation:

- Rajeharish Rajendran, Graham J Hickman, Carole C Perry, and David J Boocock (2018), Next-generation 2.5D tissue culture surfaces to study cancer cell aggregation. Royal Society of Chemistry Materials Chemistry Division Poster Symposium, 2018

Chapter 10. References

- 1 National Cancer Institute, Cancer Statistics, <https://www.cancer.gov/about-cancer/understanding/statistics>, (accessed 19 July 2024).
- 2 D. Hanahan and R. A. Weinberg, *Cell*, 2000, **100**, 57–70.
- 3 H. Masuda, D. Zhang, C. Bartholomeusz, H. Doihara, G. N. Hortobagyi and N. T. Ueno, *Breast Cancer Res Treat*, 2012, **136**, 331–345.
- 4 P. A. J. Muller, K. H. Vousden and J. C. Norman, *Journal of Cell Biology*, 2011, **192**, 209–218.
- 5 J. Roche, *Cancers (Basel)*, 2018, **10**, 52.
- 6 N. J. Robinson and W. P. Schiemann, *Cancers (Basel)*, 2022, **14**, 808.
- 7 D. J. Hicklin and L. M. Ellis, *Journal of Clinical Oncology*, 2005, **23**, 1011–1027.
- 8 S. Qian, Z. Wei, W. Yang, J. Huang, Y. Yang and J. Wang, *Front Oncol*, , DOI:10.3389/fonc.2022.985363.
- 9 D. Hanahan and R. A. Weinberg, *Cell*, 2011, **144**, 646–674.
- 10 K. Dhatchinamoorthy, J. D. Colbert and K. L. Rock, *Front Immunol*, , DOI:10.3389/fimmu.2021.636568.
- 11 G. Khusnurrokhman and F. F. Wati, *Annals of Medicine & Surgery*, , DOI:10.1016/j.amsu.2022.104022.
- 12 M. A. Nowak, N. L. Komarova, A. Sengupta, P. V. Jallepalli, I.-M. Shih, B. Vogelstein and C. Lengauer, *Proceedings of the National Academy of Sciences*, 2002, **99**, 16226–16231.
- 13 M. V. Liberti and J. W. Locasale, *Trends Biochem Sci*, 2016, **41**, 211–218.
- 14 D. Hanahan, *Cancer Discov*, 2022, **12**, 31–46.
- 15 S. Ma, Y. Zhao, W. C. Lee, L.-T. Ong, P. L. Lee, Z. Jiang, G. Oguz, Z. Niu, M. Liu, J. Y. Goh, W. Wang, M. A. Bustos, S. Ehmsen, A. Ramasamy, D. S. B. Hoon, H. J. Ditzel, E. Y. Tan, Q. Chen and Q. Yu, *Nat Commun*, 2022, **13**, 4118.
- 16 S. Okumura, Y. Konishi, M. Narukawa, Y. Sugiura, S. Yoshimoto, Y. Arai, S. Sato, Y. Yoshida, S. Tsuji, K. Uemura, M. Wakita, T. Matsudaira, T. Matsumoto, S. Kawamoto, A. Takahashi, Y. Itatani, H. Miki, M. Takamatsu, K. Obama, K. Takeuchi, M. Suematsu, N. Ohtani, Y. Fukunaga, M. Ueno, Y. Sakai, S. Nagayama and E. Hara, *Nat Commun*, 2021, **12**, 5674.
- 17 J.-W. Zhang, D. Zhang and B.-P. Yu, *Cancer Lett*, 2021, **520**, 68–79.
- 18 K. L. Woodford-Richens, A. J. Rowan, P. Gorman, S. Halford, D. C. Bicknell, H. S. Wasan, R. R. Roylance, W. F. Bodmer and I. P. M. Tomlinson, *Proceedings of the National Academy of Sciences*, 2001, **98**, 9719–9723.
- 19 K. Saginala, A. Barsouk, J. S. Aluru, P. Rawla and A. Barsouk, *Med. Sci. (Basel)*, 2021, **9**, 63.
- 20 R. L. Siegel, K. D. Miller, H. E. Fuchs and A. Jemal, *CA Cancer J. Clin.*, 2021, **71**, 7–33.
- 21 S. Raimondi, M. Suppa and S. Gandini, *Acta Derm. Venereol.*, 2020, **100**, adv00136.

- 22 A. Viros, B. Sanchez-Laorden, M. Pedersen, S. J. Furney, J. Rae, K. Hogan, M. R. Ejiama Sarah and Girotti, M. Cook and R. Dhomen Nathalie and Marais, *Nature*, 2014, **511**, 478–482.
- 23 R. C. Hennessey, A. M. Holderbaum, A. Bonilla, C. Delaney, J. E. Gillahan, K. L. Tober, T. M. Oberyszyn, J. H. Zippin and C. E. Burd, *Pigment Cell Melanoma Res.*, 2017, **30**, 477–487.
- 24 C. Bertolotto, F. Lesueur, S. Giuliano, T. Strub, M. de Lichy, K. Bille, P. Dessen, B. d’Hayer, H. Mohamdi, A. Remenieras, E. Maubec, A. de la Fouchardière, V. Molinié, P. Vabres, N. Dalle Stéphane and Poulalhon, T. Martin-Denavit, L. Thomas, P. Andry-Benzaquen, N. Dupin, F. Boitier, A. Rossi, J.-L. Perrot, B. Labeille, C. Robert, B. Escudier, O. Caron, L. Brugières, S. Saule, B. Gardie, S. Gad, S. Richard, J. Couturier, B. T. Teh, L. Ghiorzo Paola and Pastorino, S. Puig, C. Badenas, H. Olsson, C. Ingvar, E. Rouleau, R. Lidereau, P. Bahadoran, E. Vielh Philippe and Corda, H. Blanché, D. Zelenika, P. Galan, French Familial Melanoma Study Group, F. Aubin, B. Bachollet, C. Becuwe, P. Berthet, V. Bignon Yves Jean and Bonadona, J.-L. Bonafe, M.-N. Bonnet-Dupeyron, J. Cambazard Frédéric and Chevrant-Breton, I. Coupier, S. Dalac, L. Demange, M. d’Incan, C. Dugast, L. Faivre, L. Vincent-Fétita, M. Gauthier-Villars, B. Gilbert, F. Grange, J.-J. Grob, P. Humbert, N. Janin, P. Joly, D. Kerob, C. Lasset, D. Leroux, J. Levang, J.-M. Limacher, C. Livideanu, M. Longy, A. Lortholary, D. Stoppa-Lyonnet, S. Mansard, L. Mansuy, K. Marrou, C. Matéus, C. Maugard, N. Meyer, C. Nogues, P. Souteyrand, L. Venat-Bouvet, H. Zattara, V. Chaudru, G. M. Lenoir, M. Lathrop, I. Davidson, M.-F. Avril, F. Demenais and B. Ballotti Robert and Bressac-de Paillerets, *Nature*, 2011, **480**, 94–98.
- 25 F. Chang, L. S. Steelman, J. T. Lee, J. G. Shelton, P. M. Navolanic, W. L. Blalock, R. A. Franklin and J. A. McCubrey, *Leukemia*, 2003, **17**, 1263–1293.
- 26 Cancer Genome Atlas Network, *Cell*, 2015, **161**, 1681–1696.
- 27 P. M. Pollock, U. L. Harper, L. M. Hansen Katherine S and Yudt, M. Stark, T. Y. Robbins Christiane M and Moses, G. Hostetter, U. Wagner, J. Kakareka, G. Salem, T. Pohida, P. Heenan, P. Duray, O. Kallioniemi, N. K. Hayward, J. M. Trent and P. S. Meltzer, *Nat. Genet.*, 2003, **33**, 19–20.
- 28 K. Eddy, R. Shah and S. Chen, *Front Oncol*, 2021, **10**, 3357.
- 29 K. Chiba, F. K. Lorbeer, A. H. Shain, D. T. McSwiggen, E. Schruf, A. Oh, X. Ryu Jekwan and Darzacq, B. C. Bastian and D. Hockemeyer, *Science (1979)*, 2017, **357**, 1416–1420.
- 30 J. B. Loureiro, L. Raimundo, C. Calheiros Juliana and Carvalho, V. Barcherini, C. Lima Nuno R and Gomes, M. I. Almeida, M. G. Alves, J. L. Costa, M. M. M. Santos and L. Saraiva, *Cancers (Basel)*, 2021, **13**, 1648.
- 31 R. Cabrita, S. Mitra, A. Sanna, H. Ekedahl, K. Lövgren, H. Olsson, C. Ingvar, K. Isaksson, M. Lauss, A. Carneiro and G. Jönsson, *Cancers (Basel)*, 2020, **12**, 742.
- 32 M. Irvine, A. Stewart, B. Pedersen, S. Boyd, R. Kefford and H. Rizos, *Oncogenesis*, 2018, **7**, 72.
- 33 P. Redondo, E. Bandrés, T. Solano, I. Okroujnov and J. Garc\'{i}a-Foncillas, *Cytokine*, 2000, **12**, 374–378.
- 34 A. Filimon, I. A. Preda, A. F. Boloca and G. Negroiu, *Cells*, 2021, **11**, 120.
- 35 G. J. Kaunitz, T. R. Cottrell, V. Lilo Mohammed and Muthappan, J. Esandrio, H. Berry Sneha and Xu, A. Ogurtsova, A. H. Anders Robert A and Fischer, S. Kraft, M. R. Gerstenblith, C. L.

- Thompson, K. Honda, C. G. Cuda Jonathan D and Eberhart, J. T. Handa and J. M. Lipson Evan J and Taube, *Lab. Invest.*, 2017, **97**, 1063–1071.
- 36 J. Fares, M. Y. Fares, H. H. Khachfe, H. A. Salhab and Y. Fares, *Signal Transduct Target Ther*, 2020, **5**, 28.
- 37 N. Jacquelot, C. P. M. Duong, G. T. Belz and L. Zitvogel, *Front Immunol*, , DOI:10.3389/fimmu.2018.02480.
- 38 X. Ye and R. A. Weinberg, *Trends Cell Biol*, 2015, **25**, 675–686.
- 39 F. Rambow, J.-C. Marine and C. R. Goding, *Genes Dev.*, 2019, **33**, 1295–1318.
- 40 A. W. Lambert, D. R. Pattabiraman and R. A. Weinberg, *Cell*, 2017, **168**, 670–691.
- 41 S. Amintas, A. Bedel, F. Moreau-Gaudry, J. Boutin, L. Buscail, J.-P. Merlio, V. Vendrely and E. Dabernat Sandrine and Buscail, *Int. J. Mol. Sci.*, 2020, **21**, 2653.
- 42 N. Aceto, A. Bardia, D. T. Miyamoto, M. C. Donaldson, B. S. Wittner, J. A. Spencer, M. Yu, A. Pely, A. Engstrom, H. Zhu, B. W. Brannigan, R. Kapur, S. L. Stott, T. Shioda, S. Ramaswamy, D. T. Ting, C. P. Lin, M. Toner, D. A. Haber and S. Maheswaran, *Cell*, 2014, **158**, 1110–1122.
- 43 K. J. Cheung, V. Padmanaban, V. Silvestri, K. Schipper, J. D. Cohen, A. N. Fairchild, M. A. Gorin, J. E. Verdone, K. J. Pienta, J. S. Bader, A. J. Ewald, A. J. E. De-Signed, J. E. V Performed Re-Search and J. S. B. Contributed, , DOI:10.1073/pnas.1508541113.
- 44 X. Liu, R. Taftaf, M. Kawaguchi, Y.-F. Chang, W. Chen, D. Entenberg, L. Zhang Youbin and Gerratana, S. Huang, D. B. Patel, E. Tsui, V. Adorno-Cruz, S. M. Chirieleison, Y. Cao, A. S. Harney, S. Patel, A. Patsialou, Y. Shen, S. Avril, H. L. Gilmore, J. D. Lathia, D. W. Abbott, M. Cristofanilli, J. S. Condeelis and H. Liu, *Cancer Discov.*, 2019, **9**, 96–113.
- 45 A.-M. Larsson, S. Jansson, P.-O. Bendahl, C. Levin Tykjaer Jørgensen, N. Loman, C. Graffman, L. Lundgren, K. Aaltonen and L. Rydén, *Breast Cancer Research*, 2018, **20**, 48.
- 46 J.-M. Hou, M. G. Krebs, L. Lancashire, R. Sloane, A. Backen, R. K. Swain, L. J. C. Priest, A. Greystoke, C. Zhou, K. Morris, T. Ward, F. H. Blackhall and C. Dive, *Journal of Clinical Oncology*, 2012, **30**, 525–532.
- 47 N. Sawabata, Y. Susaki, T. Nakamura, T. Kawaguchi, M. Yasukawa and S. Taniguchi, *Gen Thorac Cardiovasc Surg*, 2020, **68**, 975–983.
- 48 E. Long, M. Ilie, C. Bence, C. Butori, E. Selva, S. Lalvée, C. Bonnetaud, G. Poissonnet, J.-P. Lacour, P. Bahadoran, P. Brest, E. Gilson, R. Ballotti, V. Hofman and P. Hofman, *Cancer Med*, 2016, **5**, 1022–1030.
- 49 H. Thangavel, C. De Angelis, S. Vasaikar, R. Bhat, M. K. Jolly, C. Nagi, C. J. Creighton, F. Chen, L. E. Dobrolecki, J. T. George, T. Kumar, N. M. Abdulkareem, S. Mao, A. Nardone, M. Rimawi, C. K. Osborne, M. T. Lewis, H. Levine, B. Zhang, R. Schiff, M. Giuliano and M. V. Trivedi, *J Clin Med*, 2019, **8**, 1772.
- 50 S. S. Martin and K. Vuori, *Biochimica et Biophysica Acta (BBA) - Molecular Cell Research*, 2004, **1692**, 145–157.
- 51 H. Han, J. Y. Sung, S.-H. Kim, U.-J. Yun, H. Kim, E.-J. Jang, H.-E. Yoo, E. K. Hong, S.-H. Goh, A. Moon, J.-S. Lee, S.-K. Ye, J. Shim and Y.-N. Kim, *Cancer Lett*, 2021, **508**, 59–72.
- 52 V. Spindler, C. Dehner, S. Hübner and J. Waschke, *Journal of Investigative Dermatology*, 2014, **134**, 1655–1664.

- 53 Z. Aktary and M. Pasdar, *Int J Cell Biol*, 2012, **2012**, 1–14.
- 54 R.-R. Wei, D.-N. Sun, H. Yang, J. Yan, X. Zhang, X.-L. Zheng, X.-H. Fu, M.-Y. Geng, X. Huang and J. Ding, *Acta Pharmacol. Sin.*, 2018, **39**, 1326–1337.
- 55 R. Taftaf, X. Liu, S. Singh, Y. Jia, N. K. Dashzeveg, A. D. Hoffmann, L. El-Shennawy, E. K. Ramos, V. Adorno-Cruz, E. J. Schuster, D. Scholten, D. Patel, Y. Zhang, A. A. Davis, C. Reduzzi, Y. Cao, P. D’Amico, Y. Shen, M. Cristofanilli, W. A. Muller, V. Varadan and H. Liu, *Nat Commun*, 2021, **12**, 4867.
- 56 T.-W. Lin, H.-T. Chang, C.-H. Chen, C.-H. Chen, S.-W. Lin, T.-L. Hsu and C.-H. Wong, *J. Am. Chem. Soc.*, 2015, **137**, 9685–9693.
- 57 N. Woolf, B. E. Pearson, P. A. Bondzie, R. D. Meyer, M. Lavaei, A. C. Belkina, V. Chitalia and N. Rahimi, *Oncogenesis*, 2017, **6**, e378–e378.
- 58 Q. Zhao, M. Barclay, J. Hilken, X. Guo, H. Barrow, J. M. Rhodes and L.-G. Yu, *Interaction between circulating galectin-3 and cancer-associated MUC1 enhances tumour cell homotypic aggregation and prevents anoikis*, 2010.
- 59 A. F. Sarioglu, N. Aceto, N. Kojic, M. C. Donaldson, M. Zeinali, B. Hamza, A. Engstrom, H. Zhu, T. K. Sundaresan, D. T. Miyamoto, X. Luo, A. Bardia, B. S. Wittner, S. Ramaswamy, T. Shioda, S. L. Ting David T and Stott, R. Kapur, D. A. Maheswaran Shyamala and Haber and M. Toner, *Nat. Methods*, 2015, **12**, 685–691.
- 60 N. Aceto, M. Toner, S. Maheswaran and D. A. Haber, *Trends Cancer*, 2015, **1**, 44–52.
- 61 M. Giuliano, A. Shaikh, H. C. Lo, G. Arpino, S. De Placido, X. H. Zhang, M. Cristofanilli, R. Schiff and M. V. Trivedi, *Cancer Res*, 2018, **78**, 845–852.
- 62 A. Cacciamali, R. Villa and S. Dotti, *Front Physiol*, , DOI:10.3389/fphys.2022.836480.
- 63 G. J. Hickman, D. J. Boockock, A. G. Pockley and C. C. Perry, *ACS Biomater Sci Eng*, 2016, **2**, 152–164.
- 64 G. J. Hickman, D. J. Boockock, A. G. Pockley and C. C. Perry, *ACS Biomater Sci Eng*, 2016, **2**, 152–164.
- 65 C. J. Wilson, R. E. Clegg, D. I. Leavesley and M. J. Pearcy, *Tissue Eng*, 2005, **11**, 1–18.
- 66 M. J. Sherratt, D. V. Bax, S. S. Chaudhry, N. Hodson, J. R. Lu, P. Saravanapavan and C. M. Kielty, *Biomaterials*, 2005, **26**, 7192–7206.
- 67 B. G. Keselowsky, D. M. Collard and A. J. García, *Proceedings of the National Academy of Sciences*, 2005, **102**, 5953–5957.
- 68 J. E. Phillips, T. A. Petrie, F. P. Creighton and A. J. García, *Acta Biomater*, 2010, **6**, 12–20.
- 69 J. Zhang, L. Li, Y. Peng, Y. Chen, X. Lv, S. Li, X. Qin, H. Yang, C. Wu and Y. Liu, *Biochimica et Biophysica Acta (BBA) - Molecular Cell Research*, 2018, **1865**, 172–185.
- 70 L. Glennon-Alty, R. Williams, S. Dixon and P. Murray, *Acta Biomater*, 2013, **9**, 6041–6051.
- 71 N. Al-Azzam and A. Alazzam, *PLoS One*, 2022, **17**, e0269914.
- 72 P. Weiss and B. Garber, *Proceedings of the National Academy of Sciences*, 1952, **38**, 264–280.

- 73 A. Zareidoost, M. Yousefpour, B. Ghaseme and A. Amanzadeh, *J Mater Sci Mater Med*, 2012, **23**, 1479–1488.
- 74 B. Majhy, P. Priyadarshini and A. K. Sen, *RSC Adv*, 2021, **11**, 15467–15476.
- 75 L. Damiaty, M. G. Eales, A. H. Nobbs, B. Su, P. M. Tsimbouri, M. Salmeron-Sanchez and M. J. Dalby, *J Tissue Eng*, 2018, **9**, 204173141879069.
- 76 M. J. Dalby, N. Gadegaard, R. Tare, A. Andar, M. O. Riehle, P. Herzyk, C. D. W. Wilkinson and R. O. C. Oreffo, *Nat Mater*, 2007, **6**, 997–1003.
- 77 R. McMurray, M. J and N. Gadegaar, in *Biomedical Engineering, Trends in Materials Science*, InTech, 2011.
- 78 F. Johansson, P. Carlberg, N. Danielsen, L. Montelius and M. Kanje, *Biomaterials*, 2006, **27**, 1251–1258.
- 79 J. D. Foley, E. W. Grunwald, P. F. Nealey and C. J. Murphy, *Biomaterials*, 2005, **26**, 3639–3644.
- 80 A. Ranella, M. Barberoglou, S. Bakogianni, C. Fotakis and E. Stratakis, *Acta Biomater*, 2010, **6**, 2711–2720.
- 81 M. Macgregor, R. Williams, J. Downes, A. Bachhuka and K. Vasilev, *Materials*, 2017, **10**, 1081.
- 82 T. Yeung, P. C. Georges, L. A. Flanagan, B. Marg, M. Ortiz, M. Funaki, N. Zahir, W. Ming, V. Weaver and P. A. Janmey, *Cell Motil Cytoskeleton*, 2005, **60**, 24–34.
- 83 B. S. Ludwig, H. Kessler, S. Kossatz and U. Reuning, *Cancers (Basel)*, 2021, **13**, 1711.
- 84 J.-H. Lin, H.-Y. Chang, W.-L. Kao, K.-Y. Lin, H.-Y. Liao, Y.-W. You, Y.-T. Kuo, D.-Y. Kuo, K.-J. Chu, Y.-H. Chu and J.-J. Shyue, *Langmuir*, 2014, **30**, 10328–10335.
- 85 S. P. Mitra, *Journal of Surface Science and Technology*, , DOI:10.18311/jsst/2020/23282.
- 86 V. Hlady and J. Buijs, *Curr Opin Biotechnol*, 1996, **7**, 72–77.
- 87 P. Roach, D. Farrar and C. C. Perry, *J Am Chem Soc*, 2005, **127**, 8168–8173.
- 88 S. Komasa, T. Kusumoto, Y. Taguchi, H. Nishizaki, T. Sekino, M. Umeda, J. Okazaki and T. Kawazoe, *J Nanomater*, 2014, **2014**, 1–11.
- 89 G. Mohan and N. D. Gallant, *J Biomed Mater Res A*, 2015, **103**, 2066–2076.
- 90 M. Cantini, M. Sousa, D. Moratal, J. F. Mano and M. Salmerón-Sánchez, *Biomater. Sci.*, 2013, **1**, 202–212.
- 91 L. Vroman, A. L. Adams, G. C. Fischer and P. C. Munoz, *Blood*, 1980, **55**, 156–9.
- 92 F. Fang and I. Szleifer, *Biophys J*, 2001, **80**, 2568–2589.
- 93 P. Roach, D. Farrar and C. C. Perry, *J Am Chem Soc*, 2006, **128**, 3939–3945.
- 94 M. S. Lord, B. G. Cousins, P. J. Doherty, J. M. Whitelock, A. Simmons, R. L. Williams and B. K. Milthorpe, *Biomaterials*, 2006, **27**, 4856–4862.
- 95 A. Dolatshahi-Pirouz, K. Rechendorff, M. B. Hovgaard, M. Foss, J. Chevallier and F. Besenbacher, *Colloids Surf B Biointerfaces*, 2008, **66**, 53–59.

- 96 K. Rechendorff, M. B. Hovgaard, M. Foss, V. P. Zhdanov and F. Besenbacher, *Langmuir*, 2006, **22**, 10885–10888.
- 97 R. M. Visalakshan, M. N. MacGregor, S. Sasidharan, A. Ghazaryan, A. M. Mierczynska-Vasilev, S. Morsbach, V. Mailänder, K. Landfester, J. D. Hayball and K. Vasilev, *ACS Appl Mater Interfaces*, 2019, **11**, 27615–27623.
- 98 E. Liamas, R. A. Black, P. A. Mulheran, R. Tampé, R. Wieneke, O. R. T. Thomas and Z. J. Zhang, *Sci Rep*, 2020, **10**, 15662.
- 99 D. Pellenc, H. Berry and O. Gallet, *J Colloid Interface Sci*, 2006, **298**, 132–144.
- 100 B. Li, W. Shen, H. Peng, Y. Li, F. Chen, L. Zheng, J. Xu and L. Jia, *Onco. Targets. Ther.*, 2019, **12**, 3207–3221.
- 101 J.-H. Lin, H.-Y. Chang, W.-L. Kao, K.-Y. Lin, H.-Y. Liao, Y.-W. You, Y.-T. Kuo, D.-Y. Kuo, K.-J. Chu, Y.-H. Chu and J.-J. Shyue, *Langmuir*, 2014, **30**, 10328–10335.
- 102 G. J. Hickman, A. Rai, D. J. Boocock, R. C. Rees and C. C. Perry, *J. Mater. Chem.*, 2012, **22**, 12141.
- 103 G. J. Hickman, R. C. Rees, D. J. Boocock, A. G. Pockley and C. C. Perry, *Adv Healthc Mater*, 2015, **4**, 593–601.
- 104 M. Nicklin, G. J. Hickman, A. Graham Pockley and C. C. Perry, *ACS Appl Bio Mater*, 2020, **3**, 495–504.
- 105 M. Nicklin, R. C. Rees, A. G. Pockley and C. C. Perry, *Biomater. Sci.*, 2014, **2**, 1486–1496.
- 106 N. Harner-Foreman, J. Vadakekolathu, S. A. Laversin, M. G. Mathieu, S. Reeder, A. G. Pockley, R. C. Rees and D. J. Boocock, *Sci. Rep.*, 2017, **7**, 40633.
- 107 A. L. Hellewell, S. Rosini and J. C. Adams, *J Vis Exp*, , DOI:10.3791/55051.
- 108 T. D. Schmittgen and K. J. Livak, *Nat Protoc*, 2008, **3**, 1101–1108.
- 109 E. Cerami, J. Gao, U. Dogrusoz, B. E. Gross, S. O. Sumer, A. Aksoy Bülent Arman and Jacobsen, C. J. Byrne, E. Heuer Michael L and Larsson, Y. Antipin, B. Reva, A. P. Goldberg, C. Sander and N. Schultz, *Cancer Discov.*, 2012, **2**, 401–404.
- 110 J. Anaya, *PeerJ Comput Sci*, 2016, **2**, e67.
- 111 D. Liu, B. Schilling, D. Liu, A. Sucker, E. Livingstone, L. Jerby-Arnon, L. Zimmer, R. Gutzmer, I. Satzger, C. Loquai, S. Grabbe, N. Vokes, C. A. Margolis, J. Conway, M. X. He, H. Elmarakeby, F. Dietlein, D. Miao, A. Tracy, H. Gogas, S. M. Goldinger, J. Utikal, C. U. Blank, R. Rauschenberg, D. von Bubnoff, A. Krackhardt, B. Weide, S. Haferkamp, F. Kiecker, B. Izar, A. Garraway Levi and Regev, K. Flaherty, A. Paschen, E. M. Van Allen and D. Schadendorf, *Nat. Med.*, 2019, **25**, 1916–1927.
- 112 W. S. Liang, W. Hendricks, J. Kiefer, J. Schmidt, S. Sekar, J. Carpten, D. W. Craig, J. Adkins, L. Cuyugan, Z. Manojlovic, R. F. Halperin, A. Helland, S. Nasser, C. Legendre, L. H. Hurley, K. Sivaprakasam, D. B. Johnson, H. Crandall, K. J. Busam, V. Zismann, V. Deluca, J. Lee, A. Sekulic, C. E. Ariyan, J. Sosman and J. Trent, *Genome Res.*, 2017, **27**, 524–532.
- 113 W. Hugo, J. M. Zaretsky, L. Sun, B. H. Song Chunying and Moreno, S. Hu-Lieskovan, B. Berent-Maoz, J. Pang, B. Chmielowski, E. Cherry Grace and Seja, S. Lomeli, X. Kong, M. C. Kelley, J. A. Sosman, D. B. Johnson, A. Ribas and R. S. Lo, *Cell*, 2016, **165**, 35–44.

- 114 E. M. Van Allen, D. Miao, B. Schilling, S. A. Shukla, C. Blank, L. Zimmer, A. Sucker, U. Hillen, M. H. G. Foppen, S. M. Goldinger, J. Utikal, J. C. Hassel, B. Weide, K. C. Kaehler, C. Loquai, P. Mohr, R. Gutzmer, R. Dummer, S. Gabriel, C. J. Wu, D. Schadendorf and L. A. Garraway, *Science (1979)*, 2015, **350**, 207–211.
- 115 A. Snyder, V. Makarov, T. Merghoub, J. Yuan, J. M. Zaretsky, A. Desrichard, L. A. Walsh, M. A. Postow, P. Wong, T. S. Ho, T. J. Hollmann, C. Bruggeman, K. Kannan, Y. Li, C. Elipenahli, C. Liu, C. T. Harbison, L. Wang, A. Ribas, J. D. Wolchok and T. A. Chan, *N. Engl. J. Med.*, 2014, **371**, 2189–2199.
- 116 R. Bonneville, M. A. Krook, E. A. Kautto, J. Miya, M. R. Wing, H.-Z. Chen, J. W. Reeser, L. Yu and S. Roychowdhury, *JCO Precis Oncol*, 2017, 1–15.
- 117 L. Ding, M. H. Bailey, E. Porta-Pardo, V. Thorsson, A. Colaprico, D. Bertrand, D. L. Gibbs, A. Weerasinghe, K. Huang, C. Tokheim, I. Cortés-Ciriano, R. Jayasinghe, F. Chen, L. Yu, S. Sun, C. Olsen, J. Kim, A. M. Taylor, A. D. Cherniack, R. Akbani, C. Suphavilai, N. Nagarajan, J. M. Stuart, G. B. Mills, M. A. Wyczalkowski, B. G. Vincent, C. M. Hutter, J. C. Zenklusen, K. A. Hoadley, M. C. Wendl, Ilya Shmulevich, A. J. Lazar, D. A. Wheeler, G. Getz, S. J. Caesar-Johnson, J. A. Demchok, I. Felau, M. Kasapi, M. L. Ferguson, C. M. Hutter, H. J. Sofia, R. Tarnuzzer, Z. Wang, L. Yang, J. C. Zenklusen, J. (Julia) Zhang, S. Chudamani, J. Liu, L. Lolla, R. Naresh, T. Pihl, Q. Sun, Y. Wan, Y. Wu, J. Cho, T. DeFreitas, S. Frazer, N. Gehlenborg, G. Getz, D. I. Heiman, J. Kim, M. S. Lawrence, P. Lin, S. Meier, M. S. Noble, G. Saksena, D. Voet, H. Zhang, B. Bernard, N. Chambwe, V. Dhankani, T. Knijnenburg, R. Kramer, K. Leinonen, Y. Liu, M. Miller, S. Reynolds, I. Shmulevich, V. Thorsson, W. Zhang, R. Akbani, B. M. Broom, A. M. Hegde, Z. Ju, R. S. Kanchi, A. Korkut, J. Li, H. Liang, S. Ling, W. Liu, Y. Lu, G. B. Mills, K.-S. Ng, A. Rao, M. Ryan, J. Wang, J. N. Weinstein, J. Zhang, A. Abeshouse, J. Armenia, D. Chakravarty, W. K. Chatila, I. de Bruijn, J. Gao, B. E. Gross, Z. J. Heins, R. Kundra, K. La, M. Ladanyi, A. Luna, M. G. Nissan, A. Ochoa, S. M. Phillips, E. Reznik, F. Sanchez-Vega, C. Sander, N. Schultz, R. Sheridan, S. O. Sumer, Y. Sun, B. S. Taylor, J. Wang, H. Zhang, P. Anur, M. Peto, P. Spellman, C. Benz, J. M. Stuart, C. K. Wong, C. Yau, D. N. Hayes, J. S. Parker, M. D. Wilkerson, A. Ally, M. Balasundaram, R. Bowlby, D. Brooks, R. Carlsen, E. Chuah, N. Dhalla, R. Holt, S. J. M. Jones, K. Kasaian, D. Lee, Y. Ma, M. A. Marra, M. Mayo, R. A. Moore, A. J. Mungall, K. Mungall, A. G. Robertson, S. Sadeghi, J. E. Schein, P. Sipahimalani, A. Tam, N. Thiessen, K. Tse, T. Wong, A. C. Berger, R. Beroukhir, A. D. Cherniack, C. Cibulskis, S. B. Gabriel, G. F. Gao, G. Ha, M. Meyerson, S. E. Schumacher, J. Shih, M. H. Kucherlapati, R. S. Kucherlapati, S. Baylin, L. Cope, L. Danilova, M. S. Bootwalla, P. H. Lai, D. T. Maglinte, D. J. Van Den Berg, D. J. Weisenberger, J. T. Auman, S. Balu, T. Bodenheimer, C. Fan, K. A. Hoadley, A. P. Hoyle, S. R. Jefferys, C. D. Jones, S. Meng, P. A. Mieczkowski, L. E. Mose, A. H. Perou, C. M. Perou, J. Roach, Y. Shi, J. V. Simons, T. Skelly, M. G. Soloway, D. Tan, U. Veluvolu, H. Fan, T. Hinoue, P. W. Laird, H. Shen, W. Zhou, M. Bellair, K. Chang, K. Covington, C. J. Creighton, H. Dinh, H. Doddapaneni, L. A. Donehower, J. Drummond, R. A. Gibbs, R. Glenn, W. Hale, Y. Han, J. Hu, V. Korchina, S. Lee, L. Lewis, W. Li, X. Liu, M. Morgan, D. Morton, D. Muzny, J. Santibanez, M. Sheth, E. Shinbrot, L. Wang, M. Wang, D. A. Wheeler, L. Xi, F. Zhao, J. Hess, E. L. Appelbaum, M. Bailey, M. G. Cordes, L. Ding, C. C. Fronick, L. A. Fulton, R. S. Fulton, C. Kandoth, E. R. Mardis, M. D. McLellan, C. A. Miller, H. K. Schmidt, R. K. Wilson, D. Crain, E. Curley, J. Gardner, K. Lau, D. Mallery, S. Morris, J. Paulauskis, R. Penny, C. Shelton, T. Shelton, M. Sherman, E. Thompson, P. Yena, J. Bowen, J. M. Gastier-Foster, M. Gerken, K. M. Leraas, T. M. Lichtenberg, N. C. Ramirez, L. Wise, E. Zmuda, N. Corcoran, T. Costello, C. Hovens, A. L. Carvalho, A. C. de Carvalho, J. H. Fregnani, A. Longatto-Filho, R. M. Reis, C. Scapulatempo-Neto, H. C. S. Silveira, D. O. Vidal, A. Burnette, J. Eschbacher, B. Hermes, A. Noss, R. Singh, M. L. Anderson, P. D. Castro, M. Ittmann, D.

Huntsman, B. Kohl, X. Le, R. Thorp, C. Andry, E. R. Duffy, V. Lyadov, O. Paklina, G. Setdikova, A. Shabunin, M. Tavobilov, C. McPherson, R. Warnick, R. Berkowitz, D. Cramer, C. Feltmate, N. Horowitz, A. Kibel, M. Muto, C. P. Raut, A. Malykh, J. S. Barnholtz-Sloan, W. Barrett, K. Devine, J. Fulop, Q. T. Ostrom, K. Shimmel, Y. Wolinsky, A. E. Sloan, A. De Rose, F. Giuliante, M. Goodman, B. Y. Karlan, C. H. Hagedorn, J. Eckman, J. Harr, J. Myers, K. Tucker, L. A. Zach, B. Deyarmin, H. Hu, L. Kvecher, C. Larson, R. J. Mural, S. Somiari, A. Vicha, T. Zelinka, J. Bennett, M. Iacocca, B. Rabeno, P. Swanson, M. Latour, L. Lacombe, B. Têtu, A. Bergeron, M. McGraw, S. M. Staugaitis, J. Chabot, H. Hibshoosh, A. Sepulveda, T. Su, T. Wang, O. Potapova, O. Voronina, L. Desjardins, O. Mariani, S. Roman-Roman, X. Sastre, M.-H. Stern, F. Cheng, S. Signoretti, A. Berchuck, D. Bigner, E. Lipp, J. Marks, S. McCall, R. McLendon, A. Secord, A. Sharp, M. Behera, D. J. Brat, A. Chen, K. Delman, S. Force, F. Khuri, K. Magliocca, S. Maithel, J. J. Olson, T. Owonikoko, A. Pickens, S. Ramalingam, D. M. Shin, G. Sica, E. G. Van Meir, H. Zhang, W. Eijckenboom, A. Gillis, E. Korpershoek, L. Looijenga, W. Oosterhuis, H. Stoop, K. E. van Kessel, E. C. Zwarthoff, C. Calatozzolo, L. Cuppini, S. Cuzzubbo, F. DiMeco, G. Finocchiaro, L. Mattei, A. Perin, B. Pollo, C. Chen, J. Houck, P. Lohavanichbutr, A. Hartmann, C. Stoehr, R. Stoehr, H. Taubert, S. Wach, B. Wullich, W. Kycler, D. Murawa, M. Wiznerowicz, K. Chung, W. J. Edenfield, J. Martin, E. Baudin, G. Bublely, R. Bueno, A. De Rienzo, W. G. Richards, S. Kalkanis, T. Mikkelsen, H. Noushmehr, L. Scarpacci, N. Girard, M. Aymerich, E. Campo, E. Giné, A. L. Guillermo, N. Van Bang, P. T. Hanh, B. D. Phu, Y. Tang, H. Colman, K. Evason, P. R. Dottino, J. A. Martignetti, H. Gabra, H. Juhl, T. Akeredolu, S. Stepa, D. Hoon, K. Ahn, K. J. Kang, F. Beuschlein, A. Breggia, M. Birrer, D. Bell, M. Borad, A. H. Bryce, E. Castle, V. Chandan, J. Cheville, J. A. Copland, M. Farnell, T. Flotte, N. Giama, T. Ho, M. Kendrick, J.-P. Kocher, K. Kopp, C. Moser, D. Nagorney, D. O'Brien, B. P. O'Neill, T. Patel, G. Petersen, F. Que, M. Rivera, L. Roberts, R. Smallridge, T. Smyrk, M. Stanton, R. H. Thompson, M. Torbenson, J. D. Yang, L. Zhang, F. Brimo, J. A. Ajani, A. M. A. Gonzalez, C. Behrens, J. Bondaruk, R. Broaddus, B. Czerniak, B. Esmali, J. Fujimoto, J. Gershenwald, C. Guo, A. J. Lazar, C. Logothetis, F. Meric-Bernstam, C. Moran, L. Ramondetta, D. Rice, A. Sood, P. Tamboli, T. Thompson, P. Troncso, A. Tsao, I. Wistuba, C. Carter, L. Haydu, P. Hersey, V. Jakrot, H. Kakavand, R. Kefford, K. Lee, G. Long, G. Mann, M. Quinn, R. Saw, R. Scolyer, K. Shannon, A. Spillane, J. Stretch, M. Synott, J. Thompson, J. Wilmott, H. Al-Ahmadie, T. A. Chan, R. Ghossein, A. Gopalan, D. A. Levine, V. Reuter, S. Singer, B. Singh, N. V. Tien, T. Broudy, C. Mirsaiid, P. Nair, P. Drwiega, J. Miller, J. Smith, H. Zaren, J.-W. Park, N. P. Hung, E. Kebebew, W. M. Linehan, A. R. Metwalli, K. Pacak, P. A. Pinto, M. Schiffman, L. S. Schmidt, C. D. Vocke, N. Wentzensen, R. Worrell, H. Yang, M. Moncrieff, C. Goparaju, J. Melamed, H. Pass, N. Botnariuc, I. Caraman, M. Cernat, I. Chemencedji, A. Clipca, S. Doruc, G. Gorincioi, S. Mura, M. Pirtac, I. Stancul, D. Tcaciuc, M. Albert, I. Alexopoulou, A. Arnaout, J. Bartlett, J. Engel, S. Gilbert, J. Parfitt, H. Sekhon, G. Thomas, D. M. Rassel, R. C. Rintoul, C. Bifulco, R. Tamakawa, W. Urba, N. Hayward, H. Timmers, A. Antenucci, F. Facciolo, G. Grazi, M. Marino, R. Merola, R. de Krijger, A.-P. Gimenez-Roqueplo, A. Piché, S. Chevalier, G. McKercher, K. Birsoy, G. Barnett, C. Brewer, C. Farver, T. Naska, N. A. Pennell, D. Raymond, C. Schilero, K. Smolenski, F. Williams, C. Morrison, J. A. Borgia, M. J. Liptay, M. Pool, C. W. Seder, K. Junker, L. Omberg, M. Dinkin, G. Manikhas, D. Alvaro, M. C. Bragazzi, V. Cardinale, G. Carpino, E. Gaudio, D. Chesla, S. Cottingham, M. Dubina, F. Moiseenko, R. Dhanasekaran, K.-F. Becker, K.-P. Janssen, J. Slotta-Huspenina, M. H. Abdel-Rahman, D. Aziz, S. Bell, C. M. Cebulla, A. Davis, R. Duell, J. B. Elder, J. Hilty, B. Kumar, J. Lang, N. L. Lehman, R. Mandt, P. Nguyen, R. Pilarski, K. Rai, L. Schoenfeld, K. Senecal, P. Wakely, P. Hansen, R. Lechan, J. Powers, A. Tischler, W. E. Grizzle, K. C. Sexton, A. Kastl, J. Henderson, S. Porten, J. Waldmann, M. Fassnacht, S. L. Asa, D. Schadendorf, M. Couce, M. Graefen, H. Huland, G. Sauter, T. Schlomm, R. Simon, P. Tennstedt, O. Olabode, M. Nelson, O. Bathe, P. R. Carroll, J. M. Chan, P. Disaia, P. Glenn, R. K. Kelley, C. N. Landen, J. Phillips, M. Prados, J. Simko, K.

- Smith-McCune, S. VandenBerg, K. Roggin, A. Fehrenbach, A. Kendler, S. Sifri, R. Steele, A. Jimeno, F. Carey, I. Forgie, M. Mannelli, M. Carney, B. Hernandez, B. Campos, C. Herold-Mende, C. Jungk, A. Unterberg, A. von Deimling, A. Bossler, J. Galbraith, L. Jacobus, M. Knudson, T. Knutson, D. Ma, M. Milhem, R. Sigmund, A. K. Godwin, R. Madan, H. G. Rosenthal, C. Adebamowo, S. N. Adebamowo, A. Boussioutas, D. Beer, T. Giordano, A.-M. Mes-Masson, F. Saad, T. Bocklage, L. Landrum, R. Mannel, K. Moore, K. Moxley, R. Postier, J. Walker, R. Zuna, M. Feldman, F. Valdivieso, R. Dhir, J. Luketich, E. M. M. Pinero, M. Quintero-Aguilo, C. G. Carlotti, J. S. Dos Santos, R. Kemp, A. Sankarankuty, D. Tirapelli, J. Catto, K. Agnew, E. Swisher, J. Creaney, B. Robinson, C. S. Shelley, E. M. Godwin, S. Kendall, C. Shipman, C. Bradford, T. Carey, A. Haddad, J. Moyer, L. Peterson, M. Prince, L. Rozek, G. Wolf, R. Bowman, K. M. Fong, I. Yang, R. Korst, W. K. Rathmell, J. L. Fantacone-Campbell, J. A. Hooke, A. J. Kovatich, C. D. Shriver, J. DiPersio, B. Drake, R. Govindan, S. Heath, T. Ley, B. Van Tine, P. Westervelt, M. A. Rubin, J. Il Lee, N. D. Aredes and A. Mariamidze, *Cell*, 2018, **173**, 305-320.e10.
- 118 G. D. Poore, E. Kopylova, Q. Zhu, C. Carpenter, S. Fraraccio, S. Wandro, T. Kosciolk, S. Janssen, J. Metcalf, S. J. Song, J. Kanbar, S. Miller-Montgomery, R. Heaton, R. McKay, S. P. Patel, A. D. Swafford and R. Knight, *Nature*, 2020, **579**, 567–574.
- 119 V. Bhandari, C. Hoey, L. Y. Liu, E. Lalonde, J. Ray, J. Livingstone, R. Lesurf, Y.-J. Shiah, T. Vujcic, X. Huang, S. M. G. Espiritu, L. E. Heisler, F. Yousif, V. Huang, T. N. Yamaguchi, C. Q. Yao, V. Y. Sabelnykova, M. Fraser, M. L. K. Chua, T. van der Kwast, S. K. Liu, P. C. Boutros and R. G. Bristow, *Nat Genet*, 2019, **51**, 308–318.
- 120 Q. Gao, W.-W. Liang, S. M. Foltz, G. Mutharasu, R. G. Jayasinghe, S. Cao, W.-W. Liao, S. M. Reynolds, M. A. Wyczalkowski, L. Yao, L. Yu, S. Q. Sun, K. Chen, A. J. Lazar, R. C. Fields, M. C. Wendl, B. A. Van Tine, R. Vij, F. Chen, M. Nykter, I. Shmulevich, L. Ding, S. J. Caesar-Johnson, J. A. Demchok, I. Felau, M. Kasapi, M. L. Ferguson, C. M. Hutter, H. J. Sofia, R. Tarnuzzer, Z. Wang, L. Yang, J. C. Zenklusen, J. (Julia) Zhang, S. Chudamani, J. Liu, L. Lolla, R. Naresh, T. Pihl, Q. Sun, Y. Wan, Y. Wu, J. Cho, T. DeFreitas, S. Frazer, N. Gehlenborg, G. Getz, D. I. Heiman, J. Kim, M. S. Lawrence, P. Lin, S. Meier, M. S. Noble, G. Saksena, D. Voet, H. Zhang, B. Bernard, N. Chambwe, V. Dhankani, T. Knijnenburg, R. Kramer, K. Leinonen, Y. Liu, M. Miller, S. Reynolds, I. Shmulevich, V. Thorsson, W. Zhang, R. Akbani, B. M. Broom, A. M. Hegde, Z. Ju, R. S. Kanchi, A. Korkut, J. Li, H. Liang, S. Ling, W. Liu, Y. Lu, G. B. Mills, K.-S. Ng, A. Rao, M. Ryan, J. Wang, J. N. Weinstein, J. Zhang, A. Abeshouse, J. Armenia, D. Chakravarty, W. K. Chatila, I. de Bruijn, J. Gao, B. E. Gross, Z. J. Heins, R. Kundra, K. La, M. Ladanyi, A. Luna, M. G. Nissan, A. Ochoa, S. M. Phillips, E. Reznik, F. Sanchez-Vega, C. Sander, N. Schultz, R. Sheridan, S. O. Sumer, Y. Sun, B. S. Taylor, J. Wang, H. Zhang, P. Anur, M. Peto, P. Spellman, C. Benz, J. M. Stuart, C. K. Wong, C. Yau, D. N. Hayes, J. S. Parker, M. D. Wilkerson, A. Ally, M. Balasundaram, R. Bowlby, D. Brooks, R. Carlsen, E. Chuah, N. Dhalla, R. Holt, S. J. M. Jones, K. Kasaian, D. Lee, Y. Ma, M. A. Marra, M. Mayo, R. A. Moore, A. J. Mungall, K. Mungall, A. G. Robertson, S. Sadeghi, J. E. Schein, P. Sipahimalani, A. Tam, N. Thiessen, K. Tse, T. Wong, A. C. Berger, R. Beroukhim, A. D. Cherniack, C. Cibulskis, S. B. Gabriel, G. F. Gao, G. Ha, M. Meyerson, S. E. Schumacher, J. Shih, M. H. Kucherlapati, R. S. Kucherlapati, S. Baylin, L. Cope, L. Danilova, M. S. Bootwalla, P. H. Lai, D. T. Maglinte, D. J. Van Den Berg, D. J. Weisenberger, J. T. Auman, S. Balu, T. Bodenheimer, C. Fan, K. A. Hoadley, A. P. Hoyle, S. R. Jefferys, C. D. Jones, S. Meng, P. A. Mieczkowski, L. E. Mose, A. H. Perou, C. M. Perou, J. Roach, Y. Shi, J. V. Simons, T. Skelly, M. G. Soloway, D. Tan, U. Veluvolu, H. Fan, T. Hinoue, P. W. Laird, H. Shen, W. Zhou, M. Bellair, K. Chang, K. Covington, C. J. Creighton, H. Dinh, H. Doddapaneni, L. A. Donehower, J. Drummond, R. A. Gibbs, R. Glenn, W. Hale, Y. Han, J. Hu, V. Korchina, S. Lee, L. Lewis, W. Li, X. Liu, M. Morgan, D.

Morton, D. Muzny, J. Santibanez, M. Sheth, E. Shinbrot, L. Wang, M. Wang, D. A. Wheeler, L. Xi, F. Zhao, J. Hess, E. L. Appelbaum, M. Bailey, M. G. Cordes, L. Ding, C. C. Fronick, L. A. Fulton, R. S. Fulton, C. Kandoth, E. R. Mardis, M. D. McLellan, C. A. Miller, H. K. Schmidt, R. K. Wilson, D. Crain, E. Curley, J. Gardner, K. Lau, D. Mallery, S. Morris, J. Paulauskis, R. Penny, C. Shelton, T. Shelton, M. Sherman, E. Thompson, P. Yena, J. Bowen, J. M. Gastier-Foster, M. Gerken, K. M. Leraas, T. M. Lichtenberg, N. C. Ramirez, L. Wise, E. Zmuda, N. Corcoran, T. Costello, C. Hovens, A. L. Carvalho, A. C. de Carvalho, J. H. Fregnani, A. Longatto-Filho, R. M. Reis, C. Scapulatempo-Neto, H. C. S. Silveira, D. O. Vidal, A. Burnette, J. Eschbacher, B. Hermes, A. Noss, R. Singh, M. L. Anderson, P. D. Castro, M. Ittmann, D. Huntsman, B. Kohl, X. Le, R. Thorp, C. Andry, E. R. Duffy, V. Lyadov, O. Paklina, G. Setdikova, A. Shabunin, M. Tavobilov, C. McPherson, R. Warnick, R. Berkowitz, D. Cramer, C. Feltmate, N. Horowitz, A. Kibel, M. Muto, C. P. Raut, A. Malykh, J. S. Barnholtz-Sloan, W. Barrett, K. Devine, J. Fulop, Q. T. Ostrom, K. Shimmel, Y. Wolinsky, A. E. Sloan, A. De Rose, F. Giuliante, M. Goodman, B. Y. Karlan, C. H. Hagedorn, J. Eckman, J. Harr, J. Myers, K. Tucker, L. A. Zach, B. Deyarmin, H. Hu, L. Kvecher, C. Larson, R. J. Mural, S. Somiari, A. Vicha, T. Zelinka, J. Bennett, M. Iacocca, B. Rabeno, P. Swanson, M. Latour, L. Lacombe, B. Têtu, A. Bergeron, M. McGraw, S. M. Staugaitis, J. Chabot, H. Hibshoosh, A. Sepulveda, T. Su, T. Wang, O. Potapova, O. Voronina, L. Desjardins, O. Mariani, S. Roman-Roman, X. Sastre, M.-H. Stern, F. Cheng, S. Signoretti, A. Berchuck, D. Bigner, E. Lipp, J. Marks, S. McCall, R. McLendon, A. Secord, A. Sharp, M. Behera, D. J. Brat, A. Chen, K. Delman, S. Force, F. Khuri, K. Magliocca, S. Maithel, J. J. Olson, T. Owonikoko, A. Pickens, S. Ramalingam, D. M. Shin, G. Sica, E. G. Van Meir, H. Zhang, W. Eijckenboom, A. Gillis, E. Korpershoek, L. Looijenga, W. Oosterhuis, H. Stoop, K. E. van Kessel, E. C. Zwarthoff, C. Calatozzolo, L. Cuppini, S. Cuzzubbo, F. DiMeco, G. Finocchiaro, L. Mattei, A. Perin, B. Pollo, C. Chen, J. Houck, P. Lohavanichbutr, A. Hartmann, C. Stoehr, R. Stoehr, H. Taubert, S. Wach, B. Wullich, W. Kycler, D. Murawa, M. Wiznerowicz, K. Chung, W. J. Edenfield, J. Martin, E. Baudin, G. Bublely, R. Bueno, A. De Rienzo, W. G. Richards, S. Kalkanis, T. Mikkelsen, H. Noushmehr, L. Scarpacci, N. Girard, M. Aymerich, E. Campo, E. Giné, A. L. Guillermo, N. Van Bang, P. T. Hanh, B. D. Phu, Y. Tang, H. Colman, K. Evason, P. R. Dottino, J. A. Martignetti, H. Gabra, H. Juhl, T. Akeredolu, S. Stepa, D. Hoon, K. Ahn, K. J. Kang, F. Beuschlein, A. Breggia, M. Birrer, D. Bell, M. Borad, A. H. Bryce, E. Castle, V. Chandan, J. Cheville, J. A. Copland, M. Farnell, T. Flotte, N. Giama, T. Ho, M. Kendrick, J.-P. Kocher, K. Kopp, C. Moser, D. Nagorney, D. O'Brien, B. P. O'Neill, T. Patel, G. Petersen, F. Que, M. Rivera, L. Roberts, R. Smallridge, T. Smyrk, M. Stanton, R. H. Thompson, M. Torbenson, J. D. Yang, L. Zhang, F. Brimo, J. A. Ajani, A. M. A. Gonzalez, C. Behrens, J. Bondaruk, R. Broaddus, B. Czerniak, B. Esmaeli, J. Fujimoto, J. Gershenwald, C. Guo, A. J. Lazar, C. Logothetis, F. Meric-Bernstam, C. Moran, L. Ramondetta, D. Rice, A. Sood, P. Tamboli, T. Thompson, P. Troncso, A. Tsao, I. Wistuba, C. Carter, L. Haydu, P. Hersey, V. Jakrot, H. Kakavand, R. Kefford, K. Lee, G. Long, G. Mann, M. Quinn, R. Saw, R. Scolyer, K. Shannon, A. Spillane, J. Stretch, M. Synott, J. Thompson, J. Wilmott, H. Al-Ahmadie, T. A. Chan, R. Ghossein, A. Gopalan, D. A. Levine, V. Reuter, S. Singer, B. Singh, N. V. Tien, T. Broudy, C. Mirsaidi, P. Nair, P. Drwiega, J. Miller, J. Smith, H. Zaren, J.-W. Park, N. P. Hung, E. Kebebew, W. M. Linehan, A. R. Metwalli, K. Pacak, P. A. Pinto, M. Schiffman, L. S. Schmidt, C. D. Vocke, N. Wentzensen, R. Worrell, H. Yang, M. Moncrieff, C. Goparaju, J. Melamed, H. Pass, N. Botnariuc, I. Caraman, M. Cernat, I. Chemencedji, A. Clipca, S. Doruc, G. Gorincioi, S. Mura, M. Pirtac, I. Stancul, D. Tcaciuc, M. Albert, I. Alexopoulou, A. Arnaout, J. Bartlett, J. Engel, S. Gilbert, J. Parfitt, H. Sekhon, G. Thomas, D. M. Rassi, R. C. Rintoul, C. Bifulco, R. Tamakawa, W. Urba, N. Hayward, H. Timmers, A. Antenucci, F. Facciolo, G. Grazi, M. Marino, R. Merola, R. de Krijger, A.-P. Gimenez-Roqueplo, A. Piché, S. Chevalier, G. McKercher, K. Birsoy, G. Barnett, C. Brewer, C. Farver, T. Naska, N. A. Pennell, D. Raymond, C. Schilero, K. Smolenski, F. Williams, C. Morrison, J. A. Borgia, M. J. Liptay, M. Pool, C. W.

Seder, K. Junker, L. Omberg, M. Dinkin, G. Manikhas, D. Alvaro, M. C. Bragazzi, V. Cardinale, G. Carpino, E. Gaudio, D. Chesla, S. Cottingham, M. Dubina, F. Moiseenko, R. Dhanasekaran, K.-F. Becker, K.-P. Janssen, J. Slotta-Huspenina, M. H. Abdel-Rahman, D. Aziz, S. Bell, C. M. Cebulla, A. Davis, R. Duell, J. B. Elder, J. Hilty, B. Kumar, J. Lang, N. L. Lehman, R. Mandt, P. Nguyen, R. Pilarski, K. Rai, L. Schoenfield, K. Senecal, P. Wakely, P. Hansen, R. Lechan, J. Powers, A. Tischler, W. E. Grizzle, K. C. Sexton, A. Kastl, J. Henderson, S. Porten, J. Waldmann, M. Fassnacht, S. L. Asa, D. Schadendorf, M. Couce, M. Graefen, H. Huland, G. Sauter, T. Schlomm, R. Simon, P. Tennstedt, O. Olabode, M. Nelson, O. Bathe, P. R. Carroll, J. M. Chan, P. Disaia, P. Glenn, R. K. Kelley, C. N. Landen, J. Phillips, M. Prados, J. Simko, K. Smith-McCune, S. VandenBerg, K. Roggin, A. Fehrenbach, A. Kendler, S. Sifri, R. Steele, A. Jimeno, F. Carey, I. Forgie, M. Mannelli, M. Carney, B. Hernandez, B. Campos, C. Herold-Mende, C. Jungk, A. Unterberg, A. von Deimling, A. Bossler, J. Galbraith, L. Jacobus, M. Knudson, T. Knutson, D. Ma, M. Milhem, R. Sigmund, A. K. Godwin, R. Madan, H. G. Rosenthal, C. Adebamowo, S. N. Adebamowo, A. Boussioutas, D. Beer, T. Giordano, A.-M. Mes-Masson, F. Saad, T. Bocklage, L. Landrum, R. Mannel, K. Moore, K. Moxley, R. Postier, J. Walker, R. Zuna, M. Feldman, F. Valdivieso, R. Dhir, J. Luketich, E. M. M. Pinero, M. Quintero-Aguilo, C. G. Carlotti, J. S. Dos Santos, R. Kemp, A. Sankarankuty, D. Tirapelli, J. Catto, K. Agnew, E. Swisher, J. Creaney, B. Robinson, C. S. Shelley, E. M. Godwin, S. Kendall, C. Shipman, C. Bradford, T. Carey, A. Haddad, J. Moyer, L. Peterson, M. Prince, L. Rozek, G. Wolf, R. Bowman, K. M. Fong, I. Yang, R. Korst, W. K. Rathmell, J. L. Fantacone-Campbell, J. A. Hooke, A. J. Kovatich, C. D. Shriver, J. DiPersio, B. Drake, R. Govindan, S. Heath, T. Ley, B. Van Tine, P. Westervelt, M. A. Rubin, J. Il Lee, N. D. Aredes and A. Mariamidze, *Cell Rep*, 2018, **23**, 227-238.e3.

- 121 F. Sanchez-Vega, M. Mina, J. Armenia, W. K. Chatila, A. Luna, K. C. La, S. Dimitriadoy, D. L. Liu, H. S. Kantheti, S. Saghafinia, D. Chakravarty, F. Daian, Q. Gao, M. H. Bailey, W.-W. Liang, S. M. Foltz, I. Shmulevich, L. Ding, Z. Heins, A. Ochoa, B. Gross, J. Gao, H. Zhang, R. Kundra, C. Kandoth, I. Bahceci, L. Dervishi, U. Dogrusoz, W. Zhou, H. Shen, P. W. Laird, G. P. Way, C. S. Greene, H. Liang, Y. Xiao, C. Wang, A. Iavarone, A. H. Berger, T. G. Bivona, A. J. Lazar, G. D. Hammer, T. Giordano, L. N. Kwong, G. McArthur, C. Huang, A. D. Tward, M. J. Frederick, F. McCormick, M. Meyerson, E. M. Van Allen, A. D. Cherniack, G. Ciriello, C. Sander, N. Schultz, S. J. Caesar-Johnson, J. A. Demchok, I. Felau, M. Kasapi, M. L. Ferguson, C. M. Hutter, H. J. Sofia, R. Tarnuzzer, Z. Wang, L. Yang, J. C. Zenklusen, J. (Julia) Zhang, S. Chudamani, J. Liu, L. Lolla, R. Naresh, T. Pihl, Q. Sun, Y. Wan, Y. Wu, J. Cho, T. DeFreitas, S. Frazer, N. Gehlenborg, G. Getz, D. I. Heiman, J. Kim, M. S. Lawrence, P. Lin, S. Meier, M. S. Noble, G. Saksena, D. Voet, H. Zhang, B. Bernard, N. Chambwe, V. Dhankani, T. Knijnenburg, R. Kramer, K. Leinonen, Y. Liu, M. Miller, S. Reynolds, I. Shmulevich, V. Thorsson, W. Zhang, R. Akbani, B. M. Broom, A. M. Hegde, Z. Ju, R. S. Kanchi, A. Korkut, J. Li, H. Liang, S. Ling, W. Liu, Y. Lu, G. B. Mills, K.-S. Ng, A. Rao, M. Ryan, J. Wang, J. N. Weinstein, J. Zhang, A. Abeshouse, J. Armenia, D. Chakravarty, W. K. Chatila, I. de Bruijn, J. Gao, B. E. Gross, Z. J. Heins, R. Kundra, K. La, M. Ladanyi, A. Luna, M. G. Nissan, A. Ochoa, S. M. Phillips, E. Reznik, F. Sanchez-Vega, C. Sander, N. Schultz, R. Sheridan, S. O. Sumer, Y. Sun, B. S. Taylor, J. Wang, H. Zhang, P. Anur, M. Peto, P. Spellman, C. Benz, J. M. Stuart, C. K. Wong, C. Yau, D. N. Hayes, J. S. Parker, M. D. Wilkerson, A. Ally, M. Balasundaram, R. Bowlby, D. Brooks, R. Carlsen, E. Chuah, N. Dhalla, R. Holt, S. J. M. Jones, K. Kasaian, D. Lee, Y. Ma, M. A. Marra, M. Mayo, R. A. Moore, A. J. Mungall, K. Mungall, A. G. Robertson, S. Sadeghi, J. E. Schein, P. Sipahimalani, A. Tam, N. Thiessen, K. Tse, T. Wong, A. C. Berger, R. Beroukhim, A. D. Cherniack, C. Cibulskis, S. B. Gabriel, G. F. Gao, G. Ha, M. Meyerson, S. E. Schumacher, J. Shih, M. H. Kucherlapati, R. S. Kucherlapati, S. Baylin, L. Cope, L. Danilova, M. S. Bootwalla, P. H. Lai, D. T. Maglinte, D. J. Van Den Berg, D. J. Weisenberger, J. T. Auman, S. Balu, T.

Bodenheimer, C. Fan, K. A. Hoadley, A. P. Hoyle, S. R. Jefferys, C. D. Jones, S. Meng, P. A. Mieczkowski, L. E. Mose, A. H. Perou, C. M. Perou, J. Roach, Y. Shi, J. V. Simons, T. Skelly, M. G. Soloway, D. Tan, U. Veluvolu, H. Fan, T. Hinoue, P. W. Laird, H. Shen, W. Zhou, M. Bellair, K. Chang, K. Covington, C. J. Creighton, H. Dinh, H. Doddapaneni, L. A. Donehower, J. Drummond, R. A. Gibbs, R. Glenn, W. Hale, Y. Han, J. Hu, V. Korchina, S. Lee, L. Lewis, W. Li, X. Liu, M. Morgan, D. Morton, D. Muzny, J. Santibanez, M. Sheth, E. Shinbrot, L. Wang, M. Wang, D. A. Wheeler, L. Xi, F. Zhao, J. Hess, E. L. Appelbaum, M. Bailey, M. G. Cordes, L. Ding, C. C. Fronick, L. A. Fulton, R. S. Fulton, C. Kandoth, E. R. Mardis, M. D. McLellan, C. A. Miller, H. K. Schmidt, R. K. Wilson, D. Crain, E. Curley, J. Gardner, K. Lau, D. Mallery, S. Morris, J. Paulauskis, R. Penny, C. Shelton, T. Shelton, M. Sherman, E. Thompson, P. Yena, J. Bowen, J. M. Gastier-Foster, M. Gerken, K. M. Leraas, T. M. Lichtenberg, N. C. Ramirez, L. Wise, E. Zmuda, N. Corcoran, T. Costello, C. Hovens, A. L. Carvalho, A. C. de Carvalho, J. H. Fregnani, A. Longatto-Filho, R. M. Reis, C. Scapulatempo-Neto, H. C. S. Silveira, D. O. Vidal, A. Burnette, J. Eschbacher, B. Hermes, A. Noss, R. Singh, M. L. Anderson, P. D. Castro, M. Ittmann, D. Huntsman, B. Kohl, X. Le, R. Thorp, C. Andry, E. R. Duffy, V. Lyadov, O. Paklina, G. Setdikova, A. Shabunin, M. Tavobilov, C. McPherson, R. Warnick, R. Berkowitz, D. Cramer, C. Feltmate, N. Horowitz, A. Kibel, M. Muto, C. P. Raut, A. Malykh, J. S. Barnholtz-Sloan, W. Barrett, K. Devine, J. Fulop, Q. T. Ostrom, K. Shimmel, Y. Wolinsky, A. E. Sloan, A. De Rose, F. Giuliante, M. Goodman, B. Y. Karlan, C. H. Hagedorn, J. Eckman, J. Harr, J. Myers, K. Tucker, L. A. Zach, B. Deyarmin, H. Hu, L. Kvecher, C. Larson, R. J. Mural, S. Somiari, A. Vicha, T. Zelinka, J. Bennett, M. Iacocca, B. Rabeno, P. Swanson, M. Latour, L. Lacombe, B. Têtu, A. Bergeron, M. McGraw, S. M. Staugaitis, J. Chabot, H. Hibshoosh, A. Sepulveda, T. Su, T. Wang, O. Potapova, O. Voronina, L. Desjardins, O. Mariani, S. Roman-Roman, X. Sastre, M.-H. Stern, F. Cheng, S. Signoretti, A. Berchuck, D. Bigner, E. Lipp, J. Marks, S. McCall, R. McLendon, A. Secord, A. Sharp, M. Behera, D. J. Brat, A. Chen, K. Delman, S. Force, F. Khuri, K. Magliocca, S. Maithel, J. J. Olson, T. Owonikoko, A. Pickens, S. Ramalingam, D. M. Shin, G. Sica, E. G. Van Meir, H. Zhang, W. Eijckenboom, A. Gillis, E. Korpershoek, L. Looijenga, W. Oosterhuis, H. Stoop, K. E. van Kessel, E. C. Zwarthoff, C. Calatozzolo, L. Cuppini, S. Cuzzubbo, F. DiMeco, G. Finocchiaro, L. Mattei, A. Perin, B. Pollo, C. Chen, J. Houck, P. Lohavanichbutr, A. Hartmann, C. Stoehr, R. Stoehr, H. Taubert, S. Wach, B. Wullich, W. Kycler, D. Murawa, M. Wiznerowicz, K. Chung, W. J. Edenfield, J. Martin, E. Baudin, G. Buble, R. Bueno, A. De Rienzo, W. G. Richards, S. Kalkanis, T. Mikkelsen, H. Noushmehr, L. Scarpace, N. Girard, M. Aymerich, E. Campo, E. Giné, A. L. Guillermo, N. Van Bang, P. T. Hanh, B. D. Phu, Y. Tang, H. Colman, K. Evason, P. R. Dottino, J. A. Martignetti, H. Gabra, H. Juhl, T. Akeredolu, S. Stepa, D. Hoon, K. Ahn, K. J. Kang, F. Beuschlein, A. Breggia, M. Birrer, D. Bell, M. Borad, A. H. Bryce, E. Castle, V. Chandan, J. Cheville, J. A. Copland, M. Farnell, T. Flotte, N. Giama, T. Ho, M. Kendrick, J.-P. Kocher, K. Kopp, C. Moser, D. Nagorney, D. O'Brien, B. P. O'Neill, T. Patel, G. Petersen, F. Que, M. Rivera, L. Roberts, R. Smallridge, T. Smyrk, M. Stanton, R. H. Thompson, M. Torbenson, J. D. Yang, L. Zhang, F. Brimo, J. A. Ajani, A. M. A. Gonzalez, C. Behrens, J. Bondaruk, R. Broaddus, B. Czerniak, B. Esmaeli, J. Fujimoto, J. Gershenwald, C. Guo, A. J. Lazar, C. Logothetis, F. Meric-Bernstam, C. Moran, L. Ramondetta, D. Rice, A. Sood, P. Tamboli, T. Thompson, P. Troncoso, A. Tsao, I. Wistuba, C. Carter, L. Haydu, P. Hersey, V. Jakrot, H. Kakavand, R. Kefford, K. Lee, G. Long, G. Mann, M. Quinn, R. Saw, R. Scolyer, K. Shannon, A. Spillane, J. Stretch, M. Synott, J. Thompson, J. Wilmott, H. Al-Ahmadie, T. A. Chan, R. Ghossein, A. Gopalan, D. A. Levine, V. Reuter, S. Singer, B. Singh, N. V. Tien, T. Broudy, C. Mirsaiid, P. Nair, P. Drwiega, J. Miller, J. Smith, H. Zaren, J.-W. Park, N. P. Hung, E. Kebebew, W. M. Linehan, A. R. Metwalli, K. Pacak, P. A. Pinto, M. Schiffman, L. S. Schmidt, C. D. Vocke, N. Wentzensen, R. Worrell, H. Yang, M. Moncrieff, C. Goparaju, J. Melamed, H. Pass, N. Botnariuc, I. Caraman, M. Cernat, I. Chemencedji, A. Clipca, S. Doruc, G. Gorincioi, S. Mura, M. Pirtac, I. Stancul, D. Tcaciuc, M.

Albert, I. Alexopoulou, A. Arnaout, J. Bartlett, J. Engel, S. Gilbert, J. Parfitt, H. Sekhon, G. Thomas, D. M. Rassel, R. C. Rintoul, C. Bifulco, R. Tamakawa, W. Urba, N. Hayward, H. Timmers, A. Antenucci, F. Facciolo, G. Grazi, M. Marino, R. Merola, R. de Krijger, A.-P. Gimenez-Roqueplo, A. Piché, S. Chevalier, G. McKercher, K. Birsoy, G. Barnett, C. Brewer, C. Farver, T. Naska, N. A. Pennell, D. Raymond, C. Schilero, K. Smolenski, F. Williams, C. Morrison, J. A. Borgia, M. J. Liptay, M. Pool, C. W. Seder, K. Junker, L. Omberg, M. Dinkin, G. Manikhas, D. Alvaro, M. C. Bragazzi, V. Cardinale, G. Carpino, E. Gaudio, D. Chesla, S. Cottingham, M. Dubina, F. Moiseenko, R. Dhanasekaran, K.-F. Becker, K.-P. Janssen, J. Slotta-Huspenina, M. H. Abdel-Rahman, D. Aziz, S. Bell, C. M. Cebulla, A. Davis, R. Duell, J. B. Elder, J. Hilty, B. Kumar, J. Lang, N. L. Lehman, R. Mandt, P. Nguyen, R. Pilarski, K. Rai, L. Schoenfield, K. Senecal, P. Wakely, P. Hansen, R. Lechan, J. Powers, A. Tischler, W. E. Grizzle, K. C. Sexton, A. Kastl, J. Henderson, S. Porten, J. Waldmann, M. Fassnacht, S. L. Asa, D. Schadendorf, M. Couce, M. Graefen, H. Huland, G. Sauter, T. Schlomm, R. Simon, P. Tennstedt, O. Olabode, M. Nelson, O. Bathe, P. R. Carroll, J. M. Chan, P. Disaia, P. Glenn, R. K. Kelley, C. N. Landen, J. Phillips, M. Prados, J. Simko, K. Smith-McCune, S. VandenBerg, K. Roggin, A. Fehrenbach, A. Kendler, S. Sifri, R. Steele, A. Jimeno, F. Carey, I. Forgie, M. Mannelli, M. Carney, B. Hernandez, B. Campos, C. Herold-Mende, C. Jungk, A. Unterberg, A. von Deimling, A. Bossler, J. Galbraith, L. Jacobus, M. Knudson, T. Knutson, D. Ma, M. Milhem, R. Sigmund, A. K. Godwin, R. Madan, H. G. Rosenthal, C. Adebamowo, S. N. Adebamowo, A. Boussioutas, D. Beer, T. Giordano, A.-M. Mes-Masson, F. Saad, T. Bocklage, L. Landrum, R. Mannel, K. Moore, K. Moxley, R. Postier, J. Walker, R. Zuna, M. Feldman, F. Valdivieso, R. Dhir, J. Luketich, E. M. M. Pinero, M. Quintero-Aguilo, C. G. Carlotti, J. S. Dos Santos, R. Kemp, A. Sankarankuty, D. Tirapelli, J. Catto, K. Agnew, E. Swisher, J. Creaney, B. Robinson, C. S. Shelley, E. M. Godwin, S. Kendall, C. Shipman, C. Bradford, T. Carey, A. Haddad, J. Moyer, L. Peterson, M. Prince, L. Rozek, G. Wolf, R. Bowman, K. M. Fong, I. Yang, R. Korst, W. K. Rathmell, J. L. Fantacone-Campbell, J. A. Hooke, A. J. Kovatich, C. D. Shriver, J. DiPersio, B. Drake, R. Govindan, S. Heath, T. Ley, B. Van Tine, P. Westervelt, M. A. Rubin, J. Il Lee, N. D. Aredes and A. Mariamidze, *Cell*, 2018, **173**, 321-337.e10.

- 122 J. Liu, T. Lichtenberg, K. A. Hoadley, L. M. Poisson, A. J. Lazar, A. D. Cherniack, A. J. Kovatich, C. C. Benz, D. A. Levine, A. V. Lee, L. Omberg, D. M. Wolf, C. D. Shriver, V. Thorsson, H. Hu, S. J. Caesar-Johnson, J. A. Demchok, I. Felau, M. Kasapi, M. L. Ferguson, C. M. Hutter, H. J. Sofia, R. Tarnuzzer, Z. Wang, L. Yang, J. C. Zenklusen, J. (Julia) Zhang, S. Chudamani, J. Liu, L. Lolla, R. Naresh, T. Pihl, Q. Sun, Y. Wan, Y. Wu, J. Cho, T. DeFreitas, S. Frazer, N. Gehlenborg, G. Getz, D. I. Heiman, J. Kim, M. S. Lawrence, P. Lin, S. Meier, M. S. Noble, G. Saksena, D. Voet, H. Zhang, B. Bernard, N. Chambwe, V. Dhankani, T. Knijnenburg, R. Kramer, K. Leinonen, Y. Liu, M. Miller, S. Reynolds, I. Shmulevich, V. Thorsson, W. Zhang, R. Akbani, B. M. Broom, A. M. Hegde, Z. Ju, R. S. Kanchi, A. Korkut, J. Li, H. Liang, S. Ling, W. Liu, Y. Lu, G. B. Mills, K.-S. Ng, A. Rao, M. Ryan, J. Wang, J. N. Weinstein, J. Zhang, A. Abeshouse, J. Armenia, D. Chakravarty, W. K. Chatila, I. de Bruijn, J. Gao, B. E. Gross, Z. J. Heins, R. Kundra, K. La, M. Ladanyi, A. Luna, M. G. Nissan, A. Ochoa, S. M. Phillips, E. Reznik, F. Sanchez-Vega, C. Sander, N. Schultz, R. Sheridan, S. O. Sumer, Y. Sun, B. S. Taylor, J. Wang, H. Zhang, P. Anur, M. Peto, P. Spellman, C. Benz, J. M. Stuart, C. K. Wong, C. Yau, D. N. Hayes, J. S. Parker, M. D. Wilkerson, A. Ally, M. Balasundaram, R. Bowlby, D. Brooks, R. Carlsen, E. Chuah, N. Dhalla, R. Holt, S. J. M. Jones, K. Kasaian, D. Lee, Y. Ma, M. A. Marra, M. Mayo, R. A. Moore, A. J. Mungall, K. Mungall, A. G. Robertson, S. Sadeghi, J. E. Schein, P. Sipahimalani, A. Tam, N. Thiessen, K. Tse, T. Wong, A. C. Berger, R. Beroukhim, A. D. Cherniack, C. Cibulskis, S. B. Gabriel, G. F. Gao, G. Ha, M. Meyerson, S. E. Schumacher, J. Shih, M. H. Kucherlapati, R. S. Kucherlapati, S. Baylin, L. Cope, L. Danilova, M. S. Bootwalla, P. H. Lai, D. T. Maglinte, D. J. Van Den Berg, D. J. Weisenberger, J. T. Auman, S. Balu, T. Bodenheimer, C. Fan, K. A.

Hoadley, A. P. Hoyle, S. R. Jefferys, C. D. Jones, S. Meng, P. A. Mieczkowski, L. E. Mose, A. H. Perou, C. M. Perou, J. Roach, Y. Shi, J. V. Simons, T. Skelly, M. G. Soloway, D. Tan, U. Veluvolu, H. Fan, T. Hinoue, P. W. Laird, H. Shen, W. Zhou, M. Bellair, K. Chang, K. Covington, C. J. Creighton, H. Dinh, H. Doddapaneni, L. A. Donehower, J. Drummond, R. A. Gibbs, R. Glenn, W. Hale, Y. Han, J. Hu, V. Korchina, S. Lee, L. Lewis, W. Li, X. Liu, M. Morgan, D. Morton, D. Muzny, J. Santibanez, M. Sheth, E. Shinbro, L. Wang, M. Wang, D. A. Wheeler, L. Xi, F. Zhao, J. Hess, E. L. Appelbaum, M. Bailey, M. G. Cordes, L. Ding, C. C. Fronick, L. A. Fulton, R. S. Fulton, C. Kandoth, E. R. Mardis, M. D. McLellan, C. A. Miller, H. K. Schmidt, R. K. Wilson, D. Crain, E. Curley, J. Gardner, K. Lau, D. Mallery, S. Morris, J. Paulauskis, R. Penny, C. Shelton, T. Shelton, M. Sherman, E. Thompson, P. Yena, J. Bowen, J. M. Gastier-Foster, M. Gerken, K. M. Leraas, T. M. Lichtenberg, N. C. Ramirez, L. Wise, E. Zmuda, N. Corcoran, T. Costello, C. Hovens, A. L. Carvalho, A. C. de Carvalho, J. H. Fregnani, A. Longatto-Filho, R. M. Reis, C. Scapulatempo-Neto, H. C. S. Silveira, D. O. Vidal, A. Burnette, J. Eschbacher, B. Hermes, A. Noss, R. Singh, M. L. Anderson, P. D. Castro, M. Ittmann, D. Huntsman, B. Kohl, X. Le, R. Thorp, C. Andry, E. R. Duffy, V. Lyadov, O. Paklina, G. Setdikova, A. Shabunin, M. Tavobilov, C. McPherson, R. Warnick, R. Berkowitz, D. Cramer, C. Feltmate, N. Horowitz, A. Kibel, M. Muto, C. P. Raut, A. Malykh, J. S. Barnholtz-Sloan, W. Barrett, K. Devine, J. Fulop, Q. T. Ostrom, K. Shimmel, Y. Wolinsky, A. E. Sloan, A. De Rose, F. Giuliante, M. Goodman, B. Y. Karlan, C. H. Hagedorn, J. Eckman, J. Harr, J. Myers, K. Tucker, L. A. Zach, B. Deyarmin, H. Hu, L. Kvecher, C. Larson, R. J. Mural, S. Somiari, A. Vicha, T. Zelinka, J. Bennett, M. Iacocca, B. Rabeno, P. Swanson, M. Latour, L. Lacombe, B. Têtu, A. Bergeron, M. McGraw, S. M. Staugaitis, J. Chabot, H. Hibshoosh, A. Sepulveda, T. Su, T. Wang, O. Potapova, O. Voronina, L. Desjardins, O. Mariani, S. Roman-Roman, X. Sastre, M.-H. Stern, F. Cheng, S. Signoretti, A. Berchuck, D. Bigner, E. Lipp, J. Marks, S. McCall, R. McLendon, A. Secord, A. Sharp, M. Behera, D. J. Brat, A. Chen, K. Delman, S. Force, F. Khuri, K. Magliocca, S. Maithel, J. J. Olson, T. Owonikoko, A. Pickens, S. Ramalingam, D. M. Shin, G. Sica, E. G. Van Meir, H. Zhang, W. Eijckenboom, A. Gillis, E. Korpershoek, L. Looijenga, W. Oosterhuis, H. Stoop, K. E. van Kessel, E. C. Zwarthoff, C. Calatozzolo, L. Cuppini, S. Cuzzubbo, F. DiMeco, G. Finocchiaro, L. Mattei, A. Perin, B. Pollo, C. Chen, J. Houck, P. Lohavanichbutr, A. Hartmann, C. Stoehr, R. Stoehr, H. Taubert, S. Wach, B. Wullich, W. Kycler, D. Murawa, M. Wiznerowicz, K. Chung, W. J. Edenfield, J. Martin, E. Baudin, G. Bublely, R. Bueno, A. De Rienzo, W. G. Richards, S. Kalkanis, T. Mikkelsen, H. Noushmehr, L. Scarpacci, N. Girard, M. Aymerich, E. Campo, E. Giné, A. L. Guillermo, N. Van Bang, P. T. Hanh, B. D. Phu, Y. Tang, H. Colman, K. Evason, P. R. Dottino, J. A. Martignetti, H. Gabra, H. Juhl, T. Akeredolu, S. Stepa, D. Hoon, K. Ahn, K. J. Kang, F. Beuschlein, A. Breggia, M. Birrer, D. Bell, M. Borad, A. H. Bryce, E. Castle, V. Chandan, J. Cheville, J. A. Copland, M. Farnell, T. Flotte, N. Giama, T. Ho, M. Kendrick, J.-P. Kocher, K. Kopp, C. Moser, D. Nagorney, D. O'Brien, B. P. O'Neill, T. Patel, G. Petersen, F. Que, M. Rivera, L. Roberts, R. Smallridge, T. Smyrk, M. Stanton, R. H. Thompson, M. Torbenson, J. D. Yang, L. Zhang, F. Brimo, J. A. Ajani, A. M. Angulo Gonzalez, C. Behrens, J. Bondaruk, R. Broaddus, B. Czerniak, B. Esmaeli, J. Fujimoto, J. Gershenwald, C. Guo, A. J. Lazar, C. Logothetis, F. Meric-Bernstam, C. Moran, L. Ramondetta, D. Rice, A. Sood, P. Tamboli, T. Thompson, P. Troncso, A. Tsao, I. Wistuba, C. Carter, L. Haydu, P. Hersey, V. Jakrot, H. Kakavand, R. Kefford, K. Lee, G. Long, G. Mann, M. Quinn, R. Saw, R. Scolyer, K. Shannon, A. Spillane, J. Stretch, M. Synott, J. Thompson, J. Wilmott, H. Al-Ahmadie, T. A. Chan, R. Ghossein, A. Gopalan, D. A. Levine, V. Reuter, S. Singer, B. Singh, N. V. Tien, T. Broudy, C. Mirsaidi, P. Nair, P. Drwiega, J. Miller, J. Smith, H. Zaren, J.-W. Park, N. P. Hung, E. Kebebew, W. M. Linehan, A. R. Metwalli, K. Pacak, P. A. Pinto, M. Schiffman, L. S. Schmidt, C. D. Vocke, N. Wentzensen, R. Worrell, H. Yang, M. Moncrieff, C. Goparaju, J. Melamed, H. Pass, N. Botnariuc, I. Caraman, M. Cernat, I. Chemencedji, A. Clipca, S. Doruc, G. Gorincioi, S. Mura, M. Pirtac, I. Stancul, D. Tcaciuc, M. Albert, I. Alexopoulou, A. Arnaout,

J. Bartlett, J. Engel, S. Gilbert, J. Parfitt, H. Sekhon, G. Thomas, D. M. Rassl, R. C. Rintoul, C. Bifulco, R. Tamakawa, W. Urba, N. Hayward, H. Timmers, A. Antenucci, F. Facciolo, G. Grazi, M. Marino, R. Merola, R. de Krijger, A.-P. Gimenez-Roqueplo, A. Piché, S. Chevalier, G. McKercher, K. Birsoy, G. Barnett, C. Brewer, C. Farver, T. Naska, N. A. Pennell, D. Raymond, C. Schilero, K. Smolenski, F. Williams, C. Morrison, J. A. Borgia, M. J. Liptay, M. Pool, C. W. Seder, K. Junker, L. Omberg, M. Dinkin, G. Manikhas, D. Alvaro, M. C. Bragazzi, V. Cardinale, G. Carpino, E. Gaudio, D. Chesla, S. Cottingham, M. Dubina, F. Moiseenko, R. Dhanasekaran, K.-F. Becker, K.-P. Janssen, J. Slotta-Huspenina, M. H. Abdel-Rahman, D. Aziz, S. Bell, C. M. Cebulla, A. Davis, R. Duell, J. B. Elder, J. Hilty, B. Kumar, J. Lang, N. L. Lehman, R. Mandt, P. Nguyen, R. Pilarski, K. Rai, L. Schoenfield, K. Senecal, P. Wakely, P. Hansen, R. Lechan, J. Powers, A. Tischler, W. E. Grizzle, K. C. Sexton, A. Kastl, J. Henderson, S. Porten, J. Waldmann, M. Fassnacht, S. L. Asa, D. Schadendorf, M. Couce, M. Graefen, H. Huland, G. Sauter, T. Schlomm, R. Simon, P. Tennstedt, O. Olabode, M. Nelson, O. Bathe, P. R. Carroll, J. M. Chan, P. Disaia, P. Glenn, R. K. Kelley, C. N. Landen, J. Phillips, M. Prados, J. Simko, K. Smith-McCune, S. VandenBerg, K. Roggin, A. Fehrenbach, A. Kandler, S. Sifri, R. Steele, A. Jimeno, F. Carey, I. Forgie, M. Mannelli, M. Carney, B. Hernandez, B. Campos, C. Herold-Mende, C. Jungk, A. Unterberg, A. von Deimling, A. Bossler, J. Galbraith, L. Jacobus, M. Knudson, T. Knutson, D. Ma, M. Milhem, R. Sigmund, A. K. Godwin, R. Madan, H. G. Rosenthal, C. Adebamowo, S. N. Adebamowo, A. Boussioutas, D. Beer, T. Giordano, A.-M. Mes-Masson, F. Saad, T. Bocklage, L. Landrum, R. Mannel, K. Moore, K. Moxley, R. Postier, J. Walker, R. Zuna, M. Feldman, F. Valdivieso, R. Dhir, J. Luketich, E. M. Mora Pinero, M. Quintero-Aguilo, J. C. G. Carlotti, J. S. Dos Santos, R. Kemp, A. Sankarankuty, D. Tirapelli, J. Catto, K. Agnew, E. Swisher, J. Creaney, B. Robinson, C. S. Shelley, E. M. Godwin, S. Kendall, C. Shipman, C. Bradford, T. Carey, A. Haddad, J. Moyer, L. Peterson, M. Prince, L. Rozek, G. Wolf, R. Bowman, K. M. Fong, I. Yang, R. Korst, W. K. Rathmell, J. L. Fantacone-Campbell, J. A. Hooke, A. J. Kovatich, C. D. Shriver, J. DiPersio, B. Drake, R. Govindan, S. Heath, T. Ley, B. Van Tine, P. Westervelt, M. A. Rubin, J. Il Lee, N. D. Aredes and A. Mariamidze, *Cell*, 2018, **173**, 400-416.e11.

- 123 A. M. Taylor, J. Shih, G. Ha, G. F. Gao, X. Zhang, A. C. Berger, S. E. Schumacher, C. Wang, H. Hu, J. Liu, A. J. Lazar, A. D. Cherniack, R. Beroukhim, M. Meyerson, S. J. Caesar-Johnson, J. A. Demchok, I. Felau, M. Kasapi, M. L. Ferguson, C. M. Hutter, H. J. Sofia, R. Tarnuzzer, Z. Wang, L. Yang, J. C. Zenklusen, J. (Julia) Zhang, S. Chudamani, J. Liu, L. Lolla, R. Naresh, T. Pihl, Q. Sun, Y. Wan, Y. Wu, J. Cho, T. DeFreitas, S. Frazer, N. Gehlenborg, G. Getz, D. I. Heiman, J. Kim, M. S. Lawrence, P. Lin, S. Meier, M. S. Noble, G. Saksena, D. Voet, H. Zhang, B. Bernard, N. Chambwe, V. Dhankani, T. Knijnenburg, R. Kramer, K. Leinonen, Y. Liu, M. Miller, S. Reynolds, I. Shmulevich, V. Thorsson, W. Zhang, R. Akbani, B. M. Broom, A. M. Hegde, Z. Ju, R. S. Kanchi, A. Korkut, J. Li, H. Liang, S. Ling, W. Liu, Y. Lu, G. B. Mills, K.-S. Ng, A. Rao, M. Ryan, J. Wang, J. N. Weinstein, J. Zhang, A. Abeshouse, J. Armenia, D. Chakravarty, W. K. Chatila, I. de Bruijn, J. Gao, B. E. Gross, Z. J. Heins, R. Kundra, K. La, M. Ladanyi, A. Luna, M. G. Nissan, A. Ochoa, S. M. Phillips, E. Reznik, F. Sanchez-Vega, C. Sander, N. Schultz, R. Sheridan, S. O. Sumer, Y. Sun, B. S. Taylor, J. Wang, H. Zhang, P. Anur, M. Peto, P. Spellman, C. Benz, J. M. Stuart, C. K. Wong, C. Yau, D. N. Hayes, J. S. Parker, M. D. Wilkerson, A. Ally, M. Balasundaram, R. Bowlby, D. Brooks, R. Carlsen, E. Chuah, N. Dhalla, R. Holt, S. J. M. Jones, K. Kasaian, D. Lee, Y. Ma, M. A. Marra, M. Mayo, R. A. Moore, A. J. Mungall, K. Mungall, A. G. Robertson, S. Sadeghi, J. E. Schein, P. Sipahimalani, A. Tam, N. Thiessen, K. Tse, T. Wong, A. C. Berger, R. Beroukhim, A. D. Cherniack, C. Cibulskis, S. B. Gabriel, G. F. Gao, G. Ha, M. Meyerson, S. E. Schumacher, J. Shih, M. H. Kucherlapati, R. S. Kucherlapati, S. Baylin, L. Cope, L. Danilova, M. S. Bootwalla, P. H. Lai, D. T. Maglinte, D. J. Van Den Berg, D. J. Weisenberger, J. T. Auman, S. Balu, T. Bodenheimer, C. Fan, K. A.

Hoadley, A. P. Hoyle, S. R. Jefferys, C. D. Jones, S. Meng, P. A. Mieczkowski, L. E. Mose, A. H. Perou, C. M. Perou, J. Roach, Y. Shi, J. V. Simons, T. Skelly, M. G. Soloway, D. Tan, U. Veluvolu, H. Fan, T. Hinoue, P. W. Laird, H. Shen, W. Zhou, M. Bellair, K. Chang, K. Covington, C. J. Creighton, H. Dinh, H. Doddapaneni, L. A. Donehower, J. Drummond, R. A. Gibbs, R. Glenn, W. Hale, Y. Han, J. Hu, V. Korchina, S. Lee, L. Lewis, W. Li, X. Liu, M. Morgan, D. Morton, D. Muzny, J. Santibanez, M. Sheth, E. Shinbrot, L. Wang, M. Wang, D. A. Wheeler, L. Xi, F. Zhao, J. Hess, E. L. Appelbaum, M. Bailey, M. G. Cordes, L. Ding, C. C. Fronick, L. A. Fulton, R. S. Fulton, C. Kandoth, E. R. Mardis, M. D. McLellan, C. A. Miller, H. K. Schmidt, R. K. Wilson, D. Crain, E. Curley, J. Gardner, K. Lau, D. Mallery, S. Morris, J. Paulauskis, R. Penny, C. Shelton, T. Shelton, M. Sherman, E. Thompson, P. Yena, J. Bowen, J. M. Gastier-Foster, M. Gerken, K. M. Leraas, T. M. Lichtenberg, N. C. Ramirez, L. Wise, E. Zmuda, N. Corcoran, T. Costello, C. Hovens, A. L. Carvalho, A. C. de Carvalho, J. H. Fregnani, A. Longatto-Filho, R. M. Reis, C. Scapulatempo-Neto, H. C. S. Silveira, D. O. Vidal, A. Burnette, J. Eschbacher, B. Hermes, A. Noss, R. Singh, M. L. Anderson, P. D. Castro, M. Ittmann, D. Huntsman, B. Kohl, X. Le, R. Thorp, C. Andry, E. R. Duffy, V. Lyadov, O. Paklina, G. Setdikova, A. Shabunin, M. Tavobilov, C. McPherson, R. Warnick, R. Berkowitz, D. Cramer, C. Feltmate, N. Horowitz, A. Kibel, M. Muto, C. P. Raut, A. Malykh, J. S. Barnholtz-Sloan, W. Barrett, K. Devine, J. Fulop, Q. T. Ostrom, K. Shimmel, Y. Wolinsky, A. E. Sloan, A. De Rose, F. Giuliante, M. Goodman, B. Y. Karlan, C. H. Hagedorn, J. Eckman, J. Harr, J. Myers, K. Tucker, L. A. Zach, B. Deyarmin, H. Hu, L. Kvecher, C. Larson, R. J. Mural, S. Somiari, A. Vicha, T. Zelinka, J. Bennett, M. Iacocca, B. Rabeno, P. Swanson, M. Latour, L. Lacombe, B. Têtu, A. Bergeron, M. McGraw, S. M. Staugaitis, J. Chabot, H. Hibshoosh, A. Sepulveda, T. Su, T. Wang, O. Potapova, O. Voronina, L. Desjardins, O. Mariani, S. Roman-Roman, X. Sastre, M.-H. Stern, F. Cheng, S. Signoretti, A. Berchuck, D. Bigner, E. Lipp, J. Marks, S. McCall, R. McLendon, A. Secord, A. Sharp, M. Behera, D. J. Brat, A. Chen, K. Delman, S. Force, F. Khuri, K. Magliocca, S. Maithel, J. J. Olson, T. Owonikoko, A. Pickens, S. Ramalingam, D. M. Shin, G. Sica, E. G. Van Meir, H. Zhang, W. Eijckenboom, A. Gillis, E. Korpershoek, L. Looijenga, W. Oosterhuis, H. Stoop, K. E. van Kessel, E. C. Zwarthoff, C. Calatozzolo, L. Cuppini, S. Cuzzubbo, F. DiMeco, G. Finocchiaro, L. Mattei, A. Perin, B. Pollo, C. Chen, J. Houck, P. Lohavanichbutr, A. Hartmann, C. Stoehr, R. Stoehr, H. Taubert, S. Wach, B. Wullich, W. Kycler, D. Murawa, M. Wiznerowicz, K. Chung, W. J. Edenfield, J. Martin, E. Baudin, G. Bublely, R. Bueno, A. De Rienzo, W. G. Richards, S. Kalkanis, T. Mikkelsen, H. Noushmehr, L. Scarpacci, N. Girard, M. Aymerich, E. Campo, E. Giné, A. L. Guillermo, N. Van Bang, P. T. Hanh, B. D. Phu, Y. Tang, H. Colman, K. Evason, P. R. Dottino, J. A. Martignetti, H. Gabra, H. Juhl, T. Akeredolu, S. Stepa, D. Hoon, K. Ahn, K. J. Kang, F. Beuschlein, A. Breggia, M. Birrer, D. Bell, M. Borad, A. H. Bryce, E. Castle, V. Chandan, J. Cheville, J. A. Copland, M. Farnell, T. Flotte, N. Giama, T. Ho, M. Kendrick, J.-P. Kocher, K. Kopp, C. Moser, D. Nagorney, D. O'Brien, B. P. O'Neill, T. Patel, G. Petersen, F. Que, M. Rivera, L. Roberts, R. Smallridge, T. Smyrk, M. Stanton, R. H. Thompson, M. Torbenson, J. D. Yang, L. Zhang, F. Brimo, J. A. Ajani, A. M. Angulo Gonzalez, C. Behrens, J. Bondaruk, R. Broaddus, B. Czerniak, B. Esmaeli, J. Fujimoto, J. Gershenwald, C. Guo, A. J. Lazar, C. Logothetis, F. Meric-Bernstam, C. Moran, L. Ramondetta, D. Rice, A. Sood, P. Tamboli, T. Thompson, P. Troncso, A. Tsao, I. Wistuba, C. Carter, L. Haydu, P. Hersey, V. Jakrot, H. Kakavand, R. Kefford, K. Lee, G. Long, G. Mann, M. Quinn, R. Saw, R. Scolyer, K. Shannon, A. Spillane, J. Stretch, M. Synott, J. Thompson, J. Wilmott, H. Al-Ahmadie, T. A. Chan, R. Ghossein, A. Gopalan, D. A. Levine, V. Reuter, S. Singer, B. Singh, N. V. Tien, T. Broudy, C. Mirsaidi, P. Nair, P. Drwiega, J. Miller, J. Smith, H. Zaren, J.-W. Park, N. P. Hung, E. Kebebew, W. M. Linehan, A. R. Metwalli, K. Pacak, P. A. Pinto, M. Schiffman, L. S. Schmidt, C. D. Vocke, N. Wentzensen, R. Worrell, H. Yang, M. Moncrieff, C. Goparaju, J. Melamed, H. Pass, N. Botnariuc, I. Caraman, M. Cernat, I. Chemencedji, A. Clipca, S. Doruc, G. Gorincioi, S. Mura, M. Pirtac, I. Stancul, D. Tcaciuc, M. Albert, I. Alexopoulou, A. Arnaout,

J. Bartlett, J. Engel, S. Gilbert, J. Parfitt, H. Sekhon, G. Thomas, D. M. Rassl, R. C. Rintoul, C. Bifulco, R. Tamakawa, W. Urba, N. Hayward, H. Timmers, A. Antenucci, F. Facciolo, G. Grazi, M. Marino, R. Merola, R. de Krijger, A.-P. Gimenez-Roqueplo, A. Piché, S. Chevalier, G. McKercher, K. Birsoy, G. Barnett, C. Brewer, C. Farver, T. Naska, N. A. Pennell, D. Raymond, C. Schilero, K. Smolenski, F. Williams, C. Morrison, J. A. Borgia, M. J. Liptay, M. Pool, C. W. Seder, K. Junker, L. Omberg, M. Dinkin, G. Manikhas, D. Alvaro, M. C. Bragazzi, V. Cardinale, G. Carpino, E. Gaudio, D. Chesla, S. Cottingham, M. Dubina, F. Moiseenko, R. Dhanasekaran, K.-F. Becker, K.-P. Janssen, J. Slotta-Huspenina, M. H. Abdel-Rahman, D. Aziz, S. Bell, C. M. Cebulla, A. Davis, R. Duell, J. B. Elder, J. Hilty, B. Kumar, J. Lang, N. L. Lehman, R. Mandt, P. Nguyen, R. Pilarski, K. Rai, L. Schoenfield, K. Senecal, P. Wakely, P. Hansen, R. Lechan, J. Powers, A. Tischler, W. E. Grizzle, K. C. Sexton, A. Kastl, J. Henderson, S. Porten, J. Waldmann, M. Fassnacht, S. L. Asa, D. Schadendorf, M. Couce, M. Graefen, H. Huland, G. Sauter, T. Schlomm, R. Simon, P. Tennstedt, O. Olabode, M. Nelson, O. Bathe, P. R. Carroll, J. M. Chan, P. Disaia, P. Glenn, R. K. Kelley, C. N. Landen, J. Phillips, M. Prados, J. Simko, K. Smith-McCune, S. VandenBerg, K. Roggin, A. Fehrenbach, A. Kandler, S. Sifri, R. Steele, A. Jimeno, F. Carey, I. Forgie, M. Mannelli, M. Carney, B. Hernandez, B. Campos, C. Herold-Mende, C. Jungk, A. Unterberg, A. von Deimling, A. Bossler, J. Galbraith, L. Jacobus, M. Knudson, T. Knutson, D. Ma, M. Milhem, R. Sigmund, A. K. Godwin, R. Madan, H. G. Rosenthal, C. Adebamowo, S. N. Adebamowo, A. Boussioutas, D. Beer, T. Giordano, A.-M. Mes-Masson, F. Saad, T. Bocklage, L. Landrum, R. Mannel, K. Moore, K. Moxley, R. Postier, J. Walker, R. Zuna, M. Feldman, F. Valdivieso, R. Dhir, J. Luketich, E. M. Mora Pinero, M. Quintero-Aguilo, C. G. Carlotti, J. S. Dos Santos, R. Kemp, A. Sankarankuty, D. Tirapelli, J. Catto, K. Agnew, E. Swisher, J. Creaney, B. Robinson, C. S. Shelley, E. M. Godwin, S. Kendall, C. Shipman, C. Bradford, T. Carey, A. Haddad, J. Moyer, L. Peterson, M. Prince, L. Rozek, G. Wolf, R. Bowman, K. M. Fong, I. Yang, R. Korst, W. K. Rathmell, J. L. Fantacone-Campbell, J. A. Hooke, A. J. Kovatich, C. D. Shriver, J. DiPersio, B. Drake, R. Govindan, S. Heath, T. Ley, B. Van Tine, P. Westervelt, M. A. Rubin, J. Il Lee, N. D. Aredes and A. Mariamidze, *Cancer Cell*, 2018, **33**, 676-689.e3.

- 124 K. Ellrott, M. H. Bailey, G. Saksena, K. R. Covington, C. Kandoth, C. Stewart, J. Hess, S. Ma, K. E. Chiotti, M. McLellan, H. J. Sofia, C. Hutter, G. Getz, D. Wheeler, L. Ding, S. J. Caesar-Johnson, J. A. Demchok, I. Felau, M. Kasapi, M. L. Ferguson, C. M. Hutter, H. J. Sofia, R. Tarnuzzer, Z. Wang, L. Yang, J. C. Zenklusen, J. (Julia) Zhang, S. Chudamani, J. Liu, L. Lolla, R. Naresh, T. Pihl, Q. Sun, Y. Wan, Y. Wu, J. Cho, T. DeFreitas, S. Frazer, N. Gehlenborg, G. Getz, D. I. Heiman, J. Kim, M. S. Lawrence, P. Lin, S. Meier, M. S. Noble, G. Saksena, D. Voet, H. Zhang, B. Bernard, N. Chambwe, V. Dhankani, T. Knijnenburg, R. Kramer, K. Leinonen, Y. Liu, M. Miller, S. Reynolds, I. Shmulevich, V. Thorsson, W. Zhang, R. Akbani, B. M. Broom, A. M. Hegde, Z. Ju, R. S. Kanchi, A. Korkut, J. Li, H. Liang, S. Ling, W. Liu, Y. Lu, G. B. Mills, K.-S. Ng, A. Rao, M. Ryan, J. Wang, J. N. Weinstein, J. Zhang, A. Abeshouse, J. Armenia, D. Chakravarty, W. K. Chatila, I. de Bruijn, J. Gao, B. E. Gross, Z. J. Heins, R. Kundra, K. La, M. Ladanyi, A. Luna, M. G. Nissan, A. Ochoa, S. M. Phillips, E. Reznik, F. Sanchez-Vega, C. Sander, N. Schultz, R. Sheridan, S. O. Sumer, Y. Sun, B. S. Taylor, J. Wang, H. Zhang, P. Anur, M. Peto, P. Spellman, C. Benz, J. M. Stuart, C. K. Wong, C. Yau, D. N. Hayes, Parker, M. D. Wilkerson, A. Ally, M. Balasundaram, R. Bowlby, D. Brooks, R. Carlsen, E. Chuah, N. Dhalla, R. Holt, S. J. M. Jones, K. Kasaian, D. Lee, Y. Ma, M. A. Marra, M. Mayo, R. A. Moore, A. J. Mungall, K. Mungall, A. G. Robertson, S. Sadeghi, J. E. Schein, P. Sipahimalani, A. Tam, N. Thiessen, K. Tse, T. Wong, A. C. Berger, R. Beroukhim, A. D. Cherniack, C. Cibulskis, S. B. Gabriel, G. F. Gao, G. Ha, M. Meyerson, S. E. Schumacher, J. Shih, M. H. Kucherlapati, R. S. Kucherlapati, S. Baylin, L. Cope, L. Danilova, M. S. Bootwalla, P. H. Lai, D. T. Maglinte, D. J. Van Den Berg, D. J. Weisenberger, J. T. Auman, S. Balu, T. Bodenheimer, C. Fan, K. A.

Hoadley, A. P. Hoyle, S. R. Jefferys, C. D. Jones, S. Meng, P. A. Mieczkowski, L. E. Mose, A. H. Perou, C. M. Perou, J. Roach, Y. Shi, J. V. Simons, T. Skelly, M. G. Soloway, D. Tan, U. Veluvolu, H. Fan, T. Hinoue, P. W. Laird, H. Shen, W. Zhou, M. Bellair, K. Chang, K. Covington, C. J. Creighton, H. Dinh, H. Doddapaneni, L. A. Donehower, J. Drummond, R. A. Gibbs, R. Glenn, W. Hale, Y. Han, J. Hu, V. Korchina, S. Lee, L. Lewis, W. Li, X. Liu, M. Morgan, D. Morton, D. Muzny, J. Santibanez, M. Sheth, E. Shinbrot, L. Wang, M. Wang, D. A. Wheeler, L. Xi, F. Zhao, J. Hess, E. L. Appelbaum, M. Bailey, M. G. Cordes, L. Ding, C. C. Fronick, L. A. Fulton, R. S. Fulton, C. Kandoth, E. R. Mardis, M. D. McLellan, C. A. Miller, H. K. Schmidt, R. K. Wilson, D. Crain, E. Curley, J. Gardner, K. Lau, D. Mallery, S. Morris, J. Paulauskis, R. Penny, C. Shelton, T. Shelton, M. Sherman, E. Thompson, P. Yena, J. Bowen, J. M. Gastier-Foster, M. Gerken, K. M. Leraas, T. M. Lichtenberg, N. C. Ramirez, L. Wise, E. Zmuda, N. Corcoran, T. Costello, C. Hovens, A. L. Carvalho, A. C. de Carvalho, J. H. Fregnani, A. Longatto-Filho, R. M. Reis, C. Scapulatempo-Neto, H. C. S. Silveira, D. O. Vidal, A. Burnette, J. Eschbacher, B. Hermes, A. Noss, R. Singh, M. L. Anderson, P. D. Castro, M. Ittmann, D. Huntsman, B. Kohl, X. Le, R. Thorp, C. Andry, E. R. Duffy, V. Lyadov, O. Paklina, G. Setdikova, A. Shabunin, M. Tavobilov, C. McPherson, R. Warnick, R. Berkowitz, D. Cramer, C. Feltmate, N. Horowitz, A. Kibel, M. Muto, C. P. Raut, A. Malykh, J. S. Barnholtz-Sloan, W. Barrett, K. Devine, J. Fulop, Q. T. Ostrom, K. Shimmel, Y. Wolinsky, A. E. Sloan, A. De Rose, F. Giuliante, M. Goodman, B. Y. Karlan, C. H. Hagedorn, J. Eckman, J. Harr, J. Myers, K. Tucker, L. A. Zach, B. Deyarmin, H. Hu, L. Kvecher, C. Larson, R. J. Mural, S. Somiari, A. Vicha, T. Zelinka, J. Bennett, M. Iacocca, B. Rabeno, P. Swanson, M. Latour, L. Lacombe, B. Têtu, A. Bergeron, M. McGraw, S. M. Staugaitis, J. Chabot, H. Hibshoosh, A. Sepulveda, T. Su, T. Wang, O. Potapova, O. Voronina, L. Desjardins, O. Mariani, S. Roman-Roman, X. Sastre, M.-H. Stern, F. Cheng, S. Signoretti, A. Berchuck, D. Bigner, E. Lipp, J. Marks, S. McCall, R. McLendon, A. Secord, A. Sharp, M. Behera, D. J. Brat, A. Chen, K. Delman, S. Force, F. Khuri, K. Magliocca, S. Maithel, J. J. Olson, T. Owonikoko, A. Pickens, S. Ramalingam, D. M. Shin, G. Sica, E. G. Van Meir, H. Zhang, W. Eijckenboom, A. Gillis, E. Korpershoek, L. Looijenga, W. Oosterhuis, H. Stoop, K. E. van Kessel, E. C. Zwarthoff, C. Calatozzolo, L. Cuppini, S. Cuzzubbo, F. DiMeco, G. Finocchiaro, L. Mattei, A. Perin, B. Pollo, C. Chen, J. Houck, P. Lohavanichbutr, A. Hartmann, C. Stoehr, R. Stoehr, H. Taubert, S. Wach, B. Wullich, W. Kycler, D. Murawa, M. Wiznerowicz, K. Chung, W. J. Edenfield, J. Martin, E. Baudin, G. Bublely, R. Bueno, A. De Rienzo, W. G. Richards, S. Kalkanis, T. Mikkelsen, H. Noushmehr, L. Scarpacci, N. Girard, M. Aymerich, E. Campo, E. Giné, A. L. Guillermo, N. Van Bang, P. T. Hanh, B. D. Phu, Y. Tang, H. Colman, K. Evason, P. R. Dottino, J. A. Martignetti, H. Gabra, H. Juhl, T. Akeredolu, S. Stepa, D. Hoon, K. Ahn, K. J. Kang, F. Beuschlein, A. Breggia, M. Birrer, D. Bell, M. Borad, A. H. Bryce, E. Castle, V. Chandan, J. Cheville, J. A. Copland, M. Farnell, T. Flotte, N. Giama, T. Ho, M. Kendrick, J.-P. Kocher, K. Kopp, C. Moser, D. Nagorney, D. O'Brien, B. P. O'Neill, T. Patel, G. Petersen, F. Que, M. Rivera, L. Roberts, R. Smallridge, T. Smyrk, M. Stanton, R. H. Thompson, M. Torbenson, J. D. Yang, L. Zhang, F. Brimo, J. A. Ajani, A. M. Angulo Gonzalez, C. Behrens, J. Bondaruk, R. Broaddus, B. Czerniak, B. Esmaeli, J. Fujimoto, J. Gershenwald, C. Guo, A. J. Lazar, C. Logothetis, F. Meric-Bernstam, C. Moran, L. Ramondetta, D. Rice, A. Sood, P. Tamboli, T. Thompson, P. Troncoso, A. Tsao, I. Wistuba, C. Carter, L. Haydu, P. Hersey, V. Jakrot, H. Kakavand, R. Kefford, K. Lee, G. Long, G. Mann, M. Quinn, R. Saw, R. Scolyer, K. Shannon, A. Spillane, J. Stretch, M. Synott, J. Thompson, J. Wilmott, H. Al-Ahmadie, T. A. Chan, R. Ghossein, A. Gopalan, D. A. Levine, V. Reuter, S. Singer, B. Singh, N. V. Tien, T. Broudy, C. Mirsaidi, P. Nair, P. Drwiega, J. Miller, J. Smith, H. Zaren, J.-W. Park, N. P. Hung, E. Kebebew, W. M. Linehan, A. R. Metwalli, K. Pacak, P. A. Pinto, M. Schiffman, L. S. Schmidt, C. D. Vocke, N. Wentzensen, R. Worrell, H. Yang, M. Moncrieff, C. Goparaju, J. Melamed, H. Pass, N. Botnariuc, I. Caraman, M. Cernat, I. Chemencedji, A. Clipca, S. Doruc, G. Gorincioi, S. Mura, M. Pirtac, I. Stancul, D. Tcaciuc, M. Albert, I. Alexopoulou, A. Arnaout,

J. Bartlett, J. Engel, S. Gilbert, J. Parfitt, H. Sekhon, G. Thomas, D. M. Rassl, R. C. Rintoul, C. Bifulco, R. Tamakawa, W. Urba, N. Hayward, H. Timmers, A. Antenucci, F. Facciolo, G. Grazi, M. Marino, R. Merola, R. de Krijger, A.-P. Gimenez-Roqueplo, A. Piché, S. Chevalier, G. McKercher, K. Birsoy, G. Barnett, C. Brewer, C. Farver, T. Naska, N. A. Pennell, D. Raymond, C. Schilero, K. Smolenski, F. Williams, C. Morrison, J. A. Borgia, M. J. Liptay, M. Pool, C. W. Seder, K. Junker, L. Omberg, M. Dinkin, G. Manikhas, D. Alvaro, M. C. Bragazzi, V. Cardinale, G. Carpino, E. Gaudio, D. Chesla, S. Cottingham, M. Dubina, F. Moiseenko, R. Dhanasekaran, K.-F. Becker, K.-P. Janssen, J. Slotta-Huspenina, M. H. Abdel-Rahman, D. Aziz, S. Bell, C. M. Cebulla, A. Davis, R. Duell, J. B. Elder, J. Hilty, B. Kumar, J. Lang, N. L. Lehman, R. Mandt, P. Nguyen, R. Pilarski, K. Rai, L. Schoenfield, K. Senecal, P. Wakely, P. Hansen, R. Lechan, J. Powers, A. Tischler, W. E. Grizzle, K. C. Sexton, A. Kastl, J. Henderson, S. Porten, J. Waldmann, M. Fasnacht, S. L. Asa, D. Schadendorf, M. Couce, M. Graefen, H. Huland, G. Sauter, T. Schlomm, R. Simon, P. Tennstedt, O. Olabode, M. Nelson, O. Bathe, P. R. Carroll, J. M. Chan, P. Disaia, P. Glenn, R. K. Kelley, C. N. Landen, J. Phillips, M. Prados, J. Simko, K. Smith-McCune, S. VandenBerg, K. Roggin, A. Fehrenbach, A. Kendler, S. Sifri, R. Steele, A. Jimeno, F. Carey, I. Forgie, M. Mannelli, M. Carney, B. Hernandez, B. Campos, C. Herold-Mende, C. Jungk, A. Unterberg, A. von Deimling, A. Bossler, J. Galbraith, L. Jacobus, M. Knudson, T. Knutson, D. Ma, M. Milhem, R. Sigmund, A. K. Godwin, R. Madan, H. G. Rosenthal, C. Adebamowo, S. N. Adebamowo, A. Boussioutas, D. Beer, T. Giordano, A.-M. Mes-Masson, F. Saad, T. Bocklage, L. Landrum, R. Mannel, K. Moore, K. Moxley, R. Postier, J. Walker, R. Zuna, M. Feldman, F. Valdivieso, R. Dhir, J. Luketich, E. M. Mora Pinero, M. Quintero-Aguilo, C. G. Carlotti, J. S. Dos Santos, R. Kemp, A. Sankarankuty, D. Tirapelli, J. Catto, K. Agnew, E. Swisher, J. Creaney, B. Robinson, C. S. Shelley, E. M. Godwin, S. Kendall, C. Shipman, C. Bradford, T. Carey, A. Haddad, J. Moyer, L. Peterson, M. Prince, L. Rozek, G. Wolf, R. Bowman, K. M. Fong, I. Yang, R. Korst, W. K. Rathmell, J. L. Fantacone-Campbell, J. A. Hooke, A. J. Kovatich, C. D. Shriver, J. DiPersio, B. Drake, R. Govindan, S. Heath, T. Ley, B. Van Tine, P. Westervelt, M. A. Rubin, J. Il Lee, N. D. Aredes and A. Mariamidze, *Cell Syst*, 2018, **6**, 271-281.e7.

- 125 K. A. Hoadley, C. Yau, T. Hinoue, D. M. Wolf, A. J. Lazar, E. Drill, R. Shen, A. M. Taylor, A. D. Cherniack, V. Thorsson, R. Akbani, R. Bowlby, C. K. Wong, M. Wiznerowicz, F. Sanchez-Vega, A. G. Robertson, B. G. Schneider, M. S. Lawrence, H. Noushmehr, T. M. Malta, J. M. Stuart, C. C. Benz, P. W. Laird, S. J. Caesar-Johnson, J. A. Demchok, I. Felau, M. Kasapi, M. L. Ferguson, C. M. Hutter, H. J. Sofia, R. Tarnuzzer, Z. Wang, L. Yang, J. C. Zenklusen, J. (Julia) Zhang, S. Chudamani, J. Liu, L. Lolla, R. Naresh, T. Pihl, Q. Sun, Y. Wan, Y. Wu, J. Cho, T. DeFreitas, S. Frazer, N. Gehlenborg, G. Getz, D. I. Heiman, J. Kim, M. S. Lawrence, P. Lin, S. Meier, M. S. Noble, G. Saksena, D. Voet, H. Zhang, B. Bernard, N. Chambwe, V. Dhankani, T. Knijnenburg, R. Kramer, K. Leinonen, Y. Liu, M. Miller, S. Reynolds, I. Shmulevich, V. Thorsson, W. Zhang, R. Akbani, B. M. Broom, A. M. Hegde, Z. Ju, R. S. Kanchi, A. Korkut, J. Li, H. Liang, S. Ling, W. Liu, Y. Lu, G. B. Mills, K.-S. Ng, A. Rao, M. Ryan, J. Wang, J. N. Weinstein, J. Zhang, A. Abeshouse, J. Armenia, D. Chakravarty, W. K. Chatila, I. de Bruijn, J. Gao, B. E. Gross, Z. J. Heins, R. Kundra, K. La, M. Ladanyi, A. Luna, M. G. Nissan, A. Ochoa, S. M. Phillips, E. Reznik, F. Sanchez-Vega, C. Sander, N. Schultz, R. Sheridan, S. O. Sumer, Y. Sun, B. S. Taylor, J. Wang, H. Zhang, P. Anur, M. Peto, P. Spellman, C. Benz, J. M. Stuart, C. K. Wong, C. Yau, D. N. Hayes, J. S. Parker, M. D. Wilkerson, A. Ally, M. Balasundaram, R. Bowlby, D. Brooks, R. Carlsen, E. Chuah, N. Dhalla, R. Holt, S. J. M. Jones, K. Kasaian, D. Lee, Y. Ma, M. A. Marra, M. Mayo, R. A. Moore, A. J. Mungall, K. Mungall, A. G. Robertson, S. Sadeghi, J. E. Schein, P. Sipahimalani, A. Tam, N. Thiessen, K. Tse, T. Wong, A. C. Berger, R. Beroukhim, A. D. Cherniack, C. Cibulskis, S. B. Gabriel, G. F. Gao, G. Ha, M. Meyerson, S. E. Schumacher, J. Shih, M. H. Kucherlapati, R. S. Kucherlapati, S. Baylin, L. Cope, L. Danilova,

M. S. Bootwalla, P. H. Lai, D. T. Maglinte, D. J. Van Den Berg, D. J. Weisenberger, J. T. Auman, S. Balu, T. Bodenheimer, C. Fan, K. A. Hoadley, A. P. Hoyle, S. R. Jefferys, C. D. Jones, S. Meng, P. A. Mieczkowski, L. E. Mose, A. H. Perou, C. M. Perou, J. Roach, Y. Shi, J. V. Simons, T. Skelly, M. G. Soloway, D. Tan, U. Veluvolu, H. Fan, T. Hinoue, P. W. Laird, H. Shen, W. Zhou, M. Bellair, K. Chang, K. Covington, C. J. Creighton, H. Dinh, H. Doddapaneni, L. A. Donehower, J. Drummond, R. A. Gibbs, R. Glenn, W. Hale, Y. Han, J. Hu, V. Korchina, S. Lee, L. Lewis, W. Li, X. Liu, M. Morgan, D. Morton, D. Muzny, J. Santibanez, M. Sheth, E. Shinbrot, L. Wang, M. Wang, D. A. Wheeler, L. Xi, F. Zhao, J. Hess, E. L. Appelbaum, M. Bailey, M. G. Cordes, L. Ding, C. C. Fronick, L. A. Fulton, R. S. Fulton, C. Kandath, E. R. Mardis, M. D. McLellan, C. A. Miller, H. K. Schmidt, R. K. Wilson, D. Crain, E. Curley, J. Gardner, K. Lau, D. Mallery, S. Morris, J. Paulauskis, R. Penny, C. Shelton, T. Shelton, M. Sherman, E. Thompson, P. Yena, J. Bowen, J. M. Gastier-Foster, M. Gerken, K. M. Leraas, T. M. Lichtenberg, N. C. Ramirez, L. Wise, E. Zmuda, N. Corcoran, T. Costello, C. Hovens, A. L. Carvalho, A. C. de Carvalho, J. H. Fregnani, A. Longatto-Filho, R. M. Reis, C. Scapulatempo-Neto, H. C. S. Silveira, D. O. Vidal, A. Burnette, J. Eschbacher, B. Hermes, A. Noss, R. Singh, M. L. Anderson, P. D. Castro, M. Ittmann, D. Huntsman, B. Kohl, X. Le, R. Thorp, C. Andry, E. R. Duffy, V. Lyadov, O. Paklina, G. Setdikova, A. Shabunin, M. Tavobilov, C. McPherson, R. Warnick, R. Berkowitz, D. Cramer, C. Feltmate, N. Horowitz, A. Kibel, M. Muto, C. P. Raut, A. Malykh, J. S. Barnholtz-Sloan, W. Barrett, K. Devine, J. Fulop, Q. T. Ostrom, K. Shimmel, Y. Wolinsky, A. E. Sloan, A. De Rose, F. Giuliante, M. Goodman, B. Y. Karlan, C. H. Hagedorn, J. Eckman, J. Harr, J. Myers, K. Tucker, L. A. Zach, B. Deyarmin, H. Hu, L. Kvecher, C. Larson, R. J. Mural, S. Somiari, A. Vicha, T. Zelinka, J. Bennett, M. Iacocca, B. Rabeno, P. Swanson, M. Latour, L. Lacombe, B. Têtu, A. Bergeron, M. McGraw, S. M. Staugaitis, J. Chabot, H. Hibshoosh, A. Sepulveda, T. Su, T. Wang, O. Potapova, O. Voronina, L. Desjardins, O. Mariani, S. Roman-Roman, X. Sastre, M.-H. Stern, F. Cheng, S. Signoretti, A. Berchuck, D. Bigner, E. Lipp, J. Marks, S. McCall, R. McLendon, A. Secord, A. Sharp, M. Behera, D. J. Brat, A. Chen, K. Delman, S. Force, F. Khuri, K. Magliocca, S. Maithel, J. J. Olson, T. Owonikoko, A. Pickens, S. Ramalingam, D. M. Shin, G. Sica, E. G. Van Meir, H. Zhang, W. Eijckenboom, A. Gillis, E. Korpershoek, L. Looijenga, W. Oosterhuis, H. Stoop, K. E. van Kessel, E. C. Zwarthoff, C. Calatozzolo, L. Cuppini, S. Cuzzubbo, F. DiMeco, G. Finocchiaro, L. Mattei, A. Perin, B. Pollo, C. Chen, J. Houck, P. Lohavanichbutr, A. Hartmann, C. Stoehr, R. Stoehr, H. Taubert, S. Wach, B. Wullich, W. Kycler, D. Murawa, M. Wiznerowicz, K. Chung, W. J. Edenfield, J. Martin, E. Baudin, G. Bubley, R. Bueno, A. De Rienzo, W. G. Richards, S. Kalkanis, T. Mikkelsen, H. Noushmehr, L. Scarpaccia, N. Girard, M. Aymerich, E. Campo, E. Giné, A. L. Guillermo, N. Van Bang, P. T. Hanh, B. D. Phu, Y. Tang, H. Colman, K. Evason, P. R. Dottino, J. A. Martignetti, H. Gabra, H. Juhl, T. Akeredolu, S. Stepa, D. Hoon, K. Ahn, K. J. Kang, F. Beuschlein, A. Breggia, M. Birrer, D. Bell, M. Borad, A. H. Bryce, E. Castle, V. Chandan, J. Cheville, J. A. Copland, M. Farnell, T. Flotte, N. Giama, T. Ho, M. Kendrick, J.-P. Kocher, K. Kopp, C. Moser, D. Nagorney, D. O'Brien, B. P. O'Neill, T. Patel, G. Petersen, F. Que, M. Rivera, L. Roberts, R. Smallridge, T. Smyrk, M. Stanton, R. H. Thompson, M. Torbenson, J. D. Yang, L. Zhang, F. Brimo, J. A. Ajani, A. M. A. Gonzalez, C. Behrens, olanta Bondaruk, R. Broaddus, B. Czerniak, B. Esmaeli, J. Fujimoto, J. Gershenwald, C. Guo, A. J. Lazar, C. Logothetis, F. Meric-Bernstam, C. Moran, L. Ramondetta, D. Rice, A. Sood, P. Tamboli, T. Thompson, P. Troncso, A. Tsao, I. Wistuba, C. Carter, L. Haydu, P. Hersey, V. Jakrot, H. Kakavand, R. Kefford, K. Lee, G. Long, G. Mann, M. Quinn, R. Saw, R. Scolyer, K. Shannon, A. Spillane, J. Stretch, M. Synott, J. Thompson, J. Wilmott, H. Al-Ahmadie, T. A. Chan, R. Ghossein, A. Gopalan, D. A. Levine, V. Reuter, S. Singer, B. Singh, N. V. Tien, T. Broudy, C. Mirsaidi, P. Nair, P. Drwiega, J. Miller, J. Smith, H. Zaren, J.-W. Park, N. P. Hung, E. Kebebew, W. M. Linehan, A. R. Metwalli, K. Pacak, P. A. Pinto, M. Schiffman, L. S. Schmidt, C. D. Vocke, N. Wentzensen, R. Worrell, H. Yang, M. Moncrieff, C. Goparaju, J. Melamed, H.

- Pass, N. Botnariuc, I. Caraman, M. Cernat, I. Chemencedji, A. Clipca, S. Doruc, G. Gorincioi, S. Mura, M. Pirtac, I. Stancul, D. Tcaciuc, M. Albert, I. Alexopoulou, A. Arnaout, J. Bartlett, J. Engel, S. Gilbert, J. Parfitt, H. Sekhon, G. Thomas, D. M. Rassel, R. C. Rintoul, C. Bifulco, R. Tamakawa, W. Urba, N. Hayward, H. Timmers, A. Antenucci, F. Facciolo, G. Grazi, M. Marino, R. Merola, R. de Krijger, A.-P. Gimenez-Roqueplo, A. Piché, S. Chevalier, G. McKercher, K. Birsoy, G. Barnett, C. Brewer, C. Farver, T. Naska, N. A. Pennell, D. Raymond, C. Schilero, K. Smolenski, F. Williams, C. Morrison, J. A. Borgia, M. J. Liptay, M. Pool, C. W. Seder, K. Junker, L. Omberg, M. Dinkin, G. Manikhas, D. Alvaro, M. C. Bragazzi, V. Cardinale, G. Carpino, E. Gaudio, D. Chesla, S. Cottingham, M. Dubina, F. Moiseenko, R. Dhanasekaran, K.-F. Becker, K.-P. Janssen, J. Slotta-Huspenina, M. H. Abdel-Rahman, D. Aziz, S. Bell, C. M. Cebulla, A. Davis, R. Duell, J. B. Elder, J. Hilty, B. Kumar, J. Lang, N. L. Lehman, R. Mandt, P. Nguyen, R. Pilarski, K. Rai, L. Schoenfield, K. Senecal, P. Wakely, P. Hansen, R. Lechan, J. Powers, A. Tischler, W. E. Grizzle, K. C. Sexton, A. Kastl, J. Henderson, S. Porten, J. Waldmann, M. Fassnacht, S. L. Asa, D. Schadendorf, M. Couce, M. Graefen, H. Huland, G. Sauter, T. Schlomm, R. Simon, P. Tennstedt, O. Olabode, M. Nelson, O. Bathe, P. R. Carroll, J. M. Chan, P. Disaia, P. Glenn, R. K. Kelley, C. N. Landen, J. Phillips, M. Prados, J. Simko, K. Smith-McCune, S. VandenBerg, K. Roggin, A. Fehrenbach, A. Kendler, S. Sifri, R. Steele, A. Jimeno, F. Carey, I. Forgie, M. Mannelli, M. Carney, B. Hernandez, B. Campos, C. Herold-Mende, C. Jungk, A. Unterberg, A. von Deimling, A. Bossler, J. Galbraith, L. Jacobus, M. Knudson, T. Knutson, D. Ma, M. Milhem, R. Sigmund, A. K. Godwin, R. Madan, H. G. Rosenthal, C. Adebamowo, S. N. Adebamowo, A. Boussioutas, D. Beer, T. Giordano, A.-M. Mes-Masson, F. Saad, T. Bocklage, L. Landrum, R. Mannel, K. Moore, K. Moxley, R. Postier, J. Walker, R. Zuna, M. Feldman, F. Valdivieso, R. Dhir, J. Luketich, E. M. M. Pinero, M. Quintero-Aguilo, C. G. Carlotti, J. S. Dos Santos, R. Kemp, A. Sankarankuty, D. Tirapelli, J. Catto, K. Agnew, E. Swisher, J. Creaney, B. Robinson, C. S. Shelley, E. M. Godwin, S. Kendall, C. Shipman, C. Bradford, T. Carey, A. Haddad, J. Moyer, L. Peterson, M. Prince, L. Rozek, G. Wolf, R. Bowman, K. M. Fong, I. Yang, R. Korst, W. K. Rathmell, J. L. Fantacone-Campbell, J. A. Hooke, A. J. Kovatich, C. D. Shriver, J. DiPersio, B. Drake, R. Govindan, S. Heath, T. Ley, B. Van Tine, P. Westervelt, M. A. Rubin, J. Il Lee, N. D. Aredes and A. Mariamidze, *Cell*, 2018, **173**, 291-304.e6.
- 126 A. H. Shain, M. Garrido, T. Botton, E. Talevich, I. Yeh, J. Z. Sanborn, J. Chung, N. J. Wang, H. Kakavand, G. J. Mann, J. F. Thompson, T. Wiesner, A. B. Roy Ritu and Olshen, A. Gagnon, J. W. Gray, N. Huh, J. S. Hur, K. J. Busam, R. A. Scolyer, R. J. Cho, R. Murali and B. C. Bastian, *Nat. Genet.*, 2015, **47**, 1194–1199.
- 127 A. J. Gentles, A. M. Newman, C. L. Liu, S. V. Bratman, W. Feng, D. Kim, V. S. Nair, Y. Xu, A. Khuong, C. D. Hoang, M. Diehn, R. B. West, S. K. Plevritis and A. A. Alizadeh, *Nat Med*, 2015, **21**, 938–945.
- 128 G. Jönsson, C. Busch, J. Knappskog Stian and Geisler, H. Miletic, M. Ringnér, J. R. Lillehaug, A. Borg and P. E. Lønning, *Clin. Cancer Res.*, 2010, **16**, 3356–3367.
- 129 L. Xu, S. S. Shen, Y. Hoshida, A. Subramanian, K. Ross, J.-P. Brunet, S. N. Wagner, S. Ramaswamy, J. P. Mesirov and R. O. Hynes, *Mol. Cancer Res.*, 2008, **6**, 760–769.
- 130 D. Bogunovic, D. W. O’Neill, V. Belitskaya-Levy Ilana and Vacic, Y.-L. Yu, S. Adams, F. Darvishian, R. Berman, R. Shapiro, A. C. Pavlick, S. Lonardi, J. Zavadil, I. Osman and N. Bhardwaj, *Proc. Natl. Acad. Sci. U. S. A.*, 2009, **106**, 20429–20434.
- 131 H. Mi, A. Muruganujan and P. D. Thomas, *Nucleic Acids Res.*, 2013, **41**, D377–86.

- 132 Q. Zhang, W. Liu, H.-M. Zhang, Y.-R. Xie Gui-Yan and Miao, M. Xia and A.-Y. Guo, *Genomics Proteomics Bioinformatics*, 2020, **18**, 120–128.
- 133 J. Seetharaman, A. Kanigsberg, R. Slaaby, H. Leffler, S. H. Barondes and J. M. Rini, *Journal of Biological Chemistry*, 1998, **273**, 13047–13052.
- 134 J. Fort, L. R. de la Ballina, H. E. Burghardt, C. Ferrer-Costa, J. Turnay, C. Ferrer-Orta, I. Usón, A. Zorzano, J. Fernández-Recio, M. Orozco, M. A. Lizarbe, I. Fita and M. Palacín, *Journal of Biological Chemistry*, 2007, **282**, 31444–31452.
- 135 H. Berman, K. Henrick and H. Nakamura, *Nat Struct Mol Biol*, 2003, **10**, 980–980.
- 136 D. Kozakov, D. R. Hall, B. Xia, K. A. Porter, D. Padhorny, C. Yueh, D. Beglov and S. Vajda, *Nat Protoc*, 2017, **12**, 255–278.
- 137 R. A. Laskowski and M. B. Swindells, *J Chem Inf Model*, 2011, **51**, 2778–2786.
- 138 O. D. Monera, T. J. Sereda, N. E. Zhou, C. M. Kay and R. S. Hodges, *Journal of Peptide Science*, 1995, **1**, 319–329.
- 139 D. Hillis, D. Sadava, C. Heller and Mary. Price, *Principles of Life*, W H Freeman & Co, 10th edn., 2012.
- 140 M. O. Sinnokrot, E. F. Valeev and C. D. Sherrill, *J Am Chem Soc*, 2002, **124**, 10887–10893.
- 141 D. J. Belton, R. Plowright, D. L. Kaplan and C. C. Perry, *Acta Biomater*, 2018, **73**, 355–364.
- 142 A. Barth, *Biochim. Biophys. Acta*, 2007, **1767**, 1073–1101.
- 143 K. A. Karve, E. S. Gil, S. P. McCarthy and D. L. Kaplan, *J. Memb. Sci.*, 2011, **383**, 44–49.
- 144 M. Tsukada, Y. Gotoh, M. Nagura, N. Minoura, N. Kasai and G. Freddi, *J Polym Sci B Polym Phys*, 1994, **32**, 961–968.
- 145 X. Chen, H. Cai, S. Ling, Z. Shao and Y. Huang, *Appl. Spectrosc.*, 2012, **66**, 696–699.
- 146 R. A. Hartvig, M. van de Weert, J. Østergaard, L. Jorgensen and H. Jensen, *Langmuir*, 2011, **27**, 2634–2643.
- 147 C. Macaraniag, Q. Luan, J. Zhou and I. Papautsky, *APL Bioeng*, 2022, **6**, 031501.
- 148 F. Castro-Giner and N. Aceto, *Genome Med*, 2020, **12**, 31.
- 149 Y.-T. Kang, A. Mutukuri, T. Hadlock, H. Fairbairn, T. R. Carle, S. Fouladdel, V. Murlidhar, A. Kramer, M. D. S. Reguera, E. Azizi, A. Durham, S. A. Mclean and S. Nagrath, *Adv Nanobiomed Res*, 2022, **2**, 2100083.
- 150 J. L. Orgaz and V. Sanz-Moreno, *Pigment Cell Melanoma Res*, 2013, **26**, 39–57.
- 151 A. Naba, K. R. Clauser, S. Hoersch, H. Liu, S. A. Carr and R. O. Hynes, *Molecular & Cellular Proteomics*, 2012, **11**, M111.014647.
- 152 N. Aceto, *Biomed J*, 2020, **43**, 18–23.
- 153 H. Sun, Y.-X. Zhang and Y.-M. Li, *Front Cell Dev Biol*, , DOI:10.3389/fcell.2021.709824.
- 154 P. F. Pinheiro, S. A. Pereira, I. L. Harjivan Shrika G and Martins, A. T. Marinho, M. Cipriano, C. C. Jacob, N. G. Oliveira, M. F. Castro, M. M. Marques, A. M. M. Antunes and J. P. Miranda, *Arch. Toxicol.*, 2017, **91**, 1199–1211.

- 155 F. O. Adeshakin, A. O. Adeshakin, L. O. Afolabi, D. Yan, G. Zhang and X. Wan, *Front. Oncol.*, 2021, **11**, 626577.
- 156 H. Kim, J. Y. Sung, E.-K. Park, S. Kho, K. H. Koo, S.-Y. Park, Y. K. Goh Sung-Ho and Jeon, S. Oh, B.-K. Park, Y.-K. Jung and Y.-N. Kim, *Br. J. Cancer*, 2017, **116**, 370–381.
- 157 M. Maeshiro, S. Shinriki, R. Liu, Y. Nakachi, Y. Komohara, Y. Fujiwara, K. Ohtsubo, R. Yoshida, K. Iwamoto, H. Nakayama and H. Matsui, *Sci Rep*, 2021, **11**, 6150.
- 158 K. Girigoswami, D. Saini and A. Girigoswami, *Stem Cell Rev Rep*, 2021, **17**, 739–747.
- 159 I. Malanchi, A. Santamaria-Martín, E. Susanto, H. Peng, H.-A. Lehr, J.-F. Delaloye and J. Huelsken, *Nature*, 2011, **481**, 85–89.
- 160 A. Klein, H. Schwartz, O. Sagi-Assif, T. Meshel, S. Izraely, S. Ben Menachem, R. Bengaiev, A. Ben-Shmuel, C. Nahmias, P.-O. Couraud, I. P. Witz and N. Erez, *J. Pathol.*, 2015, **236**, 116–127.
- 161 S. Varesano, M. R. Zocchi and A. Poggi, *Front Immunol.*, DOI:10.3389/fimmu.2018.00998.
- 162 E. Y. Leung, M. E. Askarian-Amiri, D. Sarkar, C. Ferraro-Peyret, W. R. Joseph, G. J. Finlay and B. C. Baguley, *Front. Oncol.*, 2017, **7**, 184.
- 163 Y. T. Phung, D. Barbone, V. C. Broaddus and M. Ho, *J. Cancer*, 2011, **2**, 507–514.
- 164 S. J. Han, S. Kwon and K. S. Kim, *Cancer Cell Int*, 2021, **21**, 152.
- 165 B. Xu, D. Fan, Y. Zhao, J. Li, Z. Wang, J. Wang, X. Wang and B. Guan Zhen and Niu, *Front. Pharmacol.*, 2019, **10**, 1576.
- 166 R. J. Ju, S. J. Stehbens and N. K. Haass, *Front Med (Lausanne)*, DOI:10.3389/fmed.2018.00307.
- 167 U. B. Hofmann, J. R. Westphal, G. N. P. van Muijen and D. J. Ruiter, *Journal of Investigative Dermatology*, 2000, **115**, 337–344.
- 168 N. R. Campbell, A. Rao, M. V. Hunter, M. K. Sznurkowska, L. Briker, M. Zhang, M. Baron, S. Heilmann, M. Deforet, C. Kenny, L. P. Ferretti, T.-H. Huang, S. Perlee, M. Garg, J. Nsengimana, M. Saini, E. Montal, M. Tagore, J. Newton-Bishop, M. R. Middleton, P. Corrie, D. J. Adams, R. Rabbie, N. Aceto, M. P. Levesque, R. A. Cornell, I. Yanai, J. B. Xavier and R. M. White, *Dev Cell*, 2021, **56**, 2808-2825.e10.
- 169 A. Genna, A. M. Vanwynsberghe, A. V. Villard, C. Pottier, J. Ancel, M. Polette and C. Gilles, *Cancers (Basel)*, 2020, **12**, 1632.
- 170 M. Pavel, M. Renna, S. J. Park, F. M. Menzies, T. Ricketts, J. Füllgrabe, A. Ashkenazi, R. A. Frake, A. C. Lombarte, C. F. Bento, K. Franze and D. C. Rubinsztein, *Nat Commun*, 2018, **9**, 2961.
- 171 Y. Tang, S. Durand, S. Dalle and J. Caramel, *Cancers (Basel)*, 2020, **12**, 2154.
- 172 A. Puliafito, A. De Simone, G. Seano, P. A. Gagliardi, L. Di Blasio, F. Chianale, A. Gamba, L. Primo and A. Celani, *Sci Rep*, 2015, **5**, 15205.
- 173 G. Jiang, R.-H. Li, C. Sun, Y.-Q. Liu and J.-N. Zheng, *PLoS One*, 2014, **9**, e111920.
- 174 Propper, DJ and al, DOI:10.1054/bjoc.2000.1141.
- 175 Y. Zhou, H. Chen, H. Li and Y. Wu, *J Cell Mol Med*, 2017, **21**, 1073–1084.

- 176 A. Datta, S. Deng, V. Gopal, K. C.-H. Yap, C. E. Halim, M. L. Lye, M. S. Ong, T. Z. Tan, G. Sethi, S. C. Hooi, A. P. Kumar and C. T. Yap, *Cancers (Basel)*, 2021, **13**, 1882.
- 177 R. Burgos-Panadero, I. Noguera, A. Cañete, S. Navarro and R. Noguera, *BMC Cancer*, 2019, **19**, 479.
- 178 I. Ortega-Martínez, J. Gardeazabal, A. Erramuzpe, A. Sanchez-Diez, J. Cortés, M. D. García-Vázquez, G. Pérez-Yarza, R. Izu, J. Luís Díaz-Ramón, I. M. de la Fuente, A. Asumendi and M. D. Boyano, *Int J Cancer*, 2016, **139**, 1598–1607.
- 179 E. Ruoslahti, *Cancer and Metastasis Review*, 1984, **3**, 43–51.
- 180 C. Gaggioli, G. Robert, C. Bertolotto, O. Bailet, P. Abbe, A. Spadafora, P. Bahadoran, J.-P. Ortonne, V. Baron, R. Ballotti and S. Tartare-Deckert, *Journal of Investigative Dermatology*, 2007, **127**, 400–410.
- 181 L. C. Sanders, B. Felding-Habermann, B. M. Mueller and D. A. Cheresh, *Cold Spring Harb Symp Quant Biol*, 1992, **57**, 233–240.
- 182 L. M. Bafetti, T. N. Young, Y. Itoh and M. S. Stack, *Journal of Biological Chemistry*, 1998, **273**, 143–149.
- 183 F. Kai, A. P. Drain and V. M. Weaver, *Dev Cell*, 2019, **49**, 332–346.
- 184 Z. Miskolczi, M. P. Smith, E. J. Rowling, J. Ferguson, J. Barriuso and C. Wellbrock, *Oncogene*, 2018, **37**, 3166–3182.
- 185 J. Yang, M. A. Price, C. L. Neudauer, C. Wilson, S. Ferrone, H. Xia, J. Iida, M. A. Simpson and J. B. McCarthy, *Journal of Cell Biology*, 2004, **165**, 881–891.
- 186 A. Naba, K. R. Clauser and R. O. Hynes, *Journal of Visualized Experiments*, , DOI:10.3791/53057.
- 187 A. Santiago-Gómez, J. I. Barrasa, N. Olmo, E. Lecona, H. Burghardt, M. Palacín, M. A. Lizarbe and J. Turnay, *Biochim. Biophys. Acta*, 2013, **1833**, 2045–2056.
- 188 P. Gao, J. L. Simpson, J. Zhang and P. G. Gibson, *Respir Res*, 2013, **14**, 136.
- 189 I. Iurisci, N. Tinari, C. Natoli, D. Angelucci, E. Cianchetti and S. Iacobelli, .
- 190 P. Vereecken, K. Zouaoui Boudjeltia, C. Debray, A. Awada, I. Legssyer, F. Sales, M. Petein, M. Vanhaeverbeek, G. Ghanem and M. Heenen, *Clin Exp Dermatol*, 2006, **31**, 105–109.
- 191 E. R. Brown, T. Doig, N. Anderson, T. Brenn, V. Doherty, Y. Xu, J. M. S. Bartlett, J. F. Smyth and D. W. Melton, *Eur J Cancer*, 2012, **48**, 865–874.
- 192 M. Stasenko, E. Smith, O. Yeku, K. J. Park, I. Laster, K. Lee, S. Walderich, E. Spriggs, B. Rueda, B. Weigelt, D. Zamarin, T. D. Rao and D. R. Spriggs, *Sci Rep*, 2021, **11**, 3718.
- 193 F. R. Zetterberg, K. Peterson, R. E. Johnsson, T. Brimert, M. Håkansson, D. T. Logan, H. Leffler and U. J. Nilsson, *ChemMedChem*, 2018, **13**, 133–137.
- 194 L. Vuong, E. Kouverianou, C. M. Rooney, B. J. McHugh, S. E. M. Howie, C. D. Gregory, S. J. Forbes, N. C. Henderson, F. R. Zetterberg, U. J. Nilsson, H. Leffler, P. Ford, A. Pedersen, L. Gravelle, S. Tantawi, H. Schambye, T. Sethi and A. C. MacKinnon, *Cancer Res*, 2019, **79**, 1480–1492.

- 195 R. Yan, Y. Li, J. Müller, Y. Zhang, S. Singer, L. Xia, X. Zhong, J. Gertsch, K.-H. Altmann and Q. Zhou, *Cell Discov*, 2021, **7**, 16.
- 196 S. Dong and R. Colin Hughes, *Glycoconj J*, 1997, **14**, 267–274.
- 197 C. De Vellis, S. Pietrobono and B. Stecca, *Cells*, 2021, **10**, 2136.
- 198 R. R. Braeuer, M. Zigler, T. Kamiya, A. S. Dobroff, L. Huang, W. Choi, D. J. McConkey, E. Shoshan, A. K. Mobley, R. Song, A. Raz and M. Bar-Eli, *Cancer Res*, 2012, **72**, 5757–5766.
- 199 J. Nieminen, A. Kuno, J. Hirabayashi and S. Sato, *Journal of Biological Chemistry*, 2007, **282**, 1374–1383.
- 200 S. Sato, *Trends in Glycoscience and Glycotechnology*, 2018, **30**, SE199–SE209.
- 201 N. Rubinstein, J. M. Ilarregui, M. A. Toscano and G. A. Rabinovich, *Tissue Antigens*, 2004, **64**, 1–12.
- 202 N. Ahmad, H.-J. Gabius, S. André, H. Kaltner, S. Sabesan, R. Roy, B. Liu, F. Macaluso and C. F. Brewer, *Journal of Biological Chemistry*, 2004, **279**, 10841–10847.
- 203 T. Sasaki, *EMBO J*, 1998, **17**, 1606–1613.
- 204 A. Lagana, J. G. Goetz, P. Cheung, A. Raz, J. W. Dennis and I. R. Nabi, *Mol Cell Biol*, 2006, **26**, 3181–3193.
- 205 J. Y. Cho, B. M. Chain, J. Vives, V. Horejsi and D. R. Katz, *Exp Cell Res*, 2003, **290**, 155–167.
- 206 G. N, Z. K, L. M, M. J, C. Z and Z. P, *Mol Immunol*, 2015, **63**, 253–263.
- 207 R. Yan, X. Zhao, J. Lei and Q. Zhou, *Nature*, 2019, **568**, 127–130.
- 208 N. Theodosakis, G. Micevic, R. Sharma, A. S. Baras, R. Lazova, M. W. Bosenberg and N. Rodić, *Pigment Cell Melanoma Res*, 2016, **29**, 385–387.
- 209 M. Furuya, J. Horiguchi, H. Nakajima, Y. Kanai and T. Oyama, *Cancer Sci*, 2012, **103**, 382–389.
- 210 M. Poettler, M. Unseld, K. Braemswig, A. Haitel, C. C. Zielinski and G. W. Prager, *Mol Cancer*, , DOI:10.1186/1476-4598-12-169.
- 211 K. KAIRA, N. ORIUCHI, H. IMAI, K. SHIMIZU, N. YANAGITANI, N. SUNAGA, T. HISADA, O. KAWASHIMA, Y. KAMIDE, T. ISHIZUKA, Y. KANAI, T. NAKAJIMA and M. MORI, *Exp Ther Med*, 2010, **1**, 799–808.
- 212 K. Hara, S. Ueda, Y. Ohno, T. Tanaka, H. Yagi, S. Okazaki, R. Kawahara, T. Masayuki, T. Enomoto, Y. Hashimoto, K. Masuko and T. Masuko, *Cancer Sci*, 2012, **103**, 1460–1466.
- 213 D. Xu and M. E. Hemler, *Molecular & Cellular Proteomics*, 2005, **4**, 1061–1071.
- 214 M. S. Parmacek, B. A. Karpinski, K. M. Gottesdiener, C. B. Thompson and J. M. Leiden, *Nucleic Acids Res*, 1989, **17**, 1915–1931.
- 215 N. C. Henderson, E. A. Collis, A. C. Mackinnon, K. J. Simpson, C. Haslett, R. Zent, M. Ginsberg and T. Sethi, *Journal of Biological Chemistry*, 2004, **279**, 54731–54741.
- 216 Y. Yan, S. Vasudevan, H. Nguyen, U. Bork, S. Sitaraman and D. Merlin, *Journal of Membrane Biology*, 2007, **215**, 15–26.

- 217 D. I. Utepbergenov, A. S. Fanning and J. M. Anderson, *Journal of Biological Chemistry*, 2006, **281**, 24671–24677.
- 218 T. Shimada, S. Yasuda, H. Sugiura and K. Yamagata, , DOI:10.3390/ijms20174171.
- 219 P. Dalton, H. C. Christian, C. W. G. Redman, I. L. Sargent and C. A. R. Boyd, *FEBS Journal*, 2007, **274**, 2715–2727.
- 220 A. Santiago-Gómez, J. I. Barrasa, N. Olmo, E. Lecona, H. Burghardt, M. Palacín, M. A. Lizarbe and J. Turnay, *Biochimica et Biophysica Acta (BBA) - Molecular Cell Research*, 2013, **1833**, 2045–2056.
- 221 Q. Zhao, M. Barclay, J. Hilkens, X. Guo, H. Barrow, J. M. Rhodes and L.-G. Yu, *Mol Cancer*, 2010, **9**, 154.
- 222 R. Yan, X. Zhao, J. Lei and Q. Zhou, *Nature*, 2019, **568**, 127–130.
- 223 L. Johannes, R. Jacob and H. Leffler, *J Cell Sci*, , DOI:10.1242/jcs.208884.
- 224 P. Vereecken, K. Zouaoui Boudjeltia, C. Debray, A. Awada, I. Legssyer, F. Sales, M. Petein, M. Vanhaeverbeek, G. Ghanem and M. Heenen, *Clin Exp Dermatol*, 2006, **31**, 105–109.
- 225 J. Hirabayashi, T. Hashidate, Y. Arata, N. Nishi, T. Nakamura, M. Hirashima, T. Urashima, T. Oka, M. Futai, W. E. G. Muller, F. Yagi and K. Kasai, *Biochimica et Biophysica Acta (BBA) - General Subjects*, 2002, **1572**, 232–254.
- 226 H. Leffler, S. Carlsson, M. Hedlund, Y. Qian and F. Poirier, *Glycoconj J*, 2002, **19**, 433–440.
- 227 M. I. Nielsen, J. Stegmayr, O. C. Grant, Z. Yang, U. J. Nilsson, I. Boos, M. C. Carlsson, R. J. Woods, C. Unverzagt, H. Leffler and H. H. Wandall, *Journal of Biological Chemistry*, 2018, **293**, 20249–20262.
- 228 A. S. Powlesland, P. G. Hitchen, S. Parry, S. A. Graham, M. M. Barrio, M. T. Elola, J. Mordoh, A. Dell, K. Drickamer and M. E. Taylor, *Glycobiology*, 2009, **19**, 899–909.
- 229 S. Kantipudi, J.-M. Jeckelmann, Z. Ucurum, P. D. Bosshart and D. Fotiadis, *Int J Mol Sci*, 2020, **21**, 7573.
- 230 D. Xu and M. E. Hemler, *Molecular & Cellular Proteomics*, 2005, **4**, 1061–1071.
- 231 N. C. Henderson, E. A. Collis, A. C. Mackinnon, K. J. Simpson, C. Haslett, R. Zent, M. Ginsberg and T. Sethi, *Journal of Biological Chemistry*, 2004, **279**, 54731–54741.
- 232 T. Baade, C. Paone, A. Baldrich and C. R. Hauck, *Sci Rep*, 2019, **9**, 5728.
- 233 J. Fort, L. R. de la Ballina, H. E. Burghardt, C. Ferrer-Costa, J. Turnay, C. Ferrer-Orta, I. Usón, A. Zorzano, J. Fernández-Recio, M. Orozco, M. A. Lizarbe, I. Fita and M. Palacín, *Journal of Biological Chemistry*, 2007, **282**, 31444–31452.
- 234 R. Lakshminarayan, C. Wunder, U. Becken, M. T. Howes, C. Benzing, S. Arumugam, S. Sales, N. Ariotti, V. Chambon, C. Lamaze, D. Loew, A. Shevchenko, K. Gaus, R. G. Parton and L. Johannes, *Nat Cell Biol*, 2014, **16**, 592–603.
- 235 P. Teriete, S. Banerji, M. Noble, C. D. Blundell, A. J. Wright, A. R. Pickford, E. Lowe, D. J. Mahoney, M. I. Tammi, J. D. Kahmann, I. D. Campbell, A. J. Day and D. G. Jackson, *Mol Cell*, 2004, **13**, 483–496.

- 236 M. Kawaguchi, N. Dashzeveg, Y. Cao, Y. Jia, X. Liu, Y. Shen and H. Liu, *Journal of Biological Chemistry*, 2020, **295**, 2640–2649.
- 237 M. Zahn-Zabal, P. A. Michel, A. Gateau, F. Nikitin, M. Schaeffer, E. Audot, P. Gaudet, P. D. Duek, D. Teixeira, V. R. De Laval, K. Samarasinghe, A. Bairoch and L. Lane, *Nucleic Acids Res*, 2020, **48**, D328–D334.
- 238 Z. Ma, S. Shi, M. Ren, C. Pang, Y. Zhan, H. An and F. Sun, *Biophys J*, 2022, **121**, 2671–2683.
- 239 Y. , Honjo, P. , Nangia-Makker, H. , Inohara and A. Raz, *Clin Cancer Res*, 2001, **7**, 661–668.
- 240 Y. K. Song, T. R. Billiar and Y. J. Lee, *American Journal of Pathology*.
- 241 K. Lindorff-Larsen, S. Piana, K. Palmo, P. Maragakis, J. L. Klepeis, R. O. Dror and D. E. Shaw, *Proteins: Structure, Function, and Bioinformatics*, 2010, **78**, 1950–1958.
- 242 J. L. Parker, J. C. Deme, D. Kolokouris, G. Kuteyi, P. C. Biggin, S. M. Lea and S. Newstead, *Nat Commun*, 2021, **12**, 7147.
- 243 A. Dietrich, E. Tanczos, W. Vanscheidt, E. Schöpf and J. C. Simon, *Eur J Cancer*, 1997, **33**, 926–930.
- 244 S.-M. Kim and J.-H. Hahn, *Exp Mol Med*, 2008, **40**, 261–270.
- 245 E. Menkhorst, N. G. Than, U. Jeschke, G. Barrientos, L. Szereday, G. Dveksler and S. M. Blois, *Front Immunol*, , DOI:10.3389/fimmu.2021.784473.
- 246 E. M. Yazawa, J. E. Geddes-Sweeney, F. Cedeno-Laurent, K. C. Walley, S. R. Barthel, M. J. Opperman, J. Liang, J. Y. Lin, T. Schatton, A. C. Laga, M. C. Mihm, A. A. Qureshi, H. R. Widlund, G. F. Murphy and C. J. Dimitroff, *Journal of Investigative Dermatology*, 2015, **135**, 1849–1862.
- 247 K. Ito, S. Onturk, K. Powell, B. Philip, J. Wilmott, R. Scolyer, P. Hersey and S. J. Ralph, *Cancer Res*, 2013, **73**, B8–B8.
- 248 T.-W. Lin, H.-T. Chang, C.-H. Chen, C.-H. Chen, S.-W. Lin, T.-L. Hsu and C.-H. Wong, *J Am Chem Soc*, 2015, **137**, 9685–9693.
- 249 T.-W. Lin, H.-T. Chang, C.-H. Chen, C.-H. Chen, S.-W. Lin, T.-L. Hsu and C.-H. Wong, *J Am Chem Soc*, 2015, **137**, 9685–9693.
- 250 R. Lakshminarayan, C. Wunder, U. Becken, M. T. Howes, C. Benzing, S. Arumugam, S. Sales, N. Ariotti, V. Chambon, C. Lamaze, D. Loew, A. Shevchenko, K. Gaus, R. G. Parton and L. Johannes, *Nat Cell Biol*, 2014, **16**, 592–603.
- 251 B. N. Stillman, D. K. Hsu, M. Pang, C. F. Brewer, P. Johnson, F.-T. Liu and L. G. Baum, *The Journal of Immunology*, 2006, **176**, 778–789.
- 252 C.-H. Li, Y.-C. Chang, M. Hsiao and S.-M. Liang, *Cancers (Basel)*, 2019, **11**, 1897.
- 253 J. T. de Oliveira, C. Ribeiro, R. Barros, C. Gomes, A. J. de Matos, C. A. Reis, G. R. Rutteman and F. Gärtner, *PLoS One*, 2015, **10**, e0134458.
- 254 E. A. Partridge, C. Le Roy, G. M. Di Guglielmo, J. Pawling, P. Cheung, M. Granovsky, I. R. Nabi, J. L. Wrana and J. W. Dennis, *Science (1979)*, 2004, **306**, 120–124.
- 255 L. G. Frigeri, R. I. Zuberi and F. T. Liu, *Biochemistry*, 1993, **32**, 7644–7649.

- 256 T. Fukumori, Y. Takenaka, N. Oka, T. Yoshii, V. Hogan, H. Inohara, H. Kanayama, H.-R. C. Kim and A. Raz, *Cancer Res*, 2004, **64**, 3376–3379.
- 257 R. Probstmeier, D. Montag and M. Schachner, *J Neurochem*, 2002, **64**, 2465–2472.
- 258 C. Paret, M. Bourouba, A. Beer, K. Miyazaki, M. Schnölzer, S. Fiedler and M. Zöller, *Int J Cancer*, 2005, **115**, 724–733.
- 259 C. S. Priglinger, C. M. Sober, S. G. Priglinger, J. Merl, K. N. Euler, M. Kernt, G. Gondi, J. Behler, A. Geerlof, A. Kampik, M. Ueffing and S. M. Hauck, *PLoS One*, 2013, **8**, e70011.
- 260 K. S. Lau, E. A. Partridge, A. Grigorian, C. I. Silvescu, V. N. Reinhold, M. Demetriou and J. W. Dennis, *Cell*, 2007, **129**, 123–134.
- 261 W.-C. Ko, C.-S. Choy, W.-N. Lin, S.-W. Chang, J.-C. Liou, T.-H. Tung, C.-Y. Hsieh and J.-F. Chang, *J Clin Med*, 2018, **7**, 300.
- 262 S. Song, N. Mazurek, C. Liu, Y. Sun, Q. Q. Ding, K. Liu, M.-C. Hung and R. S. Bresalier, *Cancer Res*, 2009, **69**, 1343–1349.
- 263 S. Dong and R. Colin Hughes, *Glycoconj J*, 1997, **14**, 267–274.
- 264 I. Rosenbergs, B. J. Cherayils, K. J. Isselbacher and S. Pillail, *Journal of Biological Chemistry*, 1991, **266**, 18731–18736.
- 265 T. Fukumori, Y. Takenaka, T. Yoshii, H.-R. Choi Kim, V. Hogan, H. Inohara, S. Kagawa and A. Raz, *Cancer Res*, 2003, **63**, 8302–8311.
- 266 J. Ochieng, M. L. Leite-Browning and P. Warfield, *Biochem Biophys Res Commun*, 1998, **246**, 788–791.
- 267 A. Markowska, F.-T. Liu and N. Panjwani, , DOI:10.1084/jem.20090121.
- 268 Y. Kariya, M. Oyama, Y. Hashimoto, J. Gu and Y. Kariya, , DOI:10.1158/1541-7786.MCR-17-0365.
- 269 J. Fukushi, I. T. Makagiansar and W. B. Stallcup, *Mol Biol Cell*, 2004, **15**, 3580–3590.
- 270 G. Elad-Sfadia, R. Haklai, E. Balan and Y. Kloog, *Journal of Biological Chemistry*, 2004, **279**, 34922–34930.
- 271 R. Taftaf, X. Liu, S. Singh, Y. Jia, N. K. Dashzeveg, A. D. Hoffmann, L. El-Shennawy, E. K. Ramos, V. Adorno-Cruz, E. J. Schuster, D. Scholten, D. Patel, Y. Zhang, A. A. Davis, C. Reduzzi, Y. Cao, P. D’Amico, Y. Shen, M. Cristofanilli, W. A. Muller, V. Varadan and H. Liu, *Nat Commun*, 2021, **12**, 4867.
- 272 T. Piyush, A. R. Chacko, P. Sindrewicz, J. Hilken, J. M. Rhodes and L.-G. Yu, *Cell Death Differ*, 2017, **24**, 1937–1947.
- 273 Q. Zhao, M. Barclay, J. Hilken, X. Guo, H. Barrow, J. M. Rhodes and L.-G. Yu, *Mol Cancer*, 2010, **9**, 154.
- 274 F. Colomb, W. Wang, D. Simpson, M. Zafar, R. Beynon, J. M. Rhodes and L.-G. Yu, *Journal of Biological Chemistry*, 2017, **292**, 8381–8389.
- 275 Ç. B. Ege, M. Akbulut, O. Zekioğlu and N. Özdemir, *Arch Gynecol Obstet*, 2011, **284**, 1231–1239.

- 276 E. Feuk-Lagerstedt, E. T. Jordan, H. Leffler, C. Dahlgren and A. Karlsson, *Journal of immunology*, 1999, **163**, 5592–5598.
- 277 N. Woolf, B. E. Pearson, P. A. Bondzie, R. D. Meyer, M. Lavaei, A. C. Belkina, V. Chitalia and N. Rahimi, *Oncogenesis*, 2017, **6**, e378–e378.
- 278 E. Yang, J. S. Shim, H.-J. Woo, K.-W. Kim and H. J. Kwon, *Biochem Biophys Res Commun*, 2007, **363**, 336–341.
- 279 H.-Y. Chen, A. Fermin, S. Vardhana, I.-C. Weng, K. F. R. Lo, E.-Y. Chang, E. Maverakis, R.-Y. Yang, D. K. Hsu, M. L. Dustin and F.-T. Liu, *Proceedings of the National Academy of Sciences*, 2009, **106**, 14496–14501.
- 280 W. Wang, H. Guo, J. Geng, X. Zheng, H. Wei, R. Sun and Z. Tian, *Journal of Biological Chemistry*, 2014, **289**, 33311–33319.
- 281 B. Wu, S. P. Crampton and C. C. W. Hughes, *Immunity*, 2007, **26**, 227–239.
- 282 P. Nangia-Makker, Y. Wang, T. Raz, L. Tait, V. Balan, V. Hogan and A. Raz, *Int J Cancer*, 2010, **127**, 2530–2541.
- 283 S. MIYAMOTO, B.-Z. KATHZ, R. M. LAFRENIE and K. M. YAMADA, *Ann N Y Acad Sci*, 1998, **857**, 119–129.
- 284 U. B. Hofmann, J. R. Westphal, E. T. Waas, A. J. W. Zendman, I. M. H. A. Cornelissen, D. J. Ruiter and G. N. P. van Muijen, *Br J Cancer*, 1999, **81**, 774–782.
- 285 R. Gendron, D. Grenier, T. Sorsa and D. Mayrand, *Clinical Diagnostic Laboratory Immunology*, 1999, **6**, 437–439.
- 286 E. Cerami, J. Gao, U. Dogrusoz, B. E. Gross, S. O. Sumer, B. A. Aksoy, A. Jacobsen, C. J. Byrne, M. L. Heuer, E. Larsson, Y. Antipin, B. Reva, A. P. Goldberg, C. Sander and N. Schultz, *Cancer Discov*, 2012, **2**, 401–404.
- 287 J. Anaya, *PeerJ Comput Sci*, 2016, **2**, e67.
- 288 J. Ochieng, R. Fridman, P. Nangia-Makker, L. A. Kleiner D E and Liotta, W. G. Stetler-Stevenson and A. Raz, *Biochemistry*, 1994, **33**, 14109–14114.
- 289 J. Ochieng, *Biochimica et Biophysica Acta (BBA) - General Subjects*, 1998, **1379**, 97–106.
- 290 A. Rotte, M. Martinka and G. Li, *Cellular Oncology*, 2012, **35**, 207–216.
- 291 J. M. Azevedo Martins, S. H. Rabelo-Santos, M. C. do Amaral Westin and L. C. Zeferino, *BMC Cancer*, 2020, **20**, 660.
- 292 E. Oviedo-Orta, A. Bermudez-Fajardo, S. Karanam, U. Benbow and A. C. Newby, *Immunology*, 2008, **124**, 42–50.
- 293 P. G. Jobin, G. S. Butler and C. M. Overall, *Biochimica et Biophysica Acta (BBA) - Molecular Cell Research*, 2017, **1864**, 2043–2055.
- 294 A. D. Kandasamy and R. Schulz, *Cardiovasc Res*, 2009, **83**, 698–706.
- 295 C. Gao, G. Xiao and J. Hu, *Cell Biosci*, 2014, **4**, 13.
- 296 S. Jain, P. Ghanghas, C. Rana and S. N. Sanyal, *Cancer Invest*, 2017, **35**, 473–483.

- 297 N. Theodosakis, G. Micevic, R. Sharma, A. S. Baras, R. Lazova, M. W. Bosenberg and N. Rodić, *Pigment Cell Melanoma Res*, 2016, **29**, 385–387.
- 298 S. Estrach, S.-A. Lee, E. Boulter, S. Pisano, A. Errante, F. S. Tissot, L. Cailleteau, C. Pons, M. H. Ginsberg and C. C. Féral, *Cancer Res*, 2014, **74**, 6878–6889.
- 299 B. J. Thompson, *BioEssays*, 2020, **42**, 1900162.
- 300 S. Loffek, O. Schilling and C.-W. Franzke, *European Respiratory Journal*, 2011, **38**, 191–208.
- 301 D. Sbardella, G. F. Fasciglione, M. Gioia, C. Ciaccio, G. R. Tundo, S. Marini and M. Coletta, *Mol Aspects Med*, 2012, **33**, 119–208.
- 302 V. G. Prieto, A. A. Mourad-Zeidan, V. Melnikova, M. M. Johnson, A. Lopez, A. H. Diwan, A. J. F. Lazar, S. S. Shen, P. S. Zhang, J. A. Reed, J. E. Gershenwald, A. Raz and M. Bar-Eli, *Clinical Cancer Research*, 2006, **12**, 6709–6715.
- 303 E. R. Brown, T. Doig, N. Anderson, T. Brenn, V. Doherty, Y. Xu, J. M. S. Bartlett, J. F. Smyth and D. W. Melton, *Eur J Cancer*, 2012, **48**, 865–874.
- 304 Z. W. , Li, Y. , Wang, W. C. , Xue, L. , C. Si, C. C. L., Z. D. F., G. L. X. and & L. A. P. J., *Zhonghua Bing Li Xue Za Zhi*, 2013, **42**, 801–805.
- 305 A. A. Mourad-Zeidan, V. O. Melnikova, H. Wang, A. Raz and M. Bar-Eli, *Am J Pathol*, 2008, **173**, 1839–1852.
- 306 M. C. Dange, A. K. Agarwal and R. D. Kalraiya, *Mol Cell Biochem*, 2015, **404**, 79–86.
- 307 S. O. Bustos, G. J. da Silva Pereira, R. de Freitas Saito, C. D. Gil, D. B. Zanatta, S. S. Smaili and R. Chammas, *Oncotarget*, 2018, **9**, 14567–14579.
- 308 D. Pedri, P. Karras, E. Landeloos, J.-C. Marine and F. Rambow, *FEBS J.*, 2022, **289**, 1352–1368.
- 309 J.-L. Duband, *Cell Adh Migr*, 2010, **4**, 458–482.
- 310 D. Yao, C. Dai and S. Peng, *Molecular Cancer Research*, 2011, **9**, 1608–1620.
- 311 M. Zeisberg and E. G. Neilson, *Journal of Clinical Investigation*, 2009, **119**, 1429–1437.
- 312 B. De Craene and G. Berx, *Nat Rev Cancer*, 2013, **13**, 97–110.
- 313 K. S. Hoek, N. C. Schlegel, P. Brafford, A. Sucker, S. Ugurel, R. Kumar, B. L. Weber, K. L. Nathanson, D. J. Phillips, M. Herlyn, D. Schadendorf and R. Dummer, *Pigment Cell Res*, 2006, **19**, 290–302.
- 314 F. Rambow, J.-C. Marine and C. R. Goding, *Genes Dev*, 2019, **33**, 1295–1318.
- 315 M. Garg, *World J Stem Cells*, 2013, **5**, 188.
- 316 F. Z. Li, A. S. Dhillon, R. L. Anderson, G. McArthur and P. T. Ferrao, *Front Oncol*, , DOI:10.3389/fonc.2015.00031.
- 317 N. Vandamme and G. Berx, *Front Oncol*, , DOI:10.3389/fonc.2014.00352.
- 318 J. Caramel, E. Papadogeorgakis, L. Hill, G. J. Browne, G. Richard, A. Wierinckx, G. Saldanha, J. Osborne, P. Hutchinson, G. Tse, J. Lachuer, A. Puisieux, J. H. Pringle, S. Ansieau and E. Tulchinsky, *Cancer Cell*, 2013, **24**, 466–480.

- 319 J. Tsoi, L. Robert, K. Paraiso, C. Galvan, K. M. Sheu, J. Lay, D. J. L. Wong, M. Atefi, R. Shirazi, X. Wang, D. Braas, C. S. Grasso, N. Palaskas, A. Ribas and T. G. Graeber, *Cancer Cell*, 2018, **33**, 890-904.e5.
- 320 C. R. Goding, *Genes Dev*, 2000, **14**, 1712–1728.
- 321 L. Guyonneau, F. Murisier, A. Rossier, A. Moulin and F. Beermann, *Mol Cell Biol*, 2004, **24**, 3396–3403.
- 322 M. L. Harris, L. L. Baxter, S. K. Loftus and W. J. Pavan, *Pigment Cell Melanoma Res.*, 2010, **23**, 496–513.
- 323 S. Carreira, J. Goodall, L. Denat, M. Rodriguez, P. Nuciforo, K. S. Hoek, A. Testori, L. Larue and C. R. Goding, *Genes Dev*, 2006, **20**, 3426–3439.
- 324 J. Landsberg, J. Kohlmeyer, M. Renn, T. Bald, M. Rogava, M. Cron, M. Fatho, V. Lennerz, T. Wölfel, M. Hölzel and T. Tüting, *Nature*, 2012, **490**, 412–416.
- 325 D. Javelaud, V.-I. Alexaki, M.-J. Pierrat, K. S. Hoek, S. Dennler, L. Van Kempen, C. Bertolotto, R. Ballotti, S. Saule, V. Delmas and A. Mauviel, *Pigment Cell Melanoma Res.*, 2011, **24**, 932–943.
- 326 E. Feige, S. Yokoyama, C. Levy, M. Khaled, V. Igras, R. J. Lin, S. Lee, H. R. Widlund, S. R. Granter, A. L. Kung and D. E. Fisher, *Proc. Natl. Acad. Sci. U. S. A.*, 2011, **108**, E924–33.
- 327 A. T. Weeraratna, Y. Jiang, G. Hostetter, K. Rosenblatt, P. Duray, M. Bittner and J. M. Trent, *Cancer Cell*, 2002, **1**, 279–288.
- 328 J. Ferguson, M. Smith, I. Zudaire, C. Wellbrock and I. Arozarena, *Oncotarget*, 2017, **8**, 32946–32959.
- 329 P. Falletta, L. Sanchez-del-Campo, J. Chauhan, M. Efferm, A. Kenyon, C. J. Kershaw, R. Siddaway, R. Lisle, R. Freter, M. J. Daniels, X. Lu, T. Tüting, M. Middleton, F. M. Buffa, A. E. Willis, G. Pavitt, Z. A. Ronai, T. Sauka-Spengler, M. Hölzel and C. R. Goding, *Genes Dev*, 2017, **31**, 18–33.
- 330 N. Bondurand, *Hum Mol Genet*, 2000, **9**, 1907–1917.
- 331 A. R. Hellström, B. Watt, S. S. Fard, D. Tenza, P. Mannström, K. Narfström, B. Ekestén, S. Ito, K. Wakamatsu, J. Larsson, M. Ulfendahl, K. Kullander, G. Raposo, S. Kerje, F. Hallböök, M. S. Marks and L. Andersson, *PLoS Genet*, 2011, **7**, e1002285.
- 332 J. Du, H. R. Widlund, M. A. Horstmann, S. Ramaswamy, K. Ross, W. E. Huber, E. K. Nishimura, T. R. Golub and D. E. Fisher, *Cancer Cell*, 2004, **6**, 565–576.
- 333 J. C. Cronin, D. E. Watkins-Chow, A. Incao, J. H. Hasskamp, N. Schönewolf, L. G. Aoude, N. K. Hayward, B. C. Bastian, R. Dummer, S. K. Loftus and W. J. Pavan, *Cancer Res*, 2013, **73**, 5709–5718.
- 334 O. Shakhova, P. Cheng, P. J. Mishra, D. Zingg, S. M. Schaefer, J. Debbache, J. Häusel, C. Matter, T. Guo, S. Davis, P. Meltzer, D. Mihic-Probst, H. Moch, M. Wegner, G. Merlino, M. P. Levesque, R. Dummer, R. Santoro, P. Cinelli and L. Sommer, *PLoS Genet*, 2015, **11**, e1004877.
- 335 X. Yang, R. Liang, C. Liu, J. A. Liu, M. P. L. Cheung, X. Liu, O. Y. Man, X.-Y. Guan, H. L. Lung and M. Cheung, *Journal of Experimental & Clinical Cancer Research*, 2019, **38**, 17.

- 336 A. Jo, S. Denduluri, B. Zhang, Z. Wang, L. Yin, Z. Yan, R. Kang, L. L. Shi, J. Mok, M. J. Lee and R. C. Haydon, *Genes Dis*, 2014, **1**, 149–161.
- 337 J.-Q. Huang, F.-K. Wei, X.-L. Xu, S.-X. Ye, J.-W. Song, P.-K. Ding, J. Zhu, H.-F. Li, X.-P. Luo, H. Gong, L. Su, L. Yang and L.-Y. Gong, *J Transl Med*, 2019, **17**, 143.
- 338 Y. Tang, S. Durand, S. Dalle and J. Caramel, *Cancers (Basel)*, 2020, **12**, 2154.
- 339 M. K. Jolly, R. J. Murphy, S. Bhatia, H. J. Whitfield, A. Redfern, M. J. Davis and E. W. Thompson, *Cells Tissues Organs*, 2022, **211**, 110–133.
- 340 M. Ennen, C. Keime, D. Kobi, G. Mengus, D. Lipsker, C. Thibault-Carpentier and I. Davidson, *Oncogene*, 2015, **34**, 3251–3263.
- 341 H.-J. Son and A. Moon, *Toxicol Res*, 2010, **26**, 245–252.
- 342 X.-X. Jie, X.-Y. Zhang and C.-J. Xu, *Oncotarget*, 2017, **8**, 81558–81571.
- 343 X. Zheng, J. L. Carstens, J. Kim, M. Scheible, J. Kaye, H. Sugimoto, C.-C. Wu, V. S. LeBleu and R. Kalluri, *Nature*, 2015, **527**, 525–530.
- 344 O. H. Ocaña, R. Córcoles, Á. Fabra, G. Moreno-Bueno, H. Acloque, S. Vega, A. Barrallo-Gimeno, A. Cano and M. A. Nieto, *Cancer Cell*, 2012, **22**, 709–724.
- 345 E. Schuster, R. Taftaf, C. Reduzzi, M. K. Albert, I. Romero-Calvo and H. Liu, *Trends Cancer*, 2021, **7**, 1020–1032.
- 346 E. Long, M. Ilie, C. Bence, C. Butori, E. Selva, S. Lalvée, C. Bonnetaud, G. Poissonnet, J.-P. Lacour, P. Bahadoran, P. Brest, E. Gilson, R. Ballotti, V. Hofman and P. Hofman, *Cancer Med*, 2016, **5**, 1022–1030.
- 347 K. J. Cheung, E. Gabrielson, Z. Werb and A. J. Ewald, *Cell*, 2013, **155**, 1639–1651.
- 348 W. Goto, S. Kashiwagi, Y. Asano, K. Takada, K. Takahashi, T. Hatano, T. Takashima, S. Tomita, H. Motomura, M. Ohsawa, K. Hirakawa and M. Ohira, *Biomark Res*, 2017, **5**, 19.
- 349 M. Yu, A. Bardia, B. S. Wittner, S. L. Stott, M. E. Smas, D. T. Ting, S. J. Isakoff, J. C. Ciciliano, M. N. Wells, A. M. Shah, K. F. Concannon, M. C. Donaldson, L. V. Sequist, E. Brachtel, D. Sgroi, J. Baselga, S. Ramaswamy, M. Toner, D. A. Haber and S. Maheswaran, *Science (1979)*, 2013, **339**, 580–584.
- 350 R. Mayor and S. Etienne-Manneville, *Nat Rev Mol Cell Biol*, 2016, **17**, 97–109.
- 351 K. Saxena, M. K. Jolly and K. Balamurugan, *Transl Oncol*, 2020, **13**, 100845.
- 352 N. R. Campbell, A. Rao, M. V. Hunter, M. K. Sznurkowska, L. Briker, M. Zhang, M. Baron, S. Heilmann, M. Deforet, C. Kenny, L. P. Ferretti, T.-H. Huang, S. Perlee, M. Garg, J. Nsengimana, M. Saini, E. Montal, M. Tagore, J. Newton-Bishop, M. R. Middleton, P. Corrie, D. J. Adams, R. Rabbie, N. Aceto, M. P. Levesque, R. A. Cornell, I. Yanai, J. B. Xavier and R. M. White, *Dev Cell*, 2021, **56**, 2808-2825.e10.
- 353 Y. Dimitrova, A. J. Gruber, N. Mittal, S. Ghosh, B. Dimitriades, D. Mathow, W. A. Grandy, G. Christofori and M. Zavolan, *Biol Direct*, 2017, **12**, 8.
- 354 J. Seoane and R. R. Gomis, *Cold Spring Harb Perspect Biol*, 2017, **9**, a022277.
- 355 J. Seoane, *Carcinogenesis*, 2006, **27**, 2148–2156.
- 356 C. D. Morrison, J. G. Parvani and W. P. Schiemann, *Cancer Lett*, 2013, **341**, 30–40.

- 357 E. Tuncer, R. R. Calçada, D. Zingg, S. Varum, P. Cheng, S. N. Freiburger, C.-X. Deng, I. Kleiter, M. P. Levesque, R. Dummer and L. Sommer, *Journal of Clinical Investigation*, 2019, **129**, 2702–2716.
- 358 X. Luo, D. Mitra, R. J. Sullivan, B. S. Wittner, A. M. Kimura, S. Pan, M. P. Hoang, B. W. Brannigan, D. P. Lawrence, K. T. Flaherty, L. V. Sequist, M. McMahon, M. W. Bosenberg, S. L. Stott, D. T. Ting, S. Ramaswamy, M. Toner, D. E. Fisher, S. Maheswaran and D. A. Haber, *Cell Rep*, 2014, **7**, 645–653.
- 359 B. Zhou, Y. Liu, M. Kahn, D. K. Ann, A. Han, H. Wang, C. Nguyen, P. Flodby, Q. Zhong, M. S. Krishnaveni, J. M. Liebler, P. Minoo, E. D. Crandall and Z. Borok, *Journal of Biological Chemistry*, 2012, **287**, 7026–7038.
- 360 S. Amini Nik, R. P. Ebrahim, K. Van Dam, J. J. Cassiman and S. Tejpar, *Exp Cell Res*, 2007, **313**, 2887–2895.
- 361 F. Löönd, M. Pirkl, M. Hisano, V. Prestigiacomo, R. K. Kalathur, N. Beerenwinkel and G. Christofori, *Life Sci Alliance*, 2022, **5**, e202101010.
- 362 M. J. Grimson, J. C. Coates, J. P. Reynolds, M. Shipman, R. L. Blanton and A. J. Harwood, *Nature*, 2000, **408**, 727–731.
- 363 J. Chen, J. Liu, R. Jin, J. Shen, Y. Liang, R. Ma, H. Lin, X. Liang, H. Yu and X. Cai, *PLoS One*, 2014, **9**, e111885.
- 364 T. L. Ng, A. M. Gown, T. S. Barry, M. C. U. Cheang, A. K. W. Chan, D. A. Turbin, F. D. Hsu, R. B. West and T. O. Nielsen, *Modern Pathology*, 2005, **18**, 68–74.
- 365 B. T. MacDonald, K. Tamai and X. He, *Dev Cell*, 2009, **17**, 9–26.
- 366 H. Aberle, A. Bauer, J. Stappert, A. Kispert and R. Kemler, *EMBO Journal*, 1997, **16**, 3797–3804.
- 367 K. M. Cadigan and M. L. Waterman, *Cold Spring Harb Perspect Biol*, 2012, **4**, a007906–a007906.
- 368 W. E. Damsky, D. P. Curley, M. Santhanakrishnan, L. E. Rosenbaum, J. T. Platt, B. E. Gould Rothberg, M. M. Taketo, D. Dankort, D. L. Rimm, M. McMahon and M. Bosenberg, *Cancer Cell*, 2011, **20**, 741–754.
- 369 T. Sinnberg, M. Menzel, D. Ewerth, B. Sauer, M. Schwarz, M. Schaller, C. Garbe and B. Schitteck, *PLoS One*, 2011, **6**, e23429.
- 370 H. R. Widlund, M. A. Horstmann, E. R. Price, J. Cui, S. L. Lessnick, M. Wu, X. He and D. E. Fisher, *Journal of Cell Biology*, 2002, **158**, 1079–1087.
- 371 R. Uka, C. Britschgi, A. Krättli, C. Matter, D. Mihic, M. J. Okoniewski, M. Gualandi, R. Stupp, P. Cinelli, R. Dummer, M. P. Levesque and O. Shakhova, *Oncogene*, 2020, **39**, 4132–4154.
- 372 A. J. Chien, E. C. Moore, A. S. Lonsdorf, R. M. Kulikauskas, B. G. Rothberg, A. J. Berger, M. B. Major, S. T. Hwang, D. L. Rimm and R. T. Moon, *Proceedings of the National Academy of Sciences*, 2009, **106**, 1193–1198.
- 373 T. Toyofuku, Z. Hong, T. Kuzuya, M. Tada and M. Hori, *Journal of Cell Biology*, 2000, **150**, 225–242.
- 374 U. Kreuser, J. Buchert, A. Haase, W. Richter and S. Diederichs, *Front Cell Dev Biol*, , DOI:10.3389/fcell.2020.581331.

- 375 P. H. Chang, M. C. Chen, Y. P. Tsai, G. Y. T. Tan, P. H. Hsu, Y. M. Jeng, Y. F. Tsai, M. H. Yang and W. W. Hwang-Verslues, *Proc Natl Acad Sci U S A*, 2021, **118**, e2014408118.
- 376 J. Park, Y. Son, N. G. Lee, K. Lee, D. G. Lee, J. Song, J. Lee, S. Kim, M. J. Cho, J.-H. Jang, J. Lee, J.-G. Park, Y.-G. Kim, J.-S. Kim, J. Lee, Y. S. Cho, Y.-J. Park, B. S. Han, K.-H. Bae, S. Han, B. Kang, S. Haam, S.-H. Lee, S. C. Lee and J.-K. Min, *Stem Cell Reports*, 2018, **11**, 115–127.
- 377 J.-J. Yu, C. Shu, H.-Y. Yang, Z. Huang, Y.-N. Li, R. Tao, Y.-Y. Chen, Q. Chen, X.-P. Chen and W. Xiao, *Front Oncol*, , DOI:10.3389/fonc.2021.734564.
- 378 S. Y. Lin, S.-C. Chang, S. Lam, R. Irene Ramos, K. Tran, S. Ohe, M. P. Salomon, A. A. S. Bhagat, C. Teck Lim, T. D. Fischer, L. J. Foshag, C. L. Boley, S. J. O’Day and D. S. B. Hoon, *Clin Chem*, 2020, **66**, 169–177.
- 379 N. Harner-Foreman, J. Vadakekolathu, S. A. Laversin, M. G. Mathieu, S. Reeder, A. G. Pockley, R. C. Rees and D. J. Boocock, *Sci Rep*, 2017, **7**, 40633.
- 380 Y.-T. Kang, A. Mutukuri, T. Hadlock, H. Fairbairn, T. R. Carle, S. Fouladdel, V. Murlidhar, A. Kramer, M. D. S. Reguera, E. Azizi, A. Durham, S. A. Mclean and S. Nagrath, *Adv Nanobiomed Res*, 2022, **2**, 2100083.
- 381 P. Schmid, P. Itin and T. Rufli, *Carcinogenesis*, 1995, **16**, 1499–1503.
- 382 S. Moretti, C. Pinzi, E. Berti, A. Spallanzani, A. Chiarugi, V. Boddi, U. M. Reali and B. Giannotti, *Melanoma Res*, 1997, **7**, 313–321.
- 383 L. Xu, W.-H. Cui, W.-C. Zhou, D.-L. Li, L.-C. Li, P. Zhao, X.-T. Mo, Z. Zhang and J. Gao, *J Cell Mol Med*, 2017, **21**, 1545–1554.
- 384 P. J. Miettinen, R. Ebner, A. R. Lopez and R. Derynck, *Journal of Cell Biology*, 1994, **127**, 2021–2036.
- 385 U. Valcourt, M. Kowanetz, H. Niimi, C.-H. Heldin and A. Moustakas, *Mol Biol Cell*, 2005, **16**, 1987–2002.
- 386 C.-Y. Loh, J. Chai, T. Tang, W. Wong, G. Sethi, M. Shanmugam, P. Chong and C. Looi, *Cells*, 2019, **8**, 1118.
- 387 M. Topalovski, M. Hagopian, M. Wang and R. A. Brekken, *Journal of Biological Chemistry*, 2016, **291**, 22244–22252.
- 388 S. Y. Tam, V. W. C. Wu and H. K. W. Law, *Front Oncol*, , DOI:10.3389/fonc.2020.00486.
- 389 M. Nicklin, G. J. Hickman, A. G. Pockley and C. C. Perry, *ACS Appl Bio Mater*, 2020, **3**, 495–504.
- 390 R. Oughtred, J. Rust, C. Chang, B. Breikreutz, C. Stark, A. Willems, L. Boucher, G. Leung, N. Kolas, F. Zhang, S. Dolma, J. Coulombe-Huntington, A. Chatr-aryamontri, K. Dolinski and M. Tyers, *Protein Science*, 2021, **30**, 187–200.
- 391 A. J. Gentles, A. M. Newman, C. L. Liu, S. V. Bratman, W. Feng, D. Kim, V. S. Nair, Y. Xu, A. Khuong, C. D. Hoang, M. Diehn, R. B. West, S. K. Plevritis and A. A. Alizadeh, *Nat Med*, 2015, **21**, 938–945.
- 392 L. Xu, S. S. Shen, Y. Hoshida, A. Subramanian, K. Ross, J.-P. Brunet, S. N. Wagner, S. Ramaswamy, J. P. Mesirov and R. O. Hynes, *Molecular Cancer Research*, 2008, **6**, 760–769.

- 393 N. Doumpas, F. Lampart, M. D. Robinson, A. Lentini, C. E. Nestor, C. Cantù and K. Basler, *EMBO J*, , DOI:10.15252/embj.201798873.
- 394 H. Mi, A. Muruganujan and P. D. Thomas, *Nucleic Acids Res*, 2012, **41**, D377–D386.
- 395 Q. Zhang, W. Liu, H.-M. Zhang, G.-Y. Xie, Y.-R. Miao, M. Xia and A.-Y. Guo, *Genomics Proteomics Bioinformatics*, 2020, **18**, 120–128.
- 396 W. J. Nelson and R. Nusse, *Science (1979)*, 2004, **303**, 1483–1487.
- 397 Y. Chen, S. Li, W. Li, R. Yang, X. Zhang, Y. Ye, J. Yu, L. Ye and W. Tang, *Sci Rep*, 2019, **9**, 7084.
- 398 P. Friedl, J. Locker, E. Sahai and J. E. Segall, *Nat Cell Biol*, 2012, **14**, 777–783.
- 399 A. Genna, A. M. Vanwynsberghe, A. V. Villard, C. Pottier, J. Ancel, M. Polette and C. Gilles, *Cancers (Basel)*, 2020, **12**, 1632.
- 400 P. Balcik-Ercin, L. Cayrefourcq, R. Soundararajan, S. A. Mani and C. Alix-Panabières, *Cancers (Basel)*, 2021, **13**, 5408.
- 401 X. Tian, Z. Liu, B. Niu, J. Zhang, T. K. Tan, S. R. Lee, Y. Zhao, D. C. H. Harris and G. Zheng, *J Biomed Biotechnol*, 2011, **2011**, 1–6.
- 402 J. Zhang, X.-J. Tian and J. Xing, *J Clin Med*, 2016, **5**, 41.
- 403 J. P. Thiery and C. T. Lim, *Cancer Cell*, 2013, **23**, 272–273.
- 404 D. Pedri, P. Karras, E. Landeloos, J. Marine and F. Rambow, *FEBS J*, 2022, **289**, 1352–1368.
- 405 C. Jamieson, M. Sharma and B. R. Henderson, *Int J Biochem Cell Biol*, 2012, **44**, 847–850.
- 406 H. Jian, X. Shen, Irwin. Liu, M. Semenov, X. He and X.-F. Wang, *Genes Dev*, 2006, **20**, 666–674.
- 407 R. Blakytyn, A. Ludlow, G. E. M. Martin, G. Ireland, L. R. Lund, M. W. J. Ferguson and G. Brunner, *J Cell Physiol*, 2004, **199**, 67–76.
- 408 G. Huai, J. F. Markmann, S. Deng and C. G. Rickert, *Clin Transl Immunology*, , DOI:10.1002/cti2.1270.
- 409 C. Y. Perrot, D. Javelaud and A. Mauviel, *Ann Dermatol*, 2013, **25**, 135.
- 410 K. Gravdal, O. J. Halvorsen, S. A. Haukaas and L. A. Akslen, *Clinical Cancer Research*, 2007, **13**, 7003–7011.
- 411 M. G. Mendez, D. Restle and P. A. Janmey, *Biophys J*, 2014, **107**, 314–323.
- 412 J.-M. Hou, M. Krebs, T. Ward, R. Sloane, L. Priest, A. Hughes, G. Clack, M. Ranson, F. Blackhall and C. Dive, *Am J Pathol*, 2011, **178**, 989–996.
- 413 M. Nicklin, R. C. Rees, A. G. Pockley and C. C. Perry, *Biomater. Sci.*, 2014, **2**, 1486–1496.
- 414 M. A. Horton, *Int J Biochem Cell Biol*, 1997, **29**, 721–725.
- 415 Y. -Q. MA, J. QIN and E. F. PLOW, *Journal of Thrombosis and Haemostasis*, 2007, **5**, 1345–1352.
- 416 S. Hou, J. Wang, W. Li, X. Hao and Q. Hang, *Front Mol Biosci*, , DOI:10.3389/fmolb.2021.708779.

- 417 L. Schaedel, C. Lorenz, A. V. Schepers, S. Klumpp and S. Köster, *Nat Commun*, 2021, **12**, 3799.
- 418 J. L. Walker, B. M. Bleaken, A. R. Romisher, A. A. Alnwibit and A. S. Menko, *Mol Biol Cell*, 2018, **29**, 1555–1570.
- 419 M. Shigyo, T. Kuboyama, Y. Sawai, M. Tada-Umezaki and C. Tohda, *Sci Rep*, 2015, **5**, 12055.
- 420 M. C. Menon, P. Y. Chuang, Z. Li, C. Wei, W. Zhang, Y. Luan, Z. Yi, H. Xiong, C. Woytovich, I. Greene, J. Overbey, I. Rosales, E. Bagiella, R. Chen, M. Ma, L. Li, W. Ding, A. Djamali, M. Saminego, P. J. O’Connell, L. Gallon, R. Colvin, B. Schroppel, J. C. He and B. Murphy, *Journal of Clinical Investigation*, 2015, **125**, 208–221.
- 421 C. Artus, F. Glacial, K. Ganeshamoorthy, N. Ziegler, M. Godet, T. Guilbert, S. Liebner and P.-O. Couraud, *Journal of Cerebral Blood Flow & Metabolism*, 2014, **34**, 433–440.
- 422 R. Fodde and T. Brabletz, *Curr Opin Cell Biol*, 2007, **19**, 150–158.
- 423 P. Salomoni and P. P. Pandolfi, *Cell*, 2002, **108**, 165–170.
- 424 V. Lallemand-Breitenbach and H. de The, *Cold Spring Harb Perspect Biol*, 2010, **2**, a000661–a000661.
- 425 V. Gottifredi and C. Prives, *Trends Cell Biol*, 2001, **11**, 184–187.
- 426 H.-K. Lin, S. Bergmann and P. P. Pandolfi, *Nature*, 2004, **431**, 205–211.
- 427 M. Shtutman, J. Zhurinsky, M. Oren, E. Levina and A. Ben-Ze’ev, *Cancer Res*, 2002, **62**, 5947–5954.
- 428 R. Satow, M. Shitashige, T. Jigami, K. Fukami, K. Honda, I. Kitabayashi and T. Yamada, *Gastroenterology*, 2012, **142**, 572–581.
- 429 J. Zhang, J. Zhai, C. C. Wong, H. Chen, X. Wang, J. Ji and J. Yu, *Oncogene*, 2021, **40**, 6641–6652.
- 430 S. Konikkat and , John L. Woolford, *Biochemical Journal*, 2017, **474**, 195–214.
- 431 K. E. Sloan, M. T. Bohnsack and N. J. Watkins, *Cell Rep*, 2013, **5**, 237–247.
- 432 R. Bernardi, P. P. Scaglioni, S. Bergmann, H. F. Horn, K. H. Vousden and P. P. Pandolfi, *Nat Cell Biol*, 2004, **6**, 665–672.
- 433 M.-S. Dai, R. Sears and H. Lu, *Cell Cycle*, 2007, **6**, 2735–2741.
- 434 F. K. Noubissi, I. Elcheva, N. Bhatia, A. Shakoory, A. Ougolkov, J. Liu, T. Minamoto, J. Ross, S. Y. Fuchs and V. S. Spiegelman, *Nature*, 2006, **441**, 898–901.
- 435 S. Cairo, F. De Falco, M. Pizzo, P. Salomoni, P. P. Pandolfi and G. Meroni, *Oncogene*, 2005, **24**, 2195–2203.
- 436 M. Gabay, Y. Li and D. W. Felsher, *Cold Spring Harb Perspect Med*, 2014, **4**, a014241–a014241.
- 437 S. Rennoll and G. Yochum, *World J Biol Chem*, 2015, **6**, 290–300.
- 438 C. Grosset, C.-Y. A. Chen, N. Xu, N. Sonenberg, H. Jacquemin-Sablon and A.-B. Shyu, *Cell*, 2000, **103**, 29–40.

- 439 J. Rosenbluh, J. Mercer, Y. Shrestha, R. Oliver, P. Tamayo, J. G. Doench, I. Tirosh, F. Piccioni, E. Hartenian, H. Horn, L. Fagbami, D. E. Root, J. Jaffe, K. Lage, J. S. Boehm and W. C. Hahn, *Cell Syst*, 2016, **3**, 302-316.e4.
- 440 H. Zhang, H.-B. Xu, E. Kurban and H.-W. Luo, *Cell Death Dis*, 2020, **11**, 646.
- 441 Y. Li, D. Guo, Y. Zhao, M. Ren, G. Lu, Y. Wang, J. Zhang, C. Mi, S. He and X. Lu, *Cell Death Dis*, 2018, **9**, 888.
- 442 K. G. Bullock, G. P. Beardsley and K. S. Anderson, *Journal of Biological Chemistry*, 2002, **277**, 22168–22174.
- 443 T. Nishimura, A. Nakata, X. Chen, K. Nishi, M. Meguro-Horike, S. Sasaki, K. Kita, S. Horike, K. Saitoh, K. Kato, K. Igarashi, T. Murayama, S. Kohno, C. Takahashi, N. Mukaida, S. Yano, T. Soga, A. Tojo and N. Gotoh, *Oncogene*, 2019, **38**, 2464–2481.
- 444 L. Corsini, S. Bonnal, J. Basquin, M. Hothorn, K. Scheffzek, J. Valcárcel and M. Sattler, *Nat Struct Mol Biol*, 2007, **14**, 620–629.
- 445 A. M. Al-Ayoubi, H. Zheng, Y. Liu, T. Bai and S. T. Eblen, *Mol Cell Biol*, 2012, **32**, 2880–2893.
- 446 D. Hu, W. Fang, A. Han, L. Gallagher, R. J. Davis, B. Xiong and W. Yang, *Carcinogenesis*, 2008, **29**, 2317–2324.
- 447 R. K. Bikkavilli, M. E. Feigin and C. C. Malbon, *J Cell Sci*, 2008, **121**, 3598–3607.
- 448 Y.-J. Chen, N. G. Mahieu, X. Huang, M. Singh, P. A. Crawford, S. L. Johnson, R. W. Gross, J. Schaefer and G. J. Patti, *Nat Chem Biol*, 2016, **12**, 937–943.
- 449 M. G. Vander Heiden, L. C. Cantley and C. B. Thompson, *Science (1979)*, 2009, **324**, 1029–1033.
- 450 G. Claps, S. Faouzi, V. Quidville, F. Chehade, S. Shen, S. Vagner and C. Robert, *Nat Rev Clin Oncol*, 2022, **19**, 749–762.
- 451 F. Petrelli, R. Ardito, B. Merelli, V. Lonati, M. Cabiddu, S. Seghezzi, S. Barni and A. Ghidini, *Melanoma Res*, 2019, **29**, 1–12.
- 452 A. Giatromanolaki, E. Sivridis, K. C. Gatter, H. Turley, A. L. Harris and M. I. Koukourakis, *Gynecol Oncol*, 2006, **103**, 912–918.
- 453 N. Yalamanchi, M. B. Klein, H. M. Pham, M. T. Longaker and J. Chang, *Plast Reconstr Surg*, 2004, **113**, 625–632.
- 454 Q. Tian, M. C. Feetham, W. A. Tao, X. C. He, L. Li, R. Aebbersold and L. Hood, *Proceedings of the National Academy of Sciences*, 2004, **101**, 15370–15375.
- 455 A. Saxena, Y. K. Banasavadi-Siddegowda, Y. Fan, S. Bhattacharya, G. Roy, D. R. Giovannucci, R. A. Frizzell and X. Wang, *Journal of Biological Chemistry*, 2012, **287**, 19158–19170.
- 456 J. N. Rauch and J. E. Gestwicki, *Journal of Biological Chemistry*, 2014, **289**, 1402–1414.
- 457 N. Yamagishi, K. Ishihara, Y. Saito and T. Hatayama, *FEBS Lett*, 2003, **555**, 390–396.
- 458 N. Yu, M. Kakunda, V. Pham, J. R. Lill, P. Du, M. Wongchenko, Y. Yan, R. Firestein and X. Huang, *Mol Cell Biol*, 2015, **35**, 1390–1400.

- 459 I. Martínez-Pena, P. Hurtado, N. Carmona-Ule, C. Abuín, A. B. Dávila-Ibáñez, L. Sánchez, M. Abal, A. Chaachou, J. Hernández-Losa, S. R. y Cajal, R. López-López and R. Piñeiro, *Int J Mol Sci*, 2021, **22**, 9279.
- 460 K. Mizukoshi, Y. Okazawa, H. Haeno, Y. Koyama, K. Sulidan, H. Komiyama, H. Saeki, N. Ohtsuji, Y. Ito, Y. Kojima, M. Goto, S. Habu, O. Hino, K. Sakamoto and A. Orimo, *Int J Cancer*, 2020, **146**, 2547–2562.
- 461 Z.-G. Wang, D. Ruggero, S. Ronchetti, S. Zhong, M. Gaboli, R. Rivi and P. P. Pandolfi, *Nat Genet*, 1998, **20**, 266–272.
- 462 E. de Stanchina, E. Querido, M. Narita, R. V Davuluri, P. P. Pandolfi, G. Ferbeyre and S. W. Lowe, *Mol Cell*, 2004, **13**, 523–535.
- 463 C. Gurrieri, P. Capodiecici, R. Bernardi, P. P. Scaglioni, K. Nafa, L. J. Rush, D. A. Verbel, C. Cordon-Cardo and P. P. Pandolfi, *JNCI Journal of the National Cancer Institute*, 2004, **96**, 269–279.
- 464 M. G. Mathieu, A. K. Miles, M. Ahmad, M. E. Buczek, A. G. Pockley, R. C. Rees and T. Regad, *Cell Death Dis*, 2014, **5**, e1061–e1061.
- 465 M. E. Buczek, A. K. Miles, W. Green, C. Johnson, D. J. Boocock, A. G. Pockley, R. C. Rees, G. Hulman, G. van Schalkwyk, R. Parkinson, J. Hulman, D. G. Powe and T. Regad, *Oncogene*, 2016, **35**, 3465–3475.
- 466 S. S. Agarwala, U. Keilholz, E. Gilles, A. Y. Bedikian, J. Wu, R. Kay, C. A. Stein, L. M. Itri, S. Suciú and A. M. M. Eggermont, *Eur J Cancer*, 2009, **45**, 1807–1814.
- 467 B. Weide, S. Richter, P. Büttner, U. Leiter, A. Forschner, J. Bauer, L. Held, T. K. Eigentler, F. Meier and C. Garbe, *PLoS One*, 2013, **8**, e81624.
- 468 J. Gil, Y. Kim, B. Szeitz, V. Doma, U. Çakır, N. Pinto de Almeida, Y. Paco Hagemeyer, V. Guryev, J. G. Johansson, Y. Sharma, I. Pla Parada, Z. Horvath, J. de Siqueira Guedes, G. Monnerat, G. Reis Alves Carneiro, F. C. Nogueira, B. Lee, H. Oskolas, E. Kuroli, J. Hársing, Y. Sugihara, M. Kuras, R. Appelqvist, E. Wieslander, G. B. Domont, B. Baldetorp, R. Hong, G. Huszty, L. Vizkeleti, J. Tímár, D. Fenyő, L. Hiram Betancourt, J. Jakobsson, J. Malm, A. Sanchez, A. Marcell Szász, P. Horvatovich, M. Rezeli, S. Kárpáti and G. Marko-Varga, , DOI:10.1101/2021.04.10.439245.
- 469 G. R. Kardos, M.-S. Dai and G. P. Robertson, *Pigment Cell Melanoma Res*, 2014, **27**, 801–812.
- 470 A. S. Soares, V. M. Costa, C. Diniz and P. Fresco, *Basic Clin Pharmacol Toxicol*, 2015, **116**, 25–36.
- 471 E. Shoshan, A. K. Mobley, R. R. Braeuer, T. Kamiya, L. Huang, M. E. Vasquez, A. Salameh, H. J. Lee, S. J. Kim, C. Ivan, G. Velazquez-Torres, K. M. Nip, K. Zhu, D. Brooks, S. J. M. Jones, I. Birol, M. Mosqueda, Y. Wen, A. K. Eterovic, A. K. Sood, P. Hwu, J. E. Gershenwald, A. Gordon Robertson, G. A. Calin, G. Markel, I. J. Fidler and M. Bar-Eli, *Nat Cell Biol*, 2015, **17**, 311–321.
- 472 Y. Liu, L. Conaway, J. Rutherford Bethard, A. M. Al-Ayoubi, A. Thompson Bradley, H. Zheng, S. A. Weed and S. T. Eblen, *Nucleic Acids Res*, 2013, **41**, 4949–4962.
- 473 K.-J. Chen, F.-Z. Li, Q. Ye, M. Jia and S. Fang, *PLoS One*, 2021, **16**, e0258053.

- 474 H.-S. Park, C.-H. Park, B.-R. Choi, M.-S. Lim, S.-H. Heo, C.-H. Kim, S.-G. Kang, K. U. Whang and M. K. Cho, *J Cutan Pathol*, 2009, **36**, 511–516.
- 475 R. Wang, C. Peng, J. Song, Y. Hua, Q. Wu, L. Deng, Y. Cao, J. Zhang, L. Zhang, L. Wu and L. Hou, *Int J Oncol*, 2022, **60**, 33.
- 476 C.-F. Li, J.-Y. Chen, Y.-H. Ho, W.-H. Hsu, L.-C. Wu, H.-Y. Lan, D. S.-S. Hsu, S.-K. Tai, Y.-C. Chang and M.-H. Yang, *Nat Cell Biol*, 2019, **21**, 251–262.
- 477 T. Valenta, G. Hausmann and K. Basler, *EMBO J*, 2012, **31**, 2714–2736.
- 478 Y. Sheng, W. Ju, Y. Huang, J. Li, H. Ozer, X. Qiao and Z. Qian, *Leukemia*, 2016, **30**, 2106–2109.
- 479 R. Murray, K. J. Veale, C. Offenhäuser and R. Z. Murray, *Commun Integr Biol*, **4**, 1370–1379.
- 480 S. Ueno, G. Weidinger, T. Osugi, A. D. Kohn, J. L. Golob, L. Pabon, H. Reinecke, R. T. Moon and C. E. Murry, *Proceedings of the National Academy of Sciences*, 2007, **104**, 9685–9690.
- 481 A. C. Mullen, D. A. Orlando, J. J. Newman, J. Lovén, R. M. Kumar, S. Bilodeau, J. Reddy, M. G. Guenther, R. P. DeKoter and R. A. Young, *Cell*, 2011, **147**, 565–576.
- 482 H. Qu, H. Zhao, X. Zhang, Y. Liu, F. Li, L. Sun and Z. Song, *Front Immunol*, , DOI:10.3389/fimmu.2020.612784.
- 483 T.-H. Pham, J. Minderjahn, C. Schmidl, H. Hoffmeister, S. Schmidhofer, W. Chen, G. Längst, C. Benner and M. Rehli, *Nucleic Acids Res*, 2013, **41**, 6391–6402.
- 484 H. Iwasaki, C. Somoza, E. A. Shigematsu Hirokazu and Duprez, J. Iwasaki-Arai, S.-I. Mizuno, Y. Arinobu, K. Geary, T. Zhang Pu and Dayaram, M. L. Fenyus, S. Elf, S. Chan, P. Kastner, C. S. Huettnner, R. Murray, D. G. Tenen and K. Akashi, *Blood*, 2005, **106**, 1590–1600.
- 485 S. H. M. Pang, C. A. de Graaf, D. J. Hilton, N. D. Huntington, S. Carotta, L. Wu and S. L. Nutt, *Front Immunol*, , DOI:10.3389/fimmu.2018.01264.
- 486 C. Le Coz, D. N. Nguyen, C. Su, B. E. Nolan, A. V. Albrecht, S. Xhani, D. Sun, B. Demaree, P. Pillarisetti, C. Khanna, F. Wright, P. A. Chen, S. Yoon, A. L. Stiegler, K. Maurer, J. P. Garifallou, A. Rymaszewski, S. H. Kroft, T. S. Olson, A. E. Seif, G. Wertheim, S. F. A. Grant, L. T. Vo, J. M. Puck, K. E. Sullivan, J. M. Routes, V. Zakharova, A. Shcherbina, A. Mukhina, N. L. Rudy, A. C. E. Hurst, T. P. Atkinson, T. J. Boggon, H. Hakonarson, A. R. Abate, J. Hajjar, S. K. Nicholas, J. R. Lupski, J. Verbsky, I. K. Chinn, M. V. Gonzalez, A. D. Wells, A. Marson, G. M. K. Poon and N. Romberg, *Journal of Experimental Medicine*, , DOI:10.1084/jem.20201750.
- 487 G. M. K. Poon and R. B. Macgregor, *J Mol Biol*, 2004, **335**, 113–127.
- 488 P. Burda, P. Laslo and T. Stopka, *Leukemia*, 2010, **24**, 1249–1257.
- 489 P. Zhang, X. Zhang, A. Iwama, C. Yu, K. A. Smith, B. U. Mueller, S. Narravula, B. E. Torbett, S. H. Orkin and D. G. Tenen, *Blood*, 2000, **96**, 2641–2648.
- 490 R. Hromas, A. Orazi, R. Neiman, R. Maki, C. Van Beveran, J. Moore and M. Klemsz, *Blood*, 1993, **82**, 2998–3004.
- 491 M. Uhlén, L. Fagerberg, B. M. Hallström, C. Lindskog, P. Oksvold, A. Mardinoglu, Å. Sivertsson, C. Kampf, E. Sjöstedt, A. Asplund, I. Olsson, K. Edlund, E. Lundberg, S. Navani, C. A.-K. Szigartyo, J. Odeberg, D. Djureinovic, J. O. Takanen, S. Hober, T. Alm, P.-H. Edqvist, H. Berling, H. Tegel, J. Mulder, J. Rockberg, P. Nilsson, J. M. Schwenk, M. Hamsten, K. von Feilitzen, M. Forsberg, L. Persson, F. Johansson, M. Zwahlen, G. von Heijne, J. Nielsen and F. Pontén, *Science (1979)*, , DOI:10.1126/science.1260419.

- 492 H. Yuki, S. Ueno, H. Tatetsu, H. Niino, T. Iino, S. Endo, Y. Kawano, Y. Komohara, M. Takeya, H. Hata, S. Okada, T. Watanabe, K. Akashi, H. Mitsuya and Y. Okuno, *Blood*, 2013, **121**, 962–970.
- 493 M. D. McKenzie, M. Ghisi, L. Cimmino, M. Erlichster, E. P. Oxley, C. Liu, M. T. Witkowski, G. Liu, A. Dakic, E. Simankowicz, L. DiRago, D. Metcalf, S. L. Nutt, M. Wall, M. E. Ritchie, J. Zuber and R. A. Dickens, *Blood*, 2016, **128**, 3930–3930.
- 494 M. P. Tschan, V. A. Reddy, A. Ressa, G. Arvidsson, M. F. Fey and B. E. Torbett, *Oncogene*, 2008, **27**, 3489–3493.
- 495 G. Rao, N. Rekhman, G. Cheng, T. Krasikov and A. I. Skoultchi, *Oncogene*, 1997, **14**, 123–131.
- 496 P. Rimmelé, M. Esposito, L. Delestré, J.-H. Guervilly, M. Ridinger-Saison, E. Despras, F. Moreau-Gachelin, F. Rosselli and C. Guillouf, *Oncotarget*, 2017, **8**, 37104–37114.
- 497 S. Gregoricchio, L. Polit, M. Esposito, J. Berthelet, L. Delestré, E. Evanno, M. Diop, I. Gallais, H. Aleth, M. Poplineau, W. Zwart, F. Rosenbauer, F. Rodrigues-Lima, E. Duprez, V. Boeva and C. Guillouf, *Nucleic Acids Res*, 2022, **50**, 7938–7958.
- 498 J. Lin, W. Liu, T. Luan, L. Yuan, W. Jiang, H. Cai, W. Yuan, Y. Wang, Q. Zhang and L. Wang, *Oncol Lett*, , DOI:10.3892/ol.2017.7204.
- 499 J. Wang, X. Wang, Y. Guo, L. Ye, D. Li, A. Hu, S. Cai, B. Yuan, S. Jin, Y. Zhou, Q. Li, L. Zheng and Q. Tong, *Clin Transl Med*, , DOI:10.1002/ctm2.588.
- 500 K. Hohenberger, D. Trufa, C. Gebbert, R. Rieker, H. Sirbu and S. Finotto, in *Lung cancer*, European Respiratory Society, 2020, p. 1642.
- 501 O. V. Kovaleva, M. A. Rashidova, D. V. Samoilo, P. A. Podlesnaya, V. V. Mochalnikova and A. N. Gratchev, *Bull Exp Biol Med*, 2021, **170**, 489–492.
- 502 D. E. Foxler, V. James, S. J. Shelton, T. Q. de A. Vallim, P. E. Shaw and T. V Sharp, *FEBS Lett.*, 2011, **585**, 1089–1096.
- 503 I. Antony-Debré, A. Paul, J. Leite, K. Mitchell, H. M. Kim, L. A. Carvajal, T. I. Todorova, K. Huang, A. Kumar, A. A. Farahat, B. Bartholdy, S.-R. Narayanagari, J. Chen, A. Ambesi-Impiombato, A. A. Ferrando, I. Mantzaris, E. Gavathiotis, A. Verma, B. Will, D. W. Boykin, W. D. Wilson, G. M. K. Poon and U. Steidl, *Journal of Clinical Investigation*, 2017, **127**, 4297–4313.
- 504 F. Cunningham, J. E. Allen, J. Allen, J. Alvarez-Jarreta, M. R. Amode, I. M. Armean, O. Austine-Orimoloye, A. G. Azov, I. Barnes, R. Bennett, A. Berry, J. Bhai, A. Bignell, K. Billis, S. Boddu, L. Brooks, M. Charkhchi, C. Cummins, L. Da Rin Fioretto, C. Davidson, K. Dodiya, S. Donaldson, B. El Houdaigui, T. El Naboulsi, R. Fatima, C. G. Giron, T. Genez, J. G. Martinez, C. Guijarro-Clarke, A. Gymer, M. Hardy, Z. Hollis, T. Hourlier, T. Hunt, T. Juettemann, V. Kaikala, M. Kay, I. Lavidas, T. Le, D. Lemos, J. C. Marugán, S. Mohanan, A. Mushtaq, M. Naven, D. N. Ogeh, A. Parker, A. Parton, M. Perry, I. Piližota, I. Prosovetkaia, M. P. Sakhivel, A. I. A. Salam, B. M. Schmitt, H. Schuilenburg, D. Sheppard, J. G. Pérez-Silva, W. Stark, E. Steed, K. Sutinen, R. Sukumaran, D. Sumathipala, M.-M. Suner, M. Szpak, A. Thormann, F. F. Tricomi, D. Urbina-Gómez, A. Veidenberg, T. A. Walsh, B. Walts, N. Willhoft, A. Winterbottom, E. Wass, M. Chakiachvili, B. Flint, A. Frankish, S. Giorgetti, L. Haggerty, S. E. Hunt, G. R. Ilesley, J. E. Loveland, F. J. Martin, B. Moore, J. M. Mudge, M. Muffato, E. Perry, M. Ruffier, J. Tate, D.

- Thybert, S. J. Trevanion, S. Dyer, P. W. Harrison, K. L. Howe, A. D. Yates, D. R. Zerbino and P. Flicek, *Nucleic Acids Res*, 2022, **50**, D988–D995.
- 505 H. A. Carey, B. E. Hildreth, D. J. Samuvel, K. A. Thies, T. J. Rosol, R. E. Toribio, J. F. Charles, M. C. Ostrowski and S. M. Sharma, *iScience*, 2019, **11**, 238–245.
- 506 M. L. Hartman and M. Czyz, *Cellular and Molecular Life Sciences*, 2015, **72**, 1249–1260.
- 507 T. Wohlfahrt, S. Rauber, S. Uebe, M. Lubber, A. Soare, A. Ekici, S. Weber, A.-E. Matei, C.-W. Chen, C. Maier, E. Karouzakis, H. P. Kiener, E. Pachera, C. Dees, C. Beyer, C. Daniel, K. Gelse, A. E. Kremer, E. Naschberger, M. Stürzl, F. Butter, M. Sticherling, S. Finotto, A. Kreuter, M. H. Kaplan, A. Jüngel, S. Gay, S. L. Nutt, D. W. Boykin, G. M. K. Poon, O. Distler, G. Schett, J. H. W. Distler and A. Ramming, *Nature*, 2019, **566**, 344–349.
- 508 K. S. Choe, O. Ujhelly, S. N. Wontakal and A. I. Skoultchi, *Journal of Biological Chemistry*, 2010, **285**, 3044–3052.
- 509 R. Feng, S. C. Desbordes, H. Xie, E. Sanchez Tillo, F. Pixley, E. R. Stanley and T. Graf, .
- 510 J. Xu, S. Lamouille and R. Derynck, *Cell Res*, 2009, **19**, 156–172.
- 511 L.-J. Song, W.-J. Zhang, Z.-W. Chang, Y.-F. Pan, H. Zong, Q.-X. Fan and L.-X. Wang, *Asian Pacific Journal of Cancer Prevention*, 2015, **16**, 3667–3671.
- 512 M. A. Bustos, R. Gross, N. Rahimzadeh, H. Cole, L. T. Tran, K. D. Tran, L. Takeshima, S. L. Stern, S. O’Day and D. S. B. Hoon, *Cancers (Basel)*, 2020, **12**, 3361.
- 513 Y. Sun, T. Zhang, C. Wang, X. Jin, C. Jia, S. Yu and J. Chen, *PLoS One*, 2015, **10**, e0119783.
- 514 S. A. Turkistany and R. P. DeKoter, *Arch Immunol Ther Exp (Warsz)*, 2011, **59**, 431–440.
- 515 J. Abernathy, C. Corkill, C. Hinojosa, X. Li and H. Zhou, *J Anim Sci Biotechnol*, 2013, **4**, 5.
- 516 J. Rhee and R. P. Dekoter, *Blood*, 2017, **130**, 2433.
- 517 M. Tseliou, A. Al-Qahtani, S. Alarifi, S. H. Alkahtani, C. Stournaras and G. Sourvinos, *Cellular Physiology and Biochemistry*, 2016, **38**, 94–109.
- 518 L. Wang, L. Yang, Y. Luo and Y. Zheng, *Journal of Biological Chemistry*, 2003, **278**, 44617–44625.
- 519 B. Boone, M. Van Gele, J. Lambert, M. Haspeslagh and L. Brochez, *J Cutan Pathol*, 2009, **36**, 629–636.
- 520 E. A. Clark, W. G. King, J. S. Brugge, M. Symons and R. O. Hynes, *Journal of Cell Biology*, 1998, **142**, 573–586.
- 521 A. Sedgwick and C. D’Souza-Schorey, *Cancers (Basel)*, 2016, **8**, 80.
- 522 M. Sharma, I. Castro-Piedras, G. E. Simmons and K. Pruitt, *Cell Signal*, 2018, **47**, 52–64.
- 523 R. Habas, Y. Kato and X. He, *Cell*, 2001, **107**, 843–854.
- 524 S. K. Mitra, D. A. Hanson and D. D. Schlaepfer, *Nat Rev Mol Cell Biol*, 2005, **6**, 56–68.
- 525 A. R. Hess, L.-M. Postovit, N. V. Margaryan, E. A. Seftor, G. B. Schneider, R. E. B. Seftor, B. J. Nickoloff and M. J. C. Hendrix, *Cancer Res*, 2005, **65**, 9851–9860.
- 526 V. Golubovskaya, A. Kaur and W. Cance, *Biochimica et Biophysica Acta (BBA) - Gene Structure and Expression*, 2004, **1678**, 111–125.

- 527 A. Kawakami and D. E. Fisher, *Laboratory Investigation*, 2017, **97**, 649–656.
- 528 H. H. Vandyck, L. M. Hillen, F. M. Bosisio, J. van den Oord, A. zur Hausen and V. Winpenninckx, *Cancer and Metastasis Reviews*, 2021, **40**, 603–624.
- 529 S. Yokoyama, E. Feige, L. L. Poling, C. Levy, H. R. Widlund, M. Khaled, A. L. Kung and D. E. Fisher, *Pigment Cell Melanoma Res*, 2008, **21**, 457–463.
- 530 B. A. Moffatt and H. Ashihara, *Arabidopsis Book*, 2002, **1**, e0018.
- 531 J. Yin, W. Ren, X. Huang, J. Deng, T. Li and Y. Yin, *Front Immunol*, , DOI:10.3389/fimmu.2018.01697.
- 532 M. H. Soflaee, R. Kesavan, U. Sahu, A. Tasdogan, E. Villa, Z. Djabari, F. Cai, D. H. Tran, H. S. Vu, E. S. Ali, H. Rion, B. P. O’Hara, S. Kelekar, J. H. Hallett, M. Martin, T. P. Mathews, P. Gao, J. M. Asara, B. D. Manning, I. Ben-Sahra and G. Hoxhaj, *Nat Commun*, 2022, **13**, 2698.
- 533 B. A. Karpinski, L.-H. Yang, P. Cacheris, G. D. Morle and J. M. Leiden, *Mol Cell Biol*, 1989, **9**, 2588–2597.
- 534 J. Hess, P. Angel and M. Schorpp-Kistner, *J Cell Sci*, 2004, **117**, 5965–5973.
- 535 I. Barozzi, M. Simonatto, S. Bonifacio, L. Yang, R. Rohs, S. Ghisletti and G. Natoli, *Mol Cell*, 2014, **54**, 844–857.
- 536 R. Gupta, R. Janostiak and N. Wajapeyee, *Oncogene*, 2020, **39**, 7093–7105.
- 537 G. F. Pierce, T. A. Mustoe, J. Lingelbach, V. R. Masakowski, G. L. Griffin, R. M. Senior and T. F. Deuel, *Journal of Cell Biology*, 1989, **109**, 429–440.
- 538 C. J. Dalton and C. A. Lemmon, *Cells*, 2021, **10**, 2443.
- 539 M. Baron, D. Norman, A. Willis and I. D. Campbell, *Nature*, 1990, **345**, 642–646.
- 540 K. Shin, B. C. Lechtenberg, Y. Fujimoto Lynn M and Yao, S. S. Bartra, G. V Plano and F. M. Marassi, *Sci. Adv.*, 2019, **5**, eaax5068.
- 541 A. Mayasundari, N. A. Whittemore, E. H. Serpersu and C. B. Peterson, *Journal of Biological Chemistry*, 2004, **279**, 29359–29366.
- 542 M. Paoli, B. F. Anderson, H. M. Baker, W. T. Morgan, A. Smith and E. N. Baker, *Nature Structural Biology 1999 6:10*, 1999, **6**, 926–931.
- 543 E. H. J. Danen, P. Sonneveld, C. Brakebusch, R. Fässler and A. Sonnenberg, *Journal of Cell Biology*, 2002, **159**, 1071–1086.
- 544 C.-T. Hsiao, H.-W. Cheng, C.-M. Huang, H.-R. Li, M.-H. Ou, J.-R. Huang, H. W. Khoo Kay-Hooi and Yu, Y.-Q. Chen, Y.-K. Wang, A. Chiou and J.-C. Kuo, *Oncotarget*, 2017, **8**, 70653–70668.
- 545 Q. Yu, W. Xiao, S. Sun, A. Sohrabi, J. Liang and S. K. Seidlits, *Front Cell Dev Biol*, , DOI:10.3389/fcell.2021.616580.
- 546 K. Wang, B. R. Seo, C. Fischbach and D. Gourdon, *Cell Mol Bioeng*, 2016, **9**, 1–11.
- 547 R. Burgos-Panadero, I. Noguera, A. Cañete, S. Navarro and R. Noguera, *BMC Cancer*, 2019, **19**, 479.
- 548 G. Efthymiou, A. Saint, M. Ruff, Z. Rekad, D. Ciais and E. Van Obberghen-Schilling, *Front Oncol*, , DOI:10.3389/fonc.2020.00641.

- 549 G. Schneider, M. Suszynska, S. Kakar and M. Z. Ratajczak, *J Cancer Stem Cell Res*, 2016, **4**, 1.
- 550 L. M. Bafetti, T. N. Young, Y. Itoh and M. S. Stack, *Journal of Biological Chemistry*, 1998, **273**, 143–149.
- 551 P. Roach, N. J. Shirtcliffe, D. Farrar and C. C. Perry, *J Phys Chem B*, 2006, **110**, 20572–20579.
- 552 P. Roach, D. Farrar and C. C. Perry, *J Am Chem Soc*, 2005, **127**, 8168–8173.
- 553 S. Ye, H. Li, W. Yang and Y. Luo, *J Am Chem Soc*, 2014, **136**, 1206–1209.
- 554 I. Noda, *J Am Chem Soc*, 1989, **111**, 8116–8118.
- 555 I. Noda, *Biomed Spectrosc Imaging*, 2015, **4**, 109–127.
- 556 Isao Noda and Yukihiko Ozaki, *Two-Dimensional Correlation Spectroscopy: Applications in Vibrational and Optical Spectroscopy*, John Wiley & Sons Ltd, 2004.
- 557 Y. Xiao, H. Donnelly, M. Sprott, J. Luo, V. Jayawarna, L. Lemgruber, P. M. Tsimbouri, R. M. D. Meek, M. Salmeron-Sanchez and M. J. Dalby, *Mater Today Bio*, 2022, **16**, 100367.
- 558 A. Guzman, M. J. Ziperstein and L. J. Kaufman, *Biomaterials*, 2014, **35**, 6954–6963.
- 559 K. Hotary, E. Allen, A. Punturieri, I. Yana and S. J. Weiss, *Journal of Cell Biology*, 2000, **149**, 1309–1323.
- 560 V. V. Artym, S. Swatkoski, K. Matsumoto, C. B. Campbell, R. J. Petrie, E. K. Dimitriadis, X. Li, S. C. Mueller, T. H. Bugge, M. Gucek and K. M. Yamada, *Journal of Cell Biology*, 2015, **208**, 331–350.
- 561 C. Tanford, 1968, pp. 121–282.
- 562 A. Dong, B. Kendrick, L. Kreilgård, J. Matsuura, M. C. Manning and J. F. Carpenter, *Arch Biochem Biophys*, 1997, **347**, 213–220.
- 563 A. V. Taubenberger, M. A. Woodruff, H. Bai, D. J. Muller and D. W. Hutmacher, *Biomaterials*, 2010, **31**, 2827–2835.
- 564 S. Vijayakumar, S. Vishveshwara, G. Ravishanker and D. L. Beveridge, *Biophys J*, 1993, **65**, 2304–2312.
- 565 G. Zandomenighi, M. R. H. Krebs, M. G. McCammon and M. Fändrich, *Protein Science*, 2009, **13**, 3314–3321.
- 566 T. M. Shin, J. M. Isas, C.-L. Hsieh, R. Kaye, C. G. Glabe, R. Langen and J. Chen, *Mol Neurodegener*, 2008, **3**, 16.
- 567 C. Xue, T. Y. Lin, D. Chang and Z. Guo, *R Soc Open Sci*, 2017, **4**, 160696.
- 568 D. J. Belton, R. Plowright, D. L. Kaplan and C. C. Perry, *Acta Biomater*, 2018, **73**, 355–364.
- 569 B. Zhu, W. Li, N. Chi, R. V. Lewis, J. Osamor and R. Wang, *ACS Omega*, 2017, **2**, 2439–2450.
- 570 T. Li, L. Hao, J. Li, C. Du and Y. Wang, *Bioact Mater*, 2020, **5**, 1044–1052.
- 571 P. Singh, C. Carraher and J. E. Schwarzbauer, *Annu Rev Cell Dev Biol*, 2010, **26**, 397–419.
- 572 N. Aceto, A. Bardia, D. T. Miyamoto, M. C. Donaldson, B. S. Wittner, J. A. Spencer, M. Yu, A. Pely, A. Engstrom, H. Zhu, B. W. Brannigan, R. Kapur, S. L. Stott, T. Shioda, S. Ramaswamy, D. T. Ting, C. P. Lin, M. Toner, D. A. Haber and S. Maheswaran, *Cell*, 2014, **158**, 1110–1122.

- 573 K. J. Cheung, V. Padmanaban, V. Silvestri, K. Schipper, J. D. Cohen, A. N. Fairchild, M. A. Gorin, J. E. Verdone, K. J. Pienta, J. S. Bader and A. J. Ewald, *Proceedings of the National Academy of Sciences*, , DOI:10.1073/pnas.1508541113.
- 574 S. Amintas, A. Bedel, F. Moreau-Gaudry, J. Boutin, L. Buscail, J.-P. Merlio, V. Vendrely, S. Dabernat and E. Buscail, *Int J Mol Sci*, 2020, **21**, 2653.
- 575 P. Mina-Osorio, I. Soto-Cruz and E. Ortega, *Biochem Biophys Res Commun*, 2007, **353**, 605–610.
- 576 R. Wei, D. Sun, H. Yang, J. Yan, X. Zhang, X. Zheng, X. Fu, M. Geng, X. Huang and J. Ding, *Acta Pharmacol Sin*, 2018, **39**, 1326–1337.
- 577 R. Taftaf, X. Liu, S. Singh, Y. Jia, N. K. Dashzeveg, A. D. Hoffmann, L. El-Shennawy, E. K. Ramos, V. Adorno-Cruz, E. J. Schuster, D. Scholten, D. Patel, Y. Zhang, A. A. Davis, C. Reduzzi, Y. Cao, P. D'Amico, Y. Shen, M. Cristofanilli, W. A. Muller, V. Varadan and H. Liu, *Nat Commun*, 2021, **12**, 4867.
- 578 N. Woolf, B. E. Pearson, P. A. Bondzie, R. D. Meyer, M. Lavaei, A. C. Belkina, V. Chitalia and N. Rahimi, *Oncogenesis*, 2017, **6**, e378–e378.
- 579 H. Ahmed and D. M. M. AlSadek, *Clin Med Insights Oncol*, 2015, **9**, 113–21.
- 580 W. S. York, R. Mazumder, R. Ranzinger, N. Edwards, R. Kahsay, M. P. Aoki-Kinoshita Kiyoko F and Campbell, R. D. Cummings, M. Feizi Ten and Martin, D. A. Natale, N. H. Packer, R. J. Woods, G. Agarwal, S. Arpinar, S. Bhat, J. Blake, L. J. G. Castro, B. Fochtman, J. Gildersleeve, X. Goldman Radoslav and Holmes, V. Jain, S. Kulkarni, R. Mahadik, A. Mehta, R. Mousavi, S. Nakarakommula, R. Navelkar, N. Pattabiraman, M. J. Pierce, K. Ross, P. Vasudev, J. Vora, T. Williamson and W. Zhang, *Glycobiology*, 2020, **30**, 72–73.
- 581 S. Löffek, O. Schilling and C.-W. Franzke, *Eur. Respir. J.*, 2011, **38**, 191–208.
- 582 K. M. Gottesdiener, B. A. Karpinski, T. Lindsten, J. L. Strominger, N. H. Jones, C. B. Thompson and J. M. Leiden, *Mol Cell Biol*, 1988, **8**, 3809–3819.
- 583 Y. Sun, J. Liu, Y. Huang, M. Li, J. Lu, N. Jin, Y. He and B. Fan, *Int J Food Prop*, 2019, **22**, 405–413.
- 584 M. Yu, A. Bardia, B. S. Wittner, S. L. Stott, M. E. Smas, D. T. Ting, J. C. Isakoff Steven J and Ciciliano, M. N. Wells, K. F. Shah Ajay M and Concannon, M. C. Donaldson, L. V. Sequist, E. Brachtel, D. Sgroi, J. Baselga, S. Ramaswamy, M. Toner, D. A. Haber and S. Maheswaran, *Science (1979)*, 2013, **339**, 580–584.
- 585 S. Hatsell, T. Rowlands, M. Hiremath and P. Cowin, *J Mammary Gland Biol Neoplasia*, 2003, **8**, 145–158.
- 586 H. Choi, Y.-S. Chun, T.-Y. Kim and J.-W. Park, *Cancer Res*, 2010, **70**, 10101–10111.
- 587 A. Vahdat Shariatpanahi, *The Importance of Macrophages, Lipid Membranes and Seeding in Experimental AA Amyloidosis*, Linköping University Electronic Press, Linköping, 2019, vol. 1687.
- 588 M. Delbianco, B. G. Davis and P. H. Seeberger, *Glycans in Nanotechnology*, Cold Spring Harbor (NY), 4th edn., 2022.

10.1 Appendix

Primers for RT-qPCR used in this project:			
Gene	Protein	Forward sequence	Reverse sequence
<i>CTNNB1</i>	β -Catenin	5'-TGGATGGGCTGCCTCCAGGTGAC-3'	5'-ACCAGCCCACCCCTCGAGCCC-3'
<i>GUBS</i>	Glucuronidase β	5'-CTCATTGGGAATTTGCCGATT-3'	5'-CCGAGTGAAGATCCCCTTTTAA-3'
<i>LGALS3</i>	Galectin-3	5'-GGCCACTGATTGTGCCTTAT-3'	5'-TCTTTCTCCCTTCCCCAGT-3'
<i>MMP2</i>	MMP2	5'-CTCAGATCCGTGGTGAGATCT-3'	5'-CTTTGGTTCTCCAGCTTCAGG-3'
<i>SLC3A2</i>	4F2hc	5'-ACCCCTGTTTTAGCTACGG-3'	5'-GGTCTTCACTCTGGCCCTTC-3'
<i>SPI1</i>	PU.1	5'-AAGTCCAGTAATGGTCGCT-3'	5'-AAGACCTGGTGCCTATGAC-3'
<i>YWHAZ</i>	KCIP-1	5'-ACCGTTACTGGCTGAGGTTGC-3'	5'-CCCAGTCTGATAGGATGTGTTGG-3'

FM3 cell lysate mass spectrometry data: FS-24h vs TCP-24h (n=4)			
UniProtKB	Protein ID	p-value	Log2FC
O15382	BCAT2	0.002264	1.863044
P42694	HELZ	0.045164	1.76627
Q9Y385	UB2J1	0.002855	1.526191
Q9Y3B9	RRP15	0.012607	1.456734
P29353	SHC1	0.03214	1.456076
O14545	TRAD1	0.014132	1.426357
P07355	ANXA2	0.017454	1.196856
P69905	HBA	0.015189	1.129354
Q15007	FL2D	0.039221	1.106202
Q15363	TMED2	0.041864	1.091522
P09601	HMOX1	0.007794	1.089179
Q6DKI1	RL7L	0.017006	1.074189
P08133	ANXA6	0.00289	0.994736
Q9NR19	ACSA	0.007227	0.955134
P09525	ANXA4	0.044073	0.918742
Q9Y5Z4	HEBP2	0.005047	0.897616
Q9Y221	NIP7	0.009803	0.868458
Q8TCT8	SPP2A	0.047156	0.82271
Q13445	TMED1	0.014818	0.797063
Q15057	ACAP2	0.023307	0.786831
A4D1P6	WDR91	0.044801	0.763077

Q8TD55	PKHO2	0.030229	0.73948
P10599	THIO	0.044454	0.697641
P15374	UCHL3	0.045295	0.697176
Q96I25	SPF45	0.001441	0.644705
P08195	4F2	0.002138	0.629641
Q9Y2X7	GIT1	0.049178	0.613484
Q5TDH0	DDI2	0.004452	0.607239
P05067	A4	0.038014	0.604539
P61201	CSN2	0.015226	0.597856
Q01650	LAT1	0.008492	0.57428
P08243	ASNS	0.018514	0.562705
P24941	CDK2	0.03157	0.55075
Q9UMX0	UBQL1	0.006614	0.531836
Q9UBT2	SAE2	0.001733	0.51973
O00566	MPP10	0.012114	0.501738
Q9Y3C1	NOP16	0.004543	0.495991
Q9Y617	SERC	0.045174	0.487961
Q9UJY1	HSPB8	0.019491	0.487927
P01111	RASN	0.04322	0.479137
Q96S97	MYADM	0.017904	0.477709
P04350	TBB4A	0.002212	0.440086
Q9UNX4	WDR3	0.003296	0.43947
O14530	TXND9	0.019058	0.424163
P04183	KITH	0.026744	0.422737
Q8NBU5	ATAD1	0.007016	0.421714
Q8WTV0	SCRB1	0.030988	0.412756
Q9NY27	PP4R2	0.046928	0.411841
Q06830	PRDX1	0.01471	0.402371
P30041	PRDX6	0.002325	0.397451
P04406	G3P	0.037359	0.39744
O00560	SDCB1	0.008305	0.395496
Q9UBF2	COPG2	0.042261	0.385831
P00558	PGK1	0.044461	0.352851
Q16543	CDC37	0.04248	0.34251
P14550	AK1A1	0.016156	0.339789

Q9NX62	IMPA3	0.035421	0.33345
O95630	STABP	0.021355	0.331923
P30740	ILEU	0.028982	0.320074
Q9HC38	GLOD4	0.034769	0.31977
Q00535	CDK5	0.035292	0.319304
O60343	TBCD4	0.045861	0.310805
P17931	LEG3	0.003143	0.306648
P98082	DAB2	0.028445	0.301949
P40763	STAT3	0.01376	0.301679
P06744	G6PI	0.037576	0.29846
Q03701	CEBPZ	0.008203	0.278179
P38606	VATA	0.023014	0.268305
P35232	PHB	0.033082	0.26802
P04075	ALDOA	0.035268	0.2667
Q9H4M9	EHD1	0.009663	0.266407
P07195	LDHB	0.003811	0.266314
P29590	PML	0.005295	0.265187
Q92734	TFG	0.009065	0.25628
Q96IU4	ABHEB	0.041866	0.251352
P16152	CBR1	0.045862	0.24683
Q92598	HS105	0.002319	0.24192
P31153	METK2	0.04399	0.241782
Q9BQE5	APOL2	0.03451	0.241446
P41250	GARS	0.00106	0.241141
Q9Y6C9	MTCH2	0.022312	0.239096
P36871	PGM1	0.023076	0.235155
P54577	SYYC	0.031141	0.234958
P31939	PUR9	0.004942	0.231547
P18085	ARF4	0.027847	0.227511
P55010	IF5	0.029146	0.225219
P51149	RAB7A	0.022931	0.224369
P11940	PABP1	0.007867	0.222547
P62495	ERF1	0.005511	0.222071
P45974	UBP5	0.012626	0.220668
O60271	JIP4	0.013346	0.219984

P41240	CSK	0.033065	0.217581
P54652	HSP72	0.024675	0.217256
Q14258	TRI25	0.032796	0.217083
P27105	STOM	0.04383	0.215163
Q8IZP0	ABI1	0.009245	0.208184
Q96P70	IPO9	0.035954	0.208174
P11766	ADHX	0.011955	0.207268
P68104	EF1A1	0.045031	0.205607
Q06124	PTN11	0.048124	0.204078
O75489	NDUS3	0.01921	0.203689
P23381	SYWC	0.030421	0.202282
O15397	IPO8	0.040703	0.199768
P55786	PSA	0.008463	0.19828
Q9UJK9	NUDT5	0.015238	0.198112
Q8NHQ9	DDX55	0.009283	0.189732
P53004	BIEA	0.03008	0.187675
P53990	IST1	0.010658	0.187323
Q9UBQ7	GRHPR	0.046106	0.186687
Q96KP4	CNDP2	0.03992	0.185337
Q96GK7	FAH2A	0.028125	0.185328
Q9Y2H2	SAC2	0.039579	0.183258
Q15435	PP1R7	0.038666	0.180918
P43490	NAMPT	0.017681	0.175885
O43776	SYNC	0.020349	0.174931
P61081	UBC12	0.002865	0.174186
P14618	KPYM	0.046562	0.172939
P13639	EF2	0.015831	0.162314
P0DMV9	HS71B	0.004898	0.161273
P50991	TCPD	0.040527	0.158296
O43707	ACTN4	0.038055	0.158247
O75955	FLOT1	0.048674	0.158006
P00390	GSHR	0.044803	0.152452
P55060	XPO2	0.02919	0.149466
O75131	CPNE3	0.04914	0.147363
P50990	TCPQ	0.042553	0.146908

Q9Y5X1	SNX9	0.004457	0.140518
P50395	GDIB	0.007383	0.139586
P26038	MOES	0.047438	0.137577
Q86VP6	CAND1	0.035625	0.131745
Q9UGP8	SEC63	0.049701	0.12957
O75874	IDHC	0.036191	0.110063
O15144	ARPC2	0.023937	0.103014
P12268	IMDH2	0.026378	0.100715
Q13617	CUL2	0.002842	0.094337
P51610	HCFC1	0.048013	-0.10624
P12270	TPR	0.012525	-0.11633
Q92974	ARHG2	0.03976	-0.12044
Q8IVM0	CCD50	0.006571	-0.13491
P35579	MYH9	0.046217	-0.135
O94776	MTA2	0.042085	-0.14584
Q96I24	FUBP3	0.011556	-0.16108
Q7L014	DDX46	0.018566	-0.18913
Q9UG63	ABCF2	0.045034	-0.20901
P31943	HNRH1	0.037137	-0.21155
Q9BUJ2	HNRL1	0.036301	-0.21341
P26358	DNMT1	0.020009	-0.2274
Q15637	SF01	0.026805	-0.23802
Q9NVJ2	ARL8B	0.021032	-0.24867
Q9Y6N5	SQOR	0.013386	-0.25711
O14578	CTRO	0.031698	-0.26219
Q96GM8	TOE1	0.036353	-0.28456
P50416	CPT1A	0.02677	-0.29168
Q14192	FHL2	0.032178	-0.29434
O60568	PLOD3	0.042638	-0.29755
P11047	LAMC1	0.003003	-0.2997
Q96GD4	AURKB	0.042717	-0.3115
Q03252	LMNB2	0.021484	-0.32136
Q9UHB6	LIMA1	0.035042	-0.34456
Q07157	ZO1	0.020011	-0.34458
Q8NFH5	NUP35	0.045425	-0.34976

O95425	SVIL	0.034539	-0.3542
Q99640	PMYT1	0.04219	-0.37316
Q9H4L4	SENP3	0.041434	-0.37768
Q6PK18	OGFD3	0.01351	-0.38129
O60462	NRP2	0.01829	-0.38243
P07942	LAMB1	0.009068	-0.38528
Q13247	SRSF6	0.013382	-0.42046
Q92599	SEPTIN8	0.021981	-0.4229
Q9HD67	MYO10	0.044252	-0.44158
P28370	SMCA1	0.015155	-0.44403
Q9UJA5	TRM6	0.010815	-0.50575
O15084	ANR28	0.048737	-0.51903
Q6NZI2	CAVN1	0.034826	-0.57214
Q9BTX1	NDC1	0.012291	-0.62277
P36915	GNL1	0.038846	-0.64001
P08572	CO4A2	0.038096	-0.80807
Q9P016	THYN1	0.024797	-0.84406
Q13523	PRP4B	0.047782	-0.9917
Q9Y4C2	TCAF1	0.033551	-1.2499
Q9NWH9	SLTM	0.033224	-1.26434
P07996	TSP1	0.006376	-1.27263
Q9Y3Z3	SAMH1	0.01731	-1.29446
Q6UX04	CWC27	0.002188	-1.9988

FM3 cell lysate mass spectrometry data: FS-72h vs FS-24h (n=4)			
UniProtKB	Protein ID	p-value	Log2FC
P16402	H13	0.000367	4.113782
Q9UHB7	AFF4	0.00474	1.815491
P05387	RLA2	0.001013	1.776279
P06703	S10A6	0.002886	1.679462
Q96P48	ARAP1	0.036512	1.537999
P16403	H12	0.000971	1.515022
Q9NZD2	GLTP	0.00605	1.448756
P49006	MRP	0.005387	1.358313

P14854	CX6B1	0.008922	1.354905
Q9Y4C2	TCAF1	0.005706	1.297726
P23297	S10A1	0.008601	1.276711
Q9P016	THYN1	0.020694	1.263961
Q15836	VAMP3	0.018236	1.243279
Q53EL6	PDCD4	0.021473	1.241346
Q6UVK1	CSPG4	0.00087	1.185535
P0CG30	GSTT2	0.04715	1.152054
P80297	MT1X	0.003098	1.144121
P05386	RLA1	0.021896	1.064345
Q92597	NDRG1	0.003112	1.042164
Q96A26	F162A	0.002948	1.037165
Q9BTC8	MTA3	0.000141	0.97563
Q14061	COX17	0.040485	0.974194
Q9UKR5	ERG28	0.032756	0.936356
Q92625	ANS1A	4.44E-05	0.929221
Q66PJ3	AR6P4	0.000495	0.911026
Q9HD67	MYO10	0.010661	0.904346
P08962	CD63	0.02772	0.89461
P35527	K1C9	0.000154	0.871875
Q86VM9	ZCH18	0.0008	0.864781
Q5ZPR3	CD276	0.016456	0.841752
P82663	RT25	0.002274	0.831646
P53999	TCP4	0.000496	0.802254
P52815	RM12	0.020954	0.789649
P14406	CX7A2	0.017097	0.765487
O00767	ACOD	0.004934	0.758642
Q9Y2Y0	AR2BP	0.038144	0.752948
Q8NBJ4	GOLM1	0.018698	0.732557
P50479	PDLI4	0.016205	0.729968
P60033	CD81	0.018929	0.726363
O60888	CUTA	0.012569	0.713155
Q16540	RM23	0.029939	0.710769
Q13938	CAYP1	0.001027	0.709692
P14209	CD99	0.003042	0.704096

Q9BTX1	NDC1	0.009305	0.686723
Q16850	CP51A	0.006921	0.641099
O00560	SDCB1	0.000149	0.626759
Q5K4L6	S27A3	0.009491	0.623518
P07225	PROS	0.043431	0.622441
O00244	ATOX1	0.015882	0.619488
P09497	CLCB	0.027732	0.616551
Q16655	36951	0.024733	0.613751
P07108	ACBP	0.006225	0.596329
Q8N129	CNPY4	0.003261	0.58428
Q96CG8	CTHR1	0.025101	0.566396
Q9H1A3	METL9	0.001299	0.564429
P49458	SRP09	0.000309	0.560234
Q9BQ61	TRIR	0.017413	0.548323
Q9P2B2	FPRP	0.018787	0.546593
P62633	CNBP	0.001287	0.542687
P05106	ITB3	0.000878	0.539007
P78324	SHPS1	0.048451	0.525578
P37268	FDFT	0.019138	0.524083
Q5DJT8	CT452	0.010651	0.521466
Q9NYH9	UTP6	0.038279	0.519524
P39687	AN32A	0.017452	0.512041
P13987	CD59	0.038679	0.510726
O14737	PDCD5	0.043304	0.509208
P07919	QCR6	0.04323	0.508671
P09972	ALDOC	0.001731	0.501581
Q14257	RCN2	0.004257	0.50124
O75223	GGCT	0.013719	0.490795
P48637	GSHB	0.005356	0.480992
P11717	MPRI	0.016048	0.459035
P56693	SOX10	0.012797	0.457636
Q13247	SRSF6	0.009643	0.457274
P09496	CLCA	0.00876	0.450172
Q92804	RBP56	0.006124	0.445256
Q9Y4F1	FARP1	0.013054	0.444618

Q8TD55	PKHO2	0.040625	0.437377
Q9UNF1	MAGD2	0.014288	0.436904
P35613	BASI	0.006703	0.436014
Q9BTT0	AN32E	0.017134	0.431988
P01011	AACT	0.040909	0.42466
Q6P6C2	ALKB5	0.026318	0.404488
Q9Y5L4	TIM13	0.026513	0.404321
P58215	LOXL3	0.042154	0.404313
P61956	SUMO2	0.016122	0.401666
P21399	ACOC	0.01783	0.392555
P29372	3MG	0.031324	0.391558
Q9NPH3	IL1AP	0.003397	0.388479
O43493	TGON2	0.020201	0.387188
P46013	KI67	0.033865	0.383663
Q6FIF0	ZFAN6	0.000961	0.382656
P37108	SRP14	0.016285	0.38238
O43765	SGTA	0.044033	0.380498
Q9Y547	IFT25	0.018644	0.377297
Q8IVM0	CCD50	0.016716	0.373841
Q14573	ITPR3	0.043538	0.373825
Q15369	ELOC	0.035666	0.369593
P40126	TYRP2	0.029318	0.365208
P16949	STMN1	0.00155	0.36384
O15240	VGf	0.026862	0.355572
Q9Y4E6	WDR7	0.006703	0.355381
Q8WW12	PCNP	0.019083	0.343678
P13686	PPA5	0.030844	0.33929
Q6UWP7	LCLT1	0.010529	0.339008
O60701	UGDH	0.003535	0.337895
Q14195	DPYL3	0.045194	0.337569
P13674	P4HA1	0.002918	0.335944
O43639	NCK2	0.029973	0.334742
P49023	PAXI	0.00138	0.333877
Q16563	SYPL1	0.019447	0.330032
Q16576	RBBP7	0.013376	0.32756

Q16831	UPP1	0.006742	0.325795
P14927	QCR7	0.009872	0.325232
Q13409	DC1I2	0.014252	0.325115
Q13867	BLMH	0.01103	0.323396
P36871	PGM1	0.00023	0.315533
Q9NZB2	F120A	0.007127	0.312474
Q9UNL2	SSRG	0.017969	0.304611
Q15637	SF01	0.025784	0.304336
O95340	PAPS2	0.004734	0.302416
Q9ULX9	MAFF	0.025674	0.301318
Q8WTV0	SCRB1	0.048951	0.298834
O75937	DNJC8	0.001608	0.296543
Q9UKK9	NUDT5	0.002981	0.294797
P08670	VIME	0.016182	0.294037
Q8WXF1	PSPC1	0.001836	0.292966
P18669	PGAM1	0.010975	0.291984
P13798	ACPH	0.002501	0.287687
Q14019	COTL1	0.024547	0.287041
Q01105	SET	0.010476	0.285494
Q9ULC4	MCTS1	0.012931	0.280534
P15586	GNS	0.023037	0.276065
Q9BUR5	MIC26	0.016624	0.27229
Q8WXI9	P66B	0.012227	0.270615
Q9BRA2	TXD17	0.009976	0.263962
Q05655	KPCD	0.0205	0.263539
P12955	PEPD	0.014702	0.262759
P13797	PLST	0.03608	0.262364
P06756	ITAV	0.035313	0.261912
Q13596	SNX1	0.014992	0.255748
Q13126	MTAP	0.005234	0.252187
P14550	AK1A1	0.00671	0.250232
O75874	IDHC	0.045097	0.248819
O60568	PLOD3	0.029738	0.246437
P19174	PLCG1	0.038502	0.242987
Q06830	PRDX1	0.003314	0.241775

Q06203	PUR1	0.039249	0.240645
Q9UKM7	MA1B1	0.043436	0.239575
Q12792	TWF1	0.020872	0.238862
P52789	HXK2	0.001106	0.232859
Q9Y274	SIA10	0.024869	0.232768
Q86U42	PABP2	0.018472	0.224794
P21912	SDHB	0.009681	0.223415
P51665	PSMD7	0.002005	0.223338
P10644	KAP0	0.031271	0.223049
Q96HE7	ERO1A	0.015646	0.217316
Q92974	ARHG2	0.03761	0.211371
Q9Y5S9	RBM8A	0.005965	0.207253
P62312	LSM6	0.042376	0.199986
P22061	PIMT	0.035786	0.196499
Q9Y2B0	CNPY2	0.018889	0.195768
O00273	DFFA	0.029602	0.192076
Q6UX53	MET7B	0.025642	0.187469
Q01082	SPTB2	0.000604	0.187038
Q06210	GFPT1	0.007049	0.177276
P05198	IF2A	0.025548	0.174579
P51153	RAB13	0.017704	0.173389
P42224	STAT1	0.03588	0.172688
P35659	DEK	0.015978	0.171312
Q9H0D6	XRN2	0.03622	0.169211
P07741	APT	0.017997	0.166132
Q4VC31	CCD58	0.034917	0.164063
P55145	MANF	0.044834	0.162221
Q9Y2Z0	SGT1	0.017446	0.160092
Q15645	PCH2	0.032136	0.159827
P78347	GTF2I	0.044777	0.157136
P46926	GNPI1	0.047471	0.154625
P61221	ABCE1	0.02318	0.131287
Q9BUJ2	HNRL1	0.025323	0.116761
O00232	PSD12	0.029144	0.107798
P20839	IMDH1	0.020639	0.106165

P47756	CAPZB	0.00386	0.10514
O60884	DNJA2	0.033478	0.085171
P50395	GDIB	0.028906	-0.0592
P49721	PSB2	0.017669	-0.06228
P41250	GARS	0.028225	-0.10348
P21281	VATB2	0.018809	-0.10729
O15144	ARPC2	0.008985	-0.13313
Q14108	SCRB2	0.045901	-0.13537
P50213	IDH3A	0.047285	-0.13738
O43684	BUB3	0.036529	-0.13847
P62249	RS16	0.034043	-0.13898
P55072	TERA	0.045815	-0.14324
P63000	RAC1	0.03188	-0.14451
P18031	PTN1	0.04978	-0.15098
P06865	HEXA	0.013707	-0.15302
P49588	SYAC	0.040214	-0.15485
P39019	RS19	0.016622	-0.15499
P51149	RAB7A	0.04283	-0.15673
O75083	WDR1	0.037658	-0.15798
O60716	CTND1	0.008892	-0.15847
Q16891	MIC60	0.038181	-0.1603
Q9Y4P3	TBL2	0.000155	-0.16391
O15533	TPSN	0.037277	-0.16437
Q12849	GRSF1	0.001338	-0.16447
P62241	RS8	0.006826	-0.16509
Q5VZM2	RRAGB	0.04016	-0.166
Q13435	SF3B2	0.029616	-0.16734
P11142	HSP7C	0.04917	-0.16739
Q6PKG0	LARP1	0.013962	-0.16821
Q9NX63	MIC19	0.030366	-0.16916
Q99623	PHB2	0.045453	-0.17236
Q12965	MYO1E	0.021143	-0.1736
Q99798	ACON	0.030539	-0.17676
P62995	TRA2B	0.042058	-0.17695
P26196	DDX6	0.005358	-0.17723

P61313	RL15	0.010871	-0.18238
Q96199	SUCB2	0.028028	-0.18256
P00387	NB5R3	0.021526	-0.18268
P35637	FUS	0.047957	-0.18339
P57088	TMM33	0.041234	-0.18358
P23246	SFPQ	0.011536	-0.18409
P62917	RL8	0.004546	-0.1845
Q9Y696	CLIC4	0.036577	-0.18521
Q04837	SSBP	0.024941	-0.18615
O15145	ARPC3	0.004198	-0.18624
Q92973	TNPO1	0.038562	-0.19034
Q13310	PABP4	0.005635	-0.19128
Q99442	SEC62	0.024826	-0.19299
P29692	EF1D	0.021631	-0.19487
P13639	EF2	0.010032	-0.20017
Q13283	G3BP1	0.021941	-0.20044
P47897	SYQ	0.007978	-0.201
Q16629	SRSF7	0.02076	-0.20108
O75947	ATP5H	0.013056	-0.20295
P05388	RLA0	0.001907	-0.20409
Q10713	MPPA	0.027536	-0.20447
P46782	RS5	0.006683	-0.2061
Q9Y3D9	RT23	0.011028	-0.2067
Q9H9B4	SFXN1	0.047422	-0.20721
P53992	SC24C	0.023017	-0.20753
P55010	IF5	0.022236	-0.20766
P62244	RS15A	0.045855	-0.20768
Q92979	NEP1	0.027456	-0.20772
P62269	RS18	0.003499	-0.20856
Q96QK1	VPS35	0.022001	-0.20858
P36542	ATPG	0.035608	-0.20886
P23396	RS3	0.00318	-0.20942
P37198	NUP62	0.034308	-0.21032
Q14974	IMB1	0.018837	-0.21045
Q15149	PLEC	0.011621	-0.21144

P30050	RL12	6.67E-05	-0.21428
Q9Y277	VDAC3	0.006198	-0.21435
P84103	SRSF3	0.018812	-0.21441
P06396	GELS	0.019247	-0.21601
Q9UMS4	PRP19	0.019835	-0.21688
Q99536	VAT1	0.029974	-0.21691
P60842	IF4A1	0.005572	-0.21713
Q1KMD3	HNRL2	0.023314	-0.21955
Q01650	LAT1	0.047349	-0.22036
P46777	RL5	0.000788	-0.22251
Q15286	RAB35	0.01777	-0.22415
P07686	HEXB	0.003024	-0.22489
P49207	RL34	0.037562	-0.22498
P34897	GLYM	0.023369	-0.2254
Q15437	SC23B	0.0448	-0.22545
P27694	RFA1	0.037209	-0.2265
O95816	BAG2	0.014634	-0.22802
O75439	MPPB	0.016321	-0.22817
P62829	RL23	0.012677	-0.2284
P62753	RS6	0.033366	-0.22876
Q99615	DNJC7	0.008836	-0.2302
P08865	RSSA	0.001528	-0.23172
Q9Y490	TLN1	0.021277	-0.23215
P19367	HXK1	0.000699	-0.23256
Q9BXK5	B2L13	0.029299	-0.23416
Q13561	DCTN2	0.033425	-0.23448
P08708	RS17	0.000456	-0.23479
P78344	IF4G2	0.012831	-0.23498
P11387	TOP1	0.013876	-0.23587
Q9H845	ACAD9	0.027832	-0.23631
Q13423	NNTM	0.032963	-0.23727
P25705	ATPA	0.02864	-0.23838
Q13813	SPTN1	0.001678	-0.2394
Q92734	TFG	0.023061	-0.24123
O75352	MPU1	0.044951	-0.24324

Q9Y399	RT02	0.048367	-0.24575
P38646	GRP75	0.019785	-0.24694
Q7KZF4	SND1	0.003063	-0.24726
Q53H12	AGK	0.046124	-0.2478
P40926	MDHM	0.02755	-0.24801
Q13505	MTX1	0.024864	-0.24915
Q9P2E9	RRBP1	0.030568	-0.24944
P55809	SCOT1	0.002913	-0.25327
P21333	FLNA	0.032491	-0.25363
P36957	ODO2	0.022839	-0.25536
P62906	RL10A	0.028321	-0.25547
P07339	CATD	0.018256	-0.25566
Q9Y4W6	AFG32	0.014044	-0.25637
Q7Z2W9	RM21	0.040866	-0.26074
O95197	RTN3	0.012027	-0.26082
P15880	RS2	0.000443	-0.26085
P25398	RS12	0.009707	-0.26119
O43707	ACTN4	0.000542	-0.26202
P27816	MAP4	0.007557	-0.26289
P62910	RL32	0.027485	-0.26329
P07203	GPX1	0.009145	-0.26414
P16435	NCPR	0.039588	-0.26424
Q05682	CALD1	0.018408	-0.26759
P62424	RL7A	0.000445	-0.26784
Q04637	IF4G1	0.012596	-0.26816
O00571	DDX3X	0.005711	-0.26829
Q13277	STX3	0.005682	-0.26952
P17844	DDX5	0.008768	-0.27
P35268	RL22	0.026058	-0.27109
P62888	RL30	0.020127	-0.27142
Q9UHQ9	NB5R1	0.007162	-0.27421
P62993	GRB2	0.012614	-0.2755
O43390	HNRPR	0.024171	-0.27591
Q92598	HS105	0.000454	-0.27662
P24752	THIL	0.010787	-0.2796

P17655	CAN2	0.005973	-0.28209
P68032	ACTC	0.045855	-0.28298
P08758	ANXA5	0.002112	-0.28434
Q96CS3	FAF2	0.030506	-0.28553
P53384	NUBP1	0.014063	-0.28651
Q969V3	NCLN	0.019413	-0.28665
O43795	MYO1B	0.035077	-0.28828
O94766	B3GA3	0.026509	-0.28895
P18124	RL7	0.001666	-0.29074
P31153	METK2	0.00346	-0.29086
P06576	ATPB	0.017094	-0.29108
Q86W42	THOC6	0.034078	-0.29133
Q6NUK1	SCMC1	0.031356	-0.29373
Q8NBX0	SCPDL	0.021982	-0.29487
P35221	CTNA1	0.006516	-0.2959
Q9UJZ1	STML2	0.007338	-0.29614
Q9NPD3	EXOS4	0.035895	-0.29717
P62899	RL31	0.013873	-0.29786
Q8NHP8	PLBL2	0.01625	-0.29802
Q8TDD1	DDX54	0.020494	-0.29929
Q9HCD5	NCOA5	0.030451	-0.29972
Q13637	RAB32	0.019891	-0.30059
P13693	TCTP	0.01172	-0.30272
Q9NR30	DDX21	0.00489	-0.30339
Q9UIJ7	KAD3	0.025949	-0.30508
P27105	STOM	0.007435	-0.30586
P62847	RS24	0.018074	-0.30843
O43464	HTRA2	0.038142	-0.30925
Q08211	DHX9	0.005695	-0.30959
P52292	IMA1	0.040528	-0.31072
P61247	RS3A	0.002493	-0.31333
Q8NOX7	SPART	0.046703	-0.31495
Q7Z434	MAVS	0.048712	-0.31557
P32969	RL9	0.000295	-0.31598
Q53FA7	QORX	0.025199	-0.31749

Q9GZR7	DDX24	0.009881	-0.31911
Q9NZJ7	MTCH1	0.019373	-0.31961
P62280	RS11	0.007761	-0.32088
P04062	GLCM	0.007263	-0.32147
P82933	RT09	0.021843	-0.32201
P68104	EF1A1	0.001366	-0.32238
P51798	CLCN7	0.013514	-0.32378
P12004	PCNA	0.00388	-0.32401
Q9NX62	IMPA3	0.016777	-0.32586
Q9NPA0	EMC7	0.003152	-0.32741
O43175	SERA	5.4E-05	-0.32762
P36578	RL4	0.004991	-0.32785
P55084	ECHB	0.014811	-0.32846
P82930	RT34	0.004243	-0.32914
P16401	H15	0.024504	-0.32922
P82650	RT22	0.01797	-0.3305
P50748	KNTC1	0.008837	-0.33183
Q16881	TRXR1	0.042867	-0.3327
P61604	CH10	0.011102	-0.33275
O76021	RL1D1	0.018943	-0.33677
P46459	NSF	0.0165	-0.33701
P61421	VA0D1	0.015013	-0.33724
P40429	RL13A	0.001143	-0.33954
P11498	PYC	0.030509	-0.34024
Q6NTF9	RHBD2	0.016082	-0.34081
Q14847	LASP1	0.004263	-0.34116
Q15424	SAFB1	0.030934	-0.34171
Q96IJ6	GMPPA	0.028918	-0.34245
P61201	CSN2	0.003948	-0.34278
P18621	RL17	0.000911	-0.34299
P26641	EF1G	0.003999	-0.34326
Q9BWU0	NADAP	0.012331	-0.34328
Q9Y512	SAM50	0.026876	-0.34373
Q13200	PSMD2	0.011863	-0.34376
Q9Y3U8	RL36	0.014033	-0.34637

P26572	MGAT1	0.043781	-0.3465
Q07020	RL18	0.001593	-0.34865
O60784	TOM1	0.024424	-0.3515
Q12769	NU160	0.020101	-0.35321
P43007	SATT	0.00545	-0.35572
Q8WUM4	PDC6I	0.031996	-0.35715
P47914	RL29	0.043621	-0.35792
Q9Y2S2	CRYL1	0.014166	-0.36029
P39023	RL3	0.019889	-0.36033
Q9C0C9	UBE2O	0.028827	-0.36112
Q9NW13	RBM28	0.000553	-0.36137
Q02218	ODO1	0.022665	-0.36189
P00505	AATM	0.001346	-0.3622
Q9BT22	ALG1	0.032628	-0.36452
P02545	LMNA	0.00977	-0.36481
P62913	RL11	2.19E-05	-0.36546
P40939	ECHA	0.031964	-0.36584
P08195	4F2	0.00137	-0.36609
Q9UG63	ABCF2	0.012097	-0.36786
Q8NBU5	ATAD1	0.0154	-0.36848
Q13838	DX39B	0.047822	-0.37653
P26358	DNMT1	0.029367	-0.38048
Q9Y679	AUP1	0.010798	-0.38141
P25205	MCM3	0.016196	-0.38208
P54886	P5CS	0.011084	-0.3829
Q9BYN8	RT26	0.009221	-0.38291
P11940	PABP1	0.001781	-0.38505
Q15050	RRS1	0.033867	-0.38569
Q9UHY1	NRBP	0.015066	-0.38621
Q00325	MPCP	0.005943	-0.39155
P60981	DEST	0.00018	-0.39315
P26440	IVD	0.015372	-0.39457
P62277	RS13	0.001087	-0.39665
Q9NQC3	RTN4	0.009548	-0.39724
P04083	ANXA1	0.012193	-0.40119

P82675	RT05	0.013961	-0.40655
Q9H0A0	NAT10	0.02112	-0.40739
Q8IY81	SPB1	0.035067	-0.41118
P08574	CY1	0.018016	-0.41276
Q9H936	GHC1	0.011892	-0.41393
Q9H074	PAIP1	0.026504	-0.41474
Q9UNH7	SNX6	0.029616	-0.41544
O75340	PDCD6	0.049943	-0.41571
P06737	PYGL	0.001919	-0.41861
P18085	ARF4	0.003533	-0.42362
P46781	RS9	0.003506	-0.42392
P18206	VINC	0.000399	-0.42992
Q6WKZ4	RFIP1	0.043445	-0.43412
Q12765	SCRN1	0.031035	-0.43614
Q9Y3T9	NOC2L	0.007317	-0.43877
Q9H6F5	CCD86	0.000608	-0.44031
Q9BVP2	GNL3	0.00377	-0.44148
P09525	ANXA4	0.037981	-0.44422
P38606	VATA	0.002576	-0.44426
Q71UI9	H2AV	0.043061	-0.44944
O75691	UTP20	0.002231	-0.45161
P67936	TPM4	0.016354	-0.45413
P23786	CPT2	0.021461	-0.4547
P43121	MUC18	0.019058	-0.45568
P63010	AP2B1	0.01131	-0.45575
Q96C57	CSTOS	0.011834	-0.45647
Q9BZL1	UBL5	0.015555	-0.46176
P14174	MIF	0.012306	-0.46181
Q9Y3L3	3BP1	0.003941	-0.46205
Q15758	AAAT	0.044976	-0.46529
P26373	RL13	0.002638	-0.46735
Q9BRF8	CPPED	0.03162	-0.46852
Q14192	FHL2	0.006564	-0.46961
P49585	PCY1A	0.047641	-0.4727
Q6NUQ4	TM214	0.017575	-0.47333

P24941	CDK2	0.027502	-0.47416
P31689	DNJA1	0.005811	-0.48289
Q9Y520	PRC2C	0.009191	-0.48509
P46087	NOP2	0.014454	-0.48614
P17858	PFKAL	0.048601	-0.48849
Q96GD4	AURKB	0.045194	-0.48854
Q92506	DHB8	0.038176	-0.48967
P30837	AL1B1	0.01204	-0.49032
P01903	DRA	0.03052	-0.49364
Q7Z3E5	ARMC9	0.022721	-0.49725
Q15397	PUM3	0.041556	-0.49734
Q9BRX2	PELO	0.024595	-0.50068
Q9NNW7	TRXR2	0.034673	-0.50104
Q9GZQ8	MLP3B	0.008308	-0.50209
P62750	RL23A	0.013473	-0.50301
P35579	MYH9	0.000109	-0.50314
P19525	E2AK2	0.000146	-0.5045
P22830	HEMH	0.041047	-0.50478
P12814	ACTN1	0.003906	-0.50544
P22570	ADRO	0.047516	-0.50753
Q9BRG1	VPS25	0.041989	-0.50984
O75127	PTCD1	0.010378	-0.51229
Q9Y4C8	RBM19	0.024383	-0.51727
Q9H3G5	CPVL	0.000245	-0.51988
P38432	COIL	0.005822	-0.52522
P0DMV9	HS71B	0.000987	-0.52868
P40616	ARL1	0.030545	-0.53271
Q9NP58	ABCB6	0.03588	-0.53523
Q15070	OXA1L	0.045058	-0.53636
Q02127	PYRD	0.021448	-0.53979
Q9H6R4	NOL6	0.026301	-0.54147
Q7L2E3	DHX30	0.0075	-0.54571
P30622	CLIP1	0.001936	-0.54878
Q03701	CEBPZ	0.000654	-0.55081
Q9Y314	NOSIP	0.046586	-0.55333

Q96KR1	ZFR	0.026775	-0.56363
Q93050	VPP1	0.011112	-0.56754
Q9UPZ3	HPS5	0.018162	-0.58166
Q9Y5S1	TRPV2	0.014912	-0.58399
Q5JTH9	RRP12	0.008227	-0.59096
O75955	FLOT1	0.000187	-0.59349
Q7Z2T5	TRM1L	0.045719	-0.59448
P07996	TSP1	0.011629	-0.59839
Q96GQ7	DDX27	0.00014	-0.60606
O75131	CPNE3	0.047515	-0.6131
Q96HC4	PDLI5	0.002436	-0.61537
Q9NY12	GAR1	0.005774	-0.61623
Q8NF37	PCAT1	0.003593	-0.62116
Q9Y646	CBPQ	0.027522	-0.62323
Q13488	VPP3	0.013244	-0.62346
Q9BXS6	NUSAP	0.020694	-0.62506
Q6P1L8	RM14	0.0041	-0.63198
Q15942	ZYX	0.000366	-0.6474
Q9UHB6	LIMA1	0.01122	-0.65934
Q9BSH5	HDHD3	0.026002	-0.67531
O00567	NOP56	0.003548	-0.67702
Q15654	TRIP6	0.005454	-0.68323
Q9Y5X2	SNX8	0.036904	-0.68619
O95169	NDUB8	0.010191	-0.69659
Q5J8M3	EMC4	0.024357	-0.70194
P11216	PYGB	0.003913	-0.71174
Q08945	SSRP1	0.009308	-0.71333
Q27J81	INF2	0.031444	-0.71457
Q13601	KRR1	0.024608	-0.73013
Q9NY93	DDX56	0.000115	-0.73241
O14773	TPP1	0.003728	-0.74704
Q14978	NOLC1	0.000307	-0.7501
O95478	NSA2	0.001453	-0.75402
P51553	IDH3G	0.032853	-0.76137
Q9P0J0	NDUAD	0.039718	-0.76218

Q9H5Q4	TFB2M	0.000865	-0.76354
Q9Y3E0	GOT1B	0.005946	-0.79324
Q9GZL7	WDR12	0.005955	-0.79439
Q9BSC4	NOL10	0.008406	-0.80365
Q15007	FL2D	0.046941	-0.80956
P48507	GSH0	0.002179	-0.80975
Q96S97	MYADM	0.002453	-0.81127
Q9NQH7	XPP3	0.043811	-0.82993
P02751	FINC	0.000163	-0.83933
P17096	HMGA1	0.033481	-0.84845
Q9Y2X3	NOP58	0.001259	-0.84947
Q15269	PWP2	0.038889	-0.86117
P04818	TYSY	0.009574	-0.8655
Q9Y5B9	SP16H	0.017429	-0.86997
Q13418	ILK	0.004712	-0.88098
Q6DKI1	RL7L	0.023087	-0.8875
P35219	CAH8	0.024926	-0.89607
Q8IXI2	MIRO1	0.038352	-0.89688
P08243	ASNS	0.00769	-0.9049
Q6IN84	MRM1	0.042492	-0.90763
O95273	CCDB1	0.028354	-0.9242
P49750	YLPM1	0.01565	-0.92465
Q6NUQ1	RINT1	0.032207	-0.95133
Q99439	CNN2	0.000525	-0.96672
Q96ER9	CCD51	0.003087	-0.97806
Q4J6C6	PPCEL	0.022994	-0.98718
Q15061	WDR43	0.008306	-0.99649
Q13501	SQSTM	0.000209	-1.00325
Q9BU89	DOHH	0.03085	-1.01
Q9NX24	NHP2	0.028362	-1.01029
P05204	HMG2	0.001656	-1.0281
O00400	ACATN	0.007217	-1.02893
Q92629	SGCD	0.047494	-1.03231
Q99698	LYST	0.044968	-1.04467
P98194	AT2C1	0.013971	-1.05651

Q02878	RL6	0.000274	-1.07444
O00461	GOLI4	0.013359	-1.08058
Q15276	RABE1	0.035374	-1.08726
Q9NZM1	MYOF	0.001081	-1.09986
P04183	KITH	0.000689	-1.10201
P22087	FBRL	0.003692	-1.10827
Q9ULH0	KDIS	0.018467	-1.12743
P52926	HMGA2	0.013518	-1.14359
Q9BZF9	UACA	0.006929	-1.14384
Q14254	FLOT2	0.009248	-1.15139
P46199	IF2M	0.033396	-1.15292
P60903	S10AA	0.026629	-1.15373
Q9H9A5	CNO10	0.04665	-1.15591
P31350	RIR2	0.001268	-1.16665
Q02338	BDH	0.003296	-1.26374
Q99541	PLIN2	0.006591	-1.33525
Q9BZF1	OSBL8	0.033759	-1.38601
Q9BRT6	LLPH	0.040557	-1.39097
O75794	CD123	0.0287	-1.40746
Q9Y385	UB2J1	0.00095	-1.42514
Q6IN85	P4R3A	0.009335	-1.48696
P57737	CORO7	0.012332	-1.48834
Q9UJY1	HSPB8	0.016598	-1.54866
Q96HW7	INT4	0.005581	-1.56796
Q09666	AHNK	0.00061	-1.61025
O43818	U3IP2	0.006424	-1.61792
A4D1P6	WDR91	0.001555	-1.6976
O43896	KIF1C	0.017786	-1.72003
P07355	ANXA2	0.000904	-1.84038
Q9Y6A9	SPCS1	0.017031	-1.91369
Q9BZQ8	NIBAN	0.002861	-1.96795
P08133	ANXA6	1.53E-06	-2.47737
P09601	HMOX1	0.002665	-2.87493
P69905	HBA	0.000793	-2.8976
O00566	MPP10	8.64E-06	-2.94202

FM3 cell ECM mass spectrometry data: FS- 24h vs TCP-24h (n=6)			
UniProtKB	Protein ID	p-value	Log2FC
O95834	EMAL2	0.001231	4.008284
P13073	COX41	0.006703	2.098046
P63241	IF5A1	0.005943	1.901673
Q15233	NONO	0.012029	1.418885
P00558	PGK1	0.012302	1.338884
P68371	TBB4B	0.04244	1.266762
P69905	HBA	0.015889	1.034933
O95445	APOM	0.045781	1.011684
P01008	ANT3	9.43E-05	0.986875
P61224	RAP1B	0.005408	0.72535
P14618	KPYM	0.005401	0.571236
P62820	RAB1A	0.03946	0.493352
P02649	APOE	0.041008	0.490942
P35527	K1C9	0.005659	-0.37606
Q15582	BGH3	0.002198	-0.47226
P35579	MYH9	0.01317	-0.63104
P38646	GRP75	0.042924	-0.76503
P09651	ROA1	0.026557	-0.79567
P99999	CYC	0.000941	-0.83176
P22626	ROA2	0.005967	-0.83624
P62857	RS28	0.023465	-0.88566
Q99623	PHB2	0.000132	-0.91602
P07195	LDHB	0.02369	-1.03065
P46783	RS10	0.015869	-1.2417
P02751	FINC	0.003016	-1.2424
Q96AG4	LRC59	0.018471	-1.26239
Q99880	H2B1L	0.021383	-1.29833
P39019	RS19	0.003057	-1.67985
Q99988	GDF15	7.97E-06	-1.96205
P08670	VIME	1.76E-05	-2.02051
P62805	H4	0.000991	-2.11465
P04004	VTNC	0.000317	-2.12173

P24539	AT5F1	0.007953	-2.39174
P35625	TIMP3	2.49E-05	-3.40401

FM3 cell ECM mass spectrometry data: FS-72h vs FS-24h (n=6)			
UniProtKB	Protein ID	p-value	Log2FC
P35625	TIMP3	6.4E-05	5.029844
P24539	AT5F1	0.046345	2.758858
P02787	TRFE	0.030503	2.559066
P22626	ROA2	9.58E-05	2.552674
P08670	VIME	3.28E-12	2.211979
Q96AG4	LRC59	0.020267	2.111244
P39019	RS19	1.13E-08	2.100408
P48047	ATPO	0.040028	2.09439
P11940	PABP1	0.023942	2.073463
P00750	TPA	0.000108	1.950184
P09651	ROA1	4.97E-05	1.920966
Q15365	PCBP1	0.016143	1.902189
P13073	COX41	6.94E-06	1.665185
P46783	RS10	0.014744	1.662312
Q92743	HTRA1	0.000166	1.487817
P17844	DDX5	0.015139	1.410857
P62857	RS28	0.000306	1.315569
P04004	VTNC	5.28E-05	1.306803
Q7KZF4	SND1	0.001348	1.274577
P07093	GDN	0.000238	1.227039
P62937	PPIA	0.046281	1.20755
Q9Y6C2	EMIL1	0.027432	1.198163
P36542	ATPG	0.00685	1.091775
Q8WUJ3	CEMIP	0.001691	1.086306
P02765	FETUA	0.02738	1.007953
Q15582	BGH3	0.000158	1.004404
P02649	APOE	6.3E-05	0.879068
P38646	GRP75	0.003194	0.862435
P21333	FLNA	0.024652	0.785443

P12273	PIP	0.031112	0.70278
P29401	TKT	0.014908	0.663072
P04406	G3P	0.002206	0.645216
P62820	RAB1A	0.003617	0.583994
P11142	HSP7C	0.028822	0.561991
P35579	MYH9	0.015217	0.370957
P52907	CAZA1	0.039515	-0.63143
P12814	ACTN1	0.017664	-0.78996
P61604	CH10	0.047048	-0.85552
P37108	SRP14	0.000997	-0.92572
Q99536	VAT1	0.016233	-1.26871
O95445	APOM	0.016563	-1.31863
P61586	RHOA	0.02622	-1.82016
Q15366	PCBP2	0.042417	-2.55202
Q9NX63	MIC19	0.007476	-3.32373

FM3 cell lysate mass spectrometry: DB2313-treated vs untreated (n=3)		
UniProtKB	p-value	log2FC
Q5PRF9	0.018411	1.26399
P61981	0.030242	1.2639
O95406	0.014498	1.101304
Q149N8	0.043609	1.086865
O00391	0.011251	1.076523
P57721	0.048664	1.00273
O95214	0.003523	1.001769
P07196	0.041212	0.925853
P31943	0.000912	0.88337
P41221	0.016428	0.882783
O95716	0.014757	0.857449
P08138	0.024333	0.844993
P26038	0.044679	0.763912
O15484	0.042225	0.755683
Q9HBA0	0.022177	0.728135

P35869	0.021865	0.727278
O95248	0.026368	0.715089
P30408	0.016503	0.6972
Q9BQ15	0.029908	0.682839
Q92685	0.049389	0.680124
Q9NRP2	0.007004	0.665575
Q8NE01	0.026175	0.618929
P26006	0.019792	0.615822
P04271	0.013125	0.602925
O00512	0.012297	0.599143
P29320	0.023445	0.584016
Q8IZ52	0.010901	0.582801
Q99879	0.02498	0.582173
Q9UBF2	0.00734	0.581197
Q8TCT8	0.011027	0.565703
P23634	0.046004	0.555111
P06703	0.025668	0.554193
O43252	0.035152	0.545806
Q9Y5U9	0.020522	0.540479
P20020	0.032828	0.536119
Q9H4I9	0.03265	0.533066
O60637	0.020311	0.529333
Q9BW72	0.036775	0.522726
P60059	0.048656	0.500947
Q96K49	0.006767	0.489626
P31327	0.015284	0.480442
P11274	0.041656	0.479713
Q13795	0.041116	0.478418
P04233	0.028698	0.477138
Q92522	0.047823	0.474518
Q9UJU2	0.040977	0.471372
Q8N6G5	0.011334	0.469709
P21291	0.018407	0.468348
Q6UX53	0.001019	0.461114
P28347	0.003404	0.458429

Q8WUM9	0.009508	0.458217
Q5JTV8	0.028705	0.454741
Q8IVF7	0.017976	0.453755
Q9NP64	0.008712	0.452267
Q9UPN3	0.013578	0.450958
P43007	0.021169	0.450412
P61803	0.030051	0.442908
Q9ULM3	0.011638	0.427337
Q9BPZ3	0.025205	0.426758
O15379	0.023968	0.426597
P84074	0.008138	0.426215
Q8TCT9	0.03446	0.423243
Q7L5N7	0.014066	0.409424
Q9NR28	0.018446	0.409168
P11217	0.007975	0.401555
Q96A26	0.01018	0.400648
Q53EU6	0.01899	0.399075
P04899	0.012095	0.386816
P48509	0.003078	0.384618
P62834	0.014965	0.383387
Q9H201	0.023975	0.382378
Q96LJ7	0.015557	0.37798
O94855	0.010378	0.374068
Q13033	0.026633	0.372495
Q14999	0.033321	0.37066
O95197	0.039396	0.367834
Q96AQ6	0.00979	0.365563
Q15035	0.009321	0.363541
P37235	0.010341	0.363442
Q9HCJ1	0.0156	0.36282
Q15149	0.002912	0.362097
Q86UU1	0.00423	0.361799
Q14738	0.023563	0.360526
Q15361	0.028544	0.358968
P50443	0.028771	0.355455

A1X283	0.024652	0.354116
Q96RU3	0.004055	0.351446
P08134	0.000994	0.343742
Q8WVC6	0.030853	0.336732
O00213	0.014553	0.334897
A8MT19	0.044214	0.334549
Q8IY63	0.046784	0.33189
Q9C004	0.013305	0.330049
P49748	0.004394	0.329679
P60033	0.011941	0.325678
Q14240	0.044242	0.324366
Q9C0C4	0.013357	0.322705
P58215	0.049404	0.319529
Q14108	0.008424	0.316974
Q9P2N7	0.04362	0.316523
Q9Y5V3	0.017778	0.315349
Q5BJH7	0.033294	0.315054
Q9ULQ0	0.002149	0.313763
Q9H4M9	0.049169	0.313525
O60488	0.045092	0.312816
Q8TCU6	0.001592	0.311877
Q07954	0.046467	0.309499
Q7Z6E9	0.012967	0.305107
Q86X83	0.04104	0.30474
P04066	0.034901	0.301783
P62873	0.008436	0.298868
P49023	0.038769	0.298513
P11233	0.003655	0.297987
P13987	0.038519	0.297794
Q9Y5B6	0.00495	0.290084
P54753	0.02983	0.288322
P62873	0.041933	0.285801
Q7LG56	0.002226	0.285532
Q99643	0.007932	0.285258
Q9Y5Z0	0.008869	0.284828

Q96CM8	0.017099	0.283968
Q14192	0.01753	0.282724
Q9H9F9	0.042133	0.281753
Q9BQB6	0.004632	0.279613
Q99538	0.017202	0.275011
O95573	0.010946	0.274948
O43707	0.02034	0.27448
P61421	0.02644	0.273357
Q969P0	0.020168	0.272173
Q96EL2	0.033186	0.271204
Q8WW01	0.04559	0.2702
Q96FZ2	0.013777	0.268287
O75354	0.043354	0.267264
Q8IV08	0.011386	0.265178
Q6UVK1	0.024001	0.265135
Q14573	0.038792	0.26209
Q9H0V9	0.018162	0.261818
Q13469	0.027897	0.259626
P55061	0.033129	0.259604
Q7L1Q6	0.002296	0.257484
Q9UHK6	0.039631	0.257261
Q12907	0.000935	0.25598
Q9P1U0	0.041754	0.252861
Q9UBI6	0.020893	0.252138
P50148	0.012309	0.251035
P63096	0.008523	0.250568
P11488	0.00547	0.249724
Q9H4A5	0.014805	0.249571
P63208	0.001245	0.249128
Q08380	0.001242	0.248391
P21964	0.029074	0.246044
P18074	0.000954	0.245802
O43760	0.007898	0.245632
Q96SI9	0.009292	0.244424
Q15418	0.013345	0.243024

P11387	0.027764	0.241622
Q9UK23	0.01598	0.240181
O60885	0.049586	0.239025
Q9NR12	0.008174	0.238225
Q9NPJ3	0.022878	0.237764
Q53EP0	0.013142	0.235846
Q5T0F9	0.007808	0.234538
O15382	0.017695	0.232848
Q96SN8	0.007212	0.232638
Q53H12	0.002936	0.232096
Q1KMD3	0.014635	0.231283
P53007	0.005516	0.231269
P56378	0.01027	0.230083
P05556	0.043644	0.22975
P42126	0.015336	0.228958
Q5MIZ7	0.036507	0.228317
P07858	0.014749	0.228124
P22830	0.00305	0.226571
O96011	0.004538	0.226486
Q9Y3Q3	0.034502	0.225976
O94973	0.000377	0.225397
O00566	0.035726	0.223199
Q9NXV2	0.044221	0.223023
Q9UBD5	0.01441	0.22281
Q9UHG3	0.02118	0.222222
Q9NX40	0.046594	0.221569
O14773	0.041546	0.220637
P15907	0.005858	0.217276
Q8IWT6	0.007124	0.217026
Q13596	0.041	0.21652
P11177	0.01624	0.215412
Q969Y2	0.044456	0.214395
Q6IAN0	0.027801	0.213967
O75427	0.008005	0.21384
Q16775	0.018802	0.213206

P60468	0.048065	0.212589
Q00013	0.028345	0.212035
Q92947	0.028149	0.211701
Q6NUK1	0.011483	0.211647
P08574	0.013902	0.211479
Q9UHQ9	0.005301	0.210954
P15559	0.006651	0.210849
P00387	0.043809	0.209286
Q9BPW8	0.04138	0.20885
Q66K74	0.029236	0.208429
P40926	0.047151	0.207081
Q9Y6C9	0.034842	0.206539
O15228	0.031287	0.206296
Q6P1M0	0.025978	0.206162
P62879	0.025105	0.205476
Q96TA2	0.019151	0.203633
O15533	0.017916	0.203528
P16615	0.045021	0.201022
Q96HW7	0.03855	0.198629
Q9UKI2	0.02799	0.198627
P62879	0.027874	0.198615
Q9HDC9	0.019243	0.197248
P03905	0.044446	0.19583
P55735	0.032542	0.194845
Q14573	0.043338	0.19455
Q9UK41	0.023111	0.194479
Q9NUS5	0.048365	0.194137
Q8N3U4	0.000441	0.193095
Q12756	0.017429	0.192955
Q9BW92	0.011927	0.192795
P10253	0.006586	0.19187
P07602	0.025201	0.191415
Q8IZL8	0.009244	0.191176
Q9Y697	0.013366	0.190952
Q53GQ0	0.011805	0.190817

O94766	0.032099	0.190132
P26440	0.030076	0.18876
O15118	0.044123	0.187722
Q92820	0.013103	0.187664
Q08426	0.043231	0.187644
Q9Y3Q8	0.017324	0.187041
Q8TEA8	0.027215	0.186784
Q9P2R7	0.002217	0.185624
Q99798	0.038713	0.184678
Q8NBZ7	0.001524	0.184146
Q9UBR2	0.004569	0.183727
Q96HY7	0.027911	0.18371
P00505	0.03091	0.182768
Q93063	0.043456	0.182494
Q02218	0.018349	0.181243
Q69YN4	0.037399	0.179701
Q9BUQ8	0.007011	0.179083
P45880	0.021179	0.178309
Q13547	0.049285	0.177694
O60684	0.018122	0.177197
P27348	0.030404	0.17685
P07686	0.002955	0.176609
Q9GZM5	0.034106	0.174634
Q96DZ1	0.033817	0.173612
Q9BRX8	0.034674	0.173205
P17655	0.001059	0.172402
Q13724	0.029924	0.171911
O00629	0.020729	0.168053
Q6ZMK1	0.028151	0.167659
P35579	0.004093	0.167614
O00217	0.048402	0.167136
Q9GZR7	0.021302	0.166213
Q16698	0.026189	0.166185
P27824	0.024974	0.165974
Q7LBC6	0.031596	0.164664

Q96ST3	0.03014	0.164489
Q8TB61	0.009128	0.163003
Q15155	0.005591	0.162298
O75489	0.044229	0.161864
P46821	0.014688	0.161848
O95696	0.018238	0.161645
Q6NUQ4	0.043323	0.161319
Q96TC7	0.022547	0.159755
Q92597	0.03748	0.159587
O75127	0.030453	0.159295
P48735	0.047013	0.158761
O43674	0.017882	0.158089
P23786	0.004353	0.157928
Q02218	0.044454	0.157727
Q9NUJ1	0.014204	0.157667
O15020	0.00772	0.15685
Q5HYK3	0.015603	0.155267
Q10471	0.011466	0.155163
Q6PI48	0.03073	0.154821
P53990	0.012647	0.154457
Q9UM00	0.006225	0.154217
P55084	0.010937	0.153662
P28290	0.034607	0.152518
O94905	0.035297	0.151097
Q14697	0.034765	0.150148
P78527	0.006298	0.149008
P00367	0.041595	0.148572
P11310	0.029547	0.148276
Q9HD45	0.037494	0.147863
Q15291	0.028437	0.146914
Q9UBG0	0.000432	0.145642
P14625	0.002659	0.1456
P29803	0.000353	0.145537
Q14165	0.001817	0.142446
P31943	0.000218	0.141736

Q9H9Y6	0.012978	0.141295
P21796	0.035632	0.141117
Q14653	0.023662	0.141029
Q9H3G5	0.047831	0.140875
P07237	0.023961	0.139275
Q13115	0.028141	0.138888
Q15067	0.013339	0.138792
Q9BRR6	0.046116	0.137628
Q9NYU2	0.034696	0.137602
Q8IWW6	0.044371	0.137355
Q8IX12	0.007518	0.136956
P32322	0.029546	0.136912
Q9H8H2	0.035879	0.136151
P30048	0.049905	0.136001
P30084	0.030597	0.133931
Q9Y4L1	0.01792	0.132207
P26368	0.039772	0.130615
P04843	0.041415	0.128835
O94804	0.02207	0.128763
P51532	0.026646	0.128443
P13667	0.026646	0.128025
O60216	0.048102	0.127725
P31040	0.041226	0.126661
Q9BVP2	0.005078	0.126145
Q8WWC4	0.012234	0.125631
P17301	0.031	0.125272
Q14019	0.013566	0.125044
Q96CS3	0.045333	0.124997
Q6NZI2	0.039595	0.124691
O60341	0.015325	0.12414
Q6P1K8	0.04421	0.122377
Q14571	0.002658	0.12181
P40939	0.033803	0.12168
P61599	0.044733	0.121485
Q15233	0.000994	0.121008

O43264	0.029749	0.119689
P98175	0.047497	0.119324
O43251	0.033335	0.118118
P45954	0.0032	0.117446
O95071	0.03526	0.116855
P63162	0.044509	0.116448
Q9UIJ7	0.031419	0.11499
P09874	0.046218	0.114085
Q9NY12	0.023806	0.113071
Q5JTH9	0.024631	0.109849
Q9HB40	0.037877	0.10933
P49419	0.015233	0.109077
P49411	0.040271	0.10802
P23246	0.04132	0.106683
Q93050	0.046913	0.106442
O75477	0.022659	0.10459
Q9Y305	0.048285	0.104207
O95340	0.009063	0.103861
Q9UJS0	0.024386	0.103415
Q96MW5	0.045338	0.103073
Q12996	0.001349	0.102239
Q9Y6E0	0.026465	0.10177
Q9UBS4	0.047121	0.099807
Q16836	0.045035	0.099639
O60610	0.036033	0.099503
P51617	0.009288	0.09907
Q9BU23	0.016916	0.099005
Q9Y512	0.011053	0.098648
P23284	0.03432	0.098278
Q13151	0.022782	0.096893
Q9NSE4	0.023253	0.096715
Q16881	0.035547	0.09367
Q92621	0.024435	0.09357
P51659	0.022414	0.093461
Q9UGI8	0.02101	0.093049

P38435	0.030595	0.092218
P48960	0.023145	0.091271
Q96A33	0.003798	0.090691
Q9UMS4	0.006117	0.089696
P62136	0.002558	0.088171
Q8IXT5	0.018352	0.085881
Q8WYA6	0.042819	0.084608
O43252	0.04321	0.084357
Q9NVH1	0.020675	0.083375
P06865	0.03909	0.081135
Q9NX47	0.015278	0.080966
Q7L8L6	0.0104	0.077337
O43837	0.045337	0.07615
Q15020	0.035096	0.075838
P82933	0.016328	0.069409
Q8TBP6	0.026221	0.064263
Q00610	0.029896	0.063941
O75400	0.022271	0.0621
O75909	0.02739	0.053591
P22307	0.040786	0.048463
Q16795	0.031967	0.04431
Q9Y2R5	0.022491	-0.03008
O60506	0.043886	-0.04926
P61163	0.04275	-0.05299
P54577	0.048738	-0.05498
Q99848	0.020084	-0.06512
P78406	0.024444	-0.06875
P31939	0.020744	-0.07087
P49588	0.028415	-0.07115
Q9BR76	0.047882	-0.07329
O00303	0.034617	-0.07353
Q9H2G2	0.044583	-0.07475
Q8NE71	0.010363	-0.07579
Q06124	0.015188	-0.07611
P62750	0.010546	-0.07653

Q96C19	0.035169	-0.07654
Q5VYK3	0.042193	-0.07909
Q8IV48	0.016073	-0.08058
P50281	0.012993	-0.08205
Q9BY32	0.016126	-0.08316
Q13045	0.000646	-0.08477
O00743	0.014079	-0.08657
P35270	0.032758	-0.0891
Q9HC38	0.023911	-0.09178
P23258	0.03221	-0.09357
Q8NFI4	0.048748	-0.09536
O94864	0.015053	-0.09561
P21980	0.047156	-0.09612
Q8N6H7	0.003357	-0.09706
P62851	0.04521	-0.09738
Q9BTD8	0.017647	-0.09856
P21108	0.008294	-0.10033
Q12788	0.005072	-0.10193
P30566	0.033763	-0.10281
Q15645	0.030261	-0.10512
P13639	0.043225	-0.10729
Q29RF7	0.045577	-0.1073
P17987	0.023155	-0.10915
Q9H223	0.025095	-0.10921
P50991	0.026116	-0.11015
Q9Y285	0.027317	-0.11025
P49915	0.024746	-0.11044
P18621	0.036694	-0.11248
Q15126	0.017246	-0.11257
Q8WXA9	0.02151	-0.11419
Q05397	0.013392	-0.11488
Q9UBL3	0.035179	-0.11673
P26373	0.030507	-0.11784
A3KN83	0.046598	-0.11807
Q9Y5X3	0.048514	-0.11827

P54727	0.008143	-0.11925
Q9P2J5	0.023141	-0.11937
Q6YHU6	0.027657	-0.1204
Q53H96	0.003493	-0.12065
Q99614	0.039329	-0.12135
O76003	0.020302	-0.12372
P78318	0.030117	-0.1247
P42166	0.049983	-0.12589
Q15785	0.031491	-0.12679
P20645	0.010147	-0.12689
P16152	0.047887	-0.12702
Q14558	0.002732	-0.12776
Q9NZ32	0.011186	-0.12842
O43633	0.014263	-0.12849
P11172	0.005541	-0.12864
P63151	0.002041	-0.12894
Q08752	0.009718	-0.12968
Q9NQ88	0.038725	-0.13014
P14550	0.044834	-0.13036
Q99575	0.022144	-0.133
P42226	0.013987	-0.13415
Q9UJK0	0.000968	-0.13458
Q96HC4	0.001017	-0.13616
P62280	0.028892	-0.13702
P40925	0.038026	-0.13727
P51688	0.04827	-0.13788
O43776	0.038266	-0.13879
Q01844	0.038733	-0.1406
O60645	0.024206	-0.14092
P61289	0.02211	-0.14126
Q96RS6	0.036575	-0.14195
Q9BY44	0.018603	-0.14249
Q14166	0.00581	-0.14304
Q5VZK9	0.026002	-0.14325
Q5SW79	0.047431	-0.14447

P11142	0.010658	-0.14554
O75879	0.041355	-0.14577
P34932	0.011797	-0.14643
P40222	0.007978	-0.14681
P42677	0.041444	-0.14741
O95396	0.041774	-0.14796
O95816	0.003378	-0.14853
P62241	0.020418	-0.14865
Q9Y3A5	0.033692	-0.14974
Q92890	0.016145	-0.1499
P31948	0.016781	-0.15004
Q27J81	0.037884	-0.15041
P46060	0.000401	-0.15209
Q9H270	0.019491	-0.15267
P60842	0.01294	-0.15322
Q16204	0.010401	-0.15378
P63279	0.003961	-0.15397
Q9BTE3	0.010861	-0.15454
P06737	0.027305	-0.155
Q9NQX3	0.025088	-0.15581
P30085	0.000529	-0.15585
P30086	0.017153	-0.15593
O60701	0.018382	-0.15593
O75534	0.00403	-0.15722
O43617	0.029573	-0.15779
P46783	0.037761	-0.16328
P16152	0.049008	-0.16403
P25685	0.022845	-0.16555
Q14651	0.041232	-0.16623
P35080	0.026297	-0.16637
P08397	0.015333	-0.16738
Q00796	0.002297	-0.16941
Q7Z4H8	0.043332	-0.16947
Q13085	0.033586	-0.17043
P30825	0.003762	-0.17093

Q9Y617	0.031415	-0.17174
Q96S44	0.04884	-0.17211
P35269	0.027932	-0.17241
P55769	0.044407	-0.17351
Q9P258	0.035452	-0.17471
Q96GD4	0.011341	-0.17475
O60573	0.010149	-0.17498
Q8IU8	0.02111	-0.17586
O60234	0.047442	-0.17614
Q12929	0.018755	-0.17634
Q86YS7	0.023534	-0.17662
Q969X6	0.04724	-0.17664
Q86TB9	0.021979	-0.17878
P78330	0.028151	-0.17968
Q9UHD8	0.007336	-0.17984
P42694	0.03784	-0.17994
P51606	0.010209	-0.18182
Q8NCH0	0.030869	-0.18274
A6NHG4	0.026706	-0.18302
Q8N8A2	0.009119	-0.18395
Q969S3	0.006841	-0.18566
P61758	0.015471	-0.18569
P08195	0.043906	-0.18645
P19525	0.037841	-0.1876
P49643	0.025509	-0.18895
P36639	0.02202	-0.189
P13984	0.027297	-0.18931
Q04206	0.006686	-0.19008
P61457	0.0098	-0.19018
Q92930	0.00707	-0.19069
Q2NL82	0.011402	-0.19078
Q15181	0.01826	-0.19107
Q99543	0.009214	-0.19176
O60361	0.030647	-0.19256
Q9Y4I1	0.00588	-0.19413

P31689	0.018671	-0.1947
P68036	0.030435	-0.19519
Q96PZ0	0.006687	-0.19571
Q9NVM4	0.020949	-0.19632
O75027	0.030782	-0.19741
P11940	0.000531	-0.19895
Q9UBP9	0.005062	-0.20052
P36543	0.014786	-0.20134
Q13153	0.012106	-0.20139
Q06203	0.008585	-0.20264
A8MWX3	0.028508	-0.203
Q16851	0.033535	-0.20372
O60869	0.004182	-0.20384
P48643	0.012257	-0.20407
Q96RL7	0.046586	-0.20449
Q8IYK4	0.035901	-0.20487
P78345	0.007819	-0.20559
P11940	0.012635	-0.206
Q14671	0.003336	-0.20732
Q14195	0.009219	-0.20882
Q14444	0.016499	-0.20941
Q5T447	0.017078	-0.2099
Q15654	0.012707	-0.21037
Q9BY42	0.044542	-0.21051
O75410	0.038836	-0.21093
Q05682	0.039064	-0.21268
P0DMV8	0.000383	-0.21617
Q9NPD8	0.033802	-0.21733
Q92615	0.025999	-0.2174
Q9Y5A9	0.031331	-0.21782
O00625	0.006677	-0.21806
Q16543	0.006124	-0.21823
Q9Y6Y0	0.03008	-0.21825
O75190	0.009198	-0.21848
P0DMV8	0.043061	-0.22003

O75828	0.011048	-0.2203
O95260	0.037427	-0.22055
Q9NTX5	0.010214	-0.22097
Q9NPH3	0.045179	-0.22163
P07910	0.045956	-0.22185
Q9H0E2	0.023745	-0.22249
Q9H267	0.014129	-0.22266
Q13895	0.017781	-0.22402
P63151	0.004256	-0.22423
Q9BXW6	0.038259	-0.2276
Q9H7B2	0.038126	-0.22811
Q8WZA0	0.031356	-0.2292
Q9BYJ9	0.013889	-0.22982
Q7L7X3	0.004712	-0.2301
Q9BRT6	0.018567	-0.23097
Q9ULX3	0.010378	-0.2311
P11802	0.002013	-0.23164
Q9BVG9	0.034372	-0.23166
P55209	0.011407	-0.23394
Q9H0C8	0.013124	-0.23477
P56182	0.00523	-0.2348
A6NDG6	0.005957	-0.23594
O15075	0.014223	-0.23751
Q9H6S0	0.015352	-0.23862
A4D1P6	0.001758	-0.23954
P12268	0.030066	-0.24138
Q9UG63	0.008205	-0.24191
Q9UHD1	0.010917	-0.24247
Q86UL3	0.008308	-0.24253
P11586	0.010575	-0.24307
Q5SW96	0.022225	-0.24376
Q92805	0.049057	-0.24696
Q86WR0	0.043137	-0.24736
Q15382	0.019427	-0.2492
Q86UY6	0.022843	-0.24962

P24941	0.039153	-0.24999
P49005	0.000591	-0.25005
P12277	0.024413	-0.25047
Q9Y2H0	8.05E-05	-0.25338
P51159	0.005385	-0.25367
O43639	0.025083	-0.25406
Q9Y4P8	0.027328	-0.25529
Q5VZE5	0.024996	-0.25535
P06276	0.032419	-0.25616
Q9NWW5	0.047012	-0.25665
Q6PHR2	0.037409	-0.2574
P35610	0.00066	-0.25747
Q6PJG6	0.044424	-0.25778
P38432	0.027432	-0.25929
Q14137	0.010244	-0.26002
P16989	0.01417	-0.26174
Q3KQV9	0.016956	-0.26324
P08237	0.009039	-0.26395
P43490	0.008833	-0.26793
P61960	0.006178	-0.2687
P30520	0.03494	-0.26898
O95721	0.015539	-0.26997
Q8N394	0.024825	-0.27009
O15540	0.007368	-0.27073
Q9Y316	0.00409	-0.271
Q96GA3	0.03532	-0.2721
O75153	2.44E-05	-0.2723
Q969Q0	0.028522	-0.27344
Q9P0K7	0.031615	-0.27425
P51452	0.001898	-0.27699
P54652	0.008178	-0.27851
Q8TF64	0.024219	-0.27924
O14578	0.012496	-0.27942
P20290	0.016486	-0.27947
O75794	0.028761	-0.28044

Q7Z3E5	0.003473	-0.2822
Q96D71	0.007363	-0.28481
Q9UH65	0.005859	-0.28506
O60749	0.01174	-0.28598
P24534	0.003825	-0.28963
Q8N392	0.021855	-0.29511
Q86WQ0	0.046732	-0.29576
Q86W92	0.027766	-0.29608
P54105	0.023806	-0.29787
P04818	0.001556	-0.2989
P31153	0.000946	-0.30068
Q7Z3T8	0.004115	-0.30164
Q16890	0.018451	-0.30196
Q8N0X7	0.012228	-0.30254
Q8TDW7	0.005865	-0.3028
Q92629	0.022485	-0.30317
Q9UKY7	0.023892	-0.30789
Q6NXE6	0.029489	-0.30848
Q15555	0.023222	-0.31238
Q9HD67	0.011954	-0.3135
P32119	0.045321	-0.3184
Q9BZQ8	0.005727	-0.32195
O60711	0.008014	-0.32352
E9PAV3	0.009473	-0.32591
Q49AR2	0.038769	-0.33308
Q9Y2Y1	0.034242	-0.33726
Q9UHR6	0.03348	-0.33827
Q9H773	0.037945	-0.33848
Q13033	0.045399	-0.33882
Q15120	0.042668	-0.33933
Q9GZT9	0.027395	-0.34678
Q16655	0.000251	-0.34763
A0MZ66	0.027981	-0.35159
P43360	0.014584	-0.35458
P63173	0.01536	-0.35911

Q9Y2V2	0.022637	-0.35943
P41162	0.006973	-0.36164
Q8N565	0.014478	-0.36416
Q8TCF1	0.002383	-0.36427
Q9BZ23	0.034782	-0.36868
Q8IVM0	0.008822	-0.37056
Q9NZE8	0.038813	-0.37298
Q9NVN8	0.010626	-0.37572
Q99502	0.027785	-0.37649
Q9NYA1	0.046328	-0.37676
Q96CB8	0.049831	-0.38071
P25391	0.021489	-0.38173
P78324	0.011982	-0.38732
Q96BK5	0.026225	-0.38924
A0A024RBG1	0.008339	-0.38989
A6NCE7	0.004321	-0.39193
P11388	0.02911	-0.40117
Q96B36	0.036866	-0.40815
Q9HA47	0.007133	-0.409
Q9H4M3	0.03683	-0.40922
Q712K3	0.044026	-0.41112
Q9UQN3	0.005127	-0.41202
Q8IV50	0.019066	-0.41327
Q9Y243	0.048401	-0.41333
Q8IUE6	0.030636	-0.4151
P98082	0.007296	-0.41955
O43734	0.015672	-0.42218
O43639	0.045936	-0.42363
O75886	0.009988	-0.42542
Q68DU8	0.016694	-0.42572
P18827	0.017057	-0.42846
Q4ZG55	0.0141	-0.42911
Q9NX74	0.033634	-0.43548
Q9Y2T4	0.03075	-0.43991
P43357	0.031987	-0.44169

Q9UHA3	0.011968	-0.44186
Q8NHU6	0.012091	-0.44545
P13284	0.013416	-0.46906
Q86TG7	0.029235	-0.47821
Q96B01	0.01636	-0.49689
Q9H6R7	0.047963	-0.49905
Q9UKJ3	0.019437	-0.50165
Q9GZN8	0.000292	-0.50552
Q9H8W4	0.01709	-0.50641
Q8N5L8	0.002817	-0.51051
P56211	0.04244	-0.51104
P35219	0.049946	-0.5229
Q02880	0.027773	-0.52342
P12882	0.003021	-0.5308
Q9P0N9	0.035644	-0.54835
O75157	0.009204	-0.56204
Q9Y608	0.012952	-0.5633
Q9Y5X0	0.038297	-0.58113
O14786	0.038751	-0.58484
Q71RS6	0.043911	-0.5943
Q9NP66	0.021493	-0.5968
P41217	0.008985	-0.60324
P49662	0.019711	-0.6042
P33981	0.009758	-0.62014
P35625	0.004196	-0.65809
Q8TBPO	0.028947	-0.66812
P78560	0.019883	-0.68724
Q08AE8	0.032007	-0.69265
P32519	0.011821	-0.70953
Q96EI5	0.001711	-0.71176
Q9NRW4	0.00257	-0.7124
Q15633	0.003246	-0.71409
Q8IU1F1	0.020326	-0.74035
O95164	0.001663	-0.74782
Q96EB1	0.018663	-0.75075

P40126	0.014035	-0.80639
O00560	0.014148	-0.80764
O75030	0.011371	-0.81459
Q5VWP3	0.00216	-0.96846
Q96G04	0.016386	-1.00561

FM3 cell lysate mass spectrometry: CHX-treated vs untreated (n=3)		
UniProtKB	p-value	Log2FC
Q96C01	0.003898	1.441526
Q9NW81	0.001338	1.297362
Q9NU23	0.038564	1.267478
Q7KZN9	0.048174	1.215658
Q9H3K2	0.003997	1.162279
O75394	0.011916	1.158104
Q9UII2	0.030107	1.102198
P17081	0.033237	1.077895
Q5JTJ3	0.006794	1.063897
Q8NI37	0.009406	1.054478
Q8IXM3	0.000363	1.017658
O95997	0.021842	0.951874
O15235	0.02551	0.9359
Q6P1L8	0.000777	0.921353
O60783	0.0011	0.910332
O95563	0.033912	0.909887
Q01469	0.01734	0.887148
Q16540	0.003869	0.885909
Q8IYB5	0.043387	0.866664
P82921	0.031293	0.857826
Q9UHI5	0.042766	0.847807
P82914	0.000983	0.842356
Q9NYZ3	0.029296	0.836717
Q9NZE8	0.012604	0.8325
Q9Y291	0.009013	0.828899

Q9BUB7	0.000906	0.809217
P43360	0.028733	0.796825
Q13309	0.017166	0.795109
Q5U5X0	0.021518	0.784661
Q9BQ48	0.011665	0.779952
Q9BW72	0.0341	0.77093
Q99595	0.00687	0.75086
P82675	0.001139	0.746639
A0PJW6	0.00334	0.726924
Q8N983	0.029914	0.718872
P49406	0.002489	0.715868
Q13084	0.004286	0.712091
Q96DP5	0.006727	0.708987
Q8N183	0.002497	0.707178
Q96C36	0.012405	0.689868
Q9Y2R0	0.002297	0.681407
Q9BYD3	0.003541	0.675955
Q9NWU5	0.006551	0.669888
O15143	0.005025	0.668575
Q96BQ5	0.015317	0.668396
Q96C36	0.003447	0.668164
O14548	0.024747	0.65954
Q9BYD1	0.000906	0.647092
Q99643	0.013637	0.64424
Q9P032	0.000505	0.642895
P50897	0.00101	0.64159
Q15526	0.011385	0.639585
Q9NPL8	0.003264	0.637378
Q8TAE8	0.007361	0.637252
Q5T653	5.79E-05	0.636993
Q99811	0.029363	0.636314
Q9NX20	0.008638	0.636183
Q9NPD8	0.006032	0.634312
P63000	0.01291	0.633285
P60602	0.008847	0.625384

Q9Y3D5	0.029004	0.624138
Q9H0U6	0.002186	0.621665
Q96E11	0.005088	0.621157
P33552	0.034444	0.617758
Q6PCB0	0.046608	0.616291
Q96DV4	0.003961	0.609917
L0R8F8	0.001367	0.606076
Q96A26	0.02935	0.606026
Q9BZE1	0.000543	0.598503
Q8IV50	0.018714	0.591037
O75208	0.010932	0.586743
Q9Y2S7	0.001448	0.585871
P09001	0.00358	0.58462
P13073	0.002475	0.582643
Q9NRX2	0.001126	0.574469
Q9HD33	0.030088	0.573121
Q96EA4	0.003477	0.573006
Q16795	3.89E-05	0.570168
O95149	0.010866	0.56955
Q96A35	0.012548	0.566919
O75251	0.003404	0.565873
Q69YH5	0.038534	0.56574
Q7Z2W9	1.35E-06	0.564119
Q9P0M9	0.009479	0.563783
O00217	0.003243	0.559558
Q5SRD1	0.000954	0.557763
Q9BRJ2	0.002266	0.556909
Q9BYC9	0.028021	0.556796
Q53S33	0.026637	0.552564
P33981	0.012832	0.552433
P52292	0.000118	0.552397
Q9Y2T4	0.04304	0.550103
Q969Z0	0.006009	0.548984
Q5HYK3	0.034668	0.548014
Q8NC60	0.018342	0.547042

Q9Y399	0.001542	0.54695
Q9BU61	0.01542	0.546126
Q9NP92	0.000138	0.545718
Q7Z7F7	0.005204	0.540537
P32322	0.005547	0.54033
P53350	0.003339	0.539505
P14854	0.03157	0.538962
Q8N5G2	0.005254	0.538513
P03915	0.046213	0.536631
Q16763	0.001565	0.536482
Q3ZCQ8	0.00223	0.53142
P82912	0.007499	0.531264
P04818	0.00039	0.528324
P51970	0.006756	0.527309
Q9NYK5	0.008055	0.526062
Q9NYY8	0.000261	0.524508
Q5U623	0.025233	0.52423
Q8NI60	0.039705	0.52213
O60671	0.031051	0.520245
Q9Y2R9	0.009433	0.520211
O75157	0.022917	0.518679
P02462	0.040237	0.510365
O75030	0.005354	0.50996
Q9P0J0	0.009404	0.509339
P35625	0.000859	0.503529
Q9P015	0.009112	0.503361
Q96EY1	0.000819	0.501389
Q9Y2Y1	0.012772	0.498831
Q9NX14	0.017268	0.495945
Q7L592	0.004016	0.493899
O96000	0.011766	0.49212
Q8TBPO	0.014024	0.491085
O00483	0.032265	0.489624
O75438	0.00288	0.485672
Q8TBP6	0.036786	0.482787

Q9UMS0	0.009231	0.478421
Q96TA2	0.003554	0.4765
Q9Y3D9	0.011632	0.470789
Q92665	0.001123	0.468868
Q9H9J2	0.001476	0.466009
O43819	0.000544	0.464713
P07996	0.034078	0.458148
P50213	0.000116	0.456229
Q8IXS6	0.018296	0.455895
Q9H2D1	0.014577	0.454156
Q96GC5	0.025889	0.453911
Q16718	0.006902	0.44961
Q9P0N9	0.025988	0.444994
O76031	0.00343	0.444177
Q9NP80	0.04034	0.442802
Q9Y320	0.005166	0.439289
P43357	0.018367	0.439065
P82663	0.014976	0.43879
P62380	0.037049	0.436984
P31350	0.005285	0.435229
P82664	0.026261	0.431993
Q15029	0.015296	0.431543
P00403	0.017636	0.431331
Q96EK7	0.002671	0.43089
Q9UI09	7.15E-05	0.428381
P23921	0.01564	0.427912
O95905	0.041306	0.425378
Q86TG7	0.038648	0.424399
Q6YN16	0.003692	0.424054
Q9H845	0.00756	0.423722
O75489	0.001343	0.423082
P28331	0.000501	0.422533
P21912	0.000394	0.420278
P56282	0.027964	0.417227
Q9Y584	0.005739	0.416668

P41247	0.029348	0.41653
Q9H0F7	0.047913	0.416428
O95298	0.020301	0.413614
P78395	0.019587	0.412745
O43676	0.047268	0.412524
Q6PJG6	0.028471	0.411743
Q8TBF2	0.031397	0.409879
Q96I51	0.005666	0.409834
O95229	0.045819	0.408683
Q9NVN8	0.01954	0.408666
Q9GZN8	0.013002	0.407876
Q9Y3B7	0.000186	0.407793
Q96EY7	0.000846	0.405582
Q6YP21	0.035437	0.404549
O95857	0.011754	0.402736
P46199	0.023505	0.402571
Q9BYD2	0.00496	0.401704
P56177	0.022571	0.400588
P82932	0.010597	0.399913
Q9H8V3	0.04349	0.399066
P20290	0.003161	0.397623
P51553	0.00345	0.397235
O43678	0.024488	0.39632
P51398	0.025567	0.394904
P56381	0.03083	0.394222
O60869	0.017817	0.3936
O14949	0.004846	0.393555
Q13405	0.02946	0.392468
Q9NQ50	0.047674	0.390597
Q96CU9	0.00549	0.388931
P09669	0.001286	0.388877
Q96B36	0.027065	0.388338
O00762	0.007653	0.38828
P82673	0.003554	0.388126
Q8NFL0	0.034993	0.384796

O43674	0.006031	0.383816
O95168	0.018922	0.383813
Q96IX5	0.020304	0.383458
Q10713	0.000261	0.383419
O14874	0.033955	0.378671
Q9BXW7	0.019938	0.377131
P13693	0.039584	0.373657
P49411	8.43E-05	0.372778
Q9P0J1	0.010961	0.372721
P56556	0.008425	0.371963
Q15036	0.043335	0.370828
P30084	0.008887	0.370332
O75380	0.020138	0.370134
O75496	0.02612	0.36831
Q9H1K1	0.022305	0.367977
P13804	0.000269	0.366659
Q6JQN1	0.001903	0.366196
P47224	0.001108	0.36559
O75027	0.002555	0.363159
O95299	0.008089	0.362197
Q99661	0.02644	0.359443
Q8WUX2	0.034964	0.358962
P10109	0.036824	0.355686
Q7L8L6	0.037417	0.35548
Q9HA47	0.017384	0.354087
Q9HBH1	0.010914	0.353869
O15091	0.007609	0.353501
O75306	0.009748	0.350492
Q9Y2Z9	0.039077	0.346737
Q9NVA1	0.037359	0.346406
Q9BQP7	0.04918	0.345838
P11940	0.006779	0.345497
Q96CG8	0.001897	0.344332
P07919	0.023658	0.342551
E9PAV3	0.012237	0.342496

Q7L3T8	0.007858	0.342344
Q9BQ95	0.040267	0.340764
Q96LI5	0.041226	0.340609
Q99714	0.008194	0.340576
Q9Y2Q9	0.007385	0.340473
Q8NHU6	0.027583	0.339977
Q9HD42	0.025249	0.338563
Q12899	0.046134	0.337747
Q9Y2R5	0.031616	0.337318
Q96EL3	0.003242	0.336755
P31153	0.001984	0.33496
Q9BZL1	0.030861	0.334291
O75439	0.002573	0.332959
P13995	0.000801	0.330635
Q5TC12	0.023562	0.329883
Q9HBU6	0.00755	0.327584
P12882	0.040336	0.326895
Q12965	0.003475	0.325091
Q9Y6M9	0.01201	0.32354
Q7L0Y3	0.002508	0.321537
P82650	0.008542	0.319652
Q15773	0.037262	0.319631
P31040	0.008352	0.319004
P49821	0.005903	0.318882
Q9GZT3	0.002326	0.314678
P0C7P4	0.003591	0.314357
Q96T88	0.009178	0.313266
P54098	0.016024	0.311967
O75503	0.031095	0.311129
Q9NYA1	0.019059	0.310127
Q96GD4	0.036711	0.30901
P82933	0.021969	0.308742
P28347	0.029257	0.306981
P19404	0.01203	0.306859
P11940	4.27E-05	0.306856

Q9NZ43	0.027613	0.305922
P82930	0.000479	0.304206
A3KN83	0.001163	0.304124
P27105	0.000178	0.299793
P22695	0.00293	0.299663
A4D1E9	0.038529	0.299542
P11310	0.002028	0.299085
O43464	0.035674	0.298635
O43615	0.025048	0.29767
P35219	0.031157	0.292096
P26440	0.032971	0.290336
Q14651	0.018693	0.287992
P11802	0.006634	0.287243
O94762	0.038939	0.286157
P02786	0.009159	0.285015
Q5JTZ9	0.000749	0.282214
Q8NEZ5	0.015459	0.28211
O75534	0.01607	0.28027
Q16875	0.048018	0.279393
Q9H223	0.003201	0.279203
P24539	0.02084	0.278079
O75879	0.046784	0.274043
Q13613	0.017023	0.273116
A6NDG6	0.004286	0.272951
Q9UG63	0.009553	0.272501
Q9BVL4	0.005342	0.270456
O43617	0.028367	0.269371
O75351	0.030416	0.267648
Q92552	0.000531	0.266436
P61513	0.035305	0.263926
O75439	0.021158	0.262958
P30626	0.011126	0.262448
P61960	0.025946	0.262356
P23443	0.024558	0.262256
O43639	0.022628	0.262102

Q8NCA5	0.045619	0.260298
Q9H9P8	0.02625	0.259986
O75964	0.016158	0.259833
Q5SW96	0.031249	0.257968
P13051	0.033226	0.256427
Q02218	0.016475	0.253313
P34897	0.023804	0.253112
Q96EH3	0.007066	0.252366
Q14444	0.003271	0.252147
Q96KB5	0.013265	0.250091
Q5JPH6	0.03456	0.248931
Q92747	0.013622	0.248679
O96005	0.006278	0.246892
P48643	0.019318	0.246779
Q9NR31	0.025346	0.245824
P50548	0.043763	0.243582
P55209	0.006044	0.243327
Q86Y56	0.010466	0.240713
P60228	0.022278	0.239934
Q12965	0.047116	0.239137
O14933	0.014484	0.23723
Q3KQV9	0.048941	0.236806
O60870	0.019913	0.235532
O95721	0.042443	0.233545
Q8TEQ6	0.03529	0.233209
Q96Q11	0.01837	0.231983
Q8N8A2	0.033738	0.231963
Q8NE86	0.020173	0.230635
Q9H1P3	0.012622	0.230242
Q9H6X2	0.04924	0.229912
Q9Y276	0.010464	0.229808
P24941	0.016395	0.229611
P40126	0.026145	0.22908
Q9ULW0	0.044524	0.22881
P24534	0.019288	0.228661

P42704	0.002486	0.228034
O75794	0.04921	0.227137
P46783	0.00049	0.226726
O75410	0.034933	0.226278
P63173	0.049666	0.225792
P11940	0.011539	0.225666
Q8NCH0	0.047833	0.225616
Q9NQ88	0.030183	0.223039
P13489	0.027351	0.221862
P36639	0.011784	0.221799
Q92882	0.042968	0.220903
P61586	0.033305	0.220129
Q9NP72	0.020152	0.219106
P06400	0.035739	0.218728
Q9Y4C2	0.019624	0.218626
Q53R41	0.02654	0.218485
P13639	0.011709	0.217709
Q9HCC0	0.022302	0.217619
P36551	0.001101	0.21691
O43837	0.014781	0.216829
Q92947	0.011861	0.21675
P48047	0.031048	0.216507
P12268	0.006388	0.216316
O95164	0.033627	0.21381
P23258	0.00477	0.212792
P52789	0.011283	0.21253
O75608	0.006092	0.211907
Q8TDW7	0.019506	0.210884
P34897	0.002599	0.209887
P31930	0.013169	0.20954
Q9Y5K6	0.037272	0.208987
P46060	0.039437	0.20857
Q9UBV2	0.03178	0.206752
Q7L1Q6	0.004685	0.206111
Q16850	0.022467	0.205271

Q05639	0.031305	0.203607
Q02318	0.000934	0.203208
O75153	5.59E-05	0.201955
Q9Y305	0.010889	0.201249
Q9BQE5	0.030051	0.199838
P36542	0.046554	0.199523
Q16659	0.025418	0.198566
P60201	0.043765	0.198362
Q9P2R7	0.008766	0.196944
O95816	0.000503	0.196521
Q13423	0.044039	0.196091
P33316	0.007732	0.196051
Q13867	0.047094	0.195271
Q96GM8	0.049931	0.194949
Q15382	0.034677	0.194792
P08397	0.015812	0.194147
P55263	0.033124	0.192958
O00505	0.034998	0.192944
Q7Z3T8	0.039943	0.192633
Q5XKP0	0.046957	0.19257
Q9NTX5	0.027986	0.190286
Q5JNZ5	0.044272	0.190237
Q7L2H7	0.049109	0.189852
P61962	0.018067	0.189253
P26641	0.048098	0.188776
P68402	0.009922	0.188284
P31689	0.01485	0.187382
Q13685	0.032611	0.186637
P62993	0.023632	0.186632
P07339	0.008343	0.183526
Q9UBB4	0.028297	0.183341
Q9Y5S1	0.009029	0.183315
Q9UH17	0.020769	0.182542
Q9Y295	0.003563	0.182467
P51606	0.030295	0.182132

Q5T447	0.039479	0.18069
O95793	0.030102	0.180481
Q99439	0.014108	0.179866
P39019	0.042042	0.179497
P30260	0.035332	0.178618
Q9BUT1	0.036812	0.178274
P54652	0.041196	0.177345
Q8WZA1	0.013359	0.176647
P27708	0.015426	0.175967
Q6GMV1	0.025074	0.174841
P26358	0.049282	0.173377
P00491	0.047288	0.173334
P62851	0.011634	0.173118
Q6NYC1	0.033705	0.172743
P60842	0.00846	0.172454
Q9Y676	0.039445	0.172452
Q9Y3F4	0.019533	0.171816
O60361	0.045719	0.170917
P22570	0.033412	0.170544
Q13153	0.034435	0.17042
O15523	0.010406	0.170269
Q9UPY3	0.048731	0.170117
Q13671	0.002517	0.169784
Q9H061	0.008195	0.169422
Q6IA86	0.04547	0.169241
P25325	0.022674	0.169079
P04181	0.002477	0.1676
P36543	0.041558	0.166311
Q8WUH1	0.034907	0.165566
O15143	0.019433	0.164848
Q92696	0.042478	0.164685
O00154	0.011231	0.164667
O00410	0.032412	0.164539
O60493	0.03262	0.164033
P55145	0.025337	0.163271

P08237	0.016814	0.163218
Q2VIQ3	0.023738	0.163101
Q15404	0.018568	0.16308
P63220	0.02775	0.162624
P25205	0.001138	0.162335
P50991	0.010073	0.162314
P33993	0.043769	0.161667
Q9UHD8	0.001276	0.161623
P31483	0.016855	0.161516
Q04206	0.005818	0.161227
P62280	0.037399	0.161127
Q15437	0.041104	0.16013
Q9BQ52	0.016818	0.159702
Q8NFV4	0.036464	0.15942
Q86TB9	0.031694	0.159135
Q9NZ32	0.010414	0.158738
Q9ULX3	0.001746	0.158663
P11586	0.027699	0.158522
Q9NVI1	0.029903	0.158513
Q14807	0.036596	0.157439
P30740	0.046308	0.156898
Q7Z3E5	0.042492	0.155318
P41227	0.048596	0.155284
O75694	0.001496	0.154767
Q12792	0.020399	0.153152
Q9Y316	0.00163	0.152634
Q99961	0.02538	0.151934
P29803	0.02827	0.150451
P08237	0.03295	0.149701
Q04637	0.019167	0.148817
Q96TA1	0.028419	0.148773
O95140	0.025697	0.14824
Q9BY44	0.039144	0.148042
Q9BY32	0.027312	0.146862
Q9Y3P9	0.033667	0.146297

O00303	0.003137	0.145809
Q00341	0.006662	0.144554
Q9Y5A9	0.025788	0.143996
O95486	0.031784	0.142679
Q9BVJ7	0.013544	0.142114
P13716	0.047959	0.141624
P30154	0.000874	0.139703
Q92890	0.042343	0.139413
P61457	0.009569	0.138101
Q8NFF5	0.009951	0.13576
O76003	0.048358	0.135699
P38571	0.046199	0.134535
P78318	0.023558	0.133573
Q9BTE3	0.009056	0.132687
Q16543	0.021014	0.132221
Q3ZCM7	0.03155	0.130882
Q04760	0.024121	0.130264
P53597	0.038502	0.127268
P21108	0.01619	0.127193
P49915	0.014002	0.12653
Q92616	0.006377	0.125787
Q9ULT8	0.017548	0.125153
O43488	0.042109	0.124588
P39748	0.029828	0.12448
Q99623	0.043319	0.122581
P68371	0.026666	0.120846
P47895	0.009919	0.120566
P78371	0.043385	0.119692
P13797	0.034934	0.118398
P11172	0.008895	0.118328
O43396	0.030807	0.116769
P67775	0.039466	0.115268
P40763	0.039372	0.114939
Q9NUQ8	0.045026	0.114333
Q14166	0.01744	0.113858

P17987	0.046456	0.111866
O60701	0.029947	0.111489
P30085	0.045558	0.1105
P28838	0.018643	0.107962
Q9P258	0.025862	0.107562
P30566	0.049706	0.107071
Q07812	0.039976	0.107065
Q15386	0.024829	0.106914
P22033	0.041362	0.106761
Q15003	0.003408	0.106326
P61163	0.042154	0.105931
P43490	0.046887	0.103608
Q8N122	0.019156	0.101854
Q15019	0.037545	0.096077
P21281	0.045935	0.091917
Q13283	0.022847	0.09164
Q8IZH2	0.026633	0.091278
Q8WWC4	0.01511	0.089451
P00367	0.026132	0.089058
P33991	0.047387	0.088373
Q9NXG2	0.044016	0.086582
P49748	0.01998	0.086023
P00367	0.018394	0.084625
Q5VTR2	0.036678	0.084023
P00505	0.045859	0.083216
O95232	0.034649	0.081137
P30837	0.020488	0.0811
Q06210	0.025729	0.07965
Q8NFI4	0.039797	0.078813
P28482	0.018408	0.076176
P61221	0.000578	0.073432
P18621	0.004176	0.071644
Q13404	0.028522	0.067841
O95347	0.012957	0.066719
Q15046	0.011022	0.038716

P19367	0.035467	-0.03528
Q12788	0.046243	-0.05068
Q9NZ45	0.044718	-0.06056
Q6P2Q9	0.047114	-0.06125
Q9UMS4	0.015535	-0.06293
Q92542	0.047306	-0.06299
P23634	0.041094	-0.06607
Q9BWF3	0.008244	-0.06638
Q9Y221	0.029652	-0.06674
P04843	0.003057	-0.06966
Q15155	0.011979	-0.07213
O43143	0.011894	-0.07815
P61978	0.040785	-0.08052
Q9NR30	0.030321	-0.08282
Q06323	0.011247	-0.08524
O75934	0.030806	-0.08883
P22830	0.040795	-0.08898
A6NHR9	0.001112	-0.08939
Q9NX40	0.028447	-0.09088
O94776	0.039008	-0.09152
Q96S52	0.043559	-0.09387
P21796	0.006879	-0.09578
P17174	0.016399	-0.09692
Q15165	0.049086	-0.09775
Q9HAB8	0.040961	-0.09913
P30101	0.021058	-0.10001
Q15434	0.039308	-0.10066
O43252	0.045534	-0.10124
P18074	0.039861	-0.10164
Q15084	0.018957	-0.10235
Q12907	0.010016	-0.10339
P30040	0.030371	-0.10477
Q86W42	0.046767	-0.10578
Q15054	0.024423	-0.10676
Q10471	0.032	-0.10862

A0FGR8	0.012951	-0.10863
O75818	0.027226	-0.10999
P13667	0.015307	-0.1104
Q12905	0.030293	-0.11062
O43707	0.018832	-0.11133
Q9Y6M1	0.030555	-0.11189
P09874	0.049756	-0.11416
Q8N684	0.010192	-0.11435
P56192	0.049961	-0.11528
Q15717	0.031553	-0.11956
Q14839	0.012524	-0.12004
Q9GZR7	0.022904	-0.12131
Q9GZT8	0.02856	-0.12191
Q8WYP5	0.024633	-0.12212
O00116	0.04692	-0.12313
Q14498	0.008133	-0.1236
P49959	0.042907	-0.12484
P49916	0.040856	-0.12615
Q6P9B6	0.003193	-0.12626
Q93009	0.005041	-0.12739
O15160	0.03717	-0.12786
Q9NR45	0.044631	-0.12798
Q8N5C6	0.044425	-0.1285
Q66K74	0.049213	-0.12861
Q13151	0.006064	-0.12912
Q7L5N7	0.015751	-0.13154
P53634	0.012003	-0.13263
P78347	0.024461	-0.13268
Q969T9	0.01564	-0.13289
Q9UPN3	0.02884	-0.13388
Q14160	0.008737	-0.13556
Q9NVP1	0.016983	-0.13585
P54802	0.020238	-0.13821
Q5T3I0	0.01758	-0.13885
Q13884	0.038702	-0.13948

P49755	0.037033	-0.13993
Q13601	0.044006	-0.14141
Q8TD19	0.028872	-0.14181
P51659	0.016887	-0.14421
P07093	0.020381	-0.14467
P07814	0.007939	-0.14583
P19338	0.013132	-0.14587
P28290	0.002071	-0.14599
P06756	0.037566	-0.14616
P11717	0.00556	-0.1467
Q96RW7	0.033762	-0.14697
P15586	0.016685	-0.14733
Q8IZL8	0.013484	-0.14777
P57740	0.033267	-0.14881
O43491	0.00638	-0.14917
P01903	0.008556	-0.14968
Q9NR12	0.045564	-0.14975
O75909	0.016815	-0.15038
O75400	0.001887	-0.1516
Q14573	0.04935	-0.15233
Q9HD45	0.049408	-0.15299
Q9Y2X3	0.017952	-0.15316
P78527	0.000475	-0.15397
Q9HC52	0.049283	-0.15792
P08670	0.015177	-0.15854
Q9BWD1	0.008183	-0.15871
P11387	0.001573	-0.15951
Q15428	0.015613	-0.16053
O43148	0.012375	-0.16125
Q9POL0	0.019828	-0.16236
Q99536	0.010457	-0.16268
Q8TDN6	0.020533	-0.16294
P52756	0.045782	-0.16324
P41223	0.048933	-0.16382
Q9BV38	0.037625	-0.16429

P16615	0.020746	-0.16481
Q96MW5	0.014527	-0.16503
Q8IX11	0.043284	-0.16607
Q9NXS2	0.025346	-0.16624
Q01780	0.008072	-0.16762
O94973	0.003834	-0.16814
Q5JTH9	0.014982	-0.16872
Q9Y2J2	0.020008	-0.16907
Q567U6	0.03568	-0.16919
Q9BTU6	0.048182	-0.16922
Q00839	0.004658	-0.16952
P15559	0.024962	-0.16983
P55265	0.002942	-0.16993
Q13428	0.036643	-0.1703
Q16629	0.025256	-0.171
Q08380	0.004417	-0.17151
P23246	0.018932	-0.17283
Q12906	0.005908	-0.17417
P22626	0.019101	-0.17429
Q9H583	0.03553	-0.17604
P19447	0.049295	-0.17703
Q8TED1	0.038784	-0.1779
Q8IX12	0.030764	-0.17793
P0DMV8	0.005123	-0.17825
Q13523	0.028999	-0.17932
Q96RQ1	0.002547	-0.18107
P31942	0.028541	-0.18125
Q5MIZ7	0.032364	-0.18203
Q5K4L6	0.021019	-0.18383
Q14697	0.006144	-0.18442
P51991	0.022514	-0.18456
Q9H8Y8	0.032576	-0.18473
P22087	0.001559	-0.18552
Q68CQ4	0.022744	-0.18626
O60832	0.038003	-0.18678

Q96GQ7	0.024106	-0.18745
O94766	0.01655	-0.18839
Q5T280	0.044232	-0.18845
O00159	0.004283	-0.18859
Q9NYU2	0.006284	-0.18917
O95425	0.036775	-0.18966
P40967	0.036143	-0.19
P02545	0.046501	-0.19251
O75475	0.022553	-0.19535
P11233	0.024106	-0.19587
P01920	0.004126	-0.19646
P08195	0.002125	-0.19761
P06865	0.00459	-0.19807
Q02790	0.012198	-0.19932
Q99943	0.027639	-0.19946
P61421	0.034466	-0.20044
P98175	0.005534	-0.20063
O94875	0.016627	-0.2013
Q6P4A7	0.014239	-0.20141
P43307	0.021299	-0.20162
Q9BRX8	0.023894	-0.20353
Q13438	0.035646	-0.20455
Q13595	0.013836	-0.20542
Q6IAN0	0.027133	-0.20624
P62873	0.041581	-0.20629
Q07955	0.042292	-0.20753
P28799	0.042312	-0.20953
Q9Y274	0.017551	-0.20973
P41250	0.000338	-0.21012
Q4G0F5	0.009839	-0.21119
Q9UHG3	0.025816	-0.21159
P04440	0.005444	-0.21187
Q9BQ39	0.008311	-0.21193
P53007	0.002647	-0.21244
Q8N2F6	0.000708	-0.213

O75427	0.032418	-0.21431
Q96PY5	0.04672	-0.21445
Q9B XK5	0.02057	-0.21494
Q9UGI8	0.001313	-0.21504
Q8NHP8	0.027362	-0.21614
Q9H8H2	0.016518	-0.21628
Q9UHQ9	0.011809	-0.21656
P17480	0.016566	-0.21673
Q8IYS2	0.006738	-0.21697
Q13330	0.049088	-0.21707
P78330	0.006435	-0.21778
P07686	0.004365	-0.21787
Q9HCD5	0.042883	-0.21844
Q13501	0.01712	-0.21923
Q9UPN3	0.016767	-0.21956
P08240	0.018469	-0.21983
O43818	0.039187	-0.22117
O60568	0.007353	-0.2222
O43390	0.022255	-0.22324
Q12996	0.00894	-0.22454
Q92922	0.014761	-0.22455
P19022	0.03848	-0.22509
Q96EP5	0.019245	-0.22598
P78316	0.043471	-0.22621
P48507	0.017246	-0.22694
Q16674	0.046166	-0.22723
O95251	0.034889	-0.22758
O14662	0.019215	-0.22862
O43175	0.01439	-0.23056
O60502	0.002243	-0.23205
Q96KR1	0.032595	-0.23366
Q15149	0.012271	-0.23431
P21266	0.032593	-0.23439
Q14956	0.04115	-0.23444
O95159	0.021746	-0.23524

Q86V88	0.012093	-0.23567
P49588	0.000683	-0.23588
Q9BVP2	0.00662	-0.23643
Q9NW08	0.035036	-0.23643
P50148	0.008509	-0.23687
P0DMV8	0.01001	-0.23757
Q9BPX7	0.046833	-0.23846
Q9BTY2	0.012156	-0.2387
Q9Y487	0.019194	-0.24183
Q7Z2K6	0.014865	-0.24419
O60294	0.034412	-0.24488
Q6UX04	0.030587	-0.24506
P24821	0.001605	-0.24634
Q9UKM7	0.031727	-0.24665
Q6NZY4	0.035866	-0.24754
O60488	0.00773	-0.2477
Q14554	0.021654	-0.24873
O75525	0.044152	-0.2496
Q9ULX9	0.034115	-0.25118
P29083	0.02297	-0.25157
Q9GZR2	0.031173	-0.25226
O75976	0.026605	-0.25237
Q9Y646	0.021369	-0.25449
P01034	0.022263	-0.25496
P46821	0.008126	-0.25565
P49589	0.001051	-0.25599
Q08426	0.048186	-0.25837
Q4G0J3	0.002705	-0.25842
P53602	0.012057	-0.25893
P07858	0.001125	-0.25972
Q5SSJ5	0.011073	-0.26173
O43933	0.024176	-0.26544
Q9Y4H2	0.021852	-0.26861
P35222	0.016808	-0.26861
P50454	0.035118	-0.27031

Q92544	0.027929	-0.27097
Q1KMD3	0.003108	-0.27432
Q9NY12	0.026601	-0.2744
Q06481	0.017681	-0.2763
Q14192	0.029719	-0.27805
P16278	0.016503	-0.28202
Q8IXI2	0.036962	-0.28293
P13929	0.030926	-0.28572
P15289	0.015056	-0.28807
P10253	0.00845	-0.29044
O15533	0.009865	-0.29119
O14734	0.009885	-0.2925
Q8IZQ5	0.038028	-0.29282
P07602	0.007663	-0.29449
Q96SI9	0.009548	-0.29791
Q8TEA8	0.011741	-0.30113
Q9H2H8	0.015154	-0.30193
P60033	0.006748	-0.30263
Q16643	0.042437	-0.30549
P48681	0.045692	-0.30716
P04062	0.00397	-0.30803
Q9UBR2	0.04213	-0.30841
P01130	0.026211	-0.31031
Q9BYN0	0.030503	-0.31137
Q8IVF7	0.045468	-0.31238
Q8WVC6	0.041046	-0.31742
Q92974	0.00165	-0.32185
Q99538	0.015837	-0.3249
Q68D91	0.004085	-0.32671
P21291	0.02073	-0.32855
Q9C0C4	0.003124	-0.32937
Q5JWF2	0.002695	-0.33373
Q6UVK1	0.000716	-0.33437
Q9BRK5	0.0191	-0.33528
Q8NDI1	0.013581	-0.33535

Q1ED39	0.033414	-0.33559
O95573	0.001232	-0.33762
Q9P270	0.045527	-0.33808
Q13263	0.013935	-0.33999
Q7Z6E9	0.024531	-0.34081
P02788	0.024361	-0.34281
Q9UBG0	0.016695	-0.34395
Q9Y3Q8	0.04629	-0.34698
Q6UX53	0.002493	-0.34982
Q567V2	0.038182	-0.35133
Q96AQ6	0.012092	-0.35604
Q9UHK6	0.022616	-0.35621
Q16881	0.002014	-0.35721
Q9H3G5	0.004664	-0.3585
Q4KMQ2	0.037545	-0.36049
Q9BYG4	0.009451	-0.36561
Q04941	0.003098	-0.37454
Q6KB66	0.003187	-0.38225
O76095	0.019654	-0.38725
Q14108	0.011149	-0.38757
P01911	0.009459	-0.38766
Q96JQ2	0.043577	-0.3914
P17028	0.007643	-0.39219
P30825	0.040084	-0.39405
P01893	0.005148	-0.39777
Q9H5H4	0.017524	-0.40751
Q15758	0.011007	-0.40985
Q8NDI1	0.032664	-0.40998
P20933	0.009876	-0.41019
P30825	0.045271	-0.41628
Q9BTC8	0.005533	-0.42533
Q9NRG9	0.034848	-0.43306
Q96KC8	0.021304	-0.43363
P17029	0.035963	-0.43942
Q629K1	0.026684	-0.44083

Q16881	0.016028	-0.44959
O75578	0.016672	-0.45358
P07711	9.5E-06	-0.45575
Q9BRU9	0.019327	-0.46001
P01768	0.013801	-0.47802
O00767	0.047432	-0.48416
Q92522	0.000702	-0.49518
P05090	0.012783	-0.50225
O15240	0.0113	-0.51496
Q9Y617	0.00059	-0.52416
Q9H1E3	0.016369	-0.53043
P23511	0.047639	-0.53484
Q96CP2	0.02556	-0.53495
P08962	0.00014	-0.56413
Q9H7Z6	0.029827	-0.56451
Q13103	0.019728	-0.56607
Q99988	0.006304	-0.59729
P02794	0.00984	-0.59875
Q8IUH5	0.028372	-0.60415
P01011	0.006989	-0.61355
P43003	0.017604	-0.69928
P02042	0.033555	-0.77044
P08243	4.58E-05	-0.80595
O00458	0.004674	-0.9872
Q9Y3B1	0.001738	-0.99921
O75683	0.037804	-1.06061
P69905	0.008487	-1.11477
P04114	0.010375	-1.12779
Q9Y6M5	1.05E-05	-1.36185
O60637	0.006105	-1.48305
Q9H3L0	0.012396	-1.62472
P09601	0.004276	-1.62872
Q8N339	0.000403	-2.45087
P02795	0.000874	-3.12516

P5B3 and P4B6B cells ECM mass spectrometry; proteins that are at least once significantly expressed in 8 comparisons conducted included here:

UniProt KB	1	2	3	4	5	6	7	8
P00338	0.0937 69	0.1606 67	0.9892 1	0.1535 94	0.2796 94	0.0139 52	0.6432 25	0.7222 29
P01008	0.0107 35	0.0081 74	0.3845 54	0.0023 28	0.1394 8	0.0006 98	0.9939 26	0.9415 41
P02545	0.1566 42	0.0453 2	0.5917 52	0.9113 76	0.2449 49	0.0364 24	0.9425 17	0.8519 15
P02768	0.0348 68	0.3346 48	0.4574 29	0.7576 23	0.8496 14	0.3178 73	0.9996 33	0.4444 79
P04004	0.0141 45	0.0065 98	0.0044 66	0.0251 16	0.2681 12	0.0005 72	0.4326 86	0.8965 76
P04083	0.0249 07	0.0192 26	0.1921 09	0.0716 77	0.2265 03	0.1199 84	0.3259 83	0.2145 56
P05783	0.2488 8	0.3707 94	0.8546 4	0.0467 73	0.1348 13	0.1280 02	0.3245 06	0.1062 89
P05121	0.2572 27	0.0403 6	0.1328 25	0.0048 21	0.6485 43	0.4287 14	0.9031 65	0.2630 86
P05787	0.8266 9	0.1190 78	0.4707 69	0.9997 74	0.2466 88	0.0033 89	0.0658 32	0.2186 06
P08670	0.8031 61	0.7268 6	0.3984 44	0.0601 23	0.3603 18	0.3147 01	0.1435 21	0.0002 81
P07996	0.8620 91	0.1108 97	0.0029 04	0.2433 37	0.1042 73	0.2555 25	0.1306 31	0.7006 49
P11142	0.6705 21	0.2904 75	0.3147 55	0.4695 15	0.2949	0.0126 82	0.2354 19	0.5014 34
P13646	0.3214 56	0.6093 76	0.2287 28	0.1920 16	0.2575 93	0.0472 97	0.0645 46	0.2033 32
P13987	0.3301 4	0.0917 97	0.2666 63	0.5820 62	0.2359 27	0.0187 22	0.0355 97	0.2431 89
P23396	0.1151 12	0.0105 96	0.3533 07	0.5931 52	0.0873 01	0.0068 78	0.6512 17	0.5674 99
P35268	0.2214 4	0.5325	0.3795 84	0.1789 28	0.1300 9	0.1862 08	0.5266 36	0.2635 33

P35527	0.2528 89	0.8964 08	0.0162 82	0.0799 46	0.9556 08	0.8771 52	0.4142 43	0.1832 05
P62805	0.0406	0.0353 38	0.7274 72	0.0814 43	0.2682 11	0.1572 35	0.3445 55	0.5723 32
P63261	0.0127 12	0.1624 66	0.6729 8	0.4519 2	0.1407 32	0.0881 47	0.2626 69	0.8892 15
P68104	0.1404 59	0.0214 57	0.8000 21	0.1160 56	0.1869 11	0.0323 62	0.4378 46	0.4183 57
P62937	0.2131 95	0.0393 49	0.9668 21	0.9351 58	0.4881 93	0.0799 61	0.8299 96	0.4511 39
Q04695	0.0900 89	0.0422 47	0.9893 05	0.0338 99	0.1539 54	0.0786 05	0.8700 48	0.2740 53
Q09666	0.0054 94	0.0247 84	0.1663 71	0.0218 39	0.2016 25	0.2851 86	0.3188 92	0.1872 19
Q13751	0.0037 54	0.3628 8	0.0020 6	0.4448 79	0.2922 3	0.0516 49	0.2222 73	0.1839 9
P84085	0.3099 55	0.3592 58	0.8696 35	0.8731 49	0.2340 88	0.0463 02	0.1750 25	0.2900 11
Q13753	0.0067 31	0.3741 94	0.0065 88	0.8010 78	0.0303 79	0.2162 96	0.8931 88	0.0396 97
Q15582	0.0058 92	0.0393 58	0.0059 19	0.0012 21	0.6026 49	0.0648 85	0.3166	0.0077 1
Q16787	0.0027 7	0.1526 72	0.0057 97	0.8759 29	0.0889 45	0.1422 85	0.7141 95	0.1208 67
Q8TF72	0.1075 67	0.8120 48	0.0998 39	0.0557 63	0.6418 22	0.0712 64	0.1996 43	0.0244 73
Q99880	0.0446 92	0.1065 21	0.5196 15	0.1862 18	0.3912 27	0.1866 24	0.3753 85	0.7789 48
Q9Y6B6	0.8523 99	0.0127 47	0.9777 44	0.6689 36	0.9227 4	0.1029 43	0.4674 38	0.3814 97
P60866	0.0287 32	0.8556 29	0.1432 59	0.5580 72	0.1024 78	0.3528 02	0.1332 83	0.0317 07
P12830	0.9411 19	0.1648 11	0.2069 36	0.4086 82	0.9335 97	0.0467 34	0.3230 98	0.7032 82

comp 1 p-value	P5 TCP-24h vs P5 FS-24h				
comp 2 p-value	P4 TCP-24h vs P4 FS-24h				
comp 3 p-value	P5-TCP-72h vs P5 FS-72h				
comp 4 p-value	P4 TCP-72h vs P4 FS-72h				
comp 5 p-value	P5 FS-24h vs P5 FS 72h				
comp 6 p-value	P4 FS-24h vs P4 FS-72h				
comp 7 p-value	P5 FS-24h vs P4 FS-24h				
comp 8 p-value	P5 FS-72h vs P4 FS-72h				